НАУЧНО ДРУШТВО СРБИЈЕ

SCIENTIFIC REVIEW

New Series

Series: Scientific and Engineering

Special Issue **Nonlinear Dynamics** S2 (2013)
Dedicated to
Milutin Milanković (1879- 1958)

Guest Editors:
Katica R. (Stevanović) Hedrih
and Žarko Mijajlović

Belgrade
2013

НАУЧНО ДРУШТВО СРБИЈЕ

SCIENTIFIC REVIEW

New Series

Series: Scientific and Engineering

Editor-in-Chief: Slobodan Perović

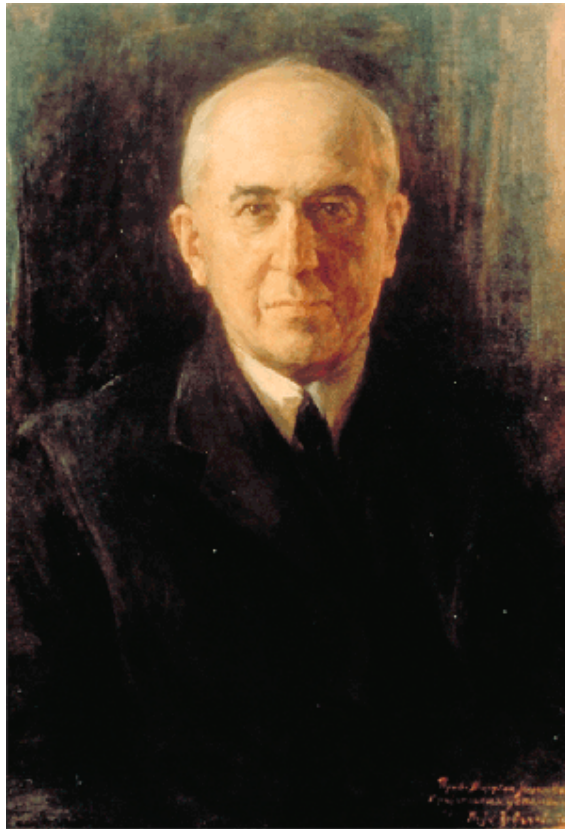**Belgrade**
2013

SCIENTIFIC REVIEW

New Series
Series: Scientific and Engineering

Special Issue **Nonlinear Dynamics** S2 (2013)

Dedicated to

Milutin Milanković (1879- 1958)

SERBIAN SCIENTIFIC
SOCIETY
Belgrade • Šafarikova 7

СЕРБСКОЕ НАУЧНОЕ
ОБЩЕСТВО
Београд   Шафарикова 7

НАУЧНО ДРУШТВО СРБИЈЕ

11000 Београд • Шафарикова 7 • Тел. 381 11 32 24 939

MILANKOVIĆ MILUTIN AND ASTRODYNAMICS

Vladan Djordjević wrote that Milutin Milanković ranks among those great scientists of the world who marked the 20th century .... The chief idea underlying his longstanding work is that climatic variations on the Earth result from regular changes in celestial mechanics (periodical change of the Earth's axis tilt, eccentricity of the Earth' orbit and change of the ecliptic angle), which in turn causes cyclic changes in the intensity of insulation [3].

In 1988., the fourth issue of the university book under the title *Foundation of Celestial Mechanics written by Milutin Milanković[2], was published by scientific book publisher «Naučna knjiga» on 97 pages. In Preface to the first issue from 1947. of this book manuscript, the author wrote that the content of the book was in accordance with the Program of the new curriculum at University of Belgrade, and also that the book contained those parts of celestial mechanics which study the motion of the planets and their secular perturbations. Also, he pointed out that by using own, proper results from own papers published in 1939 and 1941 by Serbian Academy of Sciences, the main attitudes of the expressed theory are obtained in a shorter and more synoptic way. This university book contains the following seven chapters: Newton's law of gravity, Problem of two bodies in celestial mechanics, Unperturbed planetary motions around the sun, General integrals on the motion of N-bodies, General theory of planetary perturbations, Introduction of vector elements in the calculus of perturbations, Review of the classical theory of perturbations, Secular perturbations.*

In the first Chapter of the manuscript under the title Kepler's Law, Milanković writes that by accepting Copernicus' heliocentric system and by using Tiho Brahe's results of the motion of planet Mars, Kepler in the geniuses way derived own laws and published the first two laws in the famous monograph* Astronomia nova de mortibus stellae Martis, 1609 and the third in the book Harmonices mundi, 1619. This university book concludes by the following sentences: «Numerical calculations of the secular change of the planet elements show that eccentricity and inclinations of the orbits of all big planets oscillate between narrow, defined, boundaries, as it is supposed in theory of the secular perturbations of the planets. In 1997 in edition *Choose works of Milutin Milanković* in the seven volumes, in third volume, Milanković's *Celestial mechanics* was published again.

One of the first papers written by Tatomir P. Andjelić, an honorary teaching assistant of applied mathematics at Faculty of Philosophy in Belgrade, and published in 1935, was a review entitled *Celestial mechanics* by M. Milanković. The paper was written after comments and presentation of this book by M. Milanković in Yugoslav Professors society. Milanković's *Celestial mechanics* was the first book published in this area of sciences, in which vector calculus was applied for expression, and assistant Tatomir P. Andjelić grow fond of this method, who obtained a good basis and knowledge of vectors during the study at University in Heidelberg.

In March 1984, academician Tatomira P. Andjelića gave me his newly published book *Introduction to Astrodynamics [2]*, as a present with a sentence as a dedication. This book was published in 1993, on 153 pages in the periodic edition Matematički vidici, in which special publications Monograph in a different area of mathematics and mechanics was published at Mathematical institute of SANU. In Preface to this book, the author writes that during a long period he gave lectures in astrodynamics, as a one of the subjects in postgraduate study of mechanics at Faculty of Mathematical and Natural Sciences in Belgrade. As a professor, he concluded that with the current cosmic research and challenges, it is useful, not only in the specialist publications, but also in postgraduate study, to point out the problems of astrodynamics. This is an important way for a student to obtain basic knowledge for further education and research.

In this sense, in this book academician Andjelić presented in main an introduction necessary for the next scientific research in the area of astrodynamics. His book contains elements of rocketdynamics, astronomy, celestial and rational mechanics, together with theoretical description chain of cosmic motion and some own results and application examples.

References

[1] Milutin Milanković, Kanon osunčavanja, Zavod za udzbenike i nastavna sredstva, Beograd, 1997, pp. 401.
[2] Tatomir P. Andjelić, Uvod u astrodinamiku, Matematički vidici, Matematički institut SANU, 1983., p. 158.
[3] *Djordjević Vladan,* Milutin Milanković (1879-1958), Booklet of Abstracts 6t ISNM NSA NIS 2003, p. 23.

Katica (Stevanović) Hedrih

October 13, 2013, Belgrade, Serbia

ADDREESS BY GUEST- EDITORS

Dear Reader of the Journal Scientific Review,

This Special Issue of the Journal Scientific Review published by Serbian Scientific Society contains invited/selected full papers presented at The Symposium Nonlinear Dynamics – dedicated to Milutin Milanković (Dalj, May 28, 1879-Beograd, December 12, 1958), Multidisciplinary and Interdisciplinary Applications, (SNDMIA 2012), Belgrade, October 1-5, 2012., (Eigth Serbian Symposium in area of Non-linear Sciences), (Симпозијум Нелинеарна динамика - Мулти и интердисциплинарне примене). Special Issue contains 7 full papers of Plenary Lectures, 6 full paper of Invited Lectures and 17 full papers of Contributed Lectures. Eight papers were authored by aboard scientist and other 22 full papers by Serbian scientists and researchers. Selected papers for this Special Issue are from different area of Nonlinear Dynamics: Nonlinear Mechanics, Nonlinear dynamic in Physic-chemical systems, Nonlinear biodynamical systems, Mathematical methods, and other area of sciences.

In Appendix of the Issue are few republished selected abstracts of plenary lectures which contents are published in other scientific journals aboard. Also, Appendix of the Issue contains brief review information about Symposia in Serbia and a short scientific biography of Professor Danilo P. Rašković, under which influence started research projects in area of nonlinear oscillations at Mechanical Engineering Faculty University of Niš. He established first collaboration of researchers from Serbia with academician Yuri Alekseevich Mitropolyskiy-important scientist from area of asymptotic methods on nonlinear Mechanics and main founder of and next International Conference of Nonlinear Oscillations (First ICNO Kiev 1961 – last ICNO Cracow 1990), now continued under the name European

Nonlinear Oscillation Conferences (First ENOC Hamburg 2993- next ENOC Wien 2014).

The Symposium Nonlinear Dynamics – devoted to Milutin Milanković (Dalj, May 28, 1879-Beograd, December 12, 1958), Multidisciplinary and Interdisciplinary Applications, (SNDMIA 2012), Belgrade, October 1-5, 2012., (Eigth Serbian Symposium in area of Non-linear Sciences), (Симпозијум Нелинеарна динамика - Мулти и интердисциплинарне примене) was held in Belgrade, Serbia, and is organized by the Department of Natural-Mathematical Sciences of the Serbian Scientific Society and supported by Project ON174001 (2011-2014) coordinated through Department of Mechanics at Mathematical Institute SANU, in the framework of the scientific activities of the active researchers in area of Nonlinear Dynamics in Serbia and Russia.

Scientific support to the Symposium Nonlinear Dynamics – dedicated to Milutin Milanković (Multidisciplinary and Interdisciplinary Applications, (SNDMIA 2012), Belgrade, October 1-5, 2012 (http://afrodita.rcub.bg.ac.rs/~nds/indexe.html) was given by following scientific institution in Serbia: Project ON174001 (2011-2014) coordinated through Department of Mechanics at Mathematical Institute SANU, Projet OI 172015 through Faculty of Physical Chemistry, University of Belgrade and III 45001 Institute of Chemistry, Technology and Metallurgy, University of Belgrade, Department of Catalysis and Chemical Engineering, Belgrade, Institute „Vincha", The Society of Physical Chemists of Serbia, Faculty of Physical Chemistry University of Belgrade, „Mihajilo Pupin Institute" University of Belgrade, Faculty of Technical Sciences Kosovska Mitrovica, University of Pristina with allocated place in Kosovska Mitrovica, Serbian Society of Mechanics and Section for Nonlinear Phenomena and Complex Systems (funded 27.02.1993 with President Slobodan Anić) and Society Milutin Milanković.

The objective of the SYMPOSIUM was to bring together scientists and engineers working in different areas of science to present and discuss recent developments on different problems of nonlinear dynamics with multi and interdisciplinary applications.

MAIN TOPICS OF THE SSYMPOSIUM

A* Models and methods (analytical, numerical, geometrical, experimental) in nonlinear dynamics.
Qualitative and quantitative analysis of nonlinear dynamic systems.

B* Nonlinear dynamics of continuous, discontinuous and hybrid systems.

C* Bifurcations and chaos.

D* Nonlinear stochastic systems.

E* Nonlinear dynamic phenomena.

F* Control of oscillations and chaos.

G* Applications in mechanics at different scales, and real problems from any branch of engineering science including mechanical, civil, electronic, electrical, communication, medical, materials.

H* Cross-disciplinary topics from applied mathematics, physics, biophysics, genetics, nanotechnology, finance, medicine and earth sciences.

A ROUND TABLE: Research ethics and evaluation of scientific and technological research results was held successfully and the following participants took part with corresponding address talks: Marina V. Shitikova, Pavel S. Krasilnikov, Hiroshi Yabuno, Mikhail Zakrzhevsky, Albert C. J. Luo, Marina Shitikova, Ljiljana Kolar-Anić, Slobodan Anić, Alexandra Maluckov, Ilya B. Simanovskii, Žarko Mijajlović, Željko Čupić, Stevan Maksimović, Alexander Zlenko, Katica R. (Stevanović) Hedrih and other participants.

Since 1992, the European Mechanics Society (EUROMECH) organizes *European Nonlinear Oscillations Conferences* (ENOCs) through its ENOC Committee. Actually, these events have a much longer tradition, since they are successors of the former ICNO (International Conference on Nonlinear Oscillations) series held from 1961 to 1990 in East-European countries. Starting with the 1st International Conference on Nonlinear Oscillations organized in Kiev, 1961, by Professor Yu. A. Mitropolsky, twelve ICNOs were held till 1990. Then, starting with the 1st European Nonlinear Oscillations Conference in Hamburg, 1992, six ENOCs were organized till 2008 (Prague, Copenhagen, Moscow, Eindhoven, St. Petersburg). Details are done in Appendix II.

Professor G. Rega was organizer last ENOC Rome 2011 and we point out his sentences: "It is a great privilege to host the 50th Anniversary Conference of the ICNO-ENOC series in Rome, for the first time in a South-European country".

First Serbian Scientific meeting in area of Nonlinear mechanics (nonlinear oscillations and nonlinear dynamics) was organized by Serbian
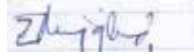
Society of Mechanics and Yugoslav society of Mechanics in 1984 in Arandjelovac. Academician Yu. Alekseevich Mitropolsky attended this Serbian Symposium and give one Plenary invited Lecture. Starting from this period Series of the scientific Symposia or Mini-Symposia were organized by Chair of Mechanics of Mechanical Engineering Faculty, University of Niš supported, by Yougoslav or Serbian Society of Mechanics. Details are done in Appendix III.

We are happy to report that our Symposium Nonlinear Dynamics – dedicated to Milutin Milanković presented 88 abstracts of the nonlinear dynamics contributions in different areas of sciences from 12 countries.

We would like to thank all authors - participants of Symposia for their scientific contribution to Symposium Nonlinear Dynamics, as well as to this Special Issue of the Journal Scientific Review of Serbia Scientific Society.

Guest- Editors of Special Issue of Journal Scientific Review of Serbia
Scientific Society

and

Katica R. (Stevanović) HEDRIH and Žarko Mijajlović
Chairs of Symposium Nonlinear Dynamics – dedicated to Milutin Milanković
and member of Serbian Scientific Society

_____

СРАВНИТЕЛЬНЫЙ АНАЛИЗ АСИМПТОТИЧЕСКИХ МЕТОДОВ ИНТЕГРИРОВАНИЯ НА ПРИМЕРЕ УРАВНЕНИЯ БЕЛЕЦКОГО

Павел Красильников

Кафедра ``Дифференциальные уравнения", МАИ Волоколамское шоссе 4, Москва, 125871, Россия   krasil06@rambler.ru

Abstract. *Small plane oscillations of the satellite in an weak elliptical orbit are investigated. The equation of oscillations of the satellite contains two small parameters: (an orbit eccentricity) and   (a measure of a deviation of a phase point from zero). It is shown that the traditional analysis using connection between yhem, has some lacks. For example, these reduction leads to a set of the shortened equations, therefore the combination of solutions of these equations is required. Moreover, if you use the reduction then equation has not Taylor expansions in a small parameter. The reduction does not allow, as a rule, to investigate a bifurcation of solutions in the space of small parameters, to give completeness information on the oscillations, to investigate the oscillations along arbitrary curves of space of small parameters.*
The small plane oscillations are investigated with the help of the generalized averaging method with small independent parameters. The oscillations in the first and second approximations of averaging method are described. It is shown that researches are free from reduction shortages.

Key words: *satellite; plane oscillations; two small parameters; generalized averaging method.*

1. ВВЕДЕНИЕ

Основы теории малых нелинейных колебаний небесных тел на слабоэллиптической орбите заложены в работах Лапласа Тиссерана, Рауса [1] -- [3], занимавшихся теорией движения Луны относительно ее центра масс. Были исследованы различные типы либраций Луны, амплитуда которых имеет первый порядок малости по e. Первые исследования вращательных движений искусственных спутников Земли на эллиптической орбите при $e = 1$ проведены в статьях [4] -- [7]. Они повторяют в основном результаты классических исследований, когда анализ эксцентриситетных колебаний основан на уравнениях

линейного приближения. В работах [8, 9] содержится вывод строгих уравнений плоских колебаний спутника на эллиптической орбите и уравнение малых колебаний, исследованы эксцентриситетные колебания в первом приближении метода усреднения, построена область параметрических колебаний. Работа [10] посвящена исследованию квазилинейных нерезонансных колебаний спутника, статьи [11, 12] содержат результаты исследований, когда в качестве независимой переменной принята средняя аномалия, при этом уравнения движения разлагаются в ряды Тейлора и Фурье, колебания спутника описываются с точностью до e^2. Подробный обзор цитируемых работ дан в монографии [13].

При исследовании малых колебаний обычно предполагают (по умолчанию) наличие связи между малыми параметрами e и ε, где ε -- мера отклонения фазовой точки от начала координат, определяемая как отношение характерного размера по угловым переменным и скоростям к фиксированным единицам измерения (заданным в системе SI, CGS или MKS). К примеру, во всех рассмотренных выше работах полагается ε : e, т.е. $\varepsilon = \alpha e$, где α -- постоянная величина порядка единицы. Наиболее интересные нелинейные резонансные эффекты вращений спутника были обнаружены в работе [14] вдоль кривой $\varepsilon = e^{1/3}$: исследована задача о существовании, бифуркациях и устойчивости периодических движений спутника с периодом, равным периоду обращения его центра масс по орбите.

Цель работы -- провести сравнительный анализ асимптотических методов интегрирования уравнения плоских колебаний спутника, использующих редукцию и свободных от редукции, описать новые эффекты вращений спутника на основе обобщенного метода усреднения с независимыми малыми параметрами.

2. ВИДЫ РЕДУКЦИЙ УРАВНЕНИЯ БЕЛЕЦКОГО

Исследуем уравнение плоских колебаний спутника

$$(1 + e\cos\nu)\frac{d^2\delta}{d\nu^2} - 2e\sin\nu\frac{d\delta}{d\nu} + 3n^2\sin\delta = 4e\sin\nu \tag{1}$$

Здесь приняты следующие обозначения: $n^2 = (A - C)/B$, A, B, C -- главные центральные моменты инерции аппарата, e -- эксцентриситет орбиты спутника, δ -- удвоенный угол между радиусом вектором центра инерции аппарата и осью z, направленной по его главной центральной оси инерции, относительно которой момент инерции равен C, ν -- истинная аномалия.

Полагаем δ малым: $\delta = \varepsilon\overline{\delta}, \delta' = \varepsilon\overline{\delta}'$. Здесь $\overline{\delta}, \overline{\delta}'$ величины порядка единицы, ε -- малый параметр. Уравнение колебаний спутника примет вид

$$\varepsilon(1 + e\cos\nu)\frac{d^2\overline{\delta}}{d\nu^2} - 2e\varepsilon\sin\nu\frac{d\overline{\delta}}{d\nu} + \omega^2\sin(\varepsilon\overline{\delta}) = 4e\sin\nu, \quad \omega = \sqrt{3}n \tag{2}$$

Линеаризуя это уравнение по δ, получим сингулярно возмущенное уравнение

$$(1+e\cos\nu)\frac{d^2\overline{\delta}}{d\nu^2} - 2e\sin\nu\frac{d\overline{\delta}}{d\nu} + \omega^2\overline{\delta} = 4\frac{e}{\varepsilon}\sin\nu, \quad \omega = \sqrt{3}n$$

частным случаем которого (при $\varepsilon = 1$) является уравнение линейных колебаний спутника, полученное в работе [8].

Рассмотрим редукции задачи, приводящие уравнение (2) к виду, содержащему один малый параметр. Будем считать, что однопараметрическое семейство кривых $f(\varepsilon, e, \alpha) = 0$, $f(0,0,\alpha) = 0$ (α -- параметр семейства), покрывает всю плоскость параметров $\{\varepsilon, e\}$, когда α пробегает область допустимых значений Λ. Вдоль каждой кривой семейства уравнение (2) зависит от одного малого параметра.

Поделив уравнение (2) на $(1+e\cos\nu)$, разложим его в ряд по малым параметрам ε, e. С этой целью представим функции $(1+e\cos\nu)^{-1}$ и $\sin(\varepsilon\overline{\delta})$ в виде рядов:

$$\frac{1}{1+e\cos\nu} = \sum_{n=0}^{\infty}(-1)^n e^n \cos^n\nu, \quad \sin(\varepsilon\overline{\delta}) = \sum_{k=0}^{\infty}(-1)^k \frac{(\varepsilon\overline{\delta})^{2k+1}}{(2k+1)!}$$

Принимая во внимание формулу Коши произведения рядов

$$\sum_{i=0}^{\infty}a_i \cdot \sum_{j=0}^{\infty}b_j = \sum_{k=0}^{\infty}\left(\sum_{s=0}^{k}a_s b_{k-s}\right)$$

получим, после преобразований, уравнение плоских колебаний спутника в виде ряда по независимым малым параметрам ε, e:

$$\overline{\delta}'' + \omega^2\overline{\delta} = 2\sin\nu\left(e\overline{\delta}' + 2\mu\right)\sum_{n=0}^{\infty}(-1)^n e^n \cos^n\nu - $$
$$-\omega^2\sum_{k=1}^{\infty}\left[(-1)^k\cos^k\nu\sum_{s=0}^{k}\frac{e^{k-s}\varepsilon^{2s}\overline{\delta}^{2s+1}}{\cos^s\nu(2s+1)!}\right] \qquad (3)$$

Здесь $\mu = e/\varepsilon$ -- сингулярный параметр. Уравнение (3) и (4) содержит его как величину нулевого порядка, поскольку сумма показателей e и ε равна нулю. Такое определение порядка малости μ является формальным, не учитывающим его сингулярный характер: числовое значение μ неопределено при $e, \varepsilon \to 0$. Порядок малости μ зависит от характера стремления малых параметров к нулю, в частности, определяется асимптотическим поведением кривых редукции в окрестности нуля. Следовательно, он зависит от вида редукции.

Удерживая члены до третьего порядка малости включительно по e и ε, будем иметь:

$$\bar{\delta}'' + \omega^2 \bar{\delta} = 4\mu \sin \nu + e\left[2\bar{\delta}' \sin \nu + \omega^2 \bar{\delta} \cos \nu - 2\mu \sin 2\nu\right] + \frac{\varepsilon^2}{6}\omega^2 \bar{\delta}^3 -$$

$$- e^2\left[\bar{\delta}' \sin 2\nu + \omega^2 \bar{\delta} \cos^2 \nu - 4\mu \cos^2 \nu \sin \nu\right] + \qquad (4)$$

$$+ e^3\left[2\bar{\delta}' \cos^2 \nu \sin \nu + \omega^2 \bar{\delta} \cos^3 \nu - 4\mu \cos^3 \nu \sin \nu\right] - e\varepsilon^2 \frac{\omega^2}{6}\bar{\delta}^3 \cos \nu$$

Для приведения уравнения (4) к регулярному случаю необходимо исключить (в плоскости малых параметров) особую прямую $\varepsilon = 0$ вместе с малой окрестностью. Для этого достаточно потребовать, чтобы при определенных значениях α кривые редукции плотно прилегали к этой прямой, формируя означенную окрестность при условии отсутствия касания их с прямой $\varepsilon = 0$ в нуле. В случае касания имеем $\varepsilon = o(e)$, поэтому $\mu \to \infty$ при $e \to 0$ вдоль кривой редукции, следовательно μ сохраняет сингулярность и за пределами указанной окрестности.

Отметим, что параметр ε играет существенную роль при исследовании малых колебаний спутника, несмотря на то, что исходное уравнение (1) не содержит его явно. Дело в том, что для большинства редукций задачи укороченные уравнения, содержащие первые главные члены разложений в ряд, имеют разный вид в зависимости от величины ε. Увеличивая ε непрерывным образом, получим переход от одного вида уравнений к другому. В дополнении к этому, при любом ε из достаточно малой окрестности, примыкающей к прямой $\varepsilon = 0$, уравнение (1) является сингулярно возмущенным, если $e \neq 0$.

Исследуем подробно различные виды редукции. Для начала рассмотрим простейший ее тип.

3. ЛИНЕЙНАЯ РЕДУКЦИЯ

Положим
$$\varepsilon = \alpha e,$$

где α - постоянная положительная величина, меняющаяся в пределах от нуля до бесконечности (напомним, что e и ε -- положительные величины). Пусть α^* - достаточная малая константа. Тогда параметр $\mu = 1/\alpha$ всюду в плоскости малых параметров, за исключением узкой конической окрестности $0,, \varepsilon < \alpha^* e$ сингулярной прямой $\varepsilon = 0$, имеет порядок малости, равный единицы, так как удовлетворяет условию полосы $0,, \mu,, 1/\alpha^*$.

Здесь следует отметить, что понятие малости μ как функции двух аргументов e, ε мы определяем через условие полосы, так, как это сделано в работах [15, 16].

Определение. Функцию $\mu(\varepsilon, e)$ будем называть функцией k -- го порядка малости по ε, e, если для любых малых положительных δ_1, δ_2 существуют постоянные $A_1(\delta_1, \delta_2) > 0$, $A_2(\delta_1, \delta_2) > 0$ и две скалярные формы k -го порядка

$$F_1(\varepsilon, e) = \sum_{s_1 + s_2 = k} \alpha_{s_1, s_2} \varepsilon^{s_1} e^{s_2}, \ \ F_2(\varepsilon, e) = \sum_{s_1 + s_2 = k} \beta_{s_1, s_2} \varepsilon^{s_1} e^{s_2}$$

положительно определенные в положительном конусе $\{\varepsilon, e : \varepsilon > 0, e > 0\}$, такие, что выполняется условие полосы

$$A_1(\delta_1, \delta_2) F_1(\varepsilon, e) \,,\, |\mu(\varepsilon, e)|, \ A_2(\delta_1, \delta_2) F_2(\varepsilon, e), \tag{5}$$

когда $0 < \varepsilon \,,\, \delta_1, 0 < e \,,\, \delta_2$

Итак, считаем, что $\varepsilon \ldots \alpha^* e$. Подставим в уравнение (4) выражение αe вместо ε, получим:

$$\overline{\delta}'' + \omega^2 \overline{\delta} = \frac{4}{\alpha} \sin \nu + e \left[2\overline{\delta}' \sin \nu + \omega^2 \overline{\delta} \cos \nu - \frac{2}{\alpha} \sin 2\nu \right] -$$

$$- e^2 \left[\overline{\delta}' \sin 2\nu + \omega^2 \overline{\delta} \cos^2 \nu - \frac{4}{\alpha} \cos^2 \nu \sin \nu - \frac{\alpha^2}{6} \omega^2 \overline{\delta}^3 \right] + \tag{6}$$

$$+ e^3 \left[2\overline{\delta}' \cos^2 \nu \sin \nu + \omega^2 \overline{\delta} \cos^3 \nu - \frac{4}{\alpha} \cos^3 \nu \sin \nu - \frac{\alpha^2}{6} \omega^2 \overline{\delta}^3 \cos \nu \right]$$

Здесь $\alpha \ldots \alpha^*$. Редуцированное уравнение (6) зависит от параметра α, однако порядок малости отдельных его членов от α не зависит, следовательно, вид уравнения не меняется при изменении α. Варьируя α непрерывным образом можно исследовать влияние малых параметров ε, e на характер плоских колебаний спутника, но с ограничениями. Дело в том, что линейная связь между ε, e делает невозможным исследование колебаний вдоль нелинейных кривых $f(\varepsilon, e, \alpha) = 0$, с которыми часто связаны наиболее интересные нелинейные эффекты.

Предельное уравнение имеет вид линейного неоднородного уравнения второго порядка:

$$\overline{\delta}'' + \omega^2 \overline{\delta} = \frac{4}{\alpha} \sin \nu$$

4. Нелинейная редукция в явном виде

Рассмотрим зависимость между малыми параметрами в виде показательной функции

$$\varepsilon = e^{\alpha}$$

При $\alpha > 1$ уравнение (2) является сингулярно возмущенным (так как μ сингулярно), неравенство $0 < \alpha \,,\, 1$ отвечает регулярному случаю.

Несложно видеть, что, если в правой части удержать первый главный член разложения, то редуцированное уравнение имеет, в зависимости от области изменения α, следующие формы представления.

Регулярный случай

$$0 < \alpha < \frac{1}{3} \qquad \frac{d^2\overline{\delta}}{d\nu^2} + \omega^2\overline{\delta} = \omega^2 e^{2\alpha}\frac{\overline{\delta}^3}{3!} \qquad (7)$$

$$\alpha = \frac{1}{3} \qquad \frac{d^2\overline{\delta}}{d\nu^2} + \omega^2\overline{\delta} = e^{2/3}\left(\omega^2\frac{\overline{\delta}^3}{3!} + 4\sin\nu\right) \qquad (8)$$

$$\frac{1}{3} < \alpha < 1 \qquad \frac{d^2\overline{\delta}}{d\nu^2} + \omega^2\overline{\delta} = 4e^{1-\alpha}\sin\nu \qquad (9)$$

$$\alpha = 1 \qquad \frac{d^2\overline{\delta}}{d\nu^2} - 2e\sin\nu\frac{d\overline{\delta}}{d\nu} + \omega^2\overline{\delta}(1 - e\cos\nu) = 4(1 - e\cos\nu)\sin\nu \quad (10)$$

Сингулярный случай

$$\alpha > 1, \alpha \in [k, k+1) \qquad \frac{d^2\overline{\delta}}{d\nu^2} + \omega^2\overline{\delta} = (-1)^{k-1}4\sin\nu\frac{\cos^{k-1}\nu}{e^{\alpha-k}} \quad (k = 1, 2, 3\ldots) \quad (11)$$

В вырожденном случае, когда $e = 0$, а параметр α удовлетворяет строгим неравенствам $0 < \alpha < 1$ (первые три уравнения), имеем

$$\frac{d^2\overline{\delta}}{d\nu^2} + \omega^2\overline{\delta} = 0 \qquad (12)$$

Это уравнение описывает малые порождающие колебания спутника на круговой орбите в окрестности положения равновесия $\overline{\delta} = 0$. Его легко получить из (1) с помощью предельного перехода $e \to 0$ и последующего разложения оставшихся функций в ряд по δ.

Случай $\alpha = 1$ стоит особняком. Его предельное уравнение ($e = 0$) имеет вид

$$\frac{d^2\overline{\delta}}{d\nu^2} + \omega^2\overline{\delta} = 4\sin\nu, \qquad (13)$$

отличный от (12). Уравнение (13) нельзя получить из (1) с помощью предельного перехода $e \to 0$ и последующего удержания членов порядка δ, поскольку указанная последовательность действий предполагает выполнения условия $\alpha < 1$, так как члены уравнения (1), содержащие эксцентрисет e сомножителем, должны стремиться к нулю быстрее, чем δ. Уравнение (13) можно получить из (1), выделяя главные члены порядка эксцентрисета -- $\delta''_\nu, \omega^2\delta$ и $4e\sin\nu$ (напомним, что $\delta = e\overline{\delta}$).

Заметим, что уравнение (13), в отличие от (12), нельзя рассматривать как уравнение малых колебаний спутника на круговой орбите. Это уравнение описывает (в первом приближении по малому параметру e) некоторые малые колебания спутника на слабо-эллиптической орбите, причем эти колебания никак

не связаны с его относительным равновесием, так как ни уравнение (10), ни его предельный случай (13) не имеют решения $\overline{\delta} = \text{const}$.

Исследуем области фазового пространства, отвечающие уравнениям регулярного случая. С этой целью рассмотрим отображение фазового пространства на себя:

$$\delta = e^{\alpha}\overline{\delta}, \delta' = e^{\alpha}\overline{\delta}', \quad e \ll 1 \qquad (14)$$

варьируя параметр α в пределах от нуля до бесконечности.

Пусть

$$K[a,b] = \left\{ \overline{\delta}, \overline{\delta}' : a^2 \,,, \; \overline{\delta}^2 + \overline{\delta}'^2 \,,, \; b^2 \right\}$$

есть кольцо, принадлежащее фазовому пространству. Здесь a - его внутренний радиус, b - внешний радиус. Полагаем, что $a, b : 1$. В этом случае, кольцо $K[a,b]$ будет представлять собой множество точек фазового пространства переменных $\overline{\delta}, \overline{\delta}'$, отстоящих от начала координат на расстояниях порядка единицы.

Очевидно, что при каждом фиксированном α отображение (14) порождает преобразование кольца в кольцо:

$$K[a,b] \to K[e^{\alpha}a, e^{\alpha}b]$$

Кольцу $K[e^{\alpha}a, e^{\alpha}b]$ соответствует область в фазовом пространстве исходных переменных δ', δ, удаленная от начала координат на величину порядка e^{α}.

Открытому интервалу $1 < \alpha < +\infty$ соответствует отображение кольца во внутренность круга радиуса eb ($e^{\alpha} \to 0$ при $\alpha \to \infty$, если $e < 1$):

$$K[a,b] \to K[0, eb]$$

Интервалу $1/3 < \alpha < 1$ отвечает отображение $K[a,b] \to K[ea, e^{1/3}b]$, а интервалу $0 < \alpha < 1/3$ -- отображение $K[a,b] \to K[e^{1/3}a, b]$

Если нанести все эти образы кольца $K[a,b]$ на фазовую плоскость, то получим некоторое семейство G колец, которое схематически можно представить набором соответствующих отрезков оси δ (см. рис. 1).
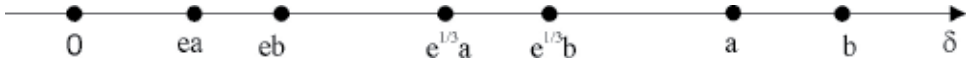

Рис.1 Семейство G

Кольцо $K[m,n]$ представлено здесь отрезком $[m,n]$. Из рисунка следует, что

$$K[ea, eb] = K[0, eb] \cap K[ea, e^{1/3}b], \; K[e^{1/3}a, e^{1/3}b] = K[ea, e^{1/3}b] \cap K[e^{1/3}a, b]$$

Это значит, что "пограничное" множество $K[ea, eb]$, отвечающее случаю $\alpha = 1$, принадлежит также областям фазового пространства, для которых $1 < \alpha < \infty$ и $1/3 < \alpha < 1$. Аналогично, "пограничное" множество $K[e^{1/3}a, e^{1/3}b]$, отвечающее случаю $\alpha = 1/3$, принадлежит областям фазового пространства, для которых $1/3 < \alpha < 1$ и $0 < \alpha < 1/3$.

Из этих рассуждений следует, что окрестность начала координат фазовых переменных δ, δ' (точнее b - окрестность) разбивается на пять кольцевых областей в зависимости от значений параметра α. Кольцу $K[0, ea]$ отвечает укороченное уравнение (11) сингулярного случая. Кольцам $K[ea, e^{1/3}b], K[e^{1/3}a, b]$ отвечают укороченные уравнения (9), (7) соответственно. "Пограничным" кольцам отвечают несколько уравнений одновременно. Так кольцо $K[ea, eb]$ связано с уравнениями (9),(10), (11), а кольцо $K[e^{1/3}a, e^{1/3}b]$ - с уравнениями (7), (8), (9). Последнее означает, что исследование решений из области $K[ea, eb]$, либо $K[e^{1/3}a, e^{1/3}b]$ можно проводить с помощью любого из трех уравнений, отвечающих выбранному кольцу, только надо следить за тем, чтобы параметр α был близок к $\alpha = 1$ в первом случае, и к $\alpha = 1/3$ - во втором.

Заметим, что решая задачу Коши для уравнения (2), необходимо следить за моментом перехода из одной кольцевой области в другую, поскольку этот переход сопровождается сменой типа укороченного уравнения.

Продолжим анализ уравнений регулярного случая, удерживая в редуцированных уравнениях члены более высокого порядка малости по e. Для этого подставим e^{α} вместо ε в уравнение (4), получим

$$\bar{\delta}'' + \omega^2 \bar{\delta} = 4e^{1-\alpha}\sin\nu + e\left[2\bar{\delta}'\sin\nu + \omega^2\bar{\delta}\cos\nu\right] - 2e^{2-\alpha}\sin 2\nu +$$
$$+ e^{2\alpha}\frac{\omega^2\bar{\delta}^3}{6} - e^2\left[\bar{\delta}'\sin 2\nu + \omega^2\bar{\delta}\cos^2\nu\right] + 4e^{3-\alpha}\cos^2\nu\sin\nu + \quad (15)$$
$$+ e^3\left[2\bar{\delta}'\cos^2\nu\sin\nu + \omega^2\bar{\delta}\cos^3\nu\right] - 4e^{4-\alpha}\cos^3\nu\sin\nu - e^{1+2\alpha}\frac{\omega^2}{6}\bar{\delta}^3\cos\nu$$

Рассмотрим случай $0 ,, \alpha < 1/3$. Тогда соотношения между малыми параметрами правой части уравнения (15) задаются неравенствами

$$e^{2\alpha} > e^{1-\alpha} > e > e^{2\alpha+1} > e^{2-\alpha} > e^2 > e^{3-\alpha} > e^3 > e^{4-\alpha}$$

Если ограничиться первыми тремя последовательными членами правой части, то, с учетом этих неравенств, получим

$$\bar{\delta}'' + \omega^2\bar{\delta} = e^{2\alpha}\frac{\omega^2\bar{\delta}^3}{6} + 4e^{1-\alpha}\sin\nu + e\left[2\bar{\delta}'\sin\nu + \omega^2\bar{\delta}\cos\nu\right] \quad (16)$$

Дальнейший анализ показывает, что удержание в уравнении (4) всех членов до 4-го порядка малости включительно вносит существенные коррективы в уравнение (16). К примеру, член 4-го порядка $\omega^2\bar{\delta}^5\varepsilon^4/120$ приводится, с помощью редукции, к виду, содержащему малый параметр $e^{4\alpha}$ сомножителем. Этот сомножитель удовлетворяет неравенствам

$$e^{2\alpha} > e^{4\alpha} > e^{1-\alpha} \quad \text{при } 0 < \alpha < \frac{1}{5}, \qquad e^{1-\alpha} > e^{4\alpha} > e \text{ при } \frac{1}{5} ,, \alpha ,, \frac{1}{4}$$

$$e > e^{4\alpha} > e^{2-\alpha} \quad \text{при } \frac{1}{4} < \alpha < \frac{1}{3},$$

поэтому соответствующий ему член необходимо удержать в правой части уравнения (16). Остальные члены уравнения имеют более высокий порядок малости. Тогда укороченное уравнение запишется в виде совокупности уравнений

$$0 < \alpha \,,\ \frac{1}{5} \qquad \bar{\delta}'' + \omega^2 \bar{\delta} = e^{2\alpha} \frac{\omega^2 \bar{\delta}^3}{6} + e^{4\alpha} \frac{\omega^2}{120} \bar{\delta}^5 + 4e^{1-\alpha} \sin \nu$$

$$\frac{1}{5} < \alpha \,,\ \frac{1}{4} \qquad \bar{\delta}'' + \omega^2 \bar{\delta} = e^{2\alpha} \frac{\omega^2 \bar{\delta}^3}{6} + 4e^{1-\alpha} \sin \nu + e^{4\alpha} \frac{\omega^2}{120} \bar{\delta}^5$$

$$\frac{1}{4} < \alpha < \frac{1}{3} \qquad \bar{\delta}'' + \omega^2 \bar{\delta} = e^{2\alpha} \frac{\omega^2 \bar{\delta}^3}{6} + 4e^{1-\alpha} \sin \nu + e \left(2\bar{\delta}' \sin \nu + \omega^2 \bar{\delta} \cos \nu \right)$$

Член шестого порядка $\omega^2 \bar{\delta}^7 \varepsilon^6 / 7!$ также оказывает влияние на уравнение (16), когда $0 < \alpha \,,\ 1/7$, увеличивая число укорочений. Окончательно, уточненное уравнение (16) предстанет в виде системы уравнений

$$0 < \alpha \,,\ \frac{1}{7} \qquad \bar{\delta}'' + \omega^2 \bar{\delta} = e^{2\alpha} \frac{\omega^2 \bar{\delta}^3}{6} + e^{4\alpha} \frac{\omega^2}{120} \bar{\delta}^5 + e^{6\alpha} \frac{\omega^2}{7!} \bar{\delta}^7$$

$$\frac{1}{7} < \alpha \,,\ \frac{1}{5} \qquad \bar{\delta}'' + \omega^2 \bar{\delta} = e^{2\alpha} \frac{\omega^2 \bar{\delta}^3}{6} + e^{4\alpha} \frac{\omega^2}{120} \bar{\delta}^5 + 4e^{1-\alpha} \sin \nu$$

$$\frac{1}{5} < \alpha \,,\ \frac{1}{4} \qquad \bar{\delta}'' + \omega^2 \bar{\delta} = e^{2\alpha} \frac{\omega^2 \bar{\delta}^3}{6} + 4e^{1-\alpha} \sin \nu + e^{4\alpha} \frac{\omega^2}{120} \bar{\delta}^5$$

$$\frac{1}{4} < \alpha < \frac{1}{3} \qquad \bar{\delta}'' + \omega^2 \bar{\delta} = e^{2\alpha} \frac{\omega^2 \bar{\delta}^3}{6} + 4e^{1-\alpha} \sin \nu + e \left(2\bar{\delta}' \sin \nu + \omega^2 \bar{\delta} \cos \nu \right)$$

На этом закончим работу с уравнением (16). Если в укороченном уравнении удержать большее число членов (четыре, пять членов и так далее), то потребуется последующая его корректировка с учетом членов четвертого, пятого, шестого порядков по e, ε и выше. Основная причина такого эффекта состоит в том, что правая часть уравнения (3) содержит ряд

$$\omega^2 \sum_{k=1}^{\infty} \frac{(-1)^k}{(2k+1)!} \varepsilon^{2k} \bar{\delta}^{2k+1},$$

каждый член которого влияет на укороченное уравнение, разбивая фиксированный интервал $(0, 1/3)$ изменения α на все более мелкие части и увеличивая число укороченных уравнений. Вызвано это тем, что $\varepsilon^{2k} = e^{2k\alpha}$ стремится к единице при $\alpha \to 0$, поэтому каждый член этого ряда проявляет себя как один из главных членов разложения.

Итак, число укороченных уравнений резко возрастает с ростом числа удерживаемых членов, что весьма затрудняет анализ системы. Сложность исследований связана также с *нетейлоровским* разложением правой части уравнения в ряд по малому параметру e и с принципиальной невозможностью приведения такого ряда к стандартному виду теории возмущений. В самом деле, рассмотрим, к примеру, укороченное уравнение, отвечающее интервалу $(1/4, 1/3)$ изменения α. Оно содержит малые параметры вида $e^{2\alpha}, e^{1-\alpha}, e$. Стандартное представление правой части предполагает наличие малого параметра Δ, удовлетворяющего условиям

$$e^{2\alpha} = \Delta^n, \, e^{1-\alpha} = \Delta^m, \, e = \Delta^p$$

где n, m, p -- целые числа, подчиненные неравенствам $n < m < p$. Отсюда явствует, что

$$\alpha = \frac{p-m}{3p-n-2m},$$

поэтому α -- рациональное число. Следовательно, при α иррациональном приведение последовательности $e^{2\alpha}, e^{1-\alpha}, e$ к стандартному виду невозможно.

Предельное уравнение имеет вид линейного осциллятора

$$\overline{\delta}'' + \omega^2 \overline{\delta} = 0 \qquad\qquad\qquad (17)$$

Пусть $\alpha = 1/3$. Положим $\Delta = e^{1/3}$, тогда укороченное уравнение, содержащее три главных члена разложения, имеет вид

$$\overline{\delta}'' + \omega^2 \overline{\delta} = \Delta^2 \left(4\sin\nu + \frac{\omega^2}{6} \overline{\delta}^3 \right) + \Delta^3 \left(2\overline{\delta}'\sin\nu + \omega^2\overline{\delta}\cos\nu \right) - \Delta^4 \frac{\omega^2}{120} \overline{\delta}^5$$

Правая часть этого уравнения приведена к стандартному виду теории возмущений, предельное уравнение имеет вид (17).

Рассмотрим случай $1/3 < \alpha < 1$. Элементарный анализ показывает, что вид укороченных уравнений зависит от области изменения α:

$$\frac{1}{3} < \alpha \,, \, \frac{1}{2} \qquad \overline{\delta}'' + \omega^2\overline{\delta} = 4e^{1-\alpha}\sin\nu + e^{2\alpha}\frac{\omega^2\overline{\delta}^3}{6} + e\left(2\overline{\delta}'\sin\nu + \omega^2\overline{\delta}\cos\nu\right)$$

$$\frac{1}{2} < \alpha \,, \, \frac{2}{3} \qquad \overline{\delta}'' + \omega^2\overline{\delta} = 4e^{1-\alpha}\sin\nu + e\left(2\overline{\delta}'\sin\nu + \omega^2\overline{\delta}\cos\nu\right) + e^{2\alpha}\frac{\omega^2\overline{\delta}^3}{6}$$

$$\frac{2}{3} \,, \, \alpha < 1 \qquad \overline{\delta}'' + \omega^2\overline{\delta} = 4e^{1-\alpha}\sin\nu + e\left(2\overline{\delta}'\sin\nu + \omega^2\overline{\delta}\cos\nu\right) - 2e^{2-\alpha}\sin 2\nu$$

Так же как и в предыдущем случае представление правой части рядом по e имеет нетейлоровский вид при иррациональном α, предельное уравнение описывается формулой (17).

Случай $\alpha = 1$. Подставим в уравнение (15) $\alpha = 1$, получим, удерживая первые три главных члена разложения,

$$\overline{\delta}'' + \omega^2\overline{\delta} \;=\; 4\sin\nu + e\left(2\overline{\delta}'\sin\nu + \omega^2\overline{\delta}\cos\nu - 2\sin 2\nu\right) +$$

$$+ e^2\left(\frac{\omega^2}{6}\overline{\delta}^3 - \overline{\delta}'\sin 2\nu + 4\cos^2\nu\sin\nu - \omega^2\overline{\delta}\cos^2\nu \right)$$

Заметим, что редуцированные уравнения можно раскладывать также в ряд по ε. Для этого достаточно выразить малый параметр e через ε, используя равенство, определяющее редукцию, и подставить это выражение в укороченные уравнения. Удерживая первые два главных члена разложения, будем иметь, при $e = \varepsilon^{1/\alpha}$

$$0 < \alpha < \frac{1}{3} \qquad \frac{d^2\overline{\delta}}{d\nu^2} + \omega^2\overline{\delta} = \omega^2\varepsilon^2\,\frac{\overline{\delta}^3}{3!}$$

$$\alpha = \frac{1}{3} \qquad \frac{d^2\overline{\delta}}{d\nu^2} + \omega^2\overline{\delta} = \varepsilon^2\left(\omega^2\,\frac{\overline{\delta}^3}{3!} + 4\sin\nu\right)$$

$$\frac{1}{3} < \alpha < 1 \qquad \frac{d^2\overline{\delta}}{d\nu^2} + \omega^2\overline{\delta} = 4\varepsilon^{(1-\alpha)/\alpha}\sin\nu$$

$$\alpha = 1 \qquad \frac{d^2\overline{\delta}}{d\nu^2} - 2\varepsilon\sin\nu\,\frac{d\overline{\delta}}{d\nu} + \omega^2\overline{\delta}\left(1 - \varepsilon\cos\nu\right) = 4\left(1 - \varepsilon\cos\nu\right)\sin\nu$$

Аналогично получаются укороченные уравнения более высоких приближений. Отношение порядка между малыми параметрами в разложение по e сохраняется и в разложение по ε, так как из неравенства

$$e^{f(\alpha)} > e^{g(\alpha)}$$

следует, при $\alpha > 0$,

$$\varepsilon^{f(\alpha)/\alpha} > \varepsilon^{g(\alpha)/\alpha}$$

Укажем также на одну характерную особенность редукции: эффект двойственности. Суть его состоит в том, что вдоль каждой кривой $\varepsilon = e^{\alpha}$ редукции сингулярный параметр μ допускает два разных значения порядка малости: γ_1 по e и γ_2 по ε, т.е.

$$\mu = e^{\gamma_1}, \quad \mu = \varepsilon^{\gamma_2}, \quad \gamma_1 \ne \gamma_2$$

Действительно, имеем

$$\mu = \frac{e}{\varepsilon} = \frac{e}{e^{\alpha}} = e^{1-\alpha}, \quad \mu = \frac{e}{\varepsilon} = \frac{\varepsilon^{1/\alpha}}{\varepsilon} = \varepsilon^{(1-\alpha)/\alpha}$$

Отсюда следует, что

$$\gamma_1 = 1-\alpha, \quad \gamma_2 = \frac{1-\alpha}{\alpha}$$

С другой стороны, существуют различные кривые, вдоль которых μ имеет одинаковый порядок малости $(1-\alpha)$. В самом деле, положим

$$\varepsilon = e^{1/(2-\alpha)}, \quad \varepsilon = e^{\alpha}$$

Вдоль первой кривой имеем

$$\mu = \frac{e}{\varepsilon} = \frac{\varepsilon^{2-\alpha}}{\varepsilon} = \varepsilon^{1-\alpha},$$

вторая кривая дает значение μ в виде $\mu = e^{1-\alpha}$.

5. Неявный вид нелинейной редукции (α)

Исследуем редукции, представленные в неявном виде. Для того, чтобы получить уравнение относительно кривых редукции, наложим дополнительное требование на параметр μ: порядок его малости должен быть постоянной

величиной во всей области изменения величин e, ε за исключением малой окрестности прямой $\varepsilon = 0$. Положим, к примеру, этот порядок, равным $2/3$. Тогда μ должен удовлетворять условию полосы

$$0 \,,\ \frac{e}{\varepsilon} \,,\ Ae^{2/3} + D\varepsilon^{2/3} \tag{18}$$

при условии, что форма, стоящая в правой части неравенства, положительно знакоопределена в положительном конусе $\varepsilon > 0, e > 0$.

Кривые редукции определим равенством

$$f(e,\varepsilon) \equiv e - \varepsilon\left(Ae^{2/3} + D\varepsilon^{2/3}\right) = 0, \tag{19}$$

описывающим одну из границ области (18) (другая граница -- ось $e = 0$).

На рис. 2 изображено семейство кривых, описываемых уравнением (19), когда $A = 1$, а D меняется в пределах от 100 безразмерных единиц до малых отрицательных значений. Кривые покрывают всю плоскость малых параметров, при этом форма

$$\left(e^{2/3} + D\varepsilon^{2/3}\right)$$

будет положительно определенной при $D > 0$ и знакопеременной, если $D < 0$. При $D > 0$ кривые редукции заметают область, ограниченную сверху кривой $\varepsilon = e^{1/3}$, отвечающей нулевому значению параметра D. В этой области вдоль каждой кривой семейства порядок малости параметра μ равен 2/3. Более того, всюду выше любой из этих кривых μ имеет тот же порядок малости, так как выполняется условие полосы (18).

Семейство кривых, отвечающее отрицательным значениям D, принадлежит области, расположенной выше кривой $\varepsilon = e^{1/3}$. Вдоль любой из этих кривых условие полосы (18) при $A = 1, D < 0$ теряет силу как определение порядка малости μ. Этот же вывод следует из поведения кривых: они не проходят через ноль и поэтому не могут задавать порядок малости μ в окрестности нуля.
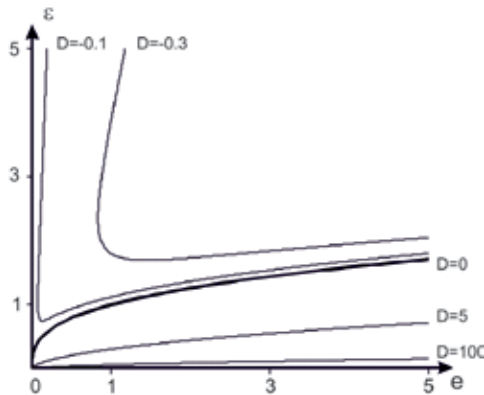

Рис.2 Кривые редукции при $A = 1$

Получим явную зависимость ε от e, ограничиваясь положительными значениями параметра D. Разрешим уравнение (19) относительно ε, рассматривая A, D как произвольные параметры. Легко видеть, что $f'_\varepsilon(e, \varepsilon) = 0$ в точке $e = \varepsilon = 0$, поэтому теорема о неявной функции неприменима.

Воспользуемся методом многоугольника Ньютона. Положим $ù = \varepsilon^{1/3}$, $\lambda = e^{1/3}$. Тогда уравнение (19) примет вид

$$g(ù, \lambda) \equiv Aù^3\lambda^2 + Dù^5 - \lambda^3 = 0 \qquad (20)$$

Будем искать решение $ù = ù(\lambda)$ в виде

$$ù = c_1\lambda^{\alpha_1} + c_2\lambda^{\alpha_2} + \cdots, \quad \alpha_2 > \alpha_1$$

Определим α_1, исходя из условия тождественного обращения уравнения (20) в ноль при подстановки в него искомого решения:

$$A\lambda^2\left(c_1\lambda^{\alpha_1} + c_2\lambda^{\alpha_2} + \cdots\right)^3 + D\left(c_1\lambda^{\alpha_1} + c_2\lambda^{\alpha_2} + \cdots\right)^5 - \lambda^3 \equiv 0$$

Раскрывая скобки, видим, что наименьшую степень имеет один или несколько членов, входящих в сумму

$$Dc_1^5\lambda^{5\alpha_1} + A\lambda^2c_1^3\lambda^{3\alpha_1} - \lambda^3$$

Чтобы уравнение (20) было тождественно равно нулю, необходимо, чтобы член с наименьшим показателем степени не был единственным, так как иначе этому члену не с чем сократиться. Поэтому α_1 следует выбирать так, чтобы среди показателей

$$5\alpha_1,\ 2+3\alpha_1,\ 3 \qquad (21)$$

параметра λ по крайней мере два имели одно и то же значение, остальные показатели должны иметь большие значения. Приравнивая между собой пары показателей, получим следующее множество возможных значений α_1:

$$\alpha_1 = 1, \frac{3}{5}, \frac{1}{3}$$

Легко видеть, что только параметр $\alpha_1 = 3/5$ удовлетворяет дополнительному условию минимальности значений соответствующей пары $\{5\alpha_1, 3\}$ на множестве показателей (21). Очевидно, что уравнение относительно c_1 имеет вид

$$Dc_1^5\lambda^3 - \lambda^3 = 0$$

Отсюда следует, что $c_1 = D^{-1/5}$, поэтому

$$\varepsilon = \left(\frac{e}{D}\right)^{3/5} + \cdots,$$

если $D \neq 0$. Для случая $D = 0$ имеем $\varepsilon = e^{1/3}$.

Построим следующее приближение для кривой $\varepsilon = \varepsilon(e)$, когда $D \neq 0$. Для этого положим

19

$$\text{и} = D^{-1/5}\lambda^{3/5} + z$$

и введем дополнительное обозначение $\theta = \lambda^{1/5}$. В новых переменных уравнение (20) примет вид

$$Dz^5 + 5D^{4/5}\theta^3 z^4 + \left(10D^{3/5}\theta^6 + A\theta^{10}\right)z^3 + \left(10D^{2/5}\theta^9 + 3AD^{-1/5}\theta^{13}\right)z^2 +$$

$$+ \left(5D^{1/5}\theta^{12} + 3AD^{-2/5}\theta^{16}\right)z + D^{-3/5}A\theta^{19} = 0$$

Ищем решение z в виде

$$z = c\theta^{\gamma}$$

Если теперь подставить это выражение в последнее уравнение и выделить в каждом из шести его мономов главные слагаемые, получим совокупность членов вида

$$Dc^5\theta^{5\gamma}, \; 5D^{4/5}c^4\theta^{3+4\gamma}, \; 10D^{3/5}c^3\theta^{6+3\gamma}, \; 10D^{2/5}c^2\theta^{9+2\gamma}, \; 5D^{1/5}c\theta^{12+\gamma}, \; D^{-3/5}A\theta^{19}$$

Несложно видеть, что при $\gamma = 7$ последние два слагаемых имеют одинаковый показатель степени величины θ, минимальный на множестве всех показателей θ для выписанных членов. Следовательно, чтобы удовлетворить алгебраическому уравнению относительно z необходимо сумму последних двух членов положить равной нулю. В результате имеем уравнение относительно c:

$$5D^{1/5}c\theta^{12+\gamma} + D^{-3/5}A\theta^{19} = 0, \quad \gamma = 7$$

Отсюда следует, что

$$c = -\frac{A}{5}D^{-4/5}, \quad \text{и} = D^{-1/5}\lambda^{3/5} - \frac{A}{5}D^{-4/5}\lambda^{7/5},$$

поэтому

$$\varepsilon = D^{-3/5}e^{3/5} - \frac{3A}{5}D^{-6/5}e^{13/15} + \cdots \tag{22}$$

Получим уравнения колебаний спутника вдоль кривых редукции. Для этого подставим найденное значение ε в правую часть уравнения (3) и разложим ее в ряд по e. Будем иметь

$$\overline{\delta}'' + \omega^2\overline{\delta} = 4D^{3/5}\sin\nu e^{2/5} + \frac{12}{5}A\sin\nu e^{2/3} + \frac{36}{25}\frac{A^2}{D^{3/5}}\sin\nu e^{14/15} +$$

$$+ \left(2\overline{\delta}'\sin\nu + \omega^2\overline{\delta}\cos\nu\right)e + \left(\frac{108}{125}\frac{A^3}{D^{6/5}}\sin\nu + \frac{\omega^2\overline{\delta}^3}{6D^{6/5}}\right)e^{6/5} + \cdots \tag{23}$$

Здесь следует положить A равным единице, если рассматривать кривые, изображенные на рис. 2, тогда D -- параметр редукции. Заметим, что он входит в знаменатель многих выражений правой части, при этом показатель его степени непрерывно растет. Следовательно, его влияние сингулярно в окрестности точки $D = 0$: с уменьшением этого параметра необходимо удерживать члены все более высокого порядка малости по e. Предельная кривая $\varepsilon = e^{1/3}$, отвечающая значению $D = 0$, является особой для уравнения Белецкого: вид уравнения вдоль этой кривой резко меняется и принимает форму

$$\overline{\delta}'' + \omega^2\,\overline{\delta} = e^{2/3}\left(4\sin\nu + \frac{\omega^2}{6}\,\overline{\delta}^3\right) + e\left(2\overline{\delta}'\sin\nu + \omega^2\,\overline{\delta}\cos\nu\right) - e^{4/3}\frac{\omega^2}{120}\,\overline{\delta}^5 + \cdots$$

Кроме того, если ограничить уравнение на кривые, расположенные в области $D < 0$, то уравнение теряет силу асимптотического описания движений при $e \to 0, \varepsilon \to 0$, так как кривые редукции не проходят через тривиальную точку $e = \varepsilon = 0$.

Заметим, что первые члены правой части уравнений (23), (24) образованны из выражения $4\mu\sin(\nu)$, поэтому они должны иметь порядок малости, равный $2/3$. Справедливость этого замечания очевидна для уравнения (24), однако уравнение (23) указывает на то, что порядок малости по e равен $2/5$. В этом нет противоречия, так как вдоль кривой (22), отвечающей параметру $\alpha = 3/5$, параметр μ имеет, в силу эффекта двойственности, два порядка малости: $\gamma_1 = 1 - \alpha = 2/5$ по e и $\gamma_2 = (1-\alpha)/\alpha = 2/3$ по ε. Это значит также, что кривые $\varepsilon = e^{1/3}$ и (22) находятся в двойственном отношении: вдоль них μ имеет один и тот же порядок малости, равный 2/3.

6. Неявный вид нелинейной редукции (β).

Рассмотрим теперь однопараметрическое семейство кривых, обобщающее нелинейную редукцию $\varepsilon = e^{\alpha}$, исследованную выше. Для этого положим

$$F(e,\varepsilon) \equiv e - \frac{\varepsilon\left(e^{1-\alpha} + A\varepsilon^{1-\alpha}\right)}{(1+A)} = 0, \quad A \ldots 0 \qquad (25)$$

Здесь A считаем заданной величиной, α -- параметр редукции.

Из определения порядка малости функции двух переменных следует, что порядок величины $\mu = e/\varepsilon$ равен $(1-\alpha)$ в замкнутой области

$$0\,,, \; e/\varepsilon\,,, \; \frac{\left(e^{1-\alpha} + A\varepsilon^{1-\alpha}\right)}{(1+A)}, \qquad (26)$$

ограниченной кривой $e = 0$ и кривой (25).

Случай $\alpha > 1$ отвечает сингулярным значениям μ, поэтому полагаем $\alpha \in (-\infty, 1]$. При $A = 0$ из представления (25) следует классическая редукция $\varepsilon = e^{\alpha}$ с ограничениями в виде $0 < \alpha\,,, \; 1$. Таким образом, обобщенная редукция снимает ограничения на область изменения α, считая нижний предел изменения α равным бесконечности.

На рис. 3 изображено семейство кривых редукции (25) при фиксированном значении параметра А, когда величина α меняется в пределах от $-\infty$ до единицы. При фиксированном α область (26) расположена выше кривой (25).

Получим явное представление кривой $F(e,\varepsilon)=0$ при $\alpha\in(-\infty,1)$ (случай $\alpha=1$ тривиален, так как имеем $e=\varepsilon$). Очевидно, что

$$\frac{\partial F}{\partial \varepsilon}=-\frac{e^{1-\alpha}+A\varepsilon^{1-\alpha}}{1+A}-(1-\alpha)\frac{A}{1+A}\varepsilon^{1-\alpha}, \quad \frac{\partial F}{\partial e}=1-\left(\frac{1-\alpha}{1+A}\right)\frac{\varepsilon}{e^{\alpha}}$$

Отсюда следует, что производная от F по ε равна нулю при $e=\varepsilon=0$, в то время как производная от F по e неопределена при $e=\varepsilon=0$, когда $0<\alpha<1$. Таким образом, функция $F(e,\varepsilon)$ неаналитична в нуле, поэтому классическая теорема о неявной функции не применима.

Заметим, что производная от F по e, вычисленная вдоль кривой (25), принимает конечное значение в нуле:

$$\frac{\partial F}{\partial e}=1-\frac{\varepsilon}{e}\frac{1-\alpha}{1+A}e^{1-\alpha}=1-\frac{1-\alpha}{1+A\left[\dfrac{1+A}{e^{1-\alpha}+A\varepsilon^{1-\alpha}}\right]^{1-\alpha}}\to 1 \text{ при } e,\varepsilon\to 0$$

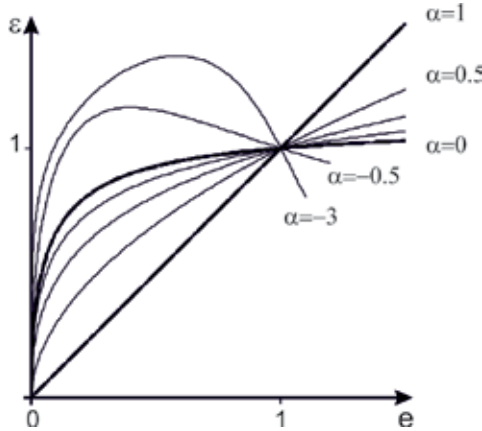Рис.3 Кривые редукции при $A=0.1$ и $\alpha\,, 1$

Это обстоятельство наводит на мысль, что возможно представление e от ε в виде ряда по ε Итак, будем искать $e(\varepsilon)$ в виде формального решения уравнения (25), которое мы запишем в виде

$$e-\frac{\varepsilon}{(1+A)}e^{1-\alpha}=\frac{A}{1+A}\varepsilon^{2-\alpha}, \quad A>0 \tag{27}$$

Заметим, что если из левой части уравнения отбросить второй член, то решение уравнения находится сразу:

$$e=\frac{A}{1+A}\varepsilon^{2-\alpha}$$

При подстановки этой формулы в уравнение (27) члены порядка $\varepsilon^{\alpha^2-3\alpha+3}$ останутся некомпенсированными. Учитывая, что при $\alpha<1$

$$\varepsilon^{\alpha^2-3\alpha+3} = o\left(\varepsilon^{2-\alpha}\right)$$

приходим к выводу, что полученная формула для e является первым членом формального ряда решения исследуемого уравнения. Если взять выражение

$$\frac{A^{1-\alpha}}{(1+A)^{2-\alpha}}\varepsilon^{\alpha^2-3\alpha+3}$$

в качестве второго члена ряда получим, что некомпенсированные члены имеют порядок малости $\alpha^2-3\alpha+3+(\alpha-1)^2$, более высокий, чем $\left(\alpha^2-3\alpha+3\right)$.

Следовательно, приближение искомого решения указанными двумя членами ряда имеет асимптотический характер.

Продолжая этот процесс далее, получим следующий вид формального решения (разложение не тейлоровское):

$$e = \frac{A}{1+A}\varepsilon^{2-\alpha} + \sum_{n=0}^{\infty} a_n \varepsilon^{\alpha^2-3\alpha+3+n(\alpha-1)^2} \qquad (28)$$

Здесь

$$a_0 = \frac{A^{1-\alpha}}{(1+A)^{2-\alpha}}, \quad a_1 = (1-\alpha)\frac{A^{1-2\alpha}}{(1+A)^{3-2\alpha}}, \quad a_2 = \frac{(1-\alpha)(2-3\alpha)}{2}\frac{A^{1-3\alpha}}{(1+A)^{4-3\alpha}}, \dots$$

Ограничим уравнение Белецкого на кривые редукции (28), удерживая первые два члена ряда (28) и первые пять главных членов правой части уравнения:

$$-\infty < \alpha < \frac{3-\sqrt{5}}{2}$$

$$\bar{\delta}'' + \omega^2\bar{\delta} = 4\left[\frac{A}{1+A}\varepsilon^{1-\alpha} + \frac{A^{1-\alpha}}{(1+A)^{2-\alpha}}\varepsilon^{\alpha^2-3\alpha+2}\right]\sin\nu + \frac{A}{1+A}\varepsilon^{2-\alpha}\left(2\bar{\delta}'\sin\nu + \omega^2\bar{\delta}\cos\nu\right)$$

$$+ \frac{\varepsilon^2}{6}\omega^2\bar{\delta}^3 + \frac{A^{1-\alpha}}{(1+A)^{2-\alpha}}\varepsilon^{\alpha^2-3\alpha+3}\left(2\bar{\delta}'\sin\nu + \omega^2\bar{\delta}\cos\nu\right)$$

$$\frac{3-\sqrt{5}}{2} \,,, \ \alpha < \frac{1}{2}$$

$$\bar{\delta}'' + \omega^2\bar{\delta} = 4\left[\frac{A}{1+A}\varepsilon^{1-\alpha} + \frac{A^{1-\alpha}}{(1+A)^{2-\alpha}}\varepsilon^{\alpha^2-3\alpha+2}\right]\sin\nu + \frac{A}{1+A}\varepsilon^{2-\alpha}\left(2\bar{\delta}'\sin\nu + \omega^2\bar{\delta}\cos\nu\right)$$

$$+ \frac{A^{1-\alpha}}{(1+A)^{2-\alpha}}\varepsilon^{\alpha^2-3\alpha+3}\left(2\bar{\delta}'\sin\nu + \omega^2\bar{\delta}\cos\nu\right) + \frac{\varepsilon^2}{6}\omega^2\bar{\delta}^3$$

$$\frac{1}{2} \,,, \ \alpha < 1$$

$$\bar{\delta}'' + \omega^2\bar{\delta} = 4\left[\frac{A}{1+A}\varepsilon^{1-\alpha} + \frac{A^{1-\alpha}}{(1+A)^{2-\alpha}}\varepsilon^{\alpha^2-3\alpha+2}\right]\sin\nu + \frac{A}{1+A}\varepsilon^{2-\alpha}\left(2\bar{\delta}'\sin\nu + \omega^2\bar{\delta}\cos\nu\right)$$

$$+ \frac{A^{1-\alpha}}{(1+A)^{2-\alpha}}\varepsilon^{\alpha^2-3\alpha+3}\left(2\bar{\delta}'\sin\nu + \omega^2\bar{\delta}\cos\nu\right) - 2\left(\frac{A}{1+A}\right)^2\varepsilon^{3-2\alpha}\sin 2\nu$$

Итак, исследуемое уравнение распадается на совокупность укороченных уравнений, в зависимости от области изменения α. Правые части уравнений представлены нетейлоровским рядом по ε.

7. ЗАКЛЮЧЕНИЕ

Анализ редукций уравнения плоских колебаний спутника на слабо-эллиптической орбите приводит к следующим выводам.

1°. Редуцированное уравнение не эквивалентно исходному. Поэтому, любое приведение исследуемого уравнения к случаю одного малого параметра не дает полной картины малых колебаний спутника, в частности, исключает всякую возможность исследовать движений вдоль кривых, не включенных в семейство редукций

2°. Редуцированное уравнение колебаний распадается, как правило, на семейство укороченных уравнений в зависимости от области изменения параметра редукции; число таких уравнений резко возрастает с увеличением числа удерживаемых главных членов разложения

3°. Представление укороченных уравнений в виде ряда по малому параметру часто имеет нетейлоровский вид, что весьма затрудняет применение методов теории возмущений в приближениях высокого порядка

4°. Редуцированные укороченные уравнения малых колебаний отвечают разным кольцевым областям фазового пространства. Поэтому необходимо следить за моментом перехода из одной кольцевой области в другую, поскольку этот переход сопровождается сменой типа укороченного уравнения, и сшивать решения в момент перехода.

5°. При редукции невозможно исследовать бифуркации решений модельных уравнений теории возмущений, за исключением вырожденного случая, когда семейство кривых редукции покрывает бифуркационную поверхность (см. [16])

8. РЕЗОНАНСНЫЕ КОЛЕБАНИЯ СПУТНИКА ПРИ НЕЗАВИСИМЫХ МАЛЫХ ПАРАМЕТРАХ.

1. Колебания при резонансе $\omega - 1 = 0$. Исследуем малые резонансные колебания спутника, описываемые уравнением (2), когда частота ω равна частоте вынуждающей силы $4\mu \sin \nu$, т.е. $\omega = 1$.

Если $\mu = e / \varepsilon$ имеет порядок малости равный единице, т.е. удовлетворяет условию полосы

$$0 ,, \ \mu ,, \ K ,$$

где K - любое конечное число, сколь угодно большое, то, проводя усреднение по быстрой переменной ν с учетом медленного изменения резонансной фазы, получим уравнение с неопределенным временным средним. Дело в том, что интеграл, описывающий временное среднее, содержит члены вида

$\cos(\theta \pm T), \cos(\theta + 3T)$, предел которых не существует при $T \to \infty$ (параметр K на этот результат не влияет).

Для того, чтобы обойти эти сложности, изменим условие полосы, рассматривая μ как малый параметр порядка $(1-\gamma)$, где γ -- любое число, меньшее единицы. Это значит, что μ удовлетворяет неравенству

$$0 \,,\; \mu \,,\; K \frac{\left(e^{1-\gamma} + A\varepsilon^{1-\gamma} \right)}{(1+A)}, \tag{29}$$

задающему некоторую замкнутую область в плоскости малых параметров e, ε. Эта область лежит выше кривой

$$\frac{e}{\varepsilon} = K \frac{\left(e^{1-\gamma} + A\varepsilon^{1-\gamma} \right)}{(1+A)}, \tag{30}$$

которая похожа на кривую (25). Область сингулярного изменения μ расположена ниже этой кривой. Уменьшая γ при фиксированном K, имеем увеличение этой области вследствие возрастающего порядка касания кривой (30) с осью ε в нуле и увеличения максимума кривой. Однако при больших K кривая (30) сильно прижимается к оси e. Таким образом, при $K ? 1$ всюду в любой области, расположенной выше кривой (30), параметр μ будет иметь порядок малости $(1-\gamma)$, за исключением очень узкой окрестности оси $\varepsilon = 0$, лежащей ниже кривой (30).

Будем считать μ и ε независимыми малыми величинами, принадлежащими замкнутой области в пространстве параметров μ, ε, описываемой неравенством (29). Тогда e, как зависимый параметр, вычисляется по формуле $e = \mu\varepsilon$. Очевидно, что e -- величина второго порядка малости. Уравнение плоских колебаний спутника, с точностью до членов третьего порядка малости, примет вид

$$\overline{\delta}'' + \overline{\delta} = 4\mu\sin\nu + \mu\varepsilon\left[2\overline{\delta}'\sin\nu + \overline{\delta}\cos\nu \right] + \frac{\varepsilon^2}{6}\overline{\delta}^3 \tag{31}$$

Порождающее уравнение имеет вид уравнения гармонических колебаний:

$$\overline{\delta}'' + \overline{\delta} = 0$$

Введем новые координаты α, θ по формулам

$$\overline{\delta} = \alpha\cos(\theta+\nu), \quad \overline{\delta}' = -\alpha\sin(\theta+\nu)$$

Тогда уравнения движения примут вид

$$\alpha' = -f(\theta,\nu)\sin(\theta+\nu), \quad \theta' = -\frac{1}{\alpha} f(\theta,\nu)\cos(\theta+\nu)$$

Здесь

$$f(\theta,\nu) = 4\mu\sin\nu - \mu\varepsilon\alpha\left[2\sin\nu\sin(\theta+\nu) - \cos\nu\cos(\theta+\nu) \right] + \frac{\varepsilon^2}{6}\alpha^3\cos(\theta+\nu)^3$$

Усредненные уравнения первого приближения приводить не будем, так как они описывают хорошо известные колебания при линейном резонансе

$$\bar{\delta}'' + \bar{\delta} = 4\mu\sin\nu, \tag{32}$$

для которого характерно неограниченное линейное нарастание амплитуды колебаний по углу $\bar{\delta}$.

Рассмотрим второе приближение метода усреднения. Используя символику усреднения стандартной по Боголюбову системы со многими малыми параметрами, считая $x = (\alpha, \theta)$, $y = (\alpha, \theta)$, получим

$$\frac{dx}{d\nu} = \mu X_{01}(x,\nu) + \varepsilon^2 X_{20}(x,\nu) + \mu\varepsilon X_{11}(x,\nu)$$

Здесь

$$X_{01}(x) = \left\| \begin{matrix} -4\sin\nu\sin(\theta+\nu) \\ -\dfrac{4}{\alpha}\sin\nu\cos(\theta+\nu) \end{matrix} \right\|, \quad X_{20}(x) = \left\| \begin{matrix} -\dfrac{\alpha^3}{6}\cos^3(\theta+\nu)\sin(\theta+\nu) \\ -\dfrac{\alpha^2}{6}\cos^4(\theta+\nu) \end{matrix} \right\|$$

$$X_{11}(x) = \left\| \begin{matrix} \alpha\left(2\sin\nu\sin(\theta+\nu)-\cos\nu\cos(\theta+\nu)\right)\sin(\theta+\nu) \\ \left(2\sin\nu\sin(\theta+\nu)-\cos\nu\cos(\theta+\nu)\right)\cos(\theta+\nu) \end{matrix} \right\|$$

Проводя усреднение по схеме, описанной в работе [16], получим усредненные уравнения второго приближения в переменных α, θ в виде

$$\begin{cases} \alpha' &= -2\mu\cos\theta \\ \theta' &= 2\mu\dfrac{\sin\theta}{\alpha} - \varepsilon^2\dfrac{\alpha^2}{16} \end{cases} \tag{33}$$

Система уравнений (33) имеет первый интеграл

$$\varepsilon^2\alpha^4 - 128\alpha\mu\sin\theta = C \tag{34}$$

Фазовый портрет системы в переменных α, θ для значений параметров $\mu = 0.004$, $\varepsilon = 0.01$ изображен на рис. 4. Жирным цветом выделена сепаратриса, отвечающая значению константы $C = 0$.

Стационарным решениям $\alpha = \alpha_*, \theta = \theta_*$ отвечают уравнения

$$-2\mu\cos\theta_* = 0, \quad 2\mu\frac{\sin\theta_*}{\alpha_*} - \varepsilon^2\frac{\alpha_*^2}{16} = 0$$

Отсюда следует, что

$$\theta_* = \frac{\pi}{2} + k\pi, \quad \alpha_* = \pm 2\sqrt[3]{\frac{4\mu}{\varepsilon^2}} \tag{35}$$

Константа C_*, отвечающая положению равновесия $\alpha = \alpha_*, \theta = \theta_*$, равна

$$C_* = -192\sqrt[3]{4\mu^4}\,\varepsilon^{-2/3}$$

Кривая сепаратрисы имеет две ветви:

$$\alpha = 0; \quad \alpha = \pm 4 \sqrt[3]{\frac{2\mu}{\varepsilon^2} \sin \theta}$$

Отсюда следует, что максимальное значение α^* амплитуды колебаний в зоне
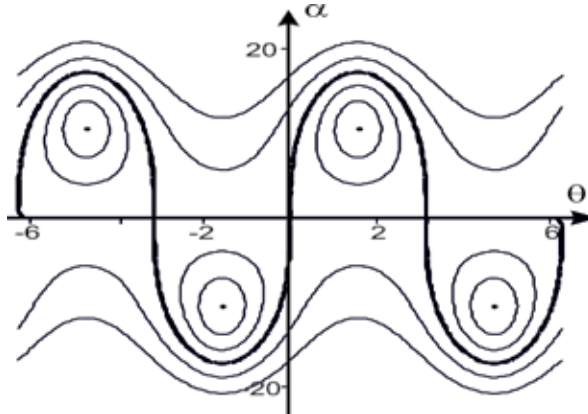

Рис.4 Фазовый портрет при резонансе $\omega = 1$

либрации описывается равенством

$$|\alpha^*| = 4 \sqrt[3]{\frac{2\mu}{\varepsilon^2}} = 4 \frac{\sqrt[3]{2e}}{\varepsilon} \tag{36}$$

Теперь можем сделать выводы. Малые резонансные колебания спутника в окрестности особой точки $\overline{\delta} = \overline{\delta}' = 0$ имеют неограниченный характер, если колебания исследовать в линейном приближении (первое приближение метода усреднения). Нелинейные члены, входящие во второе приближение метода усреднения, меняют характер колебаний: появляются зоны либрации, в которых амплитуда колебаний α и резонансная фаза θ меняется со временем периодические в окрестности стационарной точки (35), достигая максимальных значений по амплитуде (36) при $\theta = \theta_*$, и ротационные (вращательные) движения, отвечающие непрерывному росту резонансной фазы при ограниченных периодических колебаниях амплитуды α.

Как следует из формулы (36), амплитуда колебаний имеет по μ и ε порядок малости равный $(-1/3)$. Это значит, что переменная $\delta = \varepsilon\overline{\delta}$ достигает величин порядка $1/3$ по e, или $2/3$ по μ и ε.

В то же время, вдоль кривой $\mu = \varepsilon^2$ ($e = \varepsilon^3$), принадлежащей области (29), максимальная амплитуда α^* либрационных колебаний и значение α_* стационарной точки (35) не зависят от ε и, следовательно, размах колебаний по углу δ будет гораздо меньше -- порядка ε. Более того, вдоль кривой $\mu = \varepsilon^{2+\gamma}, (\gamma > 0)$ из области (29) амплитуда колебаний α стремится к нулю, когда

$\varepsilon \to 0$! Такое аномальное поведение системы в окрестности сингулярной точки $\delta = \delta' = 0$ объясняется преобладанием (вдоль указанной кривой) нелинейного члена $\varepsilon^2 \overline{\delta}^3 / 6$ над слагаемыми $4\mu \sin \nu, \mu \varepsilon \left[2\overline{\delta}' \sin \nu + \overline{\delta} \cos \nu \right]$, поэтому уравнение колебаний (31) принимает вид возмущенного уравнения Дюффинга.

Все это означает, что размах колебаний при резонансе $\omega = 1$ существенно зависит от соотношений между малыми параметрами μ, ε, несмотря на то, что колебания по углу δ зависят только от параметра e.

Результаты по исследованию резонанса $\omega = 1$ методами усреднения с одним малым параметром e описаны в работе [17]. Сравнительный анализ результатов исследования приводит к следующим выводам.

1. Исследования В.В. Белецкого относятся к случаю $\varepsilon = 1$ (уравнения (31) ,(33)совпадают с соответствующими уравнениями из [17] при $\varepsilon = 1$)

2. Как следствие, уравнения (33), описывающие колебания во втором приближении метода усреднения с двумя малыми параметрами μ, ε, совпадают с усредненными уравнениями первого приближения цитируемой работы

3. Исследование колебаний с двумя независимыми малыми параметрами содержат описание новых эффектов, обусловленных влиянием ε: увеличение максимальной амплитуды колебаний α^* в зоне либрации с уменьшением ε (μ считаем фиксированным), что непосредственно связано с явлением внешнего резонанса (см. уравнение (32)) в малой окрестности точки $\varepsilon = 0$; наличие ``аномальных'' кривых в плоскости параметров μ, ε.

Отметим также, что более подробное исследование влияния параметра ε на резонансные колебания спутника описано в работе [14], когда малые параметры связаны равенством $\varepsilon = e^{1/3}$.

2. Колебания при резонансе $2\omega - 1 = 0$

Исследуем колебания спутника в первом и во-втором приближениях метода усреднения, когда частота ω его собственных колебаний равна половине частоты вынуждающей силы $4\mu \sin \nu$, т.е. $\omega = 1/2$. С этой целью представим уравнение (4) в упрощенном виде, предполагая параметр μ величиной нулевого порядка малости: $0,, \mu,, K$, где K -- постоянная, достаточно большая величина. Удерживая члены до второго порядка малости включительно, получим:

$$\overline{\delta}'' + \omega^2 \overline{\delta} \;=\; 4\mu \sin \nu + e \left[2\overline{\delta}' \sin \nu + \omega^2 \overline{\delta} \cos \nu - 2\mu \sin 2\nu \right] + \frac{\varepsilon^2}{6} \omega^2 \overline{\delta}^3 -$$
$$- e^2 \left[\overline{\delta}' \sin 2\nu + \omega^2 \overline{\delta} \cos^2 \nu - 4\mu \cos^2 \nu \sin \nu \right]$$

Здесь, в отличие от резонанса $\omega = 1$, возмущающий член $4\mu \sin \nu$ не является резонансным, поэтому порождающее уравнение берем в виде

$$\overline{\delta}'' + \omega^2 \overline{\delta} = 4\mu \sin \nu$$

Его решение описывает периодические колебания вида

$$\overline{\delta} = \alpha\cos\varphi + \frac{4\mu}{\omega^2-1}\sin\nu, \quad \overline{\delta}' = -\alpha\omega\sin\varphi + \frac{4\mu}{\omega^2-1}\cos\nu,$$

где $\varphi = \omega\nu + \varphi_0$.

Используя эти равенства как замену переменных $\overline{\delta}, \overline{\delta}' \to \alpha, \varphi$, приведем уравнения колебаний (37) к следующей форме:

$$\frac{d\alpha}{d\nu} = -\frac{1}{\omega}f(\alpha,\varphi,\nu)\sin\varphi, \quad \frac{d\varphi}{d\nu} = \omega - \frac{1}{\alpha\omega}f(\alpha,\varphi,\nu)\cos\varphi$$

Здесь

$$f(\alpha,\varphi,\nu) = e\left[-2\alpha\omega\sin\nu\sin\varphi + \frac{6\mu}{\omega^2-1}\sin 2\nu + \omega^2\alpha\cos\nu\cos\varphi\right] + e^2[\alpha\omega\sin 2\nu\sin\varphi -$$

$$- \frac{4\mu(1+2\mu)}{\omega^2-1}\sin\nu\cos^2\nu - \omega^2\cos^2\nu\alpha\cos\varphi] + \varepsilon^2\frac{\omega^2}{6}\left[\alpha\cos\varphi + \frac{4\mu}{\omega^2-1}\sin\nu\right]^3$$

Вводим в рассмотрение резонансную расстройку $\Delta = 2\omega - \nu\left(\Delta = e\gamma, 0,, \gamma,, 1\right)$ и резонансную фазу $\theta = 2\varphi - \nu$, медленно меняющуюся со временем. В новых переменных α, θ уравнения колебаний будут иметь вид (38) при условии замены φ на $(\theta + \nu)/2$, замене первого слагаемого в уравнении по φ на Δ с удвоением второго слагаемого.

Первое приближение метода усреднения

Для того, чтобы получить усредненные уравнения первого приближения, удержим в функции (38) члены первого порядка малости. После усреднения правых частей по ν, получим систему уравнений, не содержащую ε:

$$\frac{d\alpha}{d\nu} = -\frac{\omega-2}{4}e\alpha\sin\theta$$

$$\frac{d\theta}{d\nu} = \Delta - \frac{\omega-2}{2}e\sin\theta,$$

Учитывая, что $\omega = (\Delta+1)/2$, первый интеграл усредненных уравнений примет вид

$$\alpha^2\left[-4\Delta + e\cos\theta(\Delta-3)\right] = C \tag{39}$$

Сначала рассмотрим случай строгого резонанса, когда резонансная расстройка Δ равна нулю. Тогда амплитуда колебаний будет зависеть от θ следующим образом:

$$\alpha = \sqrt{-\frac{C}{3e\cos\theta}}$$

Отсюда следует, что при $\theta = \pi/2 + k\pi$ амплитуда α принимает бесконечные значения, что приводит к недопустимой раскачке колебаний спутника. Можно показать, что амплитуда колебаний растет со временем по экспоненте при любом малом e, поэтому колебания являются параметрическими.

Если изменить частоту ω таким образом, что резонансная расстройка станет отличной от нуля, зона экспоненциального роста колебаний сохранится, вместе с тем, появится зона ограниченного изменения α. Действительно, из интеграла (39) явствует, что в случае

$$\left|\frac{4\Delta}{(3-\Delta)e}\right|\;,,\;1 \tag{40}$$

амплитуда α стремится к бесконечности при $\theta \to \theta^{\mathring{a}}$, при условии, что значение $\theta^{\mathring{a}}$ вычисляется по формуле

$$\cos\theta^{\mathring{a}} = \frac{4\Delta}{e(\Delta - 3)}$$

Если неравенство (40) выполняется с противоположным знаком, колебания имеют ограниченный характер, так как коэффициент, стоящий при α^2 в левой части интеграла (39), отличен от нуля при любых значениях θ и e.

Элементарный анализ показывает, что неравенство (40) эквивалентно неравенству

$$2\frac{(1-e)}{4-e} < \omega < 2\frac{(1+e)}{4+e},$$

определяющему область параметрического резонанса.

Второе приближение метода усреднения

Исследуем колебания спутника во втором приближение метода усреднения. Чтобы привести уравнения (38) к стандартному по Боголюбову виду, введем дополнительные переменные z,ψ по формуле

$$z = \theta - \psi, \quad \psi = \Delta\nu$$

Тогда уравнения (38) примут вид

$$\frac{d\alpha}{d\nu} = -\frac{1}{\omega}F(\alpha, z, \psi, \nu)\sin\frac{z+\psi+\nu}{2}, \quad \frac{dz}{d\nu} = -\frac{2}{\alpha\omega}F(\alpha, z, \psi, \nu)\cos\frac{z+\psi+\nu}{2}, \quad \frac{d\psi}{d\nu} = e\beta$$

где

$$F(\alpha, z, \psi, \nu) = f\left(\alpha, \frac{z+\psi+\nu}{2}, \nu\right)$$

Полагая вектор столбец x равным $(\alpha, z, \psi)^{\tau}$, преобразуем эти уравнения к следующему виду:

$$\frac{dx}{d\nu} = eX_{01} + \varepsilon^2 X_{20} + e^2 X_{02}$$

Здесь приняты следующие обозначения (угол $\varphi = (z+\psi+\nu)/2$ использован для сокращения записи):

$$X_{01} = \left\| \begin{array}{c} \left[2\alpha \sin\nu \sin\varphi - \dfrac{6\mu}{\omega(\omega^2-1)}\sin 2\nu - \omega\alpha\cos\nu\cos\varphi \right] \sin\varphi\, 5pt \\[2mm] \left[4\sin\nu \sin\varphi - \dfrac{12\mu}{\alpha\omega(\omega^2-1)}\sin 2\nu - 2\omega\cos\nu\cos\varphi \right] \cos\varphi\, 5pt \\[2mm] \beta \end{array} \right\|,$$

$$X_{20} = \left\| \begin{array}{c} -\dfrac{\omega}{6}\left[\alpha\cos\varphi + \dfrac{4\mu\sin\nu}{\omega^2-1} \right]^3 \sin\varphi\, 5pt \\[2mm] -\dfrac{\omega}{3\alpha}\left[\alpha\cos\varphi + \dfrac{4\mu\sin\nu}{\omega^2-1} \right]^3 \cos\varphi\, 5pt \\[2mm] 0 \end{array} \right\|,$$

$$X_{02} = \left\| \begin{array}{c} \left[\cos^2\nu\left(\dfrac{4\mu(1+2\mu)}{\omega(\omega^2-1)}\sin\nu + \omega\alpha\cos\varphi \right) - \alpha\sin 2\nu \sin\varphi \right] \sin\varphi\, 5pt \\[2mm] \left[\cos^2\nu\left(\dfrac{8\mu(1+2\mu)}{\alpha\omega(\omega^2-1)}\sin\nu + 2\omega\cos\varphi \right) - 2\sin 2\nu \sin\varphi \right] \cos\varphi\, 5pt \\[2mm] 0 \end{array} \right\|$$

Проведя усреднение этих уравнений ([16]), содержащих два независимых малых параметра e, ε, получим усредненные уравнения второго приближения, зависящие только от одного малого параметра e:

$$\frac{d\beta}{d\nu} = -\frac{e}{4}(\omega-2)\beta\sin\theta,$$
$$\frac{d\theta}{d\nu} = \Delta - \frac{e}{2}(\omega-2)\cos\theta - \omega\left[\frac{\beta^2}{8} + \frac{4e^2}{(\omega^2-1)^2} \right] - \frac{e^2}{2}\left[\omega - \frac{(\omega+2)^2}{8} \right] \qquad (41)$$

Здесь $\beta = \varepsilon\alpha, \theta = z + \psi$ -- резонансная фаза.

Уравнения (41) допускают интеграл

$$F(\beta,\theta) \equiv \beta^2\left(1967e^2 + 18\beta^2 + 144e\Delta\cos\theta - 432e\cos\theta - 576\Delta \right) = C \qquad (42)$$

Рассмотрим случай строгого резонанса: $\Delta = 0$. Тогда интеграл (42) упростится:

$$G(\beta,\theta) \equiv \beta^2\left(1967e^2 + 18\beta^2 - 432e\cos\theta \right) = C$$

Следует различать два принципиально разных случая колебаний. В первом случае выражение, стоящее в скобках, больше нуля при любых значениях θ и, следовательно, θ может меняться непрерывным образом от $-\infty$ до $+\infty$, при этом амплитуда β будет ограниченной функцией резонансной фазы, фазовые кривые незамкнуты. Такое поведение решений усредненной системы возможно только тогда, когда

$$1967e^2 - 432e > 0$$

т.е. при

$$e > e_*, \quad e_* = \frac{432}{1967}$$

Во-втором случае выражение, стоящее в скобках, может обращаться в ноль при некоторых значениях θ, что отвечает нулевому значению постоянной C. Появляются области на фазовой плоскости, содержащие положения равновесия и замкнутые траектории. Таким образом, характер колебаний усложняется, так как наряду с чисто вращательными движениями предыдущего случая появляются периодические колебания.

Для построения фазового портрета необходимо найти все положения равновесия уравнений (41). Проще всего это сделать, если воспользоваться теоремой Рауса, которая утверждает, что если первый интеграл уравнений движения принимает невырожденное стационарное значение в некоторой точке (на некотором многообразии), то это точка представляет собой положение равновесия системы (интегральное многообразие).

Условия стационарности функции $G(\beta, \theta)$ имеют вид

$$\frac{\partial G}{\partial \beta} \equiv \beta\left(72\beta^2 - 864e\cos\theta + 3934e^2\right) = 0$$

$$\frac{\partial G}{\partial \theta} \equiv 432\beta^2 e\sin\theta = 0$$

(43)

Отсюда следует, что

$$\theta^* = 2k\pi, \beta^* = \sqrt{12e - \frac{1967}{36}e^2}$$

Значения $\theta^* = (2k+1)\pi$ мы отбрасываем, поскольку им отвечает комплексное значение амплитуды. Очевидно, условие существование β^* задается неравенством $e < e_*$.

Из уравнений (43) также следует, что условию стационарности функции $G(\beta, \theta)$ удовлетворяет нулевое значение амплитуды β. Это значит, что многообразие $\beta = 0$ является интегральным.

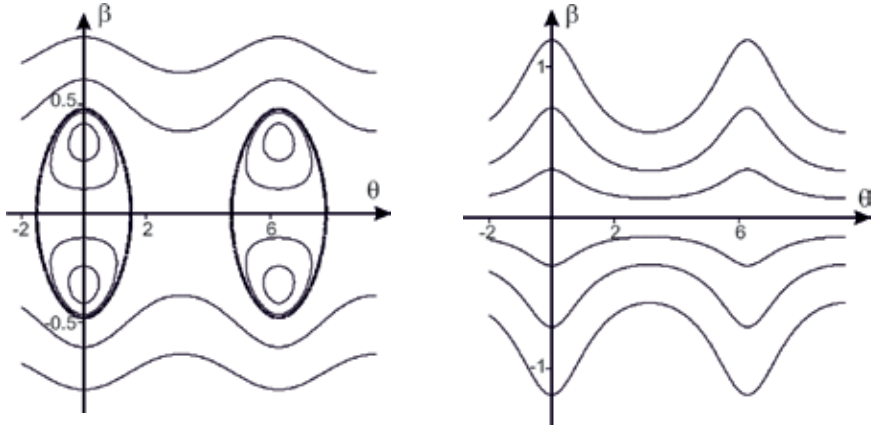На рисунке 5 изображен фазовый портрет колебаний в переменных β, θ. Жирным

Рис. 5 Фазовый портрет при резонансе $2\omega = 1$ для случаев $e < e_*$ и $e \ldots e_*$

черным цветом выделена сепаратриса, отвечающая значению $C = 0$. Ее параметрическое представление следует из интеграла $G(\beta, \theta) = 0$:

$$\beta(\theta) = \pm\sqrt{24e\cos\theta - \frac{1967}{18}e^2}$$

Отсюда вытекает, что максимальная амплитуда колебаний в зоне либрации вычисляется по формуле

$$\beta_{\max}(e) = \frac{\sqrt{432e - 1967e^2}}{\sqrt{18}}$$

Несложно найти стационарную точку этой функции и значение максимума в ней:

$$\beta_{\max}^* = \beta_{\max}(e_*/2) = \frac{36\sqrt{3934}}{1967} = 1.14793$$

Интеграл $G(\beta, \theta) = C$ позволяет исследовать эволюцию колебаний при изменении параметра e. Расчеты показывают, что при малом значении эксцентриситета появляется зона периодических движений вблизи оси $\beta = 0$ с максимальной амплитудой колебаний $\beta_{\max}$. Фазовый портрет колебаний имеет вид, изображенный на левой части рис. 5. При увеличении e высота зоны колебаний возрастает, достигая максимума $\beta_{\max}^*$ при $e = e_*/2$. Последующее возрастание эксцентриситета ведет к ее уменьшению вплоть до нулевых значений при $e = e_*$. Зона либрации исчезает и при $e \ldots e_*$ портрет колебаний представлен на правой половине рис. 5.

Фазовые кривые уравнений (41) описываются равенством

$$\beta(\theta) = \pm \frac{\sqrt{432e\cos\theta - 1967e^2 + \sqrt{\left(432e\cos\theta - 1967e^2\right)^2 + 72C}}}{6}, \qquad (44)$$

следующим из интеграла $G(\beta, \theta) = C$. Отсюда явствует, что изменение θ на $2k\pi$ радиан сохраняет значение амплитуды β, поэтому случай монотонного изменения θ (см. незамкнутые кривые на рис. 5) будем рассматривать как периодический, так как указанные приращения по θ сохраняют значения правых частей уравнений (41) и мы оказываемся в тех же условиях, что и в начальный момент $v = 0$ (на цилиндрической фазовой поверхности с локальными координатами $\beta, \theta(0,, \; \theta < 2\pi)$ кривые $\beta = \beta(\theta)$ будут замкнутыми).

Вернемся к переменным δ, δ', зависящих от β, θ:

$$\delta = \beta\cos\frac{\theta + v}{2} + \frac{4e}{\omega^2 - 1}\sin v, \quad \delta' = -\beta\omega\sin\frac{\theta + v}{2} + \frac{4e}{\omega^2 - 1}\cos v \qquad (45)$$

Очевидно, что интегральному многообразию $\beta = 0$ отвечает 2π --периодическое решение

$$\delta = \frac{4e}{\omega^2 - 1}\sin v, \quad \delta' = \frac{4e}{\omega^2 - 1}\cos v, \qquad (46)$$

стационарным точкам $\theta = 2k\pi, \beta = \beta^*$ -- 4π -- периодические решения

$$\delta = (-1)^k \beta^* \cos\frac{v}{2} + \frac{4e}{\omega^2 - 1}\sin v, \quad \delta' = (-1)^{k+1}\beta^*\omega\sin\frac{v}{2} + \frac{4e}{\omega^2 - 1}\cos v,$$

движению вдоль сепаратрисы $C = 0$ -- двояко асимптотическая к (46) траектория.

Однопараметрическому семейству $\beta = \beta(\theta, c), c = \beta(0)$ периодических решений из области либрации отвечают квазипериодические функции $\delta(v), \delta'(v)$, за исключением случая существования рациональных соотношений между периодом $T(c)$ указанного семейства и периодом изменения функций (45) по явно входящему аргументу v. Это соотношение имеет вид

$$T(c) = \frac{p}{q}4\pi, \qquad (47)$$

где p, q -- взаимно простые числа.

При выполнении этого равенства переменные δ, δ' будут $4p\pi$ -- периодическими функциями v. Учитывая, что семейство $\beta = \beta(\theta, c)$ является ляпуновским (интеграл $G(\beta, \theta)$ положительно определен в окрестности $\theta = 2k\pi, \beta = \beta^*$ при $e < e_*$), можно воспользоваться известной формулой для вычисления периода $T(c)$. Тогда из равенства (47) находим $\beta(0) = c$, интегрируем уравнения (41) с начальными условиями $\beta(0) = c$, $\theta(0) = 0$, подставляя найденные решений $\beta(v), \theta(v)$ в формулы (45), получим $4p\pi$ -- периодические функции $\delta(v), \delta'(v)$.

Случай монотонного убывания θ исследуется похожим образом. Пусть $\mathrm{T}(C)$ -- промежуток изменения ν (C -- постоянное значение первого интеграла $G(\beta,\theta)$), по истечении которого угол $\theta(\nu)$ получит приращение, равное (-4π). Тогда, если $\mathrm{T}(C)$ кратен 4π, то $\delta(\nu), \delta'(\nu)$ -- 4π--периодические функции ν. Таким образом, условие периодичности решений есть

$$\mathrm{T}(C) = 4k\pi$$

при условии, что $\mathrm{T}(C)$ вычисляется по формуле

$$\mathrm{T} = \int\limits_{0}^{-4\pi} \frac{d\theta}{\Delta - \dfrac{e}{2}(\omega-2)\cos\theta - \omega\left[\dfrac{\beta(\theta)^2}{8} + \dfrac{4e^2}{(\omega^2-1)^2}\right] - \dfrac{e^2}{2}\left[\omega - \dfrac{(\omega+2)^2}{8}\right]},$$

вытекающей из уравнений (41) после разделения переменных. Здесь $\beta(\theta)$ вычисляется по формуле (44).

Поскольку в областях монотонного изменения θ характерный размер угла β составляет величины порядка единицы, из равенства (45) следует, что замкнутая фазовая кривая $\delta' = \delta'(\delta)$, удовлетворяющая условию периодичности, близка по форме к эллипсу

$$\frac{\delta^2}{\beta^2} + \frac{\delta'^2}{(\beta\omega)^2} = 1$$

Теперь можем сделать выводы. Исследование малых колебаний на основе обобщенного метода усреднения с независимыми параметрами дает полную информацию о колебаниях спутника в первом и втором приближении метода усреднения. Точность приближения есть величина второго порядка малости по малым параметрам на асимптотически большем промежутке времени порядка $1/\mathrm{P}(\mu,\varepsilon)\mathrm{P}$ в случае резонанса $\omega=1$ и на промежутке времени порядка $1/\mathrm{P}(e,\varepsilon)\mathrm{P}$ при резонансе $\omega=1/2$. Результаты исследований свободны от редукции, содержат дополнительную информацию (в сравнении с классической схемой усреднения) о влиянии малого параметра ε на характер колебаний при резонансе $\omega=1$.

Литература

[1] *Laplace P.S.* Traité de la Mécanique Celeste, Tome II, Duprat II, Paris, 1799

[2] *Tisserand F.* Traité de la Mécanique Céleste, Tome II, ``Théorie de la Figure des Corps Célestes et de leur Mouvement de Rotation'', Paris, 1891

[3] *Routh E.L.* The Advanced Part of a Treatise on the Dynamics of a Sysytem of Rigid Bodies, London, Macmillan and Co., 1884

[4] *Baker R.M.L., Jr.* Passive stability of a satellite vihicle. ``Navigation'', 1958, 6, № 1, p. 64-65

[5] *Baker R.M.L., Jr.* Librations on a slightly eccentric orbit. ``ARS Journal'', 1960, 30, № 1, p. 124-126

[6] *Klemperer W.B., Baker R.M.L., Jr.* Satellite librations. ``Astronaut, Acta'',1957, 3, № 1, p. 16-27

[7] *Stocker T.A., Vachino R.F.* The two-dimensional librations of a dumbbell-shaped satellite in a uniform gravitational field. ``Advances in Astronaut. Sci.'',1958, vol.3

[8]*БелецкийВ.В.*Олибрацииспутника. Сб. ``Искусств. спутники Земли'', М., изд. АН СССР, 1959, № 3, с. 13-31

[9] *Белецкий В.В.* Либрация спутника на эллиптической орбите Сб. ``Искусств. спутники Земли'', М., изд. АН СССР, 1963, № 16, с. 46-56

[10] *Демин В.Г., Сингх Р.Б.* Нелинейные плоские колебания спутника на эллиптической орбите. ``Космич. исследования'', 1973, 11, № 2, с. 192-197

[11] *Schechter H.B.* Dumbbell librations in elliptic orbits. ``AIAA Journal'',1964, 2, № 6, p. 1000-1003

[12] *Liu F.C.* Periodic solution of plane libration motion of a satellite. ``AIAA Journal'', 1971, 9, № 7, с. 1240-1244

[13] *Сарычев В.А.* Итоги науки и техники. Исследование космического пространства. Т. 11. Вопросы ориентации искусственных спутников. ВИНИТИ, М., 1978, 223 стр.

[14] *Маркеев А.П.* Нелинейные колебания спутника при резонансе 1:1:1. ``Прикл. математика и механика'', 2012, Т. 76, № 1, с. 52-68

[15] *Красильников П.С.* Метод усреднения как процедура выделения главных членов в рядах решений. «Сборник научно-методических статей по теоретической механике», М., МГУ, 2009, стр. 56-68

[16] *Красильников П.С.* О нелинейных колебаниях маятника переменной длины на вибрирующем основании. ПММ, т. 76, вып. 1, 2012, с. 36-51

[17] *Белецкий В.В.* Движение спутника относительно центра масс в гравитационном поле. Изд-во МГУ, 1975, 308 стр.

A GENERALIZATION OF LAGRANGE METHOD OF VARIATION CONSTANTS

Katica R. (Stevanović) Hedrih

Mathematical Institute SANU Belgrade, Department for Mechanics
and Faculty of Mechanical Engineering, University of Niš, Serbia.
Priv. address: 18000-Niš, ul Vojvode Tankosića 3/22, Serbia,
e-mail: khedrih@eunet.rs, katicahedrih@gmail.com.khedrih@sbb.rs

Abstract. Starting from the idea of classical Lagrange method of variation constants for solving non autonomous linear differential equations describing forced vibrations of linear oscillators, in this paper a generalization of Lagrange method of variation constants in combinations with averaging method for solving nonlinear differential equations describing free and forced vibrations of fractional order nonlinear oscillators, with small nonlinearity is presented.

Key words: generalization of Lagrange method of variation constants; fractional order derivative, nonlinear terms; particular solutions; fractional order nonlinear oscillator; fractional order like cosines mode; fractional order like sinus mode; average values; slow changing; fast changing; full phase.

1. INTRODUCTION

The main idea is to develop a generalization of the method of variation constants that is inspired by classical Lagrange method of variation constants for solving non autonomous linear differential equations describing forced vibrations of linear oscillators for the case of arbitrary external excitation force. A classical Lagrange method of variation constants is presented in classical monograph university book [1] Theory of Ooscillations written by Rašković. Also, the same mwthod is presented in References [2] and [3]. In these cited references Lagrange method of variation constant is presented for solving the following linear non autonomous differential equation:

$$\ddot{x}(t) + \omega_0^2 x(t) = h f(t) \tag{1}$$

describing linear forced oscillations under an arbitrary external excitation depending only on time in the form $F(t) = F_0 f(t) = m h f(t)$.Particular integrals of homogeneous linear differential equation $\ddot{x}(t) + \omega_0^2 x(t) = 0$ are $T_1(t) = \cos \omega_0 t$ and

$T_2(t) = \sin \omega_0 t$, where ω_0 is eigen circular frequency of free harmonic oscillations. Solution of the linear non homogeneous differential equation (1) is proposed in the form of sum of products between particular solutions, $T_1(t) = \cos \omega_0 t$ and $T_2(t) = \sin \omega_0 t$, of linear autonomous differential equation and amplitudes:

$$x(t) = C(t)\cos \omega_0 t + D(t)\sin \omega_0 t \tag{2}$$

where amplitudes $C(t)$ and $D(t)$ are functions on the time, under the condition that first derivative of this solution is the same as in the case that amplitudes $C(t)$ and $D(t)$ are constants. In reference [1] solution of linear no autonomous differential equation (1) is presented in the form:

$$x(t) = C_0 \cos \omega_0 t + D_0 \sin \omega_0 t + \frac{h}{\omega_0} \int_0^t f(\tau)\sin \omega_0 (t - \tau) d\tau \tag{3}$$

For initial conditions: at $t = 0$, initial elongation $x(0) = x_0$ and initial velocity $\dot{x}(0) = \dot{x}_0$, previous solution is in the form:

$$x(t) = x_0 \cos \omega_0 t + \frac{\dot{x}_0}{\omega_0} \sin \omega_0 t + \frac{h}{\omega_0} \int_0^t f(\tau)\sin \omega_0 (t - \tau) d\tau \tag{4}$$

In the same Reference [1] for the case that linear no homogeneous differential equation is in the form:

$$\ddot{x}(t) + 2\delta \dot{x}(t) + \omega_0^2 x(t) = hf(t) \tag{5}$$

describing linear forced oscillations with energy system linear dissipation under arbitrary external excitation depending only of time in the form $F(t) = F_0 f(t) = mhf(t)$. Particular integrals of homogeneous linear differential equation $\ddot{x}(t) + 2\delta \dot{x}(t) + \omega_0^2 x(t) = 0$ are $T_1(t) = e^{\lambda_1 t}$ and $T_2(t) = e^{\lambda_2 t}$, where $\lambda_i . i = 1,2$ are eigen characteristic number of free damped oscillations and roots of system characteristic equation $\lambda^2 + 2\delta \gamma + \omega_0^2 = 0$. Roots of system characteristic equation depending on the relation between δ and ω_0 are $\lambda_{1,2} = -\delta \mp \sqrt{\delta^2 - \omega_0^2}$, for $\delta > \omega_0$ or $\lambda_{1,2} = -\delta \mp \mathbf{i}\sqrt{\omega_0^2 - \delta^2}$, $\mathbf{i} = \sqrt{-1}$, for $\delta < \omega_0$. Solution of the linear no homogeneous differential equation (5) is proposed in the form of sum of products between particular solutions, $T_1(t) = e^{\lambda_1 t}$ and $T_2(t) = e^{\lambda_2 t}$ of linear autonomous differential equation and amplitudes:

$$x(t) = C(t)e^{\lambda_1 t} + D(t)e^{\lambda_2 t} \tag{6}$$

where amplitudes $C(t)$ and $D(t)$ are functions of the time, under a condition that first derivative of this solution is same as in the case that amplitudes $C(t)$ and $D(t)$ are constants. In reference [1] solution of linear non autonomous differential equation (5) is presented in the form:

$$x(t) = C_0 e^{\lambda_1 t} + D_0 e^{\lambda_2 t} + \frac{h}{\lambda_2 - \lambda_1}\left[\int_0^t f(\tau)e^{\lambda_2(t-\tau)}d\tau - \int_0^t f(\tau)e^{\lambda_2(t-\tau)}d\tau\right] \qquad (7)$$

For the case that $\delta < \omega_0$ when eigen characteristic numbers are conjugate complex $\lambda_{1,2} = -\delta \mp \mathbf{i}\sqrt{\omega_0^2 - \delta^2}$, $\mathbf{i} = \sqrt{-1}$, previous solution take the following form:

$$x(t) = e^{-\delta t}\left(C_0 \cos p_0 t + D_0 \sin p_0 t\right) + \frac{h}{p_0}\int_0^t f(\tau)e^{-\delta(t-\tau)}\sin p_0(t-\tau)d\tau \qquad (8)$$

where $p_0 = \sqrt{\omega_0^2 - \delta^2}$.

2. EXTENSION OF THE LAGRANGE METHOD OF VARIATION CONSTANTS FOR SOLVING NON HOMOGENEOUS FRACTIONAL ORDER DIFFERENTIAL EQUATION DESCRIBING FORCED OSCILLATIONS OF THE FRACTIONAL ORDER OSCILLATOR

First, we should point out very comprehensive review papers [4-6] written by Rosikin and Shitikova, containing review and results achieved in the field of supplementing fractional order derivative in mechanics. From these papers and personal literature search, we can conclude that the results presented here are original and new.

Let's extend the Lagrange method of variation constants for solving non homogeneous fractional order differential equation describing forced oscillations of the fractional order oscillator. Then, we start from non homogeneous fractional order differential equation in the following form:

$$\ddot{x}(t) + \omega_0^2 x(t) + \omega_\alpha^2 \mathfrak{D}_t^\alpha[x(t)] = hf(t) \qquad \text{for } 0 < \alpha \leq 1 \text{ and } \alpha \neq 0 \qquad (9)$$

describing fractional order forced oscillations with energy system fractional order dissipation energy and under the arbitrary external excitation depending only of time in the form $F(t) = F_0 f(t) = mhf(t)$. Previous fractional order differential equation contain term with fractional order derivative, where α is fractional order number between zero and unit, $0 < \alpha < 1$, and $\mathfrak{D}_t^\alpha[\bullet]$ is a differential fractional order operator defined by expression:

$$\mathfrak{D}_t^\alpha[x(t)] = \frac{d^\alpha\langle x(t)\rangle}{dt^\alpha} = \frac{1}{\Gamma(1-\alpha)}\frac{d}{dt}\int_0^t \frac{x(\tau)}{(t-\tau)^\alpha}d\tau \qquad (10)$$

where $0 < \alpha < 1$ is defined by material fractional order properties as a constant, and

$$\omega_0^2 = \frac{c_0}{m}, \quad \omega_\alpha^2 = \frac{c_\alpha}{m} \quad, \quad c_0 \text{ and } c_\alpha \text{ are material rigidity constants and } m \text{ .is mass of}$$

the oscillator.

Solution of homogeneous ordinary fractional order differential equation:

$$\ddot{x}(t) + \omega_0^2 x(t) + \omega_\alpha^2 \mathfrak{D}_t^\alpha[x(t)] = 0, \qquad \text{for } 0 < \alpha \leq 1 \text{ and } \alpha \neq 0 \qquad (11)$$

is in the following form (see References [7-13]):

$$x(t,\alpha) = x_0 \sum_{k=0}^{\infty} (-1)^k \omega_\alpha^{2k} t^{2k} \sum_{j=0}^{k} \binom{k}{j} \frac{\omega_\alpha^{-2j} t^{-\alpha j}}{\omega_o^{2j} \Gamma(2k+1-\alpha j)} +$$
$$+ \dot{x}_0 \sum_{k=0}^{\infty} (-1)^k \omega_\alpha^{2k} t^{2k+1} \sum_{j=0}^{k} \binom{k}{j} \frac{\omega_\alpha^{-2j} t^{-\alpha j}}{\omega_o^{2j} \Gamma(2k+2-\alpha j)}$$
$$\text{for } 0 < \alpha \le 1 \text{ and } \alpha \ne 0 \qquad (12)$$

or in the form:

$$x(t,\alpha) == x_0 T_{\cos}(t,\alpha) + \dot{x}_0 T_{\sin}(t,\alpha), \text{ for } 0 < \alpha \le 1 \text{ and } \alpha \ne 0 \qquad (13)$$

where $T_{\cos}(t,\alpha)$ and $T_{\sin}(t,\alpha)$ particular solutions of fractional order differential equation and fractional order modes cosines like and sinus like modes of corresponding fractional order oscillator with one degree of freedom, in the form:

$$T_{\cos}(t,\alpha) = \sum_{k=0}^{\infty} (-1)^k \omega_\alpha^{2k} t^{2k} \sum_{j=0}^{k} \binom{k}{j} \frac{\omega_\alpha^{-2j} t^{-\alpha j}}{\omega_o^{2j} \Gamma(2k+1-\alpha j)} \qquad (14)$$

$$T_{\sin}(t,\alpha) = \sum_{k=0}^{\infty} (-1)^k \omega_\alpha^{2k} t^{2k+1} \sum_{j=0}^{k} \binom{k}{j} \frac{\omega_\alpha^{-2j} t^{-\alpha j}}{\omega_o^{2j} \Gamma(2k+2-\alpha j)} \qquad (15)$$

and $x_0 = x(0)$ and $\dot{x}_0 = \dot{x}(0)$ integral constant determined by initial conditions. These modes are quasiperiodic cosines like and sinus like modes with equal half period of oscillations for for $0 \le \alpha \le 1$ (approximately equal from approximation of solution) and degreasing amplitudes with time for $0 < \alpha \le 1$ and $\alpha \ne 0$.

For solving non homogeneous fractional order differential equation (9) solution is proposed in the form (13) where $T_{\cos}(t,\alpha)$ and $T_{\sin}(t,\alpha)$ are particular solutions of homogeneous fractional order differential equation (11) and fractional order modes cosines like and sinus like modes of corresponding fractional order oscillator with one degree of freedom, in the form (14) and (15) , but integral constants $x_0 \Rightarrow C(t,\alpha)$ and $\dot{x}_0 \Rightarrow D(t,\alpha)$ are function of time:

$$x(t,\alpha) = C(t,\alpha) T_{\cos}(t,\alpha) + D(t,\alpha) T_{\sin}(t,\alpha) \qquad (16)$$

First derivative $\dot{x}(t)$ and fractional order derivative $\mathfrak{D}_t^\alpha[x(t)]$ for $0 < \alpha \le 1$ and $\alpha \ne 0$ are proposed same as in the case that constants, now function time are $x_0 \Rightarrow C(t,\alpha)$ and $\dot{x}_0 \Rightarrow D(t,\alpha)$ are constant, and on the that basis we can write:

$$\dot{x}(t,\alpha) = C(t,\alpha) \dot{T}_{\cos}(t,\alpha) + D(t,\alpha) \dot{T}_{\sin}(t,\alpha) \qquad (17)$$

$$\mathfrak{D}_t^\alpha[x(t,\alpha)] = C(t,\alpha) \mathfrak{D}_t^\alpha[T_{\cos}(t,\alpha)] + D(t,\alpha) \mathfrak{D}_t^\alpha[T_{\sin}(t,\alpha)] \qquad (18)$$

under the following conditions:

$$\dot{C}(t,\alpha) T_{\cos}(t,\alpha) + \dot{D}(t,\alpha) T_{\sin}(t,\alpha) = 0 \qquad (19)$$

$$\mathfrak{D}_t^\alpha[C(t,\alpha)] T_{\cos}(t,\alpha) + \mathfrak{D}_t^\alpha[D(t,\alpha)] T_{\sin}(t,\alpha) = 0 \qquad (20)$$

Previous condition (20) must to be satisfied, and in boundary condition for $\alpha = 1$ and $\alpha \ne 0$, is same as (19).

After introducing proposed solution $x(t,\alpha)$, by (16) and corresponding derivatives, first derivative $\dot{x}(t,\alpha)$, by (17) and fractional order derivative $\mathbf{D}_t^\alpha[x(t,\alpha)]$ for $0 < \alpha \leq 1$ and $\alpha \neq 0$, by (18), and second derivative

$$\ddot{x}(t,\alpha) = C(t,\alpha)\ddot{T}_{\cos}(t,\alpha) + D(t,\alpha)\ddot{T}_{\sin}(t,\alpha) + \dot{C}(t,\alpha)\dot{T}_{\cos}(t,\alpha) + \dot{D}(t,\alpha)\dot{T}_{\sin}(t,\alpha) \tag{21}$$

into non homogeneous fractional order differential equation (9), and taking into account that particular solutions $T_{\cos}(t,\alpha)$ and $T_{\sin}(t,\alpha)$, identically satisfy the following conditions:

$$C(t,\alpha)\langle\ddot{T}_{\cos}(t,\alpha) + \omega_0^2 T_{\cos}(t,\alpha) + \omega_\alpha^2 \mathbf{D}_t^\alpha[T_{\cos}(t,\alpha)]\rangle \equiv 0$$
$$D(t,\alpha)\langle\ddot{T}_{\sin}(t,\alpha) + \omega_0^2 T_{\sin}(t,\alpha) + \omega_\alpha^2 \mathbf{D}_t^\alpha[T_{\sin}(t,\alpha)]\rangle \equiv 0$$

third condition is obtained in the following form:

$$\dot{C}(t,\alpha)\dot{T}_{\cos}(t,\alpha) + \dot{D}(t,\alpha)\dot{T}_{\sin}(t,\alpha) = hf(t) \tag{22}$$

Then determination of unknown functions: $C(t)$ and $D(t)$ is defined by three conditions: (19), (20) and (22). This system is along first derivative of the unknown functions: $\dot{C}(t)$ and $\dot{D}(t)$. Determinant of this system is:

$$\Delta(t,\alpha) = T_{\cos}(t,\alpha)\dot{T}_{\sin}(t,\alpha) - T_{\sin}(t,\alpha)\dot{T}_{\cos}(t,\alpha) \neq 0 \tag{23}$$

And solutions of the unknown functions - amplitudes $C(t)$ and $D(t)$ are in the following forms:

$$C(t,\alpha) = C_0 - h\int_0^t \frac{f(\tau)T_{\sin}(\tau,\alpha)}{\Delta(\tau,\alpha)}d\tau$$

$$D(t,\alpha) = D_0 + h\int_0^t \frac{f(\tau)T_{\cos}(\tau,\alpha)}{\Delta(\tau,\alpha)}d\tau \tag{24}$$

Solution of the ordinary fractional order differential equation (9) is in the following form:

$$x(t,\alpha) = C_0 T_{\cos}(t,\alpha) + D_0 T_{\sin}(t,\alpha) + h\int_0^t \frac{f(\tau)[T_{\cos}(\tau,\alpha)T_{\sin}(t,\alpha) - T_{\sin}(\tau,\alpha)T_{\cos}(t,\alpha)]}{T_{\cos}(\tau,\alpha)\dot{T}_{\sin}(\tau,\alpha) - T_{\sin}(\tau,\alpha)\dot{T}_{\cos}(\tau,\alpha)}d\tau \tag{25}$$

Taking into account that $\Delta(t,\alpha) = T_{\cos}(t,\alpha)\dot{T}_{\sin}(t,\alpha) - T_{\sin}(t,\alpha)\dot{T}_{\cos}(t,\alpha) \neq 0$ is slochanging function approximate calculation is possible to take for determinant of the system the following form:

$$\Delta(t,\alpha) \approx \frac{1}{2}\langle(1-\alpha)\Delta(t,\alpha=0) + \alpha\Delta(t,\alpha=1)\rangle = \frac{1}{2}\left\langle(1-\alpha)\sqrt{\omega_0^2 + \omega_\alpha^2} + \alpha e^{-\omega_\alpha^2 t}\sqrt{\omega_0^2 - \frac{1}{4}\omega_\alpha^4}\right\rangle \neq 0 \cdot$$

3. EXTENSION OF THE LAGRANGE METHOD OF VARIATION CONSTANTS FOR SOLVING FRACTIONAL ORDER DIFFERENTIAL EQUATION WITH NONLINEAR TERM DESCRIBING NONLINEAR OSCILLATIONS OF THE FRACTIONAL ORDER OSCILLATOR

3.1. For approximately solving nonlinear fractional order differential equation as it is:

$$\ddot{x}(t) + \omega_0^2 x(t) + \omega_\alpha^2 \mathbf{D}_t^\alpha[x(t)] = \pm \varepsilon x^3 \tag{26}$$

and

$$\ddot{\rho}(t) + \omega_0^2 \rho(t) + \omega_\alpha^2 \mathfrak{D}_t^\alpha[\rho(t)] = \omega_0^2 \rho_0 + \omega_\alpha^2 \mathfrak{D}_t^\alpha[\rho_0] + \dot{\phi}_0^2 \frac{\tilde{\rho}_0^4}{\rho^3(t)} \tag{27}$$

or in the form:

$$\ddot{x}(t) + \omega_0^2 x(t) + \omega_\alpha^2 \mathfrak{D}_t^\alpha[x(t)] = \pm \varepsilon f(x) \qquad \text{for } 0 < \alpha \leq 1 \text{ and } \alpha \neq 0 \tag{28}$$

containing term with fractional order derivative, where α is fractional order number between zero and unit, $0 < \alpha < 1$, and $\mathfrak{D}_t^\alpha[\bullet]$ is a differential fractional order operator defined by expression (10) and $\pm \varepsilon f\left(x, \dot{x}, \mathfrak{D}_t^\alpha[x(t)]\right)$ is nonlinear function and ε small parameter, it is possible to use combination of the Lagrange's method of variation constants and averaging method. For beginning, as in the previous part we use particular solutions $T_{\cos}(t, \alpha)$ and $T_{\sin}(t, \alpha)$ of the homogeneous fractional order differential equation (11) defined by (12) and approximate solution is supposed in the form(13) in which constants $C(t, \alpha)$ and $D(t, \alpha)$ are time functions. Using same approach ad in the previous part first derivative $\dot{x}(t)$ and fractional order derivative $\mathfrak{D}_t^\alpha[x(t)]$ for $0 < \alpha \leq 1$ and $\alpha \neq 0$ are proposed same as in the case that function of time, $C(t, \alpha)$ and $D(t, \alpha)$, are constants, and on the that basis we can write first derivative in the form (17) and fractional order derivative in the form (18) under the following conditions (19) and (20) as in the previous part. After introducing proposed solution $x(t, \alpha)$, by (16) and corresponding derivatives, first derivative $\dot{x}(t, \alpha)$, by (17) and fractional order derivative $\mathfrak{D}_t^\alpha[x(t, \alpha)]$ for $0 < \alpha \leq 1$ and $\alpha \neq 0$, by (18), and second derivative in the form (21) into non homogeneous fractional order differential equation with nonlinear term, presented by (28), and taking into account that particular solutions $T_{\cos}(t, \alpha)$ and $T_{\sin}(t, \alpha)$, identically satisfy the homogeneous fractional order differential equation, as in the previous part, the following three conditions :

$$\mathfrak{D}_t^\alpha[C(t,\alpha)]T_{\cos}(t,\alpha) + \mathfrak{D}_t^\alpha[D(t,\alpha)]T_{\sin}(t,\alpha) = 0 \quad \text{for } 0 < \alpha \leq 1 \text{ and } \alpha \neq 0$$
$$\dot{C}(t,\alpha)T_{\cos}(t,\alpha) + \dot{D}(t,\alpha)T_{\sin}(t,\alpha) = 0 \tag{29}$$
$$\dot{C}(t,\alpha)\dot{T}_{\cos}(t,\alpha) + \dot{D}(t,\alpha)\dot{T}_{\sin}(t,\alpha) = \pm \varepsilon f(C(t,\alpha), D(t,\alpha), T_{\cos}(t,\alpha), T_{\sin}(t,\alpha))$$

are obtained for determination of the unknown functions: $C(t, \alpha)$ and $D(t, \alpha)$. First derivative of the time functions $C(t, \alpha)$ and $D(t, \alpha)$ amplitudes of the

$$\dot{C}(t,\alpha) = \mp \varepsilon \frac{1}{\Delta(t,\alpha)} f(C(t,\alpha), D(t,\alpha), T_{\cos}(t,\alpha), T_{\sin}(t,\alpha))T_{\sin}(t,\alpha)$$

$$\dot{D}(t,\alpha) = \pm \varepsilon \frac{1}{\Delta(t,\alpha)} f(C(t,\alpha), D(t,\alpha), T_{\cos}(t,\alpha), T_{\sin}(t,\alpha))T_{\cos}(t,\alpha) \tag{30}$$

where determinant $\Delta(t, \alpha)$ is in same form as in previous part defined by (23).

In obtained previous system of nonlinear differential equations along first derivatives of $C(t,\alpha)$ and $D(t,\alpha)$, we separate slowchanging functions and fast changing function along one half period $\dfrac{\mathbf{T}_{harm}}{2} = \dfrac{\pi}{\sqrt{\omega_o^2 + \omega_\alpha^2}}$ of corresponding harmonic oscillations for $\alpha = 0$ or for one half period $\dfrac{\mathbf{T}_{amort}}{2} = \dfrac{\pi}{p} = \dfrac{\pi}{\sqrt{\omega_o^2 - \dfrac{1}{4}\omega_\alpha^4}}$ of

damped linear oscillations. Slowchanging functions are $C(t,\alpha)$ and $D(t,\alpha)$, and determinant $\Delta(t,\alpha) = T_{\cos}(t,\alpha)\dot{T}_{\sin}(t,\alpha) - T_{\sin}(t,\alpha)\dot{T}_{\cos}(t,\alpha) \neq 0$. Fast changing functions as oscillatory functions are: $f\big(C(t,\alpha), D(t,\alpha), T_{\cos}(t,\alpha), T_{\sin}(t,\alpha)\big)T_{\sin}(t,\alpha)$ and $f\big(C(t,\alpha), D(t,\alpha), T_{\cos}(t,\alpha), T_{\sin}(t,\alpha)\big)T_{cor}(t,\alpha)$. It is visible from numerical analysis and graphical presentation (see graphical presentations in Appendix) as well as from supposition that function $f\big(C(t,\alpha), D(t,\alpha), T_{\cos}(t,\alpha), T_{\sin}(t,\alpha)\big)$ is also an oscillatory function.

As period of harmonic oscillations is shorter, then for one period of harmonic linear oscillations, $\mathbf{T}_{harm} = \dfrac{2\pi}{\sqrt{\omega_o^2 + \omega_\alpha^2}} = \dfrac{2\pi}{\tilde{\omega}}$, for $\alpha = 0$, we can take averaging of

functions at right sides in system (30) along a period of harmonic oscillations, taking full phase $\Phi(t) = \tilde{\omega}t$, where $\tilde{\omega} = \sqrt{\omega_o^2 + \omega_\alpha^2}$, circular frequency, and in interval $\Phi(t) \in [0, 2\pi]$ which correspond to period of $\mathbf{T}_{harm}$. But, also, it is possible to take for averaging integration a period of basic harmonic oscillations: $\mathbf{T}_{0,harm} = \dfrac{2\pi}{\omega_0}$, when full

phase is $\Phi(t) = \omega_0 t$, in interval $\Phi(t) \in [0, 2\pi]$, and also it is possible to take for averaging, integration a period of damped oscillations: $\mathbf{T}_{amort} = \dfrac{2\pi}{p} = \dfrac{2\pi}{\sqrt{\omega_o^2 - \dfrac{1}{4}\omega_\alpha^4}}$,

when full phase is $\Phi(t) = pt$, where $p = \sqrt{\omega_o^2 - \dfrac{1}{4}\omega_\alpha^4}$, in interval $\Phi(t) \in [0, 2\pi]$.

Fractional order modes $T_{\cos}(t,\alpha)$ and $T_{\sin}(t,\alpha)$, are particular solutions of fractional order differential equation (11), and quasi periodic with half period $\dfrac{\mathbf{T}_{\alpha\alpha}}{2}$, for $0 \le \alpha \le 1$, in interval: $\dfrac{\mathbf{T}_{harm,\alpha=0}}{2} < \dfrac{\mathbf{T}_{\alpha\alpha}}{2} \le \dfrac{\mathbf{T}_{amprt,\alpha=1}}{2}$, or $\dfrac{\pi}{\sqrt{\omega_o^2 + \omega_\alpha^2}} \le \dfrac{\mathbf{T}_{\alpha\alpha}}{2} \le \dfrac{\pi}{\sqrt{\omega_o^2 - \frac{1}{4}\omega_\alpha^4}}$.

Then for one of the possible averaged approximation of the solutions for integral constant – time functions $C(t,\alpha)$ and $D(t,\alpha)$, for the case of fractional order differential equation with nonlinear term (28), we can made averaged values of functions $f\big(C(t,\alpha),D(t,\alpha),T_{\cos}(t,\alpha),T_{\sin}(t,\alpha)\big)T_{\sin}(t,\alpha)$ and $f\big(C(t,\alpha),D(t,\alpha),T_{\cos}(t,\alpha),T_{\sin}(t,\alpha)\big)T_{cor}(t,\alpha)$ in the right side in the system of differential equations (30) for one of the period $\mathbf{T}_\alpha$, for $0 \le \alpha \le 1$, of the fractional order differential equations depending of α and in interval $\Phi(t)\in[0,2\pi]$. Averaged values of functions $f\big(C(t,\alpha),D(t,\alpha),T_{\cos}(t,\alpha),T_{\sin}(t,\alpha)\big)T_{\sin}(t,\alpha)$ and $f\big(C(t,\alpha),D(t,\alpha),T_{\cos}(t,\alpha),T_{\sin}(t,\alpha)\big)T_{cor}(t,\alpha)$ in the right side in the system of differential equations (30) along full phases $\Phi(t)=\omega_\alpha t$, in interval from zero to $\tilde{\omega}\mathbf{T}_{harm} = 2\pi$, or $\omega_0\mathbf{T}_{0.harm} = 2\pi$ or $\omega_{\alpha\alpha}\mathbf{T}_{\alpha\alpha} = 2\pi$ or $p\mathbf{T}_{amor} = 2\pi$, depend of value $0 \le \alpha \le 1$. Then, taking into account that functions $C(t,\alpha)$ and $D(t,\alpha)$ are slowchanging, as well as determinant $\Delta(t,\alpha)=T_{\cos}(t,\alpha)\dot{T}_{\sin}(t,\alpha)-T_{\sin}(t,\alpha)\dot{T}_{\cos}(t,\alpha)\ne 0$, and that functions $T_{\cos}(t,\alpha)$ and $T_{\sin}(t,\alpha)$ are fast changeable the action of averaging in corresponding interval $\Phi(t)\in[0,2\pi]$, along full phase $\Phi(t)=\omega_\alpha t$, we take that functions $C(t,\alpha)$ and $D(t,\alpha)$ as slowchanging are constant in relation to the action of averaging, and integrating, along corresponding full phase $\Phi(t)=\omega_{\alpha\alpha}t$, system of averaged differential equations is possible to write in the following form:

$$\dot{C}(t,\alpha) \approx \mp\frac{\varepsilon}{2\pi}\int_0^{2\pi}\frac{1}{\Delta(t,\alpha)}f\big(C(t,\alpha),D(t,\alpha),T_{\cos}(\Phi(t),\alpha),T_{\sin}(\Phi(t),\alpha)\big)T_{\sin}(\Phi(t),\alpha)d\Phi(t)$$

$$\dot{D}(t,\alpha) \approx \pm\frac{\varepsilon}{2\pi}\int_0^{2\pi}\frac{1}{\Delta(t,\alpha)}f\big(C(t,\alpha),D(t,\alpha),T_{\cos}(\Phi(t),\alpha),T_{\sin}(\Phi(t),\alpha)\big)T_{\cos}(\Phi(t),\alpha)d\Phi(t) \qquad (31)$$

where

$$\Phi(t) = \omega_{\alpha\alpha}t \ \text{ for } \ 0 \le \alpha \le 1$$

$$T_{\cos}(\Phi(t),\alpha) = \sum_{k=0}^{\infty}(-1)^k\frac{\omega_\alpha^{2k}}{\omega_{\alpha\alpha}^{2k}}[\Phi(t)]^{2k}\sum_{j=0}^{k}\binom{k}{j}\frac{\omega_\alpha^{-2j}[\Phi(t)]^{-\alpha j}\omega_{\alpha\alpha}^{\alpha j}}{\omega_o^{2j}\Gamma(2k+1-\alpha j)} \qquad (32)$$

$$T_{\sin}\left(\Phi(t),\alpha\right)=\sum_{k=0}^{\infty}(-1)^k\,\frac{\omega_\alpha^{2k}}{\omega_{\alpha\alpha}^{2k+1}}[\Phi(t)]^{2k+1}\sum_{j=0}^{k}\binom{k}{j}\frac{\omega_\alpha^{-2j}[\Phi(t)]^{-\alpha j}\,\omega_{\alpha\alpha}^{\alpha j}}{\omega_o^{2j}\Gamma(2k+2-\alpha j)} \quad (33)$$

$$\Delta(t,\alpha)=T_{\cos}(t,\alpha)\dot{T}_{\sin}(t,\alpha)-T_{\sin}(t,\alpha)\dot{T}_{\cos}(t,\alpha)\neq 0 \text{ Slowchanging function} \quad (34)$$

Taking into account that determinant (34) is slowchanging function, the corresponding approximate system of averaged differential equations is possible to write in the following form:

$$\dot{C}(t,\alpha)\approx\mp\frac{\varepsilon}{2\pi}\frac{1}{\Delta(t,\alpha)}\int_0^{2\pi}f\big(C(t,\alpha),D(t,\alpha),T_{\cos}(\Phi(t),\alpha),T_{\sin}(\Phi(t),\alpha)\big)T_{\sin}(\Phi(t),\alpha)d\Phi(t)$$

$$\dot{D}(t,\alpha)\approx\pm\frac{\varepsilon}{2\pi}\frac{1}{\Delta(t,\alpha)}\int_0^{2\pi}f\big(C(t,\alpha),D(t,\alpha),T_{\cos}(\Phi(t),\alpha),T_{\sin}(\Phi(t),\alpha)\big)T_{\cos}(\Phi(t),\alpha)d\Phi(t) \quad (35)$$

3.2. Using the same approach as in the previous part, applying generalized Lagrange method of variation constant and method of averaging along full phase to the following fractional order differential equation with a nonlinear term depending of coordinate and first derivative of coordinate, in the following form:

$$\ddot{x}(t)+\omega_0^2 x(t)+\omega_\alpha^2\mathfrak{D}_t^\alpha[x(t)]=\pm\varepsilon f(x,\dot{x}) \qquad \text{for } 0<\alpha\leq 1 \text{ and } \alpha\neq 0 \quad (36)$$

it is possible to obtain approximation of the solution in the form (16) in which amplitudes $C(t,\alpha)$ and $D(t,\alpha)$ as time functions are determined by the corresponding approximate system of averaged differential equations, which is possible to write in the following form:

$$\dot{C}(t,\alpha)\approx\mp\frac{\varepsilon}{2\pi}\frac{1}{\Delta(t,\alpha)}\int_0^{2\pi}f\big(C(t,\alpha),D(t,\alpha),T_{\cos}(\Phi(t),\alpha),T_{\sin}(\Phi(t),\alpha),\dot{T}_{\cos}(\Phi(t),\alpha),\dot{T}_{\sin}(\Phi(t),\alpha)\big)T_{\sin}(\Phi(t),\alpha)d\Phi(t)$$

$$\dot{D}(t,\alpha)\approx\pm\frac{\varepsilon}{2\pi}\frac{1}{\Delta(t,\alpha)}\int_0^{2\pi}f\big(C(t,\alpha),D(t,\alpha),T_{\cos}(\Phi(t),\alpha),T_{\sin}(\Phi(t),\alpha),\dot{T}_{\cos}(\Phi(t),\alpha),\dot{T}_{\sin}(\Phi(t),\alpha)\big)T_{\cos}(\Phi(t),\alpha)d\Phi(t)$$

$$(37)$$

where

$$\dot{T}_{\cos}\left(\Phi(t),\alpha\right)=\sum_{k=0}^{\infty}(-1)^k\,\frac{\omega_\alpha^{2k}}{\omega_{\alpha\alpha}^{2k-1}}[\Phi(t)]^{2k-1}\sum_{j=0}^{k}\binom{k}{j}\frac{(2k-\alpha j)\omega_\alpha^{-2j}[\Phi(t)]^{-\alpha j}\,\omega_{\alpha\alpha}^{\alpha j}}{\omega_o^{2j}\Gamma(2k+1-\alpha j)} \quad (38)$$

$$\dot{T}_{\sin}\left(\Phi(t),\alpha\right)=\sum_{k=0}^{\infty}(-1)^k\,\frac{\omega_\alpha^{2k}}{\omega_{\alpha\alpha}^{2k}}[\Phi(t)]^{2k}\sum_{j=0}^{k}\binom{k}{j}\frac{(2k+1-\alpha j)\omega_\alpha^{-2j}[\Phi(t)]^{-\alpha j}\,\omega_{\alpha\alpha}^{\alpha j}}{\omega_o^{2j}\Gamma(2k+2-\alpha j)} \quad (39)$$

Ordinary fractional order differential equations with nonlinear term $\pm\varepsilon f(x)$ (28) and $\pm\varepsilon f(x,\dot{x})$ (36) present nonlinear, fractional order oscillator in state of free fractional order oscillations, containing a mass particle with one degree of freedom coupled by a standard light fractional order element and a parallel nonlinear elastic spring in first case (28) and with one additional parallel nonlinear dissipative element in second case (36). Both cases are very important for engineering practice and investigation od engineering system dynamics.

4. EXAMPLES

Example 1.

For first example, we can take fractional order differential equation with nonlinear cubic term:

$$\ddot{x}(t) + \omega_0^2 x(t) + \omega_\alpha^2 \mathfrak{D}_t^\alpha[x(t)] = \pm \varepsilon \omega_N^2 x^3 \qquad \text{for } 0 < \alpha \le 1 \text{ and } \alpha \ne 0 \qquad (40)$$

Previous fractional order differential equation (40) described a fractional order oscillator with small cubic nonlinearity. Physically this oscillator contain a mass particle mass m moving along ideal horizontal line and with one degree of freedom defined by coordinate x and coupled for fixed point by standard light nonlinear elastic and fractional order element with constitutive force-dilatation relation in the form:

$$F_\alpha\big(x(t), \mathfrak{D}_t^\alpha[x(t)]\big) = c_0 x(t) \mp \varepsilon c_N x^3 + c_\alpha \mathfrak{D}_t^\alpha[x(t)]$$
$$F_\alpha\big(x(t), \mathfrak{D}_t^\alpha[x(t)]\big) = m\big\langle \omega_0^2 x(t) \mp \varepsilon \omega_N^2 x^3 + \omega_\alpha^2 \mathfrak{D}_t^\alpha[x(t)]\big\rangle , \qquad (41)$$

where , $\omega_0^2 = \dfrac{c_0}{m}$, $\omega_\alpha^2 = \dfrac{c_\alpha}{m}$ and $\omega_N^2 = \dfrac{c_N}{m}$, and c_0 coefficient linear elasticity, c_N coefficient of nonlinear elasticity and c_α and α coefficients of fractional order properties.

Then, taking into account previous presentation of the combination of generalized Lagrange's method of variation constants and averaging method along full phase for one period, we propose approximation of the solution in the form (16) in which amplitudes $C(t,\alpha)$ and $D(t,\alpha)$, as time functions are determined by the corresponding approximate system of averaged differential equations, which is possible, according with (35) to write in the following form:

$$\dot{C}(t,\alpha) \approx \mp \frac{\varepsilon}{2\pi} \frac{\omega_N^2}{\Delta(t,\alpha)} \int_0^{2\pi} (C(t,\alpha)T_{\cos}(\Phi(t),\alpha) + D(t,\alpha)T_{\sin}(\Phi(t),\alpha))^3 T_{\sin}(\Phi(t),\alpha) d\Phi(t)$$

$$\dot{D}(t,\alpha) \approx \pm \frac{\varepsilon}{2\pi} \frac{\omega_N^2}{\Delta(t,\alpha)} \int_0^{2\pi} (C(t,\alpha)T_{\cos}(\Phi(t),\alpha) + D(t,\alpha)T_{\sin}(\Phi(t),\alpha))^3 T_{\cos}(\Phi(t),\alpha) d\Phi(t) \quad (42)$$

Sub-example 1.1.

For determinant $\Delta(t,\alpha) = T_{\cos}(t,\alpha)\dot{T}_{\sin}(t,\alpha) - T_{\sin}(t,\alpha)\dot{T}_{\cos}(t,\alpha) \ne 0$, we can take that for $\alpha = 0$ determinant of the system is in the following form: $\Delta(t,\alpha = 0) = \tilde{\omega}$, $\tilde{\omega} = \sqrt{\omega_0^2 + \omega_\alpha^2}$, because for $\alpha = 0$, particular solutions are: $T_{\cos}(t,\alpha = 0) = \cos \tilde{\omega} t$ and $T_{\sin}(t,\alpha = 0) = \sin \tilde{\omega} t t$. We see that determinant $\Delta(t,\alpha = 0) = \tilde{\omega}$ is constant, and amplitudes $C(t)$ and $D(t)$ are, also, slowchanging function of time determined by system of averaged differential equations first order in the form (42) where full phase is taken in the form $\Phi(t) = \tilde{\omega} t$, $\tilde{\omega} = \sqrt{\omega_0^2 + \omega_\alpha^2}$:

$$\dot{C}(t) \approx \pm \frac{\varepsilon \omega_N^2}{2\pi\tilde{\omega}} \int_0^{2\pi} \left\langle \left[[C(t)]^3 \cos^3 \Phi(t) + 3[C(t)]^2 \cos^2 \Phi(t)[D(t)]\sin\Phi(t) + 3[C(t)]\cos\Phi(t)[D(t)]^2 \sin^2 \Phi(t) + [D(t)]^3 \sin^3 \Phi(t) \right] d\langle \cos\Phi(t)\rangle \right\rangle$$

$$\dot{D}(t) \approx \pm \frac{\varepsilon \omega_N^2}{2\pi\tilde{\omega}} \int_0^{2\pi} \left\langle \left[[C(t)]^3 \cos^3 \Phi(t) + 3[C(t)]^2 \cos^2 \Phi(t)[D(t)]\sin\Phi(t) + 3[C(t)]\cos\Phi(t)[D(t)]^2 \sin^2 \Phi(t) + [D(t)]^3 \sin^3 \Phi(t) \right] d\langle \sin\Phi(t)\rangle \right\rangle$$

Taking into account that is:

$$\int_0^{2\pi} \cos^3 \Phi(t) d\langle \cos\Phi(t)\rangle = 0, \qquad \int_0^{2\pi} \cos^2 \Phi(t)\sin\Phi(t) d\langle \cos\Phi(t)\rangle - \frac{2\pi}{8}$$

$$\int_0^{2\pi} \cos\Phi(t)\sin^2 \Phi(t) d\langle \cos\Phi(t)\rangle = 0, \qquad \int_0^{2\pi} \sin^3 \Phi(t) d\langle \cos\Phi(t)\rangle = \frac{3\pi}{4}$$

$$\int_0^{2\pi} \cos^3 \Phi(t) d\langle \sin\Phi(t)\rangle = \frac{3\pi}{4}, \qquad \int_0^{2\pi} \cos^2 \Phi(t)\sin\Phi(t) d\langle \sin\Phi(t)\rangle = 0$$

$$\int_0^{2\pi} \cos\Phi(t)\sin^2 \Phi(t) d\langle \sin\Phi(t)\rangle = \frac{\pi}{4}, \qquad \int_0^{2\pi} \sin^3 \Phi(t) d\langle \sin\Phi(t)\rangle = 0$$

approximate system of averaged differential equations along unknown amplitudes $C(t, \alpha = 0)$ and $D(t, \alpha = 0)$, which are function of time, are determined by following system of averaged nonlinear differential equations first order in the form :

$$\dot{C}(t, \alpha = 0) \approx \mp \frac{3\varepsilon \omega_N^2}{8\tilde{\omega}} \left\langle [C(t, \alpha = 0)]^2 + [D(t, \alpha = 0)]^2 \right\rangle [D(t, \alpha = 0)]$$

$$\dot{D}(t, \alpha = 0) \approx \pm \frac{3\varepsilon \omega_N^2}{8\tilde{\omega}} \left\langle [C(t, \alpha = 0)]^2 + [D(t, \alpha = 0)]^2 \right\rangle [C(t, \alpha = 0)] \tag{43}$$

After transformation previous system of averaged nonlinear differential equations first order (43) into:

$$\mp \frac{\dot{C}(t, \alpha = 0)}{[D(t, \alpha = 0)]} \approx \frac{\dot{D}(t, \alpha = 0)}{[C(t, \alpha = 0)]} = \pm \frac{3\varepsilon \omega_N^2}{8\tilde{\omega}} \left\langle [C(t, \alpha = 0)]^2 + [D(t, \alpha = 0)]^2 \right\rangle \tag{44}$$

it is visible that is valid the following relation

$$[C(t, \alpha = 0)]^2 + [D(t, \alpha = 0)]^2 \approx [C(t = 0, \alpha = 0)]^2 + [D(t = 0, \alpha = 0)]^2 \approx a_0^2 = const \tag{45}$$

From previous relation (45), we conclude that amplitude of nonlinear vibrations in approximations is $a_0^2 = const$ constant , and equal to amplitude at initial moment.

$$a_0 \approx \sqrt{[C(t, \alpha = 0)]^2 + [D(t, \alpha = 0)]^2} \approx \sqrt{[C(t = 0, \alpha = 0)]^2 + [D(t = 0, \alpha = 0)]^2} \approx const \tag{46}$$

Full phase of nonlinear vibrations in first averaged approximation is:

$$\tilde{\Phi} \approx \Phi + arctg \frac{D(t, \alpha = 0)}{C(t, \alpha = 0)} = \tilde{\omega}t + arctg \frac{D(t, \alpha = 0)}{C(t, \alpha = 0)} \tag{47}$$

Circular frequency $\tilde{\omega}_{nonlin, \alpha = 0}$ of nonlinear vibrations in first averaged approximation is in the form

$$\tilde{\omega}_{nonlin, \alpha = 0} \approx \dot{\tilde{\Phi}} = \tilde{\omega} + \frac{d}{dt} arctg \frac{D(t, \alpha = 0)}{C(t, \alpha = 0)} \tag{48}$$

or

$$\tilde{\omega}_{nonlin,\alpha=0} = \dot{\tilde{\Phi}} \approx \tilde{\omega} + \frac{\dot{D}(t,\alpha=0)C(t,\alpha=0) - D(t,\alpha=0)\dot{C}(t,\alpha=0)}{\langle C(t,\alpha=0)\rangle^2 + \langle D(t,\alpha=0)\rangle^2}$$

and taking into account obtained relations (44)–(45)-(46), frequency of nonlinear vibrations finally is nonlinear function of amplitude as well as of initial amplitude a_0 in the quadratic form:

$$\tilde{\omega}_{nonlin,\alpha=0} = \dot{\tilde{\Phi}} \approx \tilde{\omega} \pm \frac{3\varepsilon\omega_N^2}{8\tilde{\omega}} a_0^2 \qquad (49)$$

Previous result is known in numerous References in nonlinear mechanics as well as in nonlinear oscillations, and obtained by different methods. One of source method is asymptotic method of nonlinear mechanics, known as asymptotic method Krilov- Bogolyibov-Mitropolsky (see References [14-23]).

Approximation of solution of nonlinear fractional order differential equation in degeneration case to the conservative nonlinear differential equation, for $\alpha=0$, is in the form:

$$x(t) \approx C(t,\alpha=0)T_{\cos}(t,\alpha=0) + D(t,\alpha=0)T_{\sin}(t,\alpha=0) \approx a_0 \cos\left\langle\left(\tilde{\omega} \pm \frac{3\varepsilon\omega_N^2}{8\tilde{\omega}} a_0^2\right)t + \tilde{\Phi}_0\right\rangle$$

$$\text{for } \alpha=0 \qquad (50)$$

Sub-example 1.2.

For $\alpha=1$, determinant $\Delta(t,\alpha) = T_{\cos}(t,\alpha)\dot{T}_{\sin}(t,\alpha) - T_{\sin}(t,\alpha)\dot{T}_{\cos}(t,\alpha) \neq 0$ of the system is in the following expression: $\Delta(t,\alpha=1) = pe^{-2\delta t} = e^{-\omega_\alpha^2 t}\sqrt{\omega_0^2 - \frac{1}{4}\omega_\alpha^4} \neq 0$

$p = \sqrt{\omega_0^2 - \frac{1}{4}\omega_\alpha^4}$ and, $2\delta = \omega_\alpha^2$, because for $\alpha=1$, particular solutions are: $T_{\cos}(t,\alpha=1) = e^{-\delta t}\cos pt$ and $T_{\sin}(t,\alpha=1) = e^{-\delta t}\sin pt$. We see that determinant $\Delta(t,\alpha=1) = pe^{-2\delta t} = e^{-\omega_\alpha^2 t}\sqrt{\omega_0^2 - \frac{1}{4}\omega_\alpha^4} \neq 0$ is slowchanging function of time, and amplitudes $C(t,\alpha=1)$ and $D(t,\alpha=1)$, also, are slowchanging functions of time determined by system of averaged differential equations first order in the form (42), where full phase is taken in the form $\Phi(t) = pt$, $p = \sqrt{\omega_0^2 - \frac{1}{4}\omega_\alpha^4}$:

$$\dot{C}(t) \approx \mp\frac{\varepsilon}{2\pi}\frac{\omega_N^2}{pe^{-2\delta t}}\int_0^{2\pi}\left(C(t,\alpha=1)e^{-\delta t}\cos\Phi(t) + D(t,\alpha=1)e^{-\delta t}\sin\Phi(t)\right)^3 e^{-\delta t}\sin\Phi d\Phi(t)$$

$$\dot{D}(t) \approx \pm\frac{\varepsilon}{2\pi}\frac{\omega_N^2}{pe^{-2\delta t}}\int_0^{2\pi}\left(C(t,\alpha=1)e^{-\delta t}\cos\Phi(t) + D(t,\alpha=1)e^{-\delta t}\sin\Phi(t)\right)^3 e^{-\delta t}cod\Phi d\Phi(t)$$

or in the form:

$$\dot{C}(t,\alpha=1) \approx \mp\frac{3\varepsilon\omega_N^2 e^{-2\delta t}}{8p}\left\langle[C(t,\alpha=1)]^2 + [D(t,\alpha=1)]^2\right\rangle[D(t,\alpha=1)]$$

$$\dot{D}(t) \approx \pm \frac{3\varepsilon\omega_N^2 e^{-2\delta t}}{8p} \left\langle [C(t,\alpha=1)]^2 + [D(t,\alpha=1)]^2 \right\rangle [C(t,\alpha=1)] \tag{51}$$

After transformation previous system of averaged nonlinear differential equations first order (51) into:

$$\mp \frac{\dot{C}(t,\alpha=1)}{[D(t,\alpha=1)]} \approx \frac{\dot{D}(t,\alpha=1)}{[C(t,\alpha=1)]} \approx \pm \frac{3\varepsilon\omega_N^2 e^{-2\delta t}}{8p} \left\langle [C(t,\alpha=1)]^2 + [D(t,\alpha=1)]^2 \right\rangle$$
$$\tag{52}$$

it is visible that is valid the following relation

$$[C(t,\alpha=1)]^2 + [D(t,\alpha=1)]^2 \approx [C(t=0,\alpha=1)]^2 + [D(t=0,\alpha=1)]^2 \approx a_0^2 = constt \tag{53}$$

From previous relation (53), we conclude that amplitude of nonlinear vibrations in approximations is $a_0^2 = const$ constant , and equal to amplitude at initial moment.

$$a_0 \approx \sqrt{[C(t,\alpha=1)]^2 + [D(t,\alpha=1)]^2} \approx \sqrt{[C(t=0,\alpha=1)]^2 + [D(t=0,\alpha=1)]^2} \approx const$$
$$\tag{54}$$

Full phase of nonlinear vibrations in first averaged approximation is:

$$\tilde{\Phi} \approx \Phi + arctg \frac{D(t,\alpha=1)}{C(t,\alpha=1)} = pt + arctg \frac{D(t,\alpha=1)}{C(t,\alpha=1)} \tag{55}$$

Circular frequency $\tilde{\omega}_{nonlin,\alpha=1}$ of nonlinear vibrations in first averaged approximation, for $\alpha=1$, is in the form:

$$\tilde{\omega}_{nonlin,\alpha=1} \approx \dot{\tilde{\Phi}} = p + \frac{d}{dt} arctg \frac{D(t,\alpha=1)}{C(t,\alpha=1)} \qquad \text{for } \alpha=1, \tag{56}$$

or

$$\tilde{\omega}_{nonlin} = \dot{\tilde{\Phi}} \approx p + \frac{\dot{D}(t,\alpha=1)C(t,\alpha=1) - D(t,\alpha=1)\dot{C}(t,\alpha=1)}{\left\langle C(t,\alpha=1) \right\rangle^2 + \left\langle D(t,\alpha=1) \right\rangle^2}$$

and taking into account obtained relations (52)–(53)-(46), circular frequency $\tilde{\omega}_{nonlin,\alpha=1}$ of nonlinear vibrations, finally, is nonlinear function of amplitude as well as of initial amplitude a_0 in the quadratic form, and elso og time:

$$\tilde{\omega}_{nonlin,\alpha=1} = \dot{\tilde{\Phi}} \approx p \pm \frac{3\varepsilon\omega_N^2 e^{-2\delta t}}{8p} a_0^2 = \sqrt{\omega_0^2 - \frac{1}{4}\omega_\alpha^4} \pm \frac{3\varepsilon\omega_N^2 e^{-\omega_\alpha^2 t}}{8p} a_0^2 \tag{57}$$

Previous result is new, and is not known from literature, only from Reference [24] as a result in solving nonlinear differential equation of dynamics of coupled two oscillators, and also in Reference [25-26] as two pages extended abstract in ICTAM 2012.

Approximation of solution of nonlinear fractional order differential equation in degeneration case to the conservative nonlinear differential equation, for $\alpha=1$, is in the form:

$$x(t) \approx C(t,\alpha=1)T_{\cos}(t,\alpha=1) + D(t,\alpha=1)T_{\sin}(t,\alpha=1) \approx a_0 e^{-\delta t} \cos\left\langle \left(pt \mp \frac{3\varepsilon\omega_N^2 e^{-2\delta t}}{16\delta p} a_0^2 \right) + \tilde{\Phi}_0 \right\rangle$$
$$\text{for } \alpha=1 \tag{58}$$

or finally

$$x(t) \approx a_0 e^{-\frac{1}{2}\omega_\alpha^2 t} \cos\left\langle \left(t\sqrt{\omega_0^2 - \frac{1}{4}\omega_\alpha^4} \mp \frac{3\varepsilon\omega_N^2 e^{-\omega_\alpha^2 t}}{8\omega_\alpha^2\sqrt{\omega_0^2 - \frac{1}{4}\omega_\alpha^4}}a_0^2\right) + \tilde{\Phi}_0 \right\rangle \quad \text{for } \alpha = 1 \tag{59}$$

Some comments and comparison of the approximation of solutions. Some comments are necessary. Previous obtained approximation (59) is approximation of solution of the following nonlinear differential equation:

$$\ddot{x}(t) + \omega_0^2 x(t) + \omega_\alpha^2 \dot{x}(t) = \pm\varepsilon\omega_N^2 x^3 \qquad \text{for } \alpha = 1 \tag{60}$$

obtained from fractional order differential equation (40) for $\alpha = 1$. One of possible first approximation of this nonlinear equation (60) is known from numerous classical books in nonlinear oscillations and nonlinear mechanics in the form:

$$x(t) \approx a_0 e^{-\delta t} \cos\left\langle \left(\omega_0 t \mp \frac{3\varepsilon\omega_N^2 e^{-2\delta t}}{16\delta p}a_0^2\right) + \tilde{\Phi}_0 \right\rangle \tag{61}$$

where circular frequency $\tilde{\omega}_{nonlin}$ of free nonlinear damped oscillations is:

$$\tilde{\omega}_{nonlin} \approx \omega_0 \pm \frac{3\varepsilon\omega_N^2 e^{-2\delta t}}{16\delta p}a_0^2 \tag{62}$$

and amplitude

$$a(t) \approx a_0 e^{-\delta t} \tag{63}$$

but different them obtained heir. Then it is necessary to compare these two obtained approximations of the same nonlinear differential equation and which two approximations of same solution.

By using two asymptotic methods from References [14] and [19], and also their proposed combination of the generalized Lagrange's method of variation constants with method of averaging and used in particular in References [24-27] starting from known analytical solutions $x(t) = R(t)e^{-\delta t}\cos(pt + \phi(t))$, $p = \sqrt{\omega_0^2 - \delta^2}$ and $x(t) = a(t)\cos[\omega_0 t + \phi(t)]$, two same first approximations of the solution of nonlinear differential equation (60) are obtained in the following forms:

$$x(t) = R_0 e^{-\delta t} \cos\left[pt \mp \frac{3}{16\delta p}\omega_{N1}^2 a_o^2(e^{-2\delta t} - 1) + \Phi_o\right], \text{for } \delta \neq 0, \varepsilon \neq 0,$$

$$\omega_0^2 > \delta^2, \quad p = \sqrt{\omega_0^2 - \delta^2} \tag{64}$$

$$x(t) = a_o e^{-\delta t} \cos\left[\omega_0 t \mp \frac{3}{16\delta\omega_0}\omega_{N1}^2 a_o^2(e^{-2\delta t} - 1) + \Phi_o\right]. \text{ for } \delta \neq 0,$$

$$\varepsilon \neq 0, \; \omega_0^2 > \delta^2 \tag{65}$$

for corresponding initial conditions. For the case that damping coefficient tends to zero, from both first approximations (64) and (65), same analytical approximation of the solution for conservative nonlinear system dynamics are obtained. For the case that

coefficient of the cubic nonlinearity tends to zero, from first approximation of the solution in the form (64) give known analytical solution of the linear no conservative system dynamics in the following form: $x(t) = R_0 e^{-\delta t} \cos(pt + \alpha_0)$, for $\delta \neq 0$, $\varepsilon = 0$, $\omega_0^2 > \delta^2$, $p = \sqrt{\omega_0^2 - \delta^2}$, $\tilde{\omega}_{N1}^2 = o$, but from the second approximation of same solution form (65) obtained solution $x(t) = a_0 e^{-\delta t} \cos(\omega_0 t + \alpha_0)$ *is not correct*. This is visible that this expression is not solution of the differential equation: $\ddot{x}(t) + 2\delta \dot{x}(t) + \omega_0^2 x(t) = 0$. Then we can conclude that, starting different known analytical solutions, for obtaining first approximations are acceptable, but limited by corresponding conditions. Approximation of the solution of nonlinear George Duffing differential equation (60) in the form (64) is better them (65) known from numerous literatures.

Comparison 1. Taking into account results presented for sub-examples 1 and 2 , and also form graphical presentation of the particular solution for $0 < \alpha < 1$ (see Figures 1 and 2 in Appendix), it is possible both particular solutions $T_{\cos}(t, \alpha)$ and $T_{\sin}(t, \alpha)$ defined by (14) and (15), of homogeneous fractional order differential equation (11) take in the form as in the case for $\alpha = 1$, $T_{\cos}(t, \alpha = 1) = e^{-\delta_\alpha t} \cos p_\alpha t$ and $T_{\sin}(t, \alpha = 1) = e^{-\delta_\alpha t} \sin p_\alpha t$, making the following comparisons:

$$T_{\cos}(t,\alpha) = \sum_{k=0}^{\infty}(-1)^k \omega_\alpha^{2k} t^{2k} \sum_{j=0}^{k}\binom{k}{j}\frac{\omega_\alpha^{-2j}t^{-\alpha j}}{\omega_o^{2j}\Gamma(2k+1-\alpha j)} \approx e^{-\delta_\alpha t}\cos p_\alpha t \qquad (66)$$

$$T_{\sin}(t,\alpha) = \sum_{k=0}^{\infty}(-1)^k \omega_\alpha^{2k} t^{2k+1} \sum_{j=0}^{k}\binom{k}{j}\frac{\omega_\alpha^{-2j}t^{-\alpha j}}{\omega_o^{2j}\Gamma(2k+2-\alpha j)} \approx e^{-\delta_\alpha t}\sin p_\alpha t \qquad (67)$$

where δ_α is coefficient of energy dissipation and p_α circular frequency for the case of fractional order system energy dissipation depending of α in interval $\alpha \in (0,1)$ and time, and we can write the following relations:

$$[T_{\cos}(t,\alpha)]^2 = \left[\sum_{k=0}^{\infty}(-1)^k \omega_\alpha^{2k} t^{2k} \sum_{j=0}^{k}\binom{k}{j}\frac{\omega_\alpha^{-2j}t^{-\alpha j}}{\omega_o^{2j}\Gamma(2k+1-\alpha j)}\right]^2 \approx e^{-2\delta_\alpha t}\cos^2 p_\alpha t \quad (68)$$

$$[T_{\sin}(t,\alpha)]^2 = \left[\sum_{k=0}^{\infty}(-1)^k \omega_\alpha^{2k} t^{2k+1} \sum_{j=0}^{k}\binom{k}{j}\frac{\omega_\alpha^{-2j}t^{-\alpha j}}{\omega_o^{2j}\Gamma(2k+2-\alpha j)}\right]^2 \approx e^{-2\delta_\alpha t}\sin^2 p_\alpha t \quad (69)$$

Then the following relations are valid:

$$e^{-2\delta_\alpha t} = [T_{\cos}(t,\alpha)]^2 + [T_{\sin}(t,\alpha)]^2 \qquad (70)$$

$$e^{-2\delta_\alpha t} = \left[\sum_{k=0}^{\infty}(-1)^k \omega_\alpha^{2k} t^{2k} \sum_{j=0}^{k}\binom{k}{j}\frac{\omega_\alpha^{-2j}t^{-\alpha j}}{\omega_o^{2j}\Gamma(2k+1-\alpha j)}\right]^2 + \left[\sum_{k=0}^{\infty}(-1)^k \omega_\alpha^{2k} t^{2k+1} \sum_{j=0}^{k}\binom{k}{j}\frac{\omega_\alpha^{-2j}t^{-\alpha j}}{\omega_o^{2j}\Gamma(2k+2-\alpha j)}\right]^2$$

and

$$p_\alpha = \frac{1}{t} arctg \frac{[T_{\sin}(t,\alpha)]}{[T_{\cos}(t,\alpha)]} = \frac{1}{t} arctg \frac{\left[\sum_{k=0}^{\infty}(-1)^k \omega_\alpha^{2k} t^{2k+1} \sum_{j=0}^{k} \binom{k}{j} \frac{\omega_\alpha^{-2j} t^{-\alpha j}}{\omega_o^{2j} \Gamma(2k+2-\alpha j)} \right]}{\left[\sum_{k=0}^{\infty}(-1)^k \omega_\alpha^{2k} t^{2k} \sum_{j=0}^{k} \binom{k}{j} \frac{\omega_\alpha^{-2j} t^{-\alpha j}}{\omega_o^{2j} \Gamma(2k+1-\alpha j)} \right]}$$ (71)

Comparison 2. As it is $\quad \Delta(t, \alpha = 0) = \tilde{\omega} = \sqrt{\omega_0^2 + \omega_\alpha^2} \quad$ for $\quad \alpha = 0 \quad$ or

$\Delta(t, \alpha = 1) = pe^{-2\delta t} = e^{-\omega_\alpha^2 t} \sqrt{\omega_0^2 - \frac{1}{4}\omega_\alpha^4} \neq 0 \quad$ for $\quad \alpha = 1$, then determinant $\Delta(t, \alpha)$ for

arbitrary α in interval $\quad 0 < \alpha \leq 1$ is slowchanging time function and it is possible to take that this function is not under the action of averaged process along full phase in interval $\quad \Phi \in [0, 2\pi]$. Then, for solving averaged values of the functions $f(C(t,\alpha), D(t,\alpha), T_{\cos}(t,\alpha), T_{\sin}(t,\alpha)) T_{\sin}(t,\alpha)$ and $f(C(t,\alpha), D(t,\alpha), T_{\cos}(t,\alpha), T_{\sin}(t,\alpha)) T_{cor}(t,\alpha)$ in the right side in the system of differential equations (30), for arbitrary α in interval $\quad 0 < \alpha \leq 1$, and for simplification if the, we take approximated value of that determinant $\Delta(t,\alpha)$

$$\Delta(t,\alpha) \approx \frac{1}{2} \langle (1-\alpha)\Delta(t,\alpha=0) + \alpha\Delta(t,\alpha=1) \rangle = \frac{1}{2} \left\langle (1-\alpha)\sqrt{\omega_0^2 + \omega_\alpha^2} + \alpha e^{-\omega_\alpha^2 t} \sqrt{\omega_0^2 - \frac{1}{4}\omega_\alpha^4} \right\rangle \neq 0 \quad (72)$$

and as a slowchanging time function no depending of phase angle, for simplification of averaging integral we can take into account the following differential equations in averaged approximation:

$$\dot{C}(t,\alpha) \approx \mp \frac{\varepsilon}{2\pi} \frac{1}{\left\langle (1-\alpha)\sqrt{\omega_0^2 + \omega_\alpha^2} + \alpha e^{-\omega_\alpha^2 t} \sqrt{\omega_0^2 - \frac{1}{4}\omega_\alpha^4} \right\rangle} \int_0^{2\pi} f(C(t,\alpha), D(t,\alpha), T_{\cos}(t,\alpha), T_{\sin}(t,\alpha)) T_{\sin}(\Phi(t),\alpha) d\Phi(t)$$

$$\dot{D}(t,\alpha) \approx \pm \frac{\varepsilon}{2\pi} \frac{1}{\left\langle (1-\alpha)\sqrt{\omega_0^2 + \omega_\alpha^2} + \alpha e^{-\omega_\alpha^2 t} \sqrt{\omega_0^2 - \frac{1}{4}\omega_\alpha^4} \right\rangle} \int_0^{2\pi} f(C(t,\alpha), D(t,\alpha), T_{\cos}(t,\alpha), T_{\sin}(t,\alpha)) T_{\cos}(\Phi(t),\alpha) d\Phi(t)$$ (73)

Comparison 3. Also, it is good to make a comparison between particular solution like cos mode $T_{s,\cos}(t,\alpha) = \sum_{k=0}^{\infty}(-1)^k \omega_{(\alpha)s}^{2k} t^{2k} \sum_{m=0}^{k} \binom{k}{m} \frac{\omega_{(\alpha)s}^{-2m} t^{-\alpha m}}{\omega_s^{2m} \Gamma(2k+1-\alpha m)}$ and its derivative

in the form minus like sin mode $\dot{T}_{\cos}(t,\alpha) = \sum_{k=1}^{\infty}(-1)^k \omega_\alpha^{2k-1} t^{2k} \sum_{m=0}^{k} \binom{k}{m} \frac{(2k-\alpha m)\omega_\alpha^{-2m} t^{-\alpha m}}{\omega_o^{2m} \Gamma(2k+1-\alpha m)}$.

Comparison is visible in Figure 1 and 2 in Appendix. Also, it is good to made a comparison between particular solution like sin mode $T_{s,\sin}(t,\alpha) = \sum_{k=0}^{\infty}(-1)^k \omega_{(\alpha)s}^{2k} t^{2k+1} \sum_{m=0}^{k} \binom{k}{m} \frac{\omega_{(\alpha)s}^{-2m} t^{-\alpha m}}{\omega_s^{2m} \Gamma(2k+2-\alpha m)}$ and its derivative in the form like cos

mode $\dot{T}_{\sin}(t,\alpha) = \sum\limits_{k=0}^{\infty}(-1)^{k}\,\omega_{\alpha}^{2k}t^{2k}\sum\limits_{m=0}^{k}\binom{k}{m}\dfrac{(2k+1-\alpha m)\omega_{\alpha}^{-2m}t^{-\alpha m}}{\omega_{o}^{2m}\Gamma(2k+2-\alpha m)}$. Comparison is visible in Figure 1 and 2 in Apendix.

Then from these comparisons it is visible that determinant $\Delta(t,\alpha)$ is slow changeable as we conclude in start.

Sub-example 1.3.

A conclusion on the basis of the previous comparisons and analysis for considered example with cubic nonlinear term and for $0 < \alpha < 1$ naturally appears. Approximation of the fractional order differential equation with nonlinear term in the form (16) in which amplitudes $C(t,\alpha)$ and $D(t,\alpha)$ are determined by system of averaged differential equations along these unknown amplitudes $C(t,\alpha)$ and $D(t,\alpha)$ - functions of time is possible to rewrite in the following form:

$$\dot{C}(t,\alpha) \approx \mp\frac{\varepsilon}{2\pi}\frac{1}{\left\langle (1-\alpha)\sqrt{\omega_0^2+\omega_\alpha^2}+\alpha e^{-\omega_\alpha^2 t}\sqrt{\omega_0^2-\frac14\omega_\alpha^4}\right\rangle}\int\limits_0^{2\pi}(C(t,\alpha)T_{\cos}(\Phi(t),\alpha)+D(t,\alpha)T_{\sin}(\Phi(t),\alpha))^3 T_{\sin}(\Phi(t),\alpha)d\Phi(t)$$

$$\dot{D}(t,\alpha) \approx \pm\frac{\varepsilon}{2\pi}\frac{1}{\left\langle (1-\alpha)\sqrt{\omega_0^2+\omega_\alpha^2}+\alpha e^{-\omega_\alpha^2 t}\sqrt{\omega_0^2-\frac14\omega_\alpha^4}\right\rangle}\int\limits_0^{2\pi}(C(t,\alpha)T_{\cos}(\Phi(t),\alpha)+(t,\alpha)T_{\sin}(\Phi(t),\alpha))^3 T_{\cos}(\Phi(t),\alpha)d\Phi(t)$$

$$(74)$$

For obtaining corresponding values of terms in sum of integrals, we need the following integrals:

$$k_{3\cos,1\sin}(\alpha)=\int\limits_0^{2\pi}[T_{\cos}(\Phi(t),\alpha)]^3 T_{\sin}(\Phi(t),\alpha)d\Phi(t),\quad k_{2\cos,2\sin}(\alpha)=\int\limits_0^{2\pi}[T_{\cos}(\Phi(t),\alpha)]^2 [T_{\sin}(\Phi(t),\alpha)]^2 d\Phi(t)$$

$$k_{1\cos,3\sin}(\alpha)=\int\limits_0^{2\pi}[T_{\cos}(\Phi(t),\alpha)][T_{\sin}(\Phi(t),\alpha)]^3 d\Phi(t),\quad k_{0\cos,4\sin}(\alpha)=\int\limits_0^{2\pi}[T_{\sin}(\Phi(t),\alpha)]^4 d\Phi(t)$$

$$k_{4\cos,0\sin}(\alpha)=\int\limits_0^{2\pi}[T_{\cos}(\Phi(t),\alpha)]^4 d\Phi(t),\quad k_{3\cos,1\sin}(\alpha)=\int\limits_0^{2\pi}[T_{\cos}(\Phi(t),\alpha)]^3 [T_{\sin}(\Phi(t),\alpha)]d\Phi(t)$$

$$k_{2\cos,2\sin}(\alpha)=\int\limits_0^{2\pi}[T_{\cos}(\Phi(t),\alpha)]^2 [T_{\sin}(\Phi(t),\alpha)]^2 d\Phi(t),\quad k_{1\cos,3\sin}(\alpha)=\int\limits_0^{2\pi}[T_{\cos}(\Phi(t),\alpha)][T_{\sin}(\Phi(t),\alpha)]^3 d\Phi(t)$$

$$k_{0\cos,4\sin}(\alpha)=\int\limits_0^{2\pi}[T_{\sin}(\Phi(t),\alpha)]^4 d\Phi(t),\quad k_{4\cos,0\sin}(\alpha)=\int\limits_0^{2\pi}[T_{\cos}(\Phi(t),\alpha)]^4 d\Phi(t)$$

$$k_{2\cos,2\sin}(\alpha)=\int\limits_0^{2\pi}[T_{\cos}(\Phi(t),\alpha)]^2 [T_{\sin}(\Phi(t),\alpha)]^2 d\Phi(t)\qquad (75)$$

Averaged differential equations along corresponding full phase s are:

$$\dot{C}(t,\alpha) \approx \mp\frac{\varepsilon}{2\pi}\frac{1}{\left\langle (1-\alpha)\sqrt{\omega_0^2+\omega_\alpha^2}+\alpha e^{-\omega_\alpha^2 t}\sqrt{\omega_0^2-\frac14\omega_\alpha^4}\right\rangle}$$
$$\left\{k_{3\cos,1\sin}(\alpha)[C(t,\alpha)]^3+3k_{2\cos,2\sin}(\alpha)[C(t,\alpha)]^3[D(t,\alpha)]+3k_{1\cos,3\sin}(\alpha)[C(t,\alpha)]^2[D(t,\alpha)]^2+k_{0\cos,4\sin}(\alpha)[D(t,\alpha)]^3\right\}$$

$$\dot{D}(t,\alpha) \approx \pm \frac{\varepsilon}{2\pi} \frac{1}{\left\langle (1-\alpha)\sqrt{\omega_0^2+\omega_\alpha^2} + \alpha e^{-\omega_\alpha^2 t}\sqrt{\omega_0^2 - \frac{1}{4}\omega_\alpha^4} \right\rangle}$$
$$\left\{ k_{4\cos,0\sin}(\alpha)[C(t,\alpha)]^3 + 3k_{3\cos,1\sin}(\alpha)[C(t,\alpha)]^2[D(t,\alpha)] + 3k_{2\cos,2\sin}(\alpha)[C(t,\alpha)]^2[D(t,\alpha)]^2 + k_{1\cos,3\sin}(\alpha)[D(t,\alpha)]^3 \right\}$$

Example 2.

Let consider the following fractional order differential equations with nonlinear term:

$$\ddot{\rho}(t) + \omega_0^2 \rho(t) + \omega_\alpha^2 \mathfrak{D}_t^\alpha[\rho(t)] = \omega_0^2 \rho_0 + \omega_\alpha^2 \mathfrak{D}_t^\alpha[\rho_0] + \dot{\varphi}_0^2 \frac{\tilde{\rho}_0^4}{\rho^3(t)} \tag{77}$$

describing distance between two mass particles coupled by standard light fractional order element, when system is moving in a plane, where ρ_0 length of standard light fractional order element in no stressed state, and $\tilde{\rho}_0$ distance between mass particles at initial moment of two mass particle motion and $\dot{\varphi}_0$ relative angular velocity of relative rotation one mass particle around other in plane at initial moment of motion.

For beginning, the nonlinear term $\dot{\varphi}_0^2 \dfrac{\tilde{\rho}_0^4}{\rho^3(t)}$ developed in the following

approximate Taylor's series around distance ρ_0:

$$\dot{\varphi}_0^2 \frac{\tilde{\rho}_0^4}{\rho^3(t)} \approx \dot{\varphi}_0^2 \frac{\tilde{\rho}_0^4}{\rho_0^3} - 3\dot{\varphi}_0^2 \frac{\tilde{\rho}_0^4}{\rho_0^4}(\rho(t)-\rho_0) + \frac{12}{2!}\dot{\varphi}_0^2 \frac{\tilde{\rho}_0^4}{\rho_0^5}(\rho(t)-\rho_0)^2 - \frac{60}{2!3!}\dot{\varphi}_0^2 \frac{\tilde{\rho}_0^4}{\rho_0^6}(\rho(t)-\rho_0)^3 + ...$$

$$\dot{\varphi}_0^2 \frac{\tilde{\rho}_0^4}{\rho^3(t)} \approx \dot{\varphi}_0^2 \frac{\tilde{\rho}_0^4}{\rho_0^3}\left\langle 1 - 3\frac{1}{\rho_0}(\rho-\rho_0) + 6\frac{1}{\rho_0^2}(\rho-\rho_0)^2 - 5\frac{1}{\rho_0^3}(\rho-\rho_0)^3 + ... \right\rangle. \tag{78}$$

Then ordinary, fractional order differential equation with nonlinear terms is possible to express in the following form:

$$\ddot{\rho}(t) + \omega_0^2 \rho(t) + \omega_\alpha^2 \mathfrak{D}_t^\alpha[\rho(t)]$$
$$\approx \omega_0^2 \rho_0 + \omega_\alpha^2 \mathfrak{D}_t^\alpha[\rho_0] + \dot{\varphi}_0^2 \frac{\tilde{\rho}_0^4}{\rho_9^3}\left\langle 1 - 3\frac{1}{\rho_0}(\rho-\rho_0) + 6\frac{1}{\rho_0^2}(\rho-\rho_0)^2 - 5\frac{1}{\rho_0^3}(\rho-\rho_0)^3 + ... \right\rangle \tag{79}$$

If we introduce the following denotation

$$(\rho - \rho_0) \Rightarrow \rho \quad \text{and} \quad \varepsilon_0 \omega_0^2 = \dot{\varphi}_0^2 \frac{\tilde{\rho}_0^4}{\rho_0^3}$$

Then previous ordinary, fractional order differential equation with nonlinear terms is in the following form:

$$\ddot{\rho}(t) + \omega_0^2 \left\langle 1 + 3\frac{\varepsilon_0}{\rho_0}\right\rangle \rho(t) + \omega_\alpha^2 \mathfrak{D}_t^\alpha[\rho(t)] \approx \varepsilon_0 \omega_0^2 \left\langle 1 + 6\frac{1}{\rho_0^2}\rho^2 - 5\frac{1}{\rho_0^3}\rho^3 + ... \right\rangle \tag{80}$$

For obtaining approximate solution of the fractional order differential equation without nonlinear terms (80, we start from corresponding homogeneous fractional order differential equation in the form

$$\ddot{\rho}(t) + \omega_0^2 \left\langle 1 + 3\frac{\varepsilon_0}{\rho_0} \right\rangle \rho(t) + \omega_\alpha^2 \mathfrak{D}_t^\alpha[\rho(t)] \approx \varepsilon_0 \omega_0^2 \tag{81}$$

with solution in the following series time form:

$$\rho(t,\alpha) = \varepsilon_0 + x_0 \sum_{k=0}^{\infty} (-1)^k \omega_\alpha^{2k} t^{2k} \sum_{j=0}^{k} \binom{k}{j} \frac{\omega_\alpha^{-2j} t^{-\alpha j}}{\omega_{o\varepsilon}^{2j} \Gamma(2k+1-\alpha j)} +$$
$$+ \dot{x}_0 \sum_{k=0}^{\infty} (-1)^k \omega_\alpha^{2k} t^{2k+1} \sum_{j=0}^{k} \binom{k}{j} \frac{\omega_\alpha^{-2j} t^{-\alpha j}}{\omega_{o\varepsilon}^{2j} \Gamma(2k+2-\alpha j)} \tag{82}$$

where

$$\omega_{0\varepsilon}^2 = \omega_0^2 \left\langle 1 + 3\frac{\varepsilon_0}{\rho_0} \right\rangle \tag{83}$$

or in the form:

$$\rho(t,\alpha) = \varepsilon_0 + x_0 T_{\cos}(t,\alpha) + \dot{x}_0 T_{\sin}(t,\alpha) \tag{84}$$

For obtaining approximate solution of the ordinary, fractional order differential equation with nonlinear terms (80), we use generalized Lagrange method of variation constants in the form:

$$\rho(t,\alpha) = \varepsilon_0 + C(t,\alpha) T_{\cos}(t,\alpha) + D(t,\alpha) T_{\sin}(t,\alpha) \tag{85}$$

where unknown amplitudes $C(t,\alpha)$ and $D(t,\alpha)$ - functions of time, are approximate determined by following system of differential equations:

$$\dot{C}(t,\alpha) \approx \mp \frac{\varepsilon}{2\pi} \int_0^{2\pi} \frac{1}{\Delta(t,\alpha)} f(C(t,\alpha)T_{\cos}(\Phi(t),\alpha) + D(t,\alpha)T_{\sin}(\Phi(t),\alpha))T_{\sin}(\Phi(t),\alpha)d\Phi(t)$$
$$\dot{D}(t,\alpha) \approx \pm \frac{\varepsilon}{2\pi} \int_0^{2\pi} \frac{1}{\Delta(t,\alpha)} f(C(t,\alpha)T_{\cos}(\Phi(t),\alpha) + D(t,\alpha)T_{\sin}(\Phi(t),\alpha))T_{\cos}(\Phi(t),\alpha)d\Phi(t) \tag{86}$$

where

$$\rho(\Phi(t),\alpha) = \varepsilon_0 + C(t,\alpha)T_{\cos}(\Phi(t),\alpha) + D(t,\alpha)T_{\sin}(\Phi(t),\alpha) \tag{87}$$

$$f(\varepsilon_0 + C(t,\alpha)T_{\cos}(\Phi(t),\alpha) + D(t,\alpha)T_{\sin}(\Phi(t),\alpha)) \approx$$
$$\approx \varepsilon_0 \omega_0^2 \frac{1}{\rho_0^2} \left\langle \varepsilon_0 + C(t,\alpha)T_{\cos}(\Phi(t),\alpha) + D(t,\alpha)T_{\sin}(\Phi(t),\alpha) \right\rangle^2 \tag{88}$$
$$\left\langle 6 - 5\frac{1}{\rho_0}(\varepsilon_0 + C(t,\alpha)T_{\cos}(\Phi(t),\alpha) + D(t,\alpha)T_{\sin}(\Phi(t),\alpha)) + ... \right\rangle$$

5. CONCLUDING REMARKS

In the paper a generalization of Lagrange variation method of constant and in combination with method of averaging for nonlinear cased, is presented by use series of the examples, and especially for fractional order differential equations.

Then in general, it is possible, to extend generalization of the Lagrange variation constant to the series of differential equations in the following forms:

$$L\{x(t)\} = hf(t)$$
$$N\{x(t)\} = hf(t)$$
$$L\{x(t)\} + \omega_\alpha^2 \mathfrak{D}_t^\alpha [x(t)] = hf(t)$$
(81)

$$L\{x(t)\} = \varepsilon h_0 f(x, \dot{x})$$
$$N\{x(t)\} = \varepsilon h_0 f(x, \dot{x})$$
$$L\{x(t)\} + \omega_\alpha^2 \mathfrak{D}_t^\alpha [x(t)] = \varepsilon h_0 f(x, \dot{x})$$
(82)

$$L\{x(t)\} = \varepsilon h_0 f(x, \dot{x}, t)$$
$$N\{x(t)\} = \varepsilon h_0 f(x, \dot{x}, t)$$
$$L\{x(t)\} + \omega_\alpha^2 \mathfrak{D}_t^\alpha [x(t)] = \varepsilon h_0 f(x, \dot{x}, t)$$
(83)

where $L\{*\}$ linear differential operator, $N\{*\}$ nonlinear differential operator, $\mathfrak{D}_t^\alpha [*]$ fractional order differential operator.

For applying generalized Lagrange method of variation constants, it is necessary to known two particular solutions $T_1(t)$ and $T_2(t)$ (or $T_1(t,\alpha)$ and $T_2(t,\alpha)$) of the corresponding homogeneous linear or nonlinear or fractional order differential equation defined by:

$$L\{x(t)\} = 0$$
$$N\{x(t)\} = 0$$
$$L\{x(t)\} + \omega_\alpha^2 \mathfrak{D}_t^\alpha [x(t)] = 0$$
(84)

Then, proposed solution in the form of combinations of known particular solutions and amplitudes $C(t)$ and $D(t)$ as functions of time, satisfying condition that first derivative of generalized coordinate is same as that amplitudes $C(t)$ and $D(t)$ are constants. Results of the applications of generalized Lagrange method of variation constants to the different non homogeneous linear or nonlinear or fractional order differential equations are listed in the following form:

1* Non homogeneous non autonomous linear differential equation:
$$L\{x(t)\} = hf(t)$$

with known particular solutions $T_1(t)$ and $T_2(t)$ of the homogeneous linear differential equation.

Solution is in the form

$$x(t) = C(t)T_1(t,\alpha) + D(t)T_2(t)$$

and amplitudes are:

$$C(t) = C_0 - h\int_0^t \frac{f(\tau)T_1(\tau)}{\Delta(\tau)}d\tau$$

$$D(t,\alpha) = D_0 + h\int_0^t \frac{f(\tau)T_2(\tau)}{\Delta(\tau)}d\tau$$

where system determinant is defined by:

$$\Delta(t) = T_1(t)\dot{T}_2(t) - T_2(t)\dot{T}_1(t) \neq 0$$

2* Non homogeneous non autonomous nonlinear differential equation

$$N\{x(t)\} = hf(t)$$

with known particular solutions $T_1(t)$ and $T_2(t)$ of the homogeneous non linear differential equation.

Solution is in the form

$$x(t) = C(t)T_1(t,\alpha) + D(t)T_2(t)$$

and amplitudes are:

$$C(t) = C_0 - h\int_0^t \frac{f(\tau)T_1(\tau)}{\Delta(\tau)}d\tau$$

$$D(t,\alpha) = D_0 + h\int_0^t \frac{f(\tau)T_2(\tau)}{\Delta(\tau)}d\tau$$

where system determinant

$$\Delta(t) = T_1(t)\dot{T}_2(t) - T_2(t)\dot{T}_1(t) \neq 0$$

3* Non homogeneous non autonomous linear fractional order differential equation

$$L\{x(t)\} + \omega_\alpha^2 \mathfrak{D}_t^\alpha[x(t)] = hf(t)$$

with known particular solutions $T_1(t,\alpha)$ and $T_2(t,\alpha)$ of the homogeneous linear fractional order differential equation.

Solution is in the form

$$x(t,\alpha) = C(t,\alpha)T_{\cos}(t,\alpha) + D(t,\alpha)T_{\sin}(t,\alpha)$$

and amplitudes are:

$$C(t,\alpha) = C_0 - h\int_0^t \frac{f(\tau)T_{\sin}(\tau,\alpha)}{\Delta(\tau,\alpha)}d\tau$$

$$D(t,\alpha) = D_0 + h\int_0^t \frac{f(\tau)T_{\cos}(\tau,\alpha)}{\Delta(\tau,\alpha)}d\tau$$

where system determinant is slowchanging function

$$\Delta(t,\alpha) = T_{\cos}(t,\alpha)\dot{T}_{\sin}(t,\alpha) - T_{\sin}(t,\alpha)\dot{T}_{\cos}(t,\alpha) \neq 0$$

4* Non homogeneous autonomous non linear differential equation with small nonlinearity:

$$L\{x(t)\} = \varepsilon h_0 f(x,\dot{x})$$

with known particular solutions $T_1(t)$ and $T_2(t)$ of the homogeneous linear differential equation.

Approximation of the solution is in the form:

$$x(t) = C(t)T_1(t,\alpha) + D(t)T_2(t)$$

and approximation of the amplitudes can be determined from the following system along unknown amplitudes $C(t)$ and $D(t)$:

$$\dot{C}(t) = \mp\varepsilon\frac{1}{\Delta(t)}f\left(C(t),D(t),T_1(\Phi(t)),T_2(\Phi(t)),\dot{T}_1(\Phi(t)),\dot{T}_2(\Phi(t))\right)T_2(\Phi(t))$$

$$\dot{D}(t) = \pm\varepsilon\frac{1}{\Delta(t)}f\left(C(t),D(t),T_1(\Phi(t)),T_2(\Phi(t)),\dot{T}_1(\Phi(t)),\dot{T}_2(\Phi(t))\right)T_2(\Phi(t))$$

where system determinant is slowchanging function

$$\Delta(t) = T_1(t)\dot{T}_2(t) - T_2(t)\dot{T}_1(t) \neq 0$$

5* Non homogeneous autonomous non linear differential equation with additional small nonlinearity:

$$N\{x(t)\} = \varepsilon h_0 f(x,\dot{x})$$

with known particular solutions $T_1(t)$ and $T_2(t)$ of the homogeneous non linear differential equation.

Approximation of the solution is in the form:

$$x(t) = C(t)T_1(t) + D(t)T_2(t)$$

and approximation of the amplitudes can be determined from the following system along unknown amplitudes $C(t)$ and $D(t)$:

$$\dot{C}(t) = \mp\varepsilon\frac{1}{\Delta(t)}f\left(C(t),D(t),T_1(\Phi(t)),T_2(\Phi(t)),\dot{T}_1(\Phi(t)),\dot{T}_2(\Phi(t))\right)T_2(\Phi(t))$$

$$\dot{D}(t) = \pm\varepsilon\frac{1}{\Delta(t)}f\left(C(t),D(t),T_1(\Phi(t)),T_2(\Phi(t)),\dot{T}_1(\Phi(t)),\dot{T}_2(\Phi(t))\right)T_2(\Phi(t))$$

where system determinant is slowchanging function

$$\Delta(t) = T_1(t)\dot{T}_2(t) - T_2(t)\dot{T}_1(t) \neq 0$$

6* Non homogeneous autonomous non linear fractional order differential equation with small nonlinearity:

$$L\{x(t)\} + \omega_\alpha^2 \mathfrak{D}_t^\alpha [x(t)] = \varepsilon h_0 f(x, \dot{x})$$

with known particular solutions $T_1(t,\alpha)$ and $T_2(t,\alpha)$ of the homogeneous linear fractional order differential equation.

Approximation of the solution is in the form:

$$x(t,\alpha) = C(t,\alpha) T_{\cos}(t,\alpha) + D(t,\alpha) T_{\sin}(t,\alpha)$$

and approximation of the amplitudes can be determined from the following system along unknown amplitudes $C(t,\alpha)$ and $D(t,\alpha)$:

$$\dot{C}(t,\alpha) = \mp \varepsilon \frac{1}{\Delta(t,\alpha)} f\left(C(t,\alpha), D(t,\alpha), T_{\cos}(\Phi(t),\alpha), T_{\sin}(\Phi(t),\alpha), \dot{T}_{\cos}(\Phi(t),\alpha), \dot{T}_{\sin}(\Phi(t),\alpha)\right) T_{\sin}(\Phi(t),\alpha)$$

$$\dot{D}(t,\alpha) = \pm \varepsilon \frac{1}{\Delta(t,\alpha)} f\left(C(t,\alpha), D(t,\alpha), T_{\cos}(\Phi(t),\alpha), T_{\sin}(\Phi(t),\alpha), \dot{T}_{\cos}(\Phi(t),\alpha), \dot{T}_{\sin}(\Phi(t),\alpha)\right) T_{\cos}(\Phi(t),\alpha)$$

where system determinant is slowchanging function

$$\Delta(t,\alpha) = T_{\cos}(t,\alpha) \dot{T}_{\sin}(t,\alpha) - T_{\sin}(t,\alpha) \dot{T}_{\cos}(t,\alpha) \neq 0$$

7* Non homogeneous non autonomous nonlinear differential equation with small nonlinearity:

$$L\{x(t)\} = \varepsilon h_0 f(x, \dot{x}, t)$$

with known particular solutions $T_1(t)$ and $T_2(t)$ of the homogeneous linear differential equation.

Approximation of the solution is in the form:

$$x(t) = C(t) T_1(t,\alpha) + D(t) T_2(t)$$

and approximation of the amplitudes is possible to determine from the following system along unknown amplitudes $C(t)$ and $D(t)$:

$$\dot{C}(t) = \mp \varepsilon \frac{1}{\Delta(t)} f\left(C(t), D(t), T_1(\Phi(t)), T_2(\Phi(t)), \dot{T}_1(\Phi(t)), \dot{T}_2(\Phi(t)), \Phi(t) + \phi(t)\right) T_2(\Phi(t))$$

$$\dot{D}(t) = \pm \varepsilon \frac{1}{\Delta(t)} f\left(C(t), D(t), T_1(\Phi(t)), T_2(\Phi(t)), \dot{T}_1(\Phi(t)), \dot{T}_2(\Phi(t)) \Phi(t) + \phi(t)\right) T_2(\Phi(t))$$

where system determinant is slowchanging function

$$\Delta(t) = T_1(t) \dot{T}_2(t) - T_2(t) \dot{T}_1(t) \neq 0$$

8* Non homogeneous non autonomous non linear differential equation with additional small nonlinearity:

$$N\{x(t)\} = \varepsilon h_0 f(x, \dot{x}, t)$$

with known particular solutions $T_1(t)$ and $T_2(t)$ of the homogeneous non linear differential equation.

Approximation of the solution is in the form:

$$x(t) = C(t)T_1(t,\alpha) + D(t)T_2(t)$$

and approximation of the amplitudes is possible to determine from the following system along unknown amplitudes $C(t)$ and $D(t)$:

$$\dot{C}(t,\alpha) = \mp\varepsilon\frac{1}{\Delta(t)}f\big(C(t),D(t),T_1(\Phi(t)),T_2(\Phi(t)),\dot{T}_1(\Phi(t)),\dot{T}_2(\Phi(t)),\Phi(t)+\phi(t)\big)T_2(\Phi(t))$$

$$\dot{D}(t,\alpha) = \pm\varepsilon\frac{1}{\Delta(t)}f\big(C(t),D(t),T_1(\Phi(t)),T_2(\Phi(t)),\dot{T}_1(\Phi(t)),\dot{T}_2(\Phi(t))\Phi(t)+\phi(t)\big)T_2(\Phi(t))$$

where system determinant is slowchanging function

$$\Delta(t) = T_1(t)\dot{T}_2(t) - T_2(t)\dot{T}_1(t) \neq 0$$

9* Non homogeneous non autonomous non linear fractional order differential equation with small nonlinearity:

$$L\{x(t)\} + \omega_\alpha^2 \mathfrak{D}_t^\alpha[x(t)] = \varepsilon h_0 f(x,\dot{x},t)$$

with known particular solutions $T_1(t,\alpha)$ and $T_2(t,\alpha)$ of the homogeneous linear fractional order differential equation.

Approximation of the solution is in the form:

$$x(t,\alpha) = C(t,\alpha)T_{\cos}(t,\alpha) + D(t,\alpha)T_{\sin}(t,\alpha)$$

and approximation of the amplitudes is possible to determine from the following system along unknown amplitudes $C(t,\alpha)$ and $D(t,\alpha)$:

$$\dot{C}(t,\alpha) = \mp\varepsilon\frac{1}{\Delta(t,\alpha)}f\big(C(t,\alpha),D(t,\alpha),T_{\cos}(\Phi(t),\alpha),T_{\sin}(\Phi(t),\alpha),\dot{T}_{\cos}(\Phi(t),\alpha),\dot{T}_{\sin}(\Phi(t),\alpha),\Phi(t)+\phi(t)\big)T_{\sin}(\Phi(t),\alpha)$$

$$\dot{D}(t,\alpha) = \pm\varepsilon\frac{1}{\Delta(t,\alpha)}f\big(C(t,\alpha),D(t,\alpha),T_{\cos}(\Phi(t),\alpha),T_{\sin}(\Phi(t),\alpha),\dot{T}_{\cos}(\Phi(t),\alpha),\dot{T}_{\sin}(\Phi(t),\alpha),\Phi(t)+\phi(t)\big)T_{\cos}(\Phi(t),\alpha)$$

where system determinant is slowchanging function

$$\Delta(t,\alpha) = T_{\cos}(t,\alpha)\dot{T}_{\sin}(t,\alpha) - T_{\sin}(t,\alpha)\dot{T}_{\cos}(t,\alpha) \neq 0$$

In the cases 7*, 8* and 9* external excitation function is periodic functions with full phase $\vartheta(t) = \Omega t + \vartheta_0 = \Phi(t) + \phi(t)$, where Ω is external excitation circular frequency in resonant range of eigen circular frequency $\tilde{\omega}_0$ of corresponding linear or nonlinear free vibrations described by corresponding homogeneous differential equation, and $\Phi(t) = \tilde{\omega}_0 t$ full phase along which it is necessary to followed averaging procedure, taking into account only fast change function under integral, as it is take in the examples 1 and 2. Slowching functions under the integrals as it is $\Delta(t)$ or $\Delta(t,\alpha)$ are no under the averaged procedure for nonlinear systems.

APENDIX - ADDITION TO THE PAPER.

The time functions – solution of a fractional order differential equation

The fractional order differential equation in the form:

$$\ddot{\rho}(t) + \omega_0^2 \rho(t) + \omega_\alpha^2 \mathfrak{D}_t^\alpha [\rho(t)] = 0 \tag{A.1}$$

is linear part with a fractional order term (in left hand side) of the fractional differential equations (9) and (26)-(27) and (77) along independent coordinate $\rho(t)$, distance between mass particles, in both considered case of the two mass particle fractional order system dynamics in plane.

As the obtained fractional differential equations (26), (27) and (28) are nonlinear, and that for small oscillations around equilibrium configurations is possible to considerate approximation of their solution around known analytical solution of linearized nonlinear fractional order differential equation as well as around other known analytical particular solutions it is possible to start with analytical solution of fractional order differential equation (A.1) and by using generalized approach of the variation constant. Then it is important to present analytical solution of the fractional order differential equation (A.1) or in the form (se References [4-13]):

$$\ddot{T}(t) + \omega_\alpha^2 T^{(\alpha)}(t) + \omega_0^2 T(t) = 0 \tag{A.2}$$

This fractional-differential equation (A.1) or (A.2) on unknown time-function $T(t)$, can be solved applying Laplace transforms (se References [7-10]). Upon that fact Laplace transform of solution is in form:

$$\mathfrak{T}(p) = \mathfrak{L}[T(t)] = \frac{pT(0) + \dot{T}(0)}{p^2 + \omega_0^2 \left[1 + \dfrac{\omega_\alpha^2}{\omega_0^2} \mathbf{R}(p)\right]} \tag{A.3}$$

where $\mathfrak{L}[\mathfrak{D}_t^\alpha[T(t)]] = \mathbf{R}(p)\mathfrak{L}[T(t)]$ is Laplace transform of a fractional derivative $\dfrac{d^\alpha T(t)}{dt^\alpha}$ for $0 \le \alpha \le 1$. For creep rheological material those Laplace transforms the form:

$$\mathfrak{L}[\mathfrak{D}_t^\alpha[T(t)]] = \mathbf{R}(p)\mathfrak{L}[T(t)] - \frac{d^{\alpha-1}}{dt^{\alpha-1}}T(0) = p^\alpha \mathfrak{L}[T(t)] - \frac{d^{\alpha-1}}{dt^{\alpha-1}}T(0) \tag{A.4}$$

where the initial value are: $\left.\dfrac{d^{\alpha-1}T(t)}{dt^{\alpha-1}}\right|_{t=0} = 0$, so, in that case Laplace transform of time-function is given by following expression:

$$\mathfrak{L}\{T(t)\} = \frac{pT_0 + \dot{T}_0}{\left[p^2 + \omega_\alpha^2 p^\alpha + \omega_0^2\right]} \tag{A.5}$$

For boundary cases, when material parameters α take following values: $\alpha = 0$ and $\alpha = 1$ we have the two special simple cases, whose corresponding

fractional-differential equations and solutions are known. In these cases fractional-differential equations are:

The solutions to equations (A.2) and (A.1) are:

$$1^* \quad T(t) = T_0 \cos t \sqrt{\omega_0^2 + \tilde{\omega}_0^2} + \frac{\dot{T}_0}{\sqrt{\omega_0^2 + \tilde{\omega}_0^2}} \sin t \sqrt{\omega_0^2 + \tilde{\omega}_0^2} \text{ , for } \alpha = 0 ; \qquad \text{(A.6)}$$

$$2^* \text{ a.} \quad T(t) = e^{-\frac{\omega_1^2}{2}t} \left\{ T_0 \cos t \sqrt{\omega_0^2 - \frac{\omega_1^4}{4}} + \frac{\dot{T}_0}{\sqrt{\omega_0^2 - \frac{\omega_1^4}{4}}} \sin t \sqrt{\omega_0^2 - \frac{\omega_1^4}{4}} \right\} \qquad \text{(A.7)}$$

for $\alpha = 1$ and for $\omega_0 > \frac{1}{2} \omega_1^2$. (for soft creep) or for strong creep:

$$2^* \text{ b.} \quad T(t) = e^{-\frac{\omega_1^2}{2}t} \left\{ T_0 Ch\, t \sqrt{\frac{\omega_1^4}{4} - \omega_0^2} + \frac{\dot{T}_0}{\sqrt{\frac{\omega_1^4}{4} - \omega_0^2}} Sh\, t \sqrt{\frac{\omega_1^4}{4} - \omega_0^2} \right\} \qquad \text{(A.8)}$$

for $\alpha = 1$ and for $\omega_0 < \frac{1}{2} \omega_1^2$.

For critical case:

$$2^* \text{ c.} \quad T(t) = e^{-\frac{\omega_1^2}{2}t} \left\{ T_0 + \frac{2\dot{T}_0}{\omega_1^2} t \right\} \text{ za } \alpha = 1 \quad \text{and za } \omega_0 = \frac{1}{2} \omega_1^2 . \qquad \text{(A.9)}$$

Fractional-differential equation (A.2) for the general case, when α is real number from interval $0 < \alpha < 1$ can be solved by using Laplace's transformation. By introducing for initial conditions of fractional derivatives in the form (A.4), and after taking Laplace's transform of the equation, we obtain the following solution:

$$T(t) = \mathfrak{L}^{-1}\{T(t)\} = T_0 \sum_{k=0}^{\infty} (-1)^k \omega_\alpha^{2k} t^{2k} \sum_{j=0}^{k} \binom{k}{j} \frac{\omega_\alpha^{-2j} t^{-\alpha j}}{\omega_o^{2j} \Gamma(2k+1-\alpha j)} + \qquad \text{(A.10)}$$
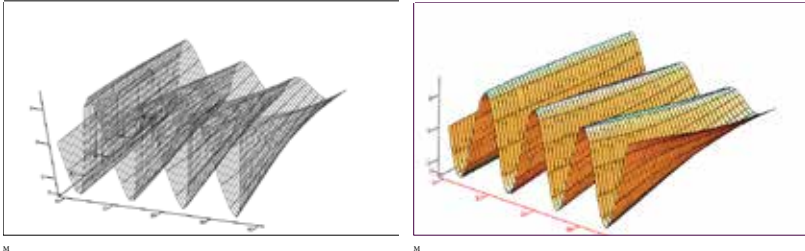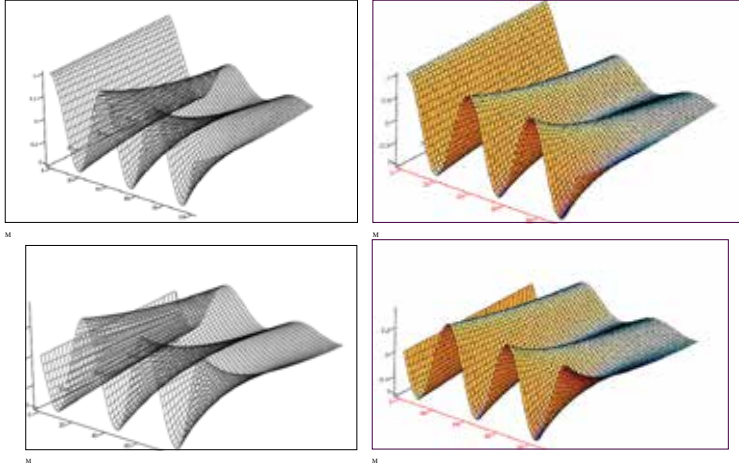
$$+ \dot{T}_0 \sum_{k=0}^{\infty} (-1)^k \omega_\alpha^{2k} t^{2k+1} \sum_{j=0}^{k} \binom{k}{j} \frac{\omega_\alpha^{-2j} t^{-\alpha j}}{\omega_o^{2j} \Gamma(2k+2-\alpha j)}$$

or

$$T(t) = \mathfrak{L}^{-1}\{T(t)\} = \sum_{k=0}^{\infty} (-1)^k \omega_\alpha^{2k} t^{2k} \sum_{j=0}^{k} \binom{k}{j} \frac{\omega_\alpha^{-2j} t^{-\alpha j}}{\omega_o^{2j}} \left[\frac{T_0}{\Gamma(2k+1-\alpha j)} + \frac{\dot{T}_0 t}{\Gamma(2k+2-\alpha j)} \right] \quad \text{(A.11)}$$

Graphical presentation of the modes of fractional order oscillator with one degree of freedom

1.a* Mode like cosines is defined by expression
$T_{s,\cos}(t,\alpha) = \sum_{k=0}^{\infty} (-1)^k \omega_{(\alpha)s}^{2k} t^{2k} \sum_{m=0}^{k} \binom{k}{m} \frac{\omega_{(\alpha)s}^{-2m} t^{-\alpha m}}{\omega_s^{2m} \Gamma(2k+1-\alpha m)}$ and for $\alpha = 0$ vibration is linear
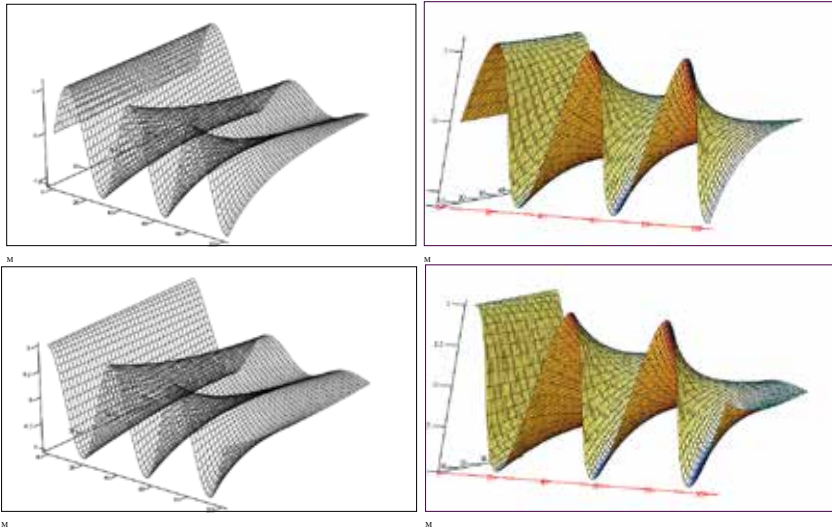
and periodic and mode is $T_{s,\cos}(t,\alpha)\big|_{\alpha=0} = \cos\left(t\sqrt{\omega_s^2 + \omega_{(\alpha=1)s}^2}\right)$ and for $\alpha = 1$ vibrations

are damped and in the form: for $\alpha = 1$, particular solutions are:
$T_{s,\cos}(t,\alpha)\big|_{\alpha=1} = e^{-\frac{1}{2}\omega_\alpha^2 t} \cos t \sqrt{\omega_0^2 - \frac{1}{4}\omega_\alpha^4}$.
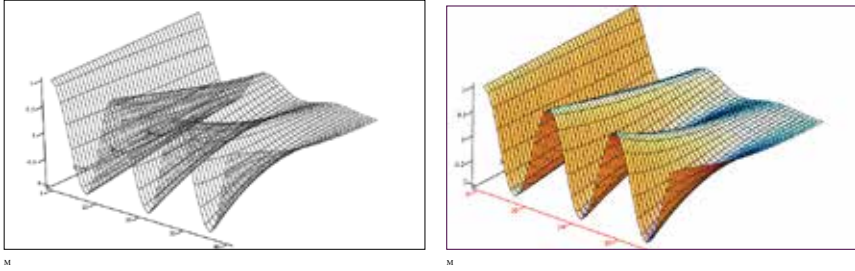
Figure 1.a* Mode like cosines is defined by expression

$$T_{s,\cos}(t,\alpha) = \sum_{k=0}^{\infty}(-1)^k \omega_{(\alpha)s}^{2k} t^{2k} \sum_{m=0}^{k}\binom{k}{m}\frac{\omega_{(\alpha)s}^{-2m} t^{-\alpha m}}{\omega_s^{2m}\Gamma(2k+1-\alpha m)}$$ and for $\alpha = 0$ vibration is linear and

periodic and mode is $T_{s,\cos}(t,\alpha)\big|_{\alpha=0} = \cos\left(t\sqrt{\omega_s^2 + \omega_{(\alpha=1)s}^2}\right)$ and for $\alpha = 1$ vibrations are

damped and in the form: for $\alpha = 1$, particular solutions are:

$$T_{s,\cos}(t,\alpha)\big|_{\alpha=1} = e^{-\frac{1}{2}\omega_\alpha^2 t}\cos t\sqrt{\omega_0^2 - \frac{1}{4}\omega_\alpha^4} \ .$$

1.b* **Derivative** **of** **the** **mods** **of** **like** **cosines**

$$T_{s,\cos}(t,\alpha) = \sum_{k=0}^{\infty}(-1)^k \omega_{(\alpha)s}^{2k} t^{2k} \sum_{m=0}^{k}\binom{k}{m}\frac{\omega_{(\alpha)s}^{-2m} t^{-\alpha m}}{\omega_s^{2m}\Gamma(2k+1-\alpha m)}$$ is minus like sine mode

$$\dot{T}_{\cos}(t,\alpha) = \sum_{k=1}^{\infty}(-1)^k \omega_\alpha^{2k} t^{2k} \sum_{m=0}^{k}\binom{k}{m}\frac{(2k-\alpha m)\omega_\alpha^{-2m} t^{-\alpha m}}{\omega_o^{2m}\Gamma(2k+1-\alpha m)}$$

Figure 1.b* Derivative of the mode of like cosines

$$T_{s,\cos}(t,\alpha) = \sum_{k=0}^{\infty}(-1)^k \omega_{(\alpha)s}^{2k} t^{2k} \sum_{m=0}^{k}\binom{k}{m}\frac{\omega_{(\alpha)s}^{-2m} t^{-\alpha m}}{\omega_s^{2m}\Gamma(2k+1-\alpha m)}$$ is minus like sine mode

$$\dot{T}_{\cos}(t,\alpha) = \sum_{k=1}^{\infty}(-1)^k \omega_\alpha^{2k} t^{2k} \sum_{m=0}^{k}\binom{k}{m}\frac{(2k-\alpha m)\omega_\alpha^{-2m} t^{-\alpha m}}{\omega_o^{2m}\Gamma(2k+1-\alpha m)} \ /$$

Figure 1.c* Comparison: Like cos mode

$$T_{s,\cos}(t,\alpha)=\sum_{k=0}^{\infty}(-1)^k\,\omega_{(\alpha)_s}^{2k}t^{2k}\sum_{m=0}^{k}\binom{k}{m}\frac{\omega_{(\alpha)_s}^{-2m}t^{-\alpha m}}{\omega_s^{2m}\Gamma(2k+1-\alpha m)}$$ and derivative in the form minus like

sin mode $$\dot{T}_{\cos}(t,\alpha)=\sum_{k=1}^{\infty}(-1)^k\,\omega_{\alpha}^{2k-1}t^{2k}\sum_{m=0}^{k}\binom{k}{m}\frac{(2k-\alpha m)\omega_{\alpha}^{-2m}t^{-\alpha m}}{\omega_o^{2m}\Gamma(2k+1-\alpha m)}$$

Figure 2.a* Comparisson

Like sin mode $$T_{s,\sin}(t,\alpha)=\sum_{k=0}^{\infty}(-1)^k\,\omega_{(\alpha)_s}^{2k}t^{2k+1}\sum_{m=0}^{k}\binom{k}{m}\frac{\omega_{(\alpha)_s}^{-2m}t^{-\alpha m}}{\omega_s^{2m}\Gamma(2k+2-\alpha m)}$$ and derivative in the form

like cos mode $$\dot{T}_{\sin}(t,\alpha)=\sum_{k=0}^{\infty}(-1)^k\,\omega_{\alpha}^{2k}t^{2k}\sum_{m=0}^{k}\binom{k}{m}\frac{(2k+1-\alpha m)\omega_{\alpha}^{-2m}t^{-\alpha m}}{\omega_o^{2m}\Gamma(2k+2-\alpha m)}$$

64

REFERENCES

[1] D. P. Rašković, Teorija oscilacija (Theory of Ooscillations), Naučna knjiga, 1952.

[2] D.P.Rašković, Analitička mehanika (Analytical Mechanics), Mašinski fakultet Kragujevac, 1974.

[3] T. Pejpvić, Diferencijalne jednacine (Differential equations), II, Univerziete u Beogradu, 1948.

[4] Rosikin Yuri and Maria Shitikova: (2010), Application of Fractional Calculus for Dynamic Problem of Solid Mechanics, Novel Trends and Resent Results, Applied Mechanics Reviews, American Society of Mechanical Enginewers –ASME, JANUAR 2010, Vol. 63/ pp. 010801-1 - 010801-52.

[5] Rosikin Yuri and Maria Shitikova:, (2002), Applications of fractional calculus to dynamic problems of linear and nonlinear hereditary mechanics of solids, Transmitted by Associate Editor Isaac Elishakoff, ASME Reprint No AMR202 $42, Appl Mech Rev vol 50, no 1, January 1997 15 © 1997 , American Society of Mechanical Engineers Downloaded**,** pp. 15-67.

[6] Rossikhin Yuriy A., (2010), Reflections on Two Parallel Ways in the Progress of Fractional Calculus in Mechanics of Solids, Applied Mechanics Reviews, Copyright © 2010 by ASME JANUARY 2010, Vol. 63 / 010701-1, pp. / (010701-1)-/(010701-12).

[7] Enelund, M., Fractional Calculus and Linear Viscoelasticity in Structural Dynamics, Division of Solid Mechanics, Chalmers tekniska Hogskola, Goteborg, Sweden, 1996., p.1-27, A1-33+B1-20+C1-19+D1-28+E1-26.

[8] Gorenflo, R., Mainardi, F., (2000) Fractional Calculus, Integral and Differential Equations of Fractional Order, CISM Lecture Notes, Udine, Italy, Preprint 54 pages, pp. 223-276.

[9] Bačlić, B. S., Atanacković, T., (2000), M., *Stability and creep of a fractional derivative order viscoelastic Rod*, Bulletin T, CXXI de L'Academie Serbe des Sciences st de Arts - 2000, Class des Sciences mathematques et naturelles Sciences mathematiques, No. 25, 115-131.

[10] K. R. Hedrih (Stevanović), A. Filipovski., (2002), *Longitudinal Vibration of a Fractional Derivative Order Rheological Rod with Variable Cross Section*, Facta Universitatis, Series Mechanics, Automatic Control and Robotics, Vol. 3 No. 12, 2002. pp.327-350.

[11] K.R. Hedtrih (Stevanović), (2008), The fractional order hybrid system vibrations, Monograph, Chap in Monograph. Advances in Nonlinear Sciences, ANN, 2008, Vol. 2, pp. 226-326.

[12] K.R. Hedtrih (Stevanović), (2011), Analytical mechanics of fractional order discrete system vibrations. Chap in Monograph. Advances in nonlinear sciences, Vол. 3, JANN, Belgrade, pp. 101-148, 2011. ISSN: 978-86-905633-3-3.

[13] K.R. Hedtrih (Stevanović), (2009), *Considering Transfer of Signals through Hybrid Fractional Order Homogeneous Structure, Keynote Lecture*, AAS-09, Ohird, Makedonija, posvecen profesoru Pane Vidincevu, prvom profesoru automatike i rachnarskih mashina u Makedoniji Special session, Applied Automatic Systems , Proceedings of selected AAS 2009 Papers. Edited by G. Dimirovski, Skopje –Istambul , 2009, ISBN -13-978-9989-2175-6-2, National Library of R. Makedonia, Skopje, Copright«2009Authors and ETAI Society, pp. 19-24.

[14] Yu. A. Mitropolyskiy, *Nonlinear Mechanics – Asymptotic Methods,* Institut matematiki NAN Ukraini, Kiev, 1995, pp. 397. (in Russian)

[15] Yu.A . Mitropolyskiy, (1964), Problemi asimptoti-cheskoy teorii nestashionarnih kolebaniy, Nauka Moskva. (in Russian).

[16] Yu.A . Mitropolyskiy, (1955), *Nestashionarnie proshesi v nelinyeynih sistemah*, AN USSR, Kiev. (in Russian)

[17] Yu.A . Mitropolyskiy and B. Mosseenkov, (1968), *Lekciyi po primenyeniyu metodov k recheniyu uravnyeniy v chastnih proizvodnih*, Int. Math. AN USSR, Kiev. (in Russian)

[18] Yu.A . Mitropolyskiy and B. Mosseenkov, (1976), *Asymptotic solutions of the Partial Differential Equations*, Kiev 1976. (in Russian).

[19] Yu.A . Mitropolyskiy (1964), Problemi asimptoti-cheskoy teorii nestashionarnih kolebaniy, Nauka Moskva. (in Russian)

[20[Yu.A . Mitropolyskiy, Nguyen Van Dao, (2003), *Lectures on Asymptotic Methods of Nonlinear Dynamics*, Vietnam National University Publishing House, Hanoi, p. 494.

[21] Yu.A . Mitropolyskiy, Some problems in the development in nonlinear mechanics theory and applications, Facta Universitatis, Series Mechanics, Automatic Control and Robotics, Vol. 1, No. 5,1995, pp. 539-560.

[22] Yu.A . Mitropolyskiy, On Application of asymptotic methods of nonlinear mechanics for solving some problems of oscillation theory, Facta Universitatis, Series Mechanics, Automatic Control and Robotics, Vol. 2, No. 6,1996, pp. 1-9.

[23] Yu.A . Mitropolyskiy, Adiabatic processes in nonlinear oscillation systems (Adiabaticheskie processi v nelinyeynih kolebatelynih sistemah), Simpozijum '83 – Nelinearni problemi dinamike, Arandjelovac, 23-25,, Novembar 1983. IT-Društvp za mehaniku Srbije, pp. I-1-I-12. (in Russia).

[24] K. R. Hedrih (Stevanović, Energy analysis in a nonlinear hybrid system containing linear and nonlinear subsystems coupled by hereditary element (Article),   NONLINEAR DYNAMICS , (2008) vol.51 br.1-2 str. 127 -140. DOI 10.1007/s11071-007-9197-2.

[25] K.R. Hedtrih (Stevanović), (2012), APPROXIMATIONS OF NONLINEAR DIFFERENTIAL EQUATION SOLUTIONS, Two pages paper, CD-Proceedings of 23rd International Congress of Theoretical and Applied Mechanics, (ICTAM Beijing 2012), 19-24 avgust 2012, SM16 Vibrations and control of structures, International Union of Theoretical and Applied Mechanics. SM16-053 pp. SM16-053:1-2, http://www.ictam2012.org/, ISBN 978-16022-3-7

[26] K.R. Hedtrih (Stevanović), (2012), APPROXIMATIONS OF NONLINEAR DIFFERENTIAL EQUATION SOLUTIONS, Abstract book of 23rd International Congress of Theoretical and Applied Mechanics, Editors: Yilon Brll, Jianxian Wang and Daining Fang, (ICTAM Beijing 2012), 19-24 avgust 2012, SM16 Vibrations and control of structures, Seminar Session, International Union of Theoretical and Applied Mechanics . SM16-053, p. 79. http://www.ictam2012.org/

[27] K.R. Hedtrih (Stevanović), (2012), Energy and Nonlinear Dynamics of Hybrid Systems, Chapter in Book: Edited by A. Luo, Dynamical Systems and Methods, 2012, Part 1, 29-83, DOI: 10.1007/978-1-4614-0454-5_2

LINEAR AND NONLINEAR REACTION SYSTEMS

Ljiljana Kolar-Anić[1], Željko Čupić[2]

[1] Faculty of Physical Chemistry, University of Belgrade, Studentski trg 12-16, 11000 Belgrade, Serbia
e-mail: ljiljana.kolar.anic@gmail.com
[2] Institute of Chemistry, Technology and Metallurgy, University of Belgrade, Department of Catalysis and Chemical Engineering, Njegoševa 12, 11000 Belgrade, Serbia
e-mail: zcupic@nanosys.ihtm.bg.ac.rs

Abstract. *The difference between linear and nonlinear reaction systems was explained on two simple examples and elaborated on autocatalator as minimal model of the reaction system as well as on the model of the real complex process: the Bray-Liebhafsky oscillatory reaction.*

1. Introduction

The nonlinear reaction systems with feedback being far from thermodynamic equilibrium can be in different self organized states. This is of crucial importance for the living systems, although this phenomenon can be found everywhere. What is the nonlinear reaction system with feedback? The difference between linear and nonlinear reaction systems will be explained on two simple examples (Sections 2, 3 and 4) and elaborated on autocatalator as minimal model of the reaction system (Section 5) as well as on the model of the real complex process: the Bray-Liebhafsky oscillatory reaction (Section 6).

2. Linear reaction system

One typical example of linear process is the following homogeneous chemical reaction realized in isothermal closed reactor:

$$A \xrightleftharpoons[k_{-1}]{k_1} X \tag{R1.1}$$

$$X \xrightleftharpoons[k_{-2}]{k_2} B . \tag{R1.2}$$

In this reaction scheme that we call model, reactant A transform to product B *via* intermediate X. The rate constants of forward reactions are denoted by k_1 and k_2, whereas the ones for reverse reactions are denoted by k_{-1} and k_{-2}. The reaction rates are the product of corresponding rate constants and concentrations of all species that take place in considered reaction ($v_1 = k_1 a$, $v_{-1} = k_{-1} x$, $v_2 = k_2 x$, and $v_{-2} = k_{-2} b$ where a, x and b stand for concentrations of A, X and B at any time t). [1-9]

Since both reactions are reversible, the overall process can be described by the summarized stoichiometric relation A $\rightarrow$ B if initial concentration of B is relatively small, or B $\rightarrow$ A if the concentration of species B is high enough at the initial moment. Hence, depending on initial conditions species A and B can be either reactants or products. As such these species are external ones and their concentrations a and b determine the dynamic state of the system and can be considered as one kind of the control parameter. On the other side, the intermediate X as the internal species does not appear in the stoichiometric relations A $\rightarrow$ B or B $\rightarrow$ A. Therefore it reflects the state of the system in any arbitrary moment t.

2.1. Equilibrium stationary state

In the equilibrium stationary state, the detailed balance of the reactions must be attained. In other words, all particular reactions (reaction steps) must be in equilibrium, that is, for every reaction in the reaction model, the rate of reactions in both directions would be equal. Such state may be attained when time tends to infinity. In the considered case, the equilibrium stationary state is reached when both relationships between reaction rates $v_1 = v_{-1}$ and $v_2 = v_{-2}$ are simultaneously satisfied. Thus we can write:

$$k_1 a_{eq} = k_{-1} x_{eq} \tag{1.1}$$

$$k_2 x_{eq} = k_{-2} b_{eq}. \tag{1.2}$$

Here, by a_{eq}, x_{eq} and b_{eq}, the equilibrium concentrations of mentioned species are denoted. The above relations give us the equilibrium concentration of intermediate species X (x_{eq})

$$x_{eq} = \frac{k_1}{k_{-1}} a_{eq} = \frac{k_{-2}}{k_2} b_{eq} \tag{2}$$

as well as the ratio between the equilibrium concentrations of reactants a_{eq} and b_{eq}

$$\frac{k_1 k_2}{k_{-1} k_{-2}} = \frac{b_{eq}}{a_{eq}}. \tag{3}$$

It means that the equilibrium stationary state is defined by the ratio of rate constants of particular reaction steps or by the ratio of the concentrations of the external species.

2.2. Nonequilibrium stationary state

Beside the equilibrium stationary state, in the above reaction system we can also analyze the nonequilibrium stationary states in which system can be during the course of reaction, that is, between $t = 0$ and $t \rightarrow \infty$. They are realized when the intermediate species X is in the stationary state. The time evolution of the concentration of this species is defined by the above model. Following the law of mass action, it is described by the following differential equation

$$\frac{\mathrm{d}x}{\mathrm{d}t} = v_1 - v_{-1} - v_2 + v_{-2} = k_1 a + k_{-2} b - (k_{-1} + k_2) x \qquad (4)$$

which can be written in the form

$$\frac{\mathrm{d}x}{\mathrm{d}t} = \lambda - kx . \qquad (5)$$

Here $k = k_{-1} + k_2$ is a constant and $\lambda = k_1 \, a + k_{-2} \, b$ is the parameter that changes during the course of reaction since it depends on the concentrations of external species A and B, and hence, depends on time.

In the nonequilibrium stationary state $\mathrm{d}x/\mathrm{d}t = 0$ whereas $\mathrm{d}r/\mathrm{d}t \neq 0$ and $\mathrm{d}b/\mathrm{d}t \neq 0$. The stationary concentration of the intermediate species X (x_{ss}) is given by the expression

$$x_{ss} = \frac{\lambda}{k} . \qquad (6)$$

Dependence of the stationary concentration of the intermediate X (x_{ss}) on the parameter λ, which is a measure of distance from equilibrium of the above considered reaction system, is given schematically in Fig 1.(a). There is a range of x_{ss} values, that is, there are a number of non-equilibrium steady states of the one system for different values of λ. As λ is a function of the reactant concentrations, there are a number of non-equilibrium steady states for different values of them. In linear reaction systems, for selected value of control parameter λ, there is only one x_{ss}. Consequently, we are dealing with monostability.

In the closed reactor (batch conditions) the stationary concentration of intermediate changes in time since the concentrations of A and B evolve during the course of reaction until their constant values at equilibrium, such that $a = a(t)$ and $b = b(t)$). Therefore, in this case, the concentrations of intermediates are only quasi- or pseudo- stationary.

In open reaction systems as it is the CSTR (Continuously fed well Stirred Tank Reactor), where concentrations of reaction species can be controlled from outside in desirable period, the nonequilibrium stationary states are really stationary and parameter λ, which is function of selected initial concentrations of species, does not change in

time. In this case we are also dealing with linear dependence between x_{ss} and λ with slope $1/k$. Therefore, such reaction systems are linear.

Nevertheless, the considered example (R1) that can be written in the form $A \rightleftharpoons X \rightleftharpoons B$ is also linear. Its dynamic states are described by the equation (4) which is first order linear differential equation. From kinetic point of view, the reaction where one molecule transforms to the other ones is the first order reaction. Besides considered example the first order reactions are also $A \rightarrow B$, $A \rightleftharpoons B$, $A \rightarrow X \rightarrow B$ and all others similar reactions but under the condition that they are all isothermal. As all other reactions are nonlinear, we can see that the number of nonlinear reaction is incomparable larger than linear ones and that we need to analyzed them with particular attention. In general, for such systems, the stationary concentration of the intermediate X (x_{ss}) is nonlinear function of the parameter λ, Figs 1.(b) and (c). However, in nonlinear reaction systems, for selected value of control parameter λ, can be one (Fig.1(b)) or more (fig1(c)) values of x_{ss}. In last case we are dealing with multistability.
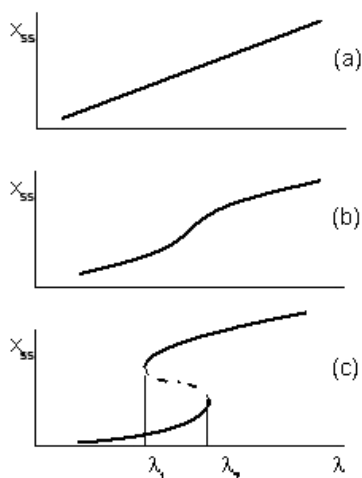
Figure 1. Steady-state concentrations of the intermediate, x_{ss}, as a function of the parameter λ, which denotes the distance of the considered dynamic state from the equilibrium. (a) Linear dependence; (b) nonlinear dependence of the monotonous form (monostability); (c) nonlinear dependence of the nonmonotonous form (multistability); dashed line denotes the region of instable steady states, that is, the instable nonequilibrium stationary states. (The figure is taken from ref. [9])

3. Nonlinear reaction system

The nonlinear dynamical system as close as possible to the previous linear one is the following model-reaction with one autocatalytic step (R2.1) [3-10]:

$$A + 2X \underset{k_{-1}}{\overset{k_1}{\rightleftharpoons}} 3X \tag{R2.1}$$

$$X \underset{k_{-2}}{\overset{k_2}{\rightleftharpoons}} B . \tag{R2.2}$$

Here, as in the previous case (R1), reactant A transform to product B *via* intermediate X. The reaction rates are now little different: $v_1 = k_1 a x^2$, $v_{-1} = k_{-1} x^3$, $v_2 = k_2 x$ and $v_{-2} = k_{-2} b$. Once more, since both reactions are reversible, the overall process can be described by the summarized stoichiometric relation A $\rightarrow$ B or B $\rightarrow$ A.

3.1. Equilibrium stationary state

In the considered case, as well as in the previous one, the equilibrium stationary state is reached when both relationships between reaction rates $v_1 = v_{-1}$ and $v_2 = v_{-2}$ are simultaneously satisfied. However, the reaction rates are different such that:

$$k_1 a_{eq} x_{eq}^2 = k_{-1} x_{eq}^3 \tag{7.1}$$

$$k_2 x_{eq} = k_{-2} b_{eq}. \tag{7.2}$$

The above relations, although different of equations (1) gives us the same relations for intermediate concentration of species X (x_{ss})

$$x_{eq} = \frac{k_1}{k_{-1}} a_{eq} = \frac{k_{-2}}{k_2} b_{eq} \tag{8}$$

as well as the ratio between the equilibrium concentrations of reactants a_{eq} and p_{eq}

$$\frac{k_1 k_2}{k_{-1} k_{-2}} = \frac{b_{eq}}{a_{eq}} \tag{9}$$

Obviously in the equilibrium stationary state there is no difference between these two considered systems. Nevertheless, the nonequilibrium stationary states are very different.

3.2. Nonequilibrium stationary state

The nonequilibrium stationary states in which system can be during the course of reaction, that is, between $t = 0$ and $t \rightarrow \infty$ can be obtained by analysis of the stationary state of the differential equation for the concentration evolution of the intermediate X:

$$\frac{dx}{dt} = k_1 a x^2 - k_{-1} x^3 - k_2 x + k_{-2} p \tag{10}$$

In the stationary state we obtain the following cubic equation

$$k_{-1} x_{ss}^3 - k_1 a x_{ss}^2 + k_2 x_{ss} - k_{-2} p = 0 \tag{11}$$

which has three stationary solutions. One is always real whereas other two can be either real or conjugate complex. Generally, cubic equation:

$$x^3 + a_1 x^2 + a_2 x + a_3 = 0 \tag{12}$$

may always be transformed to the form without quadratic term by the substitution $y = x + a_1 / 3$, which gives

$$y^3 + (a_2 - \frac{1}{3} a_1^2) y + \frac{2}{27} a_1^3 - \frac{1}{3} a_1 a_2 + a_3 = 0 \tag{13}$$

In the considered case by the following substitution

$$y_{ss} = x_{ss} - \frac{k_1 a}{3 k_{-1}} \tag{14}$$

we obtain

$$y_{ss}^3 + (\frac{k_2}{k_{-1}} - \frac{1}{3} \frac{k_1^2 a^2}{k_{-1}^2}) y_{ss} - \frac{2}{27} \frac{k_1^3 a^3}{k_{-1}^3} + \frac{1}{3} \frac{k_1 k_2 a}{k_{-1}^2} - \frac{k_{-2} b}{k_{-1}} = 0 \tag{15}$$

Because of this, the possible stationary states that appear in such nonlinear systems are often discussed in the literature by means of the abstract mathematical model which is also the basis of the considered case (R2):

$$\frac{dx}{dt} = -x^3 + \mu x + \lambda \tag{16}$$

where both μ and λ are the control parameters of the system. The cubic equation for evaluation of the stationary concentrations of intermediate X, x_{ss} written in the form:

$$x_{ss}^3 - \mu x_{ss} - \lambda = 0 \tag{17}$$

has either one real and two conjugate complex solutions or three real ones. The mutual relation between x_{ss}, μ and λ is presented in Fig. 2.(a).

Obviously, if we analyze the relation between x_{ss}, as a function that characterize steady state of the system in a function of μ and λ as a parameters representing the distance of particular steady state from equilibrium, the region with multistability can be found. It appears in the region of x_{ss}, μ and λ phase space where all three solutions of the cubic equation (17) are real. Two of them are stable, whereas the one in the middle is unstable. Therefore, we are dealing with bistability. However, is it possible that a real system is in two stable steady states simultaneously? What will be if we push the system from thermodynamic equilibrium by variation of one parameter, for example λ (Fig. 2.(b), which formally corresponds to Fig. 1. (c))? In that case, with increasing the parameter λ, x_{ss} take first the values characteristic for thermodynamic branch until $\lambda = \lambda_2$, where it suddenly shift to the other (kinetic) branch. With decreasing λ, system follows kinetic branch until $\lambda = \lambda_1$, where it shift to thermodynamic branch. Thus, in the system with bistability, hysteresis is present and system will be in one of two stable steady states depending on its history.
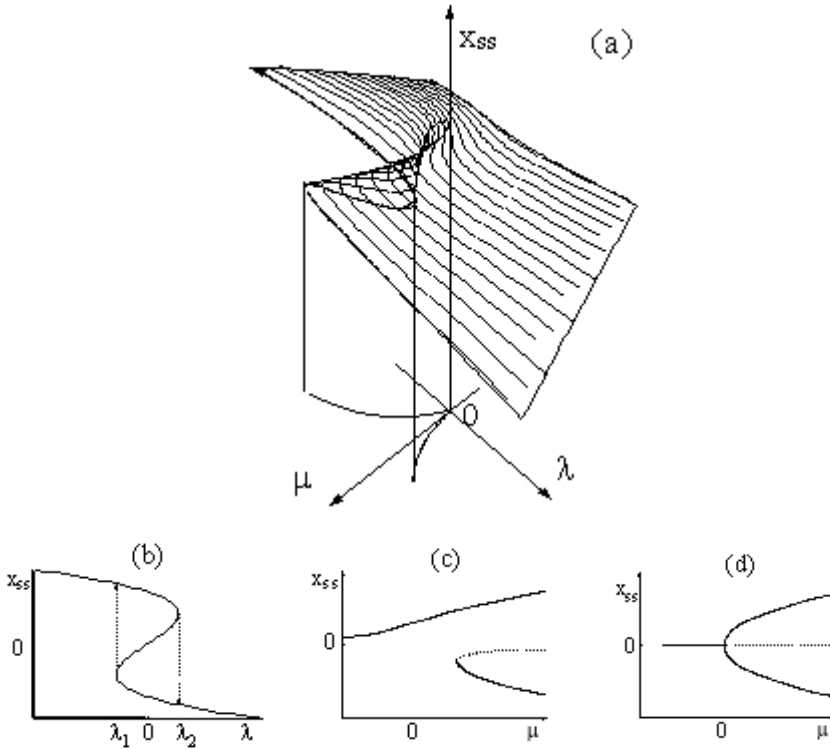
Figure 2. (a) The influence of the values of parameters μ and λ on the steady states of the intermediate x_{ss}, eq. (17); (b) Section in x_{ss}-λ plane when μ = const. > 0. (c) Section in x_{ss}-μ plane when λ = const. < 0. (d) Section in x_{ss} -μ plane when λ = 0. (The figure is taken from ref. [9])

The existence of region of multistability depends also on the parameter μ. If only one solution of equation (17) is real, x_{ss} is monotonous function of λ (Fig. 1 (b) and Figs. 2 (a), (c) and (d)) and system is always monostable. Thus, by the mathematical analysis of the considered mathematical model, as well as the corresponding model of nonlinear reaction, we can easily see that multistability is the phenomenon characteristic for some nonlinear dynamic systems in the states far from thermodynamic equilibrium.

Two examined dynamical systems selected to be as close as possible to one another but enough different to be either linear or nonlinear are compared in Table 1.

Table 1.

Linear and nonlinear reaction system

Linear

$$A \underset{k_{-1}}{\overset{k_1}{\rightleftarrows}} X$$

$$X \underset{k_{-2}}{\overset{k_2}{\rightleftarrows}} B$$

Nonlinear

$$A + 2X \underset{k_{-1}}{\overset{k_1}{\rightleftarrows}} 3X$$

$$X \underset{k_{-2}}{\overset{k_2}{\rightleftarrows}} B$$

Equilibrium stationary state:

$$\frac{k_1 k_2}{k_{-1} k_{-2}} = \frac{b_{eq}}{a_{eq}}$$

$$\frac{k_1 k_2}{k_{-1} k_{-2}} = \frac{b_{eq}}{a_{eq}}$$

Nonequilibrium stationary state:

$$dx/dt = k_1 a + k_{-2} b - (k_{-1} + k_2) x$$
$$= \lambda - kx$$

$$x_{ss} = \frac{\lambda}{k}$$

$$dx/dt = k_1 a x^2 - k_{-1} x^3 - k_2 x + k_{-2} b$$
$$= -x^3 + \mu x + \lambda$$

$$x_{ss}^3 - \mu x_{ss} - \lambda = 0$$

Mathematically speaking, the linear reaction systems are those in which the sum of the exponents on the concentrations of each addend in expressions for the reaction rate is equal to one. All others are nonlinear.

4. Nonlinear systems with feedback

In the reaction systems the feedback is the phenomenon in which the product of a reaction affects the rate of its own formation in a positive or negative sense, the autocatalysis and autoinhibition, respectively. As such, it is a crucial part of complex selforganization phenomena that occurs in nonlinear systems when they are in a state far from equilibrium. [3-10]

The feedback in the reaction system can be of chemical and thermal origin. In the first case, during the isothermal reaction, appears the chemical species, crucial for the further developing of the overall process that controls the rate of its own formation or disappearance. In the second case, the formation of the considered chemical species significantly changes the temperature of the reaction system, which influence on the rate constant of the reaction and consequently the rate of formation of this species. In addition, the change in temperature of the reaction system usually has different effects

on the rate constants of the individual elementary reactions of the mechanism, as well as their relations, which further affects the selforganization phenomena. Only nonlinear reaction systems with feedback can have instability regions. Thus, only such kind of reaction systems can be in bistable or any oscillatory state including mixed-modes and chaos. [3-13]

From the beginning, we discuss here isothermal reaction systems, only. In the already considered cases (R1) and (R2), the bistability is found only in the model with autocatalytic step, that is, in the model with one form of a feedback. The corresponding model without autocatalytic step, was linear and did not exhibit bistability.

From mathematical point of view all is clear: differential equations (4) and (10) correspond to linear and nonlinear system, respectively. From chemical point of view there are problems. First we added 2X on both sides of the same equation and obtained nonlinear system with bistability! However, addition of the same substance to both sides of the chemical reaction should not change composition of the system. Nevertheless, without these terms, the system is linear. Second, without any amount of intermediate X at the beginning of reaction, this reaction cannot begin. These two problems will be discussed in the following sections.

5. Model of minimal nonlinear reaction system with feedback: Autocatalator

Thus, we need to have autocatalytic step or any other form of feedback if we want that our model can simulate oscillatory evolution of intermediate species. However, the reaction will not start without any initial amount of this intermediate. The problem can be solved in two manners. First, we can analyze the process described by the model of the form (R2) which performs in open reactor where there is a permanent flow of the considered species through it. The other possibility, more interesting for us, is to examine the process in the closed reactor where additional reactions control the evolution of intermediate from the beginning. One such model close to (R2) but more realistic, is the autocatalator. [3,11,14] It is well-known minimal model of the chemical reaction that takes place in a closed reactor at isothermal conditions, which exhibits all the characteristics of nonlinear nonequilibrium systems. It was created by combination of cubic autocatalytic reaction (R.2.1) and a series of successive reactions:

$$R \rightarrow A \rightarrow B \rightarrow P \tag{R3}$$
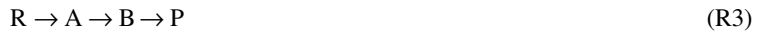
In this case reactant R transform to a product P by both autocatalytic and noncatalytic pathways parallelly. It is described by the following model

$$R \xrightarrow{\ k_0\ } A , \qquad (v_0 = k_0 r) \tag{R4.0}$$

$$A \xrightarrow{\ k_1\ } B , \qquad (v_1 = k_1 a) \tag{R4.1}$$

$$A + 2B \xrightarrow{\ k_2\ } 3B , \qquad (v_2 = k_2 ab^2) \tag{R4.2}$$

$$B \xrightarrow{\ k_3\ } P , \qquad (v_3 = k_3 b) \tag{R4.3}$$
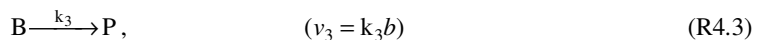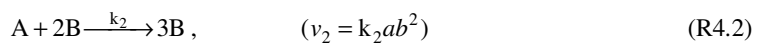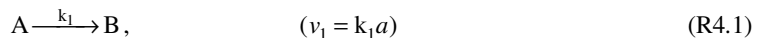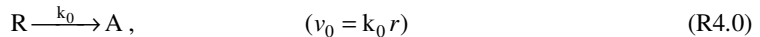
Here v_0, v_1, v_2 and v_3 denotes the reaction rates of the corresponding reaction steps, whereas k_0, k_1, k_2 and k_3 are their rate constants. The time dependent concentrations of the species R, A, B and P are denoted by r, a, b and p.

The kinetic equations for the time evolution of the concentration of r, a and b are given by the following system of differential equations of the first order:

$$\frac{\mathrm{d}r}{\mathrm{d}t} = -k_0 r \tag{18}$$

$$\frac{\mathrm{d}a}{\mathrm{d}t} = k_0 r - k_1 a - k_2 ab^2 \tag{19}$$

$$\frac{\mathrm{d}b}{\mathrm{d}t} = k_1 a + k_2 ab^2 - k_3 b \tag{20}$$

The concentration of the product P is defined by the law of conservation:

$$p = (r_0 + a_0 + b_0 + p_0) - (r + a + b) \tag{21}$$

Where the index "0" denotes the initial concentrations of relevant species.

Since all reactions in the model are irreversible, the equilibrium stationary state denoted by „eq", will be achieved when the concentrations of species R, A and B will be equal to zero. Then:

$$r_{eq} = a_{eq} = b_{eg} = 0, \qquad p_{eq} = r_0 + a_0 + b_0 + p_0. \tag{22}$$

It means that the equilibrim can be realized here only when all species are transformed to the product P.

Examination of the equilibrium stationary state is important to test the consistency of the model, only. However, we are focused on the nonequilibrium stationary states that can be realized in considered reaction system between t = 0 and the end of reaction when t → ∞.

In nonequilibrium stationary state (steady state) the rate of time evolution of intermediary concentrations is equal to zero, that is,

$$k_0 r - k_1 a_{ss} - k_2 a_{ss} b_{ss}^2 = 0 \tag{23}$$

$$k_1 a_{ss} + k_2 a_{ss} b_{ss}^2 - k_3 b_{ss} = 0 \tag{24}$$

The steady state concentrations of intermediates A and B have the following values

$$b_{ss} = \frac{k_0 r}{k_3} \tag{25}$$

$$a_{ss} = \frac{k_0 k_3^2 r}{k_0^2 k_2 r^2 + k_1 k_3^2} \tag{26}$$

As the concentration of intermediates in nonequilibrium stationary state are clearly the functions of concentration of the reactant R, they are not constant. There are a number of non-equilibrium stationary states in which the system can be during the reaction. The dependence of a_{ss} and b_{ss} on the concentration of reactant R is presented in Fig. 3.
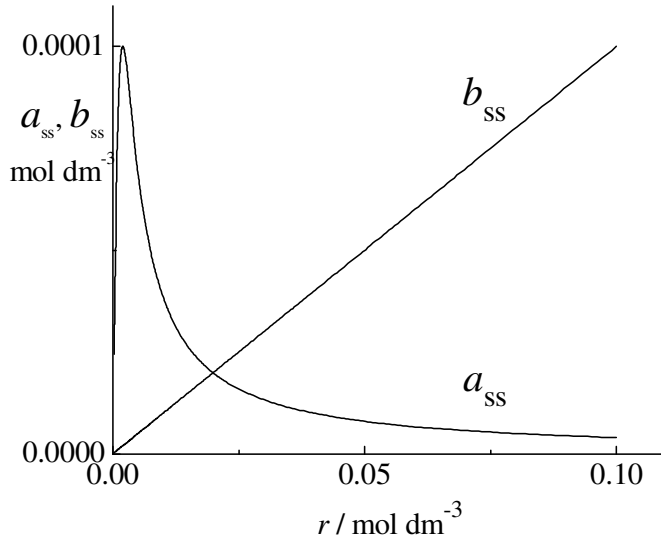
Slika 3. Steady-state concentrations of intermediates A and B, a_{ss} and b_{ss}, as a function of the concentration of reactant r. Here: $r_0 = 0.1$ mol×dm^{-3}, $k_0 = 1×10^{-3}$ s^{-1}, $k_1 = 1×10^{-2}$ s^{-1}, $k_2 = 2.5×10^9$ dm^6×mol^{-2} s^{-1}, $k_3 = 1$ s^{-1}. (The figure is taken from ref. [9])

At high values of the reactant concentration, the stationary concentration of intermediate b_{ss} is higher than the stationary concentration of intermediate a_{ss}, and *vice versa* (Fig. 3). The cross section is in the point:

$$a_{ss} = b_{ss} = \sqrt{\frac{k_3 - k_1}{k_2}} \tag{27}$$

$$r(a_{ss} = b_{ss}) = \frac{k_3}{k_0}\sqrt{\frac{k_3 - k_1}{k_2}} . \tag{28}$$

The maximal value of steady-state concentration of a_{ss}

$$a_{ss,max} = \frac{k_3}{2\sqrt{k_1 k_2}} \tag{29}$$

is achieved when

$$r_{max} = \sqrt{\frac{k_1 k_3^2}{k_0^2 k_2}} \ .$$

(30)

Reactant concentration at time t can be easily calculated by integration of equation (18) and is given by the expression

$$r = r_0 e^{-k_0 t} \ .$$

(31)

Substituting the value of r into the eqs (25) and (26), the steady state concentrations of the intermediates are obtained as a function of time:

$$b_{ss} = \frac{k_0}{k_3} r_0 e^{-k_0 t}$$

(32)

$$a_{ss} = \frac{k_0 k_3^2 r_0 e^{-k_0 t}}{k_0^2 k_2 r_0^2 e^{-2k_0 t} + k_1 k_3^2} \ .$$

(33)
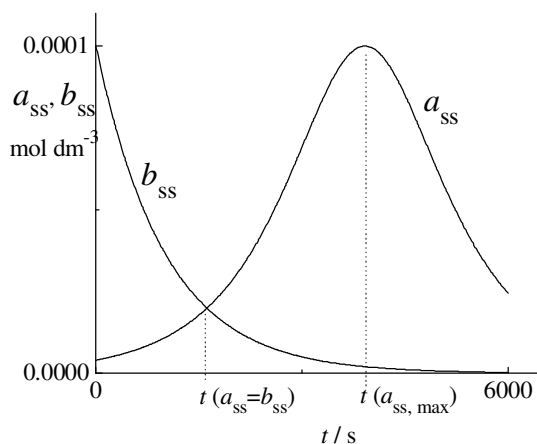
Figure 4. Steady-state concentrations of intermediates A and B, a_{ss} and b_{ss}, as a function of time. The initial conditions are equal to the ones given in Fig. 3. (The figure is taken from ref. [9])

The dependence of a_{ss} and b_{ss} on the concentration of reactant R is presented in Fig. 4. Obviously, the concentration of b_{ss} decreases exponentially during the reaction, whereas the concentration of a_{ss} changes along the curve with maximum. The moment

of intersection of the curves $t(a_{ss} = b_{ss})$ corresponds to the point where r is given by (28). In this point the following equality is satisfied

$$\frac{k_0}{k_3} r_0 e^{-k_0 t} = \sqrt{\frac{k_3 - k_1}{k_2}} \,. \tag{34}$$

Consequently

$$t(a_{ss} = b_{ss}) = \frac{1}{k_0} \ln\left(\frac{k_0 r_0}{k_3} \sqrt{\frac{k_2}{k_3 - k_1}} \right). \tag{35}$$

The maximum of the curve $a_{ss} = f(t)$ is at the time:

$$t_{max} = \frac{1}{k_0} \ln\left(\frac{k_0 r_0}{k_3} \sqrt{\frac{k_2}{k_1}} \right) = \frac{1}{2k_0} \ln \frac{k_0^2 k_2 r_0^2}{k_1 k_3^2} \,. \tag{36}$$

However, if the full integration of equations (18) - (20) is performed, we see that the evolution of the concentration may significantly deviate from the curves representing the evolution of the nonequilibrium stationary state, as illustrated in Figure 5. If the initial concentrations of intermediates A and B are zero, they first increase rapidly until reaching certain concentration values characteristic for nonequilibrium stationary states. Then they follow the course of the steady state concentration curves (Fig. 4, eqs. (32) and (33)). After some time, the concentration of intermediates begins to oscillate around the steady state. At the same point (the bifurcation point) the non-equilibrium steady state of the reaction system, which had previously been stable and attractive, becomes unstable and repulsive. Oscillations are strictly defined and have different forms depending on the given parameters. Sudden cessation of oscillations means that system crosses through the second bifurcation point, when nonequilibrium stationary state becomes stable again. Then the concentration of intermediates A and B again obey the laws (32) and (33), and continue to follow the monotonic changes as shown in Figures 4 and 5.

6. Model with feedback loop instead feedback step

The second important problem underlined at the end of Section 3 is the fact that we construct the nonlinear model by addition of 2X on both sides of equation (R2.1). Actually, this artificial chemical reaction is the summarized stoichiometric network of a small submodel where one or more additional intermediate species are present and interact one with the other. Hence the feedback loop that exists in this submodel is presented by feedback reaction (or step) where other intermediate species are invisible. To make a model more real we need to return the "invisible" intermediates what is often very complex procedure. The scientists needed about fifty years to transform the model with artificial step proposed by Lotka having idea to explain oscillatory evolution in population (15), to the model without this step but with feedback loop to explain an oscillatory reaction (16). Mentioned problem will be discussed on one such model proposed to explain dynamic states of the hydrogen peroxide decomposition in the

presence of iodate and hydrogen ions (the Bray-Liebhafskly (BL) oscillatory reaction) [17, 18]
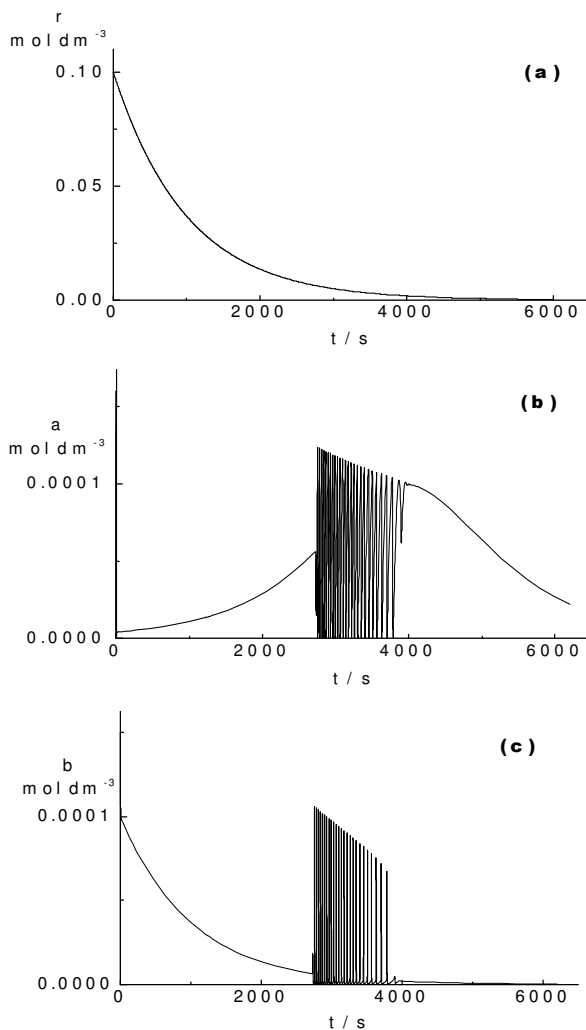
Figure 5. Time evolution of the reactant R (a), intermediate A (b) and intermediate B (c) in the case of autocatalator (R4). The initial conditions are equal to the ones given in Fig. 3. (The figure is taken from ref. [9])

$$2H_2O_2 \xrightarrow{\;IO_3^-,\, H^+\;} 2H_2O + O_2. \tag{D}$$

The first attempt to elucidate the mechanism of this very complex process was unsuccessful, although the experimental investigations together with their explanations

were excellent. Namely, already in the first report about the BL reaction, [17] Bray noticed that mentioned reaction is the result of the reduction (R) of iodate to iodine and the oxidation (O) of iodine to iodate by the following complex reaction scheme satisfied

$$2IO_3^- + 2H^+ + 5H_2O_2 \rightarrow I_2 + 5O_2 + 6H_2O . \tag{R}$$

$$I_2 + 5H_2O_2 \rightarrow 2IO_3^- + 2H^+ + 4H_2O . \tag{O}$$
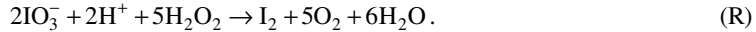
Their rates tend to become equal and we usually observe only a smooth decomposition described by reaction (D) where iodine, as intermediate species, does not appear in this stoichiometric relation. (Summing reactions (R) and (O) we obtain 5(D).) However, in a narrow range of concentrations, the alternating domination of processes (R) and (O) is also possible resulting in periodic increase and decrease of the iodine concentration during stepwise decrease of the hydrogen peroxide and increase of the oxygen concentrations (Fig.6). This apparently simple oscillatory reaction, consists of a complex homogeneous catalytic oscillatory process involving numerous iodine intermediates such as I^-, HIO, HIO_2 and I_2O beside already mentioned iodine (I_2) that all oscillates. [9, 19]
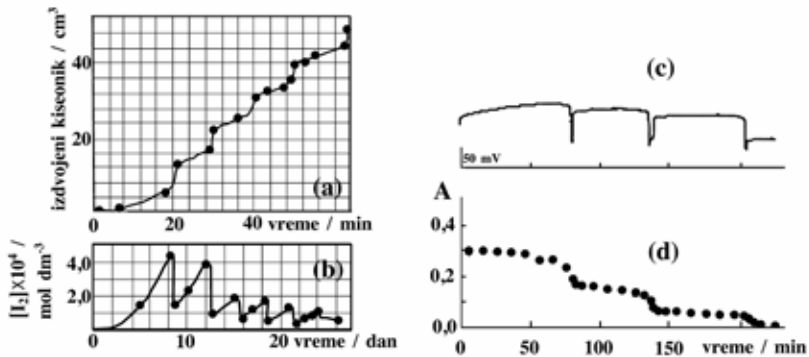
Figure 6. Time evolution of the BL oscillatory reaction in the closed reactor. In particular, time evolution of (a) the evaporated oxygen from the reaction solution, (b) iodine concentration, (c) logarithm of the iodide concentration presented by the potential of iodide-ion sensitive electrode and (d) the hydrogen peroxide concentration presented by means of absorbance of the complex between the hydrogen peroxide and titanil oxalate. Initial conditions in $mol \times dm^{-3}$ in Fig. (a): $[H_2O_2]_0 = 1.90 \times 10^{-1}$, $[KIO_3]_0 = 9.40 \times 10^{-2}$, $[H_2SO_4]_0 = 3.65 \times 10^{-2}$, ($T = 60.0$ °C); in Fig. (b): $[H_2O_2]_0 = 3.27 \times 10^{-1}$, $[HIO_3]_0 = 9.00 \times 10^{-3}$ ($T = 25.0$ °C) in Figs. (c) and (d): $[H_2O_2]_0 = 1.98 \times 10^{-2}$, $[KIO_3]_0 = 6.62 \times 10^{-2}$, $[H_2SO_4]_0 = 2.45 \times 10^{-2}$ ($T = 60.0$ °C). (Figures (a) and (b) are taken from ref. 17, and Figures (c) and (d) from ref. 20).

Consequently, the above reaction scheme had to be extended with new intermediate species and reactions between them. Among proposed models, one of the most successful in attempts to simulate numerous obtained experimental phenomena is the following one [21]:

$$IO_3^- + I^- + 2H^+ \quad \rightleftharpoons \quad HIO + HIO_2 \qquad \text{(R5.1),(R5.-1)}$$

$$HIO_2 + I^- + H^+ \quad \rightarrow \quad I_2O + H_2O \qquad \text{(R5.2)}$$

$$I_2O + H_2O \quad \rightleftharpoons \quad 2HIO \qquad \text{(R5.3),(R5.-3)}$$

$$HIO + I^- + H^+ \quad \rightleftharpoons \quad I_2 + H_2O \qquad \text{(R5.4),(R5.-4)}$$

$$HIO + H_2O_2 \quad \rightarrow \quad I^- + H^+ + O_2 + H_2O \qquad \text{(R5.5)}$$

$$I_2O + H_2O_2 \quad \rightarrow \quad HIO + HIO_2 \qquad \text{(R5.6)}$$

$$HIO_2 + H_2O_2 \quad \rightarrow \quad IO_3^- + H^+ + H_2O \qquad \text{(R5.7)}$$

$$IO_3^- + H^+ + H_2O_2 \quad \rightarrow \quad HIO_2 + O_2 + H_2O \qquad \text{(R5.8)}$$
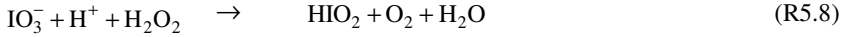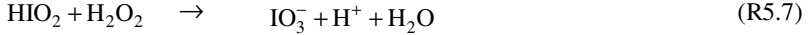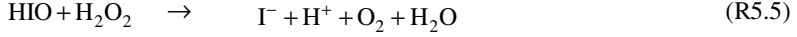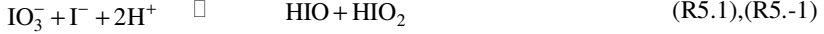
The oscillatory evolution of intermediates can be obtained by the whole model as well as by the first six reactions [16] or some other combinations of them [21-23]. However, if we want to simulate all experimentally found dynamic states, at least the model having seven reactions (first six and eight one) is necessary. [24, 25]

The above model consisting of reactions (R5.1) to (R5.8), denoted as (R5), have all the necessary features to describe the BL reaction as a complex nonlinear process with the region of multistability where different oscillatory evolutions including mixed-mode oscillations, deterministic chaos and other phenomena [9, 26-29] may be found. In fact, this model has 10 species and 11 reactions since three of them are reversible ones. Five of these ten species are independent intermediate ones such that we are dealing with the five dimensional system and need to solve simultaneously five differential equations of the first order.

With aim to present results in more mathematical language, we shall rewrite above presented model in function of independent variables only, taking into account following substitutions: $I^- \equiv X$, $HIO \equiv Y$, $HIO_2 \equiv Z$, $I_2O \equiv W$ and $I_2 \equiv Q$). Denoting the concentrations of the mentioned species by x, y, z, w and q, the time evolution of the system can be described by the following set of differential equations based on the proposed mechanism between the species included in the model and mass-action kinetics [1, 2]:

$$\frac{dq}{dt} = k_4 xy - k_{-4} q$$

$$\frac{dx}{dt} = -k_1 x - k_2 xz - k_4 xy + k_5 y + k_{-1} yz + k_{-4} q$$

$$\frac{dy}{dt} = k_1 x + 2k_3 w - k_4 xy - k_5 y + k_6 w - k_{-1} yz - 2k_{-3} y^2 + k_{-4} q \qquad (37)$$

$$\frac{dz}{dt} = k_1 x - k_2 xz + k_6 w - k_7 z + k_8 - k_{-1} yz$$

$$\frac{dw}{dt} = k_2 xz - k_3 w - k_6 w + k_{-3} y^2$$

where concentrations of external species, taken as constant, are included in the rate constants. By solving these differential equations we can simulate different dynamic states of the considered system (Fig. 7 and Fig. 8) similar to the ones found experimentally.
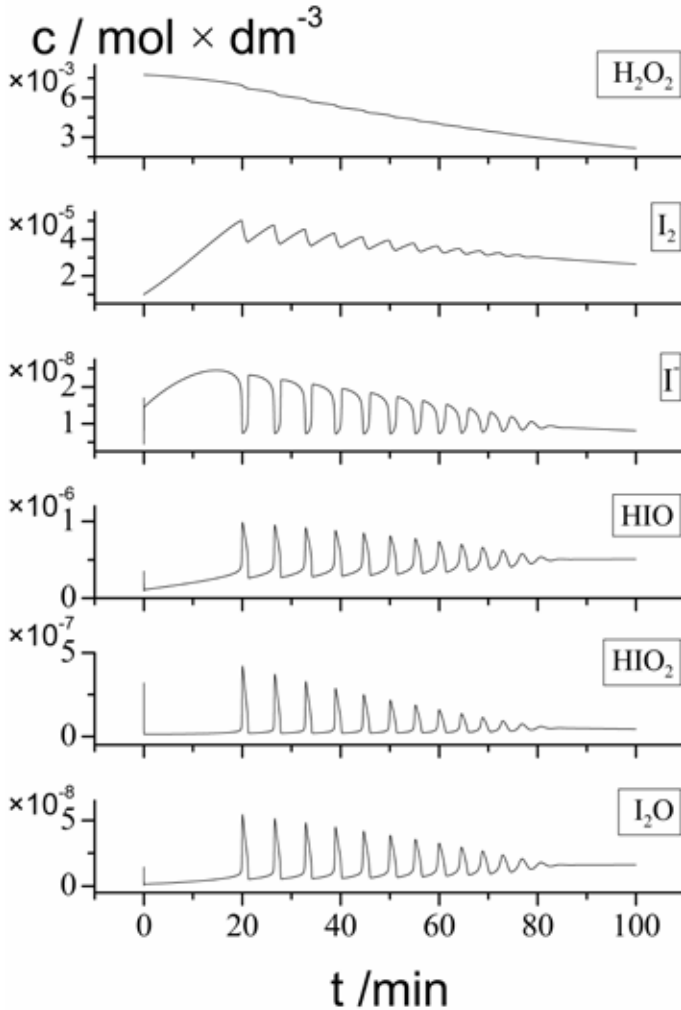

Figure 7. Time evolution of the BL oscillatory reaction in the closed reactor presented by evolution of concentrations of particular species obtained by the numerical simulations based on the model for the BL reaction (R5). (The figure is taken from ref. [9])
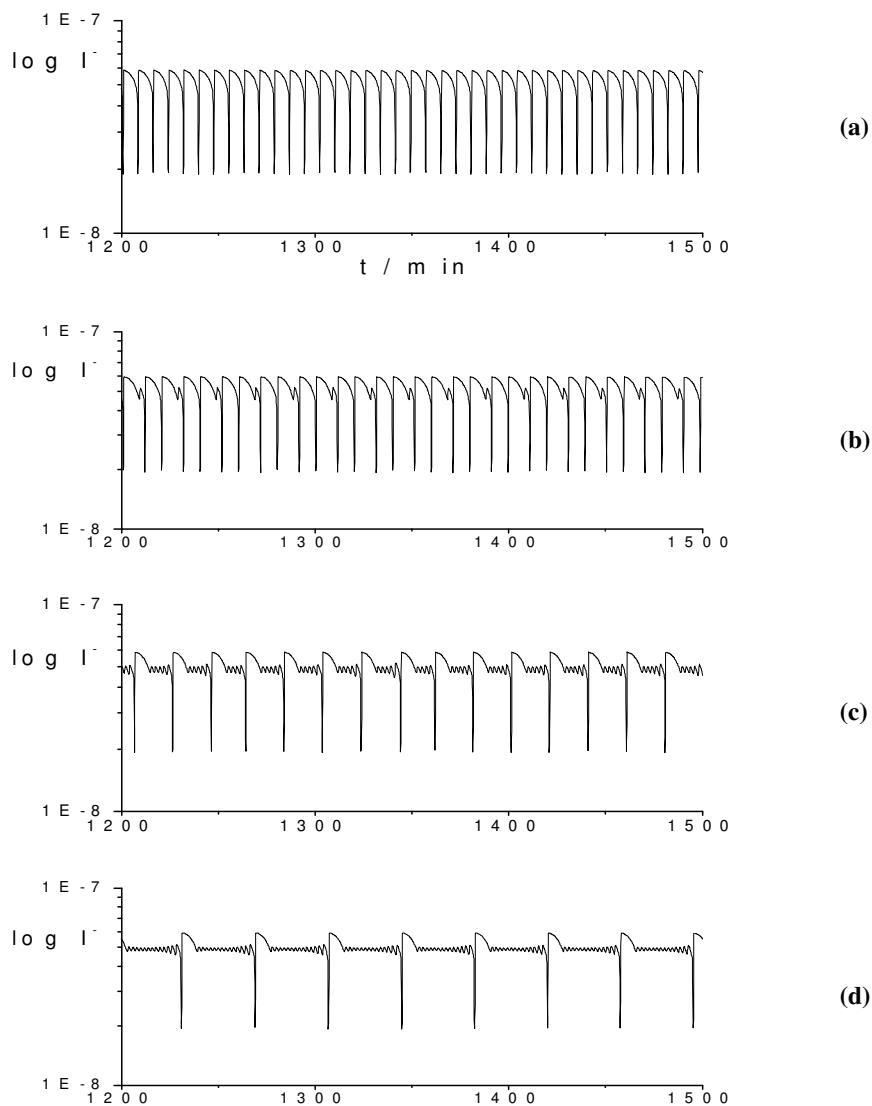
Figure 8. Numerical simulations of the oscillatory dynamics of the BL reaction realized in open reactor (segment from 1200 to 1500 min) presented by means of the iodide concentration (in $mol \times dm^{-3}$). (a) Regular oscillations, $k_f = 4.70 \times 10^{-3}$ min^{-1}; (b) and (d) mixed-mode oscillations, $k_f = 4.90 \times 10^{-3}$ min^{-1} and $k_f = 5.10 \times 10^{-3}$ min^{-1}, respectively; (c) deterministic chaos with chaotically distributed number of the small-amplitude oscillations between the large-amplitude ones, $k_f = 5.00 \times 10^{-3}$ min^{-1}. (The figure is taken from ref. [9])

On the other side, the phase space portrait similar to the one obtained by mathematical model (R2) is generated by analyzing relations between hydrogen peroxide, iodine and iodide concentrations in the selected steady states (Fig.9). A more detailed analysis of this model and its sub-variants can be found in the references [16, 21-25, 30-33].
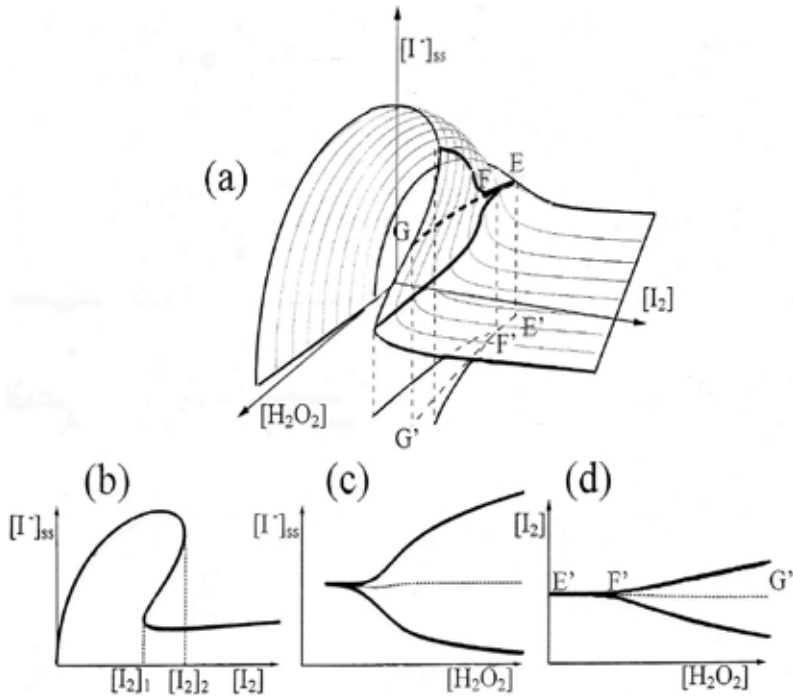
Figure 9. The effect of the concentrations of hydrogen peroxide and iodine on the steady state concentration of iodide in the vicinity of bifurcation point F. The rate constants necessary for numerical calculations are taken from ref. [21]. (a) Folded surface $F([I^-]_{ss}$, $[I_2]$, $[H_2O_2]) = 0$; (b) section in the plane $[H_2O_2] = $ const; (c) section in the plane $[I_2] = $ const = value of $[I_2]$ in bifurcation point F; (d) projection of the instability region on the $[H_2O_2]$ - $[I_2]$ plane.[8] (The figure is taken from ref. [9])

Thus, all main nonlinear phenomena found experimentally are simulated by the proposed model without any direct feedback step. However, in this model there are feedback loops. They can be obtained by different combinations of the reactions that exist in the model (R5). In particular, the autocatalysis is the overall stoichiometric relation obtained from the following subsystems

(R5.1) + (R5.2) + (R5.3) + 2(R5.5) $\Rightarrow$
$$HIO_3 + 2H_2O_2 + 2HIO \rightarrow 3HIO + 2O_2 + 2H_2O$$

(R5.-1) + (R5.2) + (R5.3) + 2(R5.8) $\Rightarrow$
$$HIO_3 + 2H_2O_2 + HIO \rightarrow 2HIO + 2O_2 + 2H_2O$$

(R5.2) + (R5.3) + (R5.4) + (R5.5) $\Rightarrow$
$$HIO_3 + 2H_2O_2 + HIO \rightarrow 2HIO + 2O_2 + 2H_2O ,$$
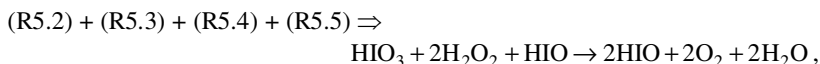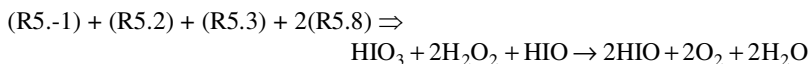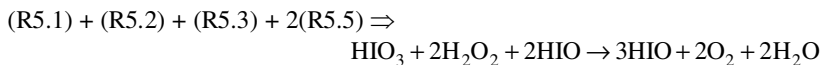
whereas the autoinhibition is the stoichiometric result of other subsystems

(R5.-3) + (R5.6) + (R5.7) $\Rightarrow$
$$2H_2O_2 + 2HIO \rightarrow HIO + HIO_3 + 2H_2O$$

(R5.-1) + (R5.2) + (R5.-3) + 2(R5.6) $\Rightarrow$
$$2H_2O_2 + 3HIO \rightarrow 2HIO + HIO_3 + 2H_2O .$$
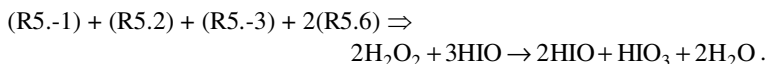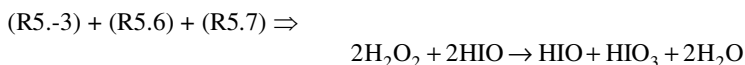
Finally, we can conclude that in the model (R5) there are both the cubic and the quadratic autocatalysis and autoinhibition in a form of feedback loop.

7. Conclusion

The difference between linear and nonlinear reaction systems was underlined and discussed on several examples. The main notions together with corresponding definitions are given on two very simple models and later elaborated on autocatalator as known minimal model of the oscillatory reaction systems as well as on the model of the real complex process: the Bray-Liebhafsky oscillatory reaction. In this way, the possible solutions of the problems that arise in mathematical models are offered and applied on a real reaction system: the Bray-Liebhafsky oscillatory one. It was shown that only nonlinear processes with feedback can be in different oscillatory self organized states.

8. References

[1] Benson S W, *The Foundations of the Chemical Kinetics*, McGraw Hill Book Company Inc., New York, (1960).
[2] Yeremin, E N, *The Foundations of the Chemical Kinetics*, MIR, Moscow, (1979).
[3] Gray, P, Scott, S. K, *Chemical Oscillations and Instabilities*, Clarendon Press, Oxford, 1990.

[4] Nicolis, G, Prigogine, I, *Self-Organization in Non-Equilibrium Systems*, J.Wiley, New-York, 1977.

[5] Nicolis, G, Prigogine, I, *Exploring Complexity*, Freeman, New York, 1989.

[6] Kolar-Anić, Lj, Čupić, Ž, Anić, S, Multistabilnost i nelinearni dinamički sistemi, *Hem. Ind*. 52 (1998) 337-342.

[7] Schmitz, G, Kolar-Anić, Lj, Anić, S, Čupić, Ž, The Ilustration of Multistability, *J. Chem. Educ*. 77 (2000) 1502-1505.

[8] Kolar-Anić, Lj, Anić, S, Vukojević, V, *Dinamika nelinearnih procesa – Od monotone do oscilatorne evolucije*, Fakultet za fizičku hemiju, Beograd 2004.

[9] Kolar-Anić, Lj, Čupić, Ž, Vukojević, V, Anić, S, *Dinamika nelinearnih procesa*, Fakultet za fizičku hemiju, Univerzitet u Beogradu, Beograd 2011, (in Serbocroat).

[10] Drazin, P. G, *Nonlinear Systems*, Cambridge University Press, 1994.

[11] Scott, S. K, *Chemical Chaos*, Oxford University Press, 1991.

[12] Nicolis, G, *Introduction to Nonlinear Science*, Cambridge University Press, Cambridge, 1995.

[13] Field, R. J, Burger, M (Eds.), *Oscillation and Traveling Waves in Chemical Systems*, J.Wiley, New York, 1985.

[14] Scott, S. Oscillations in Simple Models of Chemical Systems, *Acc. Chem. Res.*, 20 (1987) 186-191.

[15] A.J.Lotka, Undumped Oscillations Derived from the Law of Mass Action, *J. Am. Chem. Soc*., 42 (1920) 1595-1599.

[16] Schmitz, G, Cinétique de la réaction de Bray, *J. Chim. Phys.* 84 (1987) 957.

[17] Bray, W. C, A Periodic Reaction in Homogeneous Solution and Its Relation to Catalysis, *J. Am. Chem. Soc.* 43 (1921) 1262-1267.

[18] Bray, W. C, Liebhafsky, H. A, Reaction involving Hydrogen Peroxide, Iodine and Iodate Ion. I. Introduction, *J. Am. Chem.Soc*. 53 (1931) 38-44.

[19] Čupić, Ž., Ivanović-Šašić, A., S. Anić, Stanković, B., Maksimović, J., Kolar-Anić, Lj. and Schmitz, G.,Tourbillion in the Phase Space of the Bray-Liebhafsky Nonlinear Oscillatory Reaction and Related Multiple-Time-Scale Model, *MATCH Commun. Math. Comput. Chem.,***69** (2013) 805-830.

[20] Ćirić, J, Anić, S, Čupić, Ž, Kolar-Anić, Lj, The Bray-Liebhafsky Oscillatory Reaction. Kinetic Investigation in Reduction and Oxidation Pathways Based on Hydrogen Peroxide Concentration Monitoring, *Science of Sintering* **32** (2000) 187-196.

[21] Kolar-Anić, Lj, Mišljenović, Đ, Anić, S, Nicolis, G, Influence of the Reduction of Iodate by Hydrogen Peroxide on the Model of the Bray-Liebhafsky Reaction, *React. Kinet. Catal. Lett.* **54** (1995) 35-41.

[22] Kolar-Anić, Lj, Schmitz, G, Mechanism of the Bray-Liebhafsky Reaction: Effect of the Oxidation of Iodous Acid by Hydrogen Peroxide, *J. Chem. Soc. Faraday Trans.* **88** (1992) 2343-2349.

[23] Kolar-Anić, Lj, Mišljenović, Đ, Anić, S, Kinetic Model for the Bray-Liebhafsky Process without Reaction $IO_3^- + I^- + 2H^+ = HIO + HIO_2$, *React. Kinet. Catal. Lett.* **57** (1996) 37-42.

[24] Schmitz, G, Kolar-Anić, Lj, Anić, S, Čupić, Ž, Stoichometric Network Analysis and Associated Dimensionless Kinetic Equations. Application to a Model of the Bray-Liebhafsky Reaction, *J. Phys. Chem.* **112** (2008) 13452-13457.

[25] Kolar-Anić Lj, Čupić Ž, Schmitz G, Anić S, Improvement of the stoichiometric network analysis for determination of instability conditions of complex nonlinear reaction systems, *Chem. Eng. Sci.*, **65** (2010) 3718-3728.

[26] Ivanović, A. Z, Čupić, Ž. D, Janković, M. M, Kolar-Anić, Lj. Z, Anić, S. R, The chaotic sequences in the Bray-Liebhafsky reaction in an open reactor, *Phys. Chem. Chem. Phys.* **10** (2008) 5848-5858.

[27] Ivanović, A. Z, Čupić, Ž. D, Kolar-Anić, Lj. Z, Janković, M. M, Anić, S. R, Large Deviation Spectra of Chaotic Time Series from Bray-Liebhafsky Reaction, *R. J. Phys. Chem. A* **9** (2009) 1526-1530.

[28] Kissimonova K, Valent, I, Adamčiková, L, Ševšik, P, Numerical Simulations of the Oxygen Production in the Oscillating Bray-Liebhafsky Reaction, *Chem. Phys. Lett.* 341 (2001) 345-350.

[29] A. Z. Ivanović-Šašić, V. M. Marković, S. R. Anić, Lj. Z. Kolar-Anić and Ž. D. Čupić, Structures of chaos in open reaction systems, *Physical Chemistry Chemical Physics,* **13(45)** (2011) 20162-20171.

[30] Čupić, Ž, *Modelling of the mechanism of the oscillatory catalytic processes, with application on the reaction of hydrogen peroxide decomposition.* Thesis, University of Belgrade, Belgrade 1998. (in Serbo-Croatian)

[31] Čupić, Ž, Kolar-Anić, Lj, Contraction of the Model for the Bray-Liebhafsky Oscillatory Reaction by Eliminating Intermediate I_2O, *J. Chem. Phys.*, **110** (1999) 3951-3954.

[32] Kolar-Anić, Lj, Vukelić, N, Mišljenović, Đ, Anić, S, On the Instability Domains of Some Models for the Bray-Liebhafsky Oscillatory Reaction, *J. Serb. Chem. Soc.,* **60** (1995) 1005-1013, 1187.

[33] Kolar-Anić, Lj, Čupić, Ž, Anić, S, Schmitz G, Pseudo-steady States in the Model of the Bray-Liebhafsky Oscillatory Reaction, *J. Chem. Soc. Faraday Trans.* **93** (1997) 2147-2152.

_____

SHORT REVIEW ON THE MODELS OF BRAY-LIEBHAFSKY OSCILLATORY REACTION

Branislav Stanković[1], Slobodan Anić[1,2]

[1] Faculty of Physical Chemistry, University of Belgrade, Studentski trg 12-16, 11000 Belgrade, Serbia
e-mail: branislav20@yahoo.com, boban@ffh.bg.ac.rs
[2] Institute of Chemistry, Technology and Metallurgy, University of Belgrade, Department of Catalysis and Chemical Engineering, Njegoševa 12, 11000 Belgrade, Serbia

Abstract. The detailed mechanism of the Bray-Liebhafsky oscillatory reaction is not known until now, although modelling of this complex process has been one of important subjects of investigations in Nonlinear dynamics. Short overview of the main proposed models is presented here with aim to introduce readers with this subject and help in intention to find some improvements.

1. Introduction

A reaction is said to be oscillating if the concentration of one or more their intermediates does not vary monotonically, but periodically pass through maximum and minimum values [1].

The Bray-Liebhafsky reaction [2, 4], the hydrogen peroxide decomposition into the water and oxygen in the presence of hydrogen and iodate ions,

$$2H_2O_2 \xrightarrow{\quad IO_3^-,\, H^+ \quad} 2H_2O + O_2 \,. \tag{BL}$$

is the first discovered and one of the most interesting complex nonlinear (oscillatory) chemical reaction [3, 5-82].

In 1921 Bray [2] noticed that (BL) reaction can be realized by two different manners that play a role of complex reaction routes. Thus, the global reaction, BL, is the result of the reduction, R, of iodate to iodine and the oxidation, O, of iodine to iodate by the following reaction scheme:

$$2IO_3^- + 2H^+ + 5H_2O_2 \rightarrow I_2 + 5O_2 + 6H_2O \tag{R}$$

$$I_2 + 5H_2O_2 \rightarrow 2IO_3^- + 2H^+ + 4H_2O \tag{O}$$
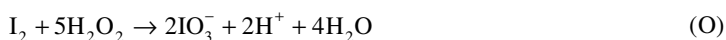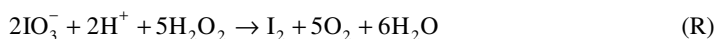
It is significant to note that this is the first, though global, model of BL reaction without possibility to generate oscillatory evolution of the concentration of species.

When the rates of processes (R) and (O) tend to become equal (or when the reaction (R) continuously dominate over reaction (O), and vice versa) we observe only a smooth decomposition described by reaction (BL). Then, iodine as intermediate species does not appear in this stoichiometric relation. However, in a narrow range of concentrations the alternating domination of processes (R) and (O) is also possible. The main reason for oscillating phenomena is the dual effects of hydrogen peroxide in the whole process. In the other words, hydrogen peroxide acts as the oxidant but also as the reductant in the reaction system. This can result in periodic increase and decrease of the iodine concentration as well as in periodic cascade decrease and increase of the hydrogen peroxide and oxygen concentrations, respectively, which is the typical behaviour of external species in homogeneous oscillatory reactions [27, 78].

Ten years after Bray wrote mentioned paper, Liebhafsky started to work with him [4] and because of their significant and extensive research the reaction of hydrogen peroxide decomposition was named the Bray-Liebhafsky reaction.

Numerous dynamic states, such as periodic and aperiodic (chaotic) oscillatory evolution (including mixed-mode oscillations and other unusual kinetic phenomena) are experimentally obtained [54, 62, 69]. This apparently simple oscillatory reaction comprises a complex homogeneous catalytic oscillatory process involving numerous iodine intermediates such as I_2, I^-, HIO and HIO_2. Hence, the more detailed model involving numerous iodine intermediates necessary for explanation of the mechanism, had to be proposed. However, detailed mechanism which would simulate all found experimental phenomena have not been presented yet, due to existence of numerous intermediaries and difficulties in theirs monitoring.

Investigation of the Bray-Liebhafsky reaction is important since it can be considered as prototype of numerous biochemical processes and oscillatory catalytic reactions. Moreover, it can be used as a matrix for catalyst characterization [34, 35, 57, 63] and quantitative analysis of numerous compounds [49, 59, 67, 73].

Short review on the models of Bray-Liebhafsky oscillatory reaction is given in Section 2. The construction of the corresponding differential equations for time evolution of the overall process through the time evolution of concentrations of each species taking part in the model is presented in Section 3.

2. The significant models of BL reaction

The model of the mechanism of one chemical reaction is a set of stoichiometric reactions that are kinetically important for the considered process. Based on such proposed model, we create a system of differential equations that describe the time evolution of the concentrations of the species involved in it, which then can be solved using numerical methods (since it is impossible to do this by analytical ones).

For an oscillatory reaction as typical nonlinear system, feedback is necessary. Feedback in reaction systems can be thermic and chemical, which is of interest in the case of Bray-Liebhafsky reaction. If the product of reaction increases its own production, we are dealing with autocatalysis and if it decreases its own production, we are dealing

with autoinhibition. Model of an oscillatory reaction may contain either direct autocatalytic step (such as $A+nB \rightarrow (n+1)B$) or autoinhibition step (such as $(n+1)B \rightarrow A+nB$), but these two steps can be also obtained by combination of several reactions, like it is in all models presented here.

Model of the Bray- Liebhafsky reaction should have to contain following reaction groups.

1) The reactions of iodine and constituents of Dushman reaction [84]

$$IO_3^- +5I^- +6H^+ \rightarrow 3I_2 +3H_2O \qquad (D)$$

2) The reactions between hydrogen peroxide and iodine species such as I_2, I^-, HIO, HIO_2, I_2O, I_2O_2 and IO_3^- [14, 15, 28, 29]. Some of these are extremely important for global reaction process and therefore, can be found in all mechanism.

Iodine and oxygen transition from solution to gas phase have been investigated for years as a significant process in the Bray-Liebhafsky reaction. Peard and Cullis [9] connected appearance of oscillations with iodine removing from the reaction system by gaseous oxygen produced in reaction. Shaw and Pritchard [13] concluded that two phases are necessary for existence of oscillations in such kind of reactions. Hence, the reaction must be treated as heterogeneous. However, even the Bray [2] showed that reaction can be carried out sufficiently slow such that gaseous oxygen can exit the system by diffusion. Laurenczy and Beck [33] investigated the effect of high pressure on the Bray-Liebhafsky reaction. They indicated that the escape of oxygen from liquid phase is not indispensable for the oscillations. Therefore, although oxygen removal may have an impact on whole reaction system, the reaction can be treated as homogeneous. Buchholtz and Broecker [44] concluded that oxygen transition to gas phase results only in changes in the location of bifurcation points and that the oscillations originate from chemical reactions. Also, by NMR spectra analysis chemical shifts were observed in the Bray-Liebhafsky reaction. Stanisavljev *et al* showed [45] that they depend on the complex combination of the effect on bubbles formation and increase in concentration of dissolved oxygen.

The difficulties in describing the reaction mechanism lie on the facts that there are only a few variables which can be varied independently in order to observe the effects and the kinetics of the overall process. Also, system is sensitive to light [19, 61], pressure [42, 46], stirring [42, 46], and microwaves [64, 65], ...

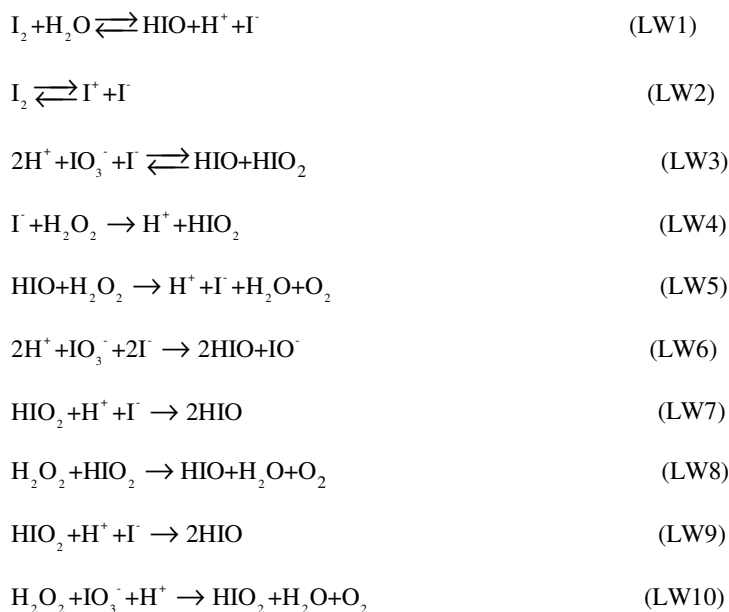*2.1. Model proposed by Liebhafsky and Wu*

The first (nonradical) model is proposed by Liebhafsky and Wu [19] in 1974 (Table 1).

As it can be seen, this model of mechanism is consisting of: three reversible reactions, (LW 1)-(LW 3), reaction of I^+ oxidation, (LW 4), HIO reduction, (LW 5), and reactions in which HIO_2 is produced, (LW 6)-(LW 10). Ninth reaction is usually negligible [23].

Although Clarke claimed that the model proposed by Liebhafsky and Wu is of a form that can generate an unstable steady state, to the best of our knowledge no one conformed his assertion. Nevertheless, this model of the Bray-Liebhafsky reaction is important as it was a basis for developing of other ones.

Table 1. Liebhafsky and Wu model [18].

$$I_2 + H_2O \rightleftharpoons HIO + H^+ + I^- \qquad\qquad (LW1)$$

$$I_2 \rightleftharpoons I^+ + I^- \qquad\qquad (LW2)$$

$$2H^+ + IO_3^- + I^- \rightleftharpoons HIO + HIO_2 \qquad\qquad (LW3)$$

$$I^- + H_2O_2 \rightarrow H^+ + HIO_2 \qquad\qquad (LW4)$$

$$HIO + H_2O_2 \rightarrow H^+ + I^- + H_2O + O_2 \qquad\qquad (LW5)$$

$$2H^+ + IO_3^- + 2I^- \rightarrow 2HIO + IO^- \qquad\qquad (LW6)$$

$$HIO_2 + H^+ + I^- \rightarrow 2HIO \qquad\qquad (LW7)$$

$$H_2O_2 + HIO_2 \rightarrow HIO + H_2O + O_2 \qquad\qquad (LW8)$$

$$HIO_2 + H^+ + I^- \rightarrow 2HIO \qquad\qquad (LW9)$$

$$H_2O_2 + IO_3^- + H^+ \rightarrow HIO_2 + H_2O + O_2 \qquad\qquad (LW10)$$

2.2. Models proposed by Sharma and Noyes and Edelson and Noyes

In 1976 Sharma and Noyes were proposed model [20] based on Deng's observation [11] that radicals participate in processes (O) (which is said to be a branched chain reaction) and own research regarding on the influence of light upon BL reaction [19]. From systematic data set of possible processes they select fourteen important for the Bray-Liebhafsky reaction (Table 2).

In 1979 Edelson and Noyes [22] (Table 3) added four reactions, (EN 15)-(EN 18), to the Sharma and Noyes model (Table 2). As can be seen by comparing these two models, in the Sharma and Noyes one, only first, seventh and last, fourteenth, processes are reversible, whereas Edelson and Noyes placed all of them to be reversible.

First four reactions, (EN 1)-(EN 4), (as well as (SN 1)-(SN 4)) represent I⁻ oxidation. Nonradical hydrogen peroxide oxidation to oxygen is given by: (EN 5) (*i.e.* (SN 5)), (EN 15) and (EN 16), whereas step (EN 15) does not contribute significantly during the most time of interest. Hydrogen peroxide reduction by the radicals containing iodine takes place by sixth and seventh reaction in both models. Although, HOO• and HO•

radicals can react in many ways, reactions (EN 8) (*i.e.* (SN 8)) and (EN 9) (*i.e.* (SN 9)) are the most probable (the fastest), and the only involved in model. Two following process that include fast reactions and sequence of following five reactions (EN 6)-(EN 11) (*i.e.* (SN 6)-(EN 11)) without EN 7 (*i.e.* SN 7), represents a chain of propagation reactions in which the final step regenerates radical necessary for the first step. In twelfth reaction, the radical species form the nonradical ones, with seventh and ninth, this reaction is there to initiate the chain sequence mentioned above. The only included chain-terminated steps are (EN 13) (*i.e.* (SN 13)), (EN 17), and (EN 18), whereas the last one is the most important. In fourteenth reaction, oxygen is removed from solution to gas phase (in all other reactions in this and models that follow, O_2 represents dissolved oxygen although it is not written as $O_{2(aq)}$.

Table 2. Sharma and Noyes model [20].

$$HIO + I^- + H^+ \rightleftharpoons I_2 + H_2O_2 \tag{SN1}$$

$$HIO_2 + H^+ + I^- \rightarrow 2HIO \tag{SN2}$$

$$2H^+ + IO_3^- + I^- \rightleftharpoons HIO + HIO_2 \tag{SN3}$$

$$2HIO_2 \rightarrow IO_3^- + HIO + H^+ \tag{SN4}$$

$$HIO + H_2O_2 \rightarrow H^+ + I^- + H_2O + O_2 \tag{SN5}$$

$$IO^\bullet + H_2O_2 \rightarrow HIO_2 + HO^\bullet \tag{SN6}$$

$$IO_2^\bullet + H_2O_2 \rightleftharpoons H^+ + IO_3^- + HO^\bullet \tag{SN7}$$

$$HOO^\bullet + I_2 \rightarrow I^- + O_2 + H^+ + I^\bullet \tag{SN8}$$

$$HO^\bullet + H_2O_2 \rightarrow H_2O + HOO^\bullet \tag{SN9}$$

$$I^\bullet + O_2 \rightarrow OOI^\bullet \tag{SN10}$$

$$OOI^\bullet + I^- + H^+ \rightarrow HIO + IO^\bullet \tag{SN11}$$

$$H^+ + IO_3^- + HIO_2 \rightarrow 2IO_2^\bullet + H_2O \tag{SN12}$$

$$2HOO^\bullet \rightarrow H_2O_2 + O_2 \tag{SN13}$$

$$O_{2(aq)} \rightleftharpoons O_{2(g)} \tag{SN14}$$
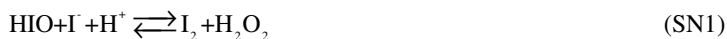
Edelson and Noyes [22] claimed that rate constants of reactions (EN 2), (EN 4), (EN 11), (EN 12), and (SN 14) are the only disposable parameters to be assigned to generate behaviour observed in the experiments, since rate constants of reactions (EN 1), (EN 3), (SN 5), (SN 9), (SN 13), and (SN 16) are known with the moderate confidence from the experiment in [20] and the other reaction rate constants ((EN 6), (EN 7), (SN 8), (SN 10), (SN 15), (SN 17), and (SN 18)) have no influence on the overall process. That is, only by changing them, one cannot obtain nonlinear phenomena. Further, they said that for oscillations existence the most important step is (EN 18).

Table 3. Edelson and Noyes model [23].

$$HIO + I^- + H^+ \rightleftharpoons I_2 + H_2O_2 \qquad \text{(EN1)}$$

$$HIO_2 + H^+ + I^- \rightarrow 2HIO \qquad \text{(EN2)}$$

$$2H^+ + IO_3^- + I^- \rightleftharpoons HIO + HIO_2 \qquad \text{(EN3)}$$

$$2HIO_2 \rightarrow IO_3^- + HIO + H^+ \qquad \text{(EN4)}$$

$$HIO + H_2O_2 \rightarrow H^+ + I^- + H_2O + O_2 \qquad \text{(EN5)}$$

$$IO^\bullet + H_2O_2 \rightarrow HIO_2 + HO^\bullet \qquad \text{(EN6)}$$

$$IO_2^\bullet + H_2O_2 \rightleftharpoons H^+ + IO_3^- + HO^\bullet \qquad \text{(EN7)}$$

$$HOO^\bullet + I_2 \rightarrow I^- + O_2 + H^+ + I^\bullet \qquad \text{(EN8)}$$

$$HO^\bullet + H_2O_2 \rightarrow H_2O + HOO^\bullet \qquad \text{(EN9)}$$

$$I^\bullet + O_2 \rightarrow OOI^\bullet \qquad \text{(EN10)}$$

$$OOI^\bullet + I^- + H^+ \rightarrow HIO + IO^\bullet \qquad \text{(EN11)}$$

$$H^+ + IO_3^- + HIO_2 \rightarrow 2IO_2^\bullet + H_2O \qquad \text{EN12)}$$

$$2HOO^\bullet \rightarrow H_2O_2 + O_2 \qquad \text{(EN13)}$$

$$O_{2(aq)} \rightleftharpoons O_{2(g)} \qquad \text{(EN14)}$$

$$HIO_2 + H_2O_2 \rightleftarrows HIO + O_2 + H_2O \qquad \text{(EN15)}$$

$$IO_3^- + H_2O_2 + H^+ \rightleftarrows HIO_2 + O_2 + H_2O \qquad \text{(EN16)}$$

$$I^\cdot + HOO^\cdot \rightleftarrows I^- + O_2 + H_2O \qquad \text{(EN17)}$$

$$2I^\cdot \rightleftarrows I_2 \qquad \text{(EN18)}$$
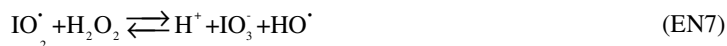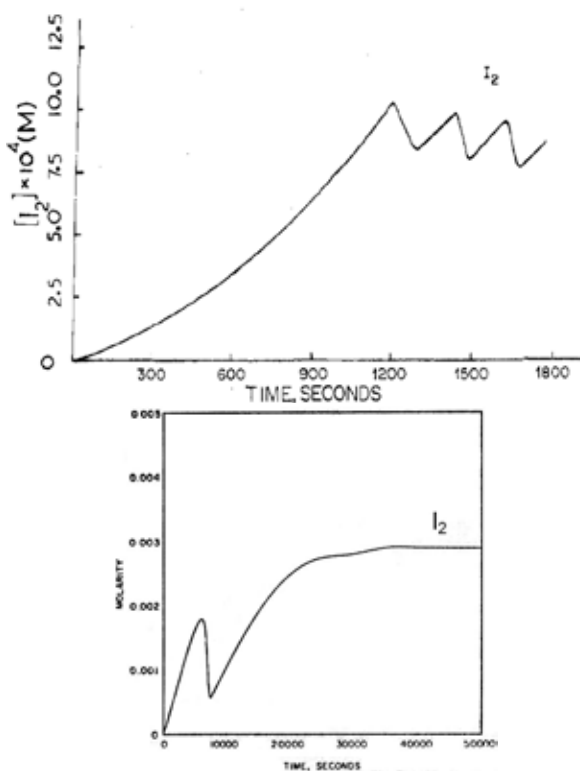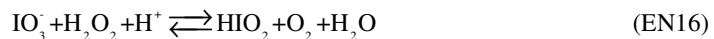
Figure 1. Experimental results (on the left side, reprinted with permission from [20]. Copyright (1976) American Chemical Society.) and numerical simulation obtained by the model proposed by Edelson and Noyes (on the right side, reprinted with permission from [22]. Copyright (1979) American Chemical Society.).

In the Bray-Liebhafsky reaction a continuous production of oxygen occurs. Hence, its concentration in solution can be much higher (than under the normal conditions) because of supersaturation [18, 19, 29, 36, 40]. Therefore, it can be written $[O_{2(aq)}]_{ss} = m[O_{2(aq)}]_{sat}$, where $[O_{2(aq)}]_{ss}$ is the oxygen steady state concentration and $m>1$. Edelson and Noyes tried to explain this process by linear supersaturation kinetics:

95

$$-\frac{d[O_{2(aq)}]}{dt} = k_{EN14}([O_{2(aq)}]-[O_{2(aq)}]_{sat})$$

(eq 1)

where $[O_{2(aq)}]$ represents total concentration of dissolved oxygen and k_{ES14} is the rate constant of reaction (EN 14). However, this required m to be order of 100, which is not realistic.

Consequently, they tried with fourth root supersaturation kinetics:

$$-\frac{d[O_{2(aq)}]}{dt} = k_{EN14}([O_{2(aq)}]-[O_{2(aq)}]_{sat})^{1/4}$$

(eq2)

Oscillations were obtained for $m=2$, but their lasting were not satisfactory (Fig. 1), since hydrogen peroxide consumption was too rapid, due to the radical processes. If we take $[H_2O_2]$ = const (CSTR conditions), still remains the problem that concentration of dissolved oxygen would be unrealistic. Edelson and Noyes believed problem was in release of supersaturation oxygen rather than in the model of chemical mechanism, so the kinetics of process (EN 14) cannot be described by (eq 1) neither (eq 2) because of the process complexity.

2.3. Model proposed by Treindl and Noyes

In 1993 Treindl and Noyes [32] composed the skeleton mechanism (Table 4), (TN 1)-(TM 10), by analysis of the known experimental results.

They claimed that only negative ions and radicals in small but non-negligible concentrations: OH⁻, OOH⁻, H•, HO• and HOO• are included in the model. Moreover, they said that I_3^- and $IO_2^•$ might be included and I• must be invoked to explain the photochemical sensitivity of the reaction [19, 20]. Also, Treindl and Noyes have chosen hydrogen peroxide to react only with HIO, due to the fact that there was no evidence about reaction between hydrogen peroxide and HIO_2.

Table 4. Treindl and Noyes model [32].

$$IO_3^- + I^- + 2H^+ \rightarrow HIO_2 + HOI \qquad\qquad (TN1)$$

$$HIO_2 + I^- + H^+ \rightarrow 2HIO \qquad\qquad (TN2)$$

$$HOI + I^- + H^+ \rightleftarrows I_2 + H_2O \qquad\qquad (TN3)$$

$$HOI + H_2O_2 \rightarrow I^- + H^+ + O_2 + H_2O \qquad\qquad (TN4)$$

$$I^- + H^+ + H_2O_2 \rightarrow HOI + H_2O \qquad\qquad (TN5)$$

$$I_2 \rightleftarrows 2I^• \qquad\qquad (TN6)$$

$$I^{\cdot} + O_2 \rightleftharpoons IOO^{\cdot} \tag{TN7}$$

$$IOO^{\cdot} \rightarrow IO_2^{\cdot} \tag{TN8}$$

$$2IO_2^{\cdot} + H_2O \rightarrow IO_3^- + H^+ + HIO_2 \tag{TN9}$$

$$O_{2(aq)} \rightarrow O_{2(g)} \tag{TN10}$$
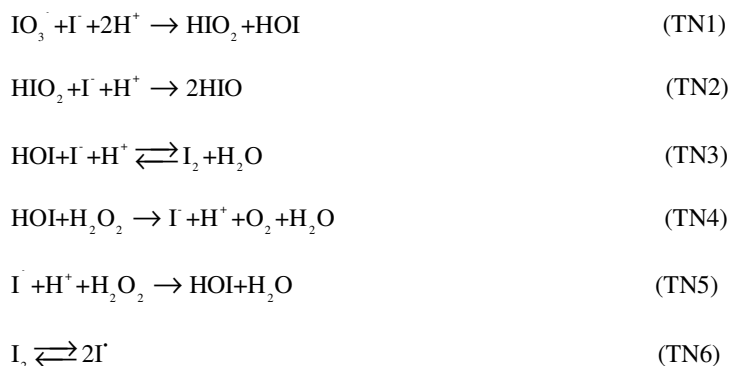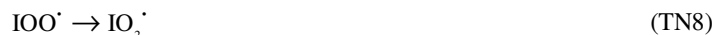
Although, Treindl and Noyes could not simulate reaction by proposed model, they had believed it can "explain at least a very large portion of the observations which have been made" in the Bray-Liebhafsky reaction system. Theirs faith in the ability of the model to provide oscillations had been based on the fact that production of iodine is autocatalytic. Noyes *et al* [37] as well as *Ren et al* [70] showed that iodine and oxygen oscillate and that oscillations do not involve a true limit cycle.

2.3. Model proposed by Schmitz and its variants

In 1987 Schmitz [29] proposed the simplest model for the Bray-Liebhafsky reaction mechanism. It is a nonradical model without any direct autocatalytic or autoinhibition step and it is the first of this kind in which oscillations were obtained. Here crucial reactions in the process of HIO oxidation into compounds with higher oxidation number occur by I_2O participation. This model downside is fact that I_2O is not found experimentally in the Bray-Liebhafsky reaction. Schmitz's model consists of reaction (M 1)-(M 6) presented in Table 5 and describes well only the reaction process in medium area of acidity [30], but no in high and low acidity solution. This lacks are solved by adding reactions (M 7) [31] and (M 8) [38] respectively. Model with mentioned improvements are also known as model 1-8 or M (1-8) and it is given in Table 5.

Except the reactions with I_2O, all of them can be found in the Liebhafsky and Wu model and earlier papers. Thus, reaction (M 1) is analysed in [3, 5, 18], (M 4) in [10, 17, 18], (M 5) in [7,16, 18], (M 7) in [4], and (M 8) in [5, 18].

Table 5. M (1-8) model [38].

$$I^- + IO_3^- + 2H^+ \rightleftharpoons HIO + HIO_2 \tag{M1}$$

$$HIO_2 + H^+ + I^- \rightarrow I_2O + H_2O \tag{M2}$$

$$I_2O + H_2O \rightleftharpoons 2HIO \tag{M3}$$

$$HIO + H^+ + I^- \rightleftharpoons I_2 + H_2O \tag{M4}$$

$$HIO + H_2O_2 \rightarrow H^+ + I^- + H_2O_2 + O_2 \tag{M5}$$

$$I_2O + H_2O_2 \rightarrow HIO + HIO_2 \tag{M6}$$

$$HIO_2 + H_2O_2 \rightarrow IO_3^- + H^+ + H_2O \tag{M7}$$

$$IO_3^- + H_2O_2 + H^+ \rightarrow HIO_2 + O_2 + H_2O \tag{M8}$$
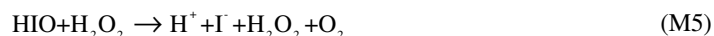
The added reactions control the appearance and duration of the induction period preceded to the oscillations occurrence. Using this model, beside the impact of acidity, successfully are simulated the impact of temperature [43], the perturbations by polymers, the occurrence of inflection in a model parameter space. In addition, the M (1-8) model provides relatively good agreement with the experimental results (Figs. 2 and 3) on the oscillations number, the shape and lasting for all reaction species that can be monitored experimentally. Agreement between the experimental findings and the model prediction proved to be quite good also in [59], where the pulsed perturbations with iodide were applied. For the M (1-8) model, the stability criteria were established [39] and it's also qualitatively consistent with the experimental data.
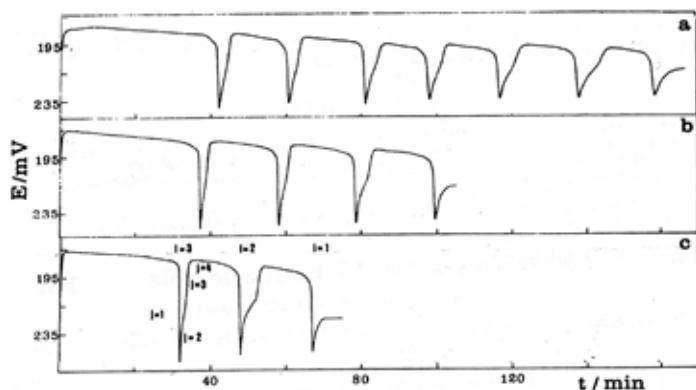
Figure 2. Iodide oscillograms of the BL reaction at the different temperatures: (a) 56.0 °C, (b) 62.0 °C, and (c) 67.0° C (Reprinted with Editors permission from [41]).

The M (1-8) model is able to describe almost all features of the Bray-Liebhafsky reaction, including simple oscillatory evolution, mixed-modes and chaos [66, 69, 74, 79, 82].

Experimental inability to prove existence of I_2O as reaction species was theoretically overcome by the elimination of I_2O from the system chemical equations [47, 50, 52]. One of the models from [47] created by the contraction of M (1-8) is presented in Table 6.
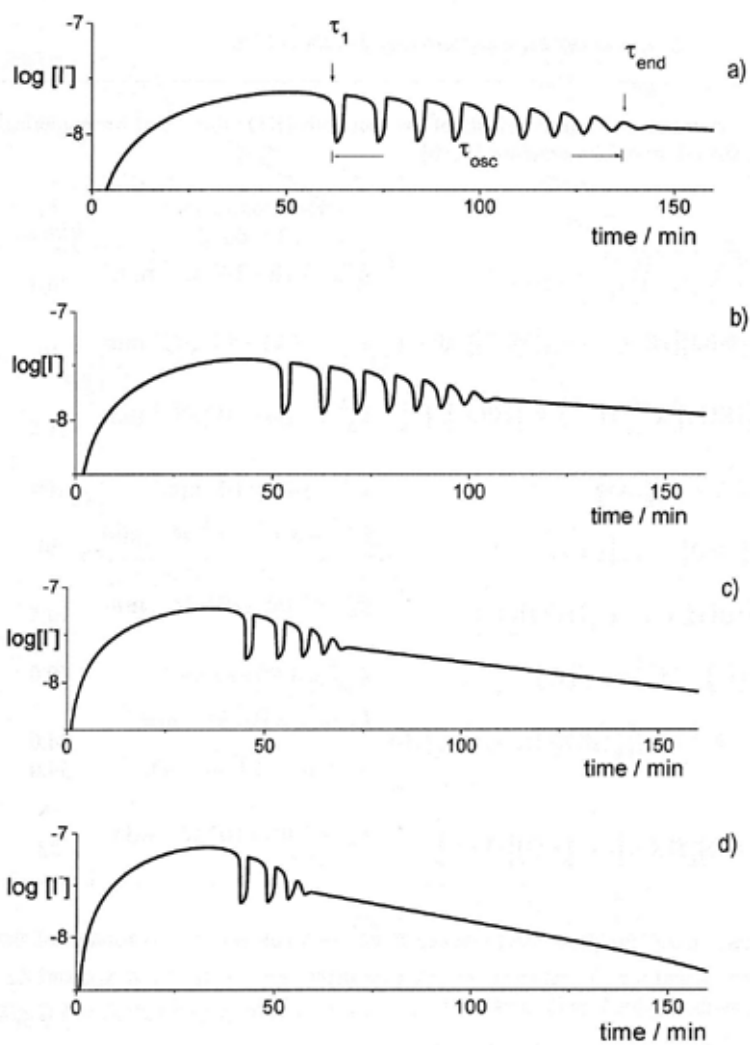
Figure 3. Simulated iodide evolution of the BL reaction based on the reaction M(1)-M-(6) at the different temperatures: (a) 54,8 °C, (b) 59.8 °C, (c) 65.8 °C, and (d) 68,8 °C (Reprinted with Edirors permission from [68]).

Table 6. Reduced M (1-8) model [47].

$$I^- + IO_3^- + 2H^+ \rightleftharpoons HIO + HIO_2 \qquad (RM1)$$

$$HIO + H^+ + I^- \rightleftharpoons I_2 + H_2O \qquad (RM2)$$

$$HIO + H_2O_2 \rightarrow I^- + O_2 + H^+ + H_2O \qquad (RM3)$$

$$HIO_2 + H_2O_2 \rightarrow IO_3^- + H^+ + H_2O \qquad (RM4)$$

$$IO_3^- + H_2O_2 + H^+ \rightarrow HIO_2 + O_2 + H_2O \qquad (RM5)$$

$$2HIO \rightleftharpoons HIO_2 + I^- + H^+ \qquad (RM6)$$

$$HIO_2 + I^- + H^+ + H_2O_2 \rightarrow HIO + HIO_2 + H_2O \qquad (RM7)$$
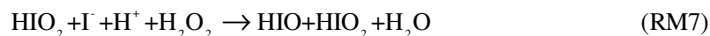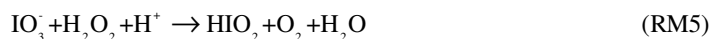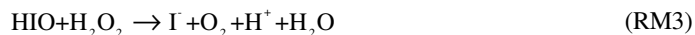
This model, like the previous one, can simulate oscillatory evolution (of every containing intermediate), but in a slightly worse agreement with experimental results. This is understandable considering the applied simplification.

Also, there are the researches treating M (1-8) model without reaction (M 7), but with changed reaction (M 8) rate constant [71, 75]. Obtained results are nearly the same.

Significant research is also the one performed by Adamčiková and Ševčík on the effects of pressure decrease, gases bubbling and stirring on the oscillating Bray-Liebhafsky reaction [42, 46]. They showed the rate of iodine interphase transport can be greatly influenced by physical processes and that they can cause the oscillatory state to be inhibited. By adding this process into the reaction mechanism, iodide is not pure catalyst anymore, because iodine is consumed in the reaction and therefore, total concentration of iodine containing species cannot be treated as a constant.

With co-workers they complemented the M (1-8) model with the reaction of iodine (AS 1) [48] and the oxygen escape (AS 2) [58] from the reaction system:

$$I_{2(aq)} \rightarrow I_{2(g)} \qquad (AS1)$$

$$O_{2(aq)} \rightarrow O_{2(g)} \qquad (AS2)$$

As they shown, the reaction of iodine (AS1) removal follows the pseudo-first-order kinetics:

$$-\frac{d[I_{2(aq)}]}{dt} = k_{AS1}[I_{2(aq)}] \qquad (eq3)$$

where $[I_{2(aq)}]$ is the iodine concentration in the solution and k_{AS1} is a constant depending on the stirring rate, while the other parameters are fixed.

The simulated the period and number of oscillations showed very good agreement when they took only a minor modification of several M (1-8) model rate constants. In [48] they also found a critical value above which oscillation cannot be observed by numerical simulation. Agreement with experiments was satisfactory.

After Schmitz conformed [52] that the escape of oxygen causes the loss of iodine into gas phase, Ševčík et al examined oxygen production in the Bray-Liebhafsky reaction [55]. Experimental data from this paper were used for comparison with the numerical results in [58] where they tried to answer on the question if the model M (1-8) with the two reactions of iodine and oxygen removal is able to correctly simulate the pulsing oxygen gas evolution. At the first approach, they assumed the first-order rate law, similarly to iodine kinetics (see eq3):

$$-\frac{d[O_{2(aq)}]}{dt} = k_{AS2}([O_{2(aq)}]-[O_{2(aq,sat)}])$$

(eq4)

where k_{AS2} is a constant depending on experimental conditions.

The results were in satisfactory good agreement with the experiments (Fig. 4), which may indicate that the kinetics of oxygen removal cannot be described by a first-order rate law and seems to be a more complicated.
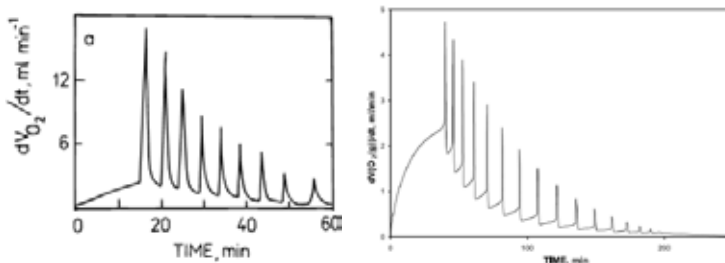
Figure 4. Experimental results (on the left side, reprinted with permission from [55]. Copyright (2000) American Chemical Society) and numerical simulation obtain by the M (1-8) model with the two reactions of iodine and oxygen removal (on the right side, Reprinted from [58] with permission from Elsevier.).
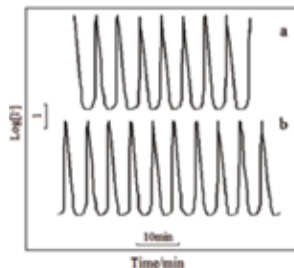
Figure 5. (a)Experimental results (originally from [20]) and (b) numerical simulation [81] obtain by the Ren et al model. (Reprinted with Editors permission from [81]).

In 2008 Ren *et al* [72] analysed model similar to the one Ševčík *et al* did, except they set all steps to be irreversible and changed a rate constants (Table 7).

They compared simulated results [81] with the experimental results presented in [20] (Fig. 5). Agreement between these two is qualitatively good; there is only a small difference in the oscillations shape. This model does not involve a true limit cycle.

Table 7. Model used by Ren *et al* [72].

$$I^- + IO_3^- + 2H^+ \rightarrow HIO + HIO_2 \tag{R1}$$

$$HIO_2 + H^+ + I^- \rightarrow I_2O + H_2O \tag{R2}$$

$$I_2O + H_2O \rightarrow 2HIO \tag{R3}$$

$$HIO + H^+ + I^- \rightarrow I_2 + H_2O \tag{R4}$$

$$HIO + H_2O_2 \rightarrow H^+ + I^- + H_2O_2 + O_2 \tag{R5}$$

$$I_2O + H_2O_2 \rightarrow HIO + HIO_2 \tag{R6}$$

$$HIO_2 + H_2O_2 \rightarrow IO_3^- + H^+ + H_2O \tag{R7}$$

$$IO_3^- + H_2O_2 + H^+ \rightarrow HIO_2 + O_2 + H_2O \tag{R8}$$

$$I_{2(aq)} \rightarrow I_{2(g)} \tag{R9}$$

$$O_{2(aq)} \rightarrow O_{2(g)} \tag{R10}$$
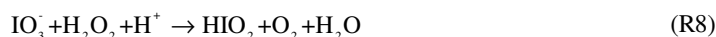
In 2010 Schmitz proposed the new model (Table 8) [76], with a set of rate constants at 25°C. He analysed [76, 80] iodine concentration impact on the rate constant of iodine interphase transport and asserted this reaction can be treated as first-order one only when iodine concentration is much larger than a steady state concentration (the one in which rates of reaction (O) and (R) are equal). Also, he discussed applicability conditions of reaction constants and adequacy of each reaction step from Table 6, i.e. under which circumstances steps can be considered as simple and under which it must be seen as the complex process consists of the simple steps. In addition, these papers show that Arrhenius law can be used if one wants to calculate a reaction constant for some other temperature. In favour goes agreement with measurements by Liebhafsky at 50°C [6] and by Schmitz at 60°C (Fig. 6) [52].

In the model presented in Table 8, reaction (M 7) is replaced by three reactions (S 7a), (S 7b), and (S 7c). Schmitz highlights that steps (S 7c) and (S 9)-(S 13) are the minor reactions, but they allow good simulation of the oxygen effect on the oscillations.

Reactions (S 11) and (S 13) can be found in [29], but since the oscillations can be obtained without them, they were neglected in the development of the model M (1-8), while the rates and kinetics law of (S 12) were obtained even by Liebhafsky and Mohammed [8].

Although, the kinetics of oxygen transport to gas phase is not simple and involves a nucleation and growth of bubbles, Schmitz used the first-order rate law as it other authors previously did.

As Bray noticed [2] oxygen production is higher during the step (O), in which it is not a product, then during (R). This statement was confirmed also in [18]. Simulation of it is thorn in the side. Schmitz claimed reaction BL always takes place during the reaction (O) and since IOH concentration is higher in the course of (O) then (R), fifth reaction may be the main source of "characteristic" oxygen production. Moreover, the simulations obtained by Schmitz last model are in appreciably agreement with measurements [18].

Table 8. Model proposed by Schmitz [76].

$$I^- + IO_3^- + 2H^+ \rightleftharpoons HIO + HIO_2 \tag{S1}$$

$$HIO_2 + H^+ + I^- \rightarrow I_2O + H_2O \tag{S2}$$

$$I_2O + H_2O \rightleftharpoons 2HIO \tag{S3}$$

$$HIO + H^+ + I^- \rightleftharpoons I_2 + H_2O \tag{S4}$$

$$HIO + H_2O_2 \rightarrow H^+ + I^- + H_2O_2 + O_2 \tag{S5}$$

$$I_2O + H_2O_2 \rightarrow HIO + HIO_2 \tag{S6}$$

$$2HIO_2 \rightleftharpoons I_2O_3 + H_2O \tag{S7a}$$

$$I_2O_3 + H_2O_2 \rightarrow IO_3^- + H^+ + HIO_2 \tag{S7b}$$

$$I_2O_3 + H_2O \rightarrow IO_3^- + H^+ + HIO \tag{S7c}$$

$$IO_3^- + H_2O_2 + H^+ \rightarrow HIO_2 + O_2 + H_2O \tag{S8}$$

$$I_{2(aq)} \rightarrow I_{2(g)} \tag{S9}$$

$$O_{2(aq)} \rightarrow O_{2(g)} \tag{S10}$$

$$HIO_2 + H_2O_2 \rightarrow IOH + O_2 + H_2O \tag{S11}$$

$$I^- + H^+ + H_2O_2 \rightarrow IOH + H_2O \tag{S12}$$

$$I^- + H^+ + \frac{1}{2}O_2 \rightarrow IOH \tag{S13}$$
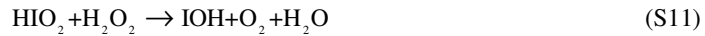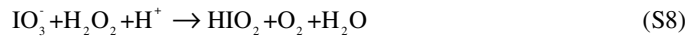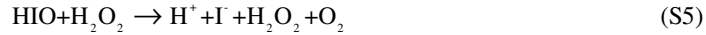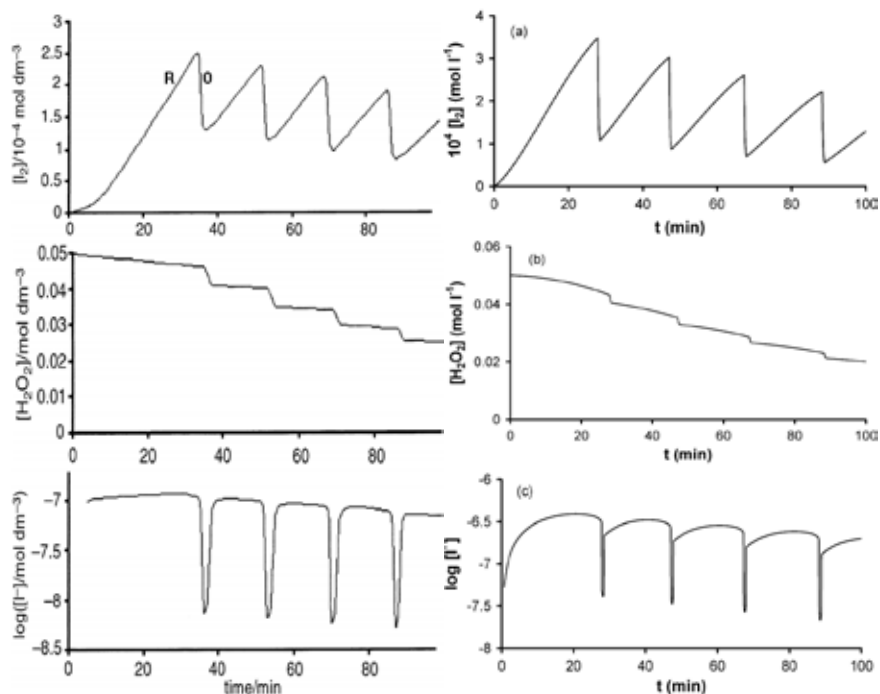
Figure 6. Experimental results [52] (on left side) and numerical simulation [80] obtain by the Schmitz's model (on the right side). Reproduced by permission of The Royal Society of Chemistry.

3. Differential equations for describing a time evolution of reaction

Generally, the above models can be associated with a set of differential equations describing the time evolution of the Bray-Liebhafsky reaction. These differential equations, which describe the rates of individual reactions, are performed directly on the basis of the mass-action law. The procedure of differential equations forming will be given for the M (1-8) model of the Bray-Liebhafsky reaction.

In the case which is of interest, the Bray-Liebhafsky reaction is considered to be homogeneous. That is, there are no chemical reactions that can be found in several phases (aggregate states). Also, the Bray-Liebhafsky reaction is deemed to be strictly determined by its chemism (only by chemical transformations) and that kinetic is not influenced by physical processes (diffusion, thermal effects, etc.).

3.1. M (1-8) model-Reaction rate equations

In the M (1-8) model, there are eight chemical reactions, three of them are reversible and five are irreversible. Irreversible reaction is one in which all reactants (starting

substances) are fully transformed into reaction products. Reversible reaction consists of two irreversible, one in which reactants are converted into products and another in which products (of the first reaction) react to become starting substances. Therefore, M (1-8) model has eleven irreversible chemical reactions. For each of them, reaction rate is determined and used to calculate overall rate of some chemical species (see below).

As an example, here is derived rate of one irreversible chemical reaction which is involved in reaction (M 1). Reaction in which reactants of (M 1) are converted into products is:

$$I^- + IO_3^- + 2H^+ \rightarrow HIO + HIO_2 \tag{R1}$$

As one can notice, it is also a first reaction in model proposed by Ren *et al* and its rate (v_1) is:

$$v_1 = k_1'[IO_3^-][H^+]^2[I^-] = k_1[I^-] \tag{eq5}$$

where k_1' is rate constant. It is rate of reaction when concentrations of all reaction species, IO_3^-, H^+ and I^-, are unity ones. In chemistry, it is commonly to denote the concentration of a species, by putting its chemical formula in square brackets. Exponents in the relations that describe the reaction rate corresponding stoichiometric coefficients (numbers which standing in front of a chemical species). If stoichiometric coefficient is 1, it is not displayed. Concentrations of IO_3^- and H^+ are considered to be negligible changed in the Bray-Liebhafsky reaction (*i.e.* they are constants) and hence, k_1 is pseudo-constant, since it contains IO_3^- and H^+ concentrations.

The same procedure was performed for each other chemical species from the M (1-8) model and the rate of each chemical process are presented in Table 9.

Table 9. Reaction rates and rate constants of M(1-8) model which are commonly used in numerical simulation of the Bray-Liebhafsky reaction. Concentration of water, $[H_2O] = 55$ M, is involved in the corresponding rate constants. Also, $[IO_3^-] = 0.0474$ and $[H^+] = 0.0958$ M are considered as constants and involved in pseudo-constants. [77]

Reaction rate	Reaction rate constant	Reaction
$v_1 = k_1 [I^-]$	$k_1 = 1,375 \times 10^2$ min^{-1}	(R 1)
$v_{-1} = k_{-1} [HIO] [HIO_2]$	$k_{-1} = 7,91 \times 10^7$ M^{-1} min^{-1}	(R -1)
$v_2 = k_2 [HIO_2] [I^-]$	$k_2 = 4,79 \times 10^{10}$ M^{-1} min^{-1}	(R 2)
$v_3 = k_3 [I_2O]$	$k_3 = 5,00 \times 10^{10}$ min^{-1}	(R 3)
$v_{-3} = k_{-3} [HIO]^2$	$k_{-3} = 3,15 \times 10^8$ M^{-1} min^{-1}	(R -3)
$v_4 = k_4 [HIO] [I^-]$	$k_4 = 3,00 \times 10^{11}$ M^{-1} min^{-1}	(R 4)
$v_{-4} = k_{-4} [I_2]$	$k_{-4} = 46,97$ min^{-1}	(R -4)
$v_5 = k_5 [HIO] [H_2O_2]$	$k_5 = 1,487 \times 10^4$ M^{-1} min^{-1}	(R 5)
$v_6 = k_6 [I_2O] [H_2O_2]$	$k_6 = 5,00 \times 10^5$ M^{-1} min^{-1}	(R 6)
$v_7 = k_7 [HIO_2] [H_2O_2]$	$k_7 = 2,00 \times 10^3$ M^{-1} min^{-1}	(R 7)
$v_8 = k_8 [H_2O_2]$	$k_8 = 2,2303 \times 10^{-4}$ min^{-1}	(R 8)

3.2. M (1-8) model- Overall rate equations of chemical species

Let us take as an example H$_2$O$_2$, it is participate in reactions (M 5), (M 6), (M 7) and (M 8). Hydrogen peroxide time derivation, $\dfrac{d[H_2O_2]}{dt}$, *i.e.* overall rate of hydrogen peroxide change, is given by the sum of all mentioned reactions, that is,

$$\frac{d[H_2O_2]}{dt} = -v_5 - v_6 - v_7 - v_8 \tag{OR1}$$

Here, minus (in the front of reaction rates) indicates that in these reactions hydrogen peroxide is consumed. But for example, overall rate of I$^-$ is:

$$\frac{d[I^-]}{dt} = v_{-1} + v_{-4} + v_5 - v_1 - v_2 - v_4 \tag{OR2}$$

where + indicates formation of iodide by the first three reactions.

In the same way, overall rate equations for other species are defined:

$$\frac{d[HIO]}{dt} = v_1 + 2v_3 + v_{-4} + v_6 - v_{-1} - 2v_{-3} - v_4 - v_5 \tag{OR3}$$

$$\frac{d[HIO_2]}{dt} = v_1 + v_6 + v_8 - v_{-1} - v_2 - v_7 \tag{OR4}$$

$$\frac{d[I_2O]}{dt} = v_2 + v_{-3} - v_3 - v_6 \tag{OR5}$$

$$\frac{d[I_2]}{dt} = v_4 - v_{-4} \tag{OR6}$$

In the mathematical sense, concentrations of chemical species can be observed as independent variables. For an example, $[H_2O_2] = x_1$, $[I^-] = x_2$, $[HIO] = x_3$, $[HIO_2] = x_4$, $[I_2O] = x_5$ and $[I_2] = x_6$. Presented set of differential equations is to be solved using a numerical method, that is, with appropriate program package. In Fig. 7, evolution of chemical species simulated on the basis of the model M (1-8) is given.
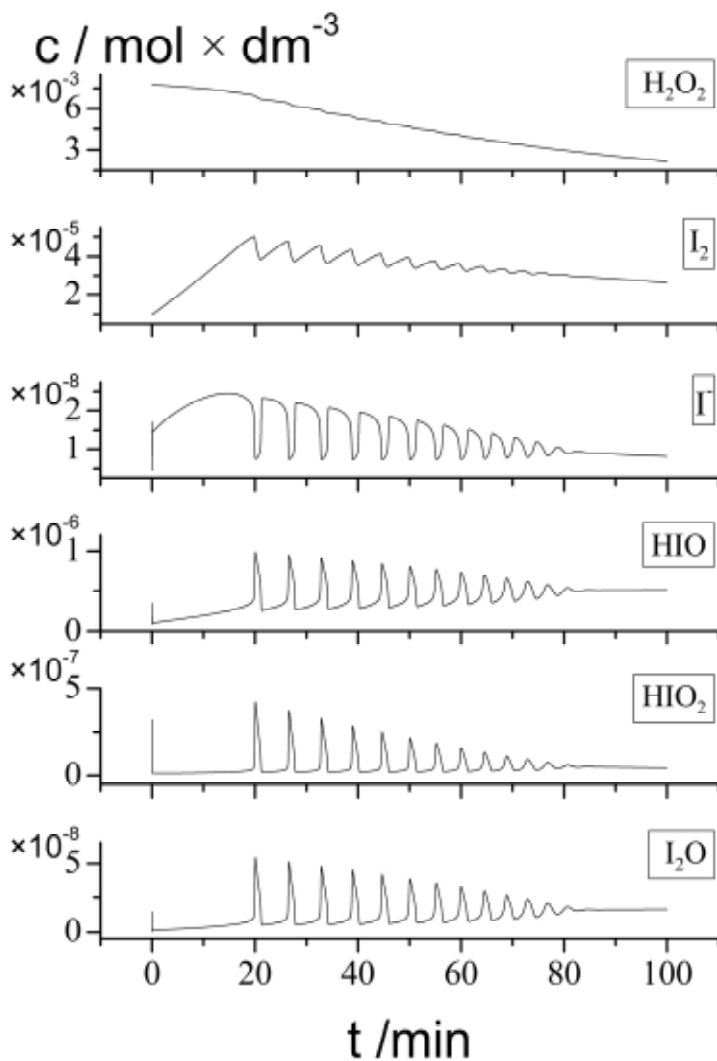
Figure 7. Numerical simulation of evolution of the chemical species concentration on the basis of M (1-8) models.

4. Conclusions

To summarize, in Liebhafsky papers one may found plenty of reactions that can take a place in reaction mechanism, but to the best of our knowledge by the model proposed by Liebhafsky and Wu the oscillations could not be obtained. In papers presenting the models

by Noyes *et al*, possible and important reactions are highlighted, but there is no good agreement with experiments. Maybe extensions of the Treindl and Noyes can give a better accordance. The M (1-8) model and its variants represent one realistic model of the Bray-Liebhafsky oscillatory reaction mechanism that well describes its phenomena and does not contain any direct autocatalytic or autoinhibition step. Moreover, it is nonradical model, so radical reactions, which rates are notably large in relation to reaction oscillatory frequency, are not responsible for oscillations.

Ševčík *et al* have made major efforts to further upgrade the M (1-8) model by the involvement of iodine and oxygen interphase transport processes, while Ren *et al* analysed the model with a different set of rate constants (with regard to experimentally obtained ones).

After almost a century of the Bray-Liebhafsky reaction investigation, we still don't know answers on many questions. One of the essential questions is how it is that during the step (O) many times more oxygen is produces than during the step (R) and still oxygen is not product of the reaction (O). To resolve this question (and many other disagreements between experiment and theory), maybe we need to add a few parallel processes.

References

[1] Laidler K J (Ed) (1996), A Glossary of Terms used in Hemical Kinetics, including Feaction Dynamics, *Pure & Appl. Chem.*, **68**, pp. 149-192

[2] Bray W C (1921), Periodic Reaction in Homogenous Solution and its Relation to Catalysis, *J. Am. Chem. Soc.*, **43**, pp. 1262-1261.

[3] Bray W C (1930), An Oxide of Iodine I$_2$O$_2$. An Intermediate compound, *J. Am. Chem. Soc.*, **52**, pp. 3580-3586.

[4] Bray W C and Liebhafsky H A (1931), Reaction involving Hydrogen Peroxide, Iodine and Iodate ion. I. Introduction, *J. Am. Chem. Soc.*, **53**, pp. 38-44.

[5] Liebhafsky H A (1931), Reaction involving Hydrogen Peroxide, Iodine and Iodate Ion. III, The Reduction of Iodate Ion by Hydrogen Peroxide, *J. Am. Chem. Soc.*, **53**, pp. 896-911.

[6] Liebhafsky H A (1931), Reaction involving Hydrogen Peroxide, Iodine and Iodate Ion. IV. The Oxidation of Iodine to Iodate Ion by Hydrogen Peroxide, *J. Am. Chem. Soc.*, **53**, pp. 2074-2090.

[7] Liebhafsky H A (1932), The Catalytic Decomposition of Hydrogen Peroxide by Iodine-Iodate Couple. II and III. The rate of Oxidation, in Neutral and in Acid Solution, of Hydrogen Peroxide by Iodide Ion, *J. Am. Chem. Soc.*, **54**, pp. 3499-3508.

[8] Liebhafsky H A and Mohammed A (1933), The Kinetics of the Reduction, in Acid Solution, of Hydrogen Peroxide by Iodide Ion, *J. Am. Chem. Soc.*, **55**, pp. 3977-3986.

[9] Peard M G and Cullis C F (1951), A Periodic Chemical Reaction - The Reaction between Hydrogen Peroxide and Iodic Acid, *Trans. Farad. Soc.*, **47**, pp. 616-630.

[10] Eigen M and Kustin K (1961), The Kinetic of Halogen Hydrolysis, *J. Am. Chem. Soc.*, **84**, pp. 1355-1361.

[11] Deng H (1967), Evidence of a Branched Chain Reaction in the Oscillating Reaction of Hydrogen Peroxide, Iodine and Iodate, *Acta. Chem. Scand.*, **21**, pp. 1057-1066.

[12] Vavalin V A and Zhabotinskii A M (1967), Oscillations in the Hydrogen Peroxide Decomposition Reaction, in Biological and Chemical System, Frank G M (Ed.), Oscillating Process, Science Publ., Moscow, pp. 220-223.

[13] Shaw D H and Pritchard H O (1968), Homogeneous periodic reaction, *J. Phys. Chem.*, **72**(4), pp. 1403-1404, **72**(7), pp. 2693.

[14] Matsuzaki I, Woodson J H, and Liebhafsky H A (1970), pH and Temperature Pulses during the Periodic Decomposition of Hydrogen Peroxide, *Bull. Chem. Soc. Jpn.*, **43**, pp. 3371

[15] Vavalin V A, Zhabotinskii A M, and Zakain A N (1970), Self-oscillation of Iodide Ion Concentration during the Iodate-Catalyzed Decomposition of Hydrogen Peroxide, *Russ .J. Phys. Chem.,* 44, pp. 1345-1346.

[16] Matzuzaki M, Simić R, and Liebhafsky H A (1972), The Mechanism of Decomposition of Hydrogen Peroxide by Iodine in Acid Solution. The Rate of Associated Reactions, *Bull. Chem. Soc. Jpn.*, **45**, pp. 3367-3371.

[17] Burger J D and Liebhafsky H A (1973), Thermodinamic Data for Aqueous Iodine Solution at Various Temperatures. Exercise in Analytical Chemistry, *Anal. Chem.*, **45**, pp. 600-602.

[18] Liebhafsky H A and Lowrence S W (1974), Reaction Involving Hydrogen Peroxide, Iodine, and Iodate Ion. V. Intraduction to the Oscillatory Decomposition of Hydrogen Peroxide, *J. Am. Chem. Soc.*, **96**, pp. 7180-7187

[19] Sharma K R and Noyes R M (1975), Oscillations in Chemical Systems. VII Effect of Light and of Oxygen at the Bray-Lebhafsky Reaction, *J. Am. Chem. Soc.*, **97,** pp. 202-204.

[20] Sharma K R and Noyes R M (1976), Oscillations in Chemical Systems. 13. A Detailed Molecular Mechanism for the Bray-Lebhafsky Reaction of Iodate and Hydrogen Peroxide, *J. Am. Chem. Soc.*, **98,** pp. 4345-4360.

[21] Chopin-Dumas J. (1978), Diagramme d'etat de la reaction Bray, *Compt. Rend. Hebd. Sniences Acad.Sci.*, Ser. C, **287**, pp. 553-556 (in French).

[22] Edelson D and Noyes R M (1979), Detailed Calculation Modeling the Oscillating Bray-Lebhafsky Reaction,*J. Phys. Chem.*, **8**3(2), pp. 212-220.

[23] Liebhafsky H A., Furuichi R, and Roe G M (1981), Reaction Involving Hydrogen Peroxide, Iodine, and Iodate Ion. 7. The Smooth Catalytic Decomposition of Hydrogen Peroxide, Mainly at 50^OC, *J. Am. Chem. Soc.*, **103**, pp. 51-56.

[24] Petrenko O E and Grinchuk A V (1982), Autooscillatory Model of Oscillating Bray-Liebhafsky Reaction Based on Sharma-Noyes Mechanism, *Kinet.Catal.,* **23**, pp. 22-25.

[25] Odutola J A, Bohlander C A, and Noyes R.M. (1982), Chemical Oscillations and Instabilities. 45. Iodide Ion Measurements on the Oscillatory Iodate-Peroxide System, *J.Phys.Chem.*, **86**, pp. 818-824.

[26] D'Alba F and Di Lorenco S (1984), Oscillatory Phenomena. Application of the D'Alba-Di Lorenco Model to the Bray-Liebhafsky System and Others Derived from It, *J.Chem.Soc.,Faraday Trans. I.,* **80**, pp. 1415-1424.

[27] Field R J and Burger M (Eds.) (1985), *Oscillations and Traveling Waves in Chemical Systems*, J.Wiley, New York.

[28] Anić S and Kolar-Anić Lj (1986), The Oscillatory Decomposition of H_2O_2 Monitored by the Potentiometric Method with Pt and Ag^+/S^{2-} Indicator Electrode, *Ber. Bunsenges. Phys. Chem.*, **90**, pp.1084-1086.

[29] Schmitz G (1987), Cinetique de la reaction de Bray, *J. Chim. Phys.*, **84**, pp. 957-965 (in French).

[30] Anić S (1987), Usmeravanje razvoja oscilatornog razlaganja vodonik peroksida (Doctoral thesis), Faculty of Science, University of Belgrade, Belgrade (in Serbian).

[31] Kolar-Anić Lj and Schmitz G (1992), Mechanism of the Bray-Liebhafsky Reaction: Effect of the Oxidation of Iodous Acid by Hydrogen Peroxide, *J. Chem. Soc. Faraday Trans.*, **88**, pp. 2343-2349.

[32] Treindl L and Noyes R M (1993), A New Explanation of the Oscillations in the Bray-Lebhafsky Reaction, *J. Phys. Chem.*, **97**, pp. 11354-11362.

[33] Laurenczy G and Beck M T (1994), Effect of High Pressure on the Bray Reaction, *J. Phys. Chem.*, **98** pp. 5188-5189.

[34] Čupić Ž, Anić S, Terlecki-Baričević A, and Kolar-Anić Lj, (1995), The Bray-Liebhafsky Reaction. The Influence of some Polymers based on Poly(4-inilpiridine), *React. Kinet. Catal. Lett,* **54**, pp. 43-49.

[35] Terlecki-Baričević A, Čupić Ž, Anić S, Kolar-Anić Lj, Mitrovski S, and Ivanović S. (1995), Polyvinylpyridine supported Iron(III) Catalyst in Hydrogen Peroxide Decomposition, *J. Serb. Chem. Soc.*, **60**, pp. 969-979.

[36] Bowers P G, Hofstetter Ch, Letter C R, and Toomey R T (1995), Supersaturation Limit for Homogeneous Nucleation of Oxygen Bubbles in Water at Elevated Pressure: "Super-Henry's Law", *J. Phys. Chem.,* **99**,pp. 9632-9637.

[37] Noyes R M, Kalachev L V, and Field R J (1995), Mathematical Model of the Bray-Lebhafsky Oscillations *J. Phys. Chem.*, **99**, pp. 3514-3520.

[38] Kolar-Anić Lj, Mišljenović Đ, Anić S, and Nicolis G (1995), Influence of the Reduction of Iodate by Hydrogen Peroxide on the Model of the Bray-Liebhafsky Reaction, *React. Kinet. Catal. Lett*., **54**, pp. 35-41.

[39] Kolar-Anić Lj, Vukelić N, Mišljenović Đ, and Anić S (1995), On the Instability Domains of Some Models for the Model of Bray-Liebhafsky reaction, J. Serb. Chem. Soc., **60**, pp. 1005-1013, pp.1187.

[40] Bowers P G, Bar-Eli K, and Noeys R M (1996), Unstable Supersaturated Solutions of Gases in Liquids and Nucleation Theory, *J. Chem. Soc. Faraday Trans.*, **92**, pp. 2843-2849.

[41] Anić S and Kolar-Anić Lj (1996), The Bray-Liebhafsky Reaction. VI. Kinetic in the Iodine Oscillations, *J. Serb. Chem. Soc.*, **61**, pp. 885-891.

[42] Ševčík P and Adamčiková L' (1997), Effect of a Pressure Decrease and Stirring on the Oscillating Bray-Liebhafsky Reaction, *Chem. Phys. Lett.*, **267**, pp. 307-312.

[43] Radenković M, Schmitz G, and Kolar-Anić Lj (1997), Simulation of Iodine Oxidation by Hydrogen Peroxide in Acid Media, on the Basis of the Model of Bray-Liebhafsky Reaction, *J. Serb. Chem. Soc*., **62**, pp. 367-369

[44] Buchholtz F G and Broecker S (1998), Oscillations of the Bray-Liebhafsky Reaction at Low Rates in a Continuous Flow Stirred Tank Reactor, *J. Phys, Chem. A*, **102**, pp. 1556-1559.

[45] Stanisavljev D, Begović N, Žujović Z, Vučelić D, and Bačić G (1998), ^{1}H NMR Monitoring of Water Behaviour duting the Bray-Liebhafsky Oscillatory Reaction, *J. Phys, Chem. A*, **102**, pp. 6883-6886.

[46] Ševčík P and Adamčiková L' (1998), Effect of a Gases Bubbling and Stirring on the Bray-Liebhafsky Reaction, J. Phys. Chem. A, **102**, pp. 1288-1291.

[47] Čupić Ž (1998), Modeliranje mehanizma oscilatornih katalitičkih procesa, sa primenom na reakciju razlaganja vodonikperoksida (Doctoral thesis), Faculty of Physical Chemistry, University of Belgrade, Belgrade (in Serbian).

[48] Valent I, Adamčiková L', and Ševčík P (1998), Simulations of the Iodine Interphase Transport Effect on the Oscillating Bray-Liebhafsky Reaction, *J. Phys. Chem. A*, **102**, pp. 7576-7579.

[49] Vukojević V B, Pejić N D, Stanisavljev D R, Anić S R, and Kolar-Anić Lj Z (1999), Determination of Cl^-, Br^-, I^-, Malonic Acid and Quercetin by Perturbation of a Nonequilibrium Stationary State in the Bray-Liebhafsky Reaction, *The Analyst*, **124**, pp. 147-152.

[50] Čupić Ž and Kolar-Anić Lj (1999), Conctraction of the Model of Bray-Liebhafsky Oscillatory Reaction by Eliminating Intermediate I_2O, *J. Chem. Phys.*,**110**, pp. 3951-3954

[51] Čupić Ž and Kolar-Anić Lj (1999), Contraction of Complex Models by the Stoichiometric Network Analysis, in Advanced Science and Technology of Sintering, Stojanović B D, Skorokhod, V V, Nikolić, M V (Eds), Kluwer Academic/Plenum Publishers, New York, pp. 75-80.

[52] Shmitz G (1999), Effect of the Oxygen on the Bray-Liebhafsky Reaction, *Phys. Chem. Chem. Phys.*, **1**,pp. 4605-4608.

[53] Genigová J, Melicherčík M, Olexová A, and L' Treindl, L' (1999), Influence of the MoO_4^{2-} Ions on the Bray-Liebhafsky Oscillatory Reaction, *J. Phys. Chem. A*, **103***, pp. 4690-4692,

[54] Vukojević V, Anić S, and Kolar-Anić Lj. (2000), Investigation of Dynamical Behaviour of the Bray-Lebhafsky Reaction in the CSTR. Determination of Bifurcation points, *J. Phys. Chem.*, **104**, pp. 10731-10739.

[55] Ševčík P, Kissimonova K, and Adamčiková L' (2000), Oxygen Production in Oscillatory Bray-Liebhafsky Reaction, *J. Phys. Chem. A*, **104**, pp. 3958-3963.

[56] Ćirić J, Anić S, Čupić Ž, and Kolar-Anić Lj (2000), The Bray-Liebhafsky Oscillatory Reaction. Kinetic Investigation in Reduction and Oxidation Pathways Based on Hydrogen Peroxide Concentration Monitoring, *Science of Sintering,* **32**, pp. 187-196.

[57] Pejić N, Čupić Ž, Anić S, Vukojević V, and Kolar-Anić Lj (2001), The Oscillatory Bray-Liebhafsky Reaction as a Matrix for Analyzing Enzyme and Polymeric Catalysts for Hydrogen Peroxide, *Sci. Sinter.*, **33**,pp. 107-115.

[58] Kissimonov K, Valent I, Adamčiková L', and Ševšík P (2001), Numerical Simulations of the Oxygen Production in the Oscillating Bray-Liebhafsky Reaction, *Chem. Phys. Lett*. **341**, pp. 345-350.

[59] Vukojević V, Anić S, and Kolar-Anić, Lj (2002), Investigation ofi Dynamic Behaviour of the Bray-Liebhafsky Reaction in the CSTR. Propreties of the System Examined by Pulsed Perturbations with I^-, *Phys. Chem. Chem. Phys*, **4**, pp. 1276-1283.

[60] Láňova B and Vřešt'ál J (2002), Study of the Bray-Liebhafsky Reaction by On-Line Mass Spectrometry, *J. Phys.Chem. A*, **106**, pp. 1228–1232.

[61] Kéki S, Székely G, and Beck M T (2003), The Effect on Light on the Bray-Lebhafsky Reaction, *J. Phys. Chem. A*, **107**, pp. 73-75.

[62] Kolar-Anić Lj, Vukojević V, Peji N, Grozdić T, and Anić S (2004), Deterministic Chaos in Open Well Stirred Bray-Lebhafsky Reaction System, in Experimental Chaos, Boccaletti, S., Gluckman, B. J., Kurths, J., Pecora, L. M., Meucci, R. and Yordanov, O.(Eds), American Institute of Physics, *AIP Conference Proceding*, Melville, New York, **742**, pp. 3-8.

[63] Kolar-Anić Lj, Anić S, and Čupić Ž (2005), Characterization of the Catalysts by means of an Oscillatory Reaction, in Finely Dispersed Particles: Micro-, Nano-, and Atto-Engineering, Spasić A, Jyh-Ping H. (Eds.), RCR-Taylor&Francis, New York, pp. 191-216.

[64] Stanisavljev D R, Djordjević, A R, and Likar-Smiljanić, V D (2005), Investigation of Microwaves on the Oscillating Bray-Lebhafsky reaction, *Chem. Phys. Lett.*, **412**, pp. 420-424.

[65] Stanisavljev D R, Djordjević A R, and Likar-Smiljanić V D (2006), Microwaves and Coherence on the Bray-Lebhafsky Reaction, *Chem. Phys. Lett.*, **423**, pp. 59-62.

[66] Schmitz G, Kolar-Anić Lj, Anić S, Grozdić T, and Vukojević V (2006), Complex and Chaotic Oscillations in a Model for the Chatalytic Hydrogen Peroxide Decomposition under Open Reactor Conditions, *J. Phys. Chem. A*, **110**, pp. 10361-10368.

[67] Pejić N D, Blagojević S M, Anić S R, Vukojević V B, Mijatović M M, Ćirić J S, Marković Z S, Marković S D; and Kolar–Anić Lj Z (2007), Kinetic Determination of Morphine by means of Bray-Liebhafsky Oscillatory Reaction System using Analyte Pulse Perturbation Technique, *Anal. Chim. Acta*, **582** (2), pp. 367-374.

[68] Anić, S., Kostić, M., Ninić, M., Blagojević, S. and Kolar-Anić, Lj. (2007), Activation Energies as the Validity Criterion of a Model for Complex Reactions that can be in Oscillatory States, *Sciene of Sintering*, **39**, 77-83.

[69] Ivanović A, Čupić Ž, Janković, M, Kolar-Anić Lj, and Anić S (2008), The Chaotic Sequences in the Bray-Lebhafsky Reaction in an Open Reactor, *Phys. Chem. Chem. Phys.*, **10**, pp. 5848-5858.

[70] Ren J, Gao J, and Yang W (2008), Computational Simulation of Bray-Liebhafsky (BL) Oscillating Chemical Reaction, *Port. Electrochim. Acta*, **26**, pp. 349-360.

[71] Schmitz G, Kolar-Anić Lj, Anić S, and Čupić Ž (2008), Stoichiometric Network Analysis and Associated Dimensionless Kinetic Equations. Application to a Model of Bray-Liebhafsky Reaction, *J. Phys. Chem.*, **112**, pp. 13452-13457.

[72] Ren J, Gao J, Qu J, Wei X, Chen X, and Yang W (2008), Nonlinear Behavior in Bray-Libhafsky Chemical Reaction, *J. Chil. Chem. Soc.*, **53**(3), pp.1620-1623.

[73] Pejić N D (2009), Analitičke primene metode pulsne perturbacije Bray-Liebhafsy oscilatorne reakcije realizovane u otvorenom reaktoru, *Hemijska industrija*, **53**, 455-465 (In Serbian).

[74] Ivanović A Z, Čupić Ž D, Kolar-Anić Lj Z, Janković M M, and Anić S R (2009), Large Deviation Spectra of Chaotic Time Series from Bray–Liebhafsky Reaction, *Russ. J. Phys. Chem. A*, **83**, pp. 1526–1530.

[75] Kolar-Anić Lj, Čupić Ž, Schmitz G, and Anić S (2010), Improvement of the Stoichiometric Network Analysis for Determination of Instability Conditions of Complex Nonlinear Reaction System, *Chem. Eng. Sci.*, **65**,pp. 3718-3728.

[76] Shmitz G (2010), Iodine Oxidation by Hydrogen Peroxide in Acidic Solution, Bray-Liebhafsky Reaction and Other Related Reactions, *Phys. Chem. Chem. Phys.*, **12**, pp. 6605-6615.

[77] Olexová A, Mrákavová M, Melicherčík M, and Treindl L' (2010), Oscillatory System I⁻, H₂O₂, HClO₄: The Modified Form of the Bray-Liebhafsky Reaction, *J. Phys. Chem. A*, **114**, pp. 7026–7029.

[78] Kolar-Anić Lj, Čupić Ž, Vukojević V, and Anić S (2011), *Dinamika nelinearnih procesa*, University of Belgrade- Faculty of Physical Chemistry, Belgrade, (in Serbian).

[79] Ivanović-Šašić A, Marković V, Anić S, Kolar-Anić Lj, and Čupić Ž (2011), Structures of Chaos in Open Reaction Systems, *Phys. Chem. Chem. Phys.*, **13**, pp. 20162–20171.

[80] Shmitz G (2011), Iodine Oxidation by Hydrogen Peroxide and Bray-Liebhafsky Reaction: Effect of the Temperature, *Phys. Chem. Chem. Phys.*, **13**, pp. 7102-7111.

[81] Ren J, Gao J, and Yang W (2012), Numerical Simulation of the Behaviour of the Bray-Liebhafsky Oscillating Chemical Reaction by a Four-variable Model, *J. Mex. Che,. Soc.*, **56**, pp. 131-138.

[82] Čupić Ž, Ivanović-Šašić A, Anić S, Stanković B, Maksimović J, Kolar-Anić Lj, and Schmitz G (2013), Tourbillion in the Phase Space of the Bray-Liebhafsky Nonlinear Oscillatory Reaction and Related Multiple-Time-Scale Model, *MATCH Commum. Math. Comput. Chem.,* **69**, pp. 805-830.

[83] Dushman S (1904), The Rate of the Reaction between Iodic and Hydriodic Acids, *J. Phys. Chem.*, **8**, pp. 453-482.

BRANISLAV STANKOVIĆ AND SLOBODAN ANIĆ

BRIGHT SOLITONS FROM DEFOCUSING NONLINEARITIES

Olga V. Borovkova[1], Yaroslav V. Kartashov[1], Lluis Torner, [1] and Boris A. Malomed[2,1]

[1]ICFO-Institut de Ciencies Fotoniques, and Universitat Politecnica de Catalunya, Mediterranean Technology Park, 08860 Castelldefels (Barcelona), Spain.
[2]Department of Physical Electronics, School of Electrical Engineering, Faculty of Engineering, Tel Aviv University, Tel Aviv 69978, Israel, e-mail: malomed@post.tau.ac.il

Abstract. *We report that defocusing cubic media with spatially inhomogeneous nonlinearity, whose strength increases rapidly enough toward the periphery, can support stable localized modes. Such nonlinearity landscapes give rise to a variety of stable solitons in all three dimensions, including 1D fundamental and multihump states, 2D vortex solitons with arbitrarily high topological charges, and fundamental solitons in 3D. Moving solitons maintain their coherence, oscillating in the nonlinear potential as robust quasi-particles and colliding elastically. In addition to numerically found soliton families, particular solutions are found in an exact analytical form, and accurate approximations are developed for the entire families, including moving solitons. The original version of this paper was published in: O. V. Borovkova, Y. V. Kartashov, L. Torner, and B. A. Malomed, Phys. Rev. E **84**, 035602 (R) (2011).*
Key words*: Bright solitons, defocusing, nonlinearities.*
PACS numbers: 42.65.Jx; 42.65.Tg; 42.65.Wi; 05.45.Yv

1. Introduction

A commonly adopted principle underlying the studies of self-sustained localized modes (bright solitons) in various physical settings is that they are supported either by the focusing nonlinearity [1], or, in the form of gap solitons, by the defocusing nonlinearity combined with periodic linear potentials [2]. The formation of bright solitons was reported also in more sophisticated systems, where the nonlinearity periodically changes its magnitude, and even the sign, along the evolution variable or in

the transverse direction(s). One thus deals with the *nonlinearity management* if it oscillates between focusing and defocusing in the course of the evolution [3], while transversely modulated nonlinearity landscapes are known as *nonlinear lattices* [4]. The latter setting readily supports stable solitons in 1D [5], while it is much harder to employ it for the stabilization of 2D and 3D solitons [6]. Note also that a hole in a uniform defocusing background was used as a support for 1D and 2D solitons in Ref. [8], but in a combination with a linear trapping potential.

Guiding bright solitons by pure defocusing nonlinearities, without the help of a linear potential, is commonly considered impossible. The primary objective of this Rapid Communication is to demonstrate that this *is nevertheless possible*, if the strength of the defocusing term is modulated in space, growing fast enough towards the periphery. The existence of bright solitons in this setting is a consequence of the fact that, in contrast to media with homogeneous nonlinearities, when the presence of decaying tails of the soliton places it into the semi-infinite spectral gap of the linearized system, where defocusing nonlinearities cannot support any self-localization, in our case the growth of the nonlinearity coefficient makes the underlying equations *non-linearizable* for the decaying tails. A similar argument explains the existence of embedded solitons inside the continuous spectrum in self-focusing media [7].

2. Bright solitons from defocusing nonlinearities

We demonstrate that the spatially modulated defocusing nonlinearity supports stable bright solitons, both quiescent and coherently moving ones, in all three dimensions. Not only fundamental solitons, but also stable 1D multipoles and 2D vortex rings are obtained. The model is based on the nonlinear-Schrödinger/Gross-Pitaevskii equation for rescaled field amplitude q in optical media of dimension $D = 1, 2$, or the wave function in a Bose-Einstein condensate (BEC) of any dimension:

$$i\partial q / \partial x = -(1/2)\tilde{\nabla}^2 q + s(\mathbf{r})|q|^2 q. \tag{1}$$

Here x is the propagation distance or time, $\mathbf{r} = (h, z, t)$ is the set of transverse coordinates, $\tilde{\nabla}^2 = \partial^2/\partial h^2 + \partial^2/\partial z^2 + \partial^2/\partial t^2$, and $s(\mathbf{r}) > 0$ is the defocusing nonlinearity strength that varies in the radial direction. In optics, spatially inhomogeneous nonlinearities can be realized in various ways [4]. In particular, in photorefractive materials, such as $LiNbO_3$, nonuniform doping with Cu or Fe may considerably enhance the local nonlinearity [9]. In BEC spatially modulated nonlinearity

landscapes can be created, via the Feshbach resonance (FR), by nonuniform external fields [10,11]. We here assume that the strength of nonlinearity grows with radius as

$$s(\mathbf{r}) = (s_0 + s_2 r^2/2)\exp(ar^2) \tag{2}$$

with $s_0, s_2 > 0$, and $a > 0$ that may be fixed by scaling (we set $a = 1/2$ below). If the nonlinearity is controlled by the FR, the divergence of the nonlinearity strength at infinity implies that the background value of the control field at $r = \yen$ corresponds to the exact resonance. In the optical realization with dopants that give rise to the two-photon resonance, the effective modulation of the nonlinearity may be achieved via the inhomogeneity of the resonance detuning, controlled by an external field, with the exact resonance occurring at $r = \yen$.

For any D, Eq. (1) with $s(\mathbf{r})$ taken as per Eq. (2) admits particular analytical solutions for fundamental solitons:

$$q(r,x) = (a^2/s_2)^{1/2}\exp(ibx - ar^2/2), \tag{3}$$

with $b = -(Da/2 + s_0 a^2/s_2)$, where b is the propagation constant. For $s_2 = 0$, exact solutions for a vortex with topological charge $m = 1$ in 2D, and a dipole soliton in 1D are available too:

$$q(r,x) = (2s_0)^{-1/2}ar \exp(ibx + if - ar^2/2), \tag{4}$$

with $b = -a(1 + D/2)$, where azimuthal coordinate f is a part of the solution for $D = 2$.

The analytical solutions correspond to the particular values of propagation constant b [multiplying Eq. (1) by q^* and integrating, one can prove that the solitons may exist only for $b < 0$]. For *families* of fundamental solitons, a variational approximation (VA) can be developed in any D by adopting the ansatz suggested by the exact solutions, $q = A\exp(ibx - ar^2/2)$ (amplitude A is a variational parameter). Using the Lagrangian of Eq. (1), the VA yields the norm of the fundamental solitons as a function of b, written here for at $s_2 = 0$ and $s_0 = 1$:

$$U \equiv \int |q(\mathbf{r})|^2 d\mathbf{r} = -(p/a)^{D/2}(b + aD/2). \tag{5}$$

The comparison with numerical results presented in Figs. 1(c) and 3(c) demonstrates that the variational dependences $U(b)$ are virtually indistinguishable, on the scale of the figures, from their numerical counterparts for all dimensions. For the soliton's width, defined as $W = 2U^{-1}\int r |q(\mathbf{r})|^2 d\mathbf{r}$, the VA gives $W_{1D} = W_{3D}/2 = 2/(pa)^{1/2}$, $W_{2D} = (p/a)^{1/2}$. Numerically found widths approach these values with the increase of U, see, e.g., Fig. 5(b).

The steep anti-Gaussian profile of the modulation of the defocusing nonlinearity postulated in Eq. (2) is not a necessary condition for the existence of solitons. In fact

$s(r) \sim r^{D+e}$ with arbitrary $e > 0$, where D is the spatial dimension, is sufficient [14]. Furthermore, for the exponential profile $s(h) = a + \sinh^2(h)$, with any $a < 1$, it is easy to find an exact 1D soliton solution $w = (1-a)^{-1/2}\operatorname{sech}(h)$ with $b = -(1+a)/[2(1-a)]$, and for $s(h) = \cosh^2(h)$ one can find the exact dipole solution $w = 3^{1/2}\sinh(h)\operatorname{sech}^2(h)$ with $b = -5/2$. The system can be also made finite, thus presenting a nonlinear counterpart of quantum-dot potentials. An example is the 1D variant of Eq. (1) with $s(h) = (1/4)(1+3h^2)^2(1-h^2)^{-3}$, defined at $h^2 < 1$, which gives rise to an exact ground-state mode, $q(h,x) = (1-h^2)^2 \exp(-9ix/4)$.

Here we report numerical results for the basic version of model (2) with $s_2 = 0$ and $s_0 \circ 1$. Fundamental solitons are sought for as $q(\mathbf{r},x) = w(r)\exp(ibx)$. The solutions were found using the standard relaxation method that quickly converges to exact solitons for a properly selected initial guess. The stability of thus found solutions was investigated by numerical computation of eigenvalues for small perturbations (with the help of an ordinary eigenvalue solver), using the linearization of Eq. (1), and then verified through direct simulations of the perturbed evolution.
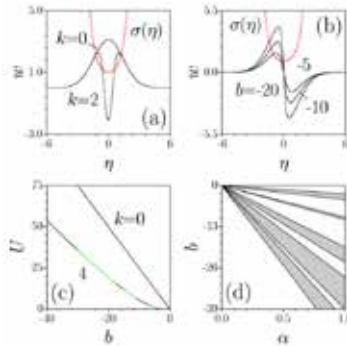
Figure 1.   (Color online) Profiles of 1D solitons: (a) with $b = -10$ and different numbers of nodes; (b) dipole solitons with different values of b. This and other figures are displayed for $a = 0.5$ in Eq. (2), with red horseshoe-shaped curves showing the nonlinearity modulation profile. (c) U vs. b for 1D solitons with different numbers of nodes, k. For $k = 0$, this dependence is indistinguishable from its variational counterpart (5) with $D = 1$. Here and in Fig. 3(c), stable and unstable portions of the soliton families are shown by black and green curves, respectively. (d) Stability (white) and instability (shaded) domains in the (a,b) plane for 1D solitons with $k = 5$. The fan-shaped structure here and in Fig. 3(d) below is a manifestation of the scaling invariance of Eq. (1).

As said above, our main result is that, in contrast to the belief that the defocusing nonlinearity cannot give rise to bright solitons, the inhomogeneous defocusing medium does support families of stable localized modes. The tails of the solitons of all types decay at $r \to \infty$ super-exponentially, irrespective of the dimension: $w|_{h \to \pm \infty} \approx (ar/2^{1/2}) \exp(-ar^2/2)$, which complies with exact solutions (4). Note that this asymptotic form does not contain the propagation constant b.

Examples of 1D solitons, with different numbers k of zeros (nodes) in the $w(h)$ shape, are displayed in Figs. 1(a) and 1(b). The solitons' amplitude increases with $|b|$, and the numerical results show that their width, at first, rapidly decreases and then saturates at $|b| \gtrsim 20$ (as predicted by the VA). For all types of the solitons, their energy flow (norm) increases with $|b|$ [Fig. 1(c)]. The solitons of higher orders have smaller norms, which is natural, taking into account the fact that, in terms of the mean-field description, the fundamental solitons, representing the ground state of the system, must minimize the chemical potential, $-b$, for a given norm.
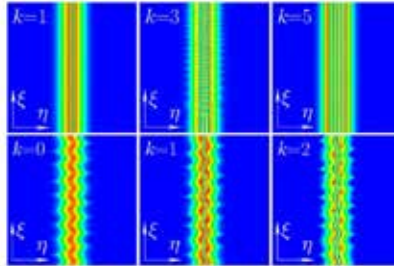
Figure 2. (Color online) Top row: Contour plots of $|q(h,x)|$ demonstrating the stable propagation of the perturbed 1D soliton with $k = 1$, $b = -10$ (left), instability of the one with $k = 3$, $b = -10$ (center), and stability of the complex mode with $k = 5$, $b = -13$ (right). Bottom row: Oscillations of 1D solitons with $k = 0, 1, 2$, $b = -20$, after the application of phase tilt $q = 1.5$.

The 1D solitons are remarkably robust. The computation of the stability eigenvalues demonstrates that the modes with $k = 0, 1, 2$ are stable at least up to $b = -40$ [in particular, this fact implies the stability of exact solution (4); it was checked that exact solution (3) is stable as well]. Only the families with $k \geq 3$ feature instability domains alternating with stability areas. The structure of the instability and stability domains becomes more complex with the increase of k, see Fig. 1(d) for

$k = 5$. We did not find any limit on the number of nodes possible in stable 1D solitons, hence even very complex structures (with $k \geq 10$) may be stable. Direct simulations of the evolution of perturbed solitons verify the predictions of the stability analysis: while stable solitons keep their shape over distances far exceeding $x = 10^3$, their unstable counterparts transform into irregularly breathing modes that remain tightly confined, see the top row in Fig. 2.

The physically relevant definition of solitons includes their ability to maintain the intrinsic coherence in the state of motion, and quasi-elastic collisions. Solitons may be set in motion multiplying them by $\exp(iqh)$, with phase tilt q. As a result, both 1D and 2D solitons start regular oscillations (see examples for 1D solitons with $k = 0, 1, 2$ in the bottom row of Fig. 2) – somewhat similar to matter-wave solitons in the cigar-shaped traps [12], with the difference that the nonlinearity is repulsive in the present setting, and the solitons oscillate in the effective nonlinear potential. An equation of motion for vectorial coordinate $\mathbf{R}(x)$ of the soliton can be readily derived in the quasi-particle approximation:

$$d^2\mathbf{R}/dx^2 = -2a(a/p)^{D/2}U_{\mathrm{D}}\exp(2aR^2)\mathbf{R},\tag{6}$$

$D = 1, 2$ (here U_{D} is the soliton's norm). As follows from Eq. (6), the squared frequency of small-amplitude oscillations of the kicked soliton is $w_{\mathrm{D}}^2 = 2a(a/p)^{D/2}U_{\mathrm{D}} + (3a/2)q^2$, which was found to be in a virtually exact agreement with results of numerical simulations. Further, we applied opposite kicks to two lobes of a 1D dipole, thus initiating oscillations and recurrent collisions of two solitons with opposite signs. It was found that the solitons keep bouncing from each other elastically. Assuming the instantaneous rebound, Eq. (6) predicts the frequency of the periodic collisions very accurately too. Thus, both 1D and 2D solitons are robust quasi-particle objects, that maintain their intrinsic coherence in the course of the motion and interact elastically.

The 2D version of the model gives rise to vortex solitons, $q(r, x) = w(r)\exp(imf + ibx)$, for all integer values of topological charge m, see Figs. 3(a) and 3(b). For the same reason as in 1D, the vortices with different m, while having completely different asymptotic forms at $r \circledR 0$, become identical at $r \circledR ¥$ (in contrast to vortex solitons in focusing media, that considerably broaden with the increase of the topological charge [13]). The increase of $|b|$ results in a gradual contraction of the vortex rings toward $r = 0$ [Fig. 3(b)]. The energy flow (norm) carried by the 2D solitons at fixed b decreases with the increase of m [Fig. 3(c)], similar to the 1D case, cf. Fig. 1(c).
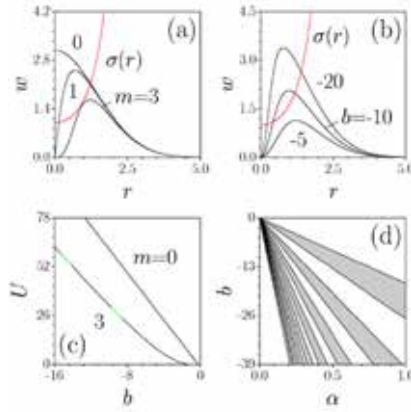
Figure 3. (Color online) Profiles of 2D solitons: (a) for $b = -10$ and different vorticities m; (b) for $m = 2$ and different values of b. (c) U vs. b for different m [the curve for $m = 0$ is indistinguishable from the variational result (5) with $D = 2$]. (d) The lowest stability (white) and instability (shaded) domains in the (a, b) plane for vortex solitons with $m = 2$.

Another essential result is that, due to the defocusing character of the nonlinearity, azimuthal instabilities, that are fatal for vortex solitons in focusing media [13], are suppressed in our system. We have found that the solitons with $m = 0$ and $m = 1$ [including the 2D exact solution (4)] are completely stable, while the vortices with $m > 1$ give rise to a complex structure of stability and instability domains. This structure can be produced upon substituting a perturbed solution,

$$q = [w(r) + u(r)\exp(inf + dx) + v^*(r)\exp(- inf + d^*x)]\exp(imf + ibx),$$

with azimuthal perturbation index n, into Eq. (1), and solving the corresponding linear eigenvalue problem. The structure of the stability domains is displayed in Fig. 3(d) for vortices with $m = 2$, that can be destroyed by perturbations with $n = 2$ at certain values of b (similarly, at $m > 2$ the most destructive perturbations pertain to $n = m, m \pm 1$). Note that the stability and instability domains are equidistantly spaced in b. We stress that conspicuous stability regions have been found for all the considered values of m. An example of the stable evolution of a perturbed vortex ring, which keeps its structure over indefinitely long distances, is shown in Fig. 4(a). Unstable vortex solitons (with $m \geq 2$) tend to split into m separate unitary vortices, that stay in a vicinity of the pivotal point, performing persistent rotation around it, which is a

consequence of the conservation of the angular momentum. Examples for $m = 2$ and 3 are displayed in Figs. 4(b) and 4(c).
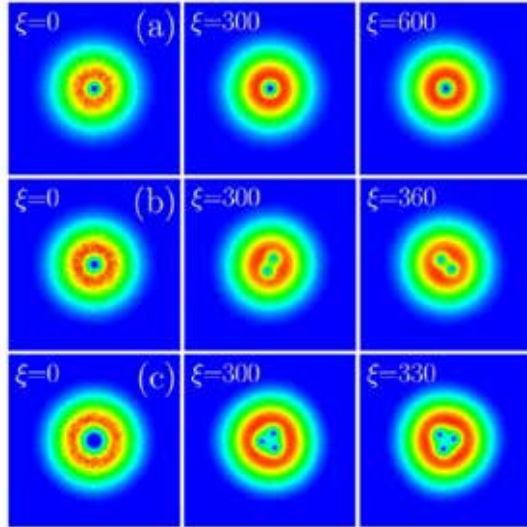
Figure 4.   (Color online) (a) Stable propagation of the perturbed vortex soliton with $m = 2$, $b = -17$. (b) Splitting of the unstable double vortex $(m = 2)$ with $b = -11$ into a steadily rotating pair of unitary vortices. (c) Splitting of the unstable vortex with $m = 3$, $b = -9$ into a rotating set of three vortices.
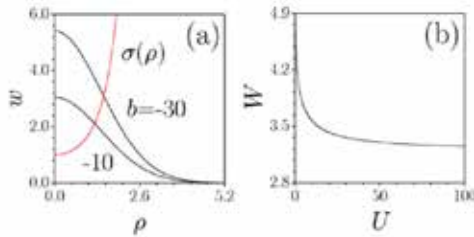
Figure 5.   (Color online) (a) Profiles of fundamental 3D solitons at $a = 0.5$. (b) The width of these solitons vs. the norm.

The 3D model also supports bright solitons with rapidly vanishing tails (recall the 3D model makes sense for BEC, but not in optics, unlike its 1D and 2D counterparts). Examples of such spherically symmetric fundamental solitons are shown

in Fig. 5(a). The norm of the 3D solitons increases almost linearly with $|b|$, in accordance with Eq. (5), while their width rapidly saturates to the aforementioned VA-predicted value, $W_{3D} = 4/(pa)^{1/2}$ [Fig. 5(b)]. The 3D fundamental solitons are completely stable in their entire existence domain, as illustrated by Fig. 6.
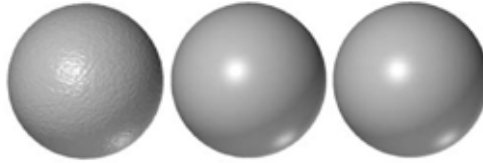
Figure 6.   Isosurface plots drawn at the level of $0.1 \max |q|$ at $x = 0$ (left), $x = 300$ (center), and $x = 600$ (right), showing stable propagation of the perturbed 3D soliton with $b = -10$.

3. Conclusions

Summarizing, it is found that, in contrast to the usual expectations, the defocusing nonlinearity, without any linear potential, may support families of stable bright solitons in all dimensions, provided that the nonlinearity strength increases rapidly enough from the center to the periphery. In addition to the fundamental solitons, we show that such media support a variety of stable higher-order modes, including 1D multipoles and 2D vortex rings with all values of the topological charge. If set in motion, the solitons move and interact as particles. The settings considered here may be implemented for matter waves in BEC and for light waves in optical materials.

References

1.   Y. S. Kivshar and G. P. Agrawal, *Optical Solitons: From Fibers to Photonic Crystals* (Academic Press, San Diego, 2003).
2.   V. A. Brazhnyi and V. V. Konotop, Mod. Phys. Lett. B **18**, 627 (2004); O. Morsch and M. Oberthaler, Rev. Mod. Phys. **78**, 179 (2006).
3.   L. Torner, IEEE Photonics Technol. Lett. **11**, 1268 (1999); I. Towers and B. A. Malomed, J. Opt. Soc. Am. **19**, 537 (2002); F. K. Abdullaev *et al.*, Phys. Rev. A **67**, 013605 (2003); H. Saito and M. Ueda, Phys. Rev. Lett. **90**, 040403 (2003); M. Centurion *et al.*, Phys. Rev. Lett. **97**, 033903 (2006); B. A. Malomed, *Soliton Management in Periodic Systems* (Springer, New York, 2006).

4. Y. V. Kartashov, B. A. Malomed, and L. Torner, Rev. Mod. Phys. **83**, 247 (2011).

5. H. Sakaguchi and B. A. Malomed, Phys. Rev. E **72**, 046610 (2005); G. Fibich, Y. Sivan, and M. I. Weinstein, Physica D **217**, 31 (2006); J. Garnier and F. K. Abdullaev, Phys. Rev. A **74**, 013604 (2006); D. L. Machacek *et al.*, Phys. Rev. E **74**, 036602 (2006); Y. Kominis and K. Hizanidis, Opt. Lett. **31**, 2888 (2006); J. Belmonte-Beitia *et al.*, Phys. Rev. Lett. **98**, 064102 (2007); P. Niarchou *et al.*, Phys. Rev. A **76**, 023615 (2007);Y. V. Kartashov, V. A. Vysloukh, and L. Torner, Opt. Lett. **33**, 1747; 2173 (2008); Y. Sivan, G. Fibich, and B. Ilan, Phys. Rev. E **77**, 045601(R) (2008); F. K. Abdullaev *et al.*, Phys. Rev. A **77**, 023615 (2008); H. A. Cruz, V. A. Brazhnyi, and V. V. Konotop, J. Phys. B **41**, 035304 (2008).

6. H. Sakaguchi and B. A. Malomed, Phys. Rev. E **73**, 026601 (2006); Y. Sivan, G. Fibich, and M. I. Weinstein, Phys. Rev. Lett. **97**, 193902 (2006); Y. V. Kartashov *et al.*, Opt. Lett. **34**, 770 (2009); N. V. Hung *et al.*, Phys. Rev. E **82**, 046602 (2010).

7. J. Yang, B. A. Malomed, and D. J. Kaup, Phys. Rev. Lett. **83**, 1958 (1999); A. R. Champneys *et al.*, Physica D **152-153**, 340 (2001); J. Yang, Phys. Rev. A **82**, 053828 (2010).

8. V. Pérez-García and R. Pardo, Physica D **238**, 1352 (2009).

9. J. Hukriede, D. Runde, and D. Kip, J. Phys. D: Appl. Phys. **36**, R1 (2003).

10. P. O. Fedichev *et al.*, Phys. Rev. Lett. **77**, 2913 (1996); S. Inouye *et al.*, Nature **392**, 151 (1998); M. Marinescu and L. You, Phys. Rev. Lett. **81**, 4596 (1998); M. Theis *et al.*, Phys. Rev. Lett. **93**, 123001 (2004).

11. I. Bloch, J. Dalibard, and W. Zwerger, Rev. Mod. Phys. **80**, 885 (2008); C. Chin *et al.*, *ibid*. **82**, 1225 (2010).

12. K. E. Strecker *et al.*, New J. Phys. **5**, 731 (2003).

13. B. A. Malomed *et al.*, J. Opt. B: Quant. Semicl. Opt. **7**, R53 (2005).

14. O. V. Borovkova *et al.*, Opt. Lett. **36**, 3088 (2011).

MODERN CONCEPTS OF ACTIVELY CONTROLLED SMART STRUCTURES – AN OVERALL DESIGN APPROACH

Tamara Nestorović

Institute of Computational Engineering, Mechanics of Adaptive Systems
Ruhr-Universität Bochum, Universitätsstraße 150, D-44801 Bochum, Germany
e-mail: tamara.nestorovic@rub.de

Abstract. *Mechanical lightweight structures often tend to unwanted vibrations due to disturbances. Passive methods for increasing the structural damping are often inadequate for the vibration suppression, since they include additional mass in the form of damping materials, additional stiffening elements or mass damper. This paper presents a modern concept for active control of smart structures using piezoelectric materials. The approach is especially well suited for light weight structures and it is presented through several subsequent steps: modeling (model identification and numerical modeling), optimization, controller design, simulation and experimental verification/testing.*

1. Introduction

High efficiency, functionality, quality and assuring a high profitability are the main requirements for products in today's world. In the field of engineering, these properties are manifested in application of thin and lightweight structures. Mechanical lightweight structures often tend to unwanted vibration, which may result in disturbing sound radiation or even in damage of components [1]. Passive methods for increasing the structural damping are often inadequate, because they always include the use of additional mass in the form of damping materials, additional stiffening designs or mass damper.

The concept of active vibration control has become a useful approach in the recent years, due to improvement of the vibration susceptibility of lightweight structures with the least possible increase in mass. For the active vibration control, supporting mechanical structure is supplied with sensors and actuators operated by a controller. High integration of the structural system with active materials (actuators/sensors) and control is regarded as a smart structure due to its ability to adapt to environmental changes. The technology of smart materials and structures, especially piezoelectric smart structures, has become mature over the last decade. One promising application of piezoelectric smart structures is the control and suppression of unwanted structural vibrations [2].

2. State of the art

Smart structures have been intensively investigated in the past years. In numerous studies the smart structure community has developed a large variety of sophisticated analysis approaches, control methods and optimization procedures. A review of the state of the art of smart structures is given by Chopra [3] and some other examples of analytical and experimental studies concerning the actuation and vibration control of smart piezoelectric structures can be found in [4]–[10]. Different approaches to modeling and vibration suppression of a piezoelectric cantilever beam have been investigated and reported in the literature. In [11] for example, the effect of different types of controllers to vibration reduction of the beam have been studied. In [12] the feedback control with a time delay was used in the investigation of vibration control for the primary resonance of a cantilever beam. The analytical results are compared with numerical simulations.

Modeling and controller design techniques presented in this paper are successfully applied for the vibration suppression of higher bending modes then investigated in [12], [13]. Proposed controller in combination with augmented plant dynamics [6]–[8] can be successfully used in the presence of combined disturbances and for the vibration suppression of even higher modes.

In [13] active vibration control of a flexible cantilever beam was studied using the Filtered-X LMS algorithm, applied to design a control law for a piezoelectric actuator. In comparison with this algorithm, we propose in this paper the technique with the optimal LQ controller and Kalman estimator which results in considerably faster controlled response in the time domain, and in higher vibration magnitude suppression in the frequency domain.

Paper by Tjahyady et al. [15] also deals with the vibration control of a flexible cantilever beam. The control technique applied here is adaptive resonant control. For the controller design purposes, the model of the beam, i.e. its first three natural frequencies were estimated using the RLS algorithm. In the present paper the model development procedure is based on the subspace based identification algorithm (n4sid). The proposed identification procedure is of special interest if a state space model of the structure is required for the subsequent design and analysis phases. State space models are especially convenient for the multiple-input multiple-output (MIMO) control design problems. Unlike in [15], where only the single-input single-output system was considered, we propose efficient methodology for MIMO systems. In one of our papers [16] we have also presented implementation of a user-defined piezoelectric finite shell element in order to model piezoelectric properties of smart structures. The element efficiency was tested through several examples of a bimorph piezoelectric beam.

3. Modeling of smart structures

In the overall design procedure of actively controlled smart structures in this paper two modeling approaches are proposed: *experimental model identification*, which requires a real or a prototype structure, and *finite element (FE) based numeric approach*.

3.1. Experimental model identification – subspace based approach

The models identified by a subspace based identification procedure are obtained in a general discrete-time state space form. This form is convenient for the controller design as well as for the comparison with the models obtained through FE procedure.

The state space representation of an nth-order system with m inputs and l outputs which should be identified from the input-output measurement data can be expressed in its general deterministic-stochastic form [17]:

$$\mathbf{x}[k+1] = \mathbf{\Phi}\mathbf{x}[k] + \mathbf{\Gamma}\mathbf{u}[k] + \boldsymbol{w}[k]$$
$$\mathbf{y}[k] = \mathbf{C}\mathbf{x}[k] + \mathbf{D}\mathbf{u}[k] + \boldsymbol{v}[k] \tag{1}$$

Since the subspace identification is based on sampled input/output measurement sequences $\mathbf{u}[k]$ and $\mathbf{y}[k]$, the method applies to a discrete-time form of the resulting state-space model, with discrete-time state and control matrices $\mathbf{\Phi}$ and $\mathbf{\Gamma}$, respectively. The process noise and the measurement noise vector sequences $\boldsymbol{w}[k]$ and $\boldsymbol{v}[k]$ are white noise with zero mean and with covariance matrix:

$$\mathcal{E}\left\{ \begin{bmatrix} \boldsymbol{w}[i] \\ \boldsymbol{v}[j] \end{bmatrix} \begin{bmatrix} \boldsymbol{w}[i]^{\text{T}} & \boldsymbol{v}[j]^{\text{T}} \end{bmatrix} \right\} = \begin{bmatrix} \mathbf{Q} & \mathbf{S} \\ \mathbf{S}^{\text{T}} & \mathbf{R} \end{bmatrix}. \tag{2}$$

The task of the subspace identification is to express the input-state-output relationships in the state space form (1) and to determine the order n of the unknown system and the system matrices $\mathbf{\Phi} \in \mathsf{R}^{n \times n}$, $\mathbf{\Gamma} \in \mathsf{R}^{n \times m}$, $\mathbf{C} \in \mathsf{R}^{l \times n}$, $\mathbf{D} \in \mathsf{R}^{l \times m}$ as well as the covariance matrices $\mathbf{Q} \in \mathsf{R}^{n \times n}$, $\mathbf{S} \in \mathsf{R}^{n \times l}$, $\mathbf{R} \in \mathsf{R}^{l \times l}$ of the noise sequences $\boldsymbol{w}[k]$ and $\boldsymbol{v}[k]$. In the subsequent derivations, only the pure deterministic case will be considered as described in [18]. Measured input and output data are arranged into block Hankel matrices [19] defined in the following way:

$$\mathbf{U} = U_{0|2i-1} = \begin{bmatrix} \mathbf{u}_0 & \mathbf{u}_1 & \mathbf{u}_2 & \cdots & \mathbf{u}_{j-1} \\ \mathbf{u}_1 & \mathbf{u}_2 & \mathbf{u}_3 & \cdots & \mathbf{u}_j \\ \vdots & \vdots & \vdots & \ddots & \vdots \\ \mathbf{u}_{i-1} & \mathbf{u}_i & \mathbf{u}_{i+1} & \cdots & \mathbf{u}_{i+j-2} \\ \hline \mathbf{u}_i & \mathbf{u}_{i+1} & \mathbf{u}_{i+2} & \cdots & \mathbf{u}_{i+j-1} \\ \mathbf{u}_{i+1} & \mathbf{u}_{i+2} & \mathbf{u}_{i+3} & \cdots & \mathbf{u}_{i+j} \\ \vdots & \vdots & \vdots & \ddots & \vdots \\ \mathbf{u}_{2i-1} & \mathbf{u}_{2i} & \mathbf{u}_{2i+1} & \cdots & \mathbf{u}_{2i+j-2} \end{bmatrix}. \tag{3}$$

The output block Hankel matrix $\mathbf{Y}$ is defined in a similar way. The purpose of writing the matrix in this manner is to build the relations between the input, output and state sequences in a matrix form. Using the matrix notation, the system equation can be written as:

$$\mathbf{Y}[k] = \mathbf{Gx}[k] + \mathbf{HU}[k].\tag{4}$$

The matrix $\mathbf{G}$ is the extended observability matrix built as

$$\mathbf{G} = \begin{bmatrix} \mathbf{C} \\ \mathbf{C\Phi} \\ \mathbf{C\Phi}^2 \\ \vdots \\ \mathbf{C\Phi}^{i-1} \end{bmatrix} \in \mathsf{R}^{li \times n}\tag{5}$$

and $\mathbf{H}$ is the lower block triangular Toeplitz matrix of impulse responses from $\mathbf{u}$ to $\mathbf{y}$:

$$\mathbf{H} = \begin{bmatrix} \mathbf{D} & 0 & 0 & \cdots & 0 \\ \mathbf{C\Gamma} & \mathbf{D} & 0 & \cdots & 0 \\ \mathbf{C\Phi\Gamma} & \mathbf{C\Gamma} & \mathbf{D} & \cdots & 0 \\ \vdots & \vdots & \vdots & \ddots & \vdots \\ \mathbf{C\Phi}^{i-2}\mathbf{\Gamma} & \mathbf{C\Phi}^{i-3}\mathbf{\Gamma} & \mathbf{C\Phi}^{i-4}\mathbf{\Gamma} & \cdots & \mathbf{D} \end{bmatrix} \in \mathsf{R}^{li \times n}.\tag{6}$$

For a deterministic case the problem is simplified to determining $\mathbf{G}$ and $\mathbf{H}$ by computing the singular value decomposition (SVD) of $\mathbf{U}$ in the first step

$$\mathbf{U} = \mathbf{PSQ}^{\mathrm{T}} = \begin{bmatrix} \mathbf{P}_{u1} & \mathbf{P}_{u2} \end{bmatrix} \begin{bmatrix} \Sigma_u & 0 \end{bmatrix} \begin{bmatrix} \mathbf{Q}_{u1}^{\mathrm{T}} \\ \mathbf{Q}_{u2}^{\mathrm{T}} \end{bmatrix}.\tag{7}$$

If matrix $\mathbf{U}$ has dimension $m \times n$ and rank r, then the partition in (7) is performed as follows:

$$\mathbf{P} = \begin{bmatrix} \mathbf{p}_1 & \cdots & \mathbf{p}_r & | & \mathbf{p}_{r+1} & \cdots & \mathbf{p}_m \end{bmatrix} = \begin{bmatrix} \mathbf{P}_{u1} & \mathbf{P}_{u2} \end{bmatrix}\tag{8}$$

$$\mathbf{Q} = \begin{bmatrix} \mathbf{q}_1 & \cdots & \mathbf{q}_r & | & \mathbf{q}_{r+1} & \cdots & \mathbf{q}_m \end{bmatrix} = \begin{bmatrix} \mathbf{Q}_{u1} & \mathbf{Q}_{u2} \end{bmatrix}\tag{9}$$

where $\mathbf{p}_i$ are the left singular vectors of $\mathbf{U}$. It can be shown that they are eigenvectors of $\mathbf{UU}^{\mathrm{T}}$. Vectors $\mathbf{q}_i$ are the right singular vectors of $\mathbf{U}$. It can be shown that they are eigenvectors of $\mathbf{U}^{\mathrm{T}}\mathbf{U}$. Multiplying (4) by $\mathbf{Q}_{u2}$, matrix $\mathbf{G}$ can be determined from a SVD of $\mathbf{YQ}_{u2}$. Then matrix $\mathbf{C}$ is obtained as the first row of the observability matrix $\mathbf{G}$, and matrix $\mathbf{\Phi}$ is calculated from: $\underline{\mathbf{G}} = \overline{\mathbf{G}}\,\mathbf{\Phi}$ applying pseudo inverse, where $\overline{\mathbf{G}}$ is obtained by dropping the last row of $\mathbf{G}$. Matrix $\underline{\mathbf{G}}$ represents the matrix obtained by dropping the first row of $\mathbf{G}$. For the calculation of $\mathbf{\Gamma}$ and $\mathbf{D}$ matrices, (4) is multiplied by the pseudo inverse of $\mathbf{U}$ on the right and by $\mathbf{P}_{u2}^{\mathrm{T}}$ from (7) on the left. Thus the equation is reduced to

$$\mathbf{P}_{u2}^{\mathrm{T}}\mathbf{Y}\mathbf{U}^{-1} = \mathbf{P}_{u2}^{\mathrm{T}}\mathbf{H} \,. \tag{10}$$

After rearranging, (10) can be solved for $\mathbf{\Gamma}$ and $\mathbf{D}$ using the least squares, see (6). In this way the system parameters in the form of state-space matrices of the model (1) are identified using the subspace-based identification method.

3.2. Finite element approach for model development of piezoelectric smart structures

If a real structure or a prototype are not available, which is especially the case in the early development phases, as well as in design review or optimization phases, another efficient modeling methodology is proposed, based on the FE approach. The FE based modeling of piezoelectric adaptive smart systems and structures represents a good basis for the overall simulation and design. This approach enables both a suitable controller design [6], [8] and the appropriate actuator/sensor placement [20].

FE based modeling of piezoelectric smart structures and systems relies on a standard modeling procedure for coupled electro-mechanical behavior. The FE analysis is based on the finite element semi-discrete form of the equations of motion of a piezoelectric smart system describing its electro-mechanical behavior. These equations can be derived using the established approximation method of displacements and electric potential and the standard finite element procedure. Here the coupled electro-mechanical behavior of smart structures will be considered. In the formulation used in this paper the temperature is assumed to be constant and electro-mechanical coupling in the domain of linear piezoelectricity is considered.

Constitutive equations in the stress-charge form (11) are used for the development of the equations of motion for a smart structure:

$$\mathbf{\sigma} = \mathbf{C}\mathbf{\varepsilon} - \mathbf{e}\mathbf{E}, \qquad \mathbf{D} = \mathbf{e}^{\mathrm{T}}\mathbf{\varepsilon} + \mathbf{\kappa}\mathbf{E} \tag{11}$$

with following notations: $\mathbf{\sigma}^{\mathrm{T}} = \begin{bmatrix} \sigma_{11} & \sigma_{22} & \sigma_{33} & \sigma_{12} & \sigma_{23} & \sigma_{31} \end{bmatrix}$ mechanical stress vector, $\mathbf{C}_{(6\times6)}$ symmetric elasticity matrix, $\mathbf{\varepsilon}^{\mathrm{T}} = \begin{bmatrix} \varepsilon_{11} & \varepsilon_{22} & \varepsilon_{33} & 2\varepsilon_{12} & 2\varepsilon_{23} & 2\varepsilon_{31} \end{bmatrix}$ strain vector, $\mathbf{E}^{\mathrm{T}} = \begin{bmatrix} E_1 & E_2 & E_3 \end{bmatrix}$ electric field vector, $\mathbf{e}_{(6\times3)}$ piezoelectric matrix, $\mathbf{D}^{\mathrm{T}} = \begin{bmatrix} D_1 & D_2 & D_3 \end{bmatrix}$ vector of electrical displacement and $\mathbf{\kappa}_{(3\times3)}$ symmetric dielectric matrix. The system of equations which describe electromechanical behavior consists of the constitutive equations (11) together with the mechanical equilibrium and electric equilibrium (charge equation of electrostatics resulting from the 4th Maxwell equation):

$$\mathbf{D}_u^{\mathrm{T}}\mathbf{\sigma} + \mathbf{P} - \rho\mathbf{v} = \mathbf{0}, \qquad \mathbf{D}_\varphi^{\mathrm{T}}\mathbf{D} = \mathbf{0} \tag{12}$$

where $\mathbf{P}^{\mathrm{T}} = \begin{bmatrix} P_1 & P_2 & P_3 \end{bmatrix}$ represents the body force vector, $\mathbf{v}^{\mathrm{T}} = \begin{bmatrix} v_1 & v_2 & v_3 \end{bmatrix}$ is the vector of mechanical displacements, ρ is the mass density and $\mathbf{D}_u$ and $\mathbf{D}_\phi$ are differentiation matrices:

$$\mathbf{D}_u^{\mathrm{T}} = \begin{bmatrix} \dfrac{\partial}{\partial x_1} & 0 & 0 & \dfrac{\partial}{\partial x_2} & 0 & \dfrac{\partial}{\partial x_3} \\[2mm] 0 & \dfrac{\partial}{\partial x_2} & 0 & \dfrac{\partial}{\partial x_1} & \dfrac{\partial}{\partial x_3} & 0 \\[2mm] 0 & 0 & \dfrac{\partial}{\partial x_3} & 0 & \dfrac{\partial}{\partial x_2} & \dfrac{\partial}{\partial x_1} \end{bmatrix}, \mathbf{D}_\varphi^{\mathrm{T}} = \begin{bmatrix} \dfrac{\partial}{\partial x_1} & \dfrac{\partial}{\partial x_2} & \dfrac{\partial}{\partial x_2} \end{bmatrix}. \quad (13)$$

Variational statement of the governing equations for the coupled electro-mechanical problem derived from the Hamilton's principle represents the basis for development of the finite element model [21]–[23]. It is obtained in the form:

$$-\int_V \left(\rho\, \delta\mathbf{v}^{\mathrm{T}} \ddot{\mathbf{v}} - \delta\boldsymbol{\varepsilon}^{\mathrm{T}} \mathbf{C}\boldsymbol{\varepsilon} + \delta\boldsymbol{\varepsilon}^{\mathrm{T}} \mathbf{e}^{\mathrm{T}} \mathbf{E} \right) dV + \int_V \left(\delta\mathbf{E}^{\mathrm{T}} \mathbf{e}\boldsymbol{\varepsilon} + \delta\mathbf{E}^{\mathrm{T}} \boldsymbol{\kappa}\mathbf{E} + \delta\mathbf{v}^{\mathrm{T}} \mathbf{F}_{\mathrm{V}} \right) dV$$
$$+\int_{\Omega_1} \delta\mathbf{v}^{\mathrm{T}} \mathbf{F}_\Omega\, d\Omega + \delta\mathbf{v}^{\mathrm{T}} \mathbf{F}_{\mathrm{P}} - \int_{\Omega_2} \delta\varphi\, q\, d\Omega - \delta\varphi Q = 0 \quad (14)$$

where F_Ω represents the surface applied forces (defined on surface Ω_1), F_P the point loads, ϕ the electric potential, q the surface charge brought on surface Ω_2 and Q the applied concentrated electric charges. Applying the approximation of displacements and electric potential with the shape functions over an element, representing the structure by a finite number of elements and adding up all elements contributions, the finite element semi-discrete form of the equations of motion is obtained:

$$\mathbf{M}\ddot{\mathbf{q}} + \mathbf{D}_d \dot{\mathbf{q}} + \mathbf{K}\mathbf{q} = \mathbf{F} = \bar{\mathbf{E}}\mathbf{f}(t) + \bar{\mathbf{B}}\mathbf{u}(t) \quad (15)$$

where vector $\mathbf{q}$ represents the vector of generalized displacements including mechanical displacements and electric potential and contains all degrees of freedom:

$$\mathbf{q}^{\mathrm{T}} = [\mathbf{u}_1^{\mathrm{T}} \quad \phi_1 \mid \mathbf{u}_2^{\mathrm{T}} \quad \phi_2 \mid \cdots \mid \mathbf{u}_n^{\mathrm{T}} \quad \phi_n]. \quad (16)$$

Matrices $\mathbf{M}$, $\mathbf{D}_d$ and $\mathbf{K}$ are the mass matrix, the damping matrix and the stiffness matrix, respectively.

The total load vector $\mathbf{F}$ in (15) is split for the purpose of the control design into the vector of external forces $\mathbf{F}_E$ and the vector of control forces $\mathbf{F}_C$:

$$\mathbf{F} = \mathbf{F}_{\mathrm{E}} + \mathbf{F}_{\mathrm{C}} = \bar{\mathbf{E}}\bar{\mathbf{f}}(t) + \bar{\mathbf{B}}\bar{\mathbf{u}}(t) = \mathbf{B}_0 \mathbf{u}. \quad (17)$$

The forces are here generalized quantities, which include also electric charges or electric potentials. Matrices $\bar{\mathbf{E}}$ and $\bar{\mathbf{B}}$ describe the positions of generalized external forces $\bar{\mathbf{f}}$ and the control parameters $\bar{\mathbf{u}}$ in the finite element structure, respectively. Matrix $\mathbf{B}_0$ represents the input matrix, and vector $\mathbf{u}$ includes all model inputs.

For the controller design purposes equation (15) is accompanied by the output equation in the form:

$$\mathbf{y} = \mathbf{C}_{0q}\mathbf{q} + \mathbf{C}_{0v}\dot{\mathbf{q}} \quad (18)$$

where in a general case $\mathbf{C}_{0q}$ represents the output displacement matrix, and $\mathbf{C}_{0v}$ the output velocity matrix. Matrices $\mathbf{C}_{0q}$ and $\mathbf{C}_{0v}$ are obtained through an FE procedure by defining appropriate sensor locations.

Solution of the equation (15) is determined in the form $\mathbf{q} = \boldsymbol{\varphi} e^{j\omega t}$ by solving the eigenvalue problem for a homogeneous case:

$$\det(\mathbf{K} - \omega^2 \mathbf{M}) = 0 \tag{19}$$

which is satisfied for n different pars ω_i, $\boldsymbol{\varphi}_i$, with $n = n_{dof}$ being the total number of degrees of freedom, ω_i the ith natural frequency and $\boldsymbol{\varphi}_i$ the ith mode shape vector. The solution can be represented in the matrix form by the matrix of natural eigenfrequencies $\boldsymbol{\Omega}$ (spectral matrix) and the modal matrix $\boldsymbol{\Phi}_{\text{m}}$:

$$\boldsymbol{\Omega} = \begin{bmatrix} \omega_1 & 0 & \cdots & 0 \\ 0 & \omega_2 & \cdots & 0 \\ \cdots & \cdots & \cdots & \cdots \\ 0 & 0 & \cdots & \omega_n \end{bmatrix}, \ \boldsymbol{\Phi}_{\text{m}} = \begin{bmatrix} \varphi_{11} & \varphi_{21} & \cdots & \varphi_{n1} \\ \varphi_{12} & \varphi_{22} & \cdots & \varphi_{n2} \\ \cdots & \cdots & \cdots & \cdots \\ \varphi_{1n_{dof}} & \varphi_{2n_{dof}} & \cdots & \varphi_{nn_{dof}} \end{bmatrix} = \begin{bmatrix} \boldsymbol{\varphi}_1 & \boldsymbol{\varphi}_2 & \cdots & \boldsymbol{\varphi}_n \end{bmatrix}. \tag{20}$$

The tools for modal reduction are also included, which enable development of appropriate models with reduced orders for the controller design. Based on the modal truncation, which was adopted as a suitable technique for the reduction of the number of equations in the FE models, a state space model of an actively controlled structure can be obtained in the form convenient for the controller design. A limited number of eigenmodes of interest is taken into account, while the remaining modes are truncated. Introducing the modal coordinates $\mathbf{z}$

$$\mathbf{q}(t) = \boldsymbol{\Phi}_{\text{m}} \mathbf{z}(t) \tag{21}$$

into equation (15), and applying the ortho-normalization with $\boldsymbol{\Phi}_{\text{m}}^{\text{T}} \mathbf{M} \boldsymbol{\Phi}_{\text{m}} = \mathbf{I}$, $\boldsymbol{\Phi}_{\text{m}}^{\text{T}} \mathbf{K} \boldsymbol{\Phi}_{\text{m}} = \boldsymbol{\Omega}$, $\boldsymbol{\Delta} = \boldsymbol{\Phi}_{\text{m}}^{\text{T}} \mathbf{D}_{\text{d}} \boldsymbol{\Phi}_{\text{m}}$, where $\boldsymbol{\Delta}$ represents the modal damping matrix and $\mathbf{D}_{\text{d}}$ is the damping matrix with Rayleigh damping $\mathbf{D}_{\text{d}} = \alpha \mathbf{M} + \beta \mathbf{K}$, the state space model of the modally reduced system can be obtained in the form:

$$\dot{\mathbf{x}} = \begin{bmatrix} \mathbf{0} & \mathbf{I} \\ -\boldsymbol{\Omega} & -\boldsymbol{\Delta} \end{bmatrix} \mathbf{x} + \begin{bmatrix} \mathbf{0} \\ \boldsymbol{\Phi}^{\text{T}} \overline{\mathbf{B}} \end{bmatrix} \mathbf{u}(t) + \begin{bmatrix} \mathbf{0} \\ \boldsymbol{\Phi}^{\text{T}} \overline{\mathbf{E}} \end{bmatrix} \mathbf{f}(t) \tag{22}$$

where $\mathbf{x}(t) = \begin{bmatrix} \mathbf{z} & \dot{\mathbf{z}} \end{bmatrix}^{\text{T}}$ represents a state-space vector. With the state and the output equations, the state space model is represented in the form:

$$\dot{\mathbf{x}}(t) = \mathbf{A}\mathbf{x}(t) + \mathbf{B}\mathbf{u}(t) + \mathbf{E}\mathbf{f}(t), \quad \mathbf{y} = \mathbf{C}\mathbf{x}(t) + \mathbf{D}\mathbf{u}(t) + \mathbf{F}\mathbf{f}(t) \tag{23}$$

which is convenient for the controller design.

Models of the form (23) obtained through modal reduction should fulfill the controllability/observability criteria. Through a balanced modal reduction such models

can be obtained. The task of the balanced reduction is actually to find such state transformation, which provides equal controllability and observability of retained modes. In other words, the controllability and observability grammians of the retained modes are diagonal and equal, and based on this criteria balanced model reduction can be performed. Ranks of the controllability and observability matrices, although relatively simple criteria, provide only an answer to the controllability/observability question in terms "yes" or "no". As very well known, if the rank of the controllability/observability matrices is equal to the number of states, the model i.e. the realization is controllable/observable. This approach gives good results only for lower system orders, otherwise numerical difficulties may be encountered.

Controllability and observability properties of the state space systems can be qualitatively expressed in terms of controllability ($\mathbf{P}$) and observability ($\mathbf{Q}$) grammians, defined in the following way:

$$\mathbf{P} = \int_0^\infty e^{\mathbf{A}t}\mathbf{B}\mathbf{B}^\mathrm{T}e^{\mathbf{A}^\mathrm{T}t}dt, \quad \mathbf{Q} = \int_0^\infty e^{\mathbf{A}t}\mathbf{C}^\mathrm{T}\mathbf{C}e^{\mathbf{A}^\mathrm{T}t}dt \tag{24}$$

$\mathbf{P}$ and $\mathbf{Q}$ satisfy algebraic Lyapunov linear matrix equations:

$$\mathbf{A}\mathbf{P} + \mathbf{P}\mathbf{A}^\mathrm{T} = -\mathbf{B}\mathbf{B}^\mathrm{T}, \quad \mathbf{A}^\mathrm{T}\mathbf{Q} + \mathbf{Q}\mathbf{A} = -\mathbf{C}^\mathrm{T}\mathbf{C} . \tag{25}$$

For an arbitrary transformation of the states by some transformation matrix, appropriate grammians are obtained, with the property that the eigenvalues of the controllability and observability grammians products remain invariant. These invariants are the Hankel singular values of the system, and they represent the basis of the balanced model reduction. In balanced realization each state (mode) is equally controllable and observable and the reduced order model is obtained by truncating the least controllable and observable modes. For more details the readers are referred to [20].

4. Controller design for smart structures

Here we propose two control techniques for smart structures, with primary aim of vibration suppression: optimal LQ controller with additional dynamics and model reference adaptive control.

4.1. Optimal LQ control with additional dynamics and Kalman filter

Optimal controller with additional dynamics includes available a priori knowledge about occurring disturbance type contained in the additional dynamics [4]. Such an a priori knowledge is available in terms of type of the disturbance function which has to be rejected or whose influence should be suppressed by the controller. Periodic disturbances with frequencies corresponding to the eigenfrequencies of a smart structure can cause resonance states and their suppression is therefore important.

As a starting point for the controller design a discrete-time state space equivalent (26) of the state space model (23) developed through the FEM procedure and modal reduction is used:

$$\mathbf{x}[k+1] = \mathbf{\Phi}\mathbf{x}[k] + \mathbf{\Gamma}\mathbf{u}[k] + \mathbf{\varepsilon}\mathbf{w}[k], \qquad \mathbf{y}[k] = \mathbf{C}\mathbf{x}[k] + \mathbf{D}\mathbf{u}[k] + \mathbf{F}\mathbf{w}[k] \qquad (26)$$

with:

$$\mathbf{\Phi} = e^{\mathbf{A}T}; \quad \mathbf{\Gamma} = \int_0^T e^{\mathbf{A}\tau}\mathbf{B}d\tau; \quad \mathbf{\varepsilon} = \int_0^T e^{\mathbf{A}\tau}\mathbf{E}d\tau \qquad (27)$$

where T represents the sampling interval for a discrete-time system.

Using the a priori knowledge about the disturbance type, which has to be suppressed, the model of the disturbance is represented in an appropriate state-space form, where the disturbance is assumed to be the output of the state-space representation. The poles λ_i of the disturbance transfer function are used to define the additional dynamics using the coefficients of the polynomial:

$$\delta(z) = \prod_i (z - e^{\lambda_i T})^{m_i} = z^s + \delta_1 z^{s-1} + \dots + \delta_s \qquad (28)$$

where m_i represents the multiplicity of the pole λ_i. Additional dynamics is expressed in a state-space form:

$$\mathbf{x}_a[k+1] = \mathbf{\Phi}_a\mathbf{x}_a[k] + \mathbf{\Gamma}_a\mathbf{e}[k] ; \qquad (29)$$

where $\mathbf{x}_a$ is the vector of the state variables for the additional dynamics, $\mathbf{e}$ is the error signal and the state-space matrices of the additional dynamics are:

$$\mathbf{\Phi}_a = \begin{bmatrix} -\delta_1 & 1 & 0 & \cdots & 0 \\ -\delta_2 & 0 & 1 & \cdots & 0 \\ \vdots & \vdots & \vdots & \ddots & \vdots \\ -\delta_{s-1} & 0 & 0 & \cdots & 1 \\ -\delta_s & 0 & 0 & \cdots & 0 \end{bmatrix}, \; \mathbf{\Gamma}_a = \begin{bmatrix} -\delta_1 \\ -\delta_2 \\ \vdots \\ -\delta_{s-1} \\ -\delta_s \end{bmatrix}. \qquad (30)$$

For multiple-input multiple-output (MIMO) systems additional dynamics is replicated q times (once per each output). In this case the replicated additional dynamics is defined as:

$$\bar{\mathbf{\Phi}} \stackrel{def}{=} diag(\underbrace{\mathbf{\Phi}_a,\dots,\mathbf{\Phi}_a}_{q\,\text{times}}), \quad \bar{\mathbf{\Gamma}} \stackrel{def}{=} diag(\underbrace{\mathbf{\Gamma}_a,\dots,\mathbf{\Gamma}_a}_{q\,\text{times}}) \qquad (31)$$

The discrete-time design model ($\mathbf{\Phi}_d$, $\mathbf{\Gamma}_d$) is formed as a cascade combination of the additional dynamics ($\mathbf{\Phi}_a$, $\mathbf{\Gamma}_a$) or ($\bar{\mathbf{\Phi}}, \bar{\mathbf{\Gamma}}$) and the discrete-time plant model ($\mathbf{\Phi}, \mathbf{\Gamma}$):

$$\mathbf{x}_d[k+1] = \mathbf{\Phi}_d\mathbf{x}_d[k] + \mathbf{\Gamma}_d\mathbf{u}[k] ; \qquad (32)$$

$$\mathbf{\Phi}_d = \begin{bmatrix} \mathbf{\Phi} & \mathbf{0} \\ \mathbf{\Gamma}^* \mathbf{C} & \mathbf{\Phi}^* \end{bmatrix}, \ \mathbf{\Gamma}_d = \begin{bmatrix} \mathbf{\Gamma} \\ \mathbf{0} \end{bmatrix}, \ \mathbf{x}_d = \begin{bmatrix} \mathbf{x}[k] \\ \mathbf{x}_a[k] \end{bmatrix} \tag{33}$$

where $\mathbf{\Phi}^*$ and $\mathbf{\Gamma}^*$ denote respectively $\mathbf{\Phi}_a$ and $\mathbf{\Gamma}_a$ in the case of single-input single-output systems or $\overline{\mathbf{\Phi}}$ and $\overline{\mathbf{\Gamma}}$ for MIMO systems. For the design model (32) the feedback gain matrix $\mathbf{L}$ of the optimal LQ controller is calculated in such a way that the feedback law $\mathbf{u}[k] = -\mathbf{L}\mathbf{x}_d[k]$ minimizes the performance index (34) subject to the constraint (32), where $\mathbf{Q}$ and $\mathbf{R}$ are symmetric, positive-definite matrices:

$$J = \frac{1}{2} \sum_{k=0}^{\infty} (\mathbf{x}_d[k]^T \mathbf{Q}\mathbf{x}_d[k] + \mathbf{u}[k]^T \mathbf{R}\mathbf{u}[k]) . \tag{34}$$

The matrices $\mathbf{Q}$ and $\mathbf{R}$ in (34) are the designer specified symmetric positive definite weighting matrices. The feedback gain matrix $\mathbf{L}$ of the optimal LQ control law for a discrete-time state space system is determined through the algorithm for the synthesis of a linear quadratic (LQ) state-feedback regulator by determining:

$$\mathbf{L} = \left(\mathbf{R} + \mathbf{\Gamma}^T \mathbf{P} \mathbf{\Gamma} \right)^{-1} \mathbf{\Gamma}^T \mathbf{P} \mathbf{\Phi}, \tag{35}$$

where $\mathbf{P}$ is obtained as a solution of the discrete-time Riccati equation [24] in the form:

$$\mathbf{\Phi}^T \mathbf{P} \mathbf{\Phi} - \mathbf{P} - \mathbf{\Phi}^T \mathbf{P} \mathbf{\Gamma} \left(\mathbf{R} + \mathbf{\Gamma}^T \mathbf{P} \mathbf{\Gamma} \right)^{-1} \mathbf{\Gamma}^T \mathbf{P} \mathbf{\Phi} + \mathbf{Q} = \mathbf{0} \tag{36}$$

which, after rearrangement, can be written in the form [4]:

$$\mathbf{P} = \mathbf{Q} + \mathbf{\Phi}^T \mathbf{P} \mathbf{\Phi} - \mathbf{\Phi}^T \mathbf{P} \mathbf{\Gamma} \left(\mathbf{R} + \mathbf{\Gamma}^T \mathbf{P} \mathbf{\Gamma} \right)^{-1} \mathbf{\Gamma}^T \mathbf{P} \mathbf{\Phi}. \tag{37}$$
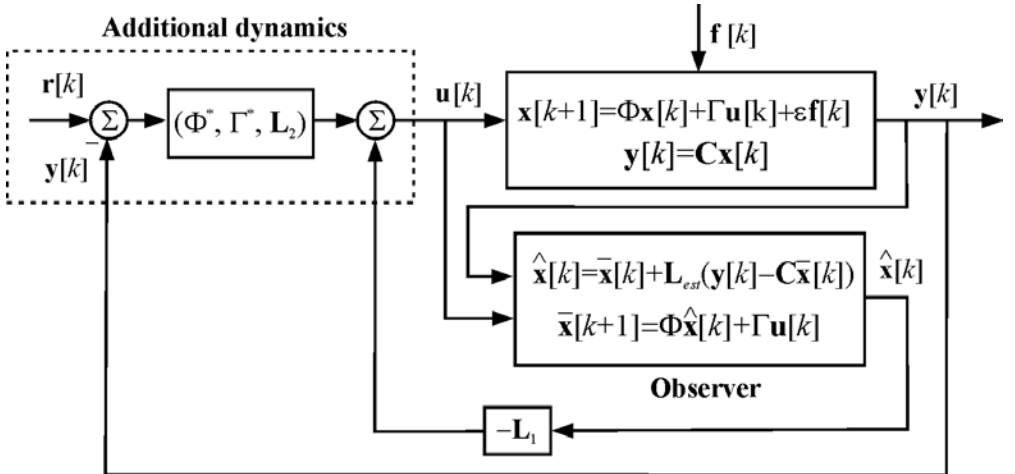
Figure 1: Optimal LQ control system with additional dynamics and observer.

The choice of the weighting matrices $\mathbf{Q}$ and $\mathbf{R}$ in the performance index is designer dependant and it is based on the relative importance of the various states and controls. The trade-off between the control effort and the system response determines the choice of the weighting matrices. In general, the weighting matrices are chosen in such a way that large input signals are penalized by increasing the value of the matrix $\mathbf{R}$ and faster response of appropriate state variables is achieved by increasing the values of appropriate elements in the weighting matrix $\mathbf{Q}$.

In the end the feedback gain matrix $\mathbf{L}$ is partitioned into:

$$\mathbf{L} = \begin{bmatrix} \mathbf{L}_1 & \mathbf{L}_2 \end{bmatrix} \tag{38}$$

so that $\mathbf{L}_1$ corresponds to the state-space model of the controlled structure, and $\mathbf{L}_2$ to the modeled additional dynamics. Block diagram of the optimal LQ control system with additional dynamics is represented in Fig. 1.

The role of the observer is to estimate the model state variables, which cannot be directly measured. For the state estimation the Kalman filter can be used. Equations for the Kalman filter design based on the current estimator assume the state-space equation of the plant in the form (26) and the measurements depending on the state variables and influenced by the measurement noise $\mathbf{y}[k] = \mathbf{C}\mathbf{x}[k] + v[k]$. The covariances of the process and measurement noise are denoted as $E(ww^{\mathrm{T}}) = \mathbf{Q}_w$ and $E(vv^{T}) = \mathbf{R}_v$, respectively. Then the Kalman estimator is defined by the following equations:

$$\hat{\mathbf{x}}[k] = \overline{\mathbf{x}}[k] + \mathbf{L}_{est}[k](\mathbf{y}[k] - \mathbf{C}\overline{\mathbf{x}}[k]), \qquad \overline{\mathbf{x}}[k+1] = \mathbf{\Phi}\hat{\mathbf{x}}[k] + \mathbf{\Gamma}\mathbf{u}[k] \tag{39}$$

with the Kalman gain matrix:

$$\mathbf{L}_{est}[k] = \mathbf{P}[k]\mathbf{C}^{\mathrm{T}}\mathbf{R}_v^{-1} \tag{40}$$

and:

$$\mathbf{P}[k] = \mathbf{M}_k[k] - \mathbf{M}_k[k]\mathbf{C}^{\mathrm{T}}(\mathbf{C}\mathbf{M}_k[k]\mathbf{C}^{\mathrm{T}} + \mathbf{R}_v)^{-1}\mathbf{C}\mathbf{M}_k[k] \tag{41}$$

$$\mathbf{M}_k[k+1] = \mathbf{\Phi}\mathbf{P}[k]\mathbf{\Phi}^{\mathrm{T}} + \mathbf{\varepsilon}\mathbf{Q}_w\mathbf{\varepsilon}^{\mathrm{T}} \tag{42}$$

Matrices $\mathbf{P}$ and $\mathbf{M}_k$ are determined by solving equations (41)–(42).

4.2. Model reference adaptive control (MRAC)

Another approach to the controller design suggested in this paper is model reference adaptive control. Controller design is based on the prescribed reference model, which defines the desired behavior of the controlled structure. In this case the available structural model is used for the investigation on the reference model prescription. Applied control technique is a direct model reference adaptive controller [6], [25], which includes the innovative integral term in the adaptation law of the adaptive gains [26], [27] to achieve robustness with respect to the boundness of the system states and adaptive gains, with small tracking errors. The model reference adaptive controller is designed as a discrete-time controller.

With general bounded, unknown and unmeasurable plant and output disturbances $\mathbf{f}_x[k]$ and $\mathbf{f}_y[k]$ respectively, discrete-time model (26) can be represented in the following form:

$$\mathbf{x}[k+1] = \mathbf{\Phi}\mathbf{x}[k] + \mathbf{\Gamma}\mathbf{u}[k] + \mathbf{f}_x[k], \quad \mathbf{y}[k] = \mathbf{C}\mathbf{x}[k] + \mathbf{D}\mathbf{u}[k] + \mathbf{f}_y[k] \tag{43}$$

For a general discrete-time state space plant model (43) the control objective of the MRAC system is to find without an explicit knowledge of the state matrices $\mathbf{\Phi}$ and $\mathbf{\Gamma}$, which contain the system parameters, such control law $\mathbf{u}[k]$ that the plant output $\mathbf{y}[k]$ follows the output $\mathbf{y}_m[k]$ of a specified reference model with the least possible error. Direct robust MRAC algorithm is derived from the general model reference adaptive tracking problem [25]. MRAC system is based on the reference model, specified by the designer, which reflects the desired behavior of the controlled structure (Fig. 2). The reference model is prescribed in a discrete-time state space form:

$$\mathbf{x}_m[k+1] = \mathbf{\Phi}_m\mathbf{x}_m[k] + \mathbf{\Gamma}_m\mathbf{u}_m[k], \quad \mathbf{y}_m[k] = \mathbf{C}_m\mathbf{x}_m[k] \tag{44}$$

where $\mathbf{\Phi}_m$ and $\mathbf{\Gamma}_m$ represent the discrete-time state and control matrices, respectively, $\mathbf{C}_m$ is the output matrix, $\mathbf{x}_m \in R^{n_m \times 1}$ is the state vector, $\mathbf{u}_m \in R^{m_m \times 1}$ the command vector and $\mathbf{y}_m \in R^{p_m \times 1}$ the output of the reference model.
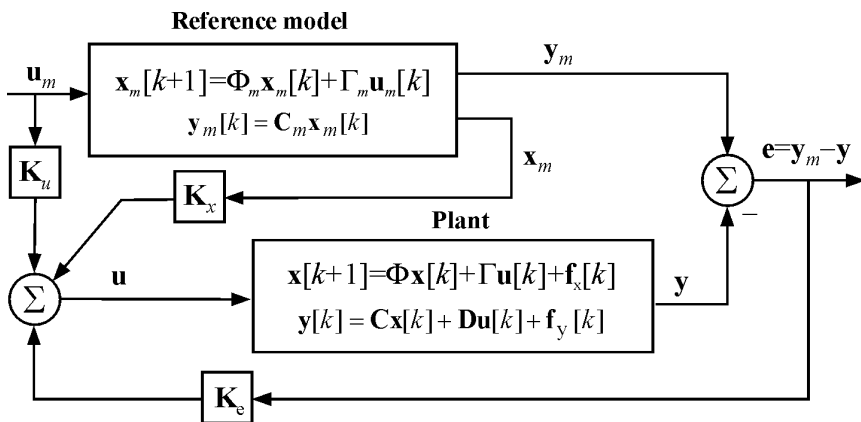
Figure 2: General form of a discrete-time MRAC system.

The output tracking error is defined as:

$$\mathbf{e}_y[k] = \mathbf{y}_m[k] - \mathbf{y}[k]. \tag{45}$$

The reference model is designed to meet some desired performance properties. Since its output prescribes the behavior of the plant output, the number of reference model outputs has to be equal to the number of the plant outputs ($p_m=p$). Otherwise it is

independent of the controlled plant. Further it is required that the reference model is asymptotically stable. The model is assumed to be bounded-input/bounded-state stable. Since the reference model only represents desired behavior of the controlled structure, the dimension n_m of the reference model state vector may be much less than the dimension n of the plant state, which is practically the case with large flexible smart structures. Regarding the stated requirements, the reference model can be designed by selecting the parameters which provide asymptotic stability. Desired responses of the reference model can be obtained by an appropriate parameter selection and confirmed through an iterative simulation and through tuning procedures. Generally it is required to achieve the desired properties of the reference model and therefore of the controlled system output, maintaining at the same time the simplicity of the control system. The lower reference model orders are preferred on one hand due to reduced computational effort. On the other hand, the simulated prescribed behavior of the reference model must comply with the real behavior of the controlled plant, i.e. of its model in the simulation. Too low orders of the reference model sometimes do not fulfill this requirement and therefore cannot be used to prescribe the controlled behavior which complies with the realistic behavior of the controlled plant. The task of the reference model selection becomes therefore a trade-off between the requirement for the lower reference model order and control algorithm simplicity on one hand, and the requirement that the reference model represents the realistic possible behavior of the controlled plant.
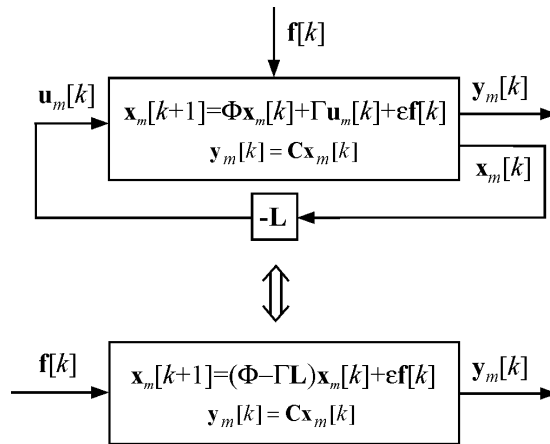
Figure 3: Equivalent representations of the reference model.

With this regard in this paper the selection of the reference model is proposed, based on the equivalent representation of the closed-loop feedback control system (Fig. 3) with an optimal LQ controller, designed using the procedure explained in section 4.1, which provides the desired behavior in the sense of the suppressed output magnitudes subjected to control in the presence of periodic excitations. Realistic prescription of the desired behavior is possible if the influence of the excitations is taken into account in the design of the reference model. In such a case the excitations represent the input of the

reference model and the reference model in turn outputs the optimally controlled behavior. In Fig. 3 the first block diagram represents the feedback system with the plant model used for the reference model design. Discrete-time plant model is defined based on the equations (26) and has the form given in the upper block of the first block-diagram in Fig. 3. Here **f** represents periodic excitations with the frequencies corresponding to selected eigenfrequencies of the plate or acoustic fluid. The feedback loop is closed by:

$$\mathbf{u}_m[k] = -\mathbf{L}\mathbf{x}_m[k]. \tag{46}$$

where **L** represents the feedback gain matrix of the optimal LQ controller, designed using the procedure explained in section 2 in such a way that the controller minimizes the performance index:

$$J = \frac{1}{2}\sum_{k=0}^{\infty}(\mathbf{x}_m[k]^T\mathbf{Q}_m\mathbf{x}_m[k] + \mathbf{u}_m[k]^T\mathbf{R}_m\mathbf{u}_m[k]) \tag{47}$$

with symmetric, positive-definite weighting matrices $\mathbf{Q}_m$ and $\mathbf{R}_m$. An equivalent representation of the closed-loop reference system in the upper block-diagram is represented in the lower block-diagram, which corresponds to the reference model designed to meet the requirements of the desired plant behavior with the reduced output.

With regard to the control objective the realization ($\boldsymbol{\Phi}$, $\boldsymbol{\Gamma}$) is supposed to be controllable and output stabilizable, the realization ($\boldsymbol{\Phi}$, **C**) is supposed to be observable and the matrix $\boldsymbol{\Gamma}$ is assumed to have a maximum rank. Then, a discrete-time direct model reference adaptive law is expressed in the following form:

$$\begin{aligned}\mathbf{u}[k] &= \mathbf{K}_r[k]\mathbf{r}[k] \\ &= \mathbf{K}_e[k]\mathbf{e}_y[k] + \mathbf{K}_x[k]\mathbf{x}_m[k] + \mathbf{K}_u[k]\mathbf{u}_m[k]\end{aligned} \tag{48}$$

where the adaptive gains as well as the vectors $\mathbf{e}_y$, $\mathbf{x}_m$ and $\mathbf{u}_m$ are concatenated within appropriate matrices of dimensions $m \times n_r$ and $n_r \times 1$, respectively:

$$\mathbf{K}_r[k] = \begin{bmatrix} \mathbf{K}_e[k] & \mathbf{K}_x[k] & \mathbf{K}_u[k] \end{bmatrix}, \quad \mathbf{r}[k] = \begin{bmatrix} \mathbf{e}_y[k] \\ \mathbf{x}_m[k] \\ \mathbf{u}_m[k] \end{bmatrix}. \tag{49}$$

The control task involves several objectives. The output tracking error $\mathbf{e}_y$ (45) should be minimized by the adaptive system. In a general case the output can be affected by an external disturbance or a measurement disturbance, which are represented by the term $\mathbf{f}_y[k]$ in the general plant output equation (43). Disturbance or excitation affecting the states of the plant $\mathbf{f}_x[k]$ is included in the state equation (43). The robust stability and performance of the controlled system in the presence of a wide class of input signals and input or output disturbances/excitations is the aim of the control. In [6] it was shown that the adaptive controller is able to maintain small tracking errors in non-ideal environment. This property reflects the robustness of the adaptive controller with respect

to boundness of the states, errors and adaptive gains. The adaptive gain $\mathbf{K}_r[k]$ in (26) is determined as a sum of proportional and integral parts $\mathbf{K}_p$ and $\mathbf{K}_I$ respectively:

$$\mathbf{K}_r[k] = \mathbf{K}_p[k] + \mathbf{K}_I[k] \tag{50}$$

According to the basic model reference adaptive algorithm the proportional and integral gains are adapted in the following way:

$$\mathbf{K}_p[k] = \mathbf{e}_y \mathbf{r}^T(t)\overline{\mathbf{T}},$$
$$\mathbf{K}_I[k+1] = \mathbf{e}_y \mathbf{r}^T[k]\mathbf{T}, \quad \mathbf{K}_I(0) = \mathbf{K}_{I0} \tag{51}$$

where $\mathbf{T}$ and $\overline{\mathbf{T}}$ are $n_r \times n_r$ time-invariant weighting matrices and $\mathbf{K}_{I0}$ is the initial integral gain.

Another aspect of the control requirements regards the convergence of the adaptive gains. In the robust model reference adaptive control approach the integral gain differs from the basic adaptive algorithm in (51). The robust model reference control system should successfully face disturbances (or the parameter variation viewed in terms of unmodeled or unknown dynamics). In ideal conditions without disturbances the integral gain increases as long as the error exists. When the integral gain reaches a certain stabilizing value the error begins to decrease and it decreases further till it reaches the zero value. Than the integral gain stops increasing and maintains some stabilizing constant value. In realistic environment due to disturbances the error does not reach the zero value and thus the integral gain never stops increasing. Although almost strictly positive real structures are theoretically proven to be stable in the presence of high gains, the infinite increase of the integral gains can lead to divergence of the adaptive control system or to numeric instability in the presence of disturbances. A modification of the integral gain in (50) by adding a σ-term is therefore introduced [6], [26], in order to guarantee the convergence. Discrete-time form of the robust adaptation with respect to the integral gain convergence is:

$$\mathbf{K}_I[k+1] = \mathbf{e}_y[k]\mathbf{r}^T[k]\mathbf{T} - \sigma\mathbf{K}_I[k]. \tag{52}$$

A condition, which the plant (43) including disturbances or excitations should fulfill in order to be globally stable with respect to boundness, is that it is almost strictly positive real [6], [27] and that the disturbances are bounded. In that case the states, gains and errors involved in the adaptive control are bounded. In order to guarantee robust stability, perfect tracking is not obtained in general, but the adaptive controller maintains a small tracking error over large ranges of non-ideal conditions and uncertainties.

5. Application examples

Implementation of the overall design procedure for vibration control of smart structures is demonstrated through several examples. Through the experimental application of control and simulation results, the possibilities of the successful vibration control are shown.

Examples include vibration control of a clamped cantilever beam, the funnel shaped inlet of the magnetic resonance tomography, and the car roof.
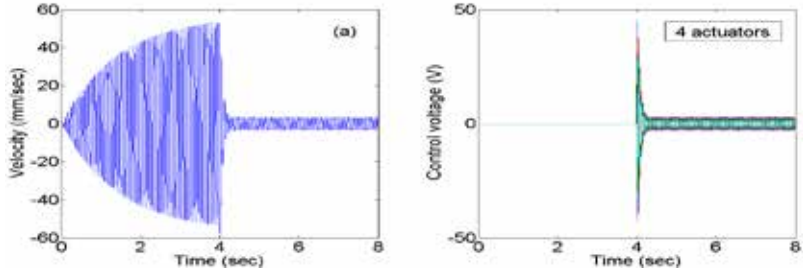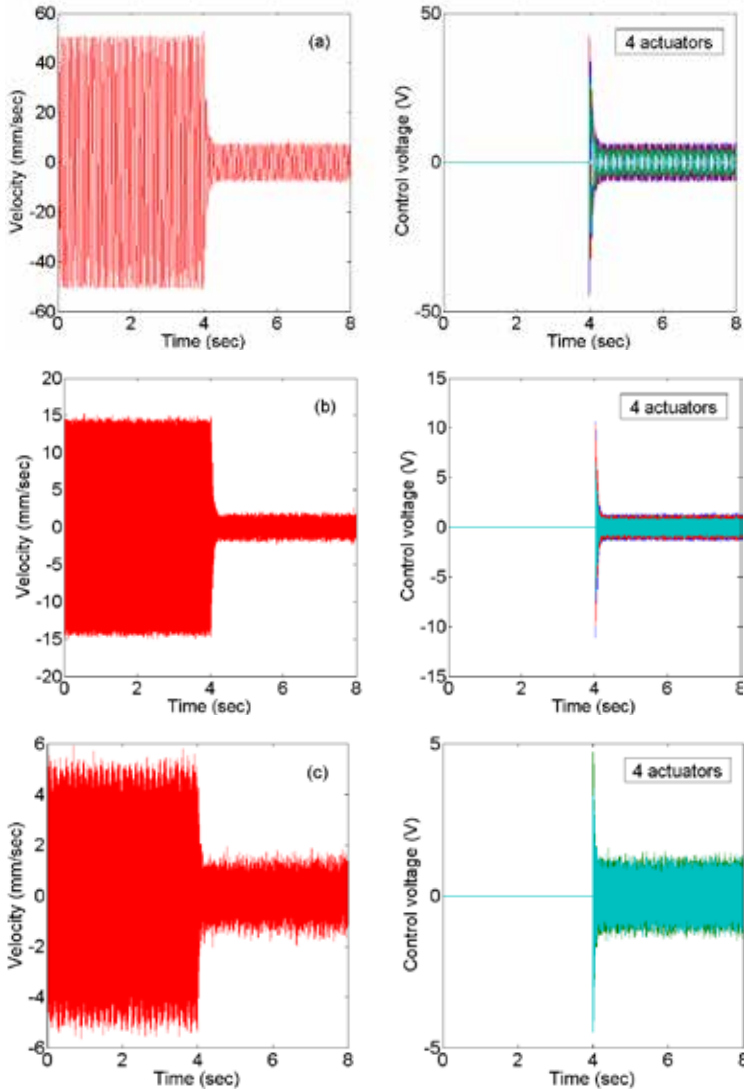

4 (a)
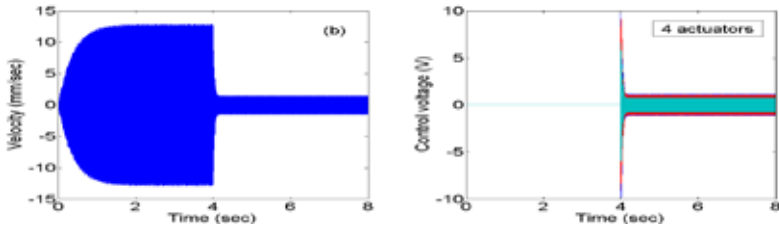
4 (b)
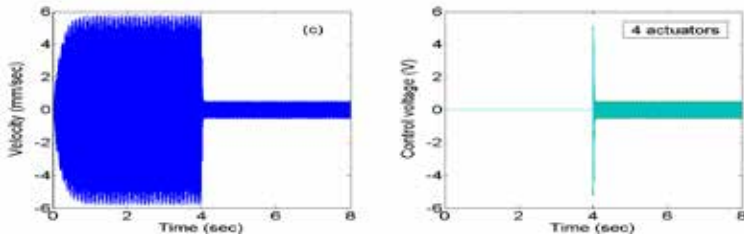
4 (c)
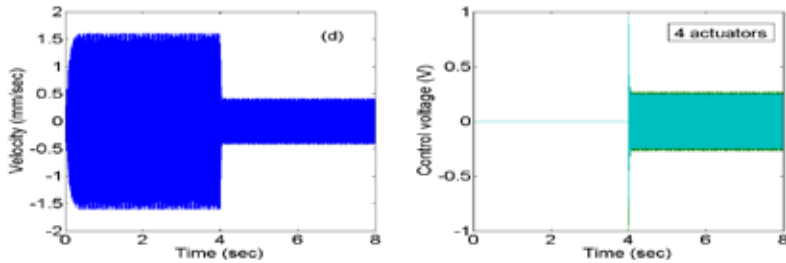
4 (d)

Figure 4: Simulated sensor signal (velocity) and control voltage signals of uncontrolled and controlled (after 4s) system, due to a harmonic excitation force:

$$F(t) = A\sin(2\pi \cdot f_i t);$$

(a) f_1=13.4 Hz, (b) f_2=72.5 Hz, (c) f_3=198 Hz, (d) f_4=392 Hz

5.1. Vibration suppression of a cantilever beam

For the solution of the control task an optimal LQ controller in combination with a Kalman filter is designed (based on the procedure in Section 4.1.) in such a way that the vibration amplitudes due to periodic excitation forces with frequencies corresponding to the eigenfrequencies of the clamped beam, are significantly suppressed in comparison with the uncontrolled case. Simulation results of the controller design, with periodical and random excitation forces are represented in Figures 4 and 5.

Simulated exciting forces $F(t) = A\sin(2\pi \cdot f_i t)$ exerted to the free end of the beam were chosen with regard to the resonant bending eigenfrequencies f_i of the beam. The optimal LQ control system was designed with the weighting matrices $\mathbf{Q} = \mathbf{C}^T\mathbf{C}$ and $\mathbf{R} = 0.1 \times \mathbf{I}_{4\times4}$. For the Kalman filter design, it is assumed in the state estimation procedure that only the sensor voltage (vibration velocity) is measured. Furthermore, a plant noise vector (force disturbance) with $\mathbf{R}_w = 100 \times \mathbf{I}_{4\times4}$ and a sensor noise disturbance with $\mathbf{R}_v = 10$ are considered for the definition of the noise correlation matrices and Kalman feedback gain design.

Diagrams 4(a) – 4(d) represent the uncontrolled and controlled (after 4s) vibration velocity of the beam, due to harmonic excitation forces with frequencies corresponding to the 1st, 2nd, 3rd and 4th bending eigenfrequency of the clamped beam respectively, as well as the corresponding control signals (actuating voltages on piezo patches). The uncontrolled and controlled (after 4s) vibration velocity of the beam due to a white noise force disturbance and the corresponding actuating voltages on piezo actuator patches are represented in Figure 5. In both cases, periodical and random excitation, a significant reduction of the vibration magnitudes can be observed in the presence of the controller.
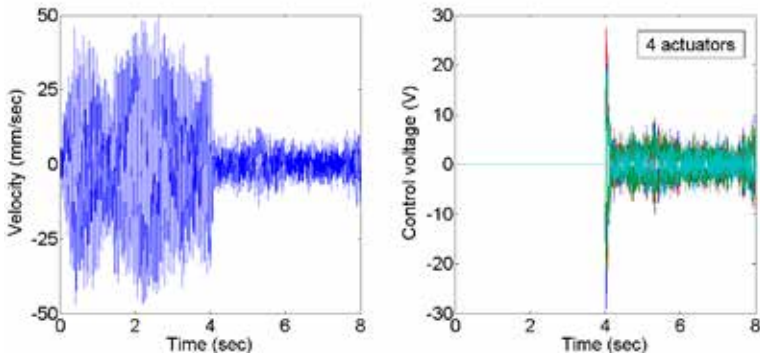
Figure 5: Simulated sensor signal (velocity) and control voltage signals of uncontrolled and controlled (after 4s) system, due to a white noise force disturbance

For the purpose of experimental validation, the identified model coupled with the Kalman state estimator and optimal LQ controller designed based on the identified model are implemented within a real time configuration. The closed loop system for the active vibration control of the beam is implemented on the real time data acquisition platform of the dSPACE system with sampling frequency of 1 kHz. The task of the control is to suppress the vibration magnitudes of the sensor signal in time domain an accordingly to reduce the resonance peaks in the frequency domain. Therefore, investigations are carried out both in the time domain and in the frequency domain by means of the experimental rig represented in Figure 6.

Figure 6: Experimental rig for validation of the control system based on the identified model

For the analysis in the time domain the shaker, represented in Figure 6, is used. The shaker is connected to the tip of beam with a rubber band, in order to excite the beam with periodic forces. The sinusoidal excitation signal for the shaker is generated in Simulink and lead out through the dSPACE DAC board. The frequency of the sine signal corresponds to the eigenfrequen-cies to be controlled. The excitation frequencies for the experimental investigation were fine adjusted experimentally to the values which cause greatest vibration magnitudes, so that disturbances correspond to the system's actual resonant states. The response of the sensor for the uncontrolled and controlled system (after 4s) and the corresponding control signals in the time domain are represented in Figure 7. Diagrams shown on the left hand side represent the velocity magnitudes of the beam measured by dSPACE ADC board and diagrams shown on the right hand side represent the voltages at the piezo actuator patches generated by dSPACE DAC board. These results were obtained using the hardware-in-the-loop system with the dSPACE Real-Time Interface platform. The experimental results show, that the application of the control results in an obvious reduction of the vibration amplitudes.

Figure 7: Sensor signal (velocity) and control voltage signals of uncontrolled and controlled (after 4s) system, due to a harmonic excitation force: $F(t) = A\sin(2\pi \cdot f_i t)$; (a) f_1=14.5 Hz, (b) f_2=72.6 Hz, (c) f_3=202 Hz

Successful performance of the controlled system is demonstrated for the case of the initial displacement disturbance type as well. Free vibrations of the beam caused by an initial displacement applied to the tip of the beam are comparable with impulse disturbance vibrations. The free vibration response (velocity) of the open-loop and

closed-loop system subjected to an initial displacement of 8mm is measured using the laser vibrometer at the point, which is located 22 mm away from the free end, and it is represented in Figure 8. Designed controller attenuates significantly the magnitudes of the free end displacement. The closed-loop 5% settling time is equal to 0.3 s, which reveals a great improvement of the response attenuation when compared with the open-loop one (7.9 s).
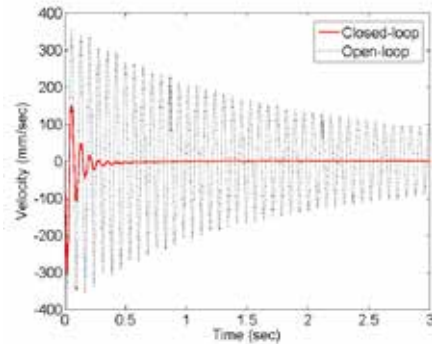
Figure 8: Free vibration response (velocity) of the controlled and uncontrolled system

The effect of the control is also documented in the frequency domain by obtaining frequency response functions from measured input and output signals. The frequency response functions between the sensor signal (laser vibrometer) as the output and the impulse excitation by an impact hammer as an input were determined using the experimental rig represented in Figure 6, in this case with the hammer instead of shaker. The free end of the beam was excited using the impact hammer and the response from the sensor was measured, for both controlled and uncontrolled case. Controlled and uncontrolled frequency response functions are represented in Figure 9 for the frequency range of up to 500 Hz. The figure shows significant vibration suppression in terms of the peak amplitudes reduction for the controlled eigenfrequencies. Especially in the lower frequency range, the designed controller significantly reduces the peak magnitude at the first resonant frequency for approximately 32dB.
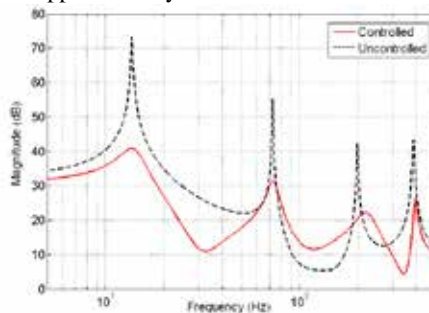
Figure 9: Frequency response of the controlled and uncontrolled system

5.2. Vibration suppression of an MRI tomograph funnel shaped inlet

Control structure in this application example is a funnel shaped piezoelectric shell structure, which represents the inlet part of the magnetic resonance tomograph (Figure 10) used in medical diagnostics.
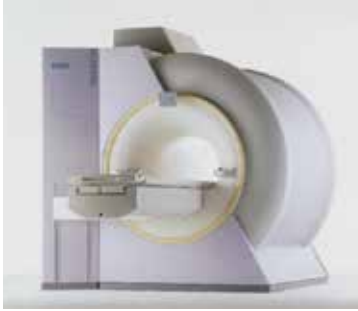
Figure 10: Magnetic resonance tomograph
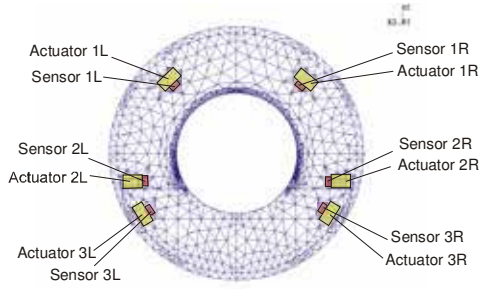
Figure 11: The finite element mesh of the funnel with actuator/sensor placement

One major problem in MRI equipment is the high-level noise that a patient must undergo during the medical treatment. The aim of the control is an attempt to reduce the noise by suppressing vibration of the magnetic resonance tomograph. The Lorenz force acting on the copper coils surrounding the cylindrical body of the tomograph excites the vibrations of the cylindrical housing. These vibrations are also transmitted to the funnel-shaped inlet of the tomograph. The need for the noise reduction through the vibration suppression imposes the idea that the vibration control of the complex funnel-shaped shell inlet of the tomograph can contribute to the overall vibration suppression of the device and therefore to the noise reduction. Since the vibrations transmitted from the copper coil around the cylindrical body of the tomograph to the funnel are viewed as a secondary source of the noise, their suppression plays an important role in the noise reduction. The present research and experimental results regard the field of the vibration suppression. Control is achieved using piezoelectric actuators and sensors glued to the surface of the funnel. The finite element mesh of the funnel with locations of the actuators and sensors is shown in Figure 11.

Vibration modes in the frequency range of interest corresponding to the modally reduced numeric model are controlled in the presence of excitations with frequencies corresponding to the eigenfrequencies of the funnel. Due to possible resonance occurrence this represents the worst case. Numeric model of the funnel is obtained using the finite element approach and modal reduction (as explained in the Section 3.2) in order to obtain a state space model convenient for the controller design. Vibration control of the selected modes in the sense of the vibration amplitudes suppression is performed applying two proposed control techniques: optimal LQ tracking system with additional dynamics (Section 4.1) and a direct robust model reference adaptive control (Section 4.2).

143

Active vibration suppression of the funnel is achieved by piezoelectric patches used as actuators and sensors. Each of the six actuators represents a group consisting of four piezoelectric patches (function modules), whereas each of the six sensors is a single piezoelectric patch. Function modules are made of piezoceramic films (PZT film Sonox P53), with standard dimensions 50×25×0.2 [mm].

Controller verification and testing was performed for several different cases. Here some representative results of the control implementation are presented.

For a single input single output case, selected actuator/sensor pair A2R−S1R (see Figure 11) is considered. In order to achieve vibration suppression of the sensor response magnitudes, in the presence of the sine excitation with the frequency equal to the first eigenfrequency (f_1=9.573 Hz), an optimal LQ controller with additional dynamics is designed, where the design model has order 13, and the weighting matrices are selected as: $\mathbf{Q}$=0.001 $\mathbf{I}_{13\times13}$ and R=100. Experimental results of the vibration suppression are shown in Figure 12, which represents the sensor response and the control signal.
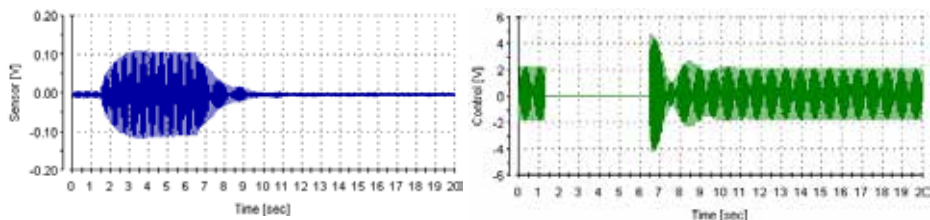
Figure 12: Sensor response and control signal for the actuator/sensor pair A2R – S1R
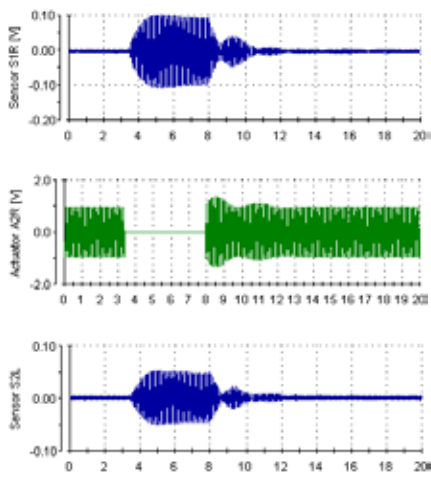
Figure 13: Actuator and sensor signals based on design model involving three eigenfrequencies of the funnel (periodic excitation with frequency f_1)
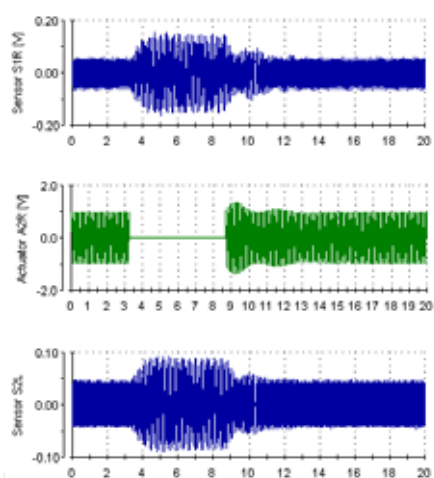
Figure 14: Actuator and sensor signals based on design model involving three eigenfrequencies of the funnel

A more general control case regards the simultaneous control of the first three eigenfrequencies. The task of the control system is to suppress vibration magnitudes measured by sensors in the presence of sinusoidal excitation, the frequency of which can be equal to any of the first three funnel eigenfrequencies, or to the combination of these sinusoidal signals.

Additional dynamics takes into account all three funnel eigenfrequencies of interest included in the reduced order state space model (f_1=9.573 Hz, f_2=23.333 Hz, f_3= 31.439Hz). Design model developed based on this additional dynamics was used to design a controller for a multiple input multiple output case. The sensors S1R, S2L and the actuator A2R were considered. The controller was tested under different excitation conditions and selected results, time responses of the sensors and the controller signal, are represented in Figures 13 and 14.

Based on the procedure for adaptive controller design described in Section 4.2, a direct robust model reference adaptive control was applied to the funnel-shaped structure in order to suppress the vibrations caused by excitations which are assumed to be sinusoidal with frequencies corresponding to selected eigenfrequencies of the funnel.
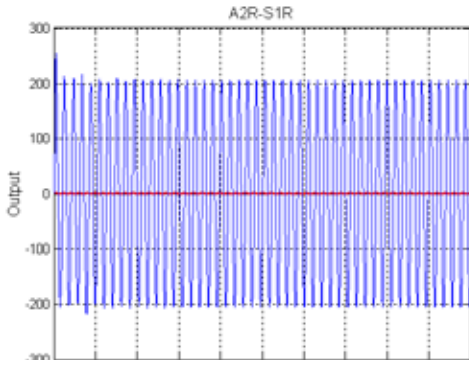
Figure 15: Uncontrolled and controlled sensor response
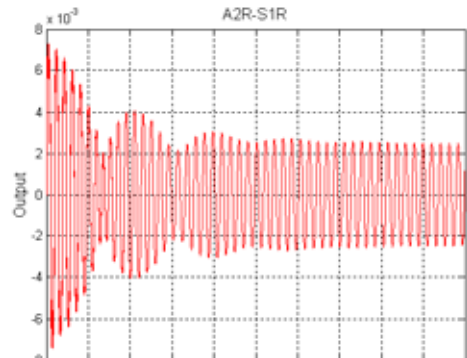
Figure 16: Zoomed controlled response of the sensor S1R
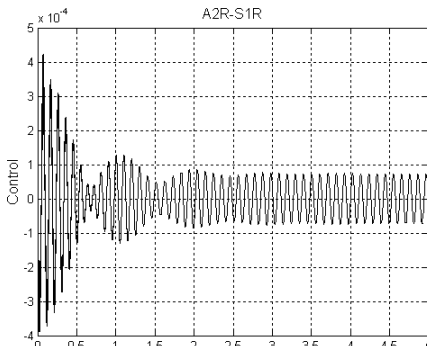
Figure 17: Control signal (actuator A2R)
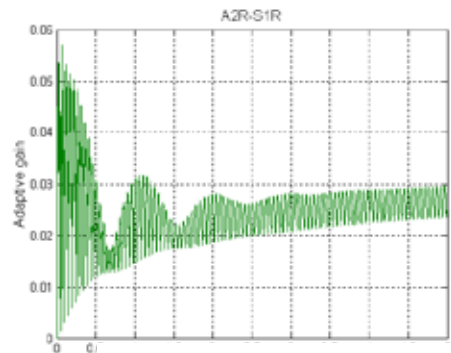
Figure 18: Adaptive gain

Coefficient σ in the modified robust algorithm (52) enables a stable control algorithm in the sense of convergence of the outputs, states and adaptive gains (see Figure 18). It is chosen to be σ=0.1. For a SISO case the coefficients of the reference model are chosen in the following way: A_m= −3, B_m=1, C_m=3. Actuator/sensor pair A2R−S1R is considered. For the presented simulation results obtained with the FE based state space model of the funnel appropriate elements of the matrices $\mathbf{T}$ and $\overline{\mathbf{T}}$ are selected to be 1000. Excitation $\sin(2\pi f_1)t$ is considered. Uncontrolled and controlled output is represented in Figure 15. Zoomed portion of the controlled response is represented in Figure 16. Actuator signal and adaptive gain K_e are represented in Figures 17 and 18, respectively.

5.3. Vibration suppression of a car roof

Vibration suppression of a car roof with attached piezoelectric patches using the optimal LQ controller with additional dynamics is demonstrated through a numerical simulation for a test structure. Piezoelectric patches attached to the surface of the car roof are used as actuators and sensors. Excitation by shakers at prescribed points is intended for the experimental investigations (Fig. 8).

Figure 19: Passenger compartment and inner surface of the car roof with attached piezoelectric patches and exciting shakers

FEM model including the piezo-electric effects of the actuator/sensor groups was obtained using the FEM software COSAR [28]. Based on the generated FEM mesh, an optimization of the actuator/sensor placement was performed under consideration of the eigenmodes of interest and the controllability index. For the controller design a modally reduced state space model was used, which takes into account five selected eigenfrequencies: f_1=48.45Hz, f_2=51.12Hz, f_3=63.23Hz, f_4=64.67Hz and f_5=68.00Hz. Using the control concept with optimal LQ controller, additional dynamics and Kalman

estimator the simulation of the vibration suppression was performed in order to show the potentials of the control strategy. The results are represented in Figure 20.

The comparison of the uncontrolled and controlled cases shows significant reduction of the vibration magnitudes in the presence of the controller. The controller was also compared with the standard optimal LQ controller without additional dynamics which compensates for the presence of the periodic sinusoidal excitations with critical frequencies. The comparison shows much better vibration suppression in the presence of the controller with additional dynamics.
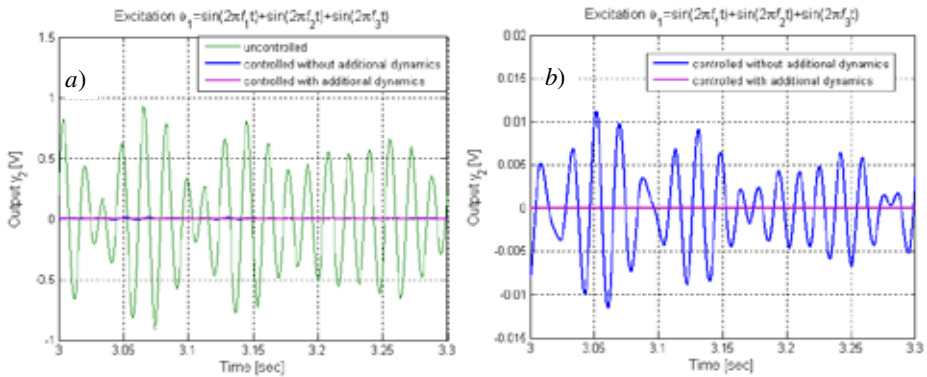
Figure 20: *a*) Controlled and uncontrolled responses of the sensor patches.
b) Zoomed portion of the controlled responses.

6. Conclusion

An overall concept for active control of smart structures using piezoelectric materials is presented in this paper. The approach is especially well suited for light weight structures and it is presented through several subsequent steps: modeling (model identification and numerical modeling), optimization, controller design, simulation and experimental verification/testing. The effectiveness of the concept is demonstrated trough application examples.

References

[1] Herold S., 2003. Simulation des dynamischen und akustischen Verhaltens aktiver Systeme im Zeitbereich. Ph.D. thesis, Darmstadt, Germany

[2] Benjeddou A., 2000. Advances in piezoelectric finite element modeling of adaptive structural elements: a survey. Computers and Structures. 76, 347-363

[3] Chopra I., 2002,Review of state of art of smart structures and integrated systems, AIAA J. 40, 2145–2187

[4] Nestorović T., 2005 Controller Design for the Vibration Suppression of Smart Structures, Fortschritt-Berichte VDI, Vol. 8, Düsseldorf, Germany

[5] Nestorović T., U. Gabbert U., 2008, Subspace-based frequency analysis of a smart acoustic structure, Facta Universitatis Series Mechanics Automatic Control and Robotics. 7, 209–220

[6] Nestorović Trajkov T., Köppe H., Gabbert U., 2008, Direct model reference adaptive control (MRAC) design and simulation for the vibration suppression of piezoelectric smart structures, Commun. Nonlinear Sci. Numer. Simul. 13, 1896–1909

[7] Nestorović Trajkov T., Gabbert U., 2006, Active control of a piezoelectric funnel-shaped structure based on subspace identification, Struct. Contr. Health Monit. 13, 1068–1079

[8] Nestorović Trajkov T., Köppe H., Gabbert U., 2005, Active Vibration Control Using Optimal LQ Tracking System with Additional Dynamics, Int. J. Control. 78, 1182–1197

[9] Vasques C.M.A., Dias Rodrigues J., 2006, Active vibration control of smart piezoelectric beams: Comparison of classical and optimal feedback control strategies, Comput. Struct. 84, 1402–1414

[10] Grasso E., Pesotski D., Janocha H., 2010 , Self-sensing piezoelectric actuators for vibration control purposes, Actuator, Proc. 12th International Conference on New Actuators Bremen, pp. 151–154

[11] Azizi A., Dourali L., Zareie S., Rad F.P., 2009, Control of Vibration Suppression of an Smart Beam by Pizoelectric Elements, Second International Conference on Environmental and Computer Science ICECS'09, pp. 165–169

[12] Maccari A., 2003, Vibration Control for the Primary Resonance of a Cantilever Beam by a Time Delay State Feedback, J. Sound Vibrat. 259 (2), 241–251

[13] Kircali O.F., Yaman Y., Nalbantoglu V., Sahin M., Karadal F.M., Ulker F.D., 2008, Spatial control of a smart beam. J. Electroceram. 20 (3–4), 175–185

[14] Jac-Eung Oh, Soo-Hong Park, Jin-Seok Hong und Jun Shin, 1998, Active vibration control of flexible cantilever beam using piezo actuator and Filtered-X LMS algorithm. KSME International Journal continued by J. Mech. Sci. Technol. 12 (4), 665–671

[15] Tjahyadi H., He F., Sammut K., 2006, Multi-mode vibration control of a flexible cantilever beam using adaptive resonant control, Smart Mater. Struct. 15, 270–278

[16] Nestorović T., Marinković D., Chandrashekar G., Marinković Z. and Trajkov M., 2012, Implementation of a user defined piezoelectric shell element for analysis of active structures, Finite Elem. Anal. Des. 52, 11-22

[17] Viberg M., 2002. Subspace-based state-space identification. Circuits Systems Signal Processing. 21, 23-37

[18] Franklin G.F., Powell J.D., Workman M.L., 1998. Digital Control of Dynamic Systems (3rd edition). Addison-Wesley Longman, Inc.

[19] Van Overschee P., De Moor B., 1996. Subspace Identification for Linear systems: Theory, Implementation, Applications. Kluwer Academic Publishers vol. 1

[20] Trajkov M., Nestorović T.: Optimal placement of piezoelectric actuators and sensors for smart structures, in Experimental Mechanics, New Trends and Perspectives, J.F. Silva Gomes and Mário A.P. Vaz, Editors, Proceedings of the 15th International Conference on Experimental Mechanics ICEM15, Porto/Portugal, 22-27 July 2012, in CD-Proceedings, Paper No. 2716, p. 1-13, ISBN: 978-972-8826-26-0

[21] Allik H., Hughes J. R., (1970), Finite Element Method for Piezoelectric Vibration, International Journal for Numerical Methods in Engineering, 2:151–157

[22] Tiersten H.F., (1967), Hamilton's principle for linear piezoelectric media, Proc. IEEE, 1523–1524

[23] Tzou H. S., Tseng C. I., (1990), Distributed piezoelectric sensor/actuator design for dynamic measurement/ control of distributed parameter system: a piezoelectric finite element approach, Journal of Sound and Vibration, 138(1), 17–34

[24] Matlab documentation, Control System Toolbox

[25] Kaufman H., Barkana I., Sobel K., 1998, Direct adaptive control algorithms: theory and applications, Second Edition, Springer-Verlag, New York

[26] Iannou P., Kokotovic P., 1983, Adaptive Systems with Reduced Models, Springer-Verlag, Berlin

[27] Iannou P., Sun J., 1996, Robust Adaptive Control, Prentice-Hall, Inc.

[28] COSAR General Purpose Finite Element Package: Manual, FEMCOS mbH Magdeburg, http://www.femcos.de

FURTHER RESULTS ON APLICATIONS OF FRACTIONAL CALCULUS IN NONLINEAR DYNAMICS - STABILITY AND CONTROL ISSUES

Mihailo Lazarević[1]

[1]Faculty of Mechanical Engineering,
The University of Belgrade, Kraljice Marije 16, 11120 Belgrade 35
e-mail: mlazarevic@mas.bg.ac.rs

Abstract. In this paper, they are presented recently obtained results which are related to applications of fractional calculus in dynamics- specially stability and control issues.In recent years**,** there have been extensive research activities related to applications of fractional calculus (FC), in nonlinear dynamics, mechatronics as well as control theory. First, they are presented the new algorithms of PID control based on fractional calculus (FC) and optimal procedure in the position control of robotic system with 3 DOFs driven by DC motors. The objective of this work is to find out optimal settings for a fractional $PI^{\alpha}D^{\beta}$ controller in order to fulfill proposed design specifications for the closed-loop system, taking advantage of the fractional orders, α and β . The effectiveness of suggested optimal fractional PID control is demonstrated with a suitable robot with three degrees of freedom as the illustrative example. Also, this paper proposes a robust fractional-order sliding mode control of a 3-DOF robot system driven by DC motors. Primarily, a conventional sliding mode controller based on PD^{α} sliding surface is designed. Numerical simulations have been carried out to show the proposed control system's robustness properties as well as compare the significance of the proposed control which resulted in reducing output oscillations (chattering-free) of the given robot. Simulations also include comparison fractional-order PD sliding mode controller with standard PD sliding-mode controller. Also, it is proposed sufficient conditions for finite time stability for the (non)homogeneous fractional order systems with time delay. New stability criteria for this class of fractional order systems will be derived using a recently obtained generalized Gronwall inequality as well as "classical" Bellman-Gronwall inequality. Last,a numerical example is provided to illustrate the application of the proposed stability procedure.

1. Introduction

Fractional calculus (FC) is a mathematical topic with more than 300 years old history, but its application to physics and engineering has been reported only in the recent years.

The fractional integro-differential operators are a generalization of integration and derivation to non-integer order (fractional) operators. It is remarkable the increasing number of studies related with the application of fractional controllers in many areas of science and engineering, where specially fractional-order systems are of interest for both modeling and controller design purposes. It has been found that in interdisciplinary fields, many systems can be described by the fractional differential equations i.e. in the fields of continuous-time modeling, fractional derivatives have proved useful in linear viscoelasticity, acoustics, rheology, polymeric chemistry, biophysics robotics, control theory of dynamical systems, electrical engineering, bioengineering and so on, [1-3].

Also, robots today are making a considerable impact on many aspects of modern life, from manufacturing to healthcare. Mobile robots, underwater and flying robots, robot networks, surgical robots, and others are playing increasing roles in society, [4]. Moreover, robots are important components in automation systems and new solutions on the system level often result in new requirements on the robot control. Sometimes new automation concepts ask for big changes in the design of the robot control, as for example in the case of automation concepts based on collaborating robots [5]. Thus, robot control development has made it possible to improve the quality of robot-based manufacturing and increase the productivity of robot automation. At the same time the robot control development has made it possible for the robot manufacturers to reduce the cost of the robots and introduce robots in applications with high requirements on motion performance. Without the efforts made to refine the robot control, there would not be one million robots working in industries world-wide today. Unlike the industrial robotics domain where the workspace of machines and humans can be segmented, applications of intelligent machines that work in contact with humans are increasing, which involve e.g. haptic interfaces and teleoperators, cooperative material-handling, power extenders and such high-volume markets as rehabilitation, physical training, entertainment. In that way, robotic systems are more and more ubiquitous in the field of direct interaction with humans, in a so called friendly home environment. For example, providing contact sensing on the whole body of a robot is a key feature to increase the safety level of physical human-robot interaction. One of these robotic systems capable of operating in human friendly environments is *NeuroArm robot*, Fig.1.
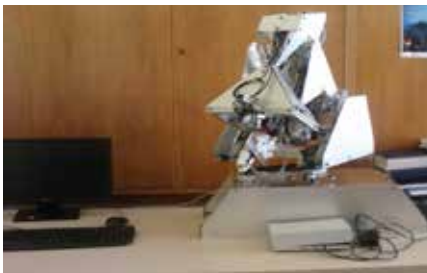
Figure 1. NeuroArm robot system,Laboratory of Mechanics at Faculty of Mechanical Engineering in Belgrade
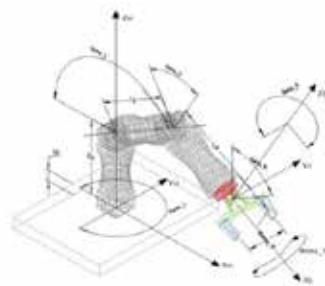
Figure 2. Model of NeuroArm with 7 DOFs

This robotic arm possesses seven degrees of freedom, which described with six parameters for rotating and one parameter for translating, Fig.2. Within NeuroArm Manipulator System there are a rich set of options that enable scientists and engineers to configure your robot that will meet the needs [6,7].

Besides, in classical control theory, state feedback and output feedback are two important techniques in system(robotic), control. Specially, due to its functional simplicity and performance robustness, the PID controller has been widely used in the process industries. Design and tuning of PID controllers have been a large research area ever since Ziegler and Nichols presented their methods in 1942, [8]. Specifications, stability, design, applications and performance of the PID controller have been widely treated since then [9,10].

However, in the recent years, emergence of effective methods to solve differentiation and integration of noninteger order equations makes fractional-order systems more and more attractive for the systems control community. The fractional controller $PI^{\beta}D^{\alpha}$ [3], the fractional PD^{α} controller [11], the fractional PI^{α} controller [12], the CRONE controllers [13,14], and the fractional lead-lag compensator [15] are some of the well-known fractional order controllers. In this paper, we suggest and obtain new algorithms of PID control based on fractional calculus (FC) in the control of robotic system driven by DC motors. The objective of this work is to find out suitable settings for a fractional $PI^{\alpha}D^{\beta}$ controller in order to achieve better transient response as well as fulfill proposed design specifications for the closed-loop system, taking advantage of the fractional orders, α and β.

Also, sliding-mode controller (SMC) is a powerful tool to robustly control incompletely modeled or uncertain systems [16] which has many attractive features such as fast response, good transient response and asymptotic stability. The conventional SMC law guarantees robustness of the sliding manifold if the model uncertainties are bounded with known bounds and comply with the matching condition. Once the system states hit the sliding surface, they stay there, and the equivalent system dynamics are predefined with a reduced order. However, SMC has some disadvantages related to well known chattering in the system. Chattering is undesirable in the control of mechanical systems, since it causes excessive control action leading to increased wear on the actuators and to excitation of the high order nonmodeled dynamics. Therefore, chattering must be eliminated from the SMC system. Since chattering is caused by the discontinuous control, there exist several techniques to reduce high switching amplitude, [17]. Recently, fractional-order sliding mode control technique, authors, Monje et al. [18] has been successfully applied for robot manipulator, as well as in [19], or in [20] results of combining sliding mode control and fractional order derivative is considered in two different approaches. In this paper, we suggest and obtain chattering-free fractional PD^{α} sliding-mode controller in the control of robotic system driven by DC motors. In that way, one has used a fractional-order sliding surface to design a fractional-order sliding mode controller for chattering-free tracking the given robot system.

.

Finally, some results of the stability criteria of fractional order systems with time-delay as well as free-delay are presented. Particularly, they are obtained and presented sufficient conditions for finite-time stability for (non)linear (non)homogeneous as well as perturbed fractional order time-delay systems. Several stability criteria for this class of fractional order systems are proposed using a recently suggested generalized Gronwall inequality as well as "classical" Bellman-Gronwall inequality. Some conclusions for stability are similar to those of classical integer-order differential equations. Lastly, numerical examples are given to illustrate the validity of the proposed procedure.

2. Preliminaries on the fractional calculus

The fractional integro-differential operators-(fractional calculus–(FC)) are a generalization of integration and derivation to non-integer order (fractional) operators. The idea of FC has been known since the development of the regular calculus, with the first reference probably being associated with Leibniz and Marquis de l'Hopital in 1695. Both Leibniz and L`Hospital, aware of ordinary calculus, raised the question of a noninteger differentiation (order $n = 1/2$) for simple functions. It had always attracted the interest of many famous ancient mathematicians, including L'Hospital, Leibniz, Liouville, Riemann, Grünward, and Letnikov [1-3]. In that way, the theory of fractional-order derivative was developed mainly in the 19th century. Since from 19th century as a foundation of fractional geometry and fractional dynamics, the theory of FO, in particular, the theory of FC and FDEs and researches of application have been developed rapidly in the world. The modern epoch started in 1974 when a consistent formalism of the fractional calculus has been developed by Oldham and Spanier,[1], and later Podlubny,[3]. Applications of FC are very wide nowadays, in rheology, viscoelasticity, acoustics, optics, chemical physics, robotics, control theory of dynamical systems, electrical engineering, bioengineering and so on, [11-20].

The modern epoch started in 1974 when a consistent formalism of the fractional calculus has been developed by Oldham and Spanier [1]. The theory of FC is a well-adapted tool to the modeling of many physical phenomena, allowing the description to take into account same peculiarities that classical integer-order models simply neglect. The main reason for the success of applications FC is that these new fractional-order models are more accurate than integer-order models and fractional derivatives provide an excellent instrument for the description of memory and hereditary properties of various materials and processes due to the existence of a "memory" term in a model. There exist today many different forms of fractional integral operators, ranging from divided-difference types to infinite-sum types, Riemann-Liouville fractional derivative,Grunwald–Letnikov fractional derivative, Caputo's, Weyl's and Erdely-Kober left and right fractional derivatives and so on, Kilbas *et al.*[21]. The three most frequently used definitions for the general fractional differintegral are: the Grunwald-Letnikov (GL) definition, the Riemann-Liouville (RL) and the Caputo definitions, [1-3]. First is the GL definition i.e Grunwald-[22], Letnikov [23] developed an approach to fractional differentiation based on the definition

$$_{GL}D_x^\alpha f(x) = \lim_{h \to 0} \frac{\left(\Delta_h^\alpha f(x)\right)}{h^\alpha}, \quad \Delta_h^\alpha f(x) = \sum_{0 \le |j| < \infty} (-1)^{|j|} \binom{\alpha}{j} f(x - jh), \quad h > 0, \quad (1)$$

which is the left Grunwald-Letnilov (GL) derivative as a limit of a fractional order backward difference. Similarly, we have the right one as

$$_{GL}D_x^\alpha f(x) = \lim_{h \to 0} \frac{\left(\Delta_{-h}^\alpha f(x)\right)}{h^\alpha}, \quad \Delta_{-h}^\alpha f(x) = \sum_{0 \le |j| < \infty} (-1)^{|j|} \binom{\alpha}{j} f(x + jh), \quad h < 0, \quad (2)$$

As indicated above, the previous definition of GL is valid for $\alpha > 0$ (fractional derivative) and for $\alpha < 0$ (fractional integral) and, commonly, these two notions are grouped into one single operator called *differintegral*. The GL derivative and RL derivative are equivalent if the functions they act on are sufficiently smooth. For generalized binomial coefficients calculation for $\alpha \in R$ and $k \in \square_0$ we can use the relation between Euler's *Gamma* function and factorial, defined as

$$\binom{\alpha}{j} = \frac{\alpha!}{j!(\alpha - j)!} = \frac{\alpha(\alpha - 1)...(\alpha - j + 1)}{j!} = \frac{\Gamma(\alpha + 1)}{\Gamma(j + 1)\Gamma(\alpha - j + 1)}, \quad \binom{\alpha}{0} = 1 \quad (3)$$

If we consider $n = t - a / h,$ where a is a real constant, which expresses a limit value, one may write

$$_{GL}D_{a,t}^\alpha f(t) = \lim_{h \to 0} \frac{1}{h^\alpha} \sum_{j=0}^{\left[\frac{t-a}{h}\right]} (-1)^j \binom{\alpha}{j} f(t - jh), \quad (4)$$

where $[x]$ means the integer part of x, a and t are the bounds of operation for $_{GL}D_{a,t}^\alpha f(t)$. For numerical calculation of fractional-order derivatives we can use the following relation (5) derived from the GL definition (4). This approach is based on the fact that for a wide class of functions, three definitions—GL, RL, and Caputo's — are equivalent. The relation to the explicit numerical approximation of α-th derivative at the points kh, $(k = 1, 2, \ldots)$ has the following form, [3]

$$_{((x-L)}D_x^{\pm\alpha} f(x) \approx h^{\mp\alpha} \sum_{j=0}^{N(x)} b_j^{(\pm\alpha)} f(x - jh) \quad (5)$$

where L is the "memory length", h is the step size of the calculation,

$$N(t) = min\left\{\left[\frac{x}{h}\right], \left[\frac{L}{h}\right]\right\}, \quad (6)$$

$[x]$ is the integer part of x and $b_j^{(\pm\alpha)}$ is the binomial coefficient given by

$$b_0^{(\pm\alpha)} = 1, \quad b_j^{(\pm\alpha)} = \left(1 - \frac{1 \pm \alpha}{j}\right) b_{j-1}^{(\pm\alpha)} \quad (7)$$

For expression of the Riemann-Liouville definition, we will consider the Riemann-Liouville *n*-fold integral for $n \in N, n > 0$ defined as

$$\underbrace{\int_a^t \int_a^{t_n} \int_a^{t_{n-1}} \dots \int_a^{t_3} \int_a^{t_2}}_{n-fold} f(t_1) \, dt_1 dt_2 \dots dt_{n-1} dt_n = \frac{1}{\Gamma(n)} \int_a^t (t-\tau)^{n-1} f(\tau) d\tau, \qquad (8)$$

Fractional Riemann-Liouville integral of order α for the function $f(t)$ for $\alpha, a \in R$ can be expressed as follows

$$_{RL}I_a^\alpha f(t) \equiv {}_{RL}D_a^{-\alpha} f(t) = \frac{1}{\Gamma(\alpha)} \int_a^t (t-\tau)^{\alpha-1} f(\tau) d\tau, \qquad (9)$$

Here, $\Gamma(.)$ is the well known Euler's gamma function which is defined by the so-called *Euler integral of the second kind*:

$$\Gamma(z) = \int_0^\infty e^{-t} t^{z-1} dt, \quad z \in \square \qquad (10)$$

For this function the *reduction formula* holds, for $z \in \square \setminus \{0, -1, -2, -3, \dots\}$:

$$\Gamma(z+1) = z\Gamma(z), \quad \Rightarrow \Gamma(n+1) = n(n-1)! = n! \quad n \in \square_0, \qquad (11)$$

The second important property of the gamma function is that has simple poles at the points $z = -n, \ (n = 0, 1, 2, \dots)$. Another important relationship for the gamma function is the Legendre formula:

$$\Gamma(z)\Gamma(z+1/2) = \sqrt{\pi} 2^{2z-1} \Gamma(2z), \quad 2z \neq 0, -1, -2, \dots, \qquad (12)$$

Taking $z = n + 1/2$ in previous relation one can obtain a set of particular values of the gamma function:

$$\Gamma(n+1/2) = \frac{\sqrt{\pi}\Gamma(2n+1)}{2^{2n}\Gamma(n+1)} = \frac{\sqrt{\pi}(2n)!}{2^{2n}n!}, \qquad (13)$$

For the case of $0 < \alpha < 1, t > 0$, and $f(t)$ being a a causal function of t, the fractional integral is presented as

$$_{RL}D_a^{-\alpha} f(t) = \frac{1}{\Gamma(\alpha)} \int_a^t \frac{f(\tau)}{(t-\tau)^{1-\alpha}} d\tau, \quad 0 < \alpha < 1, \ t > 0 \qquad (14)$$

Moreover, the *left Riemann-Liouville fractional integral* and the *right Riemann-Liouville fractional integral* are defined respectively as

$$_{RL}I_a^\alpha f\left(t\right) \equiv {}_{RL}D_a^{-\alpha} f\left(t\right) = \frac{1}{\Gamma(\alpha)}\int_a^t (t-\tau)^{\alpha-1} f(\tau)d\tau, \qquad (15)$$

$$_{RL}I_b^\alpha f\left(t\right) \equiv {}_{RL}D_b^{-\alpha} f(t) = \frac{1}{\Gamma(\alpha)}\int_t^b (\tau-t)^{\alpha-1} f(\tau)d\tau, \qquad (16)$$

where $\alpha > 0, \, n-1 < \alpha < n$. Furthermore, the *left Riemann-Liouville fractional derivative* is defined as

$$_{RL}D_{a,t}^\alpha f\left(t\right) = \frac{1}{\Gamma(n-\alpha)}\frac{d^n}{dt^n}\int_a^t (t-\tau)^{n-\alpha-1} f(\tau)d\tau, \qquad (17)$$

and the *right Riemann-Liouville fractional derivative* is defined as

$$_{RL}D_{t,b}^\alpha f\left(t\right) = \frac{(-1)^n}{\Gamma(n-\alpha)}\frac{d^n}{dt^n}\int_t^b (\tau-t)^{n-\alpha-1} f(\tau)d\tau, \qquad (18)$$

where $n-1 \le \alpha < n$, *a, b* are the terminal points of the interval $[a,b]$, which can also be $-\infty, \infty$. Also, for the RL derivative, we have

$$\lim_{\alpha\to(n-1)^+} {}_a^{RL}D_t^\alpha f(t) = \frac{d^{n-1}f(t)}{dt^{n-1}} \quad \text{and} \quad \lim_{\alpha\to n^-} {}_a^{RL}D_t^\alpha f(t) = \frac{d^n f(t)}{dt^n} \qquad (19)$$

The RL fractional derivative of a constant C takes the form

$$_{RL}D_{a,t}^\alpha C = C\frac{(t-a)^{-\alpha}}{\Gamma(1-\alpha)} \ne 0 \qquad (20)$$

But, the definitions of the fractional differentiation of Riemann-Liouville type leads a conflict between the well-established and polished mathematical theory and proper needs, such as the initial problem of the fractional differential equation, and the nonzero problem related to the Riemann-Liouville derivative of a constant. A certain solution to this conflict was proposed by Caputo first in his paper [24]. The Caputo fractional derivatives are defined as follows. The *left Caputo fractional derivative* is

$$_cD_{a,t}^\alpha f\left(t\right) = \frac{1}{\Gamma(n-\alpha)}\int_a^t (t-\tau)^{n-\alpha-1} f^{(n)}(\tau)d\tau, \qquad (21)$$

and the *right Caputo fractional derivative* is

$$_cD_{t,b}^\alpha f\left(t\right) = \frac{(-1)^n}{\Gamma(n-\alpha)}\int_t^b (\tau-t)^{n-\alpha-1} f^{(n)}(\tau)d\tau, \qquad (22)$$

155

where $f^{(n)}(\tau) = d^n f(\tau)/d\tau^n$ and $n-1 \le \alpha < n \in \Box^+$. By definition the Caputo fractional derivative of a constant is zero. Previous expressions show that the fractional-order operators are *global* operators having a memory of all past events, making them adequate for modeling hereditary and memory effects in most materials and systems. Moreover, for the Caputo derivative, we have

$$\lim_{\alpha \to (n-1)^+} {}_a^C D_t^\alpha x(t) = \frac{d^{n-1} x(t)}{dt^{n-1}} - D^{(n-1)} x(a) \tag{23}$$

and

$$\lim_{\alpha \to n^-} {}_a^C D_t^\alpha x(t) = \frac{d^n x(t)}{dt^n} \tag{24}$$

where obviously, ${}_{RL}D_a^\alpha$, $n \in (-\infty, +\infty)$ varies continuously with n, but the Caputo derivative cannot do this. Obviously, the Caputo derivative is more strict than Riemann-Liouville derivative, one reason is that the *n*-th order derivative is required to exist. On the other side, initial conditions of fractional differential equations with Caputo derivative have a clear physical meaning and Caputo derivative is extensively used in real applications. The Riemann-Liouville fractional derivatives and Caputo fractional derivatives are connected with each other by the following relations:

$$_{RL}D_{t,a}^\alpha f(t) = {}_C D_{t,a}^\alpha f(t) + \sum_{k=0}^{n-1} \frac{(-1)^k f^{(k)}(a)}{\Gamma(k-\alpha+1)} (t-a)^{k-\alpha} \tag{25}$$

$$_{RL}D_{t,b}^\alpha f(t) = {}_C D_{t,b}^\alpha f(t) + \sum_{k=0}^{n-1} \frac{(-1)^k f^{(k)}(b)}{\Gamma(k-\alpha+1)} (b-t)^{k-\alpha} \tag{26}$$

The Caputo and Riemann-Liouville formulation coincide when the initial conditions are zero,[1-3]. Besides, the RL derivative is meaningful under weaker smoothness requirements. Also, the RL derivative can be presented as:

$$_{RL}D_t^\alpha f(t) = D^n D_{a,t}^{\alpha-n} f(t), \quad \alpha \in [n-1, n), \tag{27}$$

and the Caputo derivative

$$_C D_{a,t}^\alpha f(t) = D_{a,t}^{\alpha-n} D^n f(t), \quad \alpha \in n(n-1, n), \tag{28}$$

where $n \in Z^+, D^n$ is the classical n-order derivative. For convenience, Laplace domain is usually used to describe the fractional integro-differential operation for solving engineering problems. The formula for the Laplace transform of the RL fractional derivative has the form:

$$\int_0^\infty e^{-st} {}_{RL}D_{0,t}^\alpha f(t) dt = s^\alpha F(s) - \sum_{k=0}^{n-1} s^k {}_{RL}D_{0,t}^{\alpha-k-1} f(t) \big|_{t=0} \tag{29}$$

where for $\alpha < 0$ (*i.e.*, for the case of a fractional integral) the sum in the right-hand side must be omitted). Also, Laplace transform of the Caputo fractional derivative is:

$$\int_0^\infty e^{-st} {}_C D_{0,t}^\alpha f(t) dt = s^\alpha F(s) - \sum_{k=0}^{n-1} s^{\alpha-k-1} f^{(k)}(0), \quad n-1 < \alpha < n \qquad (30)$$

which implies that all the initial values of the considered equation are presented by a set of only classical integer-order derivatives. Besides that, a geometric and physical interpretation of fractional integration and fractional differentiation can be found in Podlubny's work [25].

3. Mathematical model of a robotic system with DC motors

Robotic system is considered as an open linkage consisting of $n+1$ rigid bodies $[V_i]$ interconnected by n one-degree-of–freedom joints formed kinematical pairs of the fifth class, Fig.3, where the robotic system possesses n degrees of freedom. Here, the Rodriguez` method [26], is proposed for modeling kinematics and dynamics of the robotic system. The configuration of the mechanical model of robot can be defined by the vector of joint (internal) generalized coordinates q of dimension n, $(q) = (q^1, q^2, ..., q^n)^T$, where relative angles of rotation (in case of revolute joints) and relative displacements (in case of prismatic joints). The geometry of the system has been defined by unit vectors $\vec{e}_i$, $i = 1, 2, ..., j, .., n$ where unit vectors $\vec{e}_i$ are describing the axis of rotation (translation) of the i-th segment with respect to the previous segment and as well as vectors $\vec{\rho}_i$ and $\vec{\rho}_{ii}$, where are usually expressed in local coordinate systems connected with bodies, $\left(\vec{\rho}_i^{(i)}\right), \left(\vec{\rho}_{ii}^{(i)}\right)$. The parameters $\xi_i, \bar{\xi}_i = 1 - \xi_i$ denote parameters for recognizing joints $\xi_i, \bar{\xi}_i = 1 - \xi_i, \xi_i = 1 - prismatic, 0 - revolute$. For the entire determination of this mechanical system, it is necessary to specify masses m_i and tensors of inertia J_{Ci} expressed in local coordinate systems. In order that the kinematics of the robotic system may be described, points O_i, O_i' are noticed somewhere at the axis of the corresponding joint (i) such that they coincide in the reference configuration. The point O_i is immobile with respect to the $(i-1)$-th segment and O_i' does so with respect to the i-th one; obviously, for a revolute joint (i), the points O_i and O_i' will coincide all the time during robotic motion. For an example, the position vector of a point of interest $\vec{r}_H$ can be written as a multiplication of matrices of transformation $\left[A_{j-1,j}\right]$, position vectors $\vec{\rho}_{ii}$ and $\xi_i q^i \vec{e}_i$ is expressed by

$$\vec{r}_H(q) = \sum_{i=1}^n \left(\vec{\rho}_{ii} + \xi_i q^i \vec{e}_i\right) = \sum_{i=1}^n \left(\prod_{j=1}^i \left[A_{j-1,j}\right]\right)\left(\left(\vec{\rho}_{ii}^{(i)}\right) + \xi_i q^i \left(\vec{e}_i^{(i)}\right)\right) \qquad (31)$$

where appropriate Rodriguez' matrices of transformation are

$$\left[A_{j-1,j}\right]=\left[I\right]+\left[e_j^{d(j)}\right]^2\left(1-\cos q^j\right)+\left[e_j^{d(j)}\right]\sin\left(q^j\right) \tag{32}$$

and

$$\left(e_j^{(j)}\right)=\left(e_{\xi j},e_{\eta j},e_{\zeta j}\right)^T,\ \left[e_j^{d(j)}\right]=\begin{bmatrix} 0 & -e_{\zeta j} & e_{\eta j} \\ e_{\zeta j} & 0 & -e_{\xi j} \\ -e_{\eta j} & e_{\xi j} & 0 \end{bmatrix} \tag{33}$$

Also, it is shown,[27], regardless of the chosen theoretical approach, that we could start from different theoretical aspects (e.g. general theorems of dynamic, d`Alembert`s principle, Langrange`s equation of second kind, Appell`s equations etc.) and get equations of motion of the robotic system, which can be expressed in the identical covariant form as follows

$$\sum_{\alpha=1}^{n}a_{\alpha i}(q)\ddot{q}^{\alpha}+\sum_{\alpha=1}^{n}\sum_{\beta=1}^{n}\Gamma_{\alpha\beta,i}(q)\dot{q}^{\alpha}\dot{q}^{\beta}=Q_i \quad i=1,2,...,n. \;\square\square\square \tag{34}$$

where coefficients $a_{\alpha\beta}$ are covariant coordinates of basic metric tensor $\left[a_{\alpha\beta}\right]\in R^{n\times n}$ and $\Gamma_{\alpha\beta,\gamma}\ \alpha,\beta,\gamma=1,2,...,n$ presents Christoffel symbols of first kind. Generalized forces Q_i can be presented in the following expression (35) where $Q_i^c,Q_i^g,Q_i^{\beta},Q_i^w,Q_i^a$ denote the generalized spring forces, gravitational forces, viscous forces, semi-dry friction and generalized control forces respectively

$$Q_i = Q_i^c + Q_i^g + Q_i^{\beta} + Q_i^w + Q_i^a,\ \ i=1,2,...,n \tag{35}$$
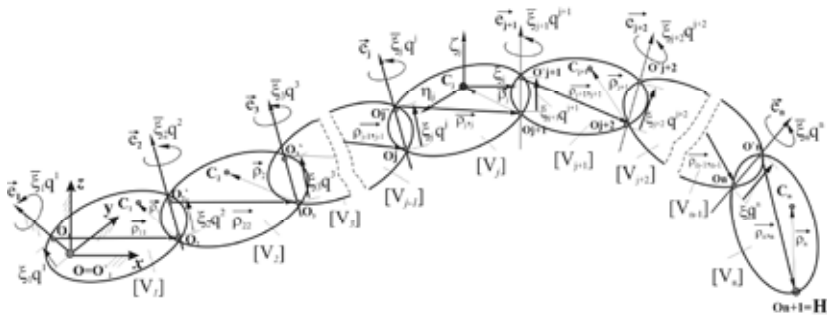
Figure 3. Open-chain structure of the robotic multi-body system

Further, on Fig 4. is the equivalent circuit of a DC motor represented.
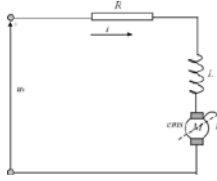
Figure 4. The equivalent circuit of a DC motor

The next equation describes the given circuit

$$R_i i_i(t) + L_i \frac{di_i(t)}{dt} + ems_i(t) = u_{vi}(t), \ i = 1, 2, 3$$

(36)

where R_i, L_i, i_i and u_{vi} are respectively resistance, inductivity, electrical current and voltage. Electromotive force is $ems_i(t) = k_e dq_m / dt$ where $k_e = const$ and $q_m(t)$ is generalized coordinate of a DC motor. If there is a reductor with a degree of reduction N_i than is $q_{mi}(t) = N_i q_i(t), \ i = 1, 2, 3$. It can be assumed that

$$Q_i^u(t) = N_i k_m i_i(t)$$

(37)

where $k_m = const$ is the torque constant. If the equation of robotic system is combined with (37) next equation can be written

$$A(q)\ddot{q} + C(q,\dot{q}) = NK_m i \ \Rightarrow i = [NK_m]^{-1} A(q)\ddot{q} + [NK_m]^{-1} C(q,\dot{q})$$

(38)

this in combination with (10) becomes

(39)

$$L[NK_m]^{-1} \left(\dot{A}(q)\ddot{q} + A(q)\dddot{q} \right) + L[NK_m]^{-1} \dot{C}(q,\dot{q}) + + R[NK_m]^{-1} \left(A(q)\ddot{q} + C(q,\dot{q}) \right) + K_e N\dot{q} = u_v(t)$$

In state space equation (39) is given with

$$\begin{bmatrix} \dot{x}_1(t) \\ \dot{x}_2(t) \\ \dot{x}_3(t) \end{bmatrix} = \begin{bmatrix} x_2(t) \\ x_3(t) \\ -A^{\bullet -1}(x_1(t))n(x(t)) \end{bmatrix} + \begin{bmatrix} 0 \\ 0 \\ -A^{\bullet -1}(x_1(t)) \end{bmatrix} u_v(t)$$

(40)

where

$$A^{\bullet}(q) = L[NK_m]^{-1} A(q)$$

$$n(q,\dot{q},\ddot{q}) = L[NK_m]^{-1} \dot{A}(q)\ddot{q} + L[NK_m]^{-1} \dot{C}(q,\dot{q}) + R[NK_m]^{-1} \left(A(q)\ddot{q} + C(q,\dot{q}) \right) + K_e N\dot{q}$$

(41)

and

$$x(t) = [x_1(t), x_2(t), x_3(t)] = [q(t), \dot{q}(t), \ddot{q}(t)]^T \in R^{3n}$$

(42)

4. Non-integer order control of robotic system

4.1 Optimal conventional and non-integer order PID control algorithm

Here, it is used robotic system with 3 DOF's ,Fig. 5, driven by 3 DC motors.
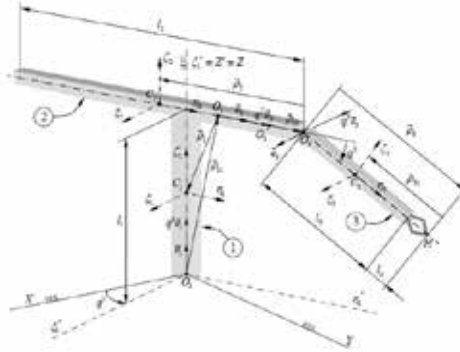
Figure 5. Robot with 3 DOF's

It is proposed the new algorithms of PID control based on fractional calculus (FC) in the control of robotic system driven by DC motors. Here, we introduce the next optimality criterion

$$J = \int |e(t)| dt \tag{43}$$

where is $e(t) = q_z(t) - q(t)$. Conventional PID control algorithm is

$$u(t) = k_p e(t) + k_d \frac{d}{dt} e(t) + k_i \int e(t) dt \tag{44}$$

while the fractional PID control algorithm is given by

$$u(t) = k_p e(t) + k_d D^{\alpha_D}[e(t)] + k_i D^{-\alpha_I}[e(t)]; \alpha_D, \alpha_I \in [0,1] \tag{45}$$
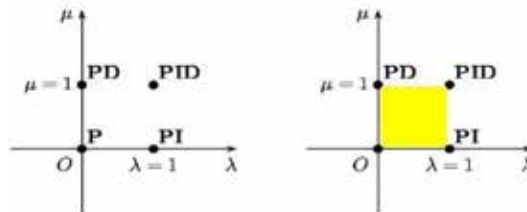
$$u(t) = K_p e(t) + T_i D_t^{-\lambda} e(t) + T_d D_t^{\mu} e(t). \quad (D_t^{(*)} \equiv_0 D_t^{(*)}). \tag{7}$$

Figure 6. Classical types of PID and fractional PID controller

The integrator term is s^α, that is to say, on a semi-logarithmic plane, there is a line having slope -20αdB. /dec. Clearly, selecting $\alpha = \beta = 1$, a classical PID controller can

be recovered. The selections of $\alpha = 1, \beta = 0,$ $\alpha = 0, \beta = 1,$ respectively corresponds conventional PI & PD controllers. All these classical types of PID controllers are the special cases of the fractional $PI^{\alpha}D^{\beta}$ controller, Fig.6. It can be expected that the controller $PI^{\alpha}D^{\beta}$ may enhance the systems control performance.

In order to determine the optimal parameters, a simulation of a given robotic system with three degrees of freedom driven by DC motors was made in *Simulink-Matlab* environment. For control of the system, voltage is used where parameters are set for each DC motor. The idea was to first determine the optimal parameters for the conventional PID control algorithm (its gains) and then to use these optimal parameters (gains) as known parameters for fractional PID control algorithm in order to determine optimal exponents of differentiation and integration. For calculation of fractional derivatives and integrals the Crone approximation of second order was used

$$s^{0.3} \approx \frac{3.981s^2 + 20.15s + 1}{s^2 + 20.15s + 3.981}, s^{0.6} \approx \frac{15.85s^2 + 40.21s + 1}{s^2 + 40.21s + 15.85} \tag{46}$$

$$s^{0.9} \approx \frac{63.1s^2 + 80.23s + 1}{s^2 + 80.23s + 63.1}, s^{-0.3} \approx \frac{25.12s^2 + 50.62s + 1}{s^3 + 50.62s^2 + 25.12s}$$
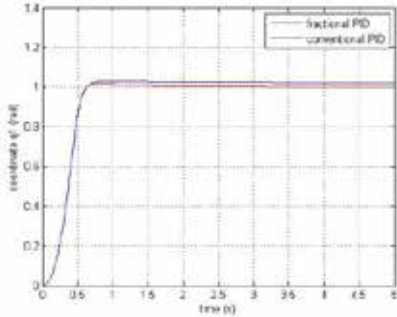
Figure7. Optimal trajectory q_1
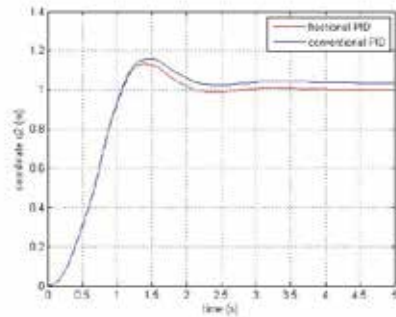
Figure 8. Optimal trajectory q_2

4.1.1 Simulation results for position control

Desired value of vector of generalized coordinate was $q_d = \begin{pmatrix} 1 & 1 & 1 \end{pmatrix}$. Optimal parameters for conventional PID and optimality criterion in this case had the following values (results are given for each DC motor):

$$k_{p1} = 50, k_{d1} = 8, k_{i1} = 4, J_1 = 0.4672, \ k_{p2} = 50, k_{d2} = 12, k_{i2} = 4, J_2 = 0.8591 \tag{47}$$

$$k_{p3} = 50, k_{d3} = 4, k_{i3} = 8, J_3 = 0.3602$$

Optimal parameters for fractional PID and optimality criterion had the following values:

$$k_{p1} = 50, k_{d1} = 8, k_{i1} = 4, \alpha_{d1} = 1, \alpha_{i1} = 0.2, J_1 = 0.3836$$
$$k_{p2} = 50, k_{d2} = 12, k_{i2} = 4, \alpha_{d2} = 1, \alpha_{i2} = 0.2, J_2 = 0.7401 \qquad (48)$$
$$k_{p3} = 50, k_{d3} = 4, k_{i3} = 8, \alpha_{d3} = 1, \alpha_{i3} = 0.8, J_3 = 0.3555$$

On Figs. 7,8 and 9 are given coordinate-time diagrams for previous optimal parameters –position control.
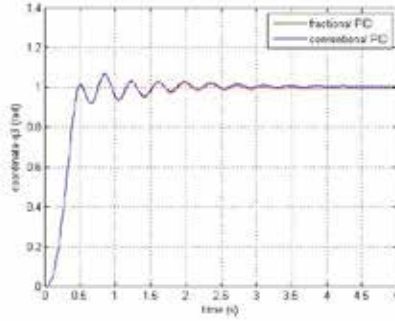
Figure 9. Optimal trajectory q_3

4.1.2 Results for tracking control

Also, we are interested in tracking control, so, we introduced vector of generalized coordinates

$$q_z = \begin{pmatrix} 0.5\sin(t - pi/2) + 0.5 \\ 0.5\sin(t - pi/2) + 0.5 \\ 0.5\sin(t - pi/2) + 0.5 \end{pmatrix}, \qquad (49)$$

Optimal parameters for conventional PID and optimality criterion had the following values:
$$k_{p1} = 50, k_{d1} = 8, k_{i1} = 22, J_1 = 0.1067 \qquad (50)$$
$$k_{p2} = 50, k_{d2} = 12, k_{i2} = 18, J_2 = 0.2115$$
$$k_{p3} = 50, k_{d3} = 18, k_{i3} = 22, J_3 = 0.1856$$

Optimal parameters for fractional PID and optimality criterion had the following values:

1) $\quad k_{p1} = 50, k_{d1} = 8, k_{i1} = 22, \alpha_{d1} = 0.6, \alpha_{i1} = 0.2, J_1 = 0.0788$

2) $\quad k_{p2} = 50, k_{d2} = 12, k_{i2} = 18, \alpha_{d2} = 0.6, \alpha_{i2} = 0.2, J_2 = 0.1386$

(51)

3) $\quad k_{p3} = 50, k_{d3} = 18, k_{i3} = 22, \alpha_{d3} = 1, \alpha_{i3} = 1, J_3 = 0.1856$

On Figs.10,11 and 12 are given coordinate-time diagrams for optimal parameters-tracking control.
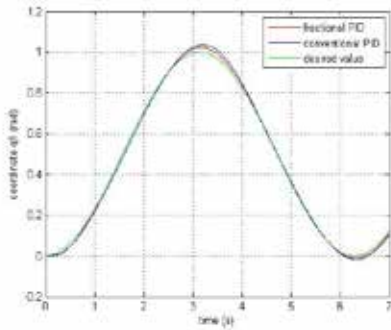
Figure 10. Optimal trajectory q_1
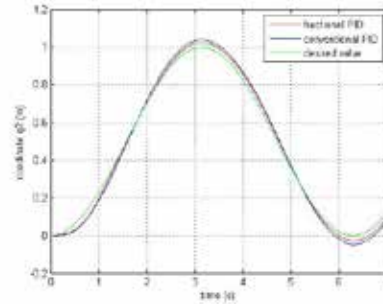
Figure 11. Optimal trajectory q_2
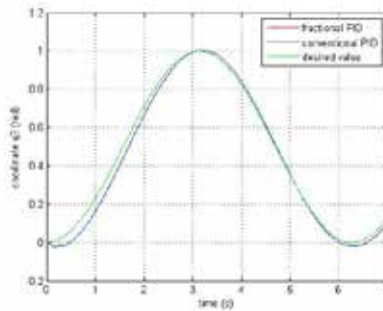
Figure 12. Optimal trajectory q_3

As, it is expected that the controller $PI^{\alpha}D^{\beta}$ may enhance the systems control performance. It has been shown, that using fractional PID gives better transient response as well as steady state error, and better tracking performances in position and tracking control of robotic system with 3 DOFs driven by DC motors.

4.2   A chattering-free sliding mode controller design based on fractional order PD$^{\alpha}$ sliding surface

Moreover, it is suggested here and obtain chattering-free fractional PD$^{\alpha}$ sliding-mode controller in the control of robotic system driven by DC motors. It is well-known that sliding-mode control is used to obtain high-performance robust control nonsensitive to disturbances and parameter variations. For a nonlinear MIMO system represented in so-called normal form

$$\dot{x} = f(x) + G(x)u \tag{52}$$

one general sliding mode control law is, [28]

$$u = -\left[\varLambda G(x)\right]^{-1} \varLambda\left[f(x) - \dot{x}_d\right] - \left[\varLambda G(x)\right]^{-1} Q\,\mathrm{sgn}(s) \tag{53}$$

consisting of continuous and discontinuous control part where switching surfaces $s = \left[s_1\, s_2\, ...s_n\right]^T$ are defined as $s = \varLambda(x - x_d)$, x_d being the vector of desired states and Q positive definite diagonal matrix. Elements of the matrix $\varLambda$ are chosen so that i-th component of sliding hypersurface has the structure

$$s_i = \left(\frac{d}{dt} + \lambda_i\right)^{(r_i - 1)}(x_i - x_{di}), \quad i = 1, 2, ..., n \tag{54}$$

where r_i is the order of the i-th subsystem and $\lambda_i > 0$. More general, considering (14) as a nominal (known) plant dynamics, we can write

$$\dot{x} = f(x) + \tilde{f}(x) + \left[G(x) + \tilde{G}(x)\right]u \tag{55}$$

where $\tilde{f}(x)$ and $\tilde{G}(x)$ represent uncertainties or unknown plant dynamics. Choosing as it is common Lyapunov function candidate to be

$$V = \frac{1}{2}s^T s \tag{56}$$

we have

$$\dot{s} = -PQ\,\mathrm{sgn}(s) + (P - I)\varLambda\left[\dot{x}_d - f(x)\right] + \varLambda\tilde{f}(x) \tag{57}$$

where $P := \varLambda\left(G + \tilde{G}\right)(\varLambda G)^{-1}$. Regardless whether $\tilde{G} \neq 0$ and/or $\tilde{f} \neq 0$, with an appropriate choice of Q, we can obtain $s^T \dot{s} < 0$ for $\|s\| > 0$, and this result indicates that the error vector defined by the difference $x - x_d$ is attracted by the subspace characterized by $s = 0$ and moves toward the origin according to what is prescribed by $s = 0$, [28]. In most cases this leads to good results but there are some disadvantages like *chattering* phenomenon. This problem could be overcome by approximating sgn(.) function in control law (53) with sat(.) or tanh(.) but here, we want to suggest one other solution. Instead of replacing sgn(.) function, we suggested to apply fractional sliding surface in order to decrease output signal oscillations. In this paper, it can be shown that without special tuning of Q for perturbed plant case, using just fractional order sliding surface and values of Q suitable for nominal plant, model uncertainties can be successfully compensated. For 3-DOF robotic system a conventional sliding manifold is of a first order *PD* structure $s_i = d\tilde{x}_i/dt + \lambda_i\tilde{x}_i$, $i = 1, 2, 3$ where $\tilde{x}_i = x_i - x_{id}$. There were some examples of using fractional *PI* and *PID* structures, [29] and now we propose a fractional PD^α structure as follows:

$$s_i = d^\alpha\tilde{x}_i/dt^\alpha + \lambda_i\tilde{x}_i, \quad i = 1, 2, 3 \tag{58}$$

4.2.1 Simulation results for position control-based on fractional PD^{α} sliding-mode control

Simulation studies have been carried out to verify the effectiveness of the proposed fractional PD^{α} sliding-mode control. Some experimental simulations were undertaken for $\alpha = 0.7, 0.8, 0.9, 0.95, 0.99$, and we found that best results are obtained with $\alpha = 0.95$, (Fig.13). Transfer function s^{ν} was realized by Crone's approximation, [30] and matrix $Q_{nom} = diag[5,5,5]$ as well as $\lambda = (5, 2.5, 2.5)^{T}$. The parameters of robot system and DC motors are set as:

$$m_1 = 6.2712 \text{ kg}, \ m_2 = 5.5575 \text{ kg}, \ m_3 = 1.8970 \text{ kg}$$

$$J_{x1} = 0.5273, \ J_{y1} = 0.5273, \ J_{z1} = 0.0164, \ J_{x2} = 1.0441, \ J_{y2} = 1.0441, \ J_{z2} = 0.0073,$$

$$J_{x3} = 0.1016, \ J_{y3} = 0.1016, \ J_{z3} = 0.0016 \left[kgm^2 \right]$$

$$K_{ei}=2, \ K_{mi}=1, \ N_i=1, \ R_i=1$$

$$(59)$$

To verify the robustness of the proposed fractional sliding/mode control we have applied corresponding parameter variation as follows:

$$\frac{\Delta m_1}{m_1} = 9.92\%, \ \frac{\Delta m_2}{m_2} = 9.47\%, \ \frac{\Delta m_3}{m_3} = 9.75\%$$

$$(60)$$

$$\frac{\Delta K_{ei}}{K_{ei}} = 5\%, \ \frac{\Delta K_{mi}}{K_{mi}} = 10\%, \ \frac{\Delta K_{ei}}{K_{ei}} = 10\%, \ \frac{\Delta K_{ei}}{K_{ei}} = 20\%$$

$$\frac{\Delta J_{x1}}{J_{x1}} = \frac{\Delta J_{y1}}{J_{y1}} = 14.39\%, \ \frac{\Delta J_{z1}}{J_{z1}} = 17.88\%, \ \frac{\Delta J_{x2}}{J_{x2}} = \frac{\Delta J_{y2}}{J_{y2}} = 9.39\%, \ \frac{\Delta J_{z2}}{J_{z2}} = 12.83\%$$

$$\frac{\Delta J_{x3}}{J_{x3}} = \frac{\Delta J_{y3}}{J_{y3}} = 14.20\%, \ \frac{\Delta J_{z3}}{J_{z3}} = 17.32\%$$
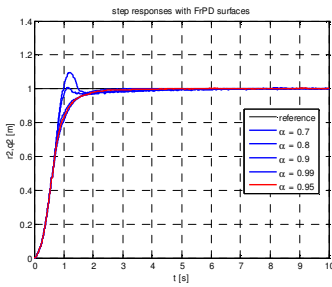
Nominal case:

Figure 13. Sliding surface s2- nominal case
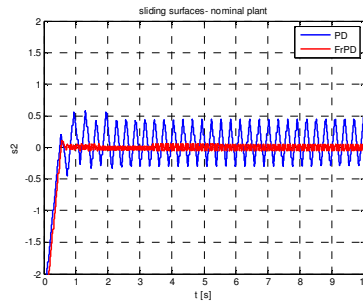
Figure 14. Step response $q_2(t)$ with PD^{α} surface

Simulation results are depicted in Figs 13 to 17 , where black lines are desired trajectories. Here, they are presented simulation data for case $i = 2$, q_2, s_2, (Fig-s.13-17). Particularly, we present comparing results for second coordinate q_2 responses with

PD and fractional PD^{α} cases and same all other conditions, for nominal object, Fig.13 and perturbed object, Fig.16.
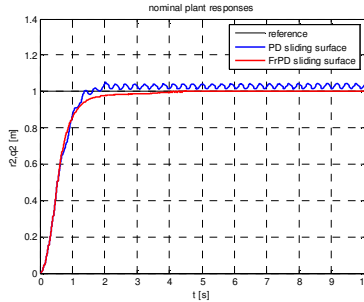
Figure 15. Stabilizing using sliding mode control PD and fractional PD^{α} -nominal case

Perturbated case:
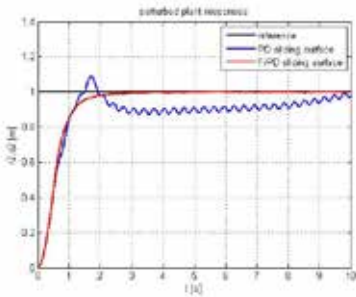
Figure 16 Stabilizing using sliding mode control PD and fractional PD^{α} -perturbed case
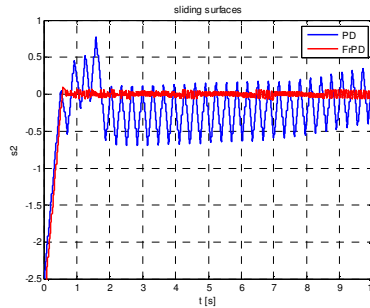
Figure 17 Sliding surface s2- perturbed case

As, it can be seen from previous figures a sliding mode control with fractional sliding surface is more robust to parameter perturbations and what is most important to emphasize output oscillations are almost completely attenuated and overall quality of transient response is much better. In that way, we obtain chattering-free tracking of the given robot system.

Also, the question of stability is of main interest in control theory. In the rest of this paper, some recently obtained results of the stability criteria of fractional order system with time delay as well as free delay are presented. They are employed the "classical" and the generalization of Gronwall Belmann lemma to obtain finite time stability and stabilization criteria for proposed class of time delay system. Also, they are presented some results on the stability of fractional order time delay systems. Finally, a numerical example is given to illustrate the validity of the proposed procedure.

5. Stability of fractional order time-delay systems

Recently, there have been some advances in control theory of fractional (non-integer order) dynamical systems for stability questions such as robust stability, bounded input–bounded output stability, internal stability, finite-time stability, practical stability, etc. Despite intensive researches, the stability of fractional order including time-delay systems remains an open problem. As for linear time invariant integer order systems, it is now well-known that stability of a linear fractional order system depends on the location of the system poles in the complex plane. Applying Matignon's stability theorem [31] one can check the system stability through the location in the complex plane of the dynamic matrix eigenvalues of the state space like system representation. But, in the case of fractional order time-delay system the characteristic function of a fractional-delay system involves fractional-order powers and exponential elements. As we know, due to the presence of the exponential function $e^{-\tau s}$, this equation has an infinite number of roots, which makes the analytical stability analysis of a time-delay system extremely difficult. In the field of infinite-dimensional fractional-delay systems most studies are concerned with the stability of a class of distributed systems, whose transfer functions involve $\sqrt{s}$ and/or $e^{-\sqrt{s}}$, [32]. Many examples of fractional differential systems with delay can be found in the literature. Simple examples such as $G(s) = \exp(-a\sqrt{s}) / s,\ a > 0$ arise in the theory of transmission lines [33], or one can find in [34] fractional delay systems with transfer function linked to the heat equation, which leads to transfer functions $G(s)$ such as

$$G(s) = \frac{\cosh(x\sqrt{s})}{\sqrt{s}\,\sinh(\sqrt{s})},\ \ \left(0 \leq x \leq 1\right)\ \ \text{or}\ \ G(s) = \frac{2e^{-a\sqrt{s}}}{b(1 - e^{-2a\sqrt{s}})} \tag{61}$$

In the literature few theorems are available for stability testing of fractional-delay systems. Chen and Moore [35] analyzed the stability of a class of fractional-delay systems, whose characteristic function can be represented as the product of factors of the form $\left(as^{\alpha} + b\right)e^{cs} + d = 0$ where the parameters a, b, c, d, and r are all real numbers. They considered the following delayed fractional equation

$$\frac{d^q y(t)}{dt^q} = K_p\, y(t - \tau) \tag{62}$$

where q and Kp are real numbers and $0 < q < 1$, time-delay τ is a positive constant and all the initial values are zeros. The stability condition is that for all possible q, r and Kp

$$\frac{q}{\tau} W\left(\frac{\tau}{r}\left(K_p\right)^{1/q}\right) \leq 0 \tag{63}$$

where in the inequality, $W(.)$ denotes the Lambert function such that $W(x)e^{W(x)} = x$. However, such a bound remains analytic and is difficult to use in practice. Further, Matignon's theorem has been used in [36] to investigate fractional differential systems

with multiple delays stability. For forced fractional-delay systems, it is usually required that BIBO stability holds, or equivalently, the characteristic function has roots with negative real parts only, while for unforced autonomous fractional delay systems, the stability usually means asymptotical stability in the sense of Lyapunov, namely, the characteristic function has roots with negative real parts only. Bonnet and Partington [37,38] analyzed the BIBO stability of fractional exponential delay systems which are of retarded or neutral type. Stability conditions can be expressed in terms of the location of the poles of the system. Also, they have handled the robust stabilization of fractional exponential delay systems of retarded type. However, all these contributions do not provide universally acceptable practical effective algebraic criteria or algorithms for testing the stability of a given general fractional delay system. Although the stability of the given general characteristic equation can be checked with the Nyquist criterion or the Mikhailov criterion, it becomes sufficiently difficult when a computer is used since one should find an angle of turn of the frequency response plot for an infinite variation of the frequency ω. A visual conclusion on stability with respect to the constructed part of the plot is not practically reliable, since, along with an infinite spiral, the delay generates loops whose number is infinite. As evidenced from the literature, the lack of universally acceptable algebraic algorithms for testing the stability of the characteristic equation has hindered the advance of control system design for fractional delay systems. This is particularly true in the case of designing fixed-structure fractional order controller, e.g., $PI^\alpha D^\beta$. On the other side, Hwang and Cheng [39] proposed a numerical algorithm that uses methods based on the Cauchy integral theorem and suggested the modified complex integral, where the stability of a given fractional-delay system can be achieved by evaluating the proposed integral and comparing its value with zero. Recently, in paper [40] the authors have studied the stability of fractional order nonlinear time-delay systems for Caputo's derivative and they extended the Lyapunov-Krasovskii theorem for the fractional nonlinear systems. Also, the Razumikhin theorem for the fractional nonlinear time-delay systems for Riemann-Liouville and Caputo derivatives was extended in [41] because the Razumikhin stability theory is more widely used to prove the stability of time-delay systems, since the construction of Lyapunov-Krasovskii functional is more difficult than that of the Lyapunov-Razumikhin function. Further, in [42] the authors proposed and proved the Mittag-Leffler stability theorem in the presence of both the Riemann-Liouville or the Caputo fractional derivatives and delay. The obtained theorems contain particular cases of the fractional calculus versions as well as the time-delay ones.

5.1 Finite-time stability of fractional order time-delay systems

All classical stability concepts, e.g., Lyapunov stability, asymptotic stability, bounded-input-bounded-output (BIBO) stability, deal with systems operating over an *infinite* interval of time. Finite-time stability is a concept that was first introduced in the 1950s and it deals with systems whose operation is limited to a *fixed finite* interval of time and requires *prescribed bounds* on system variables. Moreover, the boundedness properties of the system responses are very important from the engineering point of view. That is to say, enable system trajectories to stay within *a priori* given sets for the fractional order

time-delay systems in state-space form, i.e. system stability from the non-Lyapunov point of view is considered. From this fact and author best knowledge, he firstly introduced and defined finite-time stability for fractional order time-delay systems, [43-48]. Sufficient conditions of this kind of stability, for particular classes of fractional time-delay systems are derived. We also need the following definitions to analyze the case of fractional order systems with time-delay from non-Lyapunov point of view. First, it is introduced [43] the fractional order homogenous system with time-delay in state-space

$$_*D_{to,t}^{\alpha} x(t) = \frac{d^{\alpha} \boldsymbol{x}(t)}{dt^{\alpha}} = A_0 \boldsymbol{x}(t) + A_1 \boldsymbol{x}(t-\tau), \quad 0 < \alpha < 1, \tag{64}$$

with the associated function of initial state:

$$\boldsymbol{x}(t) = \boldsymbol{\psi}_x(t) \in C[-\tau, 0], \quad -\tau \le t \le 0. \tag{65}$$

Also, for the case of multiple time delays the state of fractional order systems can be presented as:

$$_*D_{to,t}^{\alpha} \boldsymbol{x}(t) = A_o \boldsymbol{x}(t) + \sum_{i=1}^{n} A_i \boldsymbol{x}(t-\tau_i), \quad 0 \le \tau_1 < \tau_2 < \tau_3 < ... < \tau_i < ... < \tau_n = \Delta, \tag{66}$$

and with the associated function of initial state:

$$\boldsymbol{x}(t) = \boldsymbol{\psi}_x(t), \quad -\Delta \le t \le 0. \tag{67}$$

Here, $_*D_{to,t}^{\alpha}(.)$ denotes either the Caputo fractional derivative $_C D_{to,t}^{\alpha}(.)$ or the Riemann-Liouville fractional derivative $_{RL} D_{to,t}^{\alpha}(.)$. Also, Lorenzo and Hartley [49] considered variable prehistories of $x(t)$ in $t < 0$, and its effects were taken into account in the fractional derivative in terms of the initialization function. Moreover, using the short memory principle and taking into account the initial function (65) one can obtain correct initial function, where it is assumed that there is no difficulty with questions of continuity of solutions with respect to initial data (function).

Definition 1.[43] *The system given by (64), satisfying the initial condition (65) is finite stable w.r.t* $\{t_o, J, \delta, \varepsilon, \tau\}, \quad \delta < \varepsilon$ *if and only if:*

$$\|\psi_x\|_C < \delta, \tag{68}$$

implies: $\qquad \|\mathbf{x}(t)\| < \varepsilon , \qquad \forall t \in J, \tag{69}$

Definition 2.[43] *The system given by (66), satisfying the initial condition (67) is finite stable w.r.t* $\{t_o, J, \delta, \varepsilon, \Delta\}, \quad \delta < \varepsilon$ *if and only if:*

$$\|\boldsymbol{\psi}_x\|_C < \delta, \quad \forall t \in J_\Delta, \quad J_\Delta = [-\Delta, 0] \in R, \tag{70}$$

implies: $\qquad \|\mathbf{x}(t)\| < \varepsilon , \qquad \forall t \in J, \tag{71}$

Theorem 1.(A)[43] *The autonomous system given by (64) satisfying the initial condition (65) is finite-time stable w.r.t.* $\{\delta, \varepsilon, \tau, t_o, J,\}$, $\delta < \varepsilon$, *if the following condition is satisfied*:

$$\left[1 + \frac{\sigma_{\max}^A \left(t - t_0\right)^\alpha}{\Gamma(\alpha+1)}\right] \cdot e^{\frac{\sigma_{\max}^A (t-t_0)^\alpha}{\Gamma(\alpha+1)}} \leq \varepsilon / \delta, \quad \forall t \in J. \tag{72}$$

where $\sigma_{max}(.)$ *is the largest singular value of matrix (.), namely:*

$$\sigma_{\max}^A = \sigma_{\max}\left(A_0\right) + \sigma_{\max}\left(A_1\right), \tag{73}$$

and $\Gamma(.)$ *is the Euler's gamma function.*

B) *The autonomous system given by (66) satisfying the initial condition (67) is finite-time stable w.r.t.* $\{\delta, \varepsilon, \Delta, t_o, J,\}$, $\delta < \varepsilon$, *if the following condition is satisfied*:

$$\left[1 + \frac{\sigma_{\Sigma\max}^A \left(t - t_0\right)^\alpha}{\Gamma(\alpha+1)}\right] \cdot e^{\frac{\sigma_{\Sigma\max}^A (t-t_0)^\alpha}{\Gamma(\alpha+1)}} \leq \varepsilon / \delta, \quad \forall t \in J. \tag{74}$$

where $\sigma_{\Sigma\max}^A(.) = \sum_i \sigma_i(A_i)$ *of matrices* A_i, $i = 0,1,2,...,n$ *where* $\sigma_{max}(.)$is the largest

singular value of matrix A_i, $i = 0,1,2,...,n$.

The above stability results for linear time-delay fractional differential systems are derived by applying Bellman - Gronwall's inequality. In that way, one can check system stability over finite-time interval.

Remark 1. If $\alpha = 1$, one can obtain the same conditions related to integer order time-delay systems

$$\frac{d\mathbf{x}(t)}{dt} = A_0 \mathbf{x}(t) + A_1 \mathbf{x}(t - \tau), \tag{75}$$

as follows ([50]):

$$\left[1 + \frac{\sigma_{\max}^A \left(t - t_0\right)^1}{1}\right] \cdot e^{\frac{\sigma_{\max}^A (t-t_0)^1}{1}} \leq \varepsilon / \delta, \quad \forall t \in J. , \Gamma(2) = 1 \tag{76}$$

Further, it is shown in [44] that fractional order time-delay state-space model of PD^α control of Newcastle robot can be presented by (64) in a homogenous state-space form. It is suggested using the Caputo version of the fractional derivative, where introducing $\mathbf{x}(t) = \left(x_1, x_2, x_3, x_4\right)^T$ one can obtain:

$$D_t^{1/2}\mathbf{x}(t) = \begin{bmatrix} 0 & 1 & 0 & 0 \\ 0 & 0 & 1 & 0 \\ 0 & 0 & 0 & 1 \\ -17.8 & 0 & -12.8 & 0 \end{bmatrix}\begin{bmatrix} x_1(t) \\ x_2(t) \\ x_3(t) \\ x_4(t) \end{bmatrix} + \begin{bmatrix} 0 & 0 & 0 & 0 \\ 0 & 0 & 0 & 0 \\ 0 & 0 & 0 & 0 \\ -0.04 & -0.04 & 0 & 0 \end{bmatrix}\begin{bmatrix} x_1(t-\tau) \\ x_2(t-\tau) \\ x_3(t-\tau) \\ x_4(t-\tau) \end{bmatrix} \tag{77}$$

Also, one has to check the finite-time stability w.r.t $\{t_o = 0, J = \{0,1\}, \delta = 0.06, \varepsilon = 100, \tau = 0.1\}$, where $\psi_x(t) = (0.05, 0, 0, 0)^T$, $\forall t \in [-0.1, \ 0]$. From initial data and the Eq. (77), one can easily obtain:

$$\|\psi_x(t)\|_C < 0.06,$$

$$\sigma_{\max}(A_0) = 21.95, \ \sigma_{\max}(A_1) = 0, \ \sigma_{\max} = 21.95,$$

$$\Gamma(1+1/2) = \frac{\sqrt{\pi}\,\Gamma(2+1)}{2^2\Gamma(1+1)} = \frac{\sqrt{\pi}\,(2)!}{2^2 1!} = \frac{\sqrt{\pi}}{2} = 0.886, \qquad (78)$$

From the Theorem 8(A), it immediately follows

$$\left[1 + \frac{21.95 T_e^{1/2}}{0.866} \right] \cdot e^{\frac{21.95 T_e^{1/2}}{0.866}} \le 100/0.06, \ \Rightarrow T_e = 0.05 \ \ s, \qquad (79)$$

T_e being the "estimated time" of finite-time stability. Also, in paper [51], a stability test procedure is proposed for nonhomogeneous fractional order systems with pure time-delay

$$_*D_{to,t}^\alpha x(t) = \frac{d^\alpha x(t)}{dt^\alpha} = A_0 x(t) + A_1 x(t-\tau) + B_0 u(t), \quad 0 < \alpha < 1, \qquad (80)$$

with the associated function of initial state, (65).

Definition 3. The system given by (80) satisfying the initial condition (65) is finite stable w.r.t $\{\delta, \varepsilon, \beta, \alpha_u, t_o, J,\}$, $\delta < \varepsilon$ if and only if:

$$\|\psi_x\|_C < \delta$$
$$(81)$$

$$\|u(t)\| < \alpha_u \ , \qquad \forall t \in J, \ \ \alpha_u > 0 \qquad (82)$$

implying:

$$\|x(t)\| < \varepsilon, \qquad \forall t \in J \qquad (83)$$

Theorem 2. The nonautonomous system given by (80) satisfying the initial condition (65) is finite-time stable *w.r.t.* $\{\delta, \varepsilon, \alpha_u, \alpha_0, t_o, J,\}$, $\delta < \varepsilon$, if the following condition is satisfied:

$$\left[1 + \frac{\sigma_{\max}^A (t-t_0)^\alpha}{\Gamma(\alpha+1)} \right] \cdot e^{\frac{\sigma_{\max}^A (t-t_0)^\alpha}{\Gamma(\alpha+1)}} + \gamma^\square \frac{(t-t_0)^\alpha}{\Gamma(\alpha+1)} \le \varepsilon/\delta, \quad \forall t \in J. \qquad (84)$$

where $\gamma^\square = b_0 \alpha_u / \delta$, $\|B_0\| = b_0$ and $\Gamma(.)$ Euler's gamma function.

Recently, we have studied and reported in paper [45] a stability test procedure for linear nonhomogeneous fractional order systems with pure time-delay. New stability criteria for this class of fractional order systems were derived by applying Bellman-Gronwall`s approach using for the starting point a recently obtained *generalized Gronwall*

inequality reported in [52].In that way, one can check system stability over finite-time, which is illustrated using a suitable illustrative example.

Theorem 3. ([52] *Generalized Gronwall inequality*) . Suppose $x(t), a(t)$ are nonnegative and local integrable on $0 \leq t < T, some\ T \leq +\infty$,and $g(t)$ is a nonnegative, nondecreasing continuous function defined on $0 \leq t < T$, $g(t) \leq M = const$, $\alpha > 0$ with

$$x(t) \leq a(t) + g(t) \int_0^t (t-s)^{\alpha-1} x(s) ds \qquad (85)$$

on this interval.Then

$$x(t) \leq a(t) + \int_0^t \left[\sum_{n=1}^\infty \frac{\left(g(t)\Gamma(\alpha)\right)^n}{\Gamma(n\alpha)}(t-s)^{n\alpha-1} a(s) \right] ds, \quad 0 \leq t < T \qquad (86)$$

Corollary 2.1 of Theorem 9, [52]   Under the hypothesis of Theorem 11, let $a(t)$ be a nondecreasing function on $[0,T)$. Then it holds:

$$x(t) \leq a(t) E_\alpha \left(g(t)\Gamma(\alpha) t^\alpha \right) \qquad (87)$$

Theorem 4. The linear nonautonomous system given by (80) satisfying the initial condition $\mathbf{x}(t) = \mathbf{\psi}_x(t)$, $-\tau \leq t \leq 0$ is finite-time stable w.r.t. $\{\delta, \varepsilon, \alpha_u, J_0,\}$, $\delta < \varepsilon$ if the following condition is satisfied:

$$\left(1 + \frac{\sigma_{\max 01} t^\alpha}{\Gamma(\alpha+1)} \right) E_\alpha \left(\sigma_{\max 01} t^\alpha \right) + \frac{\gamma^\bullet_{u0} t^\alpha}{\Gamma(\alpha+1)} \leq \varepsilon / \delta, \ \forall t \in J_0 = \{0,T\}, \qquad (88)$$

where $\gamma^\bullet_{u0} = \alpha_u b_0 / \delta$, and $\sigma_{max}(.)$ being the largest singular value of the matrix (.), where: $\sigma_{\max 01} = \sigma_{\max}(A_0) + \sigma_{\max}(A_1)$ and $E_\alpha(.)$ denotes Mittag-Leffler function.

Theorem 5. The linear autonomous system given by (64) satisfying the initial condition $\mathbf{x}(t) = \mathbf{\psi}_x(t)$, $-\tau \leq t \leq 0$ is finite-time stable w.r.t. $\{\delta, \varepsilon, J_0,\}$, $\delta < \varepsilon$ if the following condition is satisfied:

$$\left(1 + \frac{\sigma_{\max 01} t^\alpha}{\Gamma(\alpha+1)} \right) E_\alpha \left(\sigma_{\max 01} t^\alpha \right) \leq \varepsilon / \delta, \ \forall t \in J_0, \qquad (89)$$

Specially, the problem of finite time stability with respect to some of the variables (partial stability) is considered. Particularly, we are interested in partial stability i.e of the stability of motion with respect to some of the variables $y(t)$ where are

$$x = \left(x_1, x_2, ..., x_n\right)^T = \left(y_1, y_2, ..., y_m, z_1, ..., z_p\right)^T = \left(y^T, z^T\right)^T \tag{90}$$

$$m > 0, \, p \geq 0, \quad n = m + p$$

This class includes problems of stability to the components of the vector $y(t)$ of the equilibrium position $x = 0$ of a nonlinear system of ordinary differential equation

$$\dot{y} = Y(t, y, z), \quad \dot{z} = Z(t, y, z), \tag{91}$$

Moreover, for the vector functions Y and Z, of given system is usually assumed to be continuous in the domain

$$t \geq 0, \quad \|y\| \leq h, \quad \|z\| < L_z \leq \infty \tag{92}$$

and its solutions are assumed to be unique and z-continuable,where are $h, L_z \in R^+$ known real positive numbers,[53] .Also, one can introduce,

$$\psi_x(\theta) = \left[\psi_y(\theta), \psi_z(\theta)\right], \tag{93}$$

where is usually assumed for $\quad \forall t \in J$

$$\|\psi_y\|_C = \sup_{-\tau_M \leq \theta \leq 0} \|\psi_y(\theta)\| \leq h, \quad \|\psi_z\|_C = \sup_{-\tau_M \leq \theta \leq 0} \|\psi_z(\theta)\| < L \tag{94}$$

Definition 4: A solution $x(t) = 0$ of the time delay system given by homogenous state equation (80) ($u(t) \equiv 0, \, \forall t$) satisfying initial condition $x(t) = \psi_x(t), \, -\tau_M \leq t \leq 0$, where $\|\psi_y\|_C \leq h, \, \|\psi_z\|_C < \infty$, for all $t \geq t_0$, is

a) y –*stable* if for any $\varepsilon > 0$ and $t_0 \geq 0$, there exists $\delta(\varepsilon, t_0) > 0$ such that $\|\psi_{x0}\|_C < \delta$ implies
$$\|y(t; t_0, \psi_x(t))\| < \varepsilon, \quad \text{for all } t \geq t_0, \tag{95}$$

b) uniformly **y**-stable if δ does not depend on t_0 .

Definition 5: The time delay system given by homogenous state equation (64) (when $u(t) \equiv 0, \, \forall t$) satisfying initial condition $x(t) = \psi_x(t), \, -\tau_M \leq t \leq 0$, where $\|\psi_z\|_C < L, \, \forall t \in J$ is *finite time partially stable w.r.t* $\{\delta, \varepsilon, t_o, J, \}, \, \delta < \varepsilon$ if and only if

$$\left(\|\psi_{y0}\|_C + \|\psi_{z0}\|_C\right) < \delta \tag{96}$$

imply: $$\|y(t; t_0, \psi_x(t))\| < \varepsilon, \qquad \forall t \in J. \tag{97}$$

Definition 6: System given by (80) satisfying initial condition $x(t) = \psi_x(t), \, -\tau_M \leq t \leq 0$ where $\|\psi_z\|_C < L, \quad \forall t \in J$ is *finite time partially stable w.r.t* $\{\delta, \varepsilon, \alpha_u, t_o, J, \}, \, \delta < \varepsilon$ if and only if

$$\left(\left\|\psi_{y0}\right\|_C + \left\|\psi_{z0}\right\|_C\right) < \delta, \tag{98}$$

and
$$\left\|u(t)\right\| < \alpha_u, \quad \forall t \in J \tag{99}$$

imply
$$\left\|y(t;t_0,\psi_x(t))\right\| < \varepsilon, \quad \forall t \in J. \tag{100}$$

So, it is proposed finite time partial stability test procedure of linear (non)autonomous unknown time delay fractional order systems. Time-delay is assumed to be unknown but its upper bound is assumed to be known. System is given as follows

$$\frac{d^\alpha}{dt^\alpha}\begin{pmatrix} y(t) \\ z(t) \end{pmatrix} = \begin{bmatrix} A_{0yy} & A_{0yz} \\ A_{0zy} & A_{0zz} \end{bmatrix}\begin{pmatrix} y(t) \\ z(t) \end{pmatrix} + \begin{bmatrix} A_{1yy} & A_{1yz} \\ A_{1zy} & A_{1zz} \end{bmatrix}\begin{pmatrix} y(t-\tau) \\ z(t-\tau) \end{pmatrix} + \begin{bmatrix} B_{0y} \\ B_{0z} \end{bmatrix}u(t) \tag{101}$$

Specially, we consider stability of the following subsystem

$$\frac{d^\alpha\left(y(t)\right)}{dt^\alpha} = A_{0yy}y(t) + A_{0yz}z(t) + A_{1yy}y(t-\tau) + A_{1yz}z(t-\tau) + B_{0y}u(t) \tag{102}$$

Theorem 6: [54] The linear nonautonomous system given by (102) satisfying initial condition $x(t) = \psi_x(t), \ -\tau_M \le t \le 0$, where $\left\|\psi_z\right\|_C < L, \ \forall t \in J_0$, *is finite time partially stable w.r.t.* $\{\delta, \varepsilon, \alpha_u, J_0,\}, \ \delta < \varepsilon$, if the following condition is satisfied

$$\left(1 + \frac{\mu_{\Sigma y}t^\alpha}{\Gamma(\alpha+1)}\right)E_\alpha\left(\mu_{\Sigma y}t^\alpha\right) + \frac{\lambda_{uo}t^\alpha}{\Gamma(\alpha+1)} + \frac{\eta_{\Sigma z}t^\alpha}{\Gamma(\alpha+1)}(1+L_0) \le \varepsilon/\delta \quad \forall t \in J_0 = [0,T] \tag{103}$$

where $\mu_{\Sigma y}$ is defined by $\mu_{\Sigma y} = \sigma_{Aoyy} + \sigma_{A1yy}$, $\lambda_{u0} = \alpha_u b_0/\delta, \ L_0 = L/\delta, \eta_{\Sigma z} = a_{Aoyz} + a_{A1yz} \quad \sigma(.)$ being the largest singular value of matrix, and $E_\alpha(z)$ the Mittag-Leffler function which is defined by:

$$E_\alpha(z) = \sum_{k=0}^{\infty} \frac{z^k}{\Gamma(k\alpha+1)}, \quad \Re e\alpha > 0, z \in \square. \tag{104}$$

6   Discussion

New algorithms of PID control based on fractional calculus (FC) are studied and presented. We introduced an optimal procedure in the position control of a 3 DOF robotic system driven by DC motors as well as a robust fractional-order sliding mode control. As expected, the controller $PI^\alpha D^\beta$ may enhance the systems control performance. It has been shown that using fractional PID gives a better transient response and a steady state error as well as better tracking performances in the position control of a 3 DOF robotic system driven by DC motors. The optimal parameters for the conventional PID control algorithm (its gains) are determined first and they are used as

initial, known parameters for the fractional PID control algorithm in order to determine the optimal fractional exponents of differentiation and integration. After that, the effectiveness of the suggested optimal fractional PID control is demonstrated with a suitable robot with three degrees of freedom as an illustrative example. In addition, we proposed a robust fractional-order sliding mode control of a given robot system driven by DC motors where a fractional order sliding surface PD^{α} is introduced. It is shown that a sliding mode control with the fractional sliding surface is more robust to parameter perturbations and, what is most important to emphasize, the output oscillations are almost completely attenuated and the overall quality of the transient response is much better. While Lyapunov methods have been developed for stability analysis and control law synthesis of integer linear systems and have been extended to stability of fractional systems, only few studies deal with non-Lyapunov stability of fractional systems. Further, in this paper, we have studied and presented the finite time stability of (non)perturbed (non)linear fractional order time-delay systems. Specially, the problem of finite time stability with respect to some of the variables (partial stability) is considered. New stability criteria for this class of fractional order systems were derived using a recently obtained generalized Gronwall inequality as well as "*classical*" Bellman-Gronwall inequality to obtain finite-time stability criteria for the proposed class of time-delay systems. Finally, numerical examples are given to illustrate the validity of the proposed procedure. Some of these results are presented at the *fifth symposium of fractional differentiation and its applications* was held a t the Hohai University, Nanjing, China in the period of May 14-May 17, 2012. Also, author received awards *for the Best poster* for the paper *Finite Time Partial Stability of Fractional Order Time Delay Systems*, as well as and *the Best oral presentation* for the *paper Optimal Fractional Order PID Control Of Expansion Turbine In The Air Production Cryogenic Liquid,* [54-56].

References

[1] Oldham K B and J. Spanier, (1974)*The Fractional Calculus: Theory and Applications of Differentiation and Integration to Arbitrary Order*, Academic Press, New York, NY, USA, 1974.

[2] Hilfer R, Ed., *Applications of Fractional Calculus in Physics,*World Scientific, River Edge, NJ, USA, 2000.

[3] Podlubny I. (1999) *Fractional Differential Equations.* Academic Press, San Diego.

[4] Siciliano B, Sciavicco L Villani L. and Oriolo, G.(2009) Robotics, Springer-Verlag, London, 2009.

[5] Bredin C (2005) Team-mates, *ABB MultiMove functionality heralds a new era in robot applications.*
ABB Review, 2005. 1. URL www.abb.co.uk/

[6] Lazarević M., Mandić P and Vasić V (2011) Some applications of NeuroArm interactive robot and Webots robot simulation tool, in: *Proceedings on Accomplishments in Mechanical and Electrical Engineering and Information Technology,* 26-29.05.2011, Banjaluka, pp. 923-928.

[7] *Webots User Guide*, Cyberbotics Ltd, 2011.

[8] Astrom Kand and T Hagglund (1995)*PID controllers:Theory, design, and tuning*. Instrument Society of America, North Carolina.

[9] ChenY C Hu and K L Moore (2003) Relay Feedback Tuning of Robust PID Controllers with Iso-Damping Property, *IEEE 2003 Conference on Decision and Control*, December 9-12, 2003, Maui, HI, USA.

[10]   Astrom K J and T Hagglund (2000) The Future of PID Control," in *IFAC Workshop on Digital Control. Past, Present and Future of PID Control,* (Terrassa, Spain), pp. 19–30, April 2000.

[11]   Lazarevic M P (2006) Finite time stability analysis of PD^{α} fractional control of robotic time-delay systems, *Mech. Resch.Commun.* **33**, 269–279.

[12]   Maione G. Lino P (2007) New tuning rules for fractional PI^{α} controllers,*Nonlinear Dyn*. **49,** 251–257.

[13]   Oustaloup A, Sabatier J, Lanusse P (1999) From fractal robustness to CRONE control", *Fractional Calc. Appl. Anal***. 2**(1), 1–30.

[14]   Oustaloup A.(1991) *La Commande CRONE*. Hermes, Paris.

[15]   Monje CA., Feliu V.(2004) The fractional-order lead compensator, In: *IEEE International Conference on Computational Cybernetics*. Vienna, Austria, August 30–September 1.

[16] Edwards C. and Spurgeon S K (1998) Sliding mode control theory and applications,Taylor & Fran., NewYork.

[17] Hace, A., Jezernik, K.,.(2000) Robust position tracking   control for direct drive motor, *Industrial Electronics Society, 2000. IECON 2000. 26th Annual Conference of the IEEE.*

[18] Monje C.A., et al., *Fractional-order Systems and Controls*, Springer-Verlag, London,2010.

[19] Delavari,H. R. Ghaderi, A. Ranjbar, S. Momani,(2008) Fractional Order Controller for Two-degree of Freedom Polar Robot, 2nd Conference on Nonlinear Science and Complexity, Ankara, Turkey.

[20] Efe,M.O, (2009) Fractional Order Sliding Mode Controller Design for Fractional Order Dynamic Systems, *New Trends in Nanotech. and Frac. Calculus Applications*.

[21] Kilbas, A.A., Srivastava, H.M., Trujillo, J.J. (2006) *Theory and Applications of Fractional Differential Equations*. Elsevier, Amsterdam.

[22] Grunwald   A. K,(1867)Uber "begrenzte" Derivationen und deren Anwendung. *Zeit. fur Mathematik und Physik 12* , 441-480,.

[23] Letnikov A. V.(1868) *Theory of differentiation with an arbitrary index (Russian*), *Moscow, Matem. Sbornik*, 3:1-66.

[24] Caputo, (1969) M. *Elasticit´a e Dissipazione*. Zanichelli, Bologna.

[25] Podlubny I.,(2002) Geometric and physical interpretation of fractional integration and fractional differentiation. Fract Calc Appl Anal 5:367–386.

[26] Lazarević M.,(2005)Optimal control of redundant robots in human-like fashion:general considerations. *FME Transcation*, Faculty of Mechanical Engineering, University of Belgrade, Belgrade**. 33**(2):53-64.

[27] I. Lurie. (1961)*Analytical Mechanics.* (in Russian), G. Publishing, Moscow.

[28] Mehmet Ö.E., Kasnakoglu C, (2008) A fractional adaptation law for sliding mode control, *Int. J. Adapt. Control Signal Process.*, John Wiley & Sons.

[29] Calderon A.J., Vinagre B.M., Feliu V.- (2003)Fractional Sliding Mode Control of a DC-DC Buck Converter with Application to DC Motor Drives, *Proceedings of ICAR* 2003, Coimbra,Portugal,2003.

[30] Valerio D., (2005) *Fractional robust system control*,PhD Thesis, Technical University of Lisboa, Lisbon.

[31] D. Matignon, (1996) Stability result on fractional differential equations with applications to control processing. In *IMACS - SMC Proceeding,* July, Lille, France,pp. 963- 968.

[32] N. Ozturk,A. Uraz, (1985)An analytic stability test for a certain class of distributed parameter systems with delay, *IEEE Transactions on CAS* ,Vol.32,No.4,pp.393-39.

[33] E. Weber, *Linear Transient Analysis.* Volume II. Wiley, New York ,1956

[34] J. Loiseau, H. Mounier, Stabilisation de l'´equation de la chaleur command´ee en flux. Syst`emes Diff´erentiels Fractionnaires, Mod`eles,Methodes et Applications. *ESAIM Proceedings* 5,1998,pp.131–144.

[35] Y. Q. Chen, K. L. Moore, (2002) Analytical Stability Bound for a Class of Delayed Fractional-Order Dynamic Systems, *Nonlinear Dynamics*, Vol.29,2002,pp. 191-202.

[36] C. Hwang, C.C.Yi, (2005) Use of Lambert W Function to Stability Analysis of Time-Delay Systems,*American Control Conference, ACC2005,* June 8-10, Portland, OR, USA,2005,pp.4283-4288.

[37] C. Bonnet, J.R Partington,Stabilization of fractional exponential systems including delays,*Kybernetika,* 37,2001,pp.345-353.

[38] C. Bonnet, J.R Partington.,(2002) Analysis of fractional delay systems of retarded and neutral type, *Automatica,* 38, 2002,pp.1133-1138.

[39] Hwang C, Cheng Y-C, A numerical algorithm for stability testing of fractional delay systems. *Automatica* 42,2006,pp.825–831.

[40] D. Baleanu, A. Ranjbar N, S.J. Sadati R., H. Delavari, T. Abdeljawad, V. Gejji, (2011) Lyapunov-Krasovskii stability theorem for fractional systems with delay, *Romanian Journal of Physics*, Vol. 56. No.5-6,2011, pp.636-643

[41] D. Baleanu,S. J. Sadati, R. Ghaderi, A. Ranjbar, T. Abdeljawad (Maraaba), F. Jarad,(2010) Razumikhin Stability Theorem for Fractional Systems with Delay, *Abstract and Applied Analysis,* Volume 2010, Article ID 124812,9 pages.

[42] J. Sadati, D. Baleanu,S., A. Ranjbar,R. Ghaderi, T. Abdeljawad (Maraaba), (2010) Mittag-Leffler Stability Theorem for Fractional Systems with Delay, *Abstract and Applied Analysis*, Volume 2010, 7 pages.

[43] M. P. Lazarević, D. Debeljković,Finite Time Stability Analysis of Linear Autonomous Fractional Order Systems with Delayed State,*Asian Journal of Control*,Vol.7, No.4.2005,pp.440-447.

[44] M. P. Lazarević, Finite time stability analysis of PDα fractional control of robotic time-delay systems, *Mechanics Research Communications*,Vol.33,2006, pp.269–279.

[45] M. Lazarević, A.Spasić, Finite-Time Stability Analysis of Fractional Order Time Delay Systems: Gronwall`s Approach, *Mathematical and Computer Modelling*,2009,49,pp. 475-481.

[46] M. Lazarević, (2007) Finite-time stability analysis of fractional order time delay systems: bellman-gronwall`s approach,*Scientific Technical Review*,Vol.LVII,No.1,2007, pp.8-15.

[47] M. Lazarević, D. Debeljković, (2008) Robust Finite Time Stability of Nonlinear Fractional Order Time Delay Systems, *Int. Journal of Information and Systems Sciences*,Vol.4.No.2,2008, pp.301-315.

[48] M. Lazarević, A.Obradović,V.Vasić, (2010) Robust finite -time stability analysis of fractional order time delay systems: new results, *WSEAS2010, Control10*, May,Tunisia,2010,pp.101-106.

[49] C. Lorenzo, T. Hartley T.,Initialization,conceptualization,and application,*NASA-Tp*, Dec.,1998.

[50] M.Lazarević, D.Lj. Debeljković,Z. Nenadić,S. Milinković, Finite Time Stability of Time Delay Systems, *IMA Journal of Math. Cont. and Inf.* No.17, 2000,pp.101-109.

[51] M.P.Lazarević, On finite time stability of nonautonomous fractional order time delay systems, *Int. Jour.:Problems of Nonlinear Analysis in Engineering Systems,*Vol.1,No27,2007,pp.123-148.

[52] H. Ye., J.Gao., Y. Ding.,(2007) A generalized Gronwall inequality and its application to a fractional differential equation, *J. Math. Anal. Appl.* **328** ,pp.1075–1081.

[53] Vorotnikov, V., ,(2005) Partial Stability and Control: The State-of-the-art and Development Prospects, *Automation and Remote Control*, Vol. 66, No. 4, (2005).pp. 511-561.

[54] M.Lazarević, ,(2012) Finite Time Partial Stability of Fractional Order Time Delay Systems, No147, (2012),*FDA2012,Nanjing,*May,China.

[55] S.A. Batalov, M.P. Lazarević,A. Hace, K.Jezernik, ,(2012) A Chattering-free Fractional PDa Sliding-mode Control of a 3-DOF Robot System Driven by DC motors,No130, *FDA2012,Nanjing*,May,China.

[56] Lj. Bučanović, M. Lazarević,S. Batalov,(2012) Optimal Fractional Order PID Control Of Expansion Turbine In The Air Production Cryogenic Liquid,No128, *FDA2012, Nanjing*,May,China.

DIFFERENTIAL EQUATIONS OF MOTION FOR MECHANICAL SYSTEMS WITH NONLINEAR NONHOLONOMIC CONSTRAINTS – VARIOUS FORMS AND THEIR EQUIVALENCE

Dragomir N. Zekovic[1]

[1] University of Belgrade, Faculty of Mechanical Engineering,
Kraljice Marije 16, 11120 Belgrade, Serbia; e-mail: dzekovic@mas.bg.ac.rs

Abstract. *The paper analyzes various forms of differential equations of motion for nonlinear nonholonomic systems in terms of their equivalence. All well-known forms of differential equations of motion (Maggi, Volterra, Appell, Voronec, Chaplygin, Ferrers, Boltzmann-Hamel) are written for nonlinear nonholonomic systems and translated into the same general form, or derived from it. This way, their mutual equivalence is proved, i.e., the conclusions that hold for linear nonholonomic systems are generalized. Theoretical considerations are illustrated by a detailed example of a conservative mechanical system with a nonlinear nonholonomic constraint.*
Key words: *equation of motion, system, nonholonomic, constraint, nonlinear.*

1. First Part

In the mechanics of nonholonomic systems there are several forms of differential equations of motion [1-9] that can be translated into the same general form, i.e., it is shown that they are mutually equivalent, [10]. It is demonstrated that various forms of differential equations of motion are a consequence of the manner of incorporating nonholonomic constraints in the Lagrange-D'Alembert principle.

Let us generalize the conclusions presented in [10] to nonholonomic systems with nonlinear constraints, using standard variables (independent generalized coordinates and quasicoordinates) in contrast to the theory of Poincare's equations, where a set of operators figure, with a property of a group (conditionally speaking, those equations are written with a group variable). In Poincare's equations written in the Poincare-Chetayev variables, dependent generalized coordinates are figuring in addition to the operators mentioned.

Since considerations to follow employ the transformation of coordinates, presented in [11], it is described in brief. Let the position of a system of particles M_a $(a=1,...,N)$, in 3-dimensional Euclidean space E_3, be determined by coordinates x_a^1, x_a^2, x_a^3 $(a=1, ..., N)$. Let us incorporate new variables y^b, as in [11], by the relations

$$y^1 = \sqrt{m_1}\, x_1^1, \qquad y^2 = \sqrt{m_1}\, x_1^2, \qquad y^3 = \sqrt{m_1}\, x_1^3$$
$$\vdots \qquad\qquad \vdots \qquad\qquad \vdots$$
$$y^{3N-2} = \sqrt{m_N}\, x_N^1, \quad y^{3N-1} = \sqrt{m_N}\, x_N^2, \quad y^{3N} = \sqrt{m_N}\, x_N^3$$

where index b takes the following values: $b=1, \ldots, 3N$. After taking into account the holonomic constraints, let the system have n degrees of freedom, i.e., the determination of the position of the system requires q^i $(i=1,\ldots,n)$ generalized coordinates. All coordinates y^b can be expressed via generalized coordinates q^i by the relations

$$y^b = y^b\left(q^1,\ldots,q^n\right), \quad b = 1,\ldots,3N$$

Let us observe a mechanical system subject to the action l of nonlinear nonholonomic constraints of the form

$$\phi^\nu\left(q^i,\dot{q}^i\right) = 0 \rightarrow \dot{q}^\nu = \psi^\nu\left(q^i,\dot{q}^\alpha\right)^1 \tag{1}$$

Let us express independent generalized velocities $\dot{q}^\alpha$, using particular independent kinematic parameters $\dot{\pi}^\alpha$ by the relations

$$\dot{q}^\alpha = \theta^\alpha\left(q^i,\dot{\pi}^\beta\right) \tag{2}$$

Using the constraints (1), dependent generalized velocity $\dot{q}^\nu$ can be also expressed by means of independent kinematic parameters $\dot{\pi}^\alpha$ applying the relations

$$\dot{q}^\nu = \psi^\nu\left(q^i,\dot{q}^\alpha\right) = \psi^\nu\left[q^i,\theta^\alpha\left(q^i,\dot{\pi}^\beta\right)\right] = \theta^\nu \tag{3}$$

Based on the (2) and (3), the expression for the transformation of all velocities $\dot{q}^i$ reads

$$\dot{q}^i = \theta^i\left(q^j,\dot{\pi}^\alpha\right) \tag{4}$$

The derivation of differential equations of motion, starting from Lagrange-D'Alembert's principle, requires certain expressions and relations, therefore they are mentioned first. The expression for kinematic energy of the system reads

$$T = \frac{1}{2} g_{ij}\dot{q}^i\dot{q}^j \tag{5}$$

or considering the (4)

$$T^* = \frac{1}{2} g_{ij}\theta^i\theta^j \tag{6}$$

Countervariant coordinates of the acceleration vector in holonomic coordinates read

$$f^S = \ddot{q}^S + \Gamma_{ij}^S\dot{q}^i\dot{q}^j \tag{7}$$

---

1 Einstein summation convention is used in the paper. Indices take the following values: $\quad i, j, k, r, s=1,\ldots,n$; $\alpha,\beta,\gamma=1,\ldots,m; \quad \nu,\rho=m+1,\ldots,m+l=n$.

In accordance with the Hertz-Hölder principle

$$\delta q^i = \frac{\partial \theta^i}{\partial \dot{\pi}^\alpha} \delta \pi^\alpha \tag{8}$$

and taking into account that (considering (4), (7))

$$\ddot{q}^i = \frac{\partial \theta^i}{\partial q^j} \dot{q}^j + \frac{\partial \theta^i}{\partial \dot{\pi}^\alpha} \ddot{\pi}^\alpha = \frac{\partial \theta^i}{\partial q^j} \theta^j + \frac{\partial \theta^i}{\partial \dot{\pi}^\alpha} \ddot{\pi}^\alpha \tag{9}$$

the Lagrange-D'Alembert principle reads

$$g_{ij}\left(f^j - Q^j\right)\delta q^i = 0 \quad \rightarrow \quad \left(g_{ij}f^j - Q_i\right)\delta q^i = 0$$

$$\left(g_{ij}\frac{\partial \theta^j}{\partial \dot{\pi}^\alpha}\ddot{\pi}^\alpha + g_{ij}\frac{\partial \theta^j}{\partial q^r}\theta^r + g_{ij}\Gamma^j_{Sr}\theta^r\theta^S - Q_i\right)\frac{\partial \theta^i}{\partial \dot{\pi}^\beta}\delta \pi^\beta = 0 \tag{10}$$

Considering the independence of variations $\delta \pi^\beta$, i.e. $\delta \pi^\beta \neq 0$ it follows

$$\left(g_{ij}\frac{\partial \theta^j}{\partial \dot{\pi}^\alpha}\ddot{\pi}^\alpha + g_{ij}\frac{\partial \theta^j}{\partial q^r}\theta^r + g_{ij}\Gamma^j_{Sr}\theta^r\theta^S\right)\frac{\partial \theta^i}{\partial \dot{\pi}^\beta} = Q_i\frac{\partial \theta^i}{\partial \dot{\pi}^\beta} = Q^*_\beta \tag{11}$$

Introducing the designation

$$G_{\alpha\beta} = g_{ij}\frac{\partial \theta^i}{\partial \dot{\pi}^\alpha}\frac{\partial \theta^j}{\partial \dot{\pi}^\beta}$$

Eqs (11) finally read

$$G_{\alpha\beta}\ddot{\pi}^\alpha + g_{ij}\frac{\partial \theta^i}{\partial q^r}\frac{\partial \theta^j}{\partial \dot{\pi}^\beta}\theta^r + g_{ij}\Gamma^i_{Sr}\theta^S\theta^r\frac{\partial \theta^i}{\partial \dot{\pi}^\beta} = Q^*_\beta \tag{12}$$

Starting from the Lagrange-D'Alembert principle in the form

$$\left(\frac{d}{dt}\frac{\partial T}{\partial \dot{q}^k} - \frac{\partial T}{\partial q^k} - Q_k\right)\delta q^k = 0 \tag{13}$$

and taking into account Eq (8), Eq (13) is transformed into the equation

$$\left(\frac{d}{dt}\frac{\partial T}{\partial \dot{q}^k} - \frac{\partial T}{\partial q^k} - Q_k\right)\frac{\partial \theta^k}{\partial \dot{\pi}^\alpha}\delta \pi^\alpha = 0 \tag{14}$$

Considering the independence of variations $\delta \pi^\beta$, i.e. $\delta \pi^\beta \neq 0$, Eq (14) is decomposed into m equations (Maggi's equations)

$$\left(\frac{d}{dt}\frac{\partial T}{\partial \dot{q}^k} - \frac{\partial T}{\partial q^k} - Q_k\right)\frac{\partial \theta^k}{\partial \dot{\pi}^\alpha} = 0 \tag{15}$$

Let us transform Eq (15) using the following relations

$$\frac{\partial \theta^k}{\partial \dot{\pi}^\alpha} \frac{d}{dt} \frac{\partial T}{\partial \dot{q}^k} = \frac{d}{dt}\left(\frac{\partial \theta^k}{\partial \dot{\pi}^\alpha} \frac{\partial T}{\partial \dot{q}^k} \right) - \frac{\partial T}{\partial \dot{q}^k} \frac{d}{dt} \frac{\partial \theta^k}{\partial \dot{\pi}^\alpha}$$

(16)

$$\frac{\partial T^*}{\partial q^k} = \frac{\partial T}{\partial q^k} + \frac{\partial T}{\partial \dot{q}^i} \frac{\partial \theta^i}{\partial q^k} \quad \rightarrow \quad \frac{\partial T}{\partial q^k} = \frac{\partial T^*}{\partial q^k} - \frac{\partial T}{\partial \dot{q}^i} \frac{\partial \theta^i}{\partial q^k}$$

(17)

$$\frac{\partial \theta^k}{\partial \dot{\pi}^\alpha} \frac{\partial T}{\partial \dot{q}^k} = \frac{\partial \theta^k}{\partial \dot{\pi}^\alpha} g_{ik} \dot{q}^i = \frac{\partial \theta^k}{\partial \dot{\pi}^\alpha} g_{ik} \theta^i \quad \leftrightarrow \quad \frac{\partial T^*}{\partial \dot{\pi}^\alpha} = g_{ik} \frac{\partial \theta^k}{\partial \dot{\pi}^\alpha} \theta^i$$

(18)

Now, Eq (15) obtains the following form

$$\frac{d}{dt} \frac{\partial T^*}{\partial \dot{\pi}^\alpha} - \frac{\partial \theta^k}{\partial \dot{\pi}^\alpha} \frac{\partial T^*}{\partial q^k} - \frac{\partial T}{\partial \dot{q}^k}\left(\frac{d}{dt} \frac{\partial \theta^k}{\partial \dot{\pi}^\alpha} - \frac{\partial \theta^k}{\partial q^S} \frac{\partial \theta^S}{\partial \dot{\pi}^\alpha} \right) = Q_k \frac{\partial \theta^k}{\partial \dot{\pi}^\alpha} = Q_\alpha^*$$

(19)

Eqs (19) and (12) are equivalent, i.e., Eqs (12) represent, conditionally speaking, a direct form of Eqs (19), which is proved by the following transformations:

$$\frac{d}{dt} \frac{\partial T^*}{\partial \dot{\pi}^\alpha} = \frac{d}{dt}\left(g_{ij} \frac{\partial \theta^i}{\partial \dot{\pi}^\alpha} \theta^j \right) = \frac{\partial g_{ij}}{\partial q^S} \dot{q}^S \left(\frac{\partial \theta^i}{\partial \dot{\pi}^\alpha} \theta^j \right) + g_{ij}\left(\frac{\partial^2 \theta^i}{\partial q^r \partial \dot{\pi}^\alpha} \dot{q}^r \theta^j + \right.$$

$$\left. + \frac{\partial^2 \theta^i}{\partial \dot{\pi}^\alpha \partial \dot{\pi}^\beta} \ddot{\pi}^\beta \theta^j \right) + g_{ij} \frac{\partial \theta^i}{\partial \dot{\pi}^\alpha}\left(\frac{\partial \theta^j}{\partial q^r} \dot{q}^r + \frac{\partial \theta^j}{\partial \dot{\pi}^\beta} \ddot{\pi}^\beta \right)$$

(a)

$$\frac{\partial \theta^k}{\partial \dot{\pi}^\alpha} \frac{\partial T^*}{\partial q^k} = \frac{\partial \theta^k}{\partial \dot{\pi}^\alpha}\left(\frac{1}{2} \frac{\partial g_{ij}}{\partial q^k} \theta^i \theta^j \right) + \frac{\partial \theta^k}{\partial \dot{\pi}^\alpha}\left(g_{ij} \frac{\partial \theta^i}{\partial q^k} \theta^j \right)$$

(b)

$$\frac{\partial T}{\partial \dot{q}^k}\left(\frac{d}{dt} \frac{\partial \theta^k}{\partial \dot{\pi}^\alpha} - \frac{\partial \theta^k}{\partial q^S} \frac{\partial \theta^S}{\partial \dot{\pi}^\alpha} \right) = g_{ik} \dot{q}^i \left(\frac{\partial^2 \theta^k}{\partial \dot{\pi}^\alpha \partial \dot{\pi}^\beta} \ddot{\pi}^\beta + \frac{\partial^2 \theta^k}{\partial \dot{\pi}^\alpha \partial q^r} \dot{q}^r - \frac{\partial \theta^k}{\partial q^S} \frac{\partial \theta^S}{\partial \dot{\pi}^\alpha} \right)$$

(c)

$$\text{(a)-(b)-(c)} = G_{\alpha\beta} \ddot{\pi}^\beta + g_{ij} \frac{\partial \theta^i}{\partial \dot{\pi}^\alpha} \frac{\partial \theta^j}{\partial q^r} \theta^r + \left(\frac{\partial g_{ij}}{\partial q^S} \frac{\partial \theta^i}{\partial \dot{\pi}^\alpha} \theta^S \theta^j - \frac{1}{2} \frac{\partial g_{ij}}{\partial q^k} \frac{\partial \theta^k}{\partial \dot{\pi}^\alpha} \theta^i \theta^j \right)$$

$$\frac{\partial g_{kj}}{\partial q^i} \frac{\partial \theta^k}{\partial \dot{\pi}^\alpha} \theta^i \theta^j - \frac{1}{2} \frac{\partial g_{ij}}{\partial q^k} \frac{\partial \theta^k}{\partial \dot{\pi}^\alpha} \theta^i \theta^j = ... = \Gamma_{ij,k} \frac{\partial \theta^k}{\partial \dot{\pi}^\alpha} \theta^i \theta^j = g_{Sk} \Gamma_{ij}^S \frac{\partial \theta^k}{\partial \dot{\pi}^\alpha} \theta^i \theta^j$$

$$G_{\alpha\beta} \ddot{\pi}^\beta + g_{ij} \frac{\partial \theta^i}{\partial \dot{\pi}^\alpha} \frac{\partial \theta^j}{\partial q^r} \theta^r + g_{Sk} \Gamma_{ij}^S \frac{\partial \theta^k}{\partial \dot{\pi}^\alpha} \theta^i \theta^j = Q_\alpha^* \quad \Rightarrow \quad (19) \sim (12)$$

182

2. Second Part

(a) After we have arrived at Eqs (19) starting from Maggi's equations [1], it is evident that they are equivalent to those of Maggi's.

(b) Volterra's equations [2] are obtained when transferring from the velocity components in Cartesian coordinates to the kinematic parameters $\dot{\pi}^\alpha$. Eqs (19) will represent Volterra's equations only if we write that

$$\dot{x}^i = \theta^i \left(x^j, \dot{\pi}^\alpha \right), \quad q^i = x^i \quad \left(i = 1,...,n = 3N \right) \tag{20}$$

where $\dot{x}^i$ are independent Cartesian coordinates in which the mass of the system has been incorporated in a manner indicated in Introduction. Let us reduce Eqs (19) to Volterra's equations. For this case, kinetic energy has the form

$$T = \frac{1}{2} \delta_{ij} \dot{x}^i \dot{x}^j \tag{21}$$

or, using (20),

$$T^* = \frac{1}{2} \delta_{ij} \theta^i \theta^j \tag{22}$$

Calculating the values of the following expression from the (19), it is obtained

$$-\frac{\partial \theta^k}{\partial \dot{\pi}^\alpha} \frac{\partial T^*}{\partial q^k} + \frac{\partial T}{\partial \dot{q}^k} \frac{\partial \theta^k}{\partial q^S} \frac{\partial \theta^S}{\partial \dot{\pi}^\alpha} = -\frac{\partial \theta^k}{\partial \dot{\pi}^\alpha} g_{ij} \frac{\partial \theta^i}{\partial q^k} \theta^j - \frac{\partial \theta^k}{\partial \dot{\pi}^\alpha} \frac{1}{2} \frac{\partial g_{ij}}{\partial q^k} \theta^i \theta^j + g_{ik} \theta^i \frac{\partial \theta^k}{\partial q^S} \frac{\partial \theta^S}{\partial \dot{\pi}^\alpha} = 0$$

considering that

$$\frac{\partial g_{ij}}{\partial q^k} = \frac{\partial \delta_{ij}}{\partial q^k} = 0$$

Accordingly, Eq (19) is reduced to the form that represents Volterra's equations for nonlinear nonholonomic systems

$$\frac{d}{dt} \frac{\partial T^*}{\partial \dot{\pi}^\alpha} - \delta_{ij} \theta^i \frac{d}{dt} \frac{\partial \theta^j}{\partial \dot{\pi}^\alpha} = P_\alpha \tag{23}$$

where

$$P_\alpha = X_i \frac{\partial \theta^i}{\partial \dot{\pi}^\alpha} \tag{24}$$

Eq (23) for linear nonholonomic constraints $\left(\dot{q}^i = \beta_\alpha^i \dot{\pi}^\alpha \right)$ is reduced to the well-known form

$$\frac{d}{dt}\frac{\partial T^*}{\partial \dot{\pi}^\alpha} - b_{\beta\gamma,\alpha}\dot{\pi}^\beta\dot{\pi}^\gamma = P_\alpha \quad \left(b_{\beta\gamma,\alpha} = \delta_{rk}\beta_\beta^r\beta_\alpha^i\frac{\partial\beta_\gamma^k}{\partial x^i} \right) \tag{25}$$

(c) Further analysis shows the equivalence of Appell's equations [3] to Eqs (19), i.e., (12). Appell's acceleration function reads (in accordance with notes given above for the mass):

$$S = \frac{1}{2}(\vec{a})^2 \tag{26}$$

or

$$S = \frac{1}{2}g_{ij}f^i f^j \tag{27}$$

Taking into account that

$$f^i = \ddot{q}^i + \Gamma_{kr}^i\dot{q}^k\dot{q}^r \quad \left(\ddot{q}^i = \dot{\theta}^i\right)$$

velocity dependencies and their derivatives can be eliminated by means of constraints (4), wherefrom it follows

$$f^{*i} = \frac{\partial\theta^i}{\partial q^s}\theta^s + \frac{\partial\theta^i}{\partial\dot{\pi}^\alpha}\ddot{\pi}^\alpha + \Gamma_{kr}^i\theta^k\theta^r \tag{28}$$

Appell's equations have the form

$$\frac{\partial S^*}{\partial\ddot{\pi}^\alpha} = Q_\alpha^* \tag{29}$$

Since

$$\frac{\partial S^*}{\partial\ddot{\pi}^\alpha} = g_{ij}f^{*i}\frac{\partial f^{*j}}{\partial\ddot{\pi}^\alpha} = g_{ij}\frac{\partial\theta^j}{\partial\dot{\pi}^\alpha}\left(\frac{\partial\theta^i}{\partial q^s}\theta^s + \frac{\partial\theta^i}{\partial\dot{\pi}^\alpha}\ddot{\pi}^\alpha + \Gamma_{kr}^i\theta^k\theta^r\right) \tag{30}$$

Appell's equations can be written in the form

$$g_{ij}\frac{\partial\theta^j}{\partial\dot{\pi}^\alpha}\frac{\partial\theta^i}{\partial\dot{\pi}^\beta}\ddot{\pi}^\beta + g_{ij}\frac{\partial\theta^j}{\partial\dot{\pi}^\alpha}\frac{\partial\theta^i}{\partial q^s}\theta^s + g_{ij}\frac{\partial\theta^j}{\partial\dot{\pi}^\alpha}\Gamma_{kr}^i\theta^k\theta^r = Q_\alpha^*$$

respectively

$$G_{\alpha\beta}\ddot{\pi}^\beta + g_{ij}\frac{\partial\theta^j}{\partial\dot{\pi}^\alpha}\frac{\partial\theta^i}{\partial q^s}\theta^s + g_{ij}\frac{\partial\theta^j}{\partial\dot{\pi}^\alpha}\Gamma_{kr}^i\theta^k\theta^r = Q_\alpha^* \tag{31}$$

which coincides with the (12), i.e., with the (19)

(d) Voronec's equations have been derived with reference to real generalized velocities, i.e., $\dot{q}^1,...,\dot{q}^n$ and generalized coordinates q1,..., q^n using both expressions for kinetic energy, i.e., T and T^*, [4]. Voronec's equations for nonlinear nonholonomic constraints (1) read

$$\frac{d}{dt}\frac{\partial T^*}{\partial \dot{q}^\alpha} - \frac{\partial T^*}{\partial q^\alpha} - \frac{\partial \psi^\nu}{\partial \dot{q}^\alpha}\frac{\partial T^*}{\partial q^\nu} - \frac{\partial T}{\partial \dot{q}^\nu}\gamma_\alpha^\nu = Q_\alpha + \frac{\partial \psi^\nu}{\partial \dot{q}^\alpha}Q_\nu \tag{32}$$

where the coefficients γ_α^ν are determined by expressions

$$\gamma_\alpha^\nu = \frac{d}{dt}\frac{\partial \psi^\nu}{\partial \dot{q}^\alpha} - \frac{\partial \psi^\nu}{\partial q^\alpha} - \frac{\partial \psi^\rho}{\partial \dot{q}^\alpha}\frac{\partial \psi^\nu}{\partial q^\rho} \tag{33}$$

In the choice of kinematic parameters for real generalized velocities, i.e., $\dot{\pi}^\alpha = \dot{q}^\alpha$ Eqs (4) read

$$\dot{q}^i = \theta^i \quad \rightarrow \quad \dot{q}^\alpha = \theta^\alpha = \dot{\pi}^\alpha, \quad \dot{q}^\nu = \psi^\nu = \theta^\nu$$

while Eqs (19) then obtain the form

$$\frac{d}{dt}\frac{\partial T^*}{\partial \dot{q}^\alpha} - \frac{\partial \theta^k}{\partial \dot{q}^\alpha}\frac{\partial T^*}{\partial q^k} - \frac{\partial T}{\partial \dot{q}^k}\left(\frac{d}{dt}\frac{\partial \theta^k}{\partial \dot{q}^\alpha} - \frac{\partial \theta^k}{\partial q^S}\frac{\partial \theta^S}{\partial \dot{q}^\alpha}\right) = Q_\alpha^* \tag{34}$$

or

$$\frac{d}{dt}\frac{\partial T^*}{\partial \dot{q}^\alpha} - \frac{\partial T^*}{\partial q^\alpha} - \frac{\partial \psi^\nu}{\partial \dot{q}^\alpha}\frac{\partial T^*}{\partial q^\nu} - \frac{\partial T}{\partial \dot{q}^\beta}\left(\frac{d}{dt}\frac{\partial \theta^\beta}{\partial \dot{q}^\alpha} - \frac{\partial \theta^\beta}{\partial q^S}\frac{\partial \theta^S}{\partial \dot{q}^\alpha}\right) - \frac{\partial T}{\partial \dot{q}^\nu}\left(\frac{d}{dt}\frac{\partial \theta^\nu}{\partial \dot{q}^\alpha} - \frac{\partial \theta^\nu}{\partial q^S}\frac{\partial \theta^S}{\partial \dot{q}^\alpha}\right) = Q_\alpha^*$$

respectively

$$\frac{d}{dt}\frac{\partial T^*}{\partial \dot{q}^\alpha} - \frac{\partial T^*}{\partial q^\alpha} - \frac{\partial \psi^\nu}{\partial \dot{q}^\alpha}\frac{\partial T^*}{\partial q^\nu} - \frac{\partial T}{\partial \dot{q}^\nu}\left(\frac{d}{dt}\frac{\partial \psi^\nu}{\partial \dot{q}^\alpha} - \frac{\partial \psi^\nu}{\partial q^\beta}\frac{\partial \theta^\beta}{\partial \dot{q}^\alpha} - \frac{\partial \psi^\nu}{\partial q^\rho}\frac{\partial \theta^\rho}{\partial \dot{q}^\alpha}\right) = Q_\alpha^*$$

Finally, Eqs (19) are converted into the form

$$\frac{d}{dt}\frac{\partial T^*}{\partial \dot{q}^\alpha} - \frac{\partial T^*}{\partial q^\alpha} - \frac{\partial \psi^\nu}{\partial \dot{q}^\alpha}\frac{\partial T^*}{\partial q^\nu} - \frac{\partial T}{\partial \dot{q}^\nu}\gamma_\alpha^\nu = Q_\alpha^* = Q_i\frac{\partial \theta^i}{\partial \dot{q}^\alpha} = Q_\beta\frac{\partial \theta^\beta}{\partial \dot{q}^\alpha} + Q_\nu\frac{\partial \theta^\nu}{\partial \dot{q}^\alpha} = Q_\alpha + \frac{\partial \psi^\nu}{\partial \dot{q}^\alpha}Q_\nu$$

which coincides with Eq (32), whereby it is shown that Voronec's equations are equivalent to the initial system of equations (19), because they can be obtained from them.

(e) Since Chaplygin's equations [5] represent a special case of Voronec's equations, the conclusions on equivalence from the above analysis hold for them too.

(f) Ferrers's equations [6] are very similar to those of Volterra's and they are written for the system subject to nonholonomic constraints, whose position is determined by the $n=3N$ Cartesian coordinates x^i. Here, the mass of the system is also incorporated via coordinates in the above described manner. Velocities $\dot{x}^i$ are expressed over m independent kinematic parameters $\dot{\pi}^\alpha$ by the relations

$$\dot{x}^i = \theta^i\left(x^j, \dot{\pi}^\alpha\right) \tag{35}$$

Ferrers's equations have the following form, [6]

$$\frac{d}{dt}\frac{\partial T^*}{\partial \dot{\pi}^\alpha} - \delta_{ij}\dot{x}^j \frac{d}{dt}\frac{\partial \theta^i}{\partial \dot{\pi}^\alpha} = X_i \frac{\partial \theta^i}{\partial \dot{\pi}^\alpha} = P_\alpha \tag{36}$$

where

$$T = \frac{1}{2}\delta_{ij}\dot{x}^i\dot{x}^j, \quad T^* = T_{\left(\dot{x}^i=\theta^i\right)} = \frac{1}{2}\delta_{ij}\theta^i\theta^j \tag{37}$$

From (37) there follow the relations

$$\frac{\partial T^*}{\partial x^s} = \frac{\partial T}{\partial \dot{x}^i}\frac{\partial \dot{x}^i}{\partial x^s} = \frac{\partial T}{\partial \dot{x}^i}\frac{\partial \theta^i}{\partial x^s}, \quad \frac{\partial T}{\partial \dot{x}^i} = \delta_{ij}\dot{x}^j \tag{38}$$

Now, Eqs (36) can be written in the following manner

$$\frac{d}{dt}\frac{\partial T^*}{\partial \dot{\pi}^\alpha} - \frac{\partial \theta^i}{\partial \dot{\pi}^\alpha}\frac{\partial T^*}{\partial x^i} + \frac{\partial \theta^i}{\partial \dot{\pi}^\alpha}\frac{\partial T^*}{\partial x^i} - \delta_{ij}\dot{x}^j\frac{d}{dt}\frac{\partial \theta^i}{\partial \dot{\pi}^\alpha} = P_\alpha$$

$$\frac{d}{dt}\frac{\partial T^*}{\partial \dot{\pi}^\alpha} - \frac{\partial \theta^i}{\partial \dot{\pi}^\alpha}\frac{\partial T^*}{\partial x^i} - \frac{\partial T}{\partial \dot{x}^i}\left(\frac{d}{dt}\frac{\partial \theta^i}{\partial \dot{\pi}^\alpha} - \frac{\partial \theta^s}{\partial \dot{\pi}^\alpha}\frac{\partial \theta^i}{\partial x^s}\right) = P_\alpha \tag{39}$$

If we incorporate $x^i = q^i$ in the (39), we obtain the expression for Ferrers's equations, which coincides with the (19), whereby their equivalence to other forms of equations of motion is proved:

$$\frac{d}{dt}\frac{\partial T^*}{\partial \dot{\pi}^\alpha} - \frac{\partial \theta^i}{\partial \dot{\pi}^\alpha}\frac{\partial T^*}{\partial q^i} - \frac{\partial T}{\partial \dot{q}^i}\left(\frac{d}{dt}\frac{\partial \theta^i}{\partial \dot{\pi}^\alpha} - \frac{\partial \theta^s}{\partial \dot{\pi}^\alpha}\frac{\partial \theta^i}{\partial q^s}\right) = P_\alpha$$

(g) Generalization of Volterra's equations was performed by Voronec in his paper [7]. A mechanical system, whose position is determined by generalized coordinates $x^1,...,x^n$ and which is subject to nonholonomic constraints is observed. Velocities $\dot{x}_1,...,\dot{x}^n$ are expressed via m independent quantities $\dot{\varphi}^\alpha$ by the relations

$$\dot{x}^i = \theta^i\left(x^j, \dot{\varphi}^\alpha\right) \tag{40}$$

For nonlinear relations (40), generalized Volterra's equations read

$$\frac{d}{dt}\frac{\partial T^*}{\partial \dot{\varphi}^\alpha} - \frac{\partial \omega^\beta}{\partial \dot{x}^\gamma}\left(\frac{d}{dt}\frac{\partial \theta^\gamma}{\partial \dot{\varphi}^\alpha} - \frac{\partial \theta^\gamma}{\partial x^i}\frac{\partial \theta^i}{\partial \dot{\varphi}^\alpha}\right)\frac{\partial T^*}{\partial \dot{\varphi}^\beta} - \left[\frac{d}{dt}\frac{\partial \theta^\nu}{\partial \dot{\varphi}^\alpha} - \frac{\partial \theta^\nu}{\partial x^i}\frac{\partial \theta^i}{\partial \dot{\varphi}^\alpha} - \right.$$

$$\left. - \frac{\partial \theta^\nu}{\partial \dot{\varphi}^\beta}\frac{\partial \omega^\beta}{\partial \dot{x}^\gamma}\left(\frac{d}{dt}\frac{\partial \theta^\gamma}{\partial \dot{\varphi}^\alpha} - \frac{\partial \theta^\gamma}{\partial x^i}\frac{\partial \theta^i}{\partial \dot{\varphi}^\alpha}\right)\right]\frac{\partial T}{\partial \dot{x}^\nu} - \frac{\partial \theta^i}{\partial \dot{\varphi}^\alpha}\frac{\partial}{\partial x^i}\left(T^* + U\right) = 0 \tag{41}$$

In order to prove the equivalence of Eqs (41) to other equations of motion, let us reduce them to the form of the (19). Let us regroup the terms from (41) in the following way

$$\frac{d}{dt}\frac{\partial T^*}{\partial \dot{\varphi}^\alpha} - \frac{\partial \omega^\beta}{\partial \dot{x}^\gamma}\left(\frac{d}{dt}\frac{\partial \theta^\gamma}{\partial \dot{\varphi}^\alpha} - \frac{\partial \theta^\gamma}{\partial x^i}\frac{\partial \theta^i}{\partial \dot{\varphi}^\alpha}\right)\left(\frac{\partial T^*}{\partial \dot{\varphi}^\beta} - \frac{\partial T}{\partial \dot{x}^\nu}\frac{\partial \theta^\nu}{\partial \dot{\varphi}^\beta}\right) -$$

$$-\left(\frac{d}{dt}\frac{\partial \theta^\nu}{\partial \dot{\varphi}^\alpha} - \frac{\partial \theta^\nu}{\partial x^i}\frac{\partial \theta^i}{\partial \dot{\varphi}^\alpha}\right)\frac{\partial T}{\partial \dot{x}^\nu} - \frac{\partial \theta^i}{\partial \dot{\varphi}^\alpha}\frac{\partial}{\partial x^i}\left(T^* + U\right) = 0$$

Taking into account the relations

$$\frac{\partial T^*}{\partial \dot{\varphi}^\beta} = \frac{\partial T}{\partial \dot{x}^i}\frac{\partial \theta^i}{\partial \dot{\varphi}^\beta} = \frac{\partial T}{\partial \dot{x}^\alpha}\frac{\partial \theta^\alpha}{\partial \dot{\varphi}^\beta} + \frac{\partial T}{\partial \dot{x}^\nu}\frac{\partial \theta^\nu}{\partial \dot{\varphi}^\beta} \qquad \Big/ \cdot \frac{\partial \omega^\beta}{\partial \dot{x}^\gamma}$$

$$\dot{x}^\alpha = \theta^\alpha\left(\dot{\varphi}^\beta, x^i\right), \quad \dot{\varphi}^\beta = \omega^\beta\left(\dot{x}^\alpha, x^i\right)$$

$$\frac{\partial \theta^\alpha}{\partial \dot{\varphi}^\beta}\frac{\partial \omega^\beta}{\partial \dot{x}^\gamma} = \delta^\alpha_\gamma \quad \rightarrow \quad \frac{\partial T^*}{\partial \dot{\varphi}^\beta}\frac{\partial \omega^\beta}{\partial \dot{x}^\gamma} - \frac{\partial T}{\partial \dot{x}^\nu}\frac{\partial \theta^\nu}{\partial \dot{\varphi}^\beta}\frac{\partial \omega^\beta}{\partial \dot{x}^\gamma} = \frac{\partial T}{\partial \dot{x}^\gamma}$$

the previous equations read

$$\frac{d}{dt}\frac{\partial T^*}{\partial \dot{\varphi}^\alpha} - \frac{\partial T}{\partial \dot{x}^\gamma}\left(\frac{d}{dt}\frac{\partial \theta^\gamma}{\partial \dot{\varphi}^\alpha} - \frac{\partial \theta^\gamma}{\partial x^i}\frac{\partial \theta^i}{\partial \dot{\varphi}^\alpha}\right) - \frac{\partial T}{\partial \dot{x}^\nu}\left(\frac{d}{dt}\frac{\partial \theta^\nu}{\partial \dot{\varphi}^\alpha} - \frac{\partial \theta^\nu}{\partial x^i}\frac{\partial \theta^i}{\partial \dot{\varphi}^\alpha}\right) - \frac{\partial \theta^i}{\partial \dot{\varphi}^\alpha}\frac{\partial T^*}{\partial x^i} - \frac{\partial \theta^i}{\partial \dot{\varphi}^\alpha}Q_i = 0$$

respectively

$$\frac{d}{dt}\frac{\partial T^*}{\partial \dot{\varphi}^\alpha} - \frac{\partial \theta^i}{\partial \dot{\varphi}^\alpha}\frac{\partial T^*}{\partial x^i} - \frac{\partial T}{\partial \dot{x}^j}\left(\frac{d}{dt}\frac{\partial \theta^j}{\partial \dot{\varphi}^\alpha} - \frac{\partial \theta^j}{\partial x^i}\frac{\partial \theta^i}{\partial \dot{\varphi}^\alpha}\right) = Q^*_\alpha$$

Now, if we introduce the designations $\dot{\varphi}^\beta = \dot{\pi}^\beta$, $x^i = q^i$, the above expression obtains the form

$$\frac{d}{dt}\frac{\partial T^*}{\partial \dot{\pi}^\alpha} - \frac{\partial \theta^i}{\partial \dot{\pi}^\alpha}\frac{\partial T^*}{\partial q^i} - \frac{\partial T}{\partial \dot{q}^j}\left(\frac{d}{dt}\frac{\partial \theta^j}{\partial \dot{\pi}^\alpha} - \frac{\partial \theta^j}{\partial q^i}\frac{\partial \theta^i}{\partial \dot{\pi}^\alpha}\right) = Q^*_\alpha \tag{42}$$

which coincides with the (19).

(h) Lastly, let us show the equivalence of the Boltzmann-Hamel equations [8] to Eqs (19). In deriving the Boltzmann-Hamel equations for nonlinear nonholonomic constraints, the relations that associate kinetic parameters $\dot{\pi}^i$ with generalized velocities $\dot{q}^i$ are written in the form

$$\dot{\pi}^i = \varphi^i\left(q^j, \dot{q}^j\right), \quad \det\left[\frac{\partial \varphi^i}{\partial \dot{q}^j}\right] \neq 0 \tag{43}$$

$$\dot{q}^i = \theta^i\left(q^j, \dot{\pi}^j\right), \quad \delta q^i = \frac{\partial \theta^i}{\partial \dot{\pi}^j}\delta \pi^j \tag{44}$$

The expression for kinetic energy reads (as the function of all $\dot{q}^i$)

$$T = \frac{1}{2} g_{ij} \dot{q}^i \dot{q}^j$$

while the expression for kinetic energy $\tilde{T}$ (as the function of all $\dot{\pi}^j$)

$$\tilde{T} = \frac{1}{2} \delta_{ij} \theta^i \theta^j \tag{45}$$

Starting from Lagrange-D'Alembert's principle

$$\left(\frac{d}{dt} \frac{\partial T}{\partial \dot{q}^i} - \frac{\partial T}{\partial q^i} - Q_i \right) \frac{\partial \theta^i}{\partial \dot{\pi}^j} \delta\pi^j = 0$$

after certain transformations of Boltzmann-Hamel equations, for nonlinear relations between the velocities $\dot{q}^i$ and the quasivelocities $\dot{\pi}^i$, they read:

$$\frac{d}{dt} \frac{\partial \tilde{T}}{\partial \dot{\pi}^j} - \frac{\partial \theta^i}{\partial \dot{\pi}^j} \frac{\partial \tilde{T}}{\partial q^i} - \frac{\partial \tilde{T}}{\partial \pi^i} \left(\frac{\partial \varphi^i}{\partial q^S} \frac{\partial \theta^S}{\partial \dot{\pi}^j} + \frac{\partial \varphi^i}{\partial \dot{q}^S} \frac{d}{dt} \frac{\partial \theta^S}{\partial \dot{\pi}^j} \right) = Q_i \frac{\partial \theta^i}{\partial \dot{\pi}^j} = \tilde{Q}_j \tag{46}$$

If nonlinear nonholonomic constraints are chosen for one segment of the velocities, i.e., the condition holds for the variations

$$\delta\pi^v = 0$$

then, from Lagrange-D'Alembert's principle, we obtain *(n-l)* equations of motion for nonlinear nonholonomic system (in accordance with the (46))

$$\frac{d}{dt} \frac{\partial \tilde{T}}{\partial \dot{\pi}^\alpha} - \frac{\partial \theta^i}{\partial \dot{\pi}^\alpha} \frac{\partial \tilde{T}}{\partial q^i} - \frac{\partial \tilde{T}}{\partial \pi^i} \left(\frac{\partial \varphi^i}{\partial q^S} \frac{\partial \theta^S}{\partial \dot{\pi}^\alpha} + \frac{\partial \varphi^i}{\partial \dot{q}^S} \frac{d}{dt} \frac{\partial \theta^S}{\partial \dot{\pi}^\alpha} \right) = \tilde{Q}_\alpha \tag{47}$$

where $\dot{\pi}^v = 0$ is placed after the first differentiation.

The expression for kinetic energy, where dependent velocities are excluded (real generalized velocities and quasivelocities), is written in the form

$$T^* = T_{\left(\dot{q}^v = \psi^v \right)} = \frac{1}{2} g_{ij} \left(\dot{q}^i \dot{q}^j \right)_{\left(\dot{q}^v = \psi^v \right)}$$

$$T^* = \tilde{T}_{\left(\dot{\pi}^v = 0 \right)} = \frac{1}{2} g_{ij} \left(\theta^i \theta^j \right)_{\left(\dot{\pi}^v = 0 \right)} \tag{48}$$

Based on the (48), the following relations can be written

$$\frac{\partial \tilde{T}}{\partial \dot{\pi}^{\alpha}} = \left(g_{ij} \frac{\partial \theta^{i}}{\partial \dot{\pi}^{\alpha}} \theta^{j} \right)_{(\dot{\pi}^{\nu}=0)} = \frac{\partial T^{*}}{\partial \dot{\pi}^{\alpha}}, \quad \left(\tilde{Q}_{\alpha} \right)_{(\dot{\pi}^{\nu}=0)} = Q_{\alpha}^{*}$$

$$\frac{\partial \tilde{T}}{\partial q^{S}} = \left(\frac{1}{2} \frac{\partial g_{ij}}{\partial q^{S}} \theta^{i} \theta^{j} + g_{ij} \frac{\partial \theta^{i}}{\partial q^{S}} \theta^{j} \right)_{(\dot{\pi}^{\nu}=0)} = \frac{\partial T^{*}}{\partial q^{S}}$$

(49)

The last term in the (47) is transformed in the following manner

$$\frac{\partial \tilde{T}}{\partial \dot{\pi}^{k}} \frac{\partial \varphi^{k}}{\partial \dot{q}^{S}} = \frac{\partial T}{\partial \dot{q}^{S}} \qquad \left(\frac{\partial T}{\partial \dot{q}^{S}} = g_{iS} \dot{q}^{i} = g_{iS} \theta^{i}, \quad \frac{\partial \tilde{T}}{\partial \dot{\pi}^{k}} = g_{ij} \theta^{j} \frac{\partial \theta^{i}}{\partial \dot{\pi}^{k}} = \frac{\partial T}{\partial \dot{q}^{i}} \frac{\partial \theta^{i}}{\partial \dot{\pi}^{k}}, \quad \frac{\partial \theta^{i}}{\partial \dot{\pi}^{k}} \frac{\partial \varphi^{k}}{\partial \dot{q}^{S}} = \delta_{S}^{i} \right)$$

$$\frac{\partial \varphi^{i}}{\partial q^{S}} \frac{\partial \theta^{j}}{\partial \dot{\pi}^{i}} = -\frac{\partial \theta^{j}}{\partial \dot{q}^{S}} \qquad \left(\frac{\partial \dot{q}^{j}}{\partial q^{S}} = \frac{\partial \theta^{j}}{\partial q^{S}} + \frac{\partial \theta^{j}}{\partial \dot{\pi}^{i}} \frac{\partial \varphi^{i}}{\partial q^{S}} = 0 \quad \rightarrow \quad \frac{\partial \varphi^{i}}{\partial q^{S}} \frac{\partial \theta^{j}}{\partial \dot{\pi}^{i}} = -\frac{\partial \theta^{j}}{\partial q^{S}} \right)$$

Accordingly, after the above transformations, Eqs (47) obtain the form identical with the (19), i.e.

$$\frac{d}{dt} \frac{\partial T^{*}}{\partial \dot{\pi}^{\alpha}} - \frac{\partial \theta^{i}}{\partial \dot{\pi}^{\alpha}} \frac{\partial T^{*}}{\partial q^{i}} - \frac{\partial T}{\partial \dot{q}^{i}} \left(\frac{d}{dt} \frac{\partial \theta^{i}}{\partial \dot{\pi}^{\alpha}} - \frac{\partial \theta^{i}}{\partial q^{S}} \frac{\partial \theta^{S}}{\partial \dot{\pi}^{\alpha}} \right) = Q_{\alpha}^{*}$$

Consequently, (as established in [10] for linear nonholonomic systems) for the case of nonlinear nonholonomic systems too, various forms of differential equations of motion result from the manner of incorporating nonholonomic constraints in Lagrange-D'Alembert's principle. However, as shown by above analysis, all mentioned forms of differential equations of motion can be reduced to a common general form.

3. Third Part

Let us illustrate the considerations above using a mechanical system with a nonlinear nonholonomic constraint. The mechanical system consists of two particles M_1 and M_2 connected as shown in Fig. 1, [12].
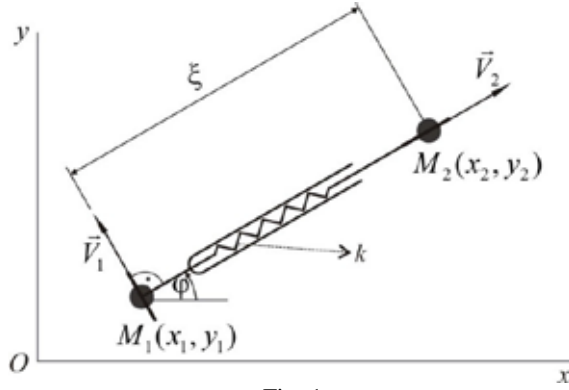
Fig. 1

Blades that are perpendicular to one another are positioned at particles M_1 and M_2, which enables the realization of nonlinear nonholonomic constraint of the type

$$\vec{V}_1 \cdot \vec{V}_2 = 0 \rightarrow \dot{x}_1 \dot{x}_2 + \dot{y}_1 \dot{y}_2 = 0 \tag{51}$$

Let the system move in a potential force field, whose potential energy depends only of the distance between particles M_1 and M_2, i.e., of ξ. For simplicity, we take that $m_1 = m_2 = m = 1$. Let us choose x_1, y_1, φ, ξ for generalized coordinates of the system (Fig. 1). The equations of nonholonomic constraints have the form

$$\dot{x}_1 \cos\varphi + \dot{y}_1 \sin\varphi = 0,$$

$$\xi\dot{\varphi} - \sqrt{\dot{x}_1^2 + \dot{y}_1^2} = \xi\dot{\varphi} - \left(\dot{x}_1 \sin\varphi - \dot{y}_1 \cos\varphi \right) = 0 \tag{52}$$

Kinetic and potential energy of the system read

$$T = \frac{1}{2} m_1 V_1^2 + \frac{1}{2} m_2 V_2^2 = \frac{1}{2} m \left(\dot{x}_1^2 + \dot{y}_1^2 \right) + \frac{1}{2} m \dot{\xi}^2, \quad V = V(\xi) = \frac{1}{2} k \left(\xi - \xi_0 \right)^2 \tag{53}$$

If $\dot{\varphi}$ and $\dot{\xi}$ are chosen from the (52) for independent generalized velocities, there follows

$$\dot{x}_1 = \xi\dot{\varphi} \sin\varphi, \quad \dot{y}_1 = -\xi\dot{\varphi} \cos\varphi \tag{54}$$

The expression for kinetic energy T^*, which is the function of independent velocities, reads

$$T^* = \frac{1}{2} \left(\xi\dot{\varphi} \right)^2 + \frac{1}{2} \dot{\xi}^2 \tag{55}$$

Considering that

$$\dot{q}^v = \psi^v \left(q^\alpha, \dot{q}^\alpha \right), \quad T = T \left(q^\alpha, \dot{q}^i \right), \quad T^* = T^* \left(q^\alpha, \dot{q}^\alpha \right), \quad V = V \left(q^\alpha \right)$$

Voronec's equations (32)

190

$$\frac{d}{dt}\frac{\partial T^*}{\partial \dot{q}^\alpha} - \frac{\partial T^*}{\partial q^\alpha} - \frac{\partial \psi^\nu}{\partial \dot{q}^\alpha}\frac{\partial T^*}{\partial q^\nu} - \frac{\partial T}{\partial \dot{q}^\nu}\gamma^\nu_\alpha = Q_\alpha + \frac{\partial \psi^\nu}{\partial \dot{q}^\alpha}Q_\nu$$

$$\gamma^\nu_\alpha = \frac{d}{dt}\frac{\partial \psi^\nu}{\partial \dot{q}^\alpha} - \frac{\partial \psi^\nu}{\partial q^\alpha} - \frac{\partial \psi^\rho}{\partial \dot{q}^\alpha}\frac{\partial \psi^\nu}{\partial q^\rho}$$

for our concrete example are transformed into Chaplygin's equations as a special case, i.e.

$$\frac{d}{dt}\frac{\partial T^*}{\partial \dot{q}^\alpha} - \frac{\partial T^*}{\partial q^\alpha} - \frac{\partial T}{\partial \dot{q}^\nu}\gamma^\nu_\alpha = Q_\alpha, \quad \gamma^\nu_\alpha = \frac{d}{dt}\frac{\partial \psi^\nu}{\partial \dot{q}^\alpha} - \frac{\partial \psi^\nu}{\partial q^\alpha}, \quad Q_\alpha = -\frac{\partial V}{\partial q^\alpha} \quad (56)$$

After certain calculations from the (56), there follow differential equations of motion for the described mechanical system

$$\dot{\xi}\dot{\varphi} + \xi\ddot{\varphi} = 0 \ \rightarrow \ \xi\dot{\varphi} = const., \quad \ddot{\xi} = -\frac{\partial V}{\partial \xi} \tag{57}$$

Let us write Appell's equations of the same system, which, in a general case, read (29)

$$\frac{\partial S^*}{\partial \ddot{\pi}^\alpha} = Q^*_\alpha$$

For independent kinematic parameters, let us choose the velocities of the particles M_1 and M_2, i.e.

$$\dot{\pi}^1 = \xi\dot{\varphi} = \dot{s}_1, \ \dot{\pi}^2 = \dot{\xi} = \dot{s}_2 \tag{58}$$

where $S_1(t)$ and $S_2(t)$ are the laws for the path of particles M_1 and M_2.
The acceleration function of the considered system reads

$$S = \frac{1}{2}a_1^2 + \frac{1}{2}a_2^2 = \frac{1}{2}\left(\ddot{x}_1^2 + \ddot{y}_1^2\right) + \frac{1}{2}\left(\ddot{x}_2^2 + \ddot{y}_2^2\right)$$

Using the equations of constraints (52) and relations

$$\dot{x}_2 = \dot{\xi}\cos\varphi, \quad \dot{y}_2 = \dot{\xi}\sin\varphi$$

we obtain

$$\ddot{x}_1 = \ddot{s}_1\sin\varphi + \dot{s}_1\dot{\varphi}\cos\varphi, \quad \ddot{y}_1 = -\ddot{s}_1\cos\varphi + \dot{s}_1\dot{\varphi}\sin\varphi,$$

$$\ddot{x}_2 = \ddot{\xi}\cos\varphi - \dot{\xi}\dot{\varphi}\sin\varphi, \quad \ddot{y}_2 = \ddot{\xi}\sin\varphi + \dot{\xi}\dot{\varphi}\cos\varphi$$

respectively

$$S^* = \frac{1}{2}\left(\ddot{s}_1^2 + \dot{s}_1^2\dot{\varphi}^2\right) + \frac{1}{2}\left(\ddot{s}_2^2 + \dot{s}_2^2\dot{\varphi}^2\right) = \frac{1}{2}\left(\ddot{s}_1^2 + \frac{\dot{s}_1^4}{\xi^2}\right) + \frac{1}{2}\left(\ddot{s}_2^2 + \frac{\dot{s}_1^2\dot{s}_2^2}{\xi^2}\right) \tag{59}$$

From the (59) there follow

$$\frac{\partial S^*}{\partial \ddot{s}_1} = Q_1^* \to \dddot{s}_1 = 0, \quad \frac{\partial S^*}{\partial \ddot{s}_2} = Q_2^* \to \dddot{s}_2 = -\frac{\partial V}{\partial \xi} \tag{60}$$

and taking into account that

$$\ddot{s}_1 = \dot{\xi}\dot{\varphi} + \xi\ddot{\varphi}, \quad \ddot{s}_2 = \ddot{\xi}$$

from the (60) there follow the equations of motion that are identical with the equations (57):

$$\dot{\xi}\dot{\varphi} + \xi\ddot{\varphi} = 0 \ \to \ \xi\dot{\varphi} = const., \quad \ddot{\xi} = -\frac{\partial V}{\partial \xi}$$

Volterra's equations are obtained by transferring from the velocities in the Cartesian coordinate system to kinematic parameters $\dot{\pi}^\alpha$. The choice for independent kinematic parameters, as in the previous case, will be performed as follows

$$\dot{\pi}^1 = \dot{s}_1, \ \dot{\pi}^2 = \dot{s}_2 \ \to \ \dot{x}^1 = \dot{x}_1 = \dot{s}_1 \sin\varphi = \theta^1, \ \dot{x}^2 = \dot{y}_1 = -\dot{s}_1 \cos\varphi = \theta^2,$$

$$\dot{x}^3 = \dot{x}_2 = \dot{s}_2 \cos\varphi = \theta^3, \ \dot{x}^4 = \dot{y}_2 = \dot{s}_2 \sin\varphi = \theta^4 \tag{61}$$

The expressions for kinematic energy T and T^* read

$$T = \frac{1}{2}\left(\dot{x}_1^2 + \dot{y}_1^2\right) + \frac{1}{2}\left(\dot{x}_2^2 + \dot{y}_2^2\right), \quad T^* = \frac{1}{2}\dot{s}_1^2 + \frac{1}{2}\dot{s}_2^2$$

whereas potential energy V is the function of distance $\overline{M_1 M_2}$, i.e.

$$V = \frac{1}{2}k\left[\sqrt{\left(x_2 - x_1\right)^2 + \left(y_2 - y_1\right)^2} - \xi_0\right]^2 \tag{62}$$

Generalized forces have the following value

$$P_1 = X_1 \frac{\partial\theta^1}{\partial\dot{s}_1} + X_2 \frac{\partial\theta^2}{\partial\dot{s}_1} + X_3 \frac{\partial\theta^3}{\partial\dot{s}_1} + X_4 \frac{\partial\theta^4}{\partial\dot{s}_1} = 0, \quad \left(X_1 = -\frac{\partial V}{\partial x_1}, \ X_2 = -\frac{\partial V}{\partial y_1}\right)$$

$$P_2 = X_1 \frac{\partial\theta^1}{\partial\dot{s}_2} + X_2 \frac{\partial\theta^2}{\partial\dot{s}_2} + X_3 \frac{\partial\theta^3}{\partial\dot{s}_2} + X_4 \frac{\partial\theta^4}{\partial\dot{s}_2} = -k\sqrt{\left(x_2 - x_1\right)^2 + \left(y_2 - y_1\right)^2} - k\xi_0, \quad \left(X_3 = -\frac{\partial V}{\partial x_2}, \ X_4 = -\frac{\partial V}{\partial y_2}\right)$$

Volterra's equations (23)

$$\frac{d}{dt}\frac{\partial T^*}{\partial\dot{\pi}^\alpha} - \delta_{ij}\theta^i \frac{d}{dt}\frac{\partial\theta^j}{\partial\dot{\pi}^\alpha} = P_\alpha$$

for the system analyzed read

$$\ddot{s}_1 - \left(\delta_{11}\theta^1 \frac{d}{dt}\frac{\partial\theta^1}{\partial\dot{s}_1} + \delta_{22}\theta^2 \frac{d}{dt}\frac{\partial\theta^2}{\partial\dot{s}_1} + \delta_{33}\theta^3 \frac{d}{dt}\frac{\partial\theta^3}{\partial\dot{s}_1} + \delta_{44}\theta^4 \frac{d}{dt}\frac{\partial\theta^4}{\partial\dot{s}_1} \right) = P_1 \rightarrow \ddot{s}_1 = 0$$

$$\ddot{s}_2 - \left(\delta_{11}\theta^1 \frac{d}{dt}\frac{\partial\theta^1}{\partial\dot{s}_2} + \delta_{22}\theta^2 \frac{d}{dt}\frac{\partial\theta^2}{\partial\dot{s}_2} + \delta_{33}\theta^3 \frac{d}{dt}\frac{\partial\theta^3}{\partial\dot{s}_2} + \delta_{44}\theta^4 \frac{d}{dt}\frac{\partial\theta^4}{\partial\dot{s}_2} \right) = P_2 \rightarrow \ddot{s}_2 = -k\left(\xi - \xi_0\right)$$

(63)

Taking into account that

$$\dot{s}_1 = \xi\dot{\varphi}, \quad \dot{s}_2 = \dot{\xi}, \quad \xi = \sqrt{\left(x_2 - x_1\right)^2 + \left(y_2 - y_1\right)^2}$$

Eqs (63) are reduced to Eqs (57) and (60), i.e.

$$\dot{\xi}\dot{\varphi} + \xi\ddot{\varphi} = 0 \rightarrow \xi\dot{\varphi} = const., \quad \ddot{\xi} = -k\left(\xi - \xi_0\right) = -\frac{\partial V}{\partial\xi}$$

Ferrers's equations (36) (differ insignificantly friom Volterra's equations)

$$\frac{d}{dt}\frac{\partial T^*}{\partial\dot{\pi}^\alpha} - \delta_{ij}\dot{x}^i \frac{d}{dt}\frac{\partial\theta^j}{\partial\dot{\pi}^\alpha} = P_\alpha$$

for the link between kinematic parameters $\dot{\pi}^1 = \dot{s}_1$, $\dot{\pi}^2 = \dot{s}_2$ and generalized velocities in Cartesian coordinates

$$\dot{x}^1 = \dot{x}_1 = \dot{s}_1 \sin\varphi = \theta^1, \quad \dot{x}^2 = \dot{y}_1 = -\dot{s}_1 \cos\varphi = \theta^2,$$

$$\dot{x}^3 = \dot{x}_2 = \dot{s}_2 \cos\varphi = \theta^3, \quad \dot{x}^4 = \dot{y}_2 = \dot{s}_2 \sin\varphi = \theta^4$$

read

$$\ddot{s}_1 - \left(\delta_{11}\dot{x}^1 \frac{d}{dt}\frac{\partial\theta^1}{\partial\dot{s}_1} + \delta_{22}\dot{x}^2 \frac{d}{dt}\frac{\partial\theta^2}{\partial\dot{s}_1} + \delta_{33}\dot{x}^3 \frac{d}{dt}\frac{\partial\theta^3}{\partial\dot{s}_1} + \delta_{44}\dot{x}^4 \frac{d}{dt}\frac{\partial\theta^4}{\partial\dot{s}_1} \right) = P_1 \rightarrow \ddot{s}_1 = 0$$

$$\ddot{s}_2 - \left(\delta_{11}\dot{x}^1 \frac{d}{dt}\frac{\partial\theta^1}{\partial\dot{s}_2} + \delta_{22}\dot{x}^2 \frac{d}{dt}\frac{\partial\theta^2}{\partial\dot{s}_2} + \delta_{33}\dot{x}^3 \frac{d}{dt}\frac{\partial\theta^3}{\partial\dot{s}_2} + \delta_{44}\dot{x}^4 \frac{d}{dt}\frac{\partial\theta^4}{\partial\dot{s}_2} \right) = P_2 \rightarrow \ddot{s}_2 = -k$$

(64)

Translated to real generalized velocities $\dot{\varphi}$, $\dot{\xi}$ and generalized accelerations $\ddot{\varphi}$, $\ddot{\xi}$ Eqs (64) read just like Eqs (57), (60) and (63)

$$\dot{\xi}\dot{\varphi} + \xi\ddot{\varphi} = 0 \rightarrow \xi\dot{\varphi} = const., \quad \ddot{\xi} = -k\left(\xi - \xi_0\right) = -\frac{\partial V}{\partial\xi}$$

The equations of Boltzmann-Hamel are given by the expression (47)

$$\frac{d}{dt}\frac{\partial\tilde{T}}{\partial\dot{\pi}^\alpha} - \frac{\partial\theta^i}{\partial\dot{\pi}^\alpha}\frac{\partial\tilde{T}}{\partial q^i} - \frac{\partial\tilde{T}}{\partial\dot{\pi}^i}\left(\frac{\partial\varphi^i}{\partial q^s}\frac{\partial\theta^s}{\partial\dot{\pi}^\alpha} + \frac{\partial\varphi^i}{\partial\dot{q}^s}\frac{d}{dt}\frac{\partial\theta^s}{\partial\dot{\pi}^\alpha} \right) = Q_\alpha^*$$

Let us choose x_1, y_1, x_2, y_2 for generalized coordinates. The relations that associate kinematic parameters with generalized velocities read

$$\dot{\pi}^1 = \dot{s}_1 = \sqrt{\dot{x}_1^2 + \dot{y}_1^2} = \varphi^1, \ \ \dot{\pi}^2 = \dot{s}_2 = \sqrt{\dot{x}_2^2 + \dot{y}_2^2} = \varphi^2,$$

$$\dot{\pi}^3 = \dot{s}_3 = \dot{x}_1 \cos\varphi + \dot{y}_1 \sin\varphi = \varphi^3, \quad \dot{\pi}^4 = \dot{s}_4 = \dot{x}_2 \sin\varphi - \dot{y}_2 \cos\varphi = \varphi^4 \quad (65)$$

$$\dot{x}_1 = \dot{s}_3 \cos\varphi + \sin\varphi\sqrt{\dot{s}_1^2 - \dot{s}_3^2} = \theta^1, \quad \dot{y}_1 = \dot{s}_3 \sin\varphi - \cos\varphi\sqrt{\dot{s}_1^2 - \dot{s}_3^2} = \theta^2$$

$$\dot{x}_2 = \dot{s}_4 \sin\varphi + \cos\varphi\sqrt{\dot{s}_2^2 - \dot{s}_4^2} = \theta^3, \quad \dot{y}_2 = -\dot{s}_4 \cos\varphi + \sin\varphi\sqrt{\dot{s}_2^2 - \dot{s}_4^2} = \theta^4 \quad (66)$$

Kinematic parameters $\dot{s}_1$ and $\dot{s}_2$ represent the velocities of the particles M_1 and M_2, while the expressions φ^3 and φ^4 are nonholonomic constraints of a given system ($\varphi^3 = 0$ and $\varphi^4 = 0$). The expressions for kinematic energy T and $\tilde{T}$ read

$$T = \frac{1}{2}\left(\dot{x}_1^2 + \dot{y}_1^2\right) + \frac{1}{2}\left(\dot{x}_2^2 + \dot{y}_2^2\right), \quad \tilde{T} = \frac{1}{2}\dot{s}_1^2 + \frac{1}{2}\dot{s}_2^2$$

so, considering that

$$\frac{\partial\tilde{T}}{\partial q^i} = 0, \quad \frac{\partial\tilde{T}}{\partial\dot{\pi}^\nu} = 0, \quad \frac{\partial\varphi^\beta}{\partial q^s} = 0$$

the equations of Boltzmann-Hamel obtain a simpler form

$$\frac{d}{dt}\frac{\partial\tilde{T}}{\partial\dot{\pi}^\alpha} - \frac{\partial\tilde{T}}{\partial\dot{\pi}^\beta}\frac{\partial\varphi^\beta}{\partial q^s}\frac{d}{dt}\frac{\partial\theta^s}{\partial\dot{\pi}^\alpha} = Q_\alpha^* \quad (67)$$

From the (67), there follow differential equations of motion for the system

$$\ddot{s}_1 = 0, \quad \ddot{s}_2 = -k\sqrt{\left(x_2 - x_1\right)^2 + \left(y_2 - y_1\right)^2} + k\xi_0$$

Taking into account that

$$\dot{s}_1 = \xi\dot{\varphi}, \quad \dot{s}_2 = \dot{\xi}, \quad \xi = \sqrt{\left(x_2 - x_1\right)^2 + \left(y_2 - y_1\right)^2}$$

the preceding equations are written in the form of identifiable expressions

$$\dot{\xi}\dot{\varphi} + \xi\ddot{\varphi} = 0 \ \rightarrow \ \xi\dot{\varphi} = const., \quad \ddot{\xi} = -k\left(\xi - \xi_0\right) = -\frac{\partial V}{\partial\xi}$$

In another variant, let us choose x_1, y_1, φ, ξ for generalized coordinates. The relations that associate kinematic parameters with generalized velocities read

$$\dot{\pi}^1 = \dot{s}_1 = \xi\dot{\varphi} = \varphi^1, \ \ \dot{\pi}^2 = \dot{s}_2 = \dot{\xi} = \varphi^2,$$

$$\dot{\pi}^3 = \dot{s}_3 = \dot{x}_1 \cos\varphi + \dot{y}_1 \sin\varphi = \varphi^3,$$

$$\dot{\pi}^4 = \dot{s}_4 = \xi\dot{\varphi} - \dot{x}_1 \sin\varphi + \dot{y}_1 \cos\varphi = 0 \quad (68)$$

$$\dot{\varphi} = \frac{\dot{s}_1}{\xi} = \theta^1, \quad \dot{\xi} = \dot{s}_2 = \theta^2, \quad \dot{x}_1 = -\sin\varphi(\dot{s}_4 - \dot{s}_1) + \cos\varphi\dot{S}_3, \quad \dot{y}_1 = \cos\varphi(\dot{s}_4 - \dot{s}_1) + \sin\varphi\dot{s}_3 \tag{69}$$

Quasicoordinates s_1 and s_2 represent the laws for the path of particles M_1 and M_2, while the expressions φ^3 and φ^4 are nonholonomic constraints of a given system ($\varphi^3 = 0$, $\varphi^4 = 0$). Kinetic *(T, $\tilde{T}$)* and potential energy of the system read

$$T = \frac{1}{2}\left(\dot{x}_1^2 + \dot{y}_1^2\right) + \frac{1}{2}\dot{\xi}^2, \quad \tilde{T} = \frac{1}{2}\left[(\dot{s}_3)^2 + (\dot{s}_4 - \dot{s}_1)^2\right] + \frac{1}{2}\dot{s}_2^2, \quad V = \frac{1}{2}k(\xi - \xi_0)^2$$

Considering that

$$\frac{\partial\tilde{T}}{\partial q^i} = 0$$

the equations of Boltzmann-Hamel are reduced to the expression

$$\frac{d}{dt}\frac{\partial\tilde{T}}{\partial\dot{\pi}^\alpha} - \frac{\partial\tilde{T}}{\partial\dot{\pi}^i}\left(\frac{\partial\varphi^i}{\partial q^S}\frac{\partial\theta^S}{\partial\dot{\pi}^\alpha} - \frac{\partial\varphi^i}{\partial\dot{q}^S}\frac{d}{dt}\frac{\partial\theta^S}{\partial\dot{\pi}^\alpha}\right) = \tilde{Q}_\alpha \tag{70}$$

From the (70) there follow the equations of motion

$$\ddot{s}_1 = 0, \quad \ddot{s}_2 = -\frac{\partial V}{\partial\xi}$$

or, in the identifiable form

$$\dot{\xi}\dot{\varphi} + \xi\ddot{\varphi} = 0 \ \rightarrow \ \xi\dot{\varphi} = const., \ \ddot{\xi} = -\frac{\partial V}{\partial\xi}$$

which is an identical form deriving from above mentioned types of differential equations of motion for nonlinear nonholonomic systems.

References

[1] Maggi G. A. Di alcune nuove forma della equayioni della dinamica applicable ai sistemi anolonomi. Atti della Reale Accademia Nazionale dei Lincei. Rendiconti classe fisiche e mathematiche, Ser. 5, v. 10, fasc. 2, p. 287-291, 1901.

[2] Volterra V. Sopra una classe di equazioni dinamiche. Atti Acd. Sci. cl. Sci fis., matem. e natur., Torino, 1898, vol 33, p. 451-542.

[3] Appell P. Sur les mouvements de roulement. Equations du mouvement anologues a celles de Lagrange. Comp. Rend. de l'Acad. de Sci. de Paris, 1899, t.129, p. 317-320

[4] Voronec P.V., On Equations of Motion for Nonholonomic Systems, Annals of Mathematics, Vol. 22, 1901. T. 22 [In Russian]

[5] Chaplygin S.A., On the Motion of Heavy Rotating Body along Horizontal Surface, Collected Works, Vol. 1, M-L, Gostehizdat, 1948. [In Russian]

[6] Ferrers N. M. Extentions of Lagrange's equations. Quart. J. Math., 1875, No 45.

[7] Voronec P.V., Equations of Motion for Hard Body Rolling without Sliding along Immovable Surface, Kiev, 1903. [In Russian]

[8] Hamel G. Die Lagrange-Eilerschen Gleichungen den Mechanik. Yeitschraft fur Math. und Phus., 1904, Bd. 50, p. 1-57.

[9] Neymark Y. I., Fufaev N. A, Dynamics of Nonholonomic systems, Nauka, Moskva, 1967, p. 520

[10] Covic V., Differential Equations and Stability of Motion of Nonholonomic Systems, Applied to Dynamic Structures, PhD thesis, Faculty of Mechanical Engineering, Belgrade, 1976. [In Serbian]

[11] Dobronravov V.V., Basics of Mechanics of Nonholonomic systems, Vissaja skola, Moskva, 1970, p. 270

[12] Zekovic D., Examples of Nonlinear Nonholonomic Constraints in Classical Mechanics, Vesn.Mosk. un-ta, Series 1, Mat.-meh., No1, 1991, p. 100-103. [In Russian]

THE NEW FORM OF FORCE FUNCTION OF TWO FINITE BODIES IN TERMS OF MODIFIED DELAUNAY'S AND ANDOYER'S ANGLE VARIABLES

Alexandr Zlenko

Department of high mathematics, Moscow automobile and road construction state
technical university (MADI), Leningradskii avenue 64, Moscow, 125319, Russia.
e – mail : zalaf121@mail.ru

Abstract. I The known earlier force function of two finite bodies in the terms of Delaunay's and Andoyer's is given to mind   when it contains only eight angle variables instead of nine and for one fixed set of coefficients of angle variables we have the only one function of cosine and the only one function of sin with summarized multipliers before them.
Key words.   force funvtion, Delaunay's and Andoyer's angle variable, regrouping, theorem, lemma, two finite bodies.

1. Introduction

Knowledge of force function of mutual gravitation   celestial bodies is very important for research of their motion. The first general result was obtained by Kondurar' [1] where the series for force function of two ellipsoids (one homogeneous and the other unhomogeneous) were presented. A method for calculating the force function of two celestial bodies was proposed by Šidlichovský [2] what is based of real Stokes constant. And also in [3] by Šidlichovský the full force function of two general rigid bodies is written in the terms of Delaunay's and Andoyer's variables. Vidyakin and Popova [4] presented expansion of force function of mutual gravitation of two rigid bodies of arbitrary form in series of spherical functions. The main purpose of our paper is to transform the force function in [3] to new form more convenient for practical use as will be seen below.

2. Presentation of the original force function

Let us describe the force function in the terms of Delaunay's and Andoyer's variables [3]:

$$U = f M_1 M_2 \sum_{j \geq 0} \sum_{n \geq 0} \sum_{m''=0}^{j} \sum_{k''=0}^{n} \frac{a_1^j a_2^n}{a^{j+n+1}} \left[\Gamma_{jm''nk''}^{CC} C_{jm''}^{(1)} C_{nk''}^{(2)} + \Gamma_{jm''nk''}^{SS} S_{jm''}^{(1)} S_{nk''}^{(2)} \right] +$$

$$+ f M_1 M_2 \sum_{j \geq 0} \sum_{n \geq 0} \sum_{m''=0}^{j} \sum_{k''=0}^{n} \frac{a_1^j a_2^n}{a^{j+n+1}} \left[\Gamma_{jm''nk''}^{SC} S_{jm''}^{(1)} C_{nk''}^{(2)} + \Gamma_{jm''nk''}^{CS} C_{jm''}^{(1)} S_{nk''}^{(2)} \right] \qquad (1)$$

where f is the universal gravitational constant, M_1 and M_2 are the masses of the bodies,

a_1 and a_2 are the characteristic diameters of the bodies, a is the Kepler's major semi axis;

$$\Gamma_{jm''nk''}^{CC} = B_{jm''nk''} \operatorname{Re} \left[Z_{jnm''k''} + (-1)^{m''} Z_{jn-m''k''} \right],$$

$$\Gamma_{jm''nk''}^{SS} = B_{jm''nk''} \operatorname{Re} \left[-Z_{jnm''k''} + (-1)^{m''} Z_{jn-m''k''} \right]$$

$$\Gamma_{jm''nk''}^{SC} = B_{jm''nk''} \operatorname{Im} \left[Z_{jnm''k''} - (-1)^{m''} Z_{jn-m''k''} \right],$$

$$\Gamma_{jm''nk''}^{CS} = B_{jm''nk''} \operatorname{Im} \left[Z_{jnm''k''} + (-1)^{m''} Z_{jn-m''k''} \right], \qquad (2)$$

$$B_{jm''nk''} = (-1)^{m''+k''} (2\pi) \left[\frac{(j+m'')!(n+k'')!}{(2j+1)(2n+1)(j-m'')!(n-k'')!} \right]^{1/2} \qquad (3)$$

$$Z_{jnm''k''} = \sum_{m=-j}^{j} \sum_{k=-n}^{n} \sum_{p=0}^{n+j} \sum_{m'=-j}^{j} \sum_{k'=-n}^{n} \sum_{q=-\infty}^{q=+\infty} D_{jnm''k''mkpm'k'q} \exp(i\alpha_{jnm''k''mkpm'k'q}) \qquad , (4)$$

$C_{jm''}^{(1)}, S_{jm''}^{(1)}$ and $C_{nk''}^{(2)}, S_{nk''}^{(2)}$ are real Stokes constants for the first and the second body respectively, $\operatorname{Re}[\ldots], \operatorname{Im}[\ldots]$ – are real and imaginary part respectively, i – imaginary unit.

$$D_{jnm''k''mkpm'k'q} = X_q^{-j-n-1, j+n-2p}(e) \cdot$$

$$\cdot \frac{1}{4\pi} \left[\frac{(2j+2n-2p)!(2p)!(j+n+m+k)!(j+n-m-k)!(2j+1)(2n+1)}{(j-m)!(j+m)!(n+k)!(n-k)!} \right]^{1/2} \cdot$$

$$\cdot \frac{(-1)^{m+m''+k+k''+j+n}}{2^{j+n} p!(j+n-p)!} \Delta_{j+n-2p,m+k}^{(j+n)}(I) \Delta_{-m',-m}^{(j)}(I_1) \Delta_{-m'',-m'}^{(j)}(J_1) \Delta_{-k',-k}^{(n)}(I_2) \Delta_{-k'',-k'}^{(n)}(J_2), \quad (5)$$

$X_q^{ns}(e)$ - coefficients of Hansen :

$$\left(\frac{r}{a} \right)^n \exp is\upsilon = \sum_{q=-\infty}^{q=\infty} X_q^{ns}(e) \exp iql, \qquad (6)$$

where r – is the distance between the centers of masses of the bodies, υ is the true anomaly, e – eccentricity of the orbit, l is the mean anomaly.

$$\Delta_{m'm}^{(j)}(\vartheta) = \sum_{\chi=max(0,m-m')}^{\chi=min(j-m',j+m)} (-1)^{\chi} \frac{[(j+m)!(j-m)!(j+m')!(j-m')!]^{1/2}}{\chi!(j-m'-\chi)!(j+m-\chi)!(\chi+m'-m)!} \cdot \qquad (7)$$

$$\cdot cos^{2j+m-m'-2\chi}(\vartheta/2) \ sin^{2\chi+m'-m}(\vartheta/2)$$

$$\alpha_{jnm''k''mkpm'k'q} = -m''l_1 - m'g_1 - mh_1 - k''l_2 - k'g_2 - kh_2 + ql + (j+n-2p)g + \\ + (m+k)h + \tfrac{1}{2}\pi(j+n-m''-k'') \qquad (8)$$

Andoyer's variables are introduced for the i-th body (i=1,2):

$L_i - \zeta_i$ component of the angular momentum vector of the i-th body (ζ_i is the axis of inertia of the i-th body with maximum moment of inertia);

G_i – the rotational angular momentum of the i-th body (absolute value);

$H_i - Z$ component of the angular momentum vector $\vec{G}_i$ of the i-th body ($M_i XYZ$ is the Koenig's coordinate system of the i-th body).

$$cos\, J_i = L_i / G_i, \quad cos\, I_i = H_i / G_i \qquad (9)$$

The Delaunay's variables L, G, H, l, g, h are introduced for describing the orbital motion of bodies. Impulses L, G, H are related to the Kepler elements a, e, I as:

$$L = M(\mu a)^{1/2},$$
$$G = M[\mu a(1 - e^2)]^{1/2}, \qquad (10)$$
$$H = M[\mu a(1 - e^2)]^{1/2} cos\, I,$$

where

$$M = \frac{M_1 M_2}{M_1 + M_2}, \ \mu = f(M_1 + M_2). \qquad (11)$$

Variable L is connected with constant of energy, G is the absolute value of the orbital angular momentum the second body around the first body, $H - Z$ component of the angular momentum vector $\vec{G}$.

3. Introducing the new angle variables

We will present the force function (1) in another way using (2) - (8) and taking finite intervals for index of summation j : 0,1,2,...,v_1; n: 0,1,2,...,v_2 ; q :-v_3 ,- v_3+1,-v_3+2, ...,0,1,2,..., v_3 (as usually do in practice).

$$U = f M_1 M_2 \sum_{j=0}^{v_1} \sum_{n=0}^{v_2} \sum_{m''=-j}^{j} \sum_{k''=0}^{n} \sum_{m=-j}^{j} \sum_{k=-n}^{n} \sum_{p=0}^{n+j} \sum_{m'=-j}^{j} \sum_{k'=-n}^{n} \sum_{q=-v_3}^{v_3} \frac{a_1^j a_2^n}{a^{j+n+1}} D_{jnm''k''mkpm'k'q} \times$$

$$\times (E_{jnm''k''} \ cos\, \alpha_{jnm''k''mkpm'k'q} + \Phi_{jnm''k''} \ sin\, \alpha_{jnm''k''mkpm'k'q}), \qquad (12)$$

where

$$E_{jnm''k''} = B_{jm''nk''}(C^{(1)}_{jm''}C^{(2)}_{nk''} - S^{(1)}_{jm''}S^{(2)}_{nk''}), \ \Phi_{jnm''k''} = B_{jm''nk''}(C^{(1)}_{jm''}S^{(2)}_{nk''} + S^{(1)}_{jm''}C^{(2)}_{nk''}),$$

$$\text{if} \quad m'' > 0 ;$$

$$E_{jnm''k''} = (-1)^{m''} B_{j-m''nk''}(C^{(1)}_{j,-m''}C^{(2)}_{nk''} + S^{(1)}_{j,-m''}S^{(2)}_{nk''}), \ \Phi_{jnm''k''} = (-1)^{m''} B_{j-m''nk''}$$

$$(C^{(1)}_{j,-m''}S^{(2)}_{nk''} - S^{(1)}_{j,-m''}C^{(2)}_{nk''}), \qquad\qquad \text{if} \quad m'' < 0 ;$$

$$E_{jn0k''} = 2 \ B_{j0nk''} \ C^{(1)}_{j0}C^{(2)}_{nk''}, \ \Phi_{jn0k''} = 2 \ B_{j0nk''} \ C^{(1)}_{j0}S^{(2)}_{nk''}, \qquad \text{if} \quad m'' = 0 . \qquad (13)$$

From (8) and (12) we can see, that in linear combination of angles $\alpha_{jnm''k''mkpm'k'q}$ there are 10 indexes of summation for 9 independent angular variables, moreover the term $\frac{1}{2}\pi(j + n - m'' - k'')$ gives us function *cosine* or *sin*. For one fixed set of coefficients $\{-m'', -m', m, -k'', -k', k, q, j+n-2p, m+k\}$ of angle variables $g_1, h_1, l_1, g_2, h_2, l_2, l, g, h$ there are several equal functions of *cosine* and *sin* with different multipliers before them. It is reasonable for one fixed set of coefficients of angle variables to have the only one function of *cosine* and the only one function of *sin* with summarized multipliers before them. From view of $\alpha_{jnm''k''mkpm'k'q}$ (8) follows that we can introduce instead of 9 variables only the 8 new angle variables:

$$l_1' = (l_1 + \pi/2), g_1' = g_1, h_1' = h - h_1, l_2' = (l_2 + \pi/2), g_2' = g_2,$$

$$h_2' = h - h_2, l' = l, g' = g + \pi/2, - \qquad\qquad (14)$$

and new coefficient q':

$$q' = j + n - 2p, \quad \text{hence} \quad p = (j + n - q')/2. \qquad\qquad (15)$$

The interval variation of q' is from $-(n+j)$ to $(n+j)$ with step of summation $\Delta q' = 2$.

Then angular linear combination $\alpha_{jnm''k''mkpm'k'q}$ will take next form in new variables:

$$\alpha_{jnm''k''mkpm'k'q} = \alpha'_{m''m'mk''k'k qq'} + p\pi,$$

where

$$\alpha'_{m''\,m'\,m\,k''k'\,k\,q\,q'} = -\,m''l'_1 - m'g'_1 + mh'_1 - k''l'_2 - k'g'_2 + kh'_2 + ql' + q'g' \quad (16)$$

This expression $\alpha'_{m''\,m'\,m\,k''k'\,k\,q\,q'}$ is the linear combination only eight new angle variables.

Then

$$cos\ \alpha_{jnm''k''mkpm'k'q} = cos\,(\,\alpha'_{m''\,m'\,m\,k''k'\,k\,q\,q'} + p\pi\,)=\left(-1\right)^{p} cos\ \alpha'_{m''\,m'\,m\,k''k'\,k\,q\,q'} =$$

$$=\left(-1\right)^{(j+n-q')/2} cos\ \alpha'_{m''\,m'\,m\,k''k'\,k\,q\,q'},$$

$$sin\ \alpha_{j\,n\,m''k''\,m\,k\,pm'k'q} = \left(-1\right)^{(j+n-q')/2} sin\ \alpha'_{m''\,m'\,m\,k''k'\,k\,q\,q'} \quad (17)$$

We rewrite the force function (12) in new notations (14)-(17):

$$U = fM_1M_2\sum_{j=0}^{v_1}\sum_{n=0}^{v_2}\sum_{m''=-j}^{j}\sum_{k''=0}^{n}\sum_{m=-j}^{j}\sum_{k=-n}^{n}\sum_{m'=-j}^{j}\sum_{k'=-n}^{n}\sum_{q=-v_3}^{v_3}\sum_{q'=-(j+n),\Delta q'=2}^{j+n}\frac{a_1^j a_2^n}{a^{j+n+1}}(-1)^p\,D_{jnm''k''mkpm'k'q}\times$$

$$\times(\,E_{jnm''k''}\ cos\ \alpha'_{m''\,m'\,m\,k''k'\,k\,q\,q'} + \Phi_{jnm''k''}\ sin\ \alpha'_{m''\,m'\,m\,k''k'\,k\,q\,q'}),\quad (18)$$

where index p is given by (15).

4. Regrouping the terms of force function

Then we change the order of summation in force function (18) in order to put together and summarize all multipliers with index j and n before functions *cosine* and *sin* with fixed set of coefficients $\{-m'',-m',m,-k'',-k',k,q,q'\}$ and obtain the next expression:

$$U = \sum_{m''=-v_1}^{v_1}\sum_{m'=-v_1}^{v_1}\sum_{m=-v_1}^{v_1}\sum_{k''=0}^{v_2}\sum_{k'=-v_2}^{v_2}\sum_{k=-v_2}^{v_2}\sum_{q=-v_3}^{v_3}\sum_{q'=-(v_1+v_2)}^{v_1+v_2}Y_{m''m'mk''k'kqq'}\quad (19)$$

where

$$Y_{m''m'mk''k'kqq'} = \quad (20)$$

$$=\left[\left(\sum_{j=v_4}^{v_1}\sum_{n=v_5,\Delta n=2}^{v_2}A'_{jnm''m'mk''k'kqq'}\right)cos\,\alpha'_{m''m'm\,k''k'\,k\,q\,q'} + \left(\sum_{j=v_4}^{v_1}\sum_{n=v_5,\Delta n=2}^{v_2}A''_{jnm''m'mk''k'kqq'}\right)sin\,\alpha'_{m''m'm\,k''k'\,k\,q\,q'}\right]$$

$$A'_{jnm''m'mk''k'kqq'} = fM_1M_2\frac{a_1^j a_2^n}{a^{j+n+1}}\,(-1)^p\,D_{jnm''k''m\,k\,pm'k'q}\ E_{jnm''k''},$$

$$A''_{jnm''m'mk''k'kqq'} = fM_1M_2\frac{a_1^j a_2^n}{a^{j+n+1}}\,(-1)^p\,D_{jnm''k''m\,k\,pm'k'q}\ \Phi_{jnm''k''},\quad (21)$$

$$v_4 = \max\left(|m''|,|m'|,|m|,|q'|-v_2\right);$$
$$v_5 = v, \text{ if } (j+v) \equiv |q'|(mod\,2), \text{ else } v_5 = v+1\ ;$$
(22)

here $v = \max\left(|k''|,|k'|,|k|,|q'|-j\right)$,

where $D_{jnm''k''mk\,pm'k'q}$ is given by formula and (5), $E_{jnm''k''}$, $\Phi_{jnm''k''}$ are given by formula (13), $p - (15)$.

In order to prove formulas (19)-(20) which has complicated indexes of summation v_4, v_5 we begin from the simple affirmations.

Lemma 1. It is true the next equality:

$$\sum_{j=0}^{v_1}\sum_{n=0}^{v_2}\sum_{m''=-j}^{j}\sum_{k''=-n}^{n}\sum_{q'=-(j+n),\Delta q'=2}^{j+n}A_{jnm''k''q'}\beta_{m''k''q'} = \sum_{m''=-v_1}^{v_1}\sum_{k''=-v_2}^{v_2}\sum_{q'=-(v_1+v_2)}^{v_1+v_2}\left(\sum_{j=v_4}^{v_1}\sum_{n=v_5,\Delta n=2}^{v_2}A_{jnm''k''q'}\right)\beta_{m''k''q'}$$
(23)

where

$$v_4 = \max\left(|m''|,|q'|-v_2\right),$$
$$v_5 = v, \text{ if } (j+v) \equiv |q'|(mod\,2), \text{ else } v_5 = v+1\ ;$$
(24)
$$v = \max\left(|k''|,|q'|-j\right)$$

In proof we use the method of mathematical induction. It easy to see that this equality is true for the next pairs of indexes of summation v_1 and v_2: (0,0), (0,1), (1,0), (1,1). Let   the equality (22) will be true for arbitrary v_1 and v_2. Then we are proving that formula (22) is true for next pairs $(v_1 + 1, v_2)$ and $(v_1, v_2 + 1)$. That's all. Note, that expression (22) is symmetrical relatively indexes j and n.

Then we prove by method of mathematical induction ***Lemma 2***, using ***Lemma 1***.

Lemma 2. It is true the next equality:

$$\sum_{j=0}^{v_1}\sum_{n=0}^{v_2}\sum_{m''=-j}^{j}\sum_{m'=-j}^{j}\sum_{k''=-n}^{n}\sum_{q'=-(j+n),\Delta q'=2}^{j+n}A_{jnm''m'k''q'}\beta_{m''m'k''q'} =$$

$$= \sum_{m''=-v_1}^{v_1}\sum_{m'=-v_1}^{v_1}\sum_{k''=-v_2}^{v_2}\sum_{q'=-(v_1+v_2)}^{v_1+v_2}\left(\sum_{j=v_4}^{v_1}\sum_{n=v_5,\Delta n=2}^{v_2}A_{jnm''m'k''q'}\right)\beta_{m''m'k''q'}\ ,$$
(25)

where

$$v_4 = \max\left(|m''|,|m'|,|q'|-v_2\right),$$
$$v_5 = v, \text{ if } (j+v) \equiv |q'|(mod\,2), \text{ else } v_5 = v+1\ ;$$
(26)
$$v = \max\left(|k''|,|q'|-j\right)$$

Then we prove by method of mathematical induction ***Lemma 3*** , using ***Lemma 2*** , and with their help the general ***Theorem*** from which follows formulas (19)-(20) for force function **U**.

Lemma 3. It is true the next equality:

$$\sum_{j=0}^{v_1}\sum_{n=0}^{v_2}\sum_{m''=-j}^{j}\sum_{m'=-j}^{j}\sum_{m=-j}^{j}\sum_{k''=-n}^{n}\sum_{q'=-(j+n),\Delta q'=2}^{j+n}A_{jnm''m'm\,k''\,q'}\beta_{m''m'm\,k''\,q'} =$$

$$= \sum_{m''=-v_1}^{v_1}\sum_{m'=-v_1}^{v_1}\sum_{m=-v_1}^{v_1}\sum_{k''=-v_2}^{v_2}\sum_{q'=-(v_1+v_2)}^{v_1+v_2}\left(\sum_{j=v_4}^{v_1}\sum_{n=v_5,\Delta n=2}^{v_2}A_{jnm''m'm\,k''q'}\right)\beta_{m''m'm\,k''q'} ,\quad (27)$$

where

$$v_4 = \max\left(\left|m''\right|,\left|m'\right|,\left|m\right|,\left|q'\right|-v_2\right),$$

$$v_5 = v,\ if\ (j+v)\equiv\left|q'\right|(mod\,2),\ else\ v_5 = v+1\ ;\qquad (28)$$

$$v = \max\left(\left|k''\right|,\left|q'\right|-j\right)$$

Theorem. It is true the next equality:

$$\sum_{j=0}^{v_1}\sum_{n=0}^{v_2}\sum_{m''=-j}^{j}\sum_{m'=-j}^{j}\sum_{m=-j}^{j}\sum_{k''=-n}^{n}\sum_{k'=-n}^{n}\sum_{k=-n}^{n}\sum_{q'=-(j+n),\Delta q'=2}^{j+n}A_{jnm''m'm\,k''k'k\,q}\beta_{m''m'm\,k''k'k\,q'} =$$

$$= \sum_{m''=-v_1}^{v_1}\sum_{m'=-v_1}^{v_1}\sum_{m=-v_1}^{v_1}\sum_{k''=-v_2}^{v_2}\sum_{k'=-v_2}^{v_2}\sum_{k=-v_2}^{v_2}\sum_{q'=-(v_1+v_2)}^{v_1+v_2}\left(\sum_{j=v_4}^{v_1}\sum_{n=v_5,\Delta n=2}^{v_2}A_{jnm''m'm\,k''k'k\,q}\beta_{m''m'm\,k''k'k\,q'}\right)\quad (29)$$

where

$$v_4 = \max\left(\left|m''\right|,\left|m'\right|,\left|m\right|,\left|q'\right|-v_2\right);$$

$$v_5 = v,\ if\ (j+v)\equiv\left|q'\right|(mod\,2),\ else\ v_5 = v+1\ ;\qquad (30)$$

here $\quad v = \max\left(\left|k''\right|,\left|k'\right|,\left|k\right|,\left|q'\right|-j\right).$

5. Converting the force function to the mind when for one fixed set of coefficients of angle variables we have the only one function of *cosine* and the only one function of *sin* with summarized multipliers before them.

It should be noted that for our purpose we can grouping the terms in force function in the various ways beginning and continuing from any index of summation. We will point out only the general method beginning on the example of k'' index (we remark if some subscript is equal zero, it is absent in the corresponding expression and there is not summation on it).

Formula (19) can be rewritten in the following way:

$$\mathbf{U} = \sum_{m''=-v_1}^{v_1}\sum_{m'=-v_1}^{v_1}\sum_{m=-v_1}^{v_1}\sum_{k''=1}^{v_2}\sum_{k'=-v_2}^{v_2}\sum_{k=-v_2}^{v_2}\sum_{q=-v_3}^{v_3}\sum_{q'=-(v_1+v_2)}^{v_1+v_2}Y_{m''m'mk''k'k\,q\,q'} + \mathbf{U}_{k''=0} ,\quad (31)$$

where

$$\mathbf{U}_{k''=0} = \sum_{m''=-v_1}^{v_1} \sum_{m'=-v_1}^{v_1} \sum_{m=-v_1}^{v_1} \sum_{k'=-v_2}^{v_2} \sum_{k=-v_2}^{v_2} \sum_{q=-v_3}^{v_3} \sum_{q'=-(v_1+v_2)}^{v_1+v_2} Y_{m''m'm\,k'k\,q\,q'} \ .$$

The first expression in (31) gives us the needed expression because for one fixed set of coefficients of angle variables we have the only one function of *cosine* and the only one function of *sin* with summarized multipliers before them.

Then we'll transform the second expression with this aim. $\mathbf{U}_{k''=0}$ we can present as the sum of three expressions:

$$\mathbf{U}_{k''=0} = \sum_{m''=-v_1}^{-1} \sum_{m'=-v_1}^{v_1} \sum_{m=-v_1}^{v_1} \sum_{k'=-v_2}^{v_2} \sum_{k=-v_2}^{v_2} \sum_{q=-v_3}^{v_3} \sum_{q'=-(v_1+v_2)}^{v_1+v_2} Y_{m''m'm\,k'k\,q\,q'} +$$

$$+ \sum_{m''=1}^{v_1} \sum_{m'=-v_1}^{v_1} \sum_{m=-v_1}^{v_1} \sum_{k'=-v_2}^{v_2} \sum_{k=-v_2}^{v_2} \sum_{q=-v_3}^{v_3} \sum_{q'=-(v_1+v_2)}^{v_1+v_2} Y_{m''m'm\,k'k\,q\,q'} + \mathbf{U}_{k''=m''=0} , \qquad (32)$$

where

$$\mathbf{U}_{k''=m''=0} = \sum_{m'=-v_1}^{v_1} \sum_{m=-v_1}^{v_1} \sum_{k'=-v_2}^{v_2} \sum_{k=-v_2}^{v_2} \sum_{q=-v_3}^{v_3} \sum_{q'=-(v_1+v_2)}^{v_1+v_2} Y_{m'm\,k'k\,q\,q'} \ . \qquad (33)$$

Transform the first expression in (32), using (20) for $Y_{m''m'mk''k'k\,q\,q'}$:

$$\sum_{m''=-v_1}^{-1} \sum_{m'=-v_1}^{v_1} \sum_{m=-v_1}^{v_1} \sum_{k'=-v_2}^{v_2} \sum_{k=-v_2}^{v_2} \sum_{q=-v_3}^{v_3} \sum_{q'=-(v_1+v_2)}^{v_1+v_2} Y_{m''m'm\,k'k\,q\,q'} =$$

$$= \sum_{m''=-v_1}^{-1} \sum_{m'=-v_1}^{v_1} \sum_{m=-v_1}^{v_1} \sum_{k'=-v_2}^{v_2} \sum_{k=-v_2}^{v_2} \sum_{q=-v_3}^{v_3} \sum_{q'=-(v_1+v_2)}^{v_1+v_2}$$

$$\left[\left(\sum_{j=v_4}^{v_1} \sum_{n=v_5,\Delta n=2}^{v_2} A'_{jnm''m'm\,k'k\,q\,q'} \right) \cos\left(\alpha'_{m'm\,k'k\,q\,q'} \right) + \left(\sum_{j=v_4}^{v_1} \sum_{n=v_5,\Delta n=2}^{v_2} A''_{jnm''m'm\,k'k\,q\,q'} \right) \sin\left(\alpha'_{m'm\,k'k\,q\,q'} \right) \right] =$$

$$= \sum_{m''=-v_1}^{-1} \sum_{m'=-v_1}^{v_1} \sum_{m=-v_1}^{v_1} \sum_{k'=-v_2}^{v_2} \sum_{k=-v_2}^{v_2} \sum_{q=-v_3}^{v_3} \sum_{q'=-(v_1+v_2)}^{v_1+v_2}$$

$$\left[\left(\sum_{j=v_4}^{v_1} \sum_{n=v_5,\Delta n=2}^{v_2} A'_{jnm''m'm\,k'k\,q\,q'} \right) \cos\left(-\alpha'_{-m'-m'-m-k'-k-q-q'} \right) + \left(\sum_{j=v_4}^{v_1} \sum_{n=v_5,\Delta n=2}^{v_2} A''_{jnm''m'm\,k'k\,q\,q'} \right) \sin\left(-\alpha'_{-m''-m'-m-k'-k-q-q'} \right) \right] =$$

$$= \sum_{m''=-v_1}^{-1} \sum_{m'=-v_1}^{v_1} \sum_{m=-v_1}^{v_1} \sum_{k'=-v_2}^{v_2} \sum_{k=-v_2}^{v_2} \sum_{q=-v_3}^{v_3} \sum_{q'=-(v_1+v_2)}^{v_1+v_2}$$

$$\left[\left(\sum_{j=v_4}^{v_1} \sum_{n=v_5,\Delta n=2}^{v_2} A'_{jnm''m'm\,k'k\,q\,q'} \right) \cos\left(\alpha'_{-m'-m'-m-k'-k-q-q'} \right) - \left(\sum_{j=v_4}^{v_1} \sum_{n=v_5,\Delta n=2}^{v_2} A''_{jnm''m'm\,k'k\,q\,q'} \right) \sin\left(\alpha'_{-m''-m'-m-k'-k-q-q'} \right) \right] =$$

$$= \sum_{m''=1}^{v_1} \sum_{m'=-v_1}^{v_1} \sum_{m=-v_1}^{v_1} \sum_{k'=-v_2}^{v_2} \sum_{k=-v_2}^{v_2} \sum_{q=-v_3}^{v_3} \sum_{q'=-(v_1+v_2)}^{v_1+v_2} \qquad (34)$$

$$\left[\left(\sum_{j=v_4}^{v_1} \sum_{n=v_5,\Delta n=2}^{v_2} A'_{jn-m''-m'-m-k'-k-q-q'} \right) \cos\left(\alpha'_{m'm\,k'k\,q\,q'} \right) - \left(\sum_{j=v_4}^{v_1} \sum_{n=v_5,\Delta n=2}^{v_2} A''_{jn-m''-m'-m-k'-k-q-q'} \right) \sin\left(\alpha'_{m'm\,k'k\,q\,q'} \right) \right]$$

Using (34) we write (32) in the new form:

$$\mathbf{U}_{k''=0} = \sum_{m''=1}^{v_1} \sum_{m'=-v_1}^{v_1} \sum_{m=-v_1}^{v_1} \sum_{k'=-v_2}^{v_2} \sum_{k=-v_2}^{v_2} \sum_{q=-v_3}^{v_3} \sum_{q'=-(v_1+v_2)}^{v_1+v_2}$$

$$\left[\sum_{j,n} \left(A'_{jnm''m'mk'kqq'} + A'_{jn-m''-m'-m-k'-k-q-q'} \right) \cos \alpha'_{m''m'mk'kqq'} + \sum_{j,n} \left(A''_{jnm''m'mk'kqq'} - A''_{jn-m''-m'-m-k'-k-q-q'} \right) \sin \alpha'_{m''m'mk'kqq'} \right] +$$

$$+ \mathbf{U}_{k''=m''=0} , \qquad (35)$$

where notation

$$\sum_{j,n} \quad \text{means} \quad \sum_{j=v_4}^{v_1} \sum_{n=v_5, \Delta n=2}^{v_2} . \qquad (36)$$

In the first expression of (35) we have for one fixed set of coefficients of angle variables the only one function of *cosine* and the only one function of *sin* with summarized multipliers before them. Thus from (31) and (35) it follows:

$$\mathbf{U} = \sum_{m''=-v_1}^{v_1} \sum_{m'=-v_1}^{v_1} \sum_{m=-v_1}^{v_1} \sum_{k''=1}^{v_2} \sum_{k'=-v_2}^{v_2} \sum_{k=-v_2}^{v_2} \sum_{q=-v_3}^{v_3} \sum_{q'=-(v_1+v_2)}^{v_1+v_2}$$

$$\left[\left(\sum_{j,n} A'_{jnm''m'mk''k'kqq'} \right) \cos \alpha'_{m''m'mk''k'kqq'} + \left(\sum_{j,n} A''_{jnm''m'mk''k'kqq'} \right) \sin \alpha'_{m''m'mk''k'kqq'} \right] +$$

$$+ \sum_{m''=1}^{v_1} \sum_{m'=-v_1}^{v_1} \sum_{m=-v_1}^{v_1} \sum_{k'=-v_2}^{v_2} \sum_{k=-v_2}^{v_2} \sum_{q=-v_3}^{v_3} \sum_{q'=-(v_1+v_2)}^{v_1+v_2}$$

$$\left[\sum_{j,n} \left(A'_{jnm''m'mk'kqq'} + A'_{jn-m''-m'-m-k'-k-q-q'} \right) \cos \alpha'_{m''m'mk'kqq'} + \sum_{j,n} \left(A''_{jnm''m'mk'kqq'} - A''_{jn-m''-m'-m-k'-k-q-q'} \right) \sin \alpha'_{m''m'mk'kqq'} \right] +$$

$$+ \mathbf{U}_{k''=m''=0} . \qquad (37)$$

Making the same procedure for $\mathbf{U}_{k''=m''=0}$ (33) with index m' as we did for m'' given by formulas (32)-(35) and so on sequentially with other indexes of summation we'll get:

$$\mathbf{U}_{k''=m''=0} = \sum_{m'=1}^{v_1} \sum_{m=-v_1}^{v_1} \sum_{k'=-v_2}^{v_2} \sum_{k=-v_2}^{v_2} \sum_{q=-v_3}^{v_3} \sum_{q'=-(v_1+v_2)}^{v_1+v_2}$$

$$\left[\sum_{j,n} \left(A'_{jnm'mk'kqq'} + A'_{jn-m'-m-k'-k-q-q'} \right) \cos \alpha'_{m'm'mk'kqq'} + \sum_{j,n} \left(A''_{jnm'mk'kqq'} - A''_{jn-m'-m-k'-k-q-q'} \right) \sin \alpha'_{m'mk'kqq'} \right] +$$

$$+ \sum_{m=1}^{v_1} \sum_{k'=-v_2}^{v_2} \sum_{k=-v_2}^{v_2} \sum_{q=-v_3}^{v_3} \sum_{q'=-(v_1+v_2)}^{v_1+v_2}$$

$$\left[\sum_{j,n} \left(A'_{jnmk'kqq'} + A'_{jn-m-k'-k-q-q'} \right) \cos \alpha'_{mk'kqq'} + \sum_{j,n} \left(A''_{jnmk'kqq'} - A''_{jn-m-k'-k-q-q'} \right) \sin \alpha'_{mk'kqq'} \right] +$$

$$+ \sum_{k'=1}^{v_2} \sum_{k=-v_2}^{v_2} \sum_{q=-v_3}^{v_3} \sum_{q'=-(v_1+v_2)}^{v_1+v_2}$$

$$\left[\sum_{j,n}\left(A'_{jnk'kqq'}+A'_{jn-k'-k-q-q'}\right)\cos\alpha'_{k'kqq'}+\sum_{j,n}\left(A''_{jnk'kqq'}-A''_{jn-k'-k-q-q'}\right)\sin\alpha'_{k'kqq'}\right]+$$

$$+\sum_{k=1}^{v_2}\sum_{q=-v_3}^{v_3}\sum_{q'=-(v_1+v_2)}^{v_1+v_2}\left[\sum_{j,n}\left(A'_{jnkqq'}+A'_{jn-k-q-q'}\right)\cos\alpha'_{kqq'}+\sum_{j,n}\left(A''_{jnkqq'}-A''_{jn-k-q-q'}\right)\sin\alpha'_{kqq'}\right]+$$

$$+\sum_{q=1}^{v_3}\sum_{q'=-(v_1+v_2)}^{v_1+v_2}\left[\sum_{j,n}\left(A'_{jnqq'}+A'_{jn-q-q'}\right)\cos\alpha'_{qq'}+\sum_{j,n}\left(A''_{jnqq'}-A''_{jn-q-q'}\right)\sin\alpha'_{qq'}\right]+$$

$$+\sum_{q'=1}^{v_1+v_2}\left[\sum_{j,n}\left(A'_{jnq'}+A'_{jn-q'}\right)\cos\alpha'_{q'}+\sum_{j,n}\left(A''_{jnq'}-A''_{jn-q'}\right)\sin\alpha'_{q'}\right]+\sum_{j,n}A'_{jn}\ . \tag{38}$$

The formulas (37) and (38) give us the desired representation of force function. It should be emphasize that this representation is not the only one. It depends on what short periodic, resonant or long periodic terms we want to extract using the method offered above.

From mechanical meaning of angular variables it is follows that variables $l'_1, g'_1, l'_2, g'_2, l$ are fast, but h'_1, h'_2, g' are slow. The term $\sum_{j,n}A'_{jn}$ is the secular term.

6. CONCLUSION

The presentation of force function of two rigid bodies given in [3] is improved in modified angle variables of Delaunay and Andoyer: 1. instead of nine angle variables of Delaunay and Andoyer we have only eight modified angle variables; 2. one fixed set of coefficients of angle variables is only in one function *cosine* and *sin*; 3. all multipliers, consisting of Kepler's elements, before *cosine* and *sin* are summarized; 4. we can easy to take the terms of needed accuracy.

The new form of force function is more convenient for elimination of the short periodic perturbations and for solving evolutional and resonant problems in celestial mechanics and astrodynamics.

References

[1] Kondurar' V (1958) Expansion of force function of mutual gravitation of two ellipsoids (one homogeneous and the other unhomogeneous), *Astron. Zh.*, **35**, No. 5, pp.763-771.
[2] Šidlichovský M (1979) The force function of two general bodies II, *Bull. Astron. Inst. Checosl.,* **30**, No. 3, pp. 152-155.
[3] Šidlichovský M (1981) The elimination of short periodic perturbations in the problem of two finite bodies, *Bull. Astron. Inst. Checosl.,* **32**, No. 3, pp. 159-167.
[4] Vidyakin V and Popova I (1999) Expansion of force function of mutual gravitation of two rigid bodies of arbitrary form in series of spherical functions, *Astron. Zh.,* **76**, pp. 641-646.
[5] Duboshin G (1975) *Nebesnaja Mekhanika. Osnovnye zadachi i metody. Nauka, Moskva.*
[6] Andoyer H (1923) *Cours de Méchanique Céleste*, Gauthier-Villars, Paris.

SOME ASPECTS OF BIRD IMPACT THEORY

Marinko Ugrčić[1]

[1] Economics Institute
Kralja Milana, 18, 11000 Belgrade, Serbia
e-mail: ugrcicmarinko@gmail.com

Abstract. In the hydrodynamic theory and finite elements method the bird body was modeled as porous water-air material in the shape of flat or hemi-spherically ended cylinder. Finite elements bird modeling was carried out by the use of the SPH method for material of different porosity. In this way, the dependence of sound speed and bulk modulus on porosity in equation of state was developed. The Lagrangian target was considered as simple flat rigid steel or elastic Al alloy plate. The comparative analysis of numerical results of bird impact for Hugoniot shock theory and SPH method was given. As well, some results of experimental data were included.

1. Introduction

One of possible and very dangerous accident is a bird strike into the aircraft in the flight. This case is characterized by the high speed impact of the bird onto aircraft structure, causing large dynamic deformations of the elements which may lead to disintegration of the construction. Assuming the variables of target (flat rigid or elastic panel) as constant, the number of variables, the bird strike analysis deals with, is high. This makes the bird strike analysis relatively complex. The various parameters include bird material and density, impact velocity, bird mass, bird material configuration, bird aspect ratio, material porosity, obliquity of impact and contact properties.

Most of the initial models of bird impact was developed on the basis of the classical impact theory and used force-impulse equation. Unfortunately, these models failed to predict the damage to its details. Further, the elementary one-dimensional theory of hydrodynamics was used to study bird impact. The mass-momentum-energy conservation equations and simple pressure-density-energy equation of state were used to describe the material behavior [1,2]. More appropriate interpretation of bird impact was carried out by involving the shock wave theory.
Regarding the finite elements methods, actually, three approaches have been successfully employed to simulate this phenomenon. These are the Lagrangian [3,4], Arbitrary Lagrangian-Eulerian (ALE) [4-7] and Smooth Particle Hydrodynamics (SPH)

formulations. The SPH formulation is a more recently developed finite element method that uses particles of mass rather than an element mesh to represent the bird [4,8,9].

The basic goals of researching presented in this work can be summarized as follows:
- brief retrospective of bird impact hydrodynamic theory coupled with shock wave equations and the definition of the elastic bulk modulus and sound speed of porous medium depending on its proper porosity,
- numerical simulation of various cases of bird impact including the variation of material density, shape and impact velocity, impact angle and parameters of target plate, and
- comparing some results of the numerical simulation and the experimental testing.

2. Elementary shock theory of bird strike

2.1 DESCRIPTION OF IMPACT

Fig. 1 depicts four phases of the impact of a cylindrical body of fluid on a rigid target at an oblique angle of 90°. More complex geometries, such as hemi-spherically ended cylinders, complicate the theory but behave in the same broad manner.
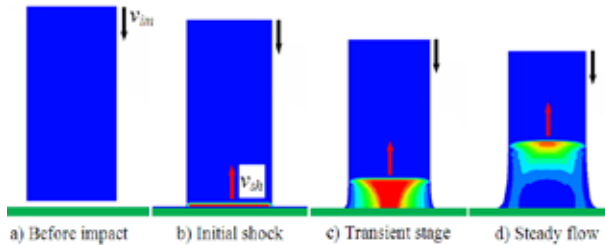
Figure 1. Bird impact phases given by numerical simulation of impact.

The four phases (Fig. 1) can be described as follows:
a) The cylinder of fluid approaches the flat target at an oblique angle and with a purely axial velocity. Its internal pressure is equal to that of the ambient atmosphere.
b) The leading face of the cylinder impacts the target and its constituent particles are instantaneously stopped, creating a violent shock wave - the Hugoniot shock - that travels back along the length of the cylinder as adjacent particles are brought to rest. The shocked region behind the wave is subject to transient shock pressure of high magnitude.
c) The huge pressure gradient between the radially unconfined free surface of the shocked region and its interior causes the generation of release waves, which trigger rapid radial expansion at the shocked end. The release or decompression waves travel at the speed of sound back towards the centre of the cylinder, reducing the strength of the shock wave as they progress.

d) The transient period ends when the release waves meet at the cylinder's central axis [10]. Steady flow is established as the cylinder flows onto the surface of the target. A steady stagnation pressure is reached, which is maximum at the centre of impact.

2.2 EOS OF WATER AND AIR

Additional useful information resulting from associating the bird to water is the equation of state (EOS) used to describe the pressure-density (p-ρ) relationship in the bird medium. A few equations are available and the one most commonly used for water-bird is a polynomial of degree 3 [1]. This polynomial EOS for the bird model corresponds to a hydrodynamic, isotropic, and non-viscous constitutive law and is given as follows:

$$p = C_0 + C_1\mu + C_2\mu^2 + C_3\mu^3 + (C_4 + C_5\mu + C_6\mu^2)E \tag{1}$$

$$\mu = \frac{\rho}{\rho_0} - 1 \tag{2}$$

where is: E - internal energy and μ - change in density during the impact.

The coefficients C_0-C_6 of polynomial equation are given by expressions based on the initial density, the speed of sound in the medium and an experimental constant k:

$$C_1 = \rho_0 c_0^2 \tag{3}$$
$$C_2 = (2k-1)C_1 \tag{4}$$
$$C_3 = (k-1)(3k-1)C_1 \tag{5}$$
$$C_0 = C_4 = C_5 = C_6 = 0 \tag{6}$$

where is: ρ_0 - density of medium (for the water $\rho_{0,w}$ = 1000 kg/m^3 and for the air $\rho_{0,a}$ = 1.225 kg/m^3), c_0 - speed of the sound in the medium (for the water $c_{0,w}$ = 1483 m/s and for the air $c_{0,a}$= 342 m/s) and k - experimental constant (for the water k_w= 2.0 and for the air k_a = 1.03).

2.3 EOS OF POROUS MATERIAL

The EOS of porous material is based on the thermodynamic equation that describes the state of matter under a given set of physical conditions $p = p(\rho,E) = p(V,E) = p(\rho,T)$. Further development of the theory for porous medium requires the elastic bulk modulus and sound speed of porous to be defined. Sound speed calculates assuming:

$$c_{por} = (1-z)^m c_{0,w} + zc_{0,a} \tag{7}$$

The Fig. 2 illustrates developed distribution for exponent values m =1-5, and m = 10. Using well-known sound speed - elasticity relation for fluid medium, the distribution of

bulk modulus K depending on porosity ($K = \rho_{por} c_{por}^2$) was calculated and shown in Fig. 3.
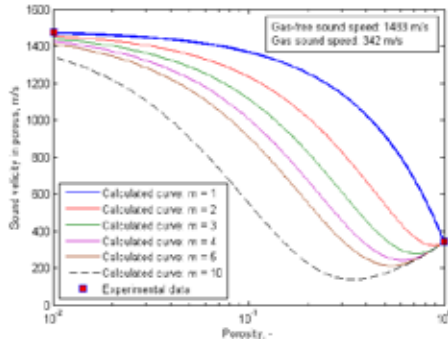
Figure 2. Sound speed distribution depending on porosity.   **Figure 3.** Bulk modulus depending on porosity.
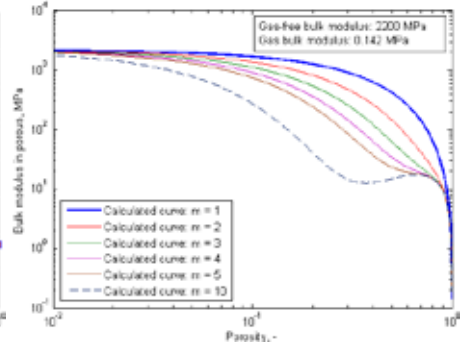
2.4 SHOCK PRESSURE AND SHOCK VELOCITY

A bird undergoing impact at high velocity behaves as a highly deformable projectile where the yield stress is much lower than the sustained stress. Accordingly, the impact can be qualified as a hydrodynamic impact. In the case of law impact velocities, i.e. at the loads below Hugoniot limit, the single elastic wave propagates through bird material. At higher impact velocities the Hugoniot shock wave appears. The pressure of the initial shock, so-called Hugoniot pressure, for incompressible and compressible bird material is given by following equations, respectively:

$$p'_{sh} = \rho c_0 v_{im} \tag{8}$$

$$p_{sh} = \rho v_{sh} v_{im} \tag{9}$$

where is: p_{sh} - shock pressure, $c_0 = c_E$ - sound speed in the fluid, v_{sh} - shock velocity of the generated shock wave, v_{im} - the translational particle velocity or simply projectile velocity and ρ_0 - initial density.

The pressure of steady flow p_{stag} (stagnation pressure) is calculated according to Bernoulli and is given by equation:

$$p_{stag} = \frac{1}{2} \rho v_{im}^2 \tag{10}$$

The equations given below apply to the bird-body with an amount of air mixed in, also called porosity, since experience has shown that porosity has a non-negligible effect on the overall results and is closer to the behavior of a bird upon impact [1,3] are given as follows:

$$\rho_1 v_{sh} = \rho_2 \left(v_{sh} - v_{im} \right) \tag{11}$$

$$p_1 + \rho_1 v_{sh}^2 = p_2 + \rho_2 (v_{sh} - v_{im})^2 \tag{12}$$

$$\frac{\rho_1}{\rho_2} = (1-z)\left(\frac{p_2}{A} + 1 \right)^{\frac{-1}{4k-1}} + z(1-q) \tag{13}$$

$$A = \frac{\rho_1 c_0^2}{4k-1} \tag{14}$$

$$\frac{\rho_2}{\rho_1} = \frac{1}{1-q} \tag{15}$$

where is: ρ_1 and ρ_2 - density of the medium before and after the impact, p_1 and p_2 - pressure before and after the impact (p_1 is negligible) and z - amount of the material porosity.

Parameter q is defined as:

$$q = 1 - \frac{\rho_1}{\rho_2} = q_1 - q_2 \tag{16}$$

where is:

$$q_1 = \left(\frac{2\bar{p}k_a + \dfrac{\rho_1 c_{0,a}^2}{p_1}}{2\bar{p}k_a^2} \right) \quad q_2 = \frac{\left[\left(2\bar{p}k_a + \dfrac{\rho_1 c_{0,a}^2}{p_1} \right)^2 - 4\bar{p}^2 k_a^2 \right]^{\frac{1}{2}}}{2\bar{p}k_a^2} \quad \bar{p} = \frac{p_2}{p_1} \tag{17}$$

Utilizing mixture theory [1] the EOS for the shock compression phase of the porous material was derived as follows:

$$\left(\frac{\rho_1}{\rho_2} \right)_{porous} = (1-z)\left(\frac{\rho_1}{\rho_2} \right)_{water} + z\left(\frac{\rho_1}{\rho_2} \right)_{air} \tag{18}$$

The solution for the shock velocity in the porous is found by isolating p_2 and ρ_2 after the shock and by the simultaneous solution of equations (9), (17) and (18). Once the shock velocity is known, the Hugoniot pressure can be found from Eq. (11). Fig. 4 and Fig. 5 show the shock velocity and the shock pressure for impact velocities ranging from 0 to 500 m/s. The shock velocity and shock pressure are plotted for four different porosities ($z = 0.1$ to 0.4) in order to illustrate the influence of that parameter.
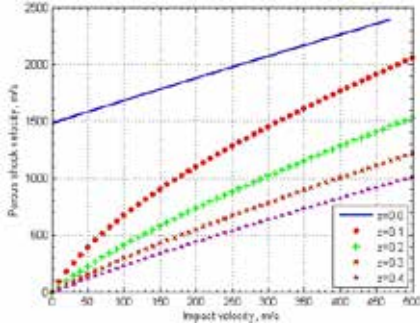
Figure 4. Theoretical dependence of shock velocity on porosity.
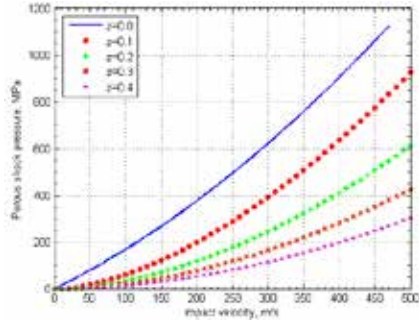
Figure 5. Theoretical dependence of shock pressure on porosity.

2.5 STAGNATION PRESSURE IN STEADY FLOW REGIME

For an uncompressible fluid like water the Eq. 10 is valuable. But for compressible materials density increases with pressure and produces higher values of stagnation pressure. In the case of compressible porous material we assume increasing factor equals $(1-z)^{-1}$:

$$p_{stag,z} = \frac{1}{1-z} \rho_{porous} \frac{v_{im}^2}{2} \tag{19}$$

$$\rho_{porous} = (1-z)\rho_{water} + z\rho_{air} \tag{20}$$

When the fluid flow reaches a steady state, it is also possible to calculate the pressure distribution along the radius, assuming exponential dependence:

$$p = p_{stag} e^{\left[-\frac{1}{2}\left(\frac{r}{R}\right)^2\right]} \tag{21}$$

where is: r - radial position and R - radius of the bird body.

The Fig. 6 and Fig. 7 illustrate the stagnation pressure depending on porosity and impact velocity, and the stagnation pressure distribution along the radius.
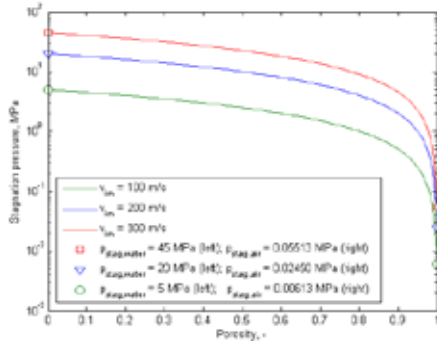
Figure 6. Stagnation pressure vs. impact velocity and porosity.
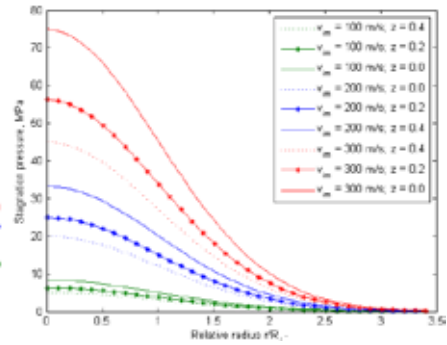
Figure 7. Stagnation pressure distribution along the radius vs. impact velocity and porosity.

Involving Eq. 19 in Eq. 20 we would get normalized diagram of stagnation pressure distribution with reduced number of curves in Fig. 7. In this case, the stagnation pressure for the same impact velocity would be identical and represented by solid line.

3. FEM modeling

3.1 BIRD MODEL

For *bird material* a homogeneous mixture of water and air was used. The porosity (volume presence of the air) was varied from $z = 0.0$ to $z = 0.4$. The effect of porosity with the P-alpha EOS [4] for porous material was investigated. The appropriate mechanical parameters of the water and water-air mixture depending on porosity are given in Table 1.

Table 1. Mechanical parameters of the water and water-air mixture

Porosity	Density	Sound speed	Bulk modulus
z	ρ	c_p (for m=1)	K (for m=1)
-	kg/m^3	m/s	MPa
0.0	1000.0	1483	2200
0.1	900.12	1368	1668
0.2	800.25	1256	1260
0.3	700.37	1142	907
0.4	600.49	1026	632

For the purpose of this research, two typical *bird shapes* that are generally used in bird strike analysis: flat and hemispherical cylinder, were considered. In each case, the height and diameter of the bird was assumed to be 200 mm and 100 mm, respectively.

The length-to-diameter ratio of 2 for each bird shape was identical. Two types of the numerical models of body shapes based on the SPH particles distributions along the symmetry axis are presented in Fig. 8.
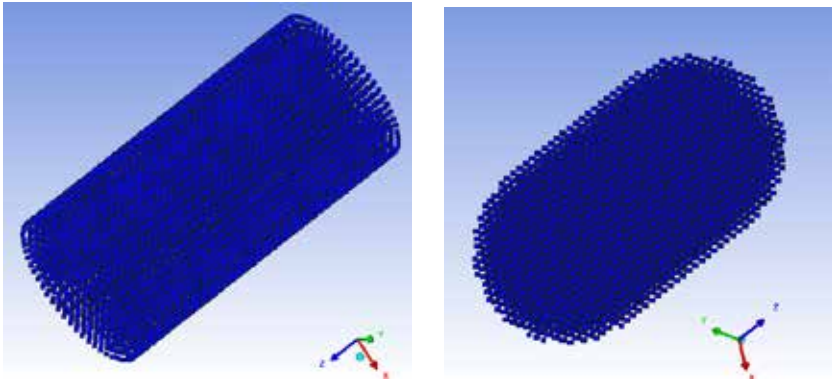
Figure 8. The SPH particles distribution along the symmetry axis of hemi-spherically ended cylinder: axial (left) and radial (right).

The cylindrical projectile model had a total of 12640 SPH particles and the cylinder with the hemi-spherical ends model had a total of 10512 SPH particles. The numerical models of bird body were built such that the nodal density of each body was approximately the same.

3.2 TARGET MODEL

For simplicity, the target structure was initially assumed to be rigid for comparative analysis of the shock pressures and shock wave velocities in the porous material. In addition, the impact velocity was assumed to be normal to the target. To simulate a rigid target, the target structure was modeled as a steel plate, with the dimensions 800×800 mm and thickness of 10 mm. All degrees of freedom of the target structure were constrained. The target structure was modeled using Belytschko-Tsay shell elements (Fig. 9) [4].
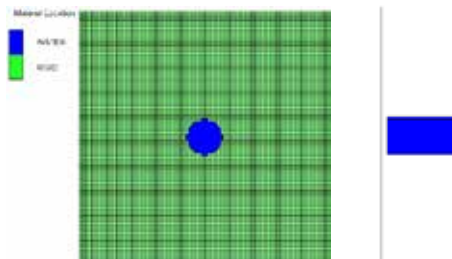
Figure 9. Lagrangian model of rigid target and SPH model of cylindrical bird projectile.

The target flexibility was introduced into the analysis, and the inherent coupling between the impact loads and the target deflection was explored. The appropriate mechanical parameters of the Al alloy are given in Table 2.

Table 2. Mechanical parameters of Al alloy target structure

Density	Poisson's ratio	Young's modulus	Shear modulus	Tensile yield strength
ρ	μ	E	G	R_{eH}
kg/m^3	-	GPa	GPa	MPa
2.785	0.33	71.00	28.60	280.00

Besides the frontal impact, the effects of oblique impact were considered on the flexible target. Specifically, the bird projectile direction of 45 degrees was simulated.
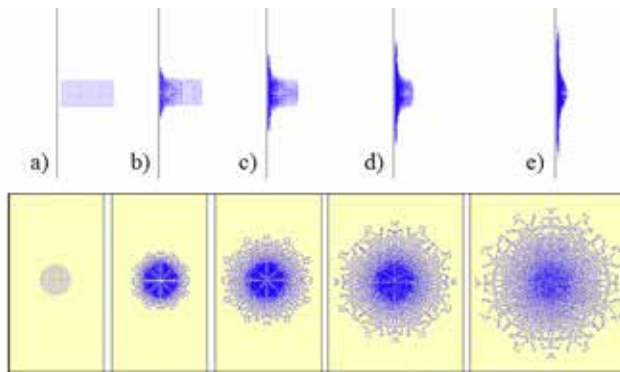
Figure 10. Deformations of cylindrical SPH body at different times during impact with rigid flat target (t= 0.0, 0.5, 1.0, 1.5, 2.0 ms).
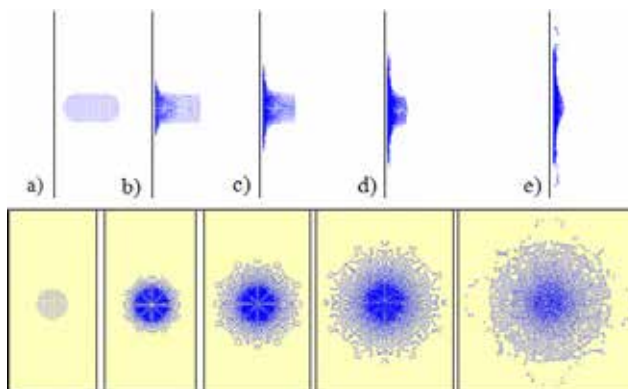
Figure 11. Deformations of hemispherical cylinder SPH body at different times during impact with rigid flat target (t= 0.0, 0.5, 1.0, 1.5, 2.0 ms).

4. Results and discussion

4.1 EFFECT OF PROJECTILE SHAPE ON A RIGID TARGET

Body deformations of artificial bird at different stages of the impact process are presented for various projectile shapes investigated in Figs. 10 and 11.

4.2 SHOCK PRESSURE AND SHOCK VELOCITY

The impact velocity for all bird projectiles was varied from 100 m/s to 500 m/s and normal to the rigid target. In addition, all the projectiles were assumed to have a porosity z of 0.4. Typical history diagram of the shock pressure distribution in the frontal plane of cylindrical body for velocities of 200 and 300 m/s impact are shown in Fig. 12.
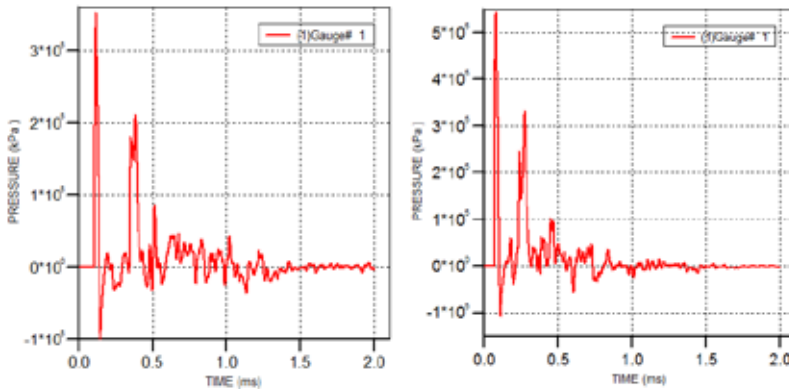
Figure 12. Shock pressure distribution along the radius for different impact velocities:
v_{im} = 200 m/s (left) and v_{im} = 300 m/s (right).

The history diagrams in Fig. 12 are similar and show appearances of two peaks on each shock pressure curve that is typical for two-phase materials such is the porous.

The SPH computed shock pressures for the cylindrical bird shape are presented in Fig. 13 and Fig. 14, for an appropriate range of projectile velocities and porosity. This last one, also, displays the experimental results from [3] for medium size birds. The exact weights of the test specimens were not given, however, it is stated that the specimens weighed between 0.5 kg to 1 kg. In addition, these figures display the computed shock pressures based on Wilbeck's theory [1].
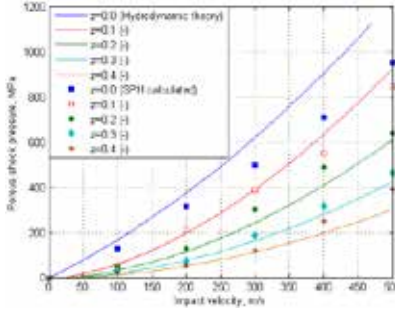
Figure 13. Comparison of Hydrodynamic theory and SPH calculated data for shock pressure distribution vs. impact velocity and porosity.
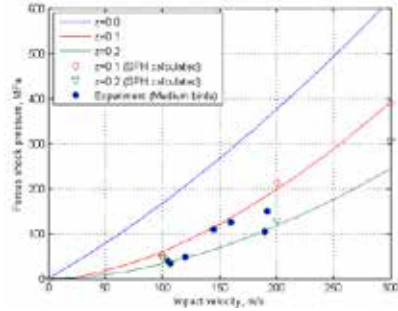
Figure 14. Computed and experimental data for shock pressure distribution vs. impact velocity and porosity.

Analysis of shock pressures calculated based on the Hydrodynamic theory and SPH method (Fig. 13) shows good correlation of computed data, specially for lower values of impact velocities ($v_{im} < 300$ m/s). Further increasing of impact velocity causes higher deviation of computed shock pressures. As well, the distribution of computed and experimental data in Fig. 14, for shock pressure in the porous, confirms validity of the predictive principle that assumes the bird body as porous medium.

4.3 STAGNATION PRESSURE IN STEADY FLOW REGIME

The steady-state flow pressure stage is considered to be more critical for bird impact events. Simplified shock pressure distribution is used to determine the stagnation pressure in steady flow regime. This diagram, implemented in the pressure history record given for 100 m/s impact velocity, will take appearance shown in Fig. 15 (smooth thick line).
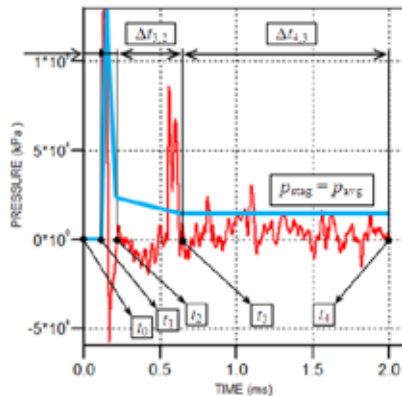
Figure 15. Simplified shock pressure distribution with typical stages.

Typical stages of pressure-time response are: $\Delta t_{1,0}$ - stage before impact, $\Delta t_{2,1}$ - shock wave stage; $\Delta t_{3,2}$ pressure release stage and $\Delta t_{4,3}$ - steady-state flow regime. Stagnation pressure calculates based on the equations:

$$p_{stag} = \frac{I_{sp}}{\Delta t_{4,3}} = \frac{I_{sp}}{\Delta t_{4,1} - \Delta t_{3,1}} = \frac{I_{sp}}{\dfrac{L}{v_{im}} - \Delta t_{3,1}} \tag{22}$$

$$I_{sp} = \int_{t_3}^{t_4} p\,dt \tag{23}$$

where is: I_{sp} - specific impulse of shock pressure during stagnation stage, $\Delta t_{4,1}$ - impact duration or so-called bird "squash-up" time, L - length of bird body and $\Delta t_{3,1}$ - time sequence of shock wave stage (up to 30% of impact time).

Stagnation pressure computed for the case of cylindrical bird shape is presented in Fig. 16, for a range of projectile velocities at $z = 0.4$. This figure displays the experimental results from [3,10] for medium size birds.
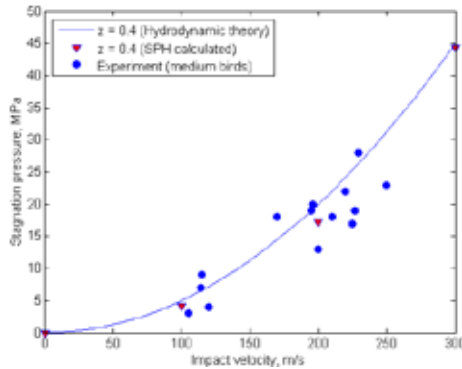
Figure 16. Stagnation pressure distribution vs. impact velocity for $z = 0.4$.

From Fig. 16, it can be seen that the computed steady state pressure from the cylindrical projectile shape match well with the experimental results. Most previous analyses [1,3,10] were capable of predicting the steady state stagnation pressures with good accuracy. In fact, Wilbeck's one-dimensional theory provides a quick way of checking the steady state pressure before performing a full numerical three-dimensional analysis.

4.4 *EFFECT OF TARGET FLEXIBILITY ON THE IMPACT LOADS AND DEFORMATIONS*

The shell model of Al alloy plate, 3 mm of thickness and the mechanical parameters

given in Table 2, was used to show the effect of target flexibility on the impact loads and plate deformations. The boundary conditions assumed all edges of the plate were fixed against displacement in any directions. Besides the frontal impact, the effects of oblique impact ($α = 45°$) were considered on the flexible target. Pressure and von Mises stress distributions for in Al plate at impact velocity 300 m/s are shown in Fig. 17.

a) Orthogonal bird impact ($α=90°$; $z=0.2$; $t=0.3$ ms)   b) Oblique bird impact ($α=45°$; $z=0.2$; $t=0.5$ ms)
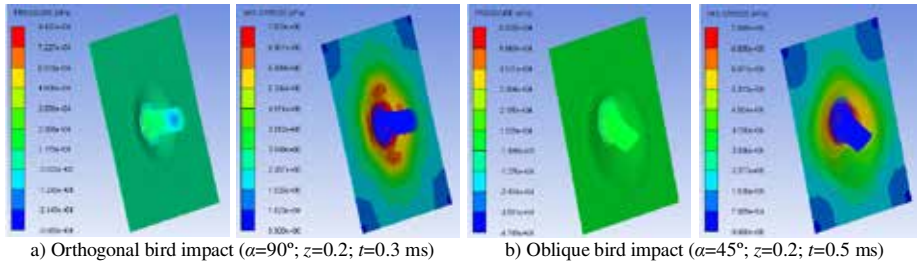
Figure 17. Pressure and von Mises stress distributions in the metallic plate at cylinder impact velocity 300 m/s.

Regarding the pressure distribution (Fig. 17), for time that provide the full contact surface will be reached in both orthogonal and oblique impact, the appearance of lower pressures characterizes the oblique impact caused by enlarged contact surface at $α = 45°$. Although, the comparative analysis of von Mises stress distributions in the metallic plate shows no difference between stress values for orthogonal and oblique impact.

Effective strain distributions along 3 mm thick Al alloy plate for orthogonal and oblique impact depending on impact velocity are shown in Fig. 18 and 19, respectively.

a) v_{im} = 100 m/s, z = 0.2; $t=T$ = 2 ms; 60° view direction (left); side view (right)   b) v_{im} = 300 m/s; z = 0.2; $t=T$ = 1 ms; 60° view direction (left); side view (right)
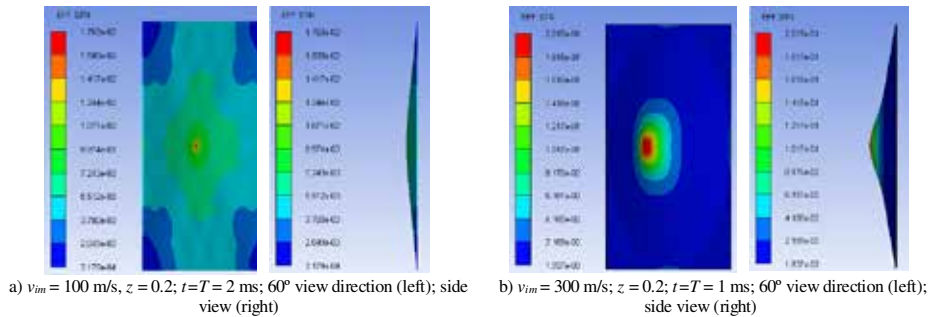
Figure 18. Effective strain distribution along 3 mm thick Al alloy plate for orthogonal cylinder impact depending on impact velocity.
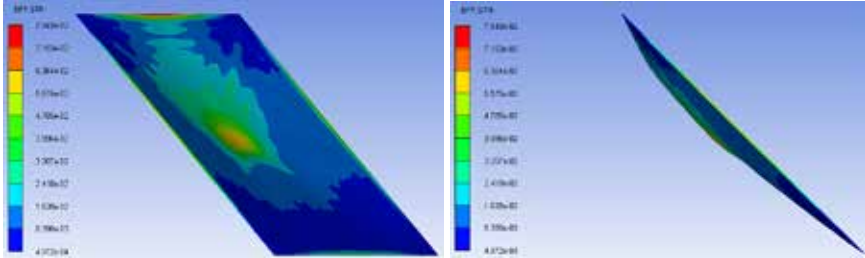
Figure 19. Effective strain distribution along 3 mm thick Al alloy plate for oblique cylinder impact (v_{im} = 300 m/s; z = 0.2; T = 1.5 ms).

From Figs. 18 and 19, it can be seen that the predicted effective strain for cylindrical bird body decreases with obliquity of impact velocity.

Finally, the pressure, von Mises stress and effective strain distributions are tested at same above mentioned impact conditions for hemispherical cylinder bird body. The relevant results of numerical simulations are given in Figs. 20, 21 and 22, respectively.
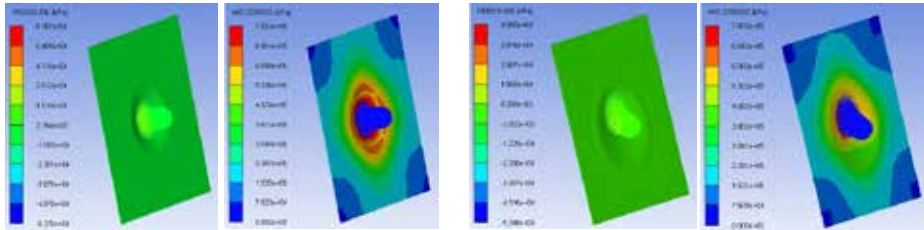
a) Orthogonal bird impact (α = 90°; z = 0.2; t = 0.3 ms) b) Oblique bird impact (α = 45°; z = 0.2; t = 0.5 ms)

Figure 20. Pressure and von Mises stress distributions in the metallic plate at hemispherical cylinder impact velocity 300 m/s.

a) v_{im} = 100 m/s, z = 0.2; t=T = 2 ms; 60° view direction (left); side view (right)   b) v_{im} = 300 m/s; z = 0.2; t=T = 1 ms; 60° view direction (left); side view (right)
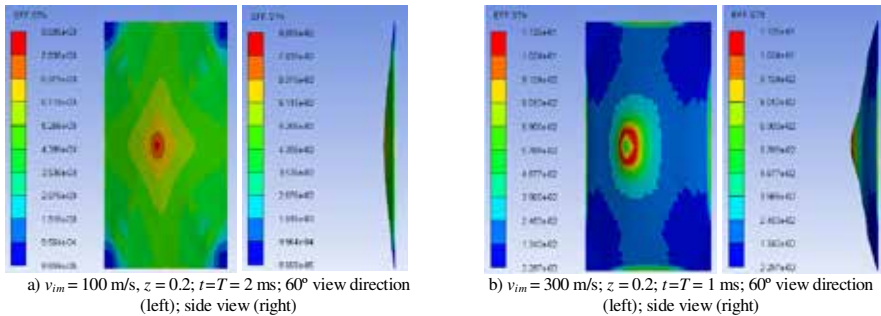
Figure 21. Effective strain distribution in 3 mm thick Al alloy plate for orthogonal hemispherical cylinder impact depending on impact velocity.
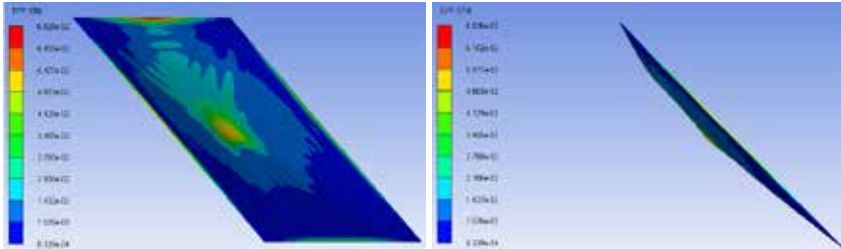
Figure 22. Effective strain distribution along 3 mm thick Al alloy plate for oblique hemispherical cylinder impact
(v_{im} = 300 m/s; z = 0.2; T = 1.5 ms).

Comparing the results of numerical simulations of bird impact on deformable target for flat cylinder and hemispherical cylinder shape of bird body it can be seen as follows:

- In the case of *orthogonal impact* maximum pressures distributions of the flat cylinder impact (Figs. 17 and 20) show for 26% higher values of pressures than for hemispherical cylinder impact, and for 38% higher values of pressures in the case of *oblique impact*;
- Von Mises stress distributions in the elastic metallic plate (Figs. 17 and 20) are practically identical relative to the stress values for orthogonal and oblique impact; and
- Effective strain distributions (Figs. 18, 19, 21 and 22) show generally that reduction of impact angle produces strain decreasing, and regarding the body shape that would be for 44% lower values of maximum strain in the case of orthogonal hemispherical cylinder impact and for 14% lower values of maximum strain in the case of oblique hemispherical cylinder impact, all at v_{im} = 300 m/s.

5. Conclusion

Brief retrospective of bird impact hydrodynamic theory coupled with Hugoniot shock wave equations was given. For bird material the homogeneous mixture of water-air mixture was used and the equation for elastic bulk modulus and sound speed of porous medium depending on porosity was involved in the analysis. Finite elements numerical simulations of bird impact were carried out by the use SPH method to represent bird body. Based on the mechanical parameters, determined by proposed equation, the effect of porosity with the P-alpha EOS for porous material was tested.

Numerical simulation of various cases of bird impact including the variation of bird material density, shape and impact velocity, impact angle and parameters of target plate was successfully performed. Comparing some results of the numerical simulation and the experimental testing, it appears that increasing the porosity might produce a better match of predicted Hugoniot shock and the FEM pressures with those observed in experiments. As well, the computed stagnation pressures in steady state regime, calculated by proposed method, match well with the experimental results. Regarding the shape, it can be seen that the predicted shock pressures associated with all of the bird

shapes produced a good correlation with the experimental results.

References

[1] Wilbeck J. S., Rand J. L., The Development of Substitute Bird Model, *ASME Journal of Engineering for Powe*r, Volume 103, (1981), pp. 725-730.

[2] Lavoie M. A., Gakwaya A., Ensan M .N., Zimcik D. G., Review of Existing Numerical Methods and Validation Procedure Available for Bird Strike Modeling, *International Conference on Computational & Experimental Engineering and Sciences*, (2007), pp. 111-118.

[3] Nizampatman L. S., Models and Methods for Bird Strike Load Predictions, *PhD Dissertation*, Faculty of Graduate School, Wichita State University, USA, (2007)

[4] ANSYS AUTODYN User's Manual *Theory manual*, ANSYS Inc. Southpointe, 275 Technology Drive, Canonsburg, PA, USA, (2010).

[5] Benson, D. J., An efficient, Accurate, Simple ALE Method for Nonlinear Finite Element Programs, *Computer Methods in Applied Mechanics and Engineering*, 72, (1989), pp. 305-350.

[6] Meo, M., Vignjević R., Maengo M., Numerical Simulations of Low-Velocity Impact on an Aircraft Sandwich Panel, *Composite Structures*, 62, (2003), pp. 353–360.

[7] Ivančević, D., Smojver, I., Hybrid Approach in Bird Strike Damage Prediction on Aeronautical Composite Structures. *Composite Structures*, 94, 1, (2011), pp. 15-23.

[8] Heimbs, S.: Bird Strike Simulations on Composite Aircraft Structures, *2011 SIMULIA Customer Conference*, Barcelona, Spain, May 17-19, (2011), pp. 73-86.

[9] Guida M., Marulo F., Meo M., Riccio M., Russo S., Fiber metal laminate for bird impact conditions. *Numerical and experimental analysis*, Proceedings of ICCST/6, Durban, South Africa, (2007), pp CD-ROM.

[10] Blair, A., Aeroengine fan blade design accounting for bird strike, *PhD Dissertation*, Department of Mechanical and Industrial Engineering, The University of Toronto, Canada, (2.

GENERALIZED VAN DER POL OSCILLATORS: FROM A LIMIT CYCLE TO THE ENTRAINMENT PHENOMENON

Ivana Kovacić

Department of Mechanics
Faculty of Technical Sciences, University of Novi Sad, 21215 Novi Sad, Serbia
e-mail: ivanakov@uns.ac.rs

Abstract. This work is concerned with generalized van der Pol oscillators, the damping-like force of which depends nonlinearly on the displacement and velocity with the powers that can be any positive real numbers. The amplitude and frequency of free limit cycle oscillations are determined first. Then, harmonically forced generalized van der Pol oscillators are considered with the aim of determining the region of entrainment, when the force is said to have entrained the limit cycle oscillations.

1. Introduction

The classical van der Pol oscillator is one of archetypal models in science and engineering. Its governing equation of motion is given by

$$\ddot{x} + x = \varepsilon\left(1 - x^2\right)\dot{x}, \tag{1}$$

where x is a generalized coordinate, dots denote differentiation with respect to time t and the coefficient ε is a positive real number (all these variables and the constant are non-dimensional). The damping-like force on the right-hand side of Eq. (1) is of a changeable sign: it is positive for smaller displacements $\left(|x| < 1\right)$ and then feeds energy into the system; however, it becomes negative for larger displacements $\left(|x| > 1\right)$ and, thus, it dissipates energy. This behaviour gives rise to self-exciting oscillations. For small values of the coefficient ε $\left(\varepsilon \ll 1\right)$, a stable limit cycle occurs with the steady-state amplitude $a_{LC} = 2$, which represents its distinctive characteristic [1, 2]. When the classical van der Pol oscillator is harmonically excited, the entrainment (locking, quenching) phenomenon can occur. It corresponds to the case when the limit cycle oscillations synchronise with the forcing frequency. Then, the force is said to have entrained the limit cycle oscillations or the limit cycle oscillations are said to have been locked/quenched [2].

This study is concerned with the investigations of the limit cycle oscillations and the entrainment phenomenon in the generalized van der Pol oscillators governed by the following equation

$$\ddot{x} + \text{sgn}(x)|x|^{\alpha} = \varepsilon\left(1 - |x|^{\beta}\right)|\dot{x}|^{\gamma}\,\text{sgn}(\dot{x}) + \varepsilon F \cos \Omega t, \tag{2}$$

where the powers α, β and γ are positive real constants, while F and Ω are related to the magnitude and frequency of harmonic excitation, respectively. Here, the restoring force and the damping-like force have a general power form: the former is an odd function in the displacement, while the latter is an even function in the displacement and an odd function in the velocity. The sign and absolute value functions are used to assure that these terms have the properties as in the classical van der Pol oscillator given by Eq. (1).

There have been few investigations concerned with the generalisation of the classical forced van der Pol equation with respect to different powers of the restoring and the damping-like force. The van der Pol oscillator with a pure cubic restoring force was investigated in [3] and [4], where the first-order harmonic balance method was applied to obtain periodic solutions, their stability was discussed and the regions of entrainment were found. Obi [5] considered a generalized version of the van der Pol equation (1a,b) in which the power of the restoring force is $2n+1$, where n is an integer, and the geometric non-linearity in the damping-like term is raised to the power $2n+2$. He showed the differences between quantitative and qualitative properties of the periodic oscillations corresponding to a linear and non-linear restoring force. He also obtained the number of periodic oscillations, their stationary amplitudes and discussed the way how they depend on the magnitude and the frequency of harmonic excitation.

In this paper, the influence of the powers of nonlinearity on the system response in studied first for small values of the coefficient ε. By applying the averaging method, the amplitude of the limit cycle is determined and its properties analysed with respect to the limit cycle amplitude of the classical van der Pol oscillator. Then, harmonically excited generalized van der Pol oscillators are investigated from the viewpoint of the occurrence of harmonic entrainment. Locked periodic motion is obtained by adjusting the averaging method. The steady-state amplitude is related to the amplitude of the limit cycle. Effects of the powers of the restoring and damping-like forces on the occurrence of this phenomenon are determined.

2. Free generalized van der Pol oscillators: Limit cycle oscillations

In this Section, the approximate analytical solution for motion of the oscillator modelled by Eqs. (2) with $F=0$ is found. To that end, the generalized Krylov-Bogoliubov method, recently extended to free purely nonlinear oscillators [6] is used. The form of the solution is taken in the form:

$$x = a\cos\psi, \quad \dot{x} = -a\omega\sin\psi, \tag{3a,b}$$

where

$$\psi = \int_0^t \omega(a)dt + \theta(t), \tag{4}$$

while the frequency ω is dependent both on the amplitude a and the power α [6]

$$\omega(a) = c\sqrt{|a|^{\alpha-1}}, \quad c = \sqrt{\frac{\pi(\alpha+1)}{2}} \frac{\Gamma\left(\frac{\alpha+3}{2(\alpha+1)}\right)}{\Gamma\left(\frac{1}{\alpha+1}\right)}, \tag{5a,b}$$

where Γ is the Euler gamma function.

Differentiating Eq. (3a) with respect to time, one obtains

$$\dot{x} = \dot{a}\cos\psi - a\omega\sin\psi - a\dot{\theta}\sin\psi, \tag{6}$$

which owing to Eq. (3b) implies that the following constraint needs to be satisfied

$$\dot{a}\cos\psi - a\dot{\theta}\sin\psi = 0. \tag{7}$$

Finding the second time derivative of Eq. (3b) and substituting it together with Eq. (3a) into Eq. (2), one obtains

$$-\dot{a}\omega\sin\psi - a\frac{d\omega}{da}\dot{a}\sin\psi - a\omega\dot{\theta}\cos\psi - a\omega^2\cos\psi + \mathrm{sgn}(a\cos\psi)|a\cos\psi|^\alpha = -\varepsilon\left(1 - |a\cos\psi|^\beta\right)\left(-a\omega\sin\psi\right)^\gamma \mathrm{sgn}\left(-a\omega\sin\psi\right). \tag{8}$$

It should be noted that the last term on the left-hand side of Eq. (8) can be approximated by the first term from the corresponding Fourier series expansion

$$\mathrm{sgn}(a\cos\psi)|a\cos\psi|^\alpha \approx |a|^\alpha b_{1_\alpha}\cos\psi, \quad b_{1_\alpha} = \frac{2}{\sqrt{\pi}}\frac{\Gamma\left(1+\frac{\alpha}{2}\right)}{\Gamma\left(\frac{3+\alpha}{2}\right)}. \tag{9}$$

Now, this term can be cancelled by the term in front of it

$$-a\omega^2\cos\psi + |a|^\alpha b_{1_\alpha}\cos\psi = 0, \tag{10}$$

i.e. it is assumed that $\omega^2 \approx b_{1_\alpha}|a|^{\alpha-1}$, although ω is given by Eqs. (5a,b) It should be noted that this approximation holds for a certain range of the values of the parameter α only (for more details, see [7] and [8]).

Further, the second term on the left-hand side of Eq. (8) contains the derivative of the frequency with respect to the amplitude, which can be obtained from Eq. (5a) [6]

$$\frac{d\omega}{da} = \frac{\alpha-1}{2a}\omega. \tag{11}$$

Substituting Eqs. (10) and (11) into Eq. (9) and combining it with Eq. (7), one derives

$$\dot{a}\left(1+\frac{\alpha-1}{2}\sin^2\psi\right)=\varepsilon\left(1-\left|a\cos\psi\right|^{\beta}\right)\left|-a\omega\sin\psi\right|^{\gamma}\mathrm{sgn}(-a\omega\sin\psi)\sin\psi, \qquad (12)$$

$$a\dot{\theta}+\dot{a}\frac{\alpha-1}{2}\sin\psi\cos\psi=\varepsilon\left(1-\left|a\cos\psi\right|^{\beta}\right)\left|-a\omega\sin\psi\right|^{\gamma}\mathrm{sgn}(-a\omega\sin\psi)\cos\psi. \qquad (13)$$

After averaging Eqs. (12) and (13), it follows that the amplitude a and the phase shift θ are defined by the following first-order differential equations

$$\dot{a}=-\frac{2\varepsilon}{\pi c(\alpha+3)|a|^{\frac{\alpha-1}{2}}}\int_0^{2\pi}\left(1-\left|a\cos\psi\right|^{\beta}\right)\left|-a\omega\sin\psi\right|^{\gamma}\mathrm{sgn}(-a\omega\sin\psi)\sin\psi\,d\psi, \qquad (14)$$

$$a\dot{\theta}=-\frac{\varepsilon}{2\pi c|a|^{\frac{\alpha-1}{2}}}\int_0^{2\pi}\left(1-\left|a\cos\psi\right|^{\beta}\right)\left|-a\omega\sin\psi\right|^{\gamma}\mathrm{sgn}(-a\omega\sin\psi)\cos\psi\,d\psi. \qquad (15)$$

By integrating them, one can derive:

$$\dot{a}=\frac{4\varepsilon c^{\gamma-1}}{\pi(\alpha+3)}\frac{|a|^{\gamma\frac{\alpha+1}{2}-\frac{\alpha-1}{2}}\Gamma\left(1+\frac{\gamma}{2}\right)\left[\sqrt{\pi}\Gamma\left(\frac{3+\beta+\gamma}{2}\right)-|a|^{\beta}\Gamma\left(\frac{1+\beta}{2}\right)\Gamma\left(\frac{3+\gamma}{2}\right)\right]}{\Gamma\left(\frac{3+\gamma}{2}\right)\Gamma\left(\frac{3+\beta+\gamma}{2}\right)}, \qquad (16)$$

$$\dot{\theta}=0. \qquad (17)$$

Equation (17) implies that in all generalized van der Pol type oscillators modelled by Eqs. (2), the phase shift is constant to terms of order ε.

The steady-state amplitude, i.e. the amplitude of the limit cycle a_{LC}, corresponds to $\dot{a}=0$ and is found to be

$$|a_{\mathrm{LC}}|=\left[\frac{\sqrt{\pi}\Gamma\left(\frac{3+\beta+\gamma}{2}\right)}{\Gamma\left(\frac{1+\beta}{2}\right)\Gamma\left(\frac{3+\gamma}{2}\right)}\right]^{1/\beta}, \qquad (18)$$

while Eqs. (5a,b) define the corresponding frequency

$$\omega_{\mathrm{LC}}=c\sqrt{|a_{\mathrm{LC}}|^{\alpha-1}}. \qquad (19)$$

The expression (18) is also found in [9], and indicates that the first approximation for the amplitude of the limit cycle depends on the values of the parameters β and γ, i.e. on the parameters appearing in the model of the damping-like force. However, in general, the amplitude of the limit-cycle actually depends on all parameters appearing in the differential equation of motion, but the ε-dependence is expected to be weak, except for the larger values of this parameter.

Equation (18) is used to plot how the amplitude of the limit cycle changes with the parameter β for two different values of the power γ (Figure 1a, b). In addition, numerically obtained amplitudes of the limit cycle are also presented in this figure for three different values of the parameter α corresponding to the linear $\alpha=1$, under-linear $\alpha=2/3$ and over-linear restoring forces $\alpha=2$. It is seen that the analytical and numerical result agree reasonably well for all the range of the powers considered, although the analytically obtained amplitude of the limit cycle can be considered as slightly under-estimated for $\alpha=2/3$ and slightly over-estimated for $\alpha=2$. These numerical results lead to the conclusion that as the power α increases, the amplitude of the limit cycle decreases and this is in general agreement with the result given in [10] for $\beta=2$, where an elliptic Krylov-Bogoliubov method is used to find the amplitude of the limit cycle. In all cases, as β increases, the amplitude of the limit cycle decreases.
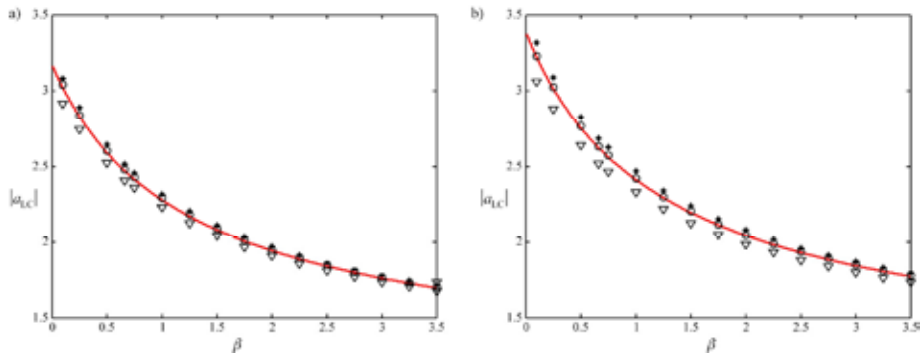
Figure 1. Amplitude of the limit cycle obtained analytically Eq. (18) (solid line) and numerically for $\varepsilon=0.1$, $\alpha=2/3$ (stars), $\alpha=1$ (circles) and $\alpha=2$ (triangles): a) $\gamma=0.8$; b) $\gamma=1.2$.

2.1 Special case: $\gamma=1$

If the velocity term in the damping force is linear, the amplitude of the limit cycle is

$$|a_{\text{LC}}| = \left[\frac{\sqrt{\pi}\Gamma\left(\frac{4+\beta}{2}\right)}{\Gamma\left(\frac{1+\beta}{2}\right)} \right]^{1/\beta} . \tag{20}$$

The change of this amplitude with the parameter β is plotted in Figure 2. Besides this, numerically obtained amplitudes of the limit cycle are also shown in this figure for different values of the parameter α.

The expression (20) is used, together with Eqs. (3a,b) and Eqs. (5a,b), to compare the analytically found phase trajectories with those calculated numerically. Figure 3 shows this for three different values of the power α corresponding (as in Figures 1 and 2) to the linear $\alpha=1$, under-linear $\alpha=2/3$ and over-linear restoring forces $\alpha=2$ (note that the case given in Figure 3a corresponds to the classical van der Pol oscillator, which is

given here to see the similarities and differences with respect to other cases considered). It is seen that the approximate analytical results obtained agree reasonably well with the numerical solutions.
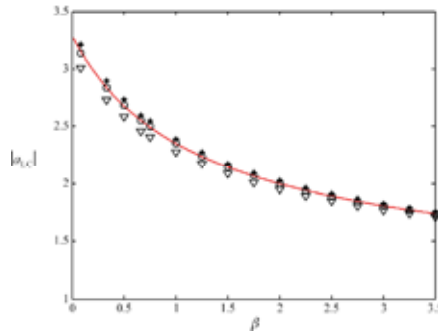
Figure 2. Amplitude of the limit cycle for $\gamma=1$, $\varepsilon=0.1$ obtained analytically Eq. (20) (solid line) and numerically: $\alpha=2/3$ (stars), $\alpha=1$ (circles) and $\alpha=2$ (triangles)
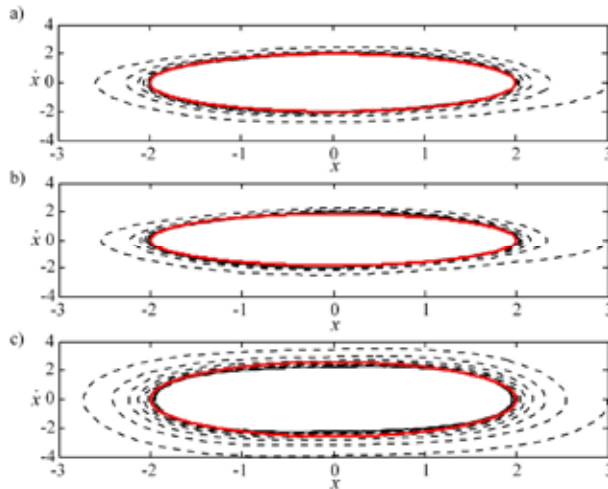
Figure 3. a) Phase trajectories calculated numerically by carrying out direct integration of the equation of motion (2) with $F=0$ (black dotted line) and the analytically obtained limit cycle (red solid line) for $\varepsilon=0.1$, $\beta=2$, $x(0)=3$, $\dot{x}(0) = 0$ and: a) $\alpha=1$; b) $\alpha=2/3$; c) $\alpha=2$.

It should also be pointed out that Eq. (20) implies that when $\beta \to 0$, $|a_{LC}| \to 2\sqrt{e}$ as well as when $\beta \to \infty$, $|a_{LC}| \to 1$. When $\beta = 2$, as is in the classical van der Pol oscillator, the amplitude is $|a_{LC}| = 2$, which is the well-known result [1, 2] also seen in Figure 3b.

3. Forced generalized van der Pol oscillator: Entrainment

In order to derive the approximation for motion for the forced generalized van der Pol oscillator (2), the method presented in the previous section is adjusted. Thus, following the methodology defined by Eqs. (3a)-(7), the equation of motion (2) becomes

$$
-\dot{a}\omega\sin\psi - a\frac{d\omega}{da}\dot{a}\sin\psi - a\omega\dot{\theta}\cos\psi - a\omega^2\cos\psi + \mathrm{sgn}(a\cos\psi)|a\cos\psi|^\alpha =
$$
$$
\varepsilon\left(1-|a\cos\psi|^\beta\right)\left(-a\omega\sin\psi\right)^\gamma\mathrm{sgn}(-a\omega\sin\psi) + \varepsilon F\cos\Omega t,
\tag{21}
$$

which due to Eqs. (10) and (11), transforms to

$$
-\left(1+\frac{\alpha-1}{2}\right)\omega\dot{a}\sin\psi - a\omega\dot{\theta}\cos\psi =
$$
$$
\varepsilon\left(1-|a\cos\psi|^\beta\right)\left(-a\omega\sin\psi\right)^\gamma\mathrm{sgn}(-a\omega\sin\psi) + \varepsilon F\cos\varphi,
\tag{22}
$$

where $\varphi = \Omega t$.

The case investigated here is the one when the frequency of excitation Ω is close to the frequency ω, i.e. $\Omega = \omega + \varepsilon\sigma$, where σ is the detuning parameter. It should be noted that this implies $\dot{\varphi} = \omega + \varepsilon\sigma$.

By solving the system formed by Eqs. (7) and (22), one obtains

$$
\dot{a}\omega\left(1+\frac{\alpha-1}{2}\sin^2\psi\right) =
$$
$$
-\varepsilon\left(1-|a\cos\psi|^\beta\right)\left(-a\omega\sin\psi\right)^\gamma\mathrm{sgn}(-a\omega\sin\psi)\sin\psi - \varepsilon F\cos\varphi\sin\psi,
\tag{23}
$$

$$
-\dot{a}\omega\frac{\alpha-1}{2}\sin\psi\cos\psi - a\omega(\dot{\psi}-\omega) =
$$
$$
\varepsilon\left(1-|a\cos\psi|^\beta\right)\left(-a\omega\sin\psi\right)^\gamma\mathrm{sgn}(-a\omega\sin\psi)\cos\psi + \varepsilon F\cos\varphi\cos\psi.
\tag{24}
$$

At this point, the phase difference $\phi = \psi - \varphi$ can be introduced and ψ replaced by $\psi = \phi + \varphi$. The phase φ can be considered as an independent variable and the transformed Eqs. (23), (24) can be averaged with respect to it. This leads to

$$
\dot{a} = \frac{4\varepsilon c^{\gamma-1}}{\pi(\alpha+3)}\frac{|a|^{\gamma\frac{\alpha+1}{2}+\frac{1-\alpha}{2}}\Gamma\left(1+\frac{\gamma}{2}\right)\left[\sqrt{\pi}\Gamma\left(\frac{3+\beta+\gamma}{2}\right)-|a|^\beta\Gamma\left(\frac{1+\beta}{2}\right)\Gamma\left(\frac{3+\gamma}{2}\right)\right]}{\Gamma\left(\frac{3+\gamma}{2}\right)\Gamma\left(\frac{3+\beta+\gamma}{2}\right)} -
$$
$$
\frac{2\varepsilon F}{c(\alpha+3)}|a|^{\frac{1-\alpha}{2}}\sin\phi,
\tag{25}
$$

$$
a\dot{\phi} = -a\varepsilon\sigma - \frac{\varepsilon F}{2c}|a|^{\frac{1-\alpha}{2}}\cos\phi.
\tag{26}
$$

The steady-state motion characterised by a_0, ϕ_0 of the forced oscillators (2) is obtained by equating the left-hand sides of Eqs. (25) and (26) with zero

$$0 = \frac{c^\gamma}{\pi} \frac{|a_0|^{\gamma \frac{\alpha+1}{2}} \Gamma\left(1 + \frac{\gamma}{2}\right)\left[\sqrt{\pi}\Gamma\left(\frac{3+\beta+\gamma}{2}\right) - |a_0|^\beta \Gamma\left(\frac{1+\beta}{2}\right)\Gamma\left(\frac{3+\gamma}{2}\right)\right]}{\Gamma\left(\frac{3+\gamma}{2}\right)\Gamma\left(\frac{3+\beta+\gamma}{2}\right)} - \frac{F}{2}\sin\phi_0, \qquad (27)$$

$$0 = a_0\varepsilon\sigma + \frac{\varepsilon F}{2c}|a_0|^{\frac{1-\alpha}{2}}\cos\phi_0. \qquad (28)$$

For $F = \Omega = \sigma = 0$, Eqs. (27) and (28) turn into Eqs. (16) and (17) for the first-order differential equations in the amplitude of the limit cycle oscillations.

3.1 Special case: $\gamma = 1$

When the damping-like force depends on the velocity linearly, Eqs. (25) and (26) give

$$\dot{a} = \frac{2\varepsilon a}{\alpha+3}\left(1 - \frac{a^\beta}{\sqrt{\pi}}\frac{\Gamma\left(\frac{\beta+1}{2}\right)}{\Gamma\left(\frac{\beta+4}{2}\right)}\right) - \frac{2\varepsilon F}{c(\alpha+3)}a^{\frac{1-\alpha}{2}}\sin\phi, \qquad (29)$$

$$a\dot{\phi} = -a\varepsilon\sigma - \frac{\varepsilon F}{2c}a^{\frac{1-\alpha}{2}}\cos\phi, \qquad (30)$$

where the notation for the absolute value has been omitted. The corresponding steady-state response a_0, ϕ_0 is defined by

$$0 = \frac{2\varepsilon a_0}{\alpha+3}\left(1 - \frac{a_0^\beta}{\sqrt{\pi}}\frac{\Gamma\left(\frac{\beta+1}{2}\right)}{\Gamma\left(\frac{\beta+4}{2}\right)}\right) - \frac{2\varepsilon F}{c(\alpha+3)}a_0^{\frac{1-\alpha}{2}}\sin\phi_0, \qquad (31)$$

$$0 = a_0\varepsilon\sigma + \frac{\varepsilon F}{2c}a_0^{\frac{1-\alpha}{2}}\cos\phi_0. \qquad (32)$$

These equations can be combined to derive the amplitude-frequency equation

$$\varepsilon^2 \frac{F^2}{c^2}a_0^{1-\alpha} = 4\left(\Omega - ca_0^{\frac{\alpha-1}{2}}\right)^2 a_0^2 + \varepsilon^2 a_0^2\left(1 - \frac{a_0^\beta}{\sqrt{\pi}}\frac{\Gamma\left(\frac{\beta+1}{2}\right)}{\Gamma\left(\frac{\beta+4}{2}\right)}\right)^2, \qquad (33)$$

Stability of this steady-state response is checked by introducing small perturbations a_1 and ϕ_1 into the steady-state amplitude a_0 and phase ϕ_0 satisfying Eqs. (31) and (32)

with $\varepsilon\sigma = \Omega - ca^{\frac{\alpha-1}{2}}$. So, by using $a = a_0 + a_1$ and $\phi = \phi_0 + \phi_1$, Eqs. (31) and (32) give the following constant coefficient system

$$\dot{a}_1 = a_1 \varepsilon \left(\frac{1+\alpha}{3+\alpha} - \frac{1+\alpha+2\beta}{3+\alpha} \frac{a_0^\beta}{\sqrt{\pi}} \frac{\Gamma\left(\frac{\beta+1}{2}\right)}{\Gamma\left(\frac{\beta+4}{2}\right)} \right) + \phi_1 \frac{4a_0}{3+\alpha}\left(\Omega - ca_0^{\frac{\alpha-1}{2}}\right), \tag{34}$$

$$\dot{\phi}_1 = a_1 \left(c\frac{\alpha-1}{2}a_0^{\frac{\alpha-3}{2}} - \frac{1+\alpha}{2}\frac{\Omega - ca_0^{\frac{\alpha-1}{2}}}{a_0} \right) + \phi_1 \varepsilon \left(\frac{1}{2} - \frac{a_0^\beta}{2\sqrt{\pi}}\frac{\Gamma\left(\frac{\beta+1}{2}\right)}{\Gamma\left(\frac{\beta+4}{2}\right)} \right). \tag{35}$$

The corresponding eigenvalues λ satisfy [2]

$$\lambda^2 - \text{tr}\cdot\lambda + \det = 0, \tag{36}$$

with the trace (tr) being:

$$\text{tr} = \varepsilon\left[\frac{1+\alpha}{3+\alpha} + \frac{1}{2} - \frac{a_0^\beta}{\sqrt{\pi}}\frac{\Gamma\left(\frac{\beta+1}{2}\right)}{\Gamma\left(\frac{\beta+4}{2}\right)}\left(\frac{1}{2} + \frac{1+\alpha+2\beta}{3+\alpha}\right) \right], \tag{37}$$

while the determinant (det) is

$$\det = \frac{1}{2(3+\alpha)}\left[4(1+\alpha)\left(\Omega - ca_0^{\frac{\alpha-1}{2}}\right)^2 - 4c(\alpha-1)a_0^{\frac{\alpha-1}{2}}\left(\Omega - ca_0^{\frac{\alpha-1}{2}}\right) + \right.$$

$$\left. \varepsilon^2(1+\alpha) - 2\varepsilon^2(1+\alpha+\beta)\frac{a_0^\beta}{\sqrt{\pi}}\frac{\Gamma\left(\frac{\beta+1}{2}\right)}{\Gamma\left(\frac{\beta+4}{2}\right)} + \varepsilon^2(1+\alpha+2\beta)\frac{a_0^{2\beta}}{\pi}\frac{\Gamma^2\left(\frac{\beta+1}{2}\right)}{\Gamma^2\left(\frac{\beta+4}{2}\right)} \right]. \tag{38}$$

By using Eqs. (33), (37) and (38), the frequency-response curves are plotted first in Fig. 4 for the classical van der Pol oscillator ($\alpha = 1$, $\beta = 2$). They are given for the convenience of the reader and also as a reference point for the comparison with other cases studied subsequently. As seen from Fig. 4, frequency-response curves can be continuous or consisting of two parts: the former corresponds to the oscillations with smaller amplitude and the latter is closed and surrounds the point corresponding to the limit cycle amplitude, Eq. (20) (this point is labelled by a star in this paper) and is located on a backbone curve $\Omega_{bc} = ca^{(\alpha-1)/2}$, which is $\Omega_{bc} = 1$ for the linear restoring force (the backbone curve is labelled by 'bc' and depicted by a double dotted-dashed line). All frequency-response curves of the classical van der Pol oscillator are symmetrical with respect to the vertical backbone curve. The line corresponding to the trace is plotted as a dashed-dotted line. It is horizontal as Eq. (37) indicates that it does not depend on the frequency. Curves defined by Eq. (38), i.e. det=0, are plotted as dotted

lines and the gray region corresponds to det<0. The boundary of the region det=0, which separates qualitatively different types of solutions, is plotted as thicker dotted line. For the stability, one requires tr<0, which is above the line corresponding to tr=0, and det>0 [2]. The parts of the frequency-response curves satisfying det>0 and tr<0 are shown as thicker lines. Thus, the entrainment can occur either between the intersection of frequency-response curves with the curve det=0 when tr<0 for smaller F or with the curve tr=0 when det>0 for higher values of F, which is confirmed numerically by solving directly the equation of motion and these numerical results are shown as black dots.
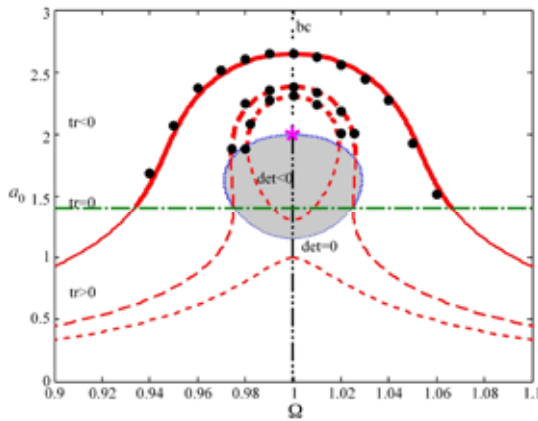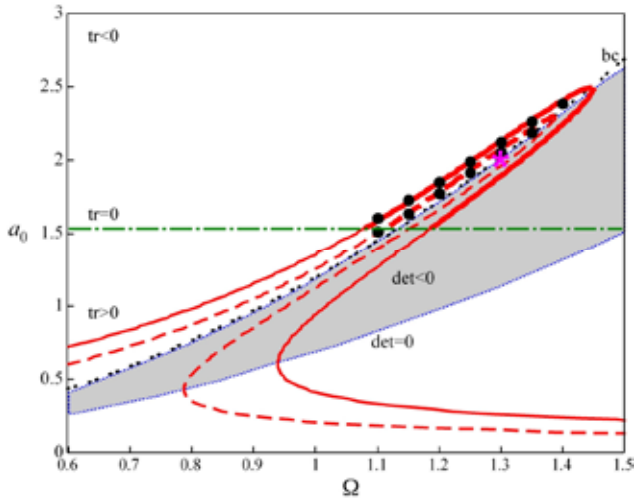

Figure 4. Frequency-response curves defined by Eq. (33) for $\varepsilon = 0.1$, $\alpha = 1$, $\beta = 2$, different values of the magnitude of the force $F=0.75$ (smaller dashes), $F=1$ (longer dashes) and $F=2$ (solid line). Numerical results are shown as black dots. The star stands for the characteristics of the limit cycle.
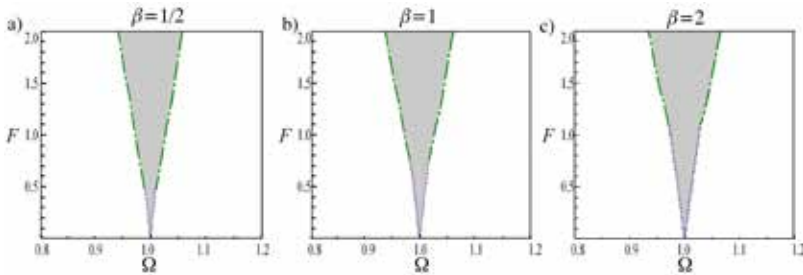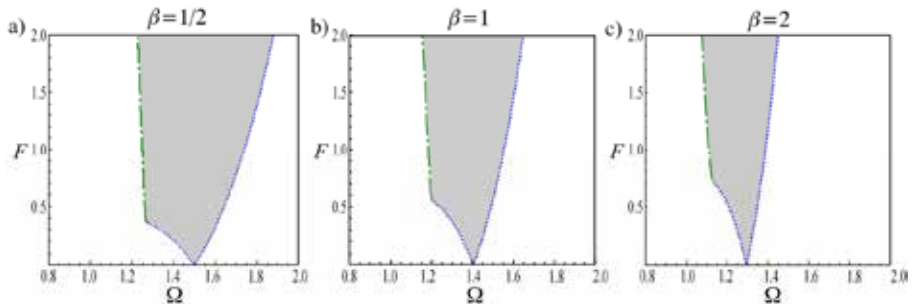

Figure 5. Entrainment regions (shaded areas) for $\varepsilon = 0.1$, $\alpha = 1$ and different values of the power β. Dotted lines depict the solutions of det=0 for which tr<0 and dashed-dotted lines the solutions of tr=0 for which det>0.

Further, the bifurcation analysis is conducted to construct the regions of entrainment. The locus of saddle-node bifurcation points is found by solving the system formed by det=0, Eq. (38) and the amplitude-frequency equation (33) and shown in the F-Ω parametric plane. This is presented in Figure 5 as a dotted line. In addition, the locus of the points along which Hopf bifurcation occurs when tr=0 and det>0 is also

presented as a dashed-dotted line. So, by considering these bifurcation curves, it turns out that stable entrainment solutions exist in the shaded region. Outside this region, beating oscillations occur [1]. Figures 5a-c show how the size of the entrainment region is affected by the change of the power β.

The case $\alpha \neq 1$ is investigated now in the same manner. First, an under-linear restoring force ($\alpha = 2/3$) is considered. The corresponding frequency-response curves are given in Figure 6. It is seen that this curves as well as the backbone curve are bent to the left. The curves corresponding to det=0 and tr=0 are also shown, so is the gray region det<0 (the same legend is used as in Fig. 4). For smaller forcing amplitudes, when the part of the frequency-response curve is closed surrounding a limit-cycle point, the region of entrainment can occur between the intersection of the frequency-response curve with det=0, which is the same situation as for the oscillator with a linear restoring force. However, for larger forcing amplitudes, when the frequency-response curve is a one-part continuous line, the entrainment occurs between the intersection of the frequency-response curve with the curve det=0 when tr<0 and the intersection with tr=0 when det>0. Note that this is the mixture of the cases existing for a linear restoring case, discussed previously.
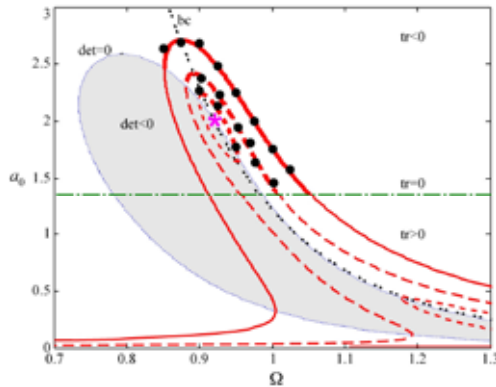
Figure 6. Frequency-response curves defined by Eq. (33) for $\varepsilon = 0.1$, $\alpha = 2/3$, $\beta = 2$, different values of the magnitude of the force $F=0.75$ (smaller dashes), $F=1$ (longer dashes) and $F=2$ (solid line) Numerical results are shown as black dots. The star stands for the characteristics of the limit cycle.
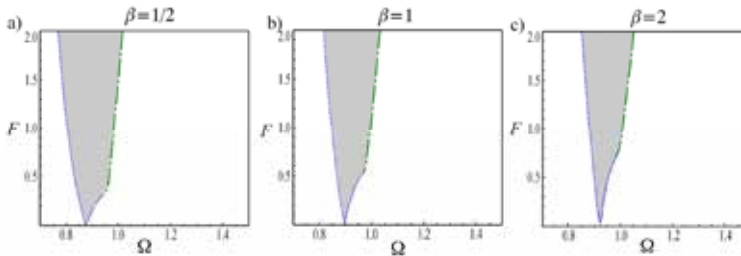
Figure 7. Entrainment regions (shaded areas) for $\varepsilon = 0.1$, $\alpha = 2/3$ and different values of the power β. Dotted lines depict the solutions of det=0 for which tr<0 and dashed-dotted lines the solutions of tr=0 for which det>0.

Figure 7a-c show how the position and the size of the entrainment region change in the F-Ω parametric plane as the power α is fixed to $\alpha = 2/3$ and β is varied. The entrainment region is shifted to lower frequencies and is wider for a lower geometric non-linearity in the damping-like force.

The frequency-response curves corresponding to a over-linear restoring force $\alpha=2$ are shown in Figure 8, while the entrainment regions are plotted in Figure 9. It is seen that the frequency-response curves are bent to the right. The entrainment region, which is wider for a lower geometric non-linearity in the damping-like force, is shifted to higher frequencies.

Figure 8. Frequency-response curves defined by Eq. (33) for $\varepsilon = 0.1$, $\alpha = 2$, $\beta = 2$, different values of the magnitude of the force $F=1$ (longer dashes) and $F=2$ (solid line). Numerical results are shown as black dots.

Figure 9. Entrainment regions (shaded areas) for $\varepsilon = 0.1$, $\alpha = 2$ and different values of the power β. Dotted lines depict the solutions of det=0 for which tr<0 and dashed-dotted lines the solutions of tr=0 for which det>0.

4. Conclusions

In this work, generalized van der Pol type oscillators have been considered. Both the restoring force and the damping-like force have a nonlinear power form: the former with respect to the displacement, and the latter with respect to the displacement and velocity. The investigations have been conducted with a view to determining the limit cycle in free generalized van der Pol oscillators and defining the entrainment region in forced generalized van der Pol oscillators.

The first approximation for the amplitude of the limit cycle is seen to be dependent on the parameters appearing in the damping-like force. The accuracy of the analytically obtained results has been confirmed numerically. In all the cases considered, it has been found that as the power of the displacement nonlinearity in the damping-like force increases, the limit cycle amplitude decreases. Further numerical results have showed that for fixed values of the power of the displacement in the damping-like force, the power of the restoring force has certain influence on the limit cycle amplitude. In the case of linear viscous damping, the higher the power of the restoring force, the smaller the limit cycle amplitude.

The forced generalized van der Pol oscillators have been studied by deriving the corresponding frequency-response equation and by performing its stability analysis. Analytical approximations for the trace and the determinant of the corresponding eigenvalue equation have been derived, on the basis of which the regions of harmonic entrainment have been obtained in the parameter plane formed by the forcing frequency and its magnitude. It has been shown that for a fixed forcing magnitude, the region of frequency in which entrainment occurs is the narrowest for the linear restoring force and is wider for non-linear restoring forces. When the restoring force is under-linear, this region is shifted towards lower frequencies and when it is over-linear, towards higher frequencies.

References

[1] Nayfeh A H and Mook D T (1979) *Nonlinear Oscillations*, Wiley, New York.
[2] Rand R H (2012) *Lecture Notes on Nonlinear Vibrations*, version 52. http://audiophile.tam.cornell.edu/randdocs/nlvibe52.pdf . Accessed 17 March 2012.
[3] Hayashi C (1964) *Nonlinear Oscillations in Physical Systems*, McGraw-Hill, NewYork.
[4] Hayashi C, Ueda Y, Akamatsu N and Itakura H (1970) On the behaviour of self-oscillatory systems with external force, *Transactions of the Japanese Institute of Electronics and Communication Engineers*, **53**-A(3), pp. 150-158.
[5] Obi C (1976) Analytical theory of nonlinear oscillations IV: the periodic oscillations of the equation $\ddot{x} - \varepsilon\left(1 - x^{2n+2}\right)\dot{x} + x^{2n+1} = \varepsilon a \cos \omega t$, $a > 0$, $\omega > 0$ independent of ε, *SIAM Journal of Applied Mathematics* **21**, pp. 345-357.

[6] Cveticanin L (2009) Oscillator with fraction order restoring force, *Journal of Sound and Vibration*, **320**, pp. 1064-1077.

[7] Kovacic I (2011) A limit cycle and relaxation oscillations in a generalized van der Pol oscillator, *Communication in Non-linear Science and Numerical Simulations*, **16**, pp. 1640–1649.

[8] Kovacic I (2011) Forced vibrations of oscillators with a purely nonlinear power-form restoring force, *Journal of Sound and Vibration*, **330**, pp. 4313–4327.

[9] Kovacic I and Mickens R E (2012) A generalized van der Pol type oscillator: Investigation of the properties of its limit cycle, *Mathematical and Computer Modelling*, **55**, pp. 645–653.

[10] Rakaric Z and Kovacic I (2011) Approximations for motion of the oscillators with a non-negative real-power restoring force, *Journal of Sound and Vibration*, **330**, pp. 321-336.

NONLINEAR OSCILLATORY FLOWS WITH DIFFERENT SYMMETRY PROPERTIES IN TWO-LAYER SYSTEMS

Ilya B. Simanovskii

Department of Mathematics, Technion - Israel Institute of
Technology, 32000 Haifa, Israel. e-mail: cesima@tx.technion.ac.il

Abstract. Nonlinear oscillatory convective regimes developed under the joint action of buoyant and thermocapillary effects in the 47v2 silicone oil - water system, are investigated. Transitions between nonlinear flows with various spatial structures have been studied. Specific types of oscillatory flows with different symmetry properties have been found. It is shown that the region of convective oscillations is observed in a finite interval of the Grashof number values bounded from below and from above.

1. Introduction

Stability of convective flows in systems with an interface has been a subject of an extensive investigation at the past few decades (for a review, see [1], [2]). Several classes of instabilities have been found.

There are two basic physical phenomena that produce convective instability in systems with an interface: buoyancy and thermocapillary effect. When heating is from below, the buoyancy instability generates Rayleigh - Bénard convection [3], while the thermocapillary effect is the origin of Marangoni - Bénard convection [4], [1]. The situation when both mechanisms of instability act simultaneously is the most typical.

It is known that the stability problem for the mechanical equilibrium in a system with an interface is not self-adjoint (see, e.g., [1], [5]), thus an oscillatory instability is possible. The mechanism of oscillations, which takes place without interfacial deformations due to the hydrodynamic and thermal interaction between convective flows on both sides of the interface, was found by Gershuni and Zhukhovitsky [6] in the case of transformer oil - formic acid system. The nonlinear oscillatory convective structures near the instability threshold for some model systems have been studied in [7], [8].

An oscillatory instability of the mechanical equilibrium can be caused by the joint action of buoyancy and thermocapillary effect in a two-layer system heated from below. This phenomenon was first discovered in [9], [1], [10]. Oscillations just above the instability threshold have been observed in experiments of Degen *et. al.* (see [11]). It should be noted that the linear stability theory for the onset of the buoyancy convection has predicted a monotonic instability [12]. In our opinion, oscillations observed in experiments [11] can be caused by the influence of the thermocapillary effect [13].

In the present paper, nonlinear oscillatory convective flows, developed under the joint action of buoyant and thermocapillary effects in the 47v2 silicone oil - water system filling the closed cavity, are studied. Specific oscillatory regimes with different symmetry properties, have been observed. New consequence of bifurcations has been found.

The paper is organized as follows. In Section 2, the mathematical formulation of the problem in the two-layer system is presented. The nonlinear approach is described in Section 3. Nonlinear simulations of the finite-amplitude convective regimes are considered in Section 4. Section 5 contains some concluding remarks.

2 Formulation of the Problem

We consider a system of two horizontal layers of immiscible viscous fluids with different physical properties. The system is bounded from above and from below by two isothermal rigid plates kept at constant different temperatures (the system is heated from below; the total temperature drop is θ). It is assumed that the interfacial tension σ decreases linearly with the increasing of the temperature: $\sigma = \sigma_0 - \alpha T$, where $\alpha > 0$. The variables referring to the top layer are marked by subscript 1, and the variables referring to the bottom layer are marked by subscript 2.

Assume that ρ_m, ν_m, η_m, κ_m, χ_m, β_m and a_m are, respectively, density, kinematic and dynamic viscosity, heat conductivity, thermal diffusivity, thermal expansion coefficient and the thickness of the m - th layer ($m = 1, 2$). Let us introduce the following non-dimensional parameters, corresponding to parameters ratios of different fluids,

$$\rho = \rho_1/\rho_2, \nu = \nu_1/\nu_2, \eta = \eta_1/\eta_2,$$

$$\kappa = \kappa_1/\kappa_2, \chi = \chi_1/\chi_2, \beta = \beta_1/\beta_2,$$

and to the ratio of layers thicknesses,

$$a = a_2/a_1.$$

As the units of length, time, velocity, pressure and temperature we choose a_1, a_1^2/ν_1, ν_1/a_1, $\rho_1\nu_1^2/a_1^2$ and θ, respectively.

The nonlinear equations of convection in the framework of the Boussinesq approximation for both fluids have the following form (see Simanovskii & Nepomnyashchy 1993):

$$\frac{\partial \vec{v}_m}{\partial t} + (\vec{v}_m \cdot \nabla)\vec{v}_m = -e_m \nabla p_m + c_m \nabla^2 \vec{v}_m + b_m G T_m \vec{\gamma},$$

$$\frac{\partial T_m}{\partial t} + \vec{v}_m \cdot \nabla T_m = \frac{d_m}{P}\nabla^2 T_m, \tag{1}$$

$$\nabla \cdot \vec{v}_m = 0.$$

Here, $\vec{v}_m = (v_{mx}, v_{my}, v_{mz})$ is the velocity vector, T_m is the temperature and p_m is the pressure in the m - th fluid; $\vec{\gamma}$ is the unit vector directed upwards; $b_1 = c_1 = d_1 = e_1 = 1$; $b_2 = 1/\beta$, $c_2 = 1/\nu$, $d_2 = 1/\chi$, $e_2 = \rho$; $G = g\beta_1\theta a_1^3/\nu_1^2$ is the Grashof number, which characterizes the buoyancy force, and $P = \nu_1/\chi_1$ is the Prandtl number for the liquid in layer 1. The conditions on the isothermal rigid horizontal boundaries are:

$$z = 1: \quad \vec{v}_1 = 0; \quad T_1 = 0, \tag{2}$$

$$z = -a: \quad \vec{v}_2 = 0; \quad T_2 = 1. \tag{3}$$

The boundary conditions on the interface include relations for the tangential stresses:

$$z = 0: \quad \eta\frac{\partial v_{1x}}{\partial z} = \frac{\partial v_{2x}}{\partial z} + \frac{\eta M}{P}\frac{\partial T_1}{\partial x}, \quad \eta\frac{\partial v_{1y}}{\partial z} = \frac{\partial v_{2y}}{\partial z} + \frac{\eta M}{P}\frac{\partial T_2}{\partial x}; \tag{4}$$

the continuity of the velocity field:

$$v_1 = v_2; \tag{5}$$

the continuity of the temperature field:

$$T_1 = T_2; \tag{6}$$

and the continuity of the heat flux normal components:

$$\kappa\frac{\partial T_1}{\partial z} - \frac{\partial T_2}{\partial z} = 0. \tag{7}$$

Here $M = \alpha\theta a_1/\eta_1\chi_1$ is the Marangoni number, which is the basic non-dimensional parameter characterizing the thermocapillary effect.

The conditions on the solid lateral boundaries, which are assumed to be thermally insulated, are

$$x = 0, L: \quad v_m = 0, \quad \frac{\partial T_m}{\partial x} = 0, \quad m = 1, 2, \tag{8}$$

where $L = l/a_1$.

The problem $(1) - (8)$ for any choice of parameters has the solution:

$$\vec{v}_m^0 = 0, \quad p_m = p_m^0(z), \quad T_m = T_m^0(z), \quad m = 1, 2, \tag{9}$$

corresponding to the quiescent state. The temperature gradients in the quiescent state are:

$$A_1 = dT_1^0/dz = -\frac{1}{(1 + \kappa a)}, \quad A_2 = dT_2^0/dz = -\frac{\kappa}{(1 + \kappa a)}. \tag{10}$$

The boundary-value problem (1) - (8) contains eight thermophysical (M, G, P, η, ν, κ, χ, β) and two geometrical (L, a) non-dimensional parameters.

3 Nonlinear approach

In order to investigate the flow regimes generated by the convective instabilities, we perform nonlinear simulations of two-dimensional flows ($v_{my} = 0$ ($m = 1, 2$); the fields of physical variables do not depend on y). In this case, we can introduce the stream function ψ

$$v_{mx} = \frac{\partial \psi_m}{\partial z}, \quad v_{mz} = -\frac{\partial \psi_m}{\partial x}, \quad (m = 1, 2).$$

Eliminating the pressure and defining the vorticity

$$\phi_m = \frac{\partial v_{mz}}{\partial x} - \frac{\partial v_{mx}}{\partial z},$$

we can rewrite the boundary value problem $(1) - (8)$ in the following form:

$$\frac{\partial \phi_m}{\partial t} + \frac{\partial \psi_m}{\partial z} \cdot \frac{\partial \phi_m}{\partial x} - \frac{\partial \psi_m}{\partial x} \cdot \frac{\partial \phi_m}{\partial z} = c_m \nabla^2 \phi_m + b_m G \frac{\partial T_m}{\partial t}, \tag{11}$$

$$\nabla^2 \psi_m = -\phi_m, \tag{12}$$

$$\frac{\partial T_m}{\partial t} + \frac{\partial \psi_m}{\partial z} \cdot \frac{\partial T_m}{\partial x} - \frac{\partial \psi_m}{\partial x} \cdot \frac{\partial T_m}{\partial z} = \frac{d_m}{P} \nabla^2 T_m \tag{13}$$
$$(m = 1, 2).$$

$$z = 1: \quad \psi_1 = \frac{\partial \psi_1}{\partial z} = 0; \quad T_1 = 0; \tag{14}$$

$$z = -a: \quad \psi_2 = \frac{\partial \psi_2}{\partial z} = 0; \quad T_2 = 1; \tag{15}$$

$$z = 0: \quad \psi_1 = \psi_2 = 0, \quad \frac{\partial \psi_1}{\partial z} = \frac{\partial \psi_2}{\partial z}, \quad \phi_2 = \eta \phi_1 + \frac{\eta M}{P} \frac{\partial T_1}{\partial x}; \tag{16}$$

$$T_1 = T_2, \quad \kappa \frac{\partial T_1}{\partial z} = \frac{\partial T_2}{\partial z}. \tag{17}$$

The calculations were performed in a finite region $0 \leq x \leq L$, $-a \leq z \leq 1$ with the rigid heat-insulated boundaries:

$$x = 0, L: \quad \psi_m = \frac{\partial \psi_m}{\partial x} = \frac{\partial T_m}{\partial x} = 0; \tag{18}$$

$$m = 1, 2.$$

The boundary conditions (18) correspond to a closed cavity. The problem (11) - (18) is integrated in time with some initial conditions for ψ_m and T_m ($m = 1, 2$) by means of a finite-difference method.

Equations and boundary conditions are approximated on a uniform mesh using a second order approximation for the spatial coordinates. The nonlinear equations are solved using an explicit scheme on a rectangular uniform mesh 112×112. The Poisson equation is solved by the iterative Liebman successive overrelaxation method on each time step. The accuracy of the solution is 10^{-5}.

The details of the numerical method can been found in the book by Simanovskii and Nepomnyashchy [1].

4   Numerical results

We investigate the nonlinear regimes of convection in the 47v2 silicone oil - water system with the following set of parameters: $\nu = 2.0$; $\eta = 1.7375$; $\kappa = 0.184$; $\chi = 0.778$; $\beta = 5.66$; $P = 25.7$. This system was used in experiments carried out by Degen $et.$ $al.$ (see [11]).

To simulate the motions in a closed cavity, we used rigid heat insulated boundary conditions (18) for $L = 2.74$. Let us take the ratio of the layers thicknesses $a = 1$.

Under the conditions of the experiment, when the geometric configuration of the system is fixed while the temperature difference θ is changed, the Marangoni number M and the Grashof number G are proportional. We define the inverse dynamic Bond number

$$K = \frac{M}{GP} = \frac{\alpha}{g\beta_1\rho_1 a_1^2}.$$

Let us fix $K = 0.027$. When the Grashof number is sufficiently small, disturbances decay in an oscillatory way and the system keeps the mechanical equilibrium. With an increase of the Grashof number ($G \geq G_* = 97$), the mechanical equilibrium state becomes unstable and perfectly symmetric standing waves (type 1) satisfying symmetry conditions

$$\psi_m(L - x, z, t) = -\psi_m(x, z, t), \quad T_m(L - x, z, t) = T_m(x, z, t), \quad m = 1, 2 \qquad (19)$$

develop near the instability threshold [13]. The snapshots of streamlines during one period of oscillations are presented in Fig. 1.

With an increase of G, the period of oscillations grows (see line 1 in Fig. 2). This prediction coincides with the observations of Degen $et.$ al [11].

With a further increase of G, the oscillations disappear. For G close to $G_* = 193.8$, the period of oscillations τ satisfies the relation $\tau^{-2} \sim G_* - G$, which is characteristic for a saddle-node bifurcation. When $G > G_*$, the steady symmetric four-vortex motion takes place in the system. Thus, the region of the Grashof number values, where symmetric oscillations take place, is bounded from below by the mechanical equilibrium state and from above by the steady state.

Now, let us take the inverse dynamic Bond number $K = 0.024$. The decrease of the inverse dynamic Bond number (weakening of the thermocapillary effect) changes the situation significantly. With an increase of the Grashof number, the mechanical equilibrium state becomes unstable and the steady flow, satisfying symmetry conditions (19) develops in the system. For $G \geq 151.5$, the steady flow becomes unstable, and the system make a transition through the homoclinic bifurcation to a specific asymmetric oscillatory flow (type 2) with an extremely high value of the period (see the left end of line 2 in Fig. 2). The snapshots of streamlines for the asymmetric oscillations (type 2) are presented in Fig. 3. The solution has a following property:

$$\psi_m(x, z, t + T/2) = -\psi_m(-x, z, t), \quad m = 1, 2. \qquad (20)$$

The period of asymmetric oscillations (type 2) changes in a non-monotonic way (line 2 in Fig. 2). For $G > 180$, the inverse period doubling bifurcation takes place - the symmetry is restored and the oscillatory flow (type 1) develops in the system (line 3 in Fig. 2). At $G > 185$, the period of oscillations grows rapidly (line 3 in Fig. 2). With a further increase of G, the oscillations disappear. For G close to $G_* = 188.2$, the period of oscillations τ satisfies the relation $\tau^{-2} \sim G_* - G$, (a saddle-node bifurcation). When $G > G_*$, the steady symmetric four-vortex flow develops in the system. Thus, for $K = 0.024$, the regions of asymmetric and symmetric oscillations are restricted by the Grashof number values from below and from above by the regions of the steady states.

Let us note, that the dependence of the period of oscillations on the Grashof number for $K = 0.025$ (lines 4 and 5 in figure 2) is similar to that described above for the case $K = 0.024$.
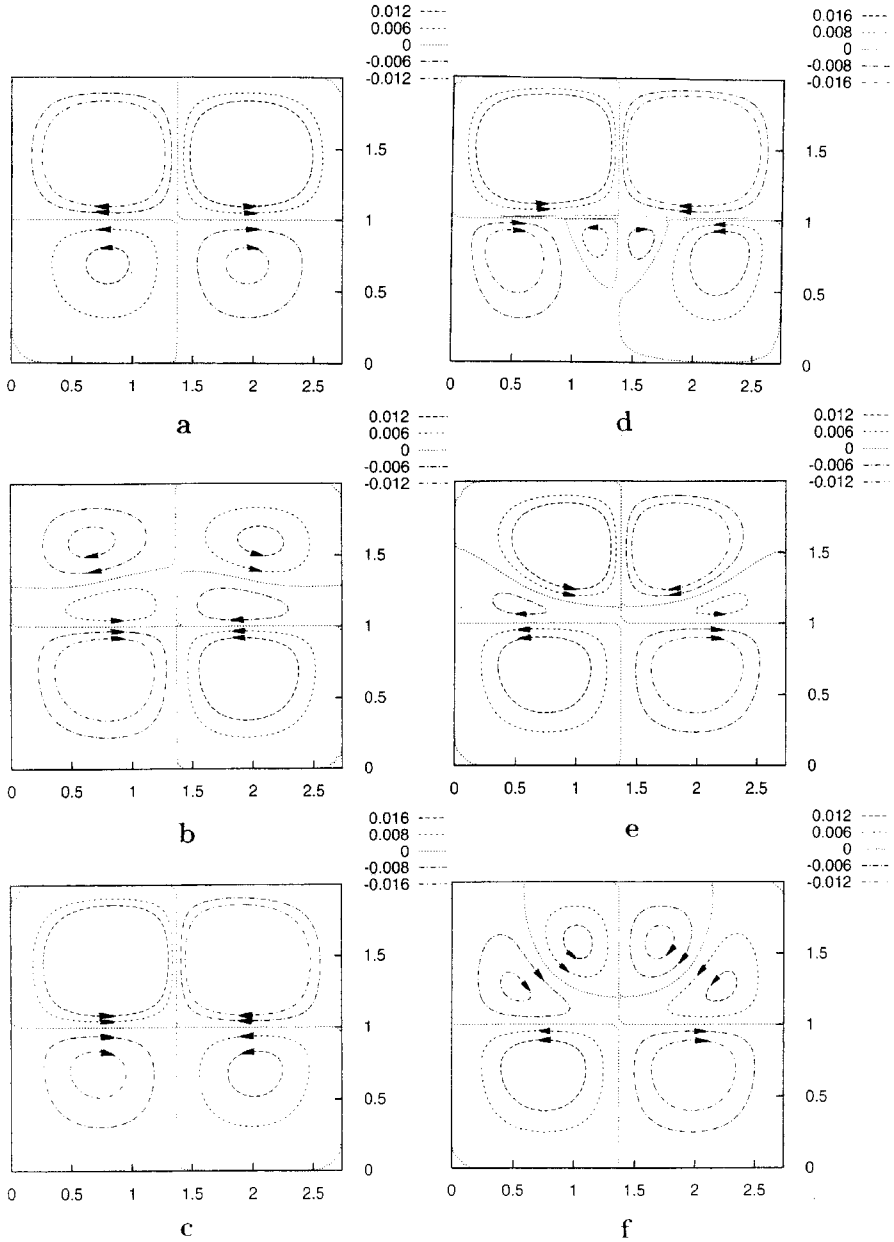
Figure 1: (a) - (f) A time sequence of snapshots of streamlines for the symmetric time-periodic motion at $G = 112$; $K = 0.027$; $L = 2.74$; $a = 1$.
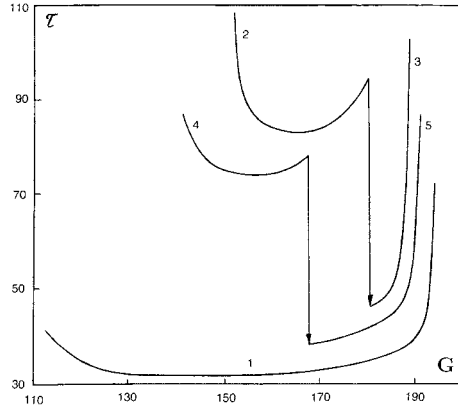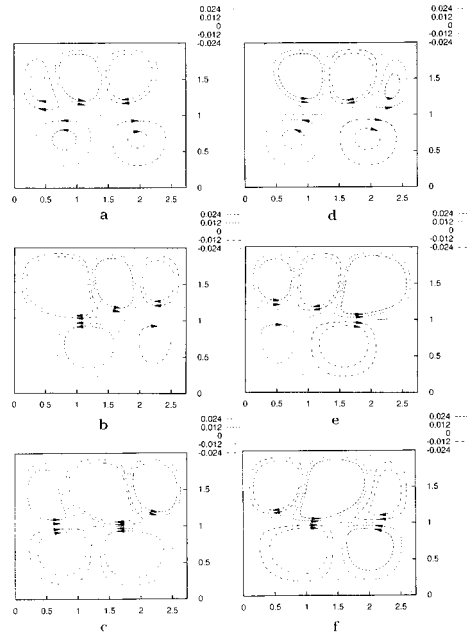
Figure 2: The dependence of the period of oscillations τ on the Grashof number G for $K = 0.027$ (line 1); 0.024 (lines 2,3); 0.025 (lines 4,5); $L = 2.74$; $a = 1$.

Figure 3: (a) - (f) A time sequence of snapshots of streamlines for the asymmetric time-periodic motion at $G = 152$; $K = 0.024$; $L = 2.74$; $a = 1$.

242

5. Conclusion

The nonlinear development of the oscillatory instability in a two-layer system in the presence of buoyancy and the thermocapillary effect, is investigated. The convective regimes are studied by the finite-difference method. It is shown that under the joint action action of buoyancy and thermocapillary effect, the development of oscillatory instability leads to specific types of nonlinear oscillations with different symmetry properties. Transitions between the flows with various spatial structures are studied. It is shown that the period of oscillations changes in a non-monotonic way for symmetric and asymmetric oscillations. It is found that in the course of the evolution of asymmetric oscillations, the violation of the symmetry property decreases and the symmetry is restored. With an increase of the Grashof number values, the oscillatory flow becomes unstable and a steady convective flow develops in the system. The region of nonlinear convective oscillations is observed in a finite interval of the Grashof number values bounded from below and from above.

References

[1] Simanovskii I. B. and Nepomnyashchy A. A. (1993) *Convective Instabilities in Systems with Interface*, Gordon and Breach, London.

[2] Nepomnyashchy A. A., Simanovskii I. B. and Legros J. C. (2012) *Interfacial Convection in Multilayer Systems*, Second Edition, Springer, New York.

[3] Gershuni G. Z. & Zhukhovitsky E. M. (1976) *Convective stability of incompressible fluid*, Keter, Jerusalem.

[4] Pearson J. R. A. (1958) On convection cells induced by surface tension, *J. Fluid Mech.*, **4**, 401.

[5] Renardy Y. Y. (1996) Pattern formation for oscillatory bulk-mode competition in a two-layer Bénard problem, ZAMP **47**, 567.

[6] Gershuni G. Z. and Zhukhovitsky E. M. (1982) On monotonic and oscillatoty instability of a two-layer immiscible fluids system heated from below, Sov. Phys. Dokl. **27**, 531.

[7] Colinet P. and Legros J. C. (1994) On the Hopf bifurcation occuring in the two-layer Rayleigh-Bénard convective instability, *Phys. Fluids*, **6**, 2631.

[8] Renardy Y., Renardy M. and Fujimura K. (1999) Takens - Bogdanov bifurcation on the hexagonal lattice for double-layer convection, Physica D **129**, 171.

[9] Nepomnyashchy A. A. and Simanovskii I. B. (1984) Thermocapillary and thermogravitational convection in a two-layer system with a distorted interface, *Fluid Dyn.* **19**, 494.

[10] Juel A., Burgess J. M., McCormick W. D., Swift J. B. and Swinney H. L. (2000) Surface-tension-driven convection patterns in two liquid layers, *Physica D* **143**, 169.

[11] Degen M. M., Colovas P. W. and Andereck C. D. (1998) Time-dependent patterns in the two-layer Rayleigh-Bénard system, *Phys. Rev. E* **57**, 6647.

[12] Nepomnyashchy A. A. and Simanovskii I. B. (2004) Influence of thermocapillary effect and interfacial heat release on convective oscillations in a two-layer system, *Phys. Fluids*, **16**, 1127.

[13] Simanovskii I. B. and Nepomnyashchy A. A. (2006) Nonlinear development of oscillatory instability in a two-layer system under the combined action of buoyancy and thermocapillary effect, *J. Fluid Mech.*, **555**, 177.

ILYA B. SIMANOVSKII

THE USE OF FINITE ELEMENTS METHOD IN VIBRATIONAL PROPERTIES CHARACTERIZATION OF MOUSE EMBRYO

Andjelka N. Hedrih[1], Marinko Ugrčić[2]

[1] State University in Novi Pazar
Vuka Karadžića bb, 36300 Novi Pazar, Serbia
e-mail: handjelka@hm.co.rs

[2] Economics Institute
Kralja Milana, 18, 11000 Belgrade, Serbia
e-mail: ugrcicmarinko@gmail.com

Abstract. To determine the vibration characteristics (natural frequencies and mode shapes) of a mouse embryo the modal analysis is used. The spherical mouse embryo 60 µm in diameter is modeled as elastic finite elements biostructure consisting of 6µm thick micromembrane and 38 µm in diameter nucleus. The modal analysis was carried out for first six modes of embryo natural frequencies by using the finite elements method and ANSYS software. The numerical analysis of dependence of embryo own frequencies on the boundary conditions are presented. The relevant illustrations of the typical variations of the shape, deformation and particle velocities of vibrating embryo are discussed.

1. Introduction

Although papers on mechanical properties of the oocyte exist (Liu et al, 2010, [1] and on structural parts of mouse embryo (Murayama et al, 2008 [2], 2006) [3], there are very few papers that regard this structure as an oscillatory system Hedrih A. (2011) [4]). Embryo vibrational characterization represents very important researching subject of modern biomechanical engineering.

Measurement of elastic properties of the biomembrane of the embryo can be done by using different techniques **(**Murayama et al, 2008 [2], 2006) [3], Sun et al, 2003, [5]). When fine glass micro-needle connected with force sensor, is used in experimental setup for probing the mechanical characteristics of the mouse embryo (Sun et al, 2003, [5]), embryo is placed in a liquid medium –eg HTF (human tubal fluid), in dish. Dish is placed on a heating plate of a special microscope that maintains the body temperature of the mouse. These are typical conditions (adequate liquid medium and temperature) to

keep the embryo alive. Embryo is fixed with vacuum micropipette on one side. On the opposite side is a fine glass micro-needle. See fig.1.

A finite elements method was used in computer-based biological training system to simulate intracytoplasmic sperm injection (ICSI) procedures in virtual environments (See ref Ladjaly et al, 2011 [6]).

The vibration properties (natural frequencies and mode shapes) of a bio structure such as an embryo could be determined by modal analysis. Results of modal analysis can also serve as a starting point for another, more detailed, dynamic analysis, such as a transient dynamic analysis in different scenarios, e.g. artificial insemination of human embryo. The natural frequencies and mode shapes are important parameters in the design of a micro-robotic cell manipulation system for dynamic loading conditions [5].

Due to the nature of modal analyses any nonlinearity in material behavior are ignored. Optionally, orthotropic and temperature-dependent material properties may be used. The critical requirement is to define stiffness as well as mass in some form. Stiffness may be specified using isotropic and orthotropic elastic material models (for example, Young's modulus and Poisson's ratio), using hyper-elastic material models (they are linearized to an equivalent combination of initial bulk and shear module), or using spring constants, for example. Mass may derive from material density or from remote masses.

The goal activities of researching presented in this paper includes:

- Create robust finite elements model of mouse embryo and basic parts of micro-robotic cell manipulation system (holding pipette, micropipette and liquid environmental medium –human tubal fluid-HTF),
- Set the contacts and boundary conditions that affect the mouse embryo vibrations,
- Run step modal analysis to simulate vibrations of embryo alone and embryo as a part assembly with other components together,
- Determine the vibrational characteristics of mouse embryo free oscillations and embryo oscillations affected by boundary conditions.

Embryo modeling and modal analysis were based on the use of the finite elements method in the modal analysis system of ANSYS WORKBENCH® products [7].

Two cases were considered: free oscillations in the frame of the abovementioned experimental setup (holding pipette, micropipette and liquid environmental medium – human tubal fluid-HTF, mouse body temperature) at *in vitro* conditions and in vacuum instead of liquid environmental medium. Micro-needle only touches, but exerts no pressure upon the biomembrane of the mouse embryo.

2. Theory of modal analysis applied in FEM

The equations of elastic structural systems without external excitation can be written in the following form:

$$[M]\{\ddot{u}\}+[C]\{\dot{u}\}+[K]\{u\}=\{0\} \tag{1}$$

246

where is: [M] - structural mass matrix, [C] - structural damping matrix, [K] - structural stiffness matrix, { ü } - nodal acceleration vector, { u̇ } - nodal velocity vector, and { u } - nodal displacement vector.

It has been recognized that performing computations in the modal subspace is more efficient than in the full eigen space. The stiffness matrix [K] can be symmetrized by rearranging the asymmetric contributions; that is, the original stiffness matrix [K] can be divided into symmetric and asymmetric parts. By dropping the damping matrix [C] and the asymmetric contributions of [K], the symmetric Block Lanczos eigen value problem is first solved to find real eigen values and the corresponding eigen vectors. In the present implementation, the asymmetric element stiffness matrix is zeroed out for Block Lanczos eigen value extraction. Following is the coordinate transformation used to transform the full eigen problem into modal subspace:

$$\{u\} = [\Phi]\{y\} \tag{2}$$

where is: [Φ] – eigen vector matrix normalized with respect to the mass matrix [M] and {y} - vector of modal coordinates

By using equation (2) in equation (1), we can write the differential equations of motion in the modal subspace as follows:

$$[I]\{\ddot{y}\} + [\Phi]^T[C][\Phi]\{\dot{y}\} + \left(\left[\Lambda^2\right] + [\Phi]^T\left[K_{asym}\right][\Phi]\right)\{y\} = \{0\} \tag{3}$$

where is: $[\Lambda^2]$ - a diagonal matrix containing the first n eigen frequencies ω_i.

For classically damped systems, the modal damping matrix $[\Phi]^T[C][\Phi]$ is a diagonal matrix with the diagonal terms being $2\xi_i\omega_i$, where ξ_i is the damping ratio of the i-th mode. For non-classically damped systems, the modal damping matrix is either symmetric or asymmetric. Asymmetric stiffness contributions of the original stiffness are projected onto the modal subspace to compute the reduced asymmetric modal stiffness matrix $[\Phi]^T[K_{asym}][\Phi]$.

Introducing the $2n$-dimensional state variable vector approach, equation (3) can be written in reduced form as follows:

$$[I]\{\dot{z}\} = [D]\{z\} \tag{4}$$

where is:

$$\{\dot{z}\} = \begin{Bmatrix} \{y\} \\ \{\dot{y}\} \end{Bmatrix} \tag{5}$$

and

$$[D] = \begin{bmatrix} 0 & I \\ -\left[\Lambda^2\right] - [\Phi]^T\left[K_{asym}\right][\Phi] & -[\Phi]^T[C][\Phi] \end{bmatrix} \tag{6}$$

The $2n$ eigen values of Equation (4) are calculated using the QR algorithm (Press et al., 1993 [7]). The inverse iteration method (Wilkinson and Reinsch, 1971 [8]) is used to calculate the complex modal subspace eigen vectors. The full complex eigen vectors, {ψ}, of original system is recovered using the following equation:

$$\{\psi\} = [\Phi]\{z\} \tag{7}$$

3. FEM modeling

In modal analysis the embryo model was considered as three-dimensional axis-symmetric problem. The mouse embryo with basic parts of micro-robotic cell manipulation system described in [9] and shown in Fig. 1 (left) is simplified according the model setup shown in the same figure (right).
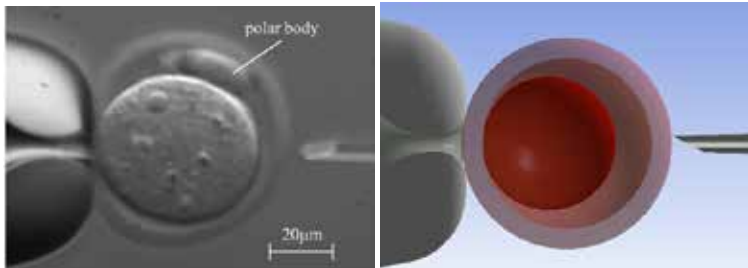
Figure 1. Photograph of cell (left) and simplified model setup of mouse embryo (right).

3.1. Embryo model

The full model setup (Fig. 2) used in the work is consisted of embryo (micromembrane with nucleus and cytoplasm) plunged into the control volume filled with liquid medium HTF. One side of embryo is connected to the holding pipette and the second is in contact with micropipette. For all time the vacuum inside the holding pipette takes the embryo fixed independently on the way of gravity and facilitates embryo manipulation.

1- Ambient (Liquid HTF)
2- Micropipette
3- Micromembrane
4- Cytoplasm
5 - Nucleus
6- Holding pipette
7- Vacuum
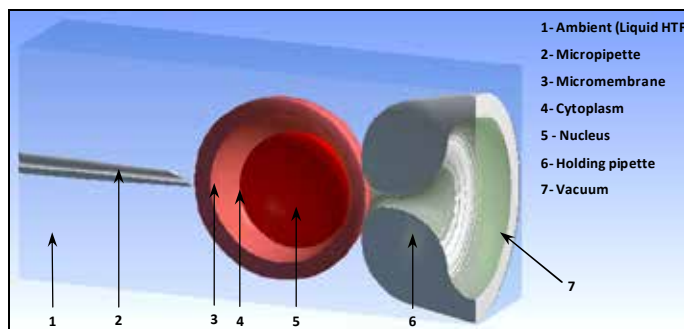
Figure 2. Axial cross-section of 3D model setup for embryo modal analysis.

The review of model setup parts with used materials and basic physical characteristics is presented in Table 1. As well, the table contains statistic data related to the number of

nodes and elements for each component after medium quality meshing procedure (Fig. 3).
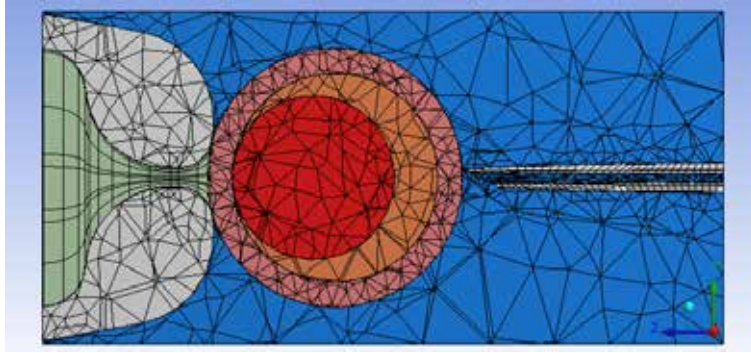
Figure 3. Details of finite elements mesh in the axial cross-section of model.

Table 1. Basic mechanical characteristics of model components with FE statistic data.

	Name	Assignment	Volume	Mass	Nodes	Elements
-	-	-	m^3	kg	-	-
1	Micromembrene	Biomembrene	5.3732E-14	5.4000E-11	7409	4288
2	Nucleus	Nucleus	2.8731E-14	2.9880E-11	685	350
3	Cytoplasm	Cytoplasm	3.0635E-14	3.1033E-11	1287	669
4	Holding pipette	Glass	1.0978E-13	2.7773E-10	3117	1776
5	Micropipette	Glass	1.4847E-15	3.7563E-12	3879	726
6	Vacuum	Air	2.8280E-14	3.4643E-14	1426	276
7	Liquid ambient	HTF	6.9430E-13	7.0333E-10	6953	3825

The initial contact regions and types of supports determine the boundary conditions of the model. All contacts regions of liquid medium HTF with micromembrane, vacuum pipette and micropipette are considered as frictional. For this kind of so-called wet friction the value 0.1 of frictional coefficient is accepted. The identical contact conditions are assumed on the contact surfaces of cytoplasm with nucleus and micromembrane.

From point of view of support boundary conditions, illustrated in Fig. 4, two types: fixed and frictionless supports, are used.

The dimensions of boundary box, represented as rectangle surface colored in dark blue in Fig. 4, filled by liquid medium HTF are 1.6E-4×7.7E-5×7.7E-5 m. Here, of shore, let to emphasize that its dimensions affect significantly the natural frequencies of embryo. All outer free faces of box are bonded by frictionless supports (E). As well, free surface of vacuum inside the holding pipette is bounded by frictionless support (D). Both the holding pipette and micropipette are constrained (fixed supports A and B) from movement in axial directions (z-axis).
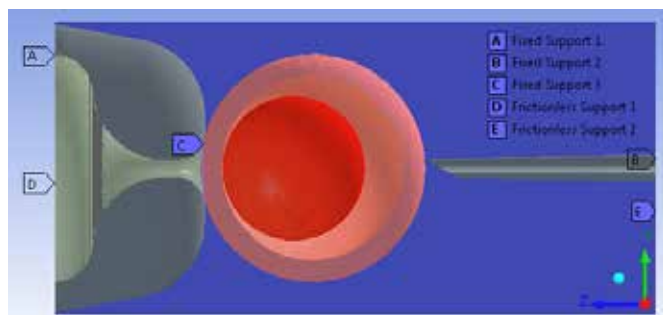
Figure 4. Details of support boundary conditions of model.

External loads of the embryo include conservative gravity force and surface force produced by 733.1 Pa vacuum on the air-micromembrane contact region. But in the modal analysis external loads make to be equal zero, so that the embryo is connected to holding pipette along initial contact edge (C).

3.2. Material data

According to the requirements of modal analysis, all materials, including bio materials (biomembrane, nucleus and cytoplasm), then medium materials (air and liquid medium HTF) and, finally, mechanical equipments materials (special glass for medical instruments) are considered as isotropic elasticity features materials.

The accepted temperature of each part of the model is same and equal to the mice body temperature of 37 ℃. Although the temperature is included in the modal analysis, it doesn't take any repercussions on the final results because of the absence of thermal loads or variations of mechanical parameters that would affect the model vibrational behavior.

Mechanical characteristics of the above mentioned materials are given in Table 2.

Table 2. Mechanical characteristics of materials

Material	Density	Reference temperature	Young's modulus	Poisson's ratio	Bulk modulus	Shear modulus
-	kg /m^3	K	Pa	-	Pa	Pa
Biomembrane	1005	310	42400	0.499	7.067E+6	14143
Nucleus	1040	310	7200	0.250	4800	2880
Cytoplasm	1013	310	17200	0.490	2.867E+5	5771,8
Liquid HTF	1013	310	1.32E+8	0.490	2.20e+9	4.430E+7
Air (vacuum)	1.225	310	3.102E+6[1]	0.490[*]	5.17E+7[*]	1.041E+6[*]
Glass	2530	310	5.448E+7	0.300	4.54E+7	2.095E+7

[1] *Given mechanical parameters of air represents the fictive values, adapted to solver requirements. It means, instead adiabatic law the linear pressure-volume dependence was assumed for small variations of air pressure up to 2E+5 Pa.*

4. Results and discussion

4.1. Natural frequences of embrio

The numerical integration of Eq. 4 facilitates the solutions for elements of diagonal matrix $[\Lambda]$ containing the first n eigen frequencies ω_i. Computed natural (own) frequences of embryo are given in Table 7.

Table 3. Natural frequencies of free and bonded embryo for first six modes.

Mode n	Natural frequences of embrio ω_i, Hz				
	Free oscillations in vacuum	Free oscillations in liquid HTF	Connection with holding pipette in vacuum	Connection with holding pipette in liquid HTF	Full connection in liquid HTF
1	0	52733	2924.2	52778	52782
2	0.0282	52839	2945.7	52882	52886
3	0.0462	53321	5868.6	53486	53491
4	600.32	54242	11888	54315	54317
5	931.50	55083	19333	55113	55116
6	940.79	55112	19353	55177	55180

The modal distribution of natural frequencies of embryo in liquid medium HTF is presented in Figs. 5. It is based on tabular data.
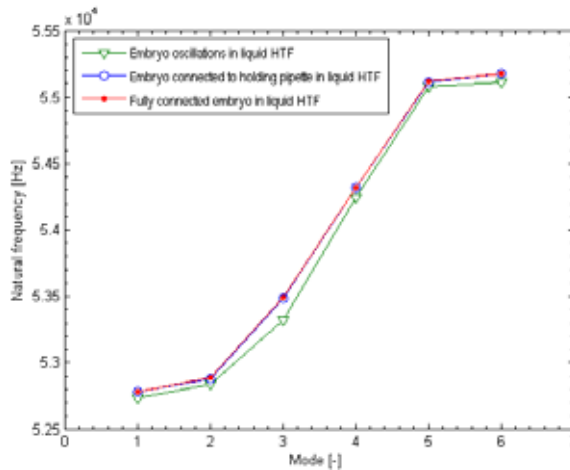
Figure 5. Modal distribution of natural frequencies of embryo vs. boundary conditions (osillations in liquid medium HTF).

Analysis of calculated results in Table 3 and represented in Figs. 5 confirms nature of boundary conditions influence on the natural frequency of embryo. In other words, the

natural frequency of embryo increases continually by involving each further boundary condition. So, In the case of contact of the embryo and liquid medium HTF the highest jump of frequency (over 52 KHz) appears and the relevant curves of frequency distribution are very close to each other (Fig. 5). Maximum frequency of 55180 Hz was reached for the embryo plunged into liquid medium and connected to micropipette and vacuum, holding pipette. Besides the abovementioned, the computed results show that oscillations of free embryo first mode are practically almost immeasurable ($\omega_i \approx 0$).

4.2. Typical variations of the vibrating embryo structural parameters

3D animations of the embryo movement relative to the corresponding mode can be describes as follows:
  - Mode 1: perpendicular oscillations along *y*-axis. Due to initial connections it looks lake rolling in *yz*-plane;
  - Mode 2 - perpendicular oscillations along *x*-axis. Due to initial connections it looks lake rolling in *xz*-plane; -presentation of this mode is very similar to mode 1
  - Mode 3 - rotation, i.e. torsion (due to initial connections) about *z*-axis;
  - Mode 4 - longitudinal oscillations along *z*-axis;
  - Mode 5 - rotation in *yz*-plane; presentation of this mode is very similar to mode 5, and
  - Mode 6 - rotation in *xz*-plane.

The appearance of scaled shape and fictive velocities distribution for typical modes 1, 4 and 6 of natural embryo oscillations are shown in Figs. 6-8.
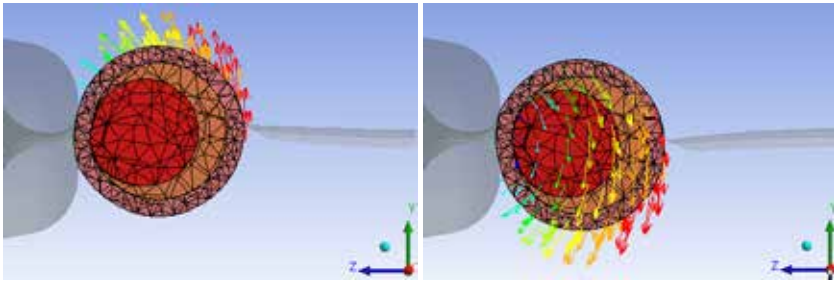
Figure 6. Shape and particle velocities distribution in extreme points of embryo vibrations in mode 1.
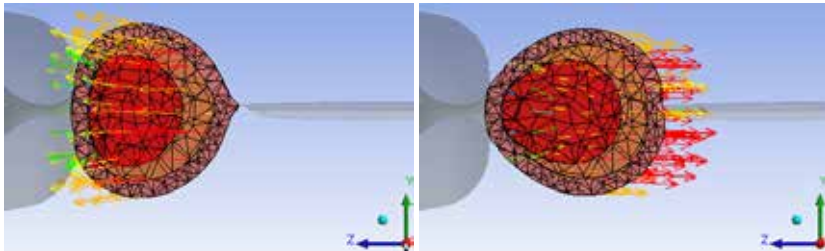
Figure 7. Shape and particle velocities distribution in extreme points of embryo vibrations in mode 4.
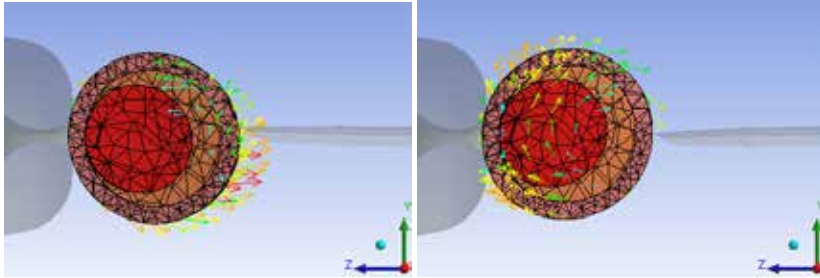
Figure 8. Shape and particle velocities distribution in extreme points of embryo vibrations in mode 6.

Real rate of total are varying from zero up to maximum 3.348 µm (Max 1.5107E+5 × 2.15E-11 m = 3.348E-6 m) in mode 4. In mode 4 micro-needle only taches the surface of embryo biomembrane.

Ladjal*y et al, 2011[5], used the method of finite elements in modelling the* Microrobotic Simulator for Assisted Biological Cell Injection, but they regarded the cell as a unified structure. Our model approximates the real phenomenon better as the cell is modelled as a three layer structure (biomembrane, cytoplasm, nucleus).

5. Conclusion

Based on the results of numerical analysis given in the paper it is shown that the robust finite elements model of mouse embryo with basic parts of ICSI system (holding pipette and micropipette) were correctly created. All necessary contacts and boundary conditions were regularly involved facilitating the modal analysis and numerical simulation of all situations of the embryo vibrations. As well, the determinations of the vibrational characteristics of mouse embryo free oscillations and embryo oscillations affected by boundary conditions for first six modes were successfully carried out.

To summarize, the work presented in the paper confirms possibility to use of the finite elements method coupled with numerical modal analysis as a powerful tools in the vibrational characterization of bio structures such as the mouse embryo. This method can be used to analyze vibrational properties of embryos of both mice and humans, and not only in physiological conditions, but also under pathological conditions, for example when artifical insemination is unsucessful, or when the implantation of the embryo does not occur. We are free to suggest that vibration properties of normal, healthy embryo differs from unhealthy embryo and vibration properties in these two cases may be distinguished. This opens new possibilities for developing an oscillation theory of reproduction in reproductive biology.

References

[1] Liu X, Fernandes R, Jurisicova A, Casperb R.F. and Sun Y. (2010) In situ mechanical characterization of mouse oocytes using a cell holding device. *The Royal Society of Chemistry, Lab Chip*, 10, pp.2154–2161.

[2] Murayama Y, Yoshida M, Mizuno J, Nakamura H, Inoue S, Watanabe Y et al. (2008) Elasticity Measurement of Zona Pellucida Using a Micro Tactile Sensor to Evaluate embrio Quality. J. Mamm. Ova Res. 25, pp.8-16.

[3] Murayama Y, Mizuno J, Kamakura H, FuetaY, Nakamura H, Akaishi H et al. s (2006) Mouse zona pellucida dynamically changes its elasticity during oocyte maturation, fertilization and early embryo development. *Human Cell* **19**, pp. 119–125.

[4] Hedrih A. (2011) Modeling oscillations of zona pelucida before and after fertilization. **ENOC** Young Scientist Prize Paper. *EUROMECH Newsletter* 40, Europian Mechanics Society, 40, pp. 6-14.

[5] Sun Y., Wan K.T., Roberts K.P., Bischof J.C., Nelson B. J. (2003) Mechanical Property Characterization of Mouse Zona Pellucida, *IEEE Transactions On Nanobioscience*, Vol. 2, **4** pp. 279-286.

[6] Ladjal*y* H, Hanus J-L, Ferreira A. (2011) . "IEEE International Conference on Robotics and Automation, San Francisco: United States " DOI : 10.1109/IROS.2011.6094965.

[7] ANSYS AUTODYN (2010)User's Manual *Theory manual*, ANSYS Inc. Southpointe, 275 Technology Drive, Canonsburg, PA, USA,

[8] Press W.H., et al., Numerical Recipes in C, (1993) *The Art of Scientific Computing*, Cambridge University Press,

[9] Wilkinson J.H., Reinsch C., Linear Algebra, (1971), *Handbook for Automatic Computation*, Springer-Verlag, New York, NY, Vol. II., pp. 418–439.

APPLICATION OF R-FUNCTIONS THEORY TO STUDY NONLINEAR VIBRATIONS OF LAMINATED SHALLOW SHELLS AND PLATES

L. Kurpa, N. Budnikov, T. Shmatko

[1] NTU "KhPI", Kharkov, Ukraine
e-mail: kurpa@kpi.kharkov.ua, l.kurpa@mail.ru

Abstract. In the present study the nonlinear vibrations of laminated plates and shallow shells are investigated. The proposed method is based on the R-functions theory and variational methods. Formulation of the problem is carried out in classical shell theory (CST). New solution structures for symmetric shallow shells with complex planform are constructed. These solution structures satisfy the boundary conditions corresponding to simply supported immovable and movable edge exactly. The nonlinear system of differential equations of motion is reduced to nonlinear system of ordinary differential equations (ODEs) by developed approach. Nonlinear forced vibrations of five-layered cross-ply plates and shallow shells with complex planform are investigated by proposed method.

1. Introduction

Research of geometrically nonlinear vibrations of the laminated plates and open shallow shells is one of important issues of nonlinear dynamics. In general case this problem may be only solved by numerical methods. Many researchers are studying this problem [1–5]. Some review of achievements in this field is presented in works [1,6,7]. The main approach which is applied to solve this problem is based on finite elements method (FEM) combined with method of harmonic balance, Bubnov-Galerkin, multiscales method and others.

One of alternatives to FEM is the effective numerically-analytical approach based on R-functions theory and variational methods (RFM). This method is a meshless one because it allows all prescribed boundary conditions to be satisfied exactly and present unknown functions in analytical form. RFM has been successfully applied to linear and nonlinear vibrations problems of plates and shallow shells [8,9,10]. In particular laminated shallow shells have been investigated in Refs. [9,10,11]. It should be observed that original approach has been proposed in Refs.[9,11] to solve geometrically nonlinear vibration problem. This approach consists of some steps. First a linear analysis is fulfilled to find natural frequencies and corresponding natural modes to be applied at

solving nonlinear problem. The second step is solving sequences of auxiliary problems like elasticity problems. The developed method uses the results of linear vibration problem essentially. The right-hand side of these equations is some functions of linear modes. The natural modes and solutions of auxiliary elasticity problems are used in the third step as a basis for expanding the nonlinear displacements. Finally the procedure by Bubnov-Galerkin is applied to reduce initial motion equations to system of ordinary differential equations (ODEs). In studies [11] single mode and solution of one auxiliary elasticity problem have been used.

First multi-mode expansion combined with R-functions theory has been proposed in paper [9]. Nonlinear free vibrations of symmetrically laminated shallow shells were investigated. First-order shell theory has been used. The analytical expressions of coefficients have been obtained for system of nonlinear ordinary differential equations. But numerical results were obtained applying single-mode. Recently in Ref. [12] multi-mode approach combined with R-functions theory for clamped isotropic shallow shells subjected to a radial harmonic excitation has been proposed. Lagrange approach is applied to obtain a system of ODEs. Numerical results were obtained by application multimode expansions. It should be noted, that systems of the basic functions satisfying only kinematic boundary conditions have been applied in Refs. [8,9].

In the present study geometrically nonlinear forced vibrations of the laminated shallow shells are investigated. New solutions structures satisfying all boundary conditions (static and kinematic) corresponding to simply supported shallow shells (movable and immovable edge) are constructed by RFM. In the present study classical non-linear shell Donnel's theory (CST) is used. Application of R-functions theory allows to study geometrically nonlinear dynamic response of the laminated shallow shells and plates with complex shape.

2. Problem formulation

Laminated shallow shells of M layers of the constant thickness h_i with radii of curvature R_x, R_y are considered. It is supposed that shells have the symmetrical structures in thickness. The principal lines of curvatures of the middle surface coincide with the coordinates x, y of the Cartesian coordinate system, and z is directed along normal to the middle surface of the shell. According to Donnel's theory it is assumed that the tangent displacements are linear functions of coordinate z and the transverse displacement w is constant through the thickness of the shell. This theory is based on Kirchhoff-Love assumptions. It means that the normal to the middle surface remains normal after deformation.

Motion equations may be represented in operator form [13]:

$$\begin{cases} L_{11}u + L_{12}v + L_{13}w = -Nl_1(w) + m_1\partial^2 u, \\ L_{21}u + L_{22}v + L_{23}w = -Nl_2(w) + m_1\partial^2 v, \\ L_{31}u + L_{32}v + L_{33}w = -Nl_3(u,v,w) + F(t) + m_1\partial^2 w. \end{cases} \tag{1}$$

Here u, v and w are displacements in directions of Ox, Oy and Oz axes relatively. Values m_1, linear differential operators L_{ij}, $i, j = \overline{1,3}$, and nonlinear differential operators Nl_i, $i = \overline{1,3}$ are defined so as in Ref. [14]. The function $F(t)$ is lateral force. Later we will consider force periodic in time.

The system (1) is supplemented by corresponding boundary conditions. In this study the following boundary conditions are considered:

a) Movable simply supported on all edges:

$$v_n = 0, \quad N_n = 0, \quad M_n = 0, \quad w = 0, \tag{2}$$

b) Immovable simply supported on all edges:

$$u = 0, \quad v = 0, \quad w = 0, \quad M_n = 0. \tag{3}$$

Expressions of N_n, M_n, and v_n are defined by known formulas [13]:

$$N_n = N_{11}l^2 + N_{22}m^2 + 2N_{12}lm, \tag{4}$$

$$M_n = M_{11}l^2 + M_{22}m^2 + 2M_{12}lm, \tag{5}$$

$$v_n = -um + vl, \tag{6}$$

where $l = \cos\alpha$, $m = \cos\beta$ are directional cosines of normal vector to boundary of the shell.

The initial conditions are taken in the form:

$$w\big|_{t=0} = w_{\max}, \partial_t w\big|_{t=0} = 0. \tag{7}$$

Components of N_{ij} and M_{ij}, $(i, j = 1,2)$ of forces $\{N\}$ and moments $\{M\}$ vectors in case of shell with symmetrical structure can be presented as follows:

$$\{N\} = \{N_{11}; N_{22}; N_{12}\}^T = [C] \cdot \{\varepsilon\}, \tag{8}$$

$$\{M\} = \{M_{11}; M_{22}; M_{12}\}^T = [D]\{\chi\}. \tag{9}$$

Here:

$$\{\varepsilon\} = \{\varepsilon_{11}; \varepsilon_{22}; \varepsilon_{12}\}^T, \quad \{\chi\} = \{\chi_{11}; \chi_{22}; \chi_{12}\}^T, \tag{10}$$

$$\varepsilon_{11} = \partial_x u + k_1 w + \frac{1}{2}(\partial_x w)^2, \quad \varepsilon_{22} = \partial_y v + k_2 w + \frac{1}{2}(\partial_y w)^2,$$

$$\varepsilon_{12} = \partial_y u + \partial_x v + (\partial_x w \cdot \partial_y w), \tag{11}$$

$$\chi_{11} = -\partial_x^2 w, \quad \chi_{22} = -\partial_y^2 w, \quad \chi_{12} = -2\partial_{xy}^2 w, \tag{12}$$

where k_1, k_2 are curvatures of the shell.

Stiffness matrices $[C]$ and $[D]$ are:

$$[C] = \begin{bmatrix} C_{11} & C_{12} & C_{16} \\ C_{12} & C_{22} & C_{26} \\ C_{16} & C_{26} & C_{66} \end{bmatrix}, \quad [D] = \begin{bmatrix} D_{11} & D_{12} & D_{16} \\ D_{12} & D_{22} & D_{26} \\ D_{16} & D_{26} & D_{66} \end{bmatrix}. \tag{13}$$

Constants C_{ij} and D_{ij} are the stiffness coefficients of the shell, which are defined by the following expressions [2,13]:

$$\left(C_{ij}, D_{ij}\right) = \sum_{s=1}^{n} \int_{h_{s-1}}^{h_s} B_{ij}^{(s)}\left(1, z^2\right) dz, \quad (ij = 11, 22, 12, 16, 26, 66). \tag{14}$$

Here $B_{ij}^{(s)}$ are stiffness coefficients of the s-th layer.

3. Method of solution

3.1. Linear vibration problem

The first step is studying the linear problem in order to find the natural frequencies and eigen functions $\left\{U^{(c)}\right\} = \left\{u^{(c)}, v^{(c)}, w^{(c)}\right\}^T$ satisfying the given boundary conditions. Note that at solving this problem we will not ignore inertia forces. Solution of linear problems has been widely discussed in [10]. Let us note that in generic case this problem can be solved by RFM [15]. We will use the Ritz's method. To obtain admissible functions, which satisfy the given boundary conditions exactly we will apply R-functions theory.

The main idea of the R-functions method is using so called solution structure of boundary value problem. These structures are basis for construction of basic functions set. The way of construction of the appropriate solution structures was proposed by V.L. Rvachev [15]. Let us construct new solution structure for the boundary conditions (2) and (3).

Movable simply supported edge. In this case the boundary conditions are described by relations (2). In order to satisfy the first boundary condition ($v_n = 0$) let us search for unknown functions u and v as follows:

$$\begin{cases} u = \Phi_1 \partial_x \omega + \omega \Phi_2, \\ v = \Phi_1 \partial_y \omega + \omega \Phi_3. \end{cases} \tag{15}$$

Here $\Phi_i \ \left(i = \overline{1,3}\right)$ are indefinite components of the solution structure. From definition of the solution structure [15], satisfying the given boundary condition it follows that indefinite components included in structure can be chosen by an arbitrary way, because the given boundary condition will be satisfied regardless of this choice. It is natural

these components should be chosen in such manner that the governing differential equations must be satisfied by the best way.

In equations (15) function $\omega(x, y)$ is normalized up to the first order, that is, it satisfies the following conditions [15]:

$$\omega(x, y) \succ 0, \forall (x, y) \in \Omega, \ \omega(x, y)\big|_{\partial\Omega} = 0, \partial_n \omega\big|_{\partial\Omega} = -1. \tag{16}$$

If we substitute (15) into expression (6) taking into account equalities

$$l = -\partial_x \omega, \ m = -\partial_y \omega, \tag{17}$$

then it is easy to show that condition $v_n = 0$ is fulfilled.

In order to satisfy the second condition

$$N_n = 0 \tag{18}$$

let us use the expression (4) for N_n. Normal forces $N_n^{(L)}$ for linear problem are defined by formulas:

$$N_n^{(L)} = N_{11}^{(L)} l^2 + N_{22}^{(L)} m^2 + 2N_{12}^{(L)} lm . \tag{19}$$

Taking into account the boundary condition for deflection function $(w = 0)$ components N_{ij} we can write down as:

$$\left\{ N_{11}^{(L)}; N_{22}^{(L)}; N_{12}^{(L)} \right\}^T = [C] \left[\partial_x u; \partial_y y; \partial_y u + \partial_x v \right]^T . \tag{20}$$

Let us transform the expression (19) for $N_n^{(L)}$ and write it in normal and tangent derivatives. It may be shown that relation (19) takes the following form:

$$N_n^{(L)} = A_1^0 \partial_n u + B_1^0 \partial_\tau u + K_1^0 \partial_n v + L_1^0 \partial_\tau v , \tag{21}$$

where

$$A_1^0 = C_{11} l^3 + 3C_{16} l^2 m + (C_{12} + 2C_{66}) lm^2 + C_{26} m^3 , \tag{22}$$

$$B_1^0 = C_{16} l^3 + (2C_{66} - C_{11}) l^2 m + (C_{26} - 2C_{16}) lm^2 - C_{12} m^3 , \tag{23}$$

$$K_1^0 = C_{16} l^3 + (C_{12} + 2C_{66}) l^2 m + 3C_{26} lm^2 + C_{22} m^3 , \tag{24}$$

$$L_1^0 = C_{12} l^3 + (2C_{66} - C_{11}) l^2 m + (C_{22} - 2C_{66}) lm^2 - C_{26} m^3 . \tag{25}$$

So the second boundary condition (18) may be written as:

$$A_1^0 \partial_n u + B_1^0 \partial_\tau u + K_1^0 \partial_n v + L_1^0 \partial_\tau v = 0, \tag{26}$$

Like Ref. [10] let us construct the extension of a functions A_1^0, B_1^0, K_1^0, L_1^0 inside of the domain with help of the formulas:

$$A_i = EC(A_i^0), \; B_i = EC(B_i^0), \; K_i = EC(K_i^0), \; L_i = EC(L_i^0), \; i = \overline{1,2}. \quad (27)$$

Derivatives with respect to normal and tangent can be extended to inside of the domain due to application of the specific differential operators D_m and T_m, at $m = 1$.

These operators are [15]:

$$D_m f(x, y) = (\nabla \omega, \nabla)^m f = \left(\partial_x \omega \cdot \partial_x + \partial_y \omega \cdot \partial_y\right)^m f, \quad (28)$$

$$T_m f(x, y) = \left(\partial_x \omega \cdot \partial_y - \partial_y \omega \cdot \partial_x\right)^m f. \quad (29)$$

So extension of the boundary condition (18) takes the following form:

$$\left(A_1 \partial_n u + B_1 \partial_\tau u + K_1 \partial_n v + L_1 \partial_\tau v\right) = \omega \Psi_1. \quad (30)$$

Substituting relation (15) into (30), one can obtain:

$$A_1 D_1 \left(\Phi_1 \partial_x \omega + \omega \Phi_2\right) + B_1 T_1 \left(\Phi_1 \partial_x \omega + \omega \Phi_2\right) + K_1 D_1 \left(\Phi_1 \partial_y \omega + \omega \Phi_3\right) +$$

$$+ L_1 T_1 \left(\Phi_1 \partial_y \omega + \omega \Phi_3\right) = \omega \Psi_1. \quad (31)$$

Using properties of operators D_1 and T_1, we get

$$\Phi_1 \left(A_1 D_1 (\partial_x \omega) + B_1 T_1 (\partial_x \omega) + K_1 D_1 (\partial_y \omega) + L_1 T_1 (\partial_y \omega)\right) +$$

$$+ \left(A_1 \partial_x \omega + K_1 \partial_y \omega\right) D_1 \Phi_1 + \left(B_1 \partial_x \omega + L_1 \partial_y \omega\right) T_1 \Phi_1 -$$

$$- A_1 \Phi_2 - K_1 \Phi_3 = \omega \Psi_2. \quad (32)$$

Let us solve the last equation in function Φ_3:

$$\Phi_3 = \frac{K_1}{K_1^2 + \omega^2} \left(\omega \Psi_2 - \Phi_1 \left(A_1 D_1 (\partial_x \omega) + B_1 T_1 (\partial_x \omega) + \right.\right.$$

$$+ K_1 D_1 (\partial_y \omega) + L_1 T_1 (\partial_y \omega)) - \left(A_1 \partial_x \omega + K_1 \partial_y \omega\right) D_1 \Phi_1 -$$

$$- \left(B_1 \partial_x \omega + L_1 \partial_y \omega\right) T_1 \Phi_1 - A_1 \Phi_2 \Big). \quad (33)$$

Then

$$u = \Phi_1 \partial_x \omega + \omega \Phi_2, \quad (34)$$

$$v = \frac{\omega K_1}{K_1^2 + \omega^2} \left(\omega \Psi_2 - \Phi_1 \left(A_1 D_1 (\partial_x \omega) + B_1 T_1 (\partial_x \omega) + \right.\right.$$

$$+ K_1 D_1 (\partial_y \omega) + L_1 T_1 (\partial_y \omega)) - \left(A_1 \partial_x \omega + K_1 \partial_y \omega\right) D_1 \Phi_1 -$$

$$- \left(B_1 \partial_x \omega + L_1 \partial_y \omega\right) T_1 \Phi_1 - A_1 \Phi_2 \Big) + \Phi_1 \partial_y \omega. \quad (35)$$

In similar fashion we can construct the solution structure for function w that satisfies the third and fourth boundary conditions ($M_n = 0$, $w = 0$). Let us write down the final form of this solution structures:

$$w = \omega\Phi_3 - \frac{\omega^2 S_1}{2(S_1^2 + \omega^2)}\left[S_1(2D_1\Phi_3 + \Phi_3 D_2\omega) + \right.$$

$$\left. + 2S_2 T_1\Phi_3 + S_3\Phi_3 T_2\omega - \omega\Psi_3\right]. \tag{36}$$

Here

$$S_1 = -D_{11}(\partial_x\omega)^4 - 4D_{16}(\partial_x\omega)^3\partial_y\omega - 2(D_{12} + 2D_{66})(\partial_x\omega)^2(\partial_y\omega)^2 - ,$$

$$- 4D_{16}\partial_x\omega(\partial_y\omega)^3 - D_{22}(\partial_y\omega)^4, \tag{37}$$

$$S_2 = -D_{16}(\partial_x\omega)^4 + (D_{11} - D_{12} - 2D_{66})(\partial_x\omega)^3\partial_y\omega +$$

$$+ 3(D_{16} - D_{26})(\partial_x\omega)^2(\partial_y\omega)^2 + D_{26}(\partial_y\omega)^4 +$$

$$+ (D_{12} - D_{22} + 2D_{26})\partial_x\omega(\partial_y\omega)^3, \tag{38}$$

$$S_3 = -D_{12}(\partial_x\omega)^4 + 2(D_{16} - D_{26})(\partial_x\omega)^3\partial_y\omega -$$

$$- (D_{11} + D_{22} - 4D_{66})(\partial_x\omega)^2(\partial_y\omega)^2 -$$

$$- 2(D_{16} - D_{26})\partial_x\omega(\partial_y\omega)^3 - D_{12}(\partial_y\omega)^4. \tag{39}$$

Formulas (36) contain special differential operators D_2, T_2 of the second order. These ones are defined by formulas (28)–(29) if $m = 2$.

Immovable simply supported edge. Analogously it may be shown that boundary conditions (3) are satisfied exactly by the following solution structure:

$$u = \omega\Phi_1, \tag{40}$$

$$v = \omega\Phi_2, \tag{41}$$

$$w = \omega\Phi_3 - \frac{\omega^2 S_1}{2(S_1^2 + \omega^2)}\left[S_1(2D_1\Phi_3 + \Phi_3 D_2\omega) + \right.$$

$$\left. + 2S_2 T_1\Phi_3 + S_3\Phi_3 T_2\omega - \omega\Psi\right]. \tag{42}$$

Here $S_i, (i = 1,2,3)$ are the same with (37–39).

In order to construct basic functions indefinite components must be expanded in truncated series:

$$\Phi_i = \sum_{k=1}^{k=n_i} a_k^{(i)} \varphi_k^{(i)}, \left(i = \overline{1,3} \right), \tag{43}$$

where $\left\{ \varphi_k^{(i)} \right\}$ are some known complete systems of the functions, for instance, power or Chebyshev's polynomials, trigonometric functions, splines or other, $\left\{ a_k^{(i)} \right\}$ are unknown coefficients that can be determined from the corresponding eigenvalue problem.

3.2. Solving the nonlinear problem

To solve the nonlinear problem unknown functions u, v, w are presented as follows:

$$\begin{cases} u(x,y,t) = \sum_{i=1}^{n} y_i(t) \cdot u_i^{(c)}(x,y) + \sum_{i=1}^{n}\sum_{j=i}^{n} y_i(t) \cdot y_j(t) \cdot u_{ij}(x,y), \\ v(x,y,t) = \sum_{i=1}^{n} y_i(t) \cdot v_i^{(c)}(x,y) + \sum_{i=1}^{n}\sum_{j=i}^{n} y_i(t) \cdot y_j(t) \cdot v_{ij}(x,y), \\ w(x,y,t) = \sum_{i=1}^{n} y_i(t) \cdot w_i^{(c)}(x,y), \end{cases} \tag{44}$$

where $u_i^{(c)}(x,y)$, $v_i^{(c)}(x,y)$ and $w_i^{(c)}(x,y)$ are eigenfunctions of linear vibrations. Functions $u_{ij}(x,y)$ and $v_{ij}(x,y)$ are solutions of the following system:

$$\begin{cases} L_{11}u_{ij} + L_{12}v_{ij} = -Nl_1^{(2)}\left(w_i^{(c)}, w_j^{(c)} \right), \\ L_{12}u_{ij} + L_{22}v_{ij} = -Nl_2^{(2)}\left(w_i^{(c)}, w_j^{(c)} \right). \end{cases} \tag{45}$$

Operators $Nl_1^{(2)}$ and $Nl_2^{(2)}$ are defined by formulas:

$$\begin{aligned} Nl_1^{(2)}\left(w_i^{(c)}, w_j^{(c)} \right) &= \partial_x w_i^{(c)}\left(C_{11}\partial_{xx}w_j^{(c)} + 2C_{16}\partial_{xy}w_j^{(c)} + C_{66}\partial_{yy}w_j^{(c)} \right) + \\ &+ \partial_y w_i^{(c)}\left(C_{16}\partial_{xx}w_j^{(c)} + \left(C_{12} + C_{66} \right)\partial_{xy}w_j^{(c)} + C_{26}\partial_{yy}w_j^{(c)} \right), \end{aligned} \tag{46}$$

$$\begin{aligned} Nl_2^{(2)}\left(w_i^{(c)}, w_j^{(c)} \right) &= \partial_x w_i^{(c)}\left(C_{16}\partial_{xx}w_j^{(c)} + \left(C_{12} + C_{66} \right)\partial_{xy}w_j^{(c)} + C_{26}\partial_{yy}w_j^{(c)} \right) + \\ &+ \partial_y w_i^{(c)}\left(C_{66}\partial_{xx}w_j^{(c)} + 2C_{26}\partial_{xy}w_j^{(c)} + C_{22}\partial_{yy}w_j^{(c)} \right). \end{aligned} \tag{47}$$

The system (45) is supplemented by the corresponding boundary conditions. For example, in case of movable simply supported edge these boundary conditions are:

$$v_{ij}^{(n)} = 0, \quad N_n = -F_1^0, \tag{48}$$

where

$$F_1^0 = N_{11}^{(N)}l^2 + N_{22}^{(N)}m^2 + 2N_{12}^{(N)}lm, \tag{49}$$

$$\left\{N^{(N)}\right\}=\left\{N_{11}^{(N)};\ N_{22}^{(N)};\ N_{12}^{(N)}\right\}^{T}=[C]\left\{\varepsilon^{(N)}\left(u_{ij},v_{ij}\right)\right\}, \tag{50}$$

$$\left\{\varepsilon^{(N)}\left(u_{ij},v_{ij}\right)\right\}=\frac{1}{2}\left\{\begin{array}{c}\partial_{x}w_{i}^{(c)}\cdot\partial_{x}w_{j}^{(c)}\\[4pt]\partial_{y}w_{i}^{(c)}\cdot\partial_{y}w_{j}^{(c)}\\[4pt]\partial_{x}w_{i}^{(c)}\cdot\partial_{y}w_{j}^{(c)}+\partial_{x}w_{j}^{(c)}\cdot\partial_{y}w_{i}^{(c)}\end{array}\right\}. \tag{51}$$

Solution of the problem (45)–(48) will be carried out by Ritz's method combined with RFM.

So the first two equations of the system (1) are satisfied identically by this choice of functions $u_{ij}(x,y)$ and $v_{ij}(x,y)$ provided that inertia forces are ignored.

Applying procedure by Bubnov-Galerkin to third equations of the system (1) one obtains the following system of non-linear ODEs:

$$y_{r}''(t)+\omega_{Lr}^{2}y_{r}(t)+\sum_{i,j=1}^{n}\beta_{ij}^{(r)}y_{i}(t)y_{j}(t)+$$

$$+\sum_{i,j,k=1}^{n}\gamma_{ijk}^{(r)}y_{i}(t)y_{j}(t)y_{k}(t)=\tilde{F}_{r}(t) \tag{52}$$

Here $r=\overline{1,n}$. Coefficients of the system (52) are defined by formulas:

$$\beta_{ij}^{(r)}=\frac{-1}{m_{1}\left\|w_{r}^{(c)}\right\|^{2}}\iint\limits_{\Omega}\left[N_{11}^{(L)}\left(u_{i}^{(c)},v_{i}^{(c)},w_{i}^{(c)}\right)\partial_{xx}w_{j}^{(c)}+\right.$$

$$+N_{22}^{(L)}\left(u_{i}^{(c)},v_{i}^{(c)},w_{i}^{(c)}\right)\partial_{yy}w_{j}^{(c)}+2N_{12}^{(L)}\left(u_{i}^{(c)},v_{i}^{(c)},w_{i}^{(c)}\right)\partial_{xy}w_{j}^{(c)}-$$

$$\left.-k_{1}N_{11}^{(Np)}-k_{2}N_{22}^{(Np)}\right]w_{r}^{(c)}d\Omega, \tag{53}$$

$$\gamma_{ijk}^{(r)}=-\frac{1}{m_{1}\left\|w_{r}^{(c)}\right\|^{2}}\iint\limits_{\Omega}\left(N_{11}^{(Np)}\left(u_{ij},v_{ij},w_{i}^{(c)}w_{j}^{(c)}\right)\partial_{xx}w_{k}^{(c)}+\right.$$

$$+N_{22}^{(Np)}\left(u_{ij},v_{ij},w_{i}^{(c)}w_{j}^{(c)}\right)\partial_{yy}w_{k}^{(c)}+$$

$$\left.+2N_{12}^{(Np)}\left(u_{ij},v_{ij},w_{i}^{(c)}w_{j}^{(c)}\right)\partial_{xy}w_{k}^{(c)}\right)w_{r}^{(c)}d\Omega, \tag{54}$$

$$\tilde{F}_{r}(t)=P_{r}\cos\Omega t,\quad P_{r}=\frac{P_{0}}{m_{1}\left\|w_{r}^{(c)}\right\|^{2}}\iint\limits_{\Omega}w_{r}^{(c)}d\Omega, \tag{55}$$

Below we present expressions of $N_{ij}^{(L)}$, $N_{ij}^{(Np)}$ in formulas (53–54):

$$\left\{N^{(L)}\left(u_{i}^{(c)},v_{i}^{(c)},w_{i}^{(c)}\right)\right\}=[C]\left\{\varepsilon^{(L)}\left(u_{i}^{(c)},v_{i}^{(c)},w_{i}^{(c)}\right)\right\}, \tag{56}$$

$$\left\{ N^{(Np)}\left(u_{ij}, v_{ij}, w_i^{(c)} w_j^{(c)} \right) \right\} = [C]\left\{ \varepsilon^{(Np)}\left(u_{ij}, v_{ij}, w_i^{(c)} w_j^{(c)} \right) \right\}, \tag{57}$$

$$\left\{ \varepsilon^{(L)}\left(u_i^{(c)}, v_i^{(c)}, w_i^{(c)} \right) \right\} = \left\{ \partial_x u_i^{(c)} + k_1 w_i^{(c)}; \partial_y v_i^{(c)} + k_2 w_i^{(c)}; \left(\partial_y u_i^{(c)} + \partial_x v_i^{(c)} \right) \right\}^T \tag{58}$$

$$\left\{ \varepsilon^{(Np)}\left(u_{ij}, v_{ij}, w_i^{(c)} w_j^{(c)} \right) \right\} = \left\{ \begin{array}{c} \partial_x u_{ij} + \dfrac{1}{2} \partial_x w_i^{(c)} \cdot \partial_x w_j^{(c)} \\[2mm] \partial_y v_{ij} + \dfrac{1}{2} \partial_y w_i^{(c)} \cdot \partial_y w_j^{(c)} \\[2mm] \partial_y u_{ij} + \partial_x v_{ij} + \partial_x w_i^{(c)} \cdot \partial_y w_j^{(c)} \end{array} \right\}. \tag{59}$$

Obtained system (52) may be investigated by the different approaches.
In particular case if take only one mode ($r = 1$) we can obtain [16] the simple dependence between amplitude $A = w_{max}/h$ and ratio Ω/ω_L :

$$\left(\Omega/\omega_L \right)^2 = 1 + \frac{8}{3\pi}\beta A + \frac{3}{4}\gamma A^2 \pm \frac{P_1}{A}. \tag{60}$$

4. Numerical results

Let us investigate the forced nonlinear vibrations of the five-layered cross-ply $\left(0^\circ /90^\circ /0^\circ /90^\circ /0^\circ \right)$ shells shown in fig.1.
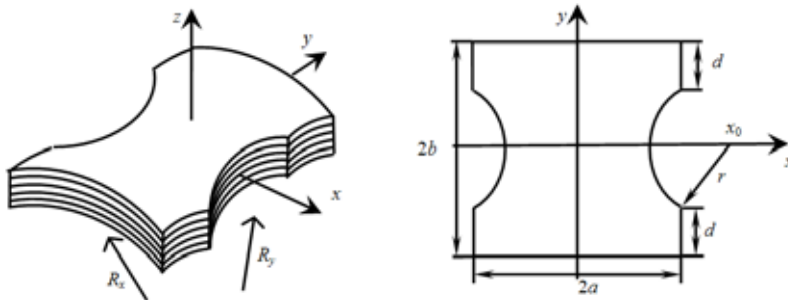
Figure 1. The geometric shape of the shell

The dimensionless material properties (typical of graphite-epoxy) are used :

$$E_1/E_2 = 40 , \ G_{12}/E_2 = 0.6 , \ \nu_{12} = 0.25 . \tag{61}$$

Geometrical parameters are:

$$R_1 = R_2 = 0.1a , \ h = 0.01a . \tag{62}$$

Further we will consider three different values of parameters d and x_0 .
case A: $d = b$,

case B: $d = b/2$, $x_0/a = 1.5$,

case C: $d = b/2$, $x_0/a = 5$.

The efficacy of the proposed method is tested by studying the nonlinear free flexural vibration of immovable simply supported square plate for which numerical results are available in the literature. The variation of nonlinear frequency ratio ω_{NL}/ω_L with non-dimensional maximum amplitude w_{max}/h is evaluated and shown in Table 1. It is observed that present results obtained by using two different of solution structures (40) – (42) which satisfy all the boundary conditions and the solution structures:

$$u = \omega\Phi_1, \quad v = \omega\Phi_2, \quad w = \omega\Phi_3, \tag{63}$$

which satisfy only the main (kinematic) boundary conditions are in close agreement with available solutions [17].

Table 1. The non-linear frequency ratio ω_{NL}/ω_L

of the square composite plate $\left(0^\circ/90^\circ/0^\circ/90^\circ/0^\circ\right)$

$\dfrac{w_{max}}{h}$	[17]	RFM (63)	RFM (40)–(42)
0.2	1.03147	1.03126	1.03129
0.4	1.12099	1.11983	1.11991
0.6	1.25723	1.25361	1.25378
0.8	1.42805	1.41988	1.42015
1.0	1.62368	1.60860	1.60897
1.2	1.83697	1.81277	1.81325

Similar results for shallow spherical shells of the complex planform (Fig. 1) are presented in Table 2.

Table 2. The non-linear frequency ratio ω_{NL}/ω_L of cross-ply spherical shells (Fig. 1)

$\dfrac{w_{max}}{h}$	Case A		Case B		Case C	
	RFM (63)	RFM (40)–(42)	RFM (63)	RFM (40)–(42)	RFM (63)	RFM (40)–(42)
0.5	0.81952	0.81974	0.81911	0.81911	0.80069	0.80069
1.0	0.64525	0.64563	0.64596	0.64596	0.62404	0.62404
1.5	0.48391	0.48433	0.48884	0.48884	0.49494	0.49494
2.0	0.35369	0.35382	0.36885	0.36885	0.45577	0.45577
2.5	0.29854	0.29781	0.32942	0.32942	0.52698	0.52698
3.0	0.35532	0.35366	0.39544	0.39544	0.67447	0.67447
3.5	0.48630	0.48408	0.52878	0.52878	0.85984	0.85984
4.0	0.64794	0.64535	0.69154	0.69154	1.06347	1.06347

Next the nonlinear forced vibration amplitudes $w_{\max} / h$ of immovable simply supported shells (Fig. 1) under transverse harmonic pressure $P = P_0 \cos \Omega t$ are studied. The backbone curves are represented in Fig. 2 by dotted lines. The nonlinear forced vibration amplitudes $w_{\max} / h$ under non-dimensional excitation frequency Ω / ω_L and load parameter $P_0 = 0.1$ are presented as full color lines for varies geometric parameters of the given shells corresponding to cases A and C.

a)   b)
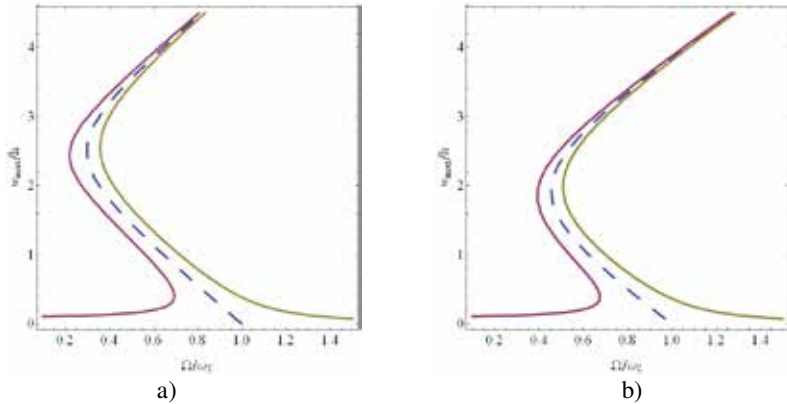
Figure 2. Resonance curves of forced vibrations of spherical shallow shells
a) Case A, b) Case C.

It should be noted that for solving the problem a single-mode approximation of the unknown functions is used. Therefore obtained results we can consider as the first approximation to real results. To clarify these results it is needed to continue research using multi-mode approximation.

5. Conclusions

New solution structures satisfying exactly all boundary conditions corresponding to simply supported (immovable and movable edge) of the symmetric laminated shallow shell with complex planform are constructed. The obtained solution structures are needed to construct a system of basic functions which are applied to reduce nonlinear motion equation of laminated shallow shells to system of ODEs. The proposed approach and new solution structures are applied to investigate nonlinear forced vibration of shallow shells with complex planform. In order to realize the proposed method for multimode approximation
it is assumed to create the corresponding software.

References

[1]   Amabili M. (2008) *Nonlinear Vibrations and Stability of Shells and Plates*, University of Parma, Italy.

[2] Qatu M.S. (2004) *Vibration of Laminated Shells and Plates*, Elsevier Ltd., Oxford.

[3] Reddy J.N., Arciniega R.A. (2004) Shear Deformation Plate and Shell Theories: From Stavsky to Present. *J. Mechanics of Advanced Materials and Structures, 11,* pp. 535–582.

[4] Abe A., Kobayashi Y., Yamada G. (2007) Nonlinear dynamic behaviors of clamped laminated shallow shells with one-to-one internal resonance, *Journal of Sound and Vibration*, **304,** pp. 957–968.

[5] T. Manoj, M. Ayyappan, K. S. Krishnan, B. NageswaraRao. (2000) Nonlinear Vibration Analysis of Thin Laminated Rectangular Plates on Elastic Foundations. *ZAMM Z. Angew. Math. Mech., 80 (3)*, pp. 183–192.

[6] Zhang Y.X., Yang C.H. (2009) Recent developments in finite element analysis for laminated composite plates, *Composite Structures, 88*, pp. 147–157.

[7] Sharma, Avadesh K.; Mittal, N. D. (2010) Review on Stress and Vibration Analysis of Composite Plates, *Journal of Applied Sciences*, vol. **10**, iss. 23, pp. 3156–3166.

[8] Kurpa L., Pilgun G., Amabili M. (2007) Nonlinear vibrations of shallow shells with complex boundary. R-functions method and experiments, *Journal of Sound and Vibration*, Vol. **306**, Iss. 3–5, pp. 580–600.

[9] Kurpa L.V. (2009) Nonlinear free vibrations of multilayer shallow shells with a symmetric structure and with a complicated form of the plan. *Journal of Mathematical Sciences, 162*, №1: 85–98.

[10] Kurpa L.V. (2009) *The R-Functions method for solving the linear problems of bending and vibrations of the plates and shells* (in Russian), Kharkov, NTU "KhPI".

[11] Kurpa L.V., Timchenko G.N. (2007) Investigation of nonlinear vibrations of the laminated composite plates using thr R-functions theory (in Russian), Strength problems, **5**, pp. 101–113.

[12] Pilgun G., Amabili M. (2012) Non-linear vibrations of shallow circular cylindrical panels with complex geometry. Meshless discretization with the R-functions method, *International Journal of Non-Linear Mechanics, 47*, pp. 137–152.

[13] Ambartsumian S.A.(1974) *The general theory of anisotropic shells,* Moscow, Nauka (in Russian).

[14] Awrejcewicz J., Kurpa L., Shmatko T. (2011) Nonlinear vibration of orthotropic shallow shells of the complex shape with variable thickness, *Dynamical systems Analytical/Numerical Metods, Stability, Bifurcation and Chaos,* Book 1, Jan Awrejcewicz and others, Wydawnictwo politechniki Lodzkiej, Poland, December 5-8, pp.243-248.

[15] Rvachev V.L. (1982) *The R-Functions theory and its Some Application* (in Russian), Naukova Dumka, Kiev.

[16] Volmir A.S. (1972) *Nonlinear dynamics of plates and shells* (in Russian), Moscow, Nauka.

[17] Singha M.K., Daripa R. (2009) Nonlinear vibration and dynamic stability analysis of composite plates, *Journal of Sound and Vibration*, **328,** pp. 541–554.

L. KURPA, N. BUDNIKOV, T. SHMATKO

EMULSIONS AND DOUBLE EMULSIONS AS PARTICULAR EXAMPLES OF MEMRISTIVE SYSTEMS

Aleksandar M. Spasić

Institute for Technology of Nuclear and Other Mineral Raw Materials, Dept. of Chem.Engng., 86 F. d'Esperey St., P.O. Box 390, 11000 Belgrade, Serbia e-mail: a.spasic@itnms.ac.rs

Abstract. The objective of this research was a try to provide a new or different approach to elaborate the complex phenomena that occur at developed liquid-liquid interfaces. Since some phenomena that occur, for example, during the processes of breaking of emulsions or double emulsions, and coalescence are not well understood the introduction of theoretical models known in electrodynamics were needed. A theory of electroviscoelasticity was developed and it is shown that the electroviscoelastic droplet, and/or droplet-film structure, that is emulsion or double emulsion may be considered as the particular example of memristive systems. All that means that for a deeper elucidation of complex phenomena at developed interfaces, that is at small separations, for example in emulsions and/or double emulsions, it is necessary to consider the electron transfer phenomenon beside the heat, mass, and momentum transfer phenomena commonly used in classical chemical engineering. Finally, the probable discussion and/or elucidation of the problems in the theoretical and experimental status of decoherence is mentioned.

1. Introduction

This presentation contains a recent development in basic and applied science and engineering of liquid-liquid finely dispersed systems, that is, in particular the selected emulsions and/or double emulsions are discussed. Since the events at the interfaces of finely dispersed systems, or at small separations, have to be considered at the molecular, atomic, and/or entities level it is inevitable to introduce the electron transfer phenomenon beside the heat, mass, and momentum transfer phenomena commonly used in classical chemical engineering.

The objective of this research was a try to provide a new or different approach to elaborate the complex phenomena that occur at developed liquid-liquid interfaces. Since some phenomena that occur, for example, during the processes of breaking of emulsions or double emulsions, and coalescence are not well understood the introduction of theoretical models known in electrodynamics are needed. Such an approach can

contribute to the deeper elucidation of the complex phenomena that occur at smaller separations, because the forces of electrical origin become dominant compared to the forces of mechanical origin, for example. the terms electrical forces and electrical interfacial potential (EIP) could be more appropriate than the terms mechanical forces and interfacial tension.

New concepts were introduced, the first is a concept of an *entity*, and the corresponding classification of finely dispersed systems and the second concept consider the introduction of an almost forgotten basic electrodynamics element *memristor*, and the corresponding memristive systems. Based on these concepts a theory of electroviscoelasticity was proposed and experimentally corroborated using the selected representative liquid-liquid system.

Three possible mathematical formalisms have been derived and discussed related to the proposed physical formalism, that is, to the developed theory of electroviscoelasticity. The first is stretching tensor model, where the normal and tangential forces are considered, only in mathematical formalism, regardless to their origin, mechanical and/or electrical. The second is classical integer order van der Pol derivative model. Finally, the third model comprise an effort to generalize the van der Pol differential equations, both, linear and nonlinear; where the ordinary time derivatives and integrals are replaced by the corresponding fractional-order time derivatives and integrals. In order to justify and corroborate more general approach the obtained calculated results were compared to those experimentally measured [1-16].

Then after, a new idea to consider emulsions and double emulsions as memristive systems is suggested. Finally, a probably possible further development related to the elucidation of the problems in the theoretical and experimental status of decoherence is mentioned [1, 14-16].
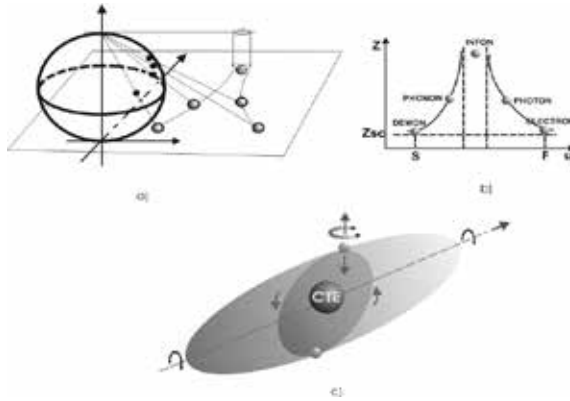
Figure 1. a) a stereographic projection/mapping from Riemann sphere; b) hierarchy of entities, correlation viscosity/impedance Z - characteristic velocity u_0, S-slow/demon (superfluid) and F-fast/electron (superconductor); c) entity as an energetic ellipsoid (at the same time macroscopic and microscopic), CTE – center of total energy, motions (translation, rotation, vibration, precession, angle rotation). From Ref. [1, 2], p. 8, p. 20, courtesy of CRC Press/Taylor & Francis.

2. Previous work

2.1. Classification of finely dispersed systems based on entities

Figure 1a shows a stereographic projection/mapping from Riemann sphere, representing *the first philosophical breakpoint*; Fig. 1b shows a "hierarchy" of entities, which have to be understood as a limit value of the ratio u_0/Z; this ratio is withdrawn from magnetic Reynolds criteria $[Re_m=4\pi l Gu_0/c^2]$, where the conductivity G is expressed as a reciprocal of the viscosity/impedance Z $(G=1/Z)$, l is the path length that an entity "overrides", u_0 is the characteristic velocity, and c is the velocity of light.

In general, S corresponds to the slow system or superfluid, and F corresponds to the fast system or superconductor; now, it is possible to propose that all real dynamic systems are situated between these limits. Also, it seems sensible to think about the further structure of entities, representing *the second philosophical breakpoint,* for example, the basic entity can be understood as an energetic ellipsoid shown in Figure 1c, that is, according to the model of electrons following Maxwell-Dirac isomorphism (MDI): an electron is an entity at the same time quantum-mechanical/microscopic N = -2 and electrodynamics/macroscopic N=3 [1, 2, and 7].

2.2. Physical formalism-the classical approach and a new approach

Formation and rupture processes of the secondary liquid/liquid droplet-film structures will be discussed considering mechanical and electrical principles. The analogy interfacial tension-interfacial electric potential will be illustrated considering the physical model of the processes appearing during the secondary separation of the droplet-film structure submerged in the droplet homophase continuum (double emulsion) on an inclined plate. Figure 2 shows the physical model of the processes involved; approach, rest, disturbance, rupture, and flow up.
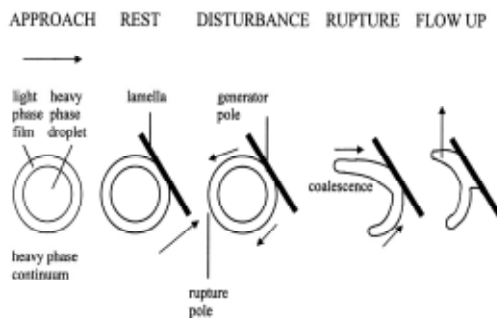
Figure 2. Physical model of the processes during the secondary separation of the double emulsion at an inclined plate; approach, rest, disturbance, rupture, and flow up (heavy phase-phosphoric acid H_3PO_4, light phase-sinergistic mixture D2EHPA-TOPO in dearomatized kerosene).

The generator pole is the origin/source of the disturbance, and the rupture pole is the point where the electrical and mechanical waves change the direction of traveling (feed into feed back).

Following a classical deterministic approach, the phases that constitute a multiphase dispersed system are assumed to be a continuum, i.e., without discontinuities inside the entire phase, that is considered homogenous and isotropic [1-5, 7-9, 14-16]. Therefore, the basic laws, e.g., conservation of mass, first and second Cauchy's laws of motion, first and second laws of thermodynamics, are applicable.

According to the classical approach, the behavior of liquid-liquid interfaces in fine dispersed systems is based on an interrelation between three forms of "instabilities". These are sedimentation, flocculation/coagulation, and coalescence. These events can be understood as a kind of interaction between the liquid phases involved.

Furthermore, the forces responsible for sedimentation and flocculation are gravity and van der Waals forces of attraction, respectively, and the forces responsible for coalescence are not well known, although some suggestions have been made recently [1-5, 7-9, 14-16].

A new approach discusses the behavior of liquid-liquid interfaces in fine dispersed systems as an interrelation between three other forms of "instabilities". These are rigid, elastic, and plastic. Figure 3 show the events that are understood as interactions between the internal/immanent and the external/incident periodical physical fields.
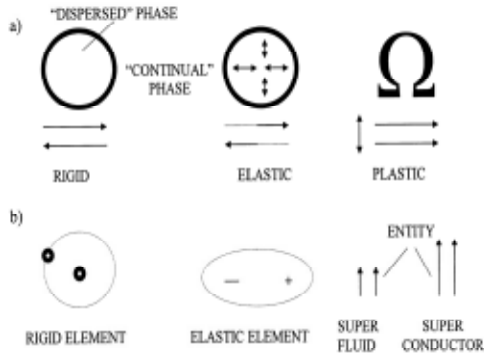
Figure 3. A new approach, a) "instabilities", rigid, elastic, plastic; b) the constructive elements of phases.

Since both electric/electromagnetic and mechanical physical fields are present in a droplet, they are considered as immanent or internal, and ultrasonic, temperature, or any other applied periodical physical fields are considered as incident or external. Hereafter, the rigid form of instability comprises the possibility of two-way disturbance spreading, or dynamic equilibrium. This form of instability, when all forces involved are in equilibrium, permits a two-way disturbance spreading (propagation or transfer) of entities either by tunneling (low energy dissipation and occurrence probability) or by induction (medium or high energy dissipation and occurrence probability). A classical

particle or system could not penetrate region in which its energy would be negative, that is, barrier regions in which the potential energy is greater than the system energy. In the real world, however, a wave function of significant amplitude may extend into and beyond such region. If the wave function extends into another region of positive energy, then the barrier is crossed with some probability; this process is termed tunneling (since the barrier is penetrated rather than climbed). The elastic form of instability comprises the possibility of reversible disturbance spreading, with or without hysteresis. Finally, the plastic form of instability comprises the possibility of irreversible disturbance spreading with a low or high intensity of influence between two entities. Entity is the smallest indivisible element of matter that is related to the particular transfer phenomena. The entity can be either differential element of mass/demon, or ion, or phonon as quanta of acoustic energy, or infon as quanta of information, or photon, or electron.

Now, a disperse system consists of two phases, "continuous" and "dispersed". The continuous phase is modeled as an infinitely large number of harmonic electromechanical oscillators with low strength interactions among them. Furthermore, the dispersed phase is a macrocollective consisting of a finite number of microcollectives/harmonic electromechanical oscillators (clusters) with strong interactions between them. The cluster can be defined as the smallest repetitive unit that has a character of integrity. Clusters appear in a micro and nano dispersed systems. The microcollective consists of the following elements: rigid elements (atoms or molecules), the elastic elements (dipoles or ions that may be recombined), and entities (as the smallest elements) [1-5, 7-9, 14-16].

2.3. Structure – mechanism – dynamics: theory of electroviscoelasticity

If the liquid-liquid interface, e.g. emulsion or double emulsion, is taken as a central and representative finely dispersed system it is possible to propose a theory of electroviscoelasticity based on a new constitutive model of liquids [1-5, 7-9, 14-16]. Thus, a hydrodynamic and electrodynamics motions are considered in the presence of both potential (elastic forces) and nonpotential (resistance forces) fields. The elastic forces are gravitational, buoyancy, and electrostatic/electrodynamics (Lorentz), and the resistance forces are continuum resistance/viscosity and electrical resistance/impedance. The principles of conservation of momentum, energy, mass, and charge are used to define the state of a real fluid system quantitatively. In addition to the conservation equations, which are insufficient to define the system uniquely, statements on the material behavior are also required; these statements are termed constitutive relations, e.g. Newton's law, Fourier's law, Fick's law, and Ohm's law.

Now, the droplet or droplet-film structure is considered as a macroscopic system with internal structure determined by the way the molecules (ions) are tuned (structured) into the primary components of a cluster configuration. After rearrangement or coupling at resonant/characteristic frequency a probable equivalent circuit is shown in Fig. 4. a. and b.. Electrical analogue Fig. 4. a., consists of passive elements (R, L, and C), and an active element (emitter-coupled oscillator W). Further on the emitter-coupled oscillator is represented by the equivalent circuit as shown in Fig. 4. b.. Figure 4.c.

shows the electrical (oscillators) and/or mechanical (structural volumes V_j) analogues when they are coupled to each other, e.g. in the droplet. Hence, the droplet consists of a finite number of structural volumes or spaces/electro-mechanical oscillators (clusters) V_j, and of a finite number of excluded surface volumes or interspaces V_s, and of a finite number of excluded bulk volumes or interspaces V_b. Furthermore, the interoscillator/cluster distance or internal separation S_i represents the equilibrium of all forces involved (electrostatic, solvation, van der Waals, and steric or fluctuation). The external separation S_e is introduced as a permitted distance when the droplet is in interaction with any external periodical physical field. The rigid droplet boundary R presents a form of droplet instability when all forces involved are in equilibrium. Nevertheless, two-way disturbance spreading (propagation or transfer) of entities occur, either by tunneling mechanism (low energy dissipation and occurrence probability) or by induction mechanism (medium or high energy dissipation and occurrence probability). The elastic droplet boundary E represents a form of droplet instability when equilibrium of all forces involved is disturbed by the action of any external periodical physical field, but the droplet still exists as a dispersed phase. In the region between the rigid and elastic droplet boundaries, a reversible disturbance spreading occurs with or without hysteresis. After the elastic droplet boundary, the plastic form of droplet instability takes place, then electro-mechanical oscillators/clusters do not exist any more and the beams of entities or atto-clusters appear. Atto-clusters are the entities that appear in the atto-dispersed systems. In this region one-way propagation of entities occurs.
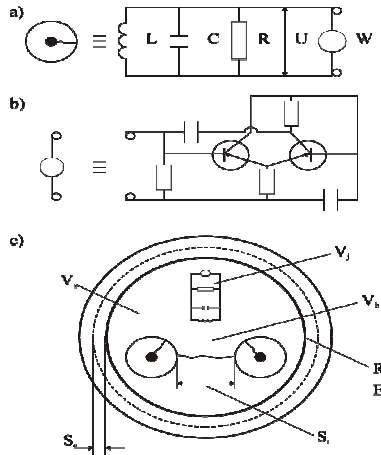
Figure 4. Graphical interpretation of the structural model: a) electrical and mechanical analog of the micro collective/cluster; b) equivalent circuit for the emitter coupled oscillator; c) the macrocollective: a schematic cross-section of the droplet and its characteristics (V_j – structural volumes/clusters; V_s – excluded surface volumes/interspaces; V_b – excluded bulk volumes/interspaces; S_i – internal separation; S_e – external separation; R – rigid droplet boundary; E – elastic droplet boundary).

3. Mathematical formalisms

3.1. The stretching tensor model

According to Newton's second law, the general equation of fluid dynamics in diferential form is given by

$$\rho \frac{D\tilde{u}}{Dt} = \sum_i \tilde{F}_i (dxdydz) + d\tilde{F}_s \tag{1}$$

When a droplet or droplet-film structure rests, for example, on the inclined plate, the term on the left-hand side of Eq. (1) becomes equal to zero, furthermore, since the droplet or droplet-film structure is in the state of "forced" levitation, and the volume forces balance each other, then the volume force term is also equal to zero. It is assumed that the surface forces are, for the general case that includes the electroviscoelastic fluids, composed of interaction terms expressed by

$$d\tilde{F}_s = \tilde{T}^{\,ij} d\tilde{A} \tag{2}$$

where the tensor T^{ij} is given by

$$\overline{T}^{\,ij} = -\alpha_0 \delta^{ij} + \alpha_1 \delta^{ij} + \alpha_2 \zeta^{ij} + \alpha \zeta_k^{\,i} \zeta^{kj} \tag{3}$$

where T^{ij} is composed of four tensors, δ^{ij} is the Kronecker symbol, and ζ^{ij} is the stretching tensor, and $\zeta_k^{\,i} \zeta^{kj}$ is the stretching coupling tensor. In the first isotropic tensor the potentiostatic pressure $\alpha_0 = \alpha_0(\rho, U)$ is dominant and the contribution of the other elements is neglected. Here U represents hydrostatic or electrostatic potential. In the second isotropic tensor, the resistance $\alpha_1 = \alpha_1(\rho, U)$ is dominant and the contribution of the other elements is neglected. In the third stretching tensor, its normal elements $\alpha_2 \sigma$ are due to the interfacial tensions and the tangential elements $\alpha_2 \tau$ are presumed to be of the same origin as the dominant physical field involved. In the fourth stretching coupling tensor, there are normal, $\alpha_3 \dot{\sigma}_k^i$, and $\alpha_3 \sigma^{kj}$ elements, and tangential $\alpha_3 \dot{\tau}_k^i$ and $\alpha_3 \tau^{kj}$ elements that are attributed to the first two dominant periodical physical fields involved. Now, the general equilibrium condition for the dispersed system with two periodical physical fields involved may be derived from Eq. (3), and may be expressed by

$$\tau_d = \frac{-\alpha_0 + \alpha_1 + \alpha_2 \left(\dfrac{\sigma}{d}\right) + \alpha_3 \left(\dfrac{\sigma}{d}\right)}{2(\alpha_2 + \alpha_3)} \tag{4}$$

where τ_d are the tangential elements of the same origin as those of the dominant periodical physical field involved. Note that for dispersed systems consisting of, or behaving as Newtonian fluids, $\alpha_3 = \alpha_3(\rho, U)$ is equal to zero.

The processes of formation and destruction of the droplet or droplet-film structure are nonlinear. Therefore, the viscosity coefficients are complex functions μ_i $(i = 0, 1, 2)$, where each consists of the real bulk component, and imaginary shear and tensile components, when correlated to the tangential tensions of mechanical origin τ_v can be written as

$$\tau_v = \mu_0 \frac{du}{dx} + \mu_1 \frac{d^2u}{dx^2} + \mu_2 \left(\frac{du}{dx}\right)^2 \qquad (5)$$

where u is the velocity, and x is one of the space coordinates.

Using the electrical analog, the impedance coefficients Z_i $(i = 0, 1, 2)$, where each consists of the real Ohmic component, and imaginary capacitive and inductive components, will be correlated with the tangential tensions of electrical origin τ_e, as following:

$$\tau_e = Z_0 \frac{d\phi_e}{dt} + Z_1 \frac{d^2\phi_e}{dt^2} + Z_2 \left(\frac{d\phi_e}{dt}\right)^2 \qquad (6)$$

where ϕ_e is the electron flux density, and t is the time coordinate.

3.2. Integer order van der Pol derivative model

Postulated assumptions for an electrical analogue:

1. The droplet is a macro system (collective of particles) consisting of structural elements that may be considered as electro-mechanical oscillators, named clusters.

2. Droplets as micro collectives undergo tuning or coupling processes, and so build the droplet as a macro collective.

3. The external physical fields (temperature, ultrasonic, electromagnetic, or any other periodic) cause the excitation of a macro system through the excitation of micro-systems at the resonant/characteristic frequency, where elastic and/or plastic deformations may occur.

Hence, the study of the electro-mechanical oscillators is based on electromechanical and electrodynamics principles. At first, during the droplet formation it is possible that the serial analog circuits are more probable, but later, as a consequence of tuning and coupling processes the parallel circuitry become dominant. Also, since the transfer of entities by tunneling (although with low energy dissipation) is much less probable it is sensible to consider the transfer of entities by induction (medium or high energy dissipation). Figure 5 presents the resultant equivalent electrical circuit, rearranged under the influence of an applied physical field, such as an antenna output circuit.

A nonlinear integral-differential equation of the Van der Pol type is selected as the convenient to represent the initial electromagnetic oscillation

$$C \frac{dv}{dt} + \left(\frac{v}{R} - \alpha v\right) + \gamma v^3 + \frac{1}{L} \int v dt = 0 \qquad (7)$$

where v is the overall potential difference at the junction point of the spherical capacitor C and the plate, L is the inductance caused by potential difference, and R is the ohm resistance (resistance of the energy transformation, electromagnetic into the mechanical or damping resistance), t is time; α and γ are constants determining the linear and

nonlinear parts of the characteristic current and potential curves. v_0, the primary steady-state solution of this equation is a sinusoid of frequency close to $\omega_0=1/(LC)^{0.5}$ and amplitude $A_0=[(\alpha-1)/R/3\gamma/4]^{0.5}$.
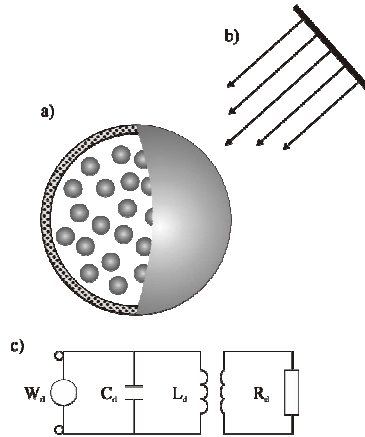
Figure 5. Definition sketch for easier understanding of the theory of electroviscoelasticity: a) rigid droplet; b) incident physical field, e.g., electromagnetic; c) equivalent electrical circuit-antenna output circuit. W_d represents the emitter-coupled oscillator, C_d, L_d, and Rd are capacitive, inductive, and resistive elements of the equivalent electrical circuit, respectively. Subscript d is related to the particular diameter of the droplet under consideration. Courtesy of Marcel Dekker, Inc. and CRC Press-Taylor & Francis Group (From Ref. 1, 2, 5, 9).

The noise in this system, due to linear amplification of the source noise (the electromagnetic force assumed to be the incident external force, which initiates the mechanical disturbance), causes the oscillations of the "continuum" particle (molecule surrounding the droplet or droplet-film structure), which can be represented by the particular integral

$$C \frac{dv}{dt} + \left(\frac{1}{R} - \alpha \right) v + \gamma v^3 + \frac{1}{L} \int v \, dt = -2A_n \cos \omega t \quad (8)$$

where ω is the frequency of the incident oscillations.

Finally, considering the droplet or droplet-film structure formation, "breathing", and/or destruction processes, and taking into account all the noise frequency components, which are included in the driving force, the corresponding equation is given by

$$C \frac{dv}{dt} + \left(\frac{1}{R} - \alpha \right) v + \frac{1}{L} \int v \, dt + \gamma v^3 = i(t) = \frac{1}{2\pi} \int_{-\infty}^{\infty} \exp(j\omega t) A_n(\omega) d\omega \quad (9)$$

where $i(t)$ is the noise current and $A_n(\omega)$ is the spectral distribution of the noise current as a function of frequency.

In the case of nonlinear oscillators, however, the problem of determining of the noise output is complicated by the fact that the output is fed back into the system thus modifying in a complicated manner the effective noise input. The noise output appears as an induced anisotropic effect.

Now again, the initial electromagnetic oscillation is represented by the differential equations, Eqs. (7) and (8), and when the nonlinear terms are omitted and/or superposed, the simpler linear equation is given by

$$C\frac{dv}{dt} + \left(\frac{1}{R} - \alpha\right)v + \frac{1}{L}\int vdt = -2A_n \cos \omega t \tag{10}$$

with a particular solution resulting in the following expression for the amplitude:

$$A = \frac{2\omega CA_n}{\left[4(\omega_0 - \omega)^2 + \left(\frac{1}{R} - \alpha\right)^2\right]^{0.5}} \tag{11}$$

and for all the noise frequency components, the simpler linear equation is given by

$$C\frac{dv}{dt} + \left(\frac{1}{R} - \alpha\right)v + \frac{1}{L}\int vdt = i(t) = \frac{1}{2\pi}\int_{-\infty}^{\infty} \exp(j\omega t)A_n(\omega)d\omega \tag{12}$$

with the particular solution expressed by

$$v_n = \frac{i\omega A_n \exp(i\omega t)}{C(\omega_0^2 - \omega^2) + i\left(\frac{1}{R} - \alpha\right)\omega} - \frac{i\omega A_n \exp(-i\omega t)}{C(\omega_0^2 - \omega^2) + i\left(\frac{1}{R} - \alpha\right)\omega} \tag{13}$$

Now, considering Eqs. (7)-(13) and Fig. 5. after the cluster's rearrangement the resultant equivalent electrical circuit can be represented as shown in Fig. 5c. Figure 6. shows, the behavior of the circuit depicted in Fig. 5c, using the correlation impedance-frequency-arbitrary droplet diameter.
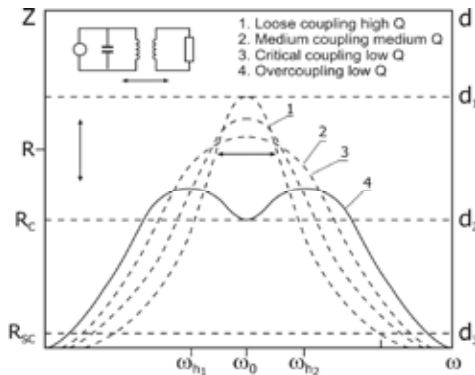
Figure 6. Impedance of the equivalent electric circuit versus its frequency. (From Ref. 4. 1997, p. 441, with permission from Academic Press).

Since all events occur at the resonant or characteristic frequency, depending on the amount of coupling, the shape of the impedance-frequency curve is judged using the factor of merit or Q factor [1-5, 7-9, 14-16]. The Q factor primarily determines the sharpness of resonance of a tuned circuit, and may be represented as the ratio of the reactance to the resistance, as follows:

$$Q = \frac{2\pi f L}{R} = \frac{\omega L}{R} \tag{14}$$

Furthermore, the impedance Z can be related to the factor of merit Q as it is given by equations

$$Z = \frac{(2\pi f R)^2}{R} = \frac{(\omega L)^2}{R} \tag{15}$$

and

$$Z = \omega L Q \tag{16}$$

From these expressions and Fig. 6. it can be seen that the impedance of a circuit is directly proportional to its effective Q at resonance. Also at the resonant frequency ω_0 the impedance Z is equal to the resistance R, R_c meaning critical, and R_{sc} meaning supercritical, respectively. These resistances and Z-ω curves correspond to the various levels of coupling (1) loose coupling and high Q; (2) medium coupling and medium Q; (3) critical coupling and low Q; (4) over-coupling and low Q). ω_{h1} and ω_{h2} represent the hump frequencies that appear during the over-coupling, curve (4) in Fig. 6. On the right axes of the Fig. 6. the corresponding critical diameters d_1, d_2, and d_3 are arbitrary plotted.

The experimental simulation of the antenna output circuit was performed in the Bruker MSL 400 spectrometer; Magnet 9.395 T, H_3PO Standard Solution, [31]P Frequency 161.924 MHz, Applied Sweep Witdh 15000 Hz – (Shift - 10 – 90 ppm), Pick at 7 ppm D2EHPA, Pick at 63 ppm TOPO [1-5, 9, 15, 16]. The obtained experimental results were in a good agreement with the developed and calculated theoretical predictions.

3.3. Recent development: van der Pol fractional order derivative model - linearized

In an effort to generalize equations (7 and 8) the ordinary time derivatives and integrals are now replaced with corresponding fractional-order time derivatives and integrals [1-8, 13- 15]. Here, the capacitive and inductive elements, using fractional–order p<2 (p = n − δ, n = 1, 2, δ << 1) enable formation of the fractional differential equation, i.e. more flexible or general model of liquid-liquid interfaces behaviour. Now, a differ-integral form using Riemann-Liouville definition is given by

$$_0D_t^p[v(t)] = \frac{d^p v}{dt^p} = \frac{1}{\Gamma(1-p)}\frac{d}{dt}\int_0^t \frac{v(\tau)}{(t-\tau)^p}d\tau; \quad _0D_t^{-p}[v(t)] = \frac{1}{\Gamma(p)}\int_0^t \frac{v(\tau)}{(t-\tau)^{1-p}}d\tau; \quad (17)$$

$$0 < p < 1 \qquad\qquad\qquad\qquad p > 0$$

Further on, a linear fractional differential equation with zeros initial conditions is obtained

$$C\,_0D_t^p[v(t)] + \left(\frac{1}{R}-\alpha\right)v + \frac{1}{L}\,_0D_t^{-p}[v(t)] = i(t) \qquad (18)$$

Further evaluation and calculation related to the solutions of the linearised, both homogeneous and nonhomogeneous, fractional integro-differential equations is presented in references [1-9].

In the case of nonhomogeneous solution obtained result appears as a band because the input (cos) is of the fractional order too; and output is in a damped oscillatory mode at high frequencies!

3.4. Van der Pol fractional order derivative model - nonlinear case

Nonlinear fractional differential equations have received rather less attention in the literature, partly because many of the model equations proposed have been linear. Here, both cases a nonlinear homogeneous *i(t)=0* and nonhomogeneous *i(t) ≠ 0* are considered. Equivalent nonlinear problem applying differentiation of Eq. (7) is presented by

$$C\frac{dv}{dt} + \left(\frac{v}{R}-\alpha v\right) + \gamma v^3 + \frac{1}{L}\int v\,dt = 0 \qquad (19)$$

In an effort to generalize the previous equation fractional order van der Pol equation become

$$_0^c D_t^{2p}v(t) = -\frac{1}{C}\left(\frac{1}{R}-\alpha\right)_0^c D_t^p v(t) - \frac{3\gamma}{C}v(t)^2\,_0^c D_t^p v(t) - \frac{1}{CL}v(t) \qquad (20)$$

Further evaluation and calculation related to the solutions of the nonlinear, both homogeneous and nonhomogeneous, fractional integro-differential equations is presented in references [1-9].

4. "Missing" basic element- memristor

Based on the definition of a "missing" basic element *memristor* for electrical circuit analysis, and taking into account four fundamental circuit variables, electric current *i*, electromotive force *v*, charge *q*, and magnetic flux *φ* the set of fundamental functional relations is given by [10]:

$$dv = R\,di \qquad (21)$$

$$dq = Cdv \tag{22}$$
$$d\varphi = Ldi \tag{23}$$
$$d\varphi = Mdq \tag{24}$$
$$d\varphi = vdt \tag{25}$$
$$dq = idt \tag{26}$$

Hence, the memristor as a current-controlled device is defined with the Eqs. (27) and (28), where w is the state variable of the device and R is a generalized resistance that depends upon the internal state of the device. In 1976 Chua and Kang generalized the memristor concept to a much broader class of nonlinear dynamical systems, named memristive systems, described by the Eqs. (29) and (30), where w is a set of state variables and R and f can, in general, be explicit functions of time [10].

$$v = R(w)i \tag{27}$$

and

$$\frac{dw}{dt} = i \tag{28}$$

$$v = R(w,i)i \tag{29}$$

and

$$\frac{dw}{dt} = f(w,i) \tag{30}$$

Further on, when an incidental uniform physical field, for example electromagnetic, is applied on the system emulsion/droplet or double emulsion/droplet-film-structure, causing the motions of both electrons and ions, than the memristance may be obtained as:

the application of an external bias $v\,(t)$ across the device (droplet or droplet-film structure) will move the boundary between the two regions (I and II). For the simplest case of ohmic electronic conduction and linear ionic drift in a uniform field with average ion mobility μ_i,

$$v(t) = \left[R_{int} \frac{w(t)}{D} + R_{bul} \left(1 - \frac{w(t)}{D} \right) \right] i(t) \tag{31}$$

$$\frac{dw(t)}{dt} = \mu_i \frac{R_{int}}{D} i(t) \tag{32}$$

now $w\,(t)$ is given by

$$w(t) = \mu_i \frac{R_{int}}{D} q(t) \tag{33}$$

By inserting Eq. (33) into Eq (31) the memristance for this system, which for $R_{int} << R_{bul}$ become

$$M(q) = R_{bul}\left[1 - \frac{\mu_i R_{int}}{D^2} q(t)\right] \tag{34}$$

where R_{int} is the low resistance at the interface and close to the interface layers (region I), R_{bul} is the much higher resistance in the bulk layers (region II), μ_i is the average ion mobility, D is the thickness of the considered fragment/"device". The $q(t)$ term present the most important contribution to the memristance, and it becomes larger in absolute value for the higher ion mobilities μ_i and smller device thickness D. This term is substantially larger (~10^6 times) in absolute value at the nanometer scale than it is at the micrometer scale, because of the factor of $1/D^2$, and the memristance is correspondingly more significant.

4.1. Emulsions and double emulsions as memristive systems

Now, according to the presented electrohydrodynamic approach, emulsions and double emulsions will be considered as the composite system "droplet + film" or "droplet-film structure + droplet homophase (S + E)". The history of this system consists of the initial/formation, intermediate/transition, and final/rigid states. 1. Every stationary state (initial, intermediate, and final) is characterized by interaction in the composite system that is of the same kind – being able to give rise to the occurrence of decoherence with the cluster arrangements as the "pointer basis states". 2. The nonstationary state is characterized by the change in the character of interaction in the composite system. The net effect takes the following "phases" each having its own characteristic time: a) under the action of an external or incidental physical field a formation, excitation, of the droplet-film structure occurs, producing the nonstationary state; b) the transition, relaxation, of the electroviscoelastic droplet-film structure into the rigid one, establishing the new final stationary state, this transition or relaxation process may be considered as a kind of a memory storage process, therefore, the system either electroviscoelastic droplet or droplet-film structure submerged into the other immiscible liquid phase, could be considered as the particular example of memristive systems; c) decoherence process, the final stationary state.

Based on these statements, and looking at figure 5c, following important propositions may be withdrawn:

- for every nonstationary state (excitation and relaxation) the resistor R_D have to be exchanged with the memristor M_D;

- for every stationary state (initial, intermediate, and final) the nonlinear memristance M (the generalized resistance) degenerate into the linear resistance R.

5. Probably possible further development: classical limit of quantum mechanics

This part will treat one important question of the classical limit of quantum mechanics, that is, is a quantum mechanics applicable at macroscopic level? This question resulted

during the research of complex systems by the end of the last century. According to the developed strategy, the proposition appeared is: if the macroscopic physical systems are only the special case of quantum-mechanical systems than it is possible to observe, under specified conditions, their quantum mechanical behavior [11].

The behavior of a droplet-film structure submerged into the droplet homophase or double emulsion, including its formation-existence-destruction states, described in this presentation will be considered as a close to the representative open macroscopic quantum system (OMQS), under the specified conditions. Hence, OMQS are quantum subsystems, that is, open quantum systems that are in inevitable permanent interaction with other physical systems, which may be named environment [11]. Does the theory of electroviscoelasticity, here presented, may be useful in discussion and/or further elucidation related to the problems of the experimental and theoretical status of decoherence?

Some needed definitions [11]:

1. The choice of an OMQS has to be in accordance to the criteria that confirm its description by the motion equation in a "classical domain".

2. It is convenient that the classical motion equation of the OMQS contain dissipative term.

3. The motion equation of the OMQS must be related, clearly and unequally, to the physical units whose values define distinguishable macroscopic states of the system.

4. The choice of a needed conditions for the following of the behavior of one OMQS have to be limited by the condition that some of the parameters values may correspond to the limit of the correspondence principle, that is, the condition $n \to \infty$ is invalid.

5. It is convenient to consider, theoretically, the behavior of the choused OMQS, and therefore to prepare possible predictions comparable with experimentally attainable situations.

The Leggett's Program:

These five points present a Leggett's task and basis for exploration of the macroscopic quantum phenomena of the second kind, that is, the confirmed quantum mechanical nature of the OMQS is related to these physical situations where the quantum effects are unequally linked to the macroscopically distinguishable states [11].

5.1. Suggested Problem – The Model

Finely dispersed system, emulsion and double emulsion, discussed, now will be considered as the composite system "droplet-film structure + droplet homophase (S + E)". The equivalent electrical circuits of the composite system are presented in Figures

4.a and 4.b and 5c; the history of this system consists of the initial/formation, intermediate/transition, and final/rigid states.

Keeping in mind all the requirements, the needed definitions and Leggett's program the model assumptions are [11-16]:

1. Every stationary state (initial, intermediate, and final) is characterized by interaction in the composite system that is of the same kind – being able to give rise to the occurrence of decoherence with the cluster arrangements as the "pointer basis states".

2. The nonstationary state is characterized by the change in the character of interaction in the composite system. The net effect takes the following "phases" each having its own characteristic time:

    a) Under the action of an external or incidental physical field a formation of the droplet-film structure occurs, producing the nonstationary state, taking time $t_{ext} = 125$ ms. This time was measured using developed liquid-liquid contact cell (LLCC) [1-5, 7-9, 14-16]; the measured variations of the EIP with time, for the representative system, are shown in Figure 7.

    b) The transition or relaxation of the electroviscoelastic droplet-film structure into the rigid one, establishing the new final stationary state, taking time $t_{relax} = 8$ min. This time was measured using developed LLCC; measured spontaneous oscillations of the EIP with time are shown in Figure 8. Now, this transition or relaxation process may be considered as a kind of the memory storage process;
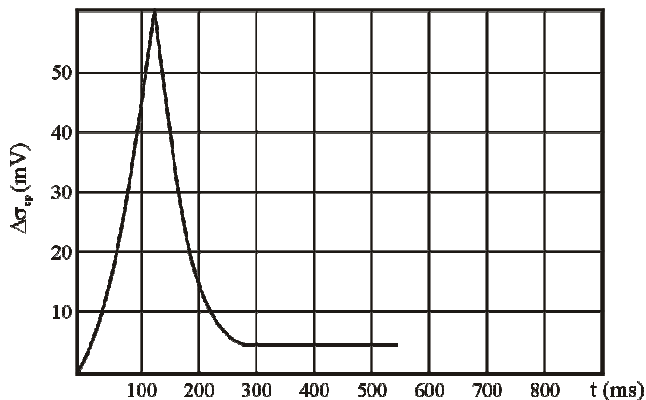
Figure 7. Measured variations of the EIP with time for the examined system: phosphoric acid/D2EHPA-TOPO-kerosene at the spherical interface.

therefore, the system electroviscoelastic droplet and/or droplet-film
structure could be considered as the particular example of memristive systems, which is shown in figure 8.

c) Decoherence process, in the final stationary state, taking time t_D., (decoherence time).

Therefore, the complete generation of the dispersed system or, for example, a double emulsion, takes overall time expressed by:

$$t_o = t_{ext} + t_{relax} + t_D \qquad (35)$$
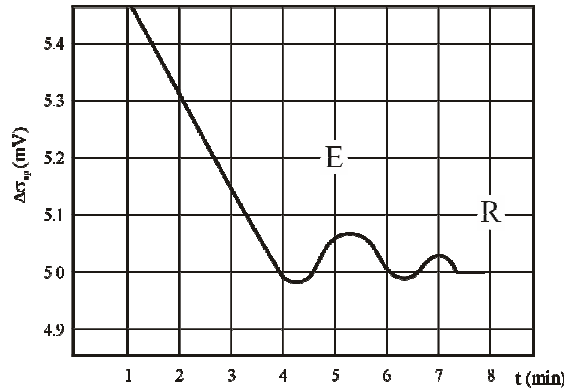
Figure 8. Measured spontaneous oscillations of the EIP during the "breathing" period; transformation of the electroviscoelastic sphere into the rigid sphere.

5.2. Suggested experimental confirmation

Since the equivalent electrical circuit, Fig 5.a may be considered as a kind of Superconducting Quantum Interference Device (SQUID), probably, it may be possible to couple, at the resonant frequency, where all events occur, one adjusted, sensitive tunnel diode oscillator as one detector of Macroscopic Quantum Tunneling Effect (MQTE). Also, the circuitry, described in the sections *2.3.* and *3.2.*, Fig. 4. and Fig. 5. may be modified, when taking into account definition of a current-controlled memristor, sections *3.*[1-5, 7-9, 14-16] and *4.* [1, 10, 15, 16], by replacement of the linear resistance (electro-viscose) with nonlinear memristance (electro-elastic) during the nonstationary periods; that is during the formation of electroviscoelastic sphere and its transition or relaxation into the rigid one.

285

6. Conclusions and implications

Three possible mathematical formalisms have been developed and discussed related to the developed theory of electroviscoelasticity. The first is stretching tensor model where the normal and tangential forces are considered, only in mathematical formalism, regardless to their origin, mechanical and/or elctricacal. The second is classical integer order van der Pol derivative model. Finally, the third model comprise an effort to generalize the previous van der Pol integral-differential equations, both linear and nonlinear; where the ordinary time derivatives and integrals are replaced by corresponding fractional-order time derivatives and integrals of order p<2 (p = n- δ, n = 1, 2, δ<<1).

Each of these mathematical formalisms, although related to the same physical formalism, facilitates better understanding of different aspects of a droplet existence, that is, its formation, life, and destruction states.

Stretching tensor model discusses the force equilibrium at the interfaces, either deformable or rigid, but its solution is difficult because the tensor contain nonlinear and complex elements.

The van der Pol derivative model is convenient for discussion of the "antenna output circuit", the resulting equivalent electrical circuit; but, since in the case of nonlinear oscillators, that is here the realistic one, the problem of determining the noise output is complicated by the fact that the output is fed back into the system, thus modifying in a complicated manner the effective noise input. The noise output appears as an induced anisotropic effect.

The theory of electroviscoelasticity using generalization of van der Pol derivative model applying fractional approach constitutes a new interdisciplinary tool to the colloid and interface science. Hence, 1-more degrees of freedom are in the model, 2-memory storage considerations and hereditary properties are included in the model, and 3-history or the impact to the present and future is in the game!

Finally, the electroviscoelastic droplet, and/or droplet-film structure, that is, emulsion or double emulsion may be considered as the particular example of memristive systems. All that means that for the elucidation of developed interfaces, for example, in colloids it is necessary to include the electron transfer phenomenon beside the heat, mass and momentum transfer phenomena commonly used in the classical chemical engineering.

All this research may have impact, for example, to the entrainment problems in solvent extraction, breaking of emulsions, deeper elucidation of adhesive processes, rupture processes, and coalescence; colloid and interface science, chemical and biological sensors, electro-analytical methods, biology or biomedicine (hematology, genetics, electroneurophysiology), classical limit of quantum mechanics, ionics, spintronics, fractional-quantum Hall effect-fluids, decoherence sensitivity, quantum computation, entities-quantum particles entanglement, [1-5, 7-9, 14-16].

References

[1] Spasic A M, Jovanovic J.M, Jovanovic M (2012) Modeling Selected Emulsions and Double Emulsions as Memristive Systems, *Advances in Colloid and Interface Science,* **174,** pp. 31-49.

[2] Hsu J-P and Spasic A M (2010) *Interfacial Electroviscoelasticity and Electrophoresis,* CRC Press-Taylor & Francis, Boca Raton London New York.

[3] Spasic A M, Lazarevic M P (2007) A New Approach to the Phenomena at the Interfaces of Finely Dispersed Systems, *Journal of Colloid and Interface Science*, **316**, pp. 984-995.

[4] Spasic A M, Jokanovic V, Krstic D N (1997) A Theory of Electroviscoelasticity: A New Approach for Quantifying the Behavior of Liquid-Liquid Interfaces under Applied Fields, *Journal of Colloid and Interface Science,* **186,** pp. 434-446.

[5] Spasic A M, Lazarevic M P, Krstic D N (2006) Theory of Electroviscoelasticity, *Finely Dispersed Particles: Micro-, Nano-, and Atto-Engineering,* CRC Press-Taylor & Francis, Boca Raton London New York, Spasic A M and Hsu J-P (Eds), pp. 371-393.

[6] Lazarevic M P, Spasic A M (2009) Finite-Time Stability Analysis of Fractional Time-Delay Systems: Gronwall's Approach, *Mathematical and Computer Modelling,* **49**, pp. 475-481.

[7] Spasic A M, Djokovic N N, Babic M D, Marinko M M, Jovanovic G N (1997) Performance of Demulsions: Entrainment Problems in Solvent Extraction, *Chemical Engineering Science*, **52**, pp. 657-675.

[8] Spasic A M (1992) Mechanism of the Secondary Liquid-Liquid Droplet-Film Rupture on Inclined Plate, *Chemical Engineering Science,* **47**, pp. 3949-3957.

[9] Spasic A M (2002) Electroviscoelasticity of Liquid/Liquid Interfaces, *Interfacial Electrokinetics & Electrophoresis,* Marcel Dekker, New York, Delgado A V (Ed), pp. 837-868.

[10] Strukov D B, Snider G S, Stewart D R, Williams R S (2008) The Missing Memristor Found, *Nature* **453/1,** pp. 80-83.

[11] Dugic M (2004) *Decoherence in a classical limit of quantum mechanics,* Notebooks of Physical Sciences, SFIN XVII (2), Institute of Physics, Belgrade,:.

[12] Elze H T (2003) Selected lectures from DICE 2002, *Decoherence and Entropy in Complex Systems*, Springer, Lecture Notes in Physics, Berlin Heidelberg New York, Elze H T (Ed.).

[13] Dugic M, Rakovic D, Plavsic M A (2006) The Polymer Conformational Stability and Transitions: A Quantum Decoherence Theory Approach, *Finely Dispersed Particles: Micro-, Nano-, and Atto-Engineering,* CRC Press-Taylor & Francis, Boca Raton London New York, Spasic A M and Hsu J-P (Eds), pp. 317-331.

[14] Spasic A M (2009) Electrohydrodynamics of Developed Liquid/Liquid Interfaces: Fractional Order Time Delay Systems, *Russian Journal of Physical Chemistry A*, **85**, pp. 1563-1570.

[15] Spasic A M. (2012) Emulsions and Double Emulsions as Memristive Systems, *CD of the 20th International Congress of Chemical and Process Engineering,* Prague, Czech Republic, B3.1.

[16] Spasic A M. (2012) Memory Storage Processes in Selected Emulsions and Double Emulsions, *Proceedings of the 11th International Conference on Fundamental and Applied Aspects of Physical Chemistry,VOL 1,* The society of Physical Chemists of Serbia, Belgrade, Serbia, pp 255-257.

ON STABILITY OF SINGULAR TIME DELAY SYSTEMS OVER THE FINITE TIME INTERVAL: CLASSICAL AND LMI CRITERIA

S. B. Stojanović[1], D. LJ. Debeljković[2]

[1] Department of Engineering Sciences and Mathematics, Faculty of Technology,
The University of Nis, Bulevar Oslobodjenja 124, 16000 Leskovac
e-mail: ssreten@ptt.rs
[2] Department of Control Engineering, Faculty of Mechanical Engineering,
The University of Belgrade, Kraljice Marije 16, 11120 Belgrade 35
e-mail: ddebeljkovic@mas.bg.ac.rs

Abstract. In this paper, finite-time stability problems for a class of singular time-delay systems are studied. The concept of finite-time stability is extended to singular time-delay systems and some conditions have been derived using two approach based on the Lyapunov-like functions: classical and LMI approach. The first approach is based on the algebraic matrix transformations, while the second approach uses the linear matrix inequalities. LMI approach provides a simple numerical solution and does not impose additional restriction on the state vector. Numerical example is given to show the effectiveness of the proposed approaches.

1. Introduction

A singular system describes a natural representation for physical systems. In general, the singular representation consists of differential and algebraic equations, and hence it is a generalized representation of the state-space system. The class of singular systems is more appropriate to describe the behavior of some practical systems like electrical systems [1], mechanical systems [2], and chemical systems [3-5]. It is well known that study of singular systems is much more complicated than that of regular ones.

It has been observed that variety of singular systems is characterized by the phenomena of time delay. Such systems are called singular systems with time delay. Time delay can appear in the input variables, output variables and/or the state space vector. In general, the dynamic behavior of continuous-time singular systems with delays is more complicated than that of system without any time-delay because the continuous time-delay system is infinite dimensional. For this reason, over the past decades, there has been increasing interest in the stability analysis for singular time-delay systems and many results have been reported in the literature [6–11].

Often Lyapunov asymptotic stability is not enough for practical applications, because there are some cases where large values of the state are not acceptable, for instance in the presence of saturations. For this purposes, the concept of the finite-time stability (FTS) and practical stability are used. A system is said to be FTS if, once a time interval is fixed, its state does not exceed some bounds during this time interval. A little work has been done for the finite-time stability and stabilization of singular time-delay systems. Some results on FTS and practical stability can be found in [12-18] (singular systems) and [19-20] (singular time-delay systems). However, according to the author's knowledge, there is no result available yet on finite-time stability and stabilization for a class of linear time-delay systems using linear matrix inequality.

In this article, we consider the problem of finite-time stability for a class of linear singular time-delay systems. The concept of finite-time stability is extended to singular time-delay systems. New conditions have been derived using two approach based on the Lyapunov-like functions: classical and LMI approach. The first approach is based on the algebraic matrix transformations, while the second approach uses the linear matrix inequalities. Numerical example is given to show the effectiveness of the proposed approaches.

2. Notation and preliminaries

The following notations will be used throughout the paper. $\Re^n$ denotes the n-dimensional Euclidean space, C^n complex vector space and $\Re^{n \times m}$ is the set of all real matrices of dimension $n \times m$. Superscript "T" stands for matrix transposition. $X > 0$ means that X is real symmetric and positive definite and $X > Y$ means that the matrix $X - Y$ is positive definite. In symmetric block matrices or long matrix expressions, we use an asterisk (*) to represent a term that is induced by symmetry. I stands identity matrix and $\lambda(X)$ eigenvalue of matrix X. Matrices, if their dimensions are not explicitly stated, are assumed to be compatible for algebraic operations.

Consider a linear continuous singular system with state delay, described by

$$\hat{E}\dot{\hat{x}}(t) = \hat{A}\hat{x}(t) + \hat{A}_d \hat{x}(t - \tau) \tag{1}$$

with a known compatible vector valued function of the initial conditions

$$\hat{x}(t) = \hat{\varphi}(t), \quad -\tau \le t \le 0 \tag{2}$$

where $\hat{x}(t) \in \Re^n$ is the state vector, τ is constant time delay, $\hat{A} \in \Re^{n \times n}$ and $\hat{A}_d \in \Re^{n \times n}$ are known constant matrices. The matrix $\hat{E} \in \Re^{n \times n}$ may be singular, and it is assumed that $\mathrm{rank}(\hat{E}) = r \le n$.

It is known ([12]) that there exist invertible matrices M and N such that

$$E = M\hat{E}N = \begin{bmatrix} I_r & 0 \\ 0 & 0 \end{bmatrix}, \quad A = M\hat{A}N = \begin{bmatrix} A_{11} & A_{12} \\ A_{21} & A_{22} \end{bmatrix}, \quad A_d = M\hat{A}_d N = \begin{bmatrix} A_d^{11} & A_d^{12} \\ A_d^{21} & A_d^{22} \end{bmatrix} \tag{3}$$

Then, by the nonsingular transformation

$$x = N^{-1}\hat{x} \tag{4}$$

the system (1) can be described by the following system:

$$E\dot{x}(t) = Ax(t) + A_d x(t - \tau)$$

$$x(t) = \varphi(t), \quad \varphi(t) = N^{-1}\hat{\varphi}(t), \quad t \in [-\tau, 0]$$

(5)

The following definition will be used in the proof of the main results.

Definition 1. Matrix pair (E, A) is said to be regular if $\det(sE - A)$ is not identically zero [6].

Definition 2. The matrix pair (E, A) is said to be impulse-free if $deg\det(sE - A) = rank\ E$ [6].

The linear continuous singular time delay system (5) may have an impulsive solution. However, the regularity and the absence of impulses of the matrix pair (E, A) ensure the existence and uniqueness of an impulse-free solution of the system. The existence of the solutions is defined in the following Lemma.

Lemma 1. Suppose that the matrix pair (E, A) $((\hat{E}, \hat{A}))$ is regular and impulsive free, then the solution to (5) ((1)) exists and is impulse-free and unique on [0, ∞) [6].

In view of this, we introduce the following definition for singular time-delay system (5) or (1).

Definition 3. The singular continuous system with state delay (5) ((1)) is said to be regular and impulse-free, if the matrix pair (E, A) $((\hat{E}, \hat{A}))$ is regular and impulse-free [6].

Then, based on Definition 3, the singular continuous time-delay systems (1) and (5) are regular and impulse-free.

Lemma 2. For any symmetric, positive definite matrix $\Xi = \Xi^T > 0$ the following condition is satisfied:

$$2u^T(t)v(t) \le u^T(t)\Gamma^{-1}u(t) + v^T(t)\Gamma v(t)$$

(6)

3. Main results

Lemma 3. Continuous singular time-delay systems (1) and (5) are regular and impulse-free if matrix A_{22}, which is defined by (3), is invertible.

Proof. Let A_{22} is invertible. Then

$$\begin{aligned}
\det(s\hat{E} - \hat{A}) &= \det(M^{-1})\det(sE - A)\det(N^{-1}) \\
&= \det(M^{-1})\det\left(\begin{bmatrix} sI_r - A_{11} & -A_{12} \\ -A_{21} & -A_{22} \end{bmatrix}\right)\det(N^{-1}) \\
&= \det(M^{-1})\det\left(\begin{bmatrix} sI_r - A_{11} & -A_{12} \\ -A_{21} & -A_{22} \end{bmatrix}\begin{bmatrix} I_r & 0 \\ -A_{22}^{-1}A_{21} & I_{n-r} \end{bmatrix}\right)\det(N^{-1}) \\
&= \det(M^{-1})\det\left(\begin{bmatrix} sI_r - A_{11} + A_{12}A_{22}^{-1}A_{21} & -A_{12} \\ 0 & -A_{22} \end{bmatrix}\right)\det(N^{-1}) \\
&= \det(M^{-1})\det(-\hat{A}_{22})\det\left(sI_r - (A_{11} - A_{12}A_{22}^{-1}A_{21})\right)\det(N^{-1})
\end{aligned}$$

(7)

which implies

$$\det(sE - A) \not\equiv 0, \quad \deg \det(sE - A) = r, \quad \det(s\hat{E} - \hat{A}) \not\equiv 0, \quad \deg \det(s\hat{E} - \hat{A}) = r \qquad (8)$$

Definition 4. Singular time delayed *s*ystem (5) is finite-time stable with respect to $\{\alpha, \beta, T\}, \ \alpha < \beta$, if

$$\sup_{t \in [-\tau, 0]} \varphi^T(t)\varphi(t) \leq \alpha \qquad (9)$$

implies

$$x^T(t) E^T E x(t) < \beta, \quad \forall t \in [0, T] \qquad (10)$$

2.1. Classical approach

The classical approach is based on Lyapunov-like functions using algebraic matrix transformations.

Theorem 1. Consider a singular time-delay *s*ystem (5) with

$$x^T(t - \theta) x(t - \theta) < q x^T(t) x(t), \quad q > 0, \quad \theta \in [-\tau, 0], \quad \forall t \in [0, T] \qquad (11)$$

If the matrix A_{22} is invertible and if there exists a positive scalar $\wp$, matrix P and positive define symmetric matrices Q and R, such that the following conditions hold:

$$PE = E^T P^T \geq 0 \qquad (12)$$

$$PE = E^T R E \qquad (13)$$

$$\beta e^{-\Lambda_m T} \lambda_{\min}(R) - \alpha[\lambda_{\max}(PE) + \tau \lambda_{\max}(Q)] < 0 \qquad (14)$$

where:

$$\Lambda_m = \max[x^T(t) \Xi x(t): \quad x^T(t) PE x(t) = 1] \qquad (15)$$

$$\Xi = A^T P^T + PA + Q + PA_d \wp^{-1} A_d^T P^T + q\lambda_{\max}\{\wp I - Q\} I \qquad (16)$$

then system (1) is regular, impulse free and finite-time stable with respect to $\{\alpha, \beta, T\}, \ \alpha < \beta$ for all $T > 0$.

Proof. Based on Lemma 3, the condition $A_{22} \neq 0$ provides that the system (5) is regular and impulse free.

Next, we show the stability. Let us consider the following Lyapunov-like function:

$$V(x(t)) = x^T(t) PE x(t) + \int_{t-\tau}^{t} x^T(s) Q x(s) ds \qquad (17)$$

Total derivative $\dot{V}(x(t))$ along the trajectories of the system (5) is:

$$\begin{aligned} \dot{V}(x(t)) &= \dot{x}^T(t) E^T P^T x(t) + x^T(t) PE \dot{x}(t) + x^T(t) Q x(t) - x^T(t-\tau) Q x(t-\tau) \\ &= x^T(t)(A^T P^T + PA) x(t) + 2x^T(t) PA_d x(t-\tau) \\ &\quad + x^T(t) Q x(t) - x^T(t-\tau) Q x(t-\tau) \\ &= x^T(t)(A^T P^T + PA + Q) x(t) + 2x^T(t) PA_d x(t-\tau) - x^T(t-\tau) Q x(t-\tau) \end{aligned} \qquad (18)$$

Based on Lemma 2, we get:

$$2x^T(t) PA_d x(t-\tau) \leq x^T(t) PA_d \wp^{-1} A_d^T P^T x(t) + x^T(t-\tau) \wp x(t-\tau) \qquad (19)$$

so

$$\dot{V}\left(x(t)\right) \leq x^{T}\left(t\right)\left(A^{T}P^{T}+PA+Q\right)x(t)+x^{T}\left(t\right)PA_{d}\wp^{-1}A_{d}^{T}P^{T}x(t)$$
$$+x^{T}\left(t-\tau\right)\left(\wp I-Q\right)x(t-\tau) \tag{20}$$

Using (11), it is clear that (20) is reduced to:

$$\dot{V}\left(x(t)\right) \leq x^{T}\left(t\right)\left(A^{T}P^{T}+PA+Q\right)x(t)$$
$$+x^{T}\left(t\right)PA_{d}\wp^{-1}A_{d}^{T}P^{T}x(t)+x^{T}\left(t-\tau\right)\left(\wp I-Q\right)x(t-\tau)$$
$$\leq x^{T}\left(t\right)\left(A^{T}P^{T}+PA+Q+PA_{d}\wp^{-1}A_{d}^{T}P^{T}\right)x(t)$$
$$+\lambda_{\max}\left\{\wp I-Q\right\}x^{T}\left(t-\tau\right)x(t-\tau)$$
$$< x^{T}\left(t\right)\left(A^{T}P^{T}+PA+Q+PA_{d}\wp^{-1}A_{d}^{T}P^{T}\right)x(t)+q\lambda_{\max}\left\{\wp I-Q\right\}x^{T}\left(t\right)x(t) \tag{21}$$
$$= x^{T}\left(t\right)\left(A^{T}P^{T}+PA+Q+PA_{d}\wp^{-1}A_{d}^{T}P^{T}+q\lambda_{\max}\left\{\wp I-Q\right\}I\right)x(t)$$
$$= x^{T}\left(t\right)\Xi x(t)$$
$$\Xi = A^{T}P^{T}+PA+Q+PA_{d}\wp^{-1}A_{d}^{T}P^{T}+q\lambda_{\max}\left\{\wp I-Q\right\}I$$

From (21) we have

$$\frac{dV\left(x(t)\right)}{V\left(x(t)\right)} < \frac{x^{T}\left(t\right)\Xi x(t)}{V\left(x(t)\right)}dt < \frac{x^{T}\left(t\right)\Xi x(t)}{x^{T}\left(t\right)PE\,x(t)}dt \leq \max\left\{\frac{x^{T}\left(t\right)\Xi x(t)}{x^{T}\left(t\right)PE\,x(t)}\right\}dt = \Lambda_{m}dt \tag{22}$$

where:

$$\Lambda_{m} = \max\left[x^{T}\left(t\right)\Xi x(t): \quad x^{T}\left(t\right)PE\,x(t)=1\right] \tag{23}$$

After integrating the previous inequality we get:

$$V\left(x(t)\right) < V\left(x(0)\right)e^{\Lambda_{m}t} \tag{24}$$

Then:

$$V\left(x(0)\right) = x^{T}\left(0\right)PEx(0)+\int_{-\tau}^{0}x^{T}(s)Qx(s)ds$$
$$\leq \lambda_{\max}\left(PE\right)x^{T}\left(0\right)x(0)+\lambda_{\max}\left(Q\right)\int_{-\tau}^{0}x^{T}(s)x(s)ds \tag{25}$$
$$\leq \alpha\lambda_{\max}\left(PE\right)+\alpha\lambda_{\max}\left(Q\right)\int_{-\tau}^{0}d\theta$$
$$\leq \alpha\left[\lambda_{\max}\left(PE\right)+\tau\lambda_{\max}\left(Q\right)\right]$$

On the other hand,

$$V\left(x(t)\right) = x^{T}\left(t\right)PEx(t)+\int_{t-\tau}^{t}x^{T}(s)Qx(s)ds \geq x^{T}\left(t\right)E^{T}REx(t) \tag{26}$$
$$> \lambda_{\min}\left(R\right)x^{T}\left(t\right)E^{T}E^{T}x(t) > \beta\,\lambda_{\min}\left(R\right)$$

Combining (24)-(26) we get:

$$\lambda_{\min}\left(R\right)x^{T}\left(t\right)E^{T}E^{T}x(t) < \alpha\left[\lambda_{\max}\left(PE\right)+\tau\lambda_{\max}\left(Q\right)\right]\cdot e^{\Lambda_{m}t} \tag{27}$$

If the following condition is satisfied:

$$\alpha\left[\lambda_{\max}(PE) + \tau\lambda_{\max}(Q)\right]\cdot e^{\Lambda_m t} < \beta\lambda_{\min}(R), \quad \forall t\in[0,T] \tag{28}$$

then:

$$x^T(t)E^T Ex(t) < \beta, \text{ for all } t\in[0,T] \tag{29}$$

From (28) follows (14). This completes the proof.

In order to improve the previous result, we formulate the following theorem.

Theorem 2. Consider a singular time-delay *s*ystem (5) with

$$x^T(t-\theta)x(t-\theta) < qx^T(t)x(t), \quad q>0, \quad \theta\in[-\tau,0], \quad \forall t\in[0,T] \tag{30}$$

If the matrix A_{22} is invertible and if there exists a positive scalar $\wp$, matrix P, positive define block diagonal matrix $Q = diag\{Q_1,Q_2\}$ and positive define matrix R, such that the following conditions hold:

$$PE = E^T P^T \geq 0 \tag{31}$$

$$PE = E^T RE \tag{32}$$

$$\beta\left[\lambda_{\min}(R) + \rho\lambda_{\min}(Q)\right]e^{-\Lambda_m T} - \alpha\left[\lambda_{\max}(PE) + \rho\lambda_{\max}(Q)\right] < 0 \tag{33}$$

where:

$$\Lambda_m = \max\left[x^T(t)\Xi x(t): \quad x^T(t)PE\,x(t)=1\right] \tag{34}$$

$$\Xi = A^T P^T + PA + Q + PA_d\wp^{-1}A_d^T P^T + q\lambda_{\max}\{\wp I - Q\}I \tag{35}$$

then system (1) is regular, impulse free and finite-time stable with respect to $\{\alpha,\beta,T\}$, $\alpha<\beta$ for all $T>0$.

Proof. From (17), based on properties of matrices $E = diag\{I_r,0\}$ and $Q = diag\{Q_1,Q_2\}$, we have:

$$V(x(t)) = x^T(t)PEx(t) + \int_{t-\tau}^{t} x^T(\theta)Qx(\theta)d\theta \geq x^T(t)E^T REx(t)$$

$$+ \int_{t-\tau}^{t} x^T(\theta)E^T QEx(\theta)d\theta \tag{36}$$

$$> \lambda_{\min}(R)x^T(t)E^T E^T x(t) + \lambda_{\min}(Q)\int_{t-\tau}^{t} x^T(\theta)E^T Ex(\theta)d\theta$$

Combining (24), (25) and (36) we get:

$$\lambda_{\min}(R)x^T(t)E^T E^T x(t) + \lambda_{\min}(Q)\int_{t-\tau}^{t} x^T(\theta)E^T Ex(\theta)d\theta < e^{\Lambda_m t}\alpha\left[\lambda_{\max}(PE) + \rho\,\lambda_{\max}(Q)\right] \tag{37}$$

If the following condition is satisfied:

$$\alpha\left[\lambda_{\max}(PE) + \rho\lambda_{\max}(Q)\right]e^{\Lambda_m t} < \beta\left[\lambda_{\min}(R) + \rho\lambda_{\min}(Q)\right], \quad \forall t\in[0,T] \tag{38}$$

then:

$$x^T(t)E^T Ex(t) < \beta, \text{ for all } t\in[0,T] \tag{39}$$

From (38) follows:

$$\alpha\left[\lambda_{\max}(PE) + \rho\lambda_{\max}(Q)\right]e^{\Lambda_m T} < \beta\left[\lambda_{\min}(R) + \rho\lambda_{\min}(Q)\right] \tag{40}$$

and (33).

Remark 1. Expressions (15) and (34) are known as Rayleigh quotient which minimum can be determined using appropriate standard numerical methods.

Remark 2. Conditions (11) and (30) are main sources of the conservatism in Theorem 1 and 2. Namely, it is difficult to determine the parameter q so that (11) or (30) are satisfied because it is considered that the solution of the system (1) is not known. One way to estimate the parameter q is the simulation of system (5) for known initial conditions.

Furthermore, it is very difficult to numerically solve the inequality (12)-(16) (Theorem 1) and (31)-(35) (Theorem 2). Therefore, the above mentioned theorems have more theoretical than practical significance.

2.1. LMI approach

Finally, by using linear matrix inequalities, we give the sufficient conditions under which the system (5) will be regular, impulse free and finite time stable. LMI approach has been applied in order to get less conservative conditions and to easier solve numerically this problem. These stability conditions have a great practical importance because they are based on standard numerical optimization methods.

Theorem 3. Singular time delayed *s*ystem (5) is regular, impulse free and finite time stable with respect to $\{\alpha, \beta, T\}$, $\alpha < \beta$ if there exist a positive scalar $\wp$, nonsingular matrix P and two positive definite matrices R and Q, such that the following conditions hold:

$$PE = E^T P^T \geq 0 \tag{41}$$

$$PE = E^T R E \tag{42}$$

$$\Xi = \begin{bmatrix} A^T P^T + PA + Q - \wp PE & PA_d \\ A_d^T P^T & -Q \end{bmatrix} < 0 \tag{43}$$

$$\lambda_1 I < R, \quad \lambda_2 I > PE, \quad \lambda_3 I > Q \tag{44}$$

$$\begin{bmatrix} -\beta e^{-\wp T}\lambda_1 & \sqrt{\alpha}\lambda_2 & \sqrt{\alpha\tau}\lambda_3 \\ * & -\lambda_2 & 0 \\ * & * & -\lambda_3 \end{bmatrix} < 0 \tag{45}$$

Proof. The proof of this theorem is divided into two parts. First, we deal with the regularity and impulse-free properties. Second, we treat the finite-time stability property. First we show that the singular delay system (1) is regular and impulse-free. Using (43), it is easy to see that the following holds:

$$A^T P^T + PA - \wp PE < 0 \tag{46}$$

By (41)-(42) we have

$$PE = \begin{bmatrix} P_{11} & 0 \\ P_{21} & 0 \end{bmatrix} = E^T P^T = \begin{bmatrix} P_{11}^{\ T} & P_{21}^{\ T} \\ 0 & 0 \end{bmatrix}, \quad PE = \begin{bmatrix} P_{11} & 0 \\ P_{21} & 0 \end{bmatrix} = E^T RE = \begin{bmatrix} R_{11} & 0 \\ 0 & 0 \end{bmatrix} \tag{47}$$

i.e.

$$P_{11} = P_{11}^{\ T}, \quad P_{21} = 0, \quad R_{11} = P_{11} \tag{48}$$

Based on (46) and (48) we have

$$\begin{bmatrix} \square & \square \\ \square & A_{22}^{\ T} P_{22}^T + P_{22} A_{22} \end{bmatrix} < 0 \tag{49}$$

where the symbol "$\square$" stands for a matrix irrelevant to the following development. From (49) we deduce that

$$A_{22}^{\ T} P_{22}^T + P_{22} A_{22} < 0 \tag{50}$$

i.e. $A_{22} \neq 0$, because $P_{22} \neq 0$ (P is regular matrix). Therefore, based on Lemma 3, we conclude that the system (5) is regular and impulse-free.

Next, we show the stability. Let us consider the Lyapunov-like function (17). Total derivative $\dot{V}(x(t))$ along the trajectories of the system (5) is

$$\begin{aligned} \dot{V}(x(t)) &= \dot{x}^T(t) PE x(t) + x^T(t) PE \dot{x}(t) + \frac{d}{dt} \int_{t-\tau}^{t} x^T(s) Q x(s) d\vartheta \\ &= x^T(t)(A^T P^T + PA) x(t) + 2x^T(t) PA_d x(t-\tau) \\ &\quad + x^T(t) Q x(t) - x^T(t-\tau) Q x(t-\tau) \\ &= \zeta^T(t) \Gamma \zeta^T(t) \end{aligned} \tag{51}$$

where:

$$\zeta^T(t) = \begin{bmatrix} x^T(t) & x^T(t-\tau) \end{bmatrix}, \quad \Gamma = \begin{bmatrix} A^T P^T + PA + Q & PA_d \\ A_d^T P^T & -Q \end{bmatrix} \tag{52}$$

From (43) and (51), one can have:

$$\begin{aligned} \dot{V}(x(t)) &= \zeta^T(t) \Gamma \zeta(t) = \zeta^T(t) \left(\Xi + \begin{bmatrix} \wp PE & 0 \\ 0 & 0 \end{bmatrix} \right) \zeta(t) \\ &= \zeta^T(t) \Xi \zeta(t) + \zeta^T(t) \begin{bmatrix} \wp PE & 0 \\ 0 & 0 \end{bmatrix} \zeta(t) \\ &< \wp x^T(t) PE x < \wp \left(x^T(t) PE x(t) + \wp \int_{t-\tau}^{t} x^T(\vartheta) Q x(\vartheta) d\vartheta \right) \\ &= \wp V(x(t)) \end{aligned} \tag{53}$$

Integrating (53) from 0 to $t \leq T$, follows:

$$V(x(t)) < e^{\wp t} V(x(0)) \tag{54}$$

Then:

$$V\big(x(0)\big) = x^T\,(0)\,PE\,x(0) + \int\limits_{-\tau}^{0} x^T\,(\vartheta)\,Q\,x(\vartheta)\,d\vartheta$$

$$\leq \lambda_{\max}\,(PE)\,x^T\,(0)\,x(0) + \lambda_{\max}\,(Q)\int\limits_{-\tau}^{0}\varphi^T\,(\vartheta)\,\varphi(\vartheta)\,d\vartheta \tag{55}$$

$$\leq \lambda_{\max}\,(PE)\cdot\alpha + \lambda_{\max}\,(Q)\cdot\alpha\int\limits_{-\tau}^{0} d\vartheta \leq \alpha\big(\lambda_{\max}\,(PE) + \tau\cdot\lambda_{\max}\,(Q)\big)$$

On the other hand, we have:

$$V\big(x(t)\big) = x^T\,(t)\,PE\,x(t) + \int\limits_{t-\tau}^{t} x^T\,(s)\,Q\,x(s)\,ds$$

$$= x^T\,(t)\,E^T R\,Ex(t) + \int\limits_{t-\tau}^{t} x^T\,(s)\,Q\,x(s)\,ds \tag{56}$$

$$> \lambda_{\min}\,(R)\,x^T\,(t)\,E^T Ex(t) + \lambda_{\min}\,(Q)\int\limits_{t-\tau}^{t} x^T\,(s)\,x(s)\,ds$$

Combining (25), (26) and (54) leads to:

$$\lambda_{\min}\,(R)\,x^T\,(t)\,E^T E^T\,x(t) < \alpha\big[\lambda_{\max}\,(PE) + \tau\lambda_{\max}\,(Q)\big]\cdot e^{\wp t} \tag{57}$$

If the following condition is satisfied:

$$\alpha\big[\lambda_{\max}\,(PE) + \tau\lambda_{\max}\,(Q)\big]\cdot e^{\wp t} < \beta\lambda_{\min}\,(R), \quad \forall t \in \big[0,T\big] \tag{58}$$

then:

$$x^T\,(t)\,E^T E\,x(t) < \beta, \quad \forall t \in \big[0,T\big] \tag{59}$$

From (58) follows:

$$-\beta\lambda_{\min}\,(R)\,e^{-\wp t} + \alpha\big[\lambda_{\max}\,(PE) + \tau\lambda_{\max}\,(Q)\big] < 0 \tag{60}$$

Let

$$0 < \lambda_1 < \lambda_{\min}\,(R), \quad \lambda_2 > \lambda_{\max}\,(PE), \quad \lambda_3 > \lambda_{\max}\,(Q) \tag{61}$$

then

$$\lambda_1 I < R, \quad \lambda_2 I > PE, \quad \lambda_3 I > Q \tag{62}$$

$$-\beta e^{-\alpha T}\lambda_1 + \alpha\lambda_2 + \alpha\tau\lambda_3 < 0 \tag{63}$$

From (63) we have:

$$-\beta e^{-\wp T}\lambda_1 + \alpha\tau\lambda_3 - \sqrt{\alpha}\lambda_2\,(-\lambda_2)^{-1}\sqrt{\alpha}\lambda_2 < 0 \tag{64}$$

and using Schur complement:

$$\begin{bmatrix} -\beta e^{-\wp T}\lambda_1 + \alpha\tau\gamma_3 & \sqrt{\alpha}\lambda_2 \\ \sqrt{\alpha}\lambda_2 & -\lambda_2 \end{bmatrix} < 0 \tag{65}$$

$$\begin{bmatrix} -\beta e^{-\wp T}\lambda_1 + \alpha\tau\lambda_3 & \sqrt{\alpha} \\ \sqrt{\alpha} & -\lambda_2 \end{bmatrix} - \begin{bmatrix} \sqrt{\alpha\tau}\lambda_3 \\ 0 \end{bmatrix}(-\lambda_3)^{-1}\begin{bmatrix} \sqrt{\alpha\tau}\lambda_3 & 0 \end{bmatrix} < 0 \tag{66}$$

we get (45). This completes the proof.

In order to improve the previous result, we formulate the following theorem.

Theorem 4. Singular time delayed *s*ystem (5) is regular, impulse free and finite time stable with respect to $\{\alpha, \beta, T\}$, $\alpha < \beta$ if there exist a positive scalar $\wp$, nonsingular matrix P, positive definite matrix R and positive definite block diagonal matrix $Q = diag\{Q_1, Q_2\}$, such that the following conditions hold:

$$PE = E^T P^T \geq 0 \tag{67}$$

$$PE = E^T R E \tag{68}$$

$$\Xi = \begin{bmatrix} A^T P^T + PA + Q - \wp PE & PA_d \\ A_d^T P^T & -Q \end{bmatrix} < 0 \tag{69}$$

$$\lambda_1 I < R, \quad \lambda_2 I > PE, \quad \lambda_3 I < Q < \lambda_4 I \tag{70}$$

$$\begin{bmatrix} -\beta[\lambda_1 + \tau\lambda_3]e^{-\gamma T} & \sqrt{\alpha}\lambda_2 & \sqrt{\alpha\tau}\lambda_4 \\ * & -\lambda_2 & 0 \\ * & * & -\lambda_4 \end{bmatrix} < 0 \tag{71}$$

Proof. Combining, (54), (55) and (36) we get:

$$\lambda_{\min}(R)x^T(t)E^T E^T x(t) + \lambda_{\min}(Q)\int_{t-\tau}^{t} x^T(\theta)E^T Ex(\theta)d\theta < e^{\wp t}\alpha[\lambda_{\max}(PE) + \tau\lambda_{\max}(Q)] \tag{72}$$

If the following condition is satisfied:

$$\alpha[\lambda_{\max}(PE) + \tau\lambda_{\max}(Q)]e^{\wp t} < \beta[\lambda_{\min}(R) + \tau\lambda_{\min}(Q)], \quad \forall t \in [0, T] \tag{73}$$

then:

$$x^T(t)E^T Ex(t) < \beta, \text{ for all } t \in [0, T] \tag{74}$$

From (73) follows:

$$-\beta[\lambda_{\min}(R) + \tau\lambda_{\min}(Q)]e^{-\wp t} + \alpha[\lambda_{\max}(PE) + \tau\lambda_{\max}(Q)] < 0 \tag{75}$$

Let

$$0 < \lambda_1 < \lambda_{\min}(R), \quad \lambda_2 > \lambda_{\max}(PE), \quad \lambda_3 < \lambda_{\min}(Q), \quad \lambda_4 > \lambda_{\max}(Q) \tag{76}$$

then

$$\lambda_1 I < R, \quad \lambda_2 I > PE, \quad \lambda_3 I > Q > \lambda_4 I \tag{77}$$

$$-\beta[\lambda_1 + \tau\lambda_3]e^{-\gamma T} + \alpha[\lambda_2 + \tau\lambda_4] < 0 \tag{78}$$

Finally, using a complement, from (78) we get (71).

Remark 3. According to our knowledge, there are no results available yet on finite-time stability in the sense of Definition 4 for a class of linear continuous time-delay systems which use linear matrix inequality and therefore we cannot to compare our results with existing ones.

4. Numerical example

The effectiveness of the results presented in the previous section is now shown by means of numerical example. Due to numerical problems, Theorem 1 and Theorem 2 have

more theoretical than practical significance (Remark 2). For this reason, in the following example, we only consider the stability conditions derived in Theorems 3 and 4.

Example 1. Consider following singular continuous time-delay system:

$$E\dot{x}(t) = Ax(t) + A_d x(t - \tau)$$

$$E = \begin{bmatrix} 1 & 0 & 0 \\ 0 & 1 & 0 \\ 0 & 0 & 0 \end{bmatrix}, \quad A = \begin{bmatrix} -2 & 1 & 0 \\ 0 & -2 & 0 \\ -1 & 0 & -2 \end{bmatrix}, \quad A_d = \begin{bmatrix} 1 & 1 & 1 \\ 1 & 1 & 1 \\ 1 & 1 & 1 \end{bmatrix}, \quad \tau = 1 \tag{79}$$

In order to verify stability properties of the system (79), the system operation is simulated under the conditions $\phi(t) = \begin{bmatrix} 1 & 1 & 1 \end{bmatrix}^T$, $t \in [-\tau, 0]$. Figures 1-2 show the initial state response and the norm of initial state response of the system (79). It is observed that the values of state variables $x_i \to \infty$, $i = 1, 2, 3$ when $t \to \infty$, which proves that the system (79) is not asymptotically stable.

Now we seek the maximum allowed upper bound of T, T_m, for the time interval $[0, T]$ so system (79) is regular, impulse free and FTS with respect (α, β, T), $\alpha = 3$, $\beta = 100$ using Theorem 3 and Theorem 4.

Based on Theorem 3, for fixed $\wp = 2.93$, we can obtain the following feasible solutions:

$$P = \begin{bmatrix} 1366.3 & -210.6 & -479.4 \\ -210.6 & 1808.0 & 1131.8 \\ 0.0 & 0.0 & 1394.6 \end{bmatrix}, \quad Q = \begin{bmatrix} 2699.7 & 137.2 & 1636.7 \\ 137.2 & 3070.4 & 1265.7 \\ 1636.7 & 1265.7 & 1556.9 \end{bmatrix},$$

$$R = \begin{bmatrix} 1366.3 & -210.6 & 0.0 \\ -210.6 & 1808.0 & 0.0 \\ 0.0 & 0.0 & 4133.3 \end{bmatrix}, \quad \begin{array}{l} \lambda_1 = 1281.9, \ \lambda_2 = 1892.8, \\ \lambda_3 = 4469.1, \\ T_m = 0.65 \end{array}$$
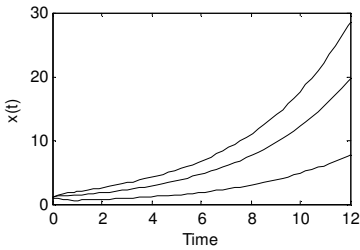
Fig. 1 The initial state response $(x(t))$ of the system (79).
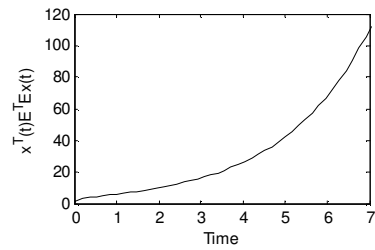
Fig. 2 The norm of initial state response $(x^T(t)E^T Ex(t))$ of the system (79).

Using Theorem 4, for fixed $\wp = 2.68$ we get:

$$P = \begin{bmatrix} 14.00 & -1.88 & -5.85 \\ -1.88 & 27.27 & 12.78 \\ 0.0 & 0.0 & 30.13 \end{bmatrix}, \quad Q = \begin{bmatrix} 69.24 & -0.13 & 0.00 \\ -0.13 & 71.65 & 0.00 \\ 0.00 & 0.00 & 71.54 \end{bmatrix},$$

$$R = \begin{bmatrix} 14.00 & -1.88 & 0.00 \\ -1.88 & 27.27 & 0.00 \\ \hline 0.00 & 0.00 & 52.37 \end{bmatrix}, \quad \begin{array}{ll} \lambda_1 = 13.67, & \lambda_2 = 27.61, \\ \lambda_3 = 69.16, & \lambda_4 = 71.79 \\ T_m = 1.24 \end{array}$$

Further, based on simulation of the system (79), the parameter T_m is estimated (T_{est}) from the norm of initial state response $(x^T(t)E^T Ex(t))$ and the following value is obtained: $T_{est} = 6.8$.

According to data, it can be seen that the condition of Theorem 4 is less conservative ($T_m = 1.24$) than the condition of Theorem 3 ($T_m = 0.65$), because it gives T_m that is nearer to the estimated value, $T_{est} = 6.8$.

5. CONCLUSION

This paper extends some of the basic results in the area of the non-Lyapunov stability to the particular class of linear singular time-delay systems. The finite-time stability problems of linear singular time-delay systems are studied. Using classical and LMI approaches novel sufficient conditions for finite-time stability are presented. The obtained LMI conditions can be checked by using the standard numerical optimization methods. Finally, numerical example is given to show the effectiveness of the proposed approaches.

References

[1] Campbell S L (1980) *Singular Systems of Differential Equations*, Pitman, London.
[2] Müller P C (1993) Stability of Linear Mechanical Systems with Holonomic Constraints, *Appl. Mech. Rev*., 46 (11) pp. 60–164.
[3] Pantelides C C, Gridsis D, Morison K R and Sargent R W H (1988) The mathematical modeling of transient systems using differential-algebraic equations, *Comp. & Chem. Eng*., 12 pp. 449–454.
[4] Kumar A and Daoutidis P (1997) Control of nonlinear differential algebraic equation systems: an overview, Proc. NATO Advanced Study Institute on Nonlinear Model Based Process Control, Antalya, Turkey, August 10-20, pp. 311-344.
[5] Rehm A and Allgower F (2004) H-Infinity Control of Descriptor Systems: An Application from Binary Distillation Control, *Proc. 7 International Symposium on Advanced Control of Chemical Processes*, Hong Kong, 11-14 January.
[6] Xu S, Dooren P V, Stefan R and Lam J (2002) Robust stability and stabilization for singular systems with state delay and parameter uncertainty, *IEEE Trans. Autom. Control*, 47(7) pp. 122–1128.
[7] Xu S, Lam J, Yang C (2003) Robust H∞ control for uncertain singular systems with state delay, Int. J. Robust Nonlinear Control, 13(13) pp. 1213–1223.
[8] Fridman E (2002) Stability of linear descriptor systems with delay: a Lyapunov-based approach, *J. Math. Anal. Appl*., 273 pp. 24–44.
[9] Yue D and Han Q L (2005) Delay-dependent robust H∞ controller design for uncertain descriptor systems with time-varying discrete and distributed delays, *IEE Proc. Control Theory Appl*., 152(6) pp. 628–638.
[10] Zhu S, Zhang C, Cheng Z and Feng J (2007) Delay-dependent robust stability criteria for two classes of uncertain singular time-delay systems, *IEEE Trans. Autom. Control*, 52(5) pp. 880–885.

[11] Xu S, Lam J and Zou Y (2008) An improved characterization of bounded realness for singular delay systems and its applications, *Int. J. Robust Nonlinear Control*, 18(3) pp. 263–277.

[12] Dai L (1981) Singular Control Systems, Springer, Berlin.

[13] Debeljkovic D Lj, Lazarevic M P, Koruga Dj and Tomasevic S (1997) Finite time stability of singular systems operating under perturbing forces: Matrix measure approach, *Proc. AMSE Conference, Melbourne Australia*, October 29 – 31 pp. 447–450.

[14] Kablar N A and Debeljkovic D Lj (1998) Non-Lyapunov stability of linear singular systems: Matrix measure approach, *Proc. Mathematical Theory of Networks and Systems*, Padova, Italy, July 6-10.

[15] Kablar N A, Debeljkovic D Lj (1998) Finite time stability of time varying singular systems, *Proc IEEE Decision and Control*, Florida, USA, December 10-12 pp. 3831-3836.

[16] Yangy C, Zhang Y Q, Linz Y and Zhouy L (2006) Practical stability of closed-loop descriptor systems, *Int. J. Syst. Sci.*, 37(14) pp. 1059–1067.

[17] Jun-E F, Zhen W, Jia-Bing S (2005) Finite-time control of linear singular systems subject to parametric uncertain and disturbances, Acta Autom. Sin., 31(4) pp. 634-637.

[18] Yang C Y, Jing X, Zhang Q L and Zhou L N, Practical stability analysis and synthesis of linear descriptor systems with disturbances, *Int. J. Autom. Comput.*, 5(2) (2008) pp. 138–144.

[19] Yang C, Zhang Q and Zhou L, Practical stability of descriptor systems with time delays in terms of two measurements, *J. Franklin Inst.*, 343 (2006) pp. 635–646.

[20] Su M, Wang S and Zhang X, Finite-Time Stabilization for Singular Linear Time-delay Systems with Time-varying Exogenous Disturbance, *Adv. Mater. Res.*, 490-495 (2012) pp. 2459-2463.

S. B. STOJANOVIČ, D. LJ. DEBELJKOVIĆ

MATHEMATICAL MODEL OF AERIAL ROBOTS AS THE BASIS FOR NEW RESEARCH

Mirjana Filipović

[1] *Mihajlo Pupin Institute, The University of Belgrade, Volgina 15, 11060 Belgrade, Serbia, e-mails: mirjana.filipovic@pupin.rs*

Abstract. *The aim of this paper is a detailed* synthesis *and analysis Cable-suspended Parallel Robot – CPR (aerial robot), which should enable their strong progress. This would be reflected in the implementation of highly-automated system that would lead the camera precisely in space with minimum participation of human labor. Setting and achieving this goal provides a much wider possibilities for its future use. The unique general type of the CPR-B mathematical model is defined. Kinematic model is generated for the system via Jacobi matrix. An adequate choice of generalized coordinates (in this paper, the internal coordinates), provides a mathematical model that illuminates the mapping of internal (resultant forces acting on the shaft of each motor) and external forces (acting on a camera carrier) by the Jacobi matrix on motion dynamics of each motors. Such an operation of this system can provide only with application of his high-fidelity mathematical model during the synthesis and analysis, which would further enable the development and application of modern control law. Several numerical examples are used for the CPR model validation.*

Nomenclature

DOF	degree of freedom
CPR	Cable-suspended Parallel Robot
$t(s)$	time
$dt = 0.0001[s]$	sample time
$g = 9.81[m/s^2]$	gravitational acceleration
$p = [x \quad y \quad z]^T[m]$	position of camera carrier in space of Cartesian coordinates (external coordinate)
$i = 1, 2, 3...$	total number of DOF
$\phi = [\theta_1 \quad \theta_2 \quad \theta_3]^T[rad]$	vector of internal coordinates
$F_b = [F_1 \quad F_2 \quad F_3]^T[N]$	vector resultant force acting on the shaft of each motor (motor force load)

$F_p = [F_x \quad F_y \quad F_z]^T [N]$ — force acting on the camera carrier

$P_p = [P_{px} \quad P_{py} \quad P_{pz}]^T [N]$ — perturbation force acting on the camera carrier

$F = (F_p + P_p)[N]$ — whole forces acting on a camera carrier

$M_b = [M_1 \quad M_2 \quad M_3]^T [Nm]$ — motor moment load

$\theta_i (\theta_i^o)[rad]$ — rotation angle of the motor shaft after the reducer (desired value)

$R_i = 0.15[m]$ — winch radius (it is assumed that all 3 winch have the same radius, than in *Example 3*)

J_b — Jacobi matrix

$R_{ri} = 0.917(\Omega)$ — rotor circuit resistance

$u_i[V]$ — voltage

$i_i[A]$ — rotor current

$C_{Ei} = 3.3942[V/(rad/s)]$ — proportionality constant of electromotive force

$C_{Mi} = 2.5194[Nm/A]$ — proportionality constant of the moment

$B_{Ci} = 0.0670[Nm/(rad/s)]$ — coefficient of viscous friction

$J_{ri} = 1.5859[kgm^2]$ — inertia moment of the rotor and reducer

$G_{vi} = \dfrac{J_{ri} \cdot R_{ri}}{C_{Mi}} = 0.1787$ — characteristic of motor inertia

$L_{vi} = \dfrac{R_{ri} \cdot B_{Ci}}{C_{Mi}} + C_{Ei} = 3.4186$ — characteristic of motor damping

$S_{vi} = \dfrac{R_{ri}}{C_{Mi}} = 0.364$ — geometric characteristic of the motor

$m = 1[kg]$ — mass of the camera carrier

$d = 3.2[m]$ — length of the recorded field

$s = 2.2[m]$ — width of the recorded field

$v = 2.0[m]$ — height of the recorded field

$\delta\theta_i(t_o)=0(rad), \delta\dot{\theta}_i(t_o)=0[rad/s]$ — initial deviation of motor rotating angle

$K_{lp} = diag[800 \quad 3500 \quad 3000]$ — positional, velocity amplification for motion control

$K_{lv} = diag[60 \quad 120 \quad 110]$

$\Diamond = 0.5$ — factor that characterizes two parallel guided ropes

1. Introduction

The goal of this research is to show modeling and control of the Cable-suspended Parallel Robot (CPR). Similar systems were analyzed and modeled as presented by the following publications.

In paper [1], the design of a planar three-degree-of- freedom parallel manipulator is considered from a kinematic viewpoint. Four different design criteria are established and used to produce designs having optimum characteristics.

The paper [2] presents the first and second order kinematic analysis of a three-degree-of-freedom 3-RPS parallel robot mechanism. The position and orientation parameters of the moving platform of this mechanism are six.

In paper [3] authors present algorithms that enable precise trajectory control of NIMS3D, an under constrained, three-dimensional cabled robot intended for use in actuated sensing. They begin by offering a brief system overview and then describe methods to determine the range of operation of the robot. Next, a discrete-time model of the system is resented.

In paper [4] author presents several prototypes of wire-driven parallel robots, recently designed and which use two different actuation schemes. Two of them have been completed and submitted to extensive tests. These tests have allowed determining interesting open problems related to kinematics that are presented.

The wrench-closure workspace of parallel cable-driven mechanisms is the set poses of their mobile platform for which the cables can balance any external wrench. The determination of this workspace is an important issue in [5] since the cables can only pull and not push on the mobile platform.

Parallel cable-driven Stewart-Gough platforms consist of an end-effector which is connected to the machine frame by motor driven cables. Since cables can transmit only tension forces, at least $m = n + 1$ cables are needed to tense a system having n degrees-of-freedom. This results in a kinematical redundancy and leads to a $(m - n)$-dimensional solution space for the cable force distribution presented in [6].

This paper presents the recent results from a newly designed parallel wire robot which is currently under construction. Firstly, an overview of the system architecture is given and technically relevant requirements for the realization are identified. A technique to compute and transfer an estimation of the workspace to CAD tools is presented in [7].

The paper [8] presents an auto-calibration method for over constrained cable-driven parallel robots using internal position sensors located in the motors. A calibration workflow is proposed and implemented including pose selection, measurement, and parameter adjustment.

Wire-driven parallel robot has attracted the interest of researchers since the very beginning of the study of parallel robots [9]. This type of robot has the advantage of having light mobile mass, simple linear actuators with possibly relatively large stroke and less risk of interference between the legs. On the other hand their major drawback is that wire actuator can only pull and not push.

A nonlinear dynamic analysis of the suspended cable system is carried out with some sensible results presented in [10] that could be useful to the real engineering of LSRT.

Integrated mechanical, electronic, optic and automatic control technologies are employed to make considerable improvement upon the same system.

For the requirement of trajectory tracking of large spherical radio telescopes, a large fine tuning platform based on the Stewart platform is presented in papers [11] and [12]. The mathematical model for kinematic control is developed with coordinate transformation, and a dynamic analysis is carried out using the Jacobi matrix, which, with a singularity analysis, built a solid base for the tracking control.

This work was done for the suspension system in four points, i.e. to be hung on all four edges of the workspace shape parallelepiped. It is a necessary geometric condition so as to provide camera motion through the entire space. See Fig. 1.

Camera's carrier moves in space freely allowing the capture of objects from above. It gives a unique feeling to the event viewer to follow smoothly from an unusual proximity, and that is very close to the action regardless of the size of observed space. Free motion in space opens up completely new and unique perspective. The commands for the synchronized motion of each winch are provided, with control of motion of each motor, which ultimately provides three-dimensional continuous camera motion.

The gyro sensor, which is installed in the carrier, is stabilized towards the horizon.

The CPR system should fly over the audience without being able to be off and fall to the ground. The whole system is very reliable in the physical sense, because there is only minimal possibility that the camera carrier falls to the shot ground.

This would happen only if both ropes broke at the same time. Two parallel guided ropes through the system are inevitable for the physical functioning of the system in Fig. 1.

Winch 4 is driven by a motor that generates the angular displacement θ_4 for winding or unwinding fiber-optic cable, depending on the position of the camera carrier in the space.

The purpose of the motor angular displacement θ_4 is used to ensure that the fiber-optic cable is never too tight or too loose and it is used to control the position of the camera relative to the moving objects.

The CPR system has different areas of applications and promising research future. Our goal is to implement this system with maximum precision.

The Section II represents a detailed description of the CPR-B system. The same Section describes the mathematical model for the CPR-B. The samples of the system responses are analyzed for different conditions in section III. In the section IV there are concluding remarks.

2. Mathematical Model of the Cable-suspended Parallel Robot – CPR-B

In this paper, a new original CPR-B has been developed. Over the pulley system, ropes are run on the winches (reel) 1, 2, 3, powered by motors.

First and second motors are used to wind up the ropes about the coils. During the rotation one side is winding while another side is unwinding. See Fig. 2.

The third motor is used to wind up the two ropes about the coil only in one direction. Those motion produce winding or unwinding of both ropes at the same time. This can be seen in Figure 1. Ropes coil on winches has radius R.

Synchronous motion of the motors produces camera carrier to move in the x, y, z

Cartesian space.
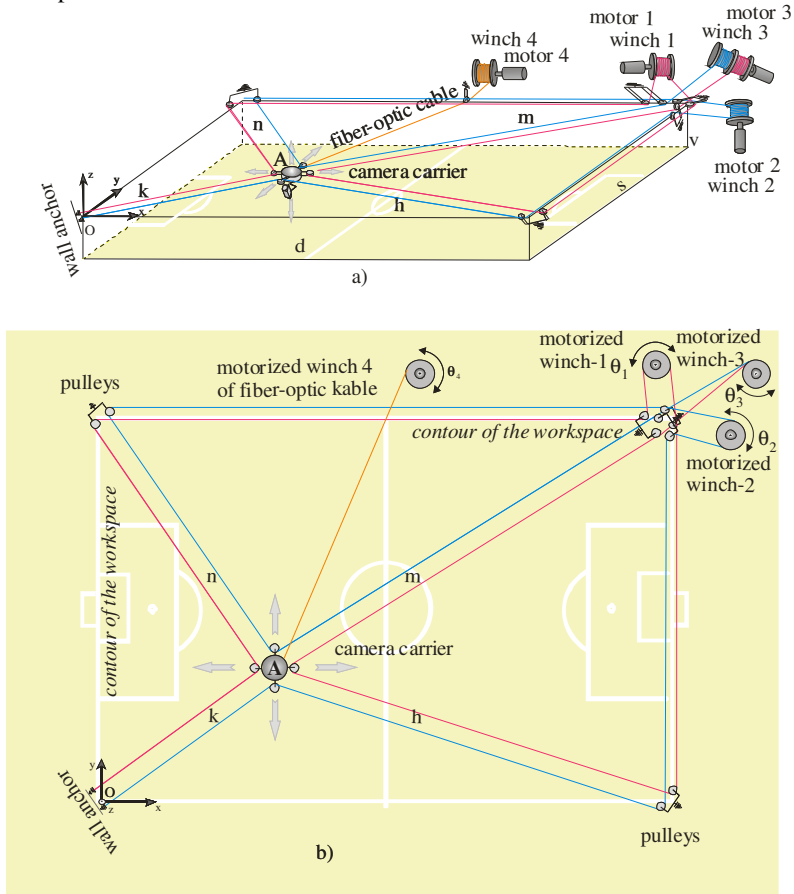
Figure 1. CPR-B, a) in 3D, b) top view.

The desired motion trajectory of the camera is defined in x, y, z, Cartesian coordinates, and it is generated by motion of three motors θ_1, θ_2, θ_3. The kinematic model of the CPR-B has been developed as essential part for solving the CPR-B dynamics. See Figure 1.

The relation between the camera motion in the Cartesian space x, y, z and angular positions of each motor θ_1, θ_2, θ_3 is solved by the Jacobi matrix J_b, which connects velocities of external coordinates changes $\dot{p} = [\dot{x} \quad \dot{y} \quad \dot{z}]^T$ with velocities of internal coordinates changes $\dot{\phi} = [\dot{\theta}_1 \quad \dot{\theta}_2 \quad \dot{\theta}_3]^T$. For generation of any trajectory in x, y, z space, it is necessary to provide very precise and mutually coordinated motion of all three motors θ_1, θ_2, θ_3.

The geometrical relationship between the lengths k, h, m, n, and Cartesian coordinates x, y, z, is defined by the following equations:

$$k = \sqrt{x^2 + y^2 + z^2} \ . \tag{1}$$

$$h = \sqrt{(d - x)^2 + y^2 + z^2} \ . \tag{2}$$

$$m = \sqrt{(d - x)^2 + (s - y)^2 + z^2} \ . \tag{3}$$

$$n = \sqrt{x^2 + (s - y)^2 + z^2} \ . \tag{4}$$

For every sampling time the relations are defined:

$$\frac{\Delta\theta_1}{\Delta t} \cdot R = \frac{\Delta k}{\Delta t} + \frac{\Delta n}{\Delta t} \ . \tag{5}$$

$$\frac{\Delta\theta_2}{\Delta t} \cdot R = \frac{\Delta k}{\Delta t} + \frac{\Delta h}{\Delta t} \ . \tag{6}$$

$$\begin{aligned}\frac{\Delta\theta_3}{\Delta t} \cdot R &= \frac{\Delta m}{\Delta t} + \frac{\Delta n}{\Delta t} + \frac{\Delta\theta_2}{\Delta t} \cdot R \\ \frac{\Delta\theta_3}{\Delta t} \cdot R &= \frac{\Delta m}{\Delta t} + \frac{\Delta h}{\Delta t} + \frac{\Delta\theta_1}{\Delta t} \cdot R\end{aligned} \ . \tag{7}$$

The equation (8) is obtained by substituting (5) and (6) into the (7):

$$\frac{\Delta\theta_3}{\Delta t} \cdot R = + \frac{\Delta k}{\Delta t} + \frac{\Delta h}{\Delta t} + \frac{\Delta m}{\Delta t} + \frac{\Delta n}{\Delta t} \ . \tag{8}$$

If the sampling time Δt is small enough it follows that:

$$\dot{\theta}_1 \cdot R = \dot{k} + \dot{n} \ . \tag{9}$$

$$\dot{\theta}_2 \cdot R = \dot{k} + \dot{h} \ . \tag{10}$$

$$\dot{\theta}_3 \cdot R = \dot{k} + \dot{h} + \dot{m} + \dot{n} \ . \tag{11}$$

By differentiating (1)-(4) and substituting them into the (9)-(11), the relationship between velocities of external coordinates changes $\dot{p} = [\dot{x} \quad \dot{y} \quad \dot{z}]^T$ and velocities of internal coordinates changes $\dot{\phi} = [\dot{\theta}_1 \quad \dot{\theta}_2 \quad \dot{\theta}_3]^T$ has been obtained:

$$\dot{\phi} = J_b \cdot \dot{p} \ . \tag{12}$$

$$J_b = \begin{bmatrix} J_{b11} & J_{b12} & J_{b13} \\ J_{b21} & J_{b22} & J_{b23} \\ J_{b31} & J_{b32} & J_{b33} \end{bmatrix}.$$
(13)

It is evident that Jacobi matrix J_b in (13) is not diagonal but full matrix. The elements of this matrix beyond diagonal show the strong coupling between the external and internal coordinates.

The kinetic energy E_k and potential E_p energy of the camera carrier motion with mass m are given in the following equations:

$$E_k = \frac{1}{2} \cdot m \cdot \dot{x}^2 + \frac{1}{2} \cdot m \cdot \dot{y}^2 + \frac{1}{2} \cdot m \cdot \dot{z}^2.$$
(14)

$$E_p = m \cdot g \cdot z.$$
(15)

First the analysis was done where the ropes are rigid. In that case a system mathematical model has the following form:

$$u = G_v \cdot \ddot{\phi} + L_v \cdot \dot{\phi} + S_v \cdot M_b.$$
(16)

Vector equation (16) is given by applying Lagrange's equation on generalized coordinates θ_1, θ_2, θ_3.
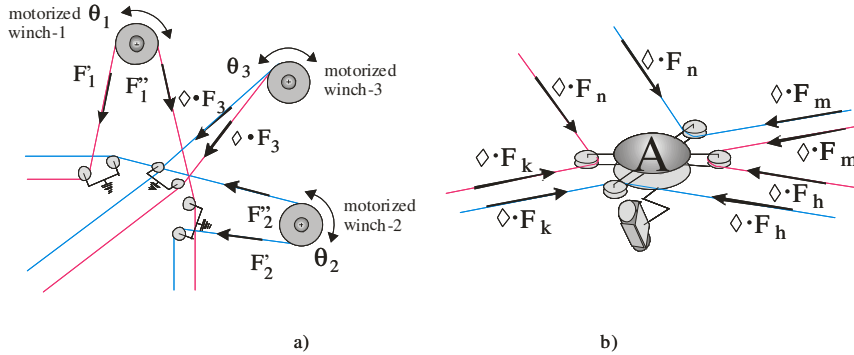
Figure 2. a) The ropes forces before motor 1, motor 2 and motor 3 and after motor 1 and motor 2, b) the ropes forces which carry a camera.

Where: $u = [u_1 \quad u_2 \quad u_3]^T$, $G_{v(3x3)} = diag\, G_{vi}$, $L_{v(3x3)} = diag\, L_{vi}$, $S_{v(3x3)} = diag\, S_{vi}$,
$a_{cc} = [0 \quad 0 \quad -g]^T$.

$$M_b = F_b \cdot R.$$
(17)

$$F_b = \frac{\left((J_{\diamond b})^T \right)^{-1}}{R} \cdot F.$$
(18)

$$F = \left(F_p + P_p \right) \cdot \tag{19}$$

$$F_p = m \cdot (\ddot{p} + a_{cc}) \,. \tag{20}$$

$$C_b = \frac{\left(\left(J_{\Diamond b} \right)^T \right)^{-1}}{R} \,. \tag{21}$$

$$J_{\Diamond b} = f(\Diamond, J_b) \,. \tag{22}$$

Since the CPR-B has two parallel ropes, suspending cameras in all four directions, then (22) has the following form:

$$J_{\Diamond b} = \Diamond \cdot J_b \,. \tag{23}$$

The presence of factors $\Diamond$ is a consequence of structural systems with Fig. 1.

$\Diamond = \dfrac{1}{2}$ is a factor which multiplies only the direction of two parallel ropes. In this direction, a force in each rope is a half of the force impact F that is acting on the camera carrier. Observed CPR-B model has two ropes from a camera carrier to all four-point suspension (line k, h, m, n).

The relation between the resultant forces F_b and total force F acting on a camera carrier in Cartesian space is given by (18). This is a geometrical relationship, which is uniquely defined.

In order to obtain the relationship between internal and external forces, the virtual work principle can be applied. Equation (18) is particularly important because it participates in the configuration of the CPR-B dynamic model.

Vector resultant force acting on the shaft of each motor is $F_b = [F_1 \quad F_2 \quad F_3]^T$.

Substituting (17)-(23) into the (16) produce a dynamic model of CPR-B which is expressed in (24):

$$u = G_v \cdot \ddot{\phi} + L_v \cdot \dot{\phi} + S_v \cdot R \cdot C_b \cdot F \,. \tag{24}$$

Matrix C_b describes a strong coupling between the presented motors.

Control law is selected by the local feedback loop for position and velocity of the motor shaft in the following form:

$$u_i = K_{lpi} \cdot (\theta_i^o - \theta_i) + K_{lvi} \cdot (\dot{\theta}_i^o - \dot{\theta}_i) \,. \tag{25}$$

3. Simulation Examples

The example CPR-B from Fig. 1 is analyzed. In order to make results comparable, they are made for the same desired trajectory and the same all other system parameters, as defined in the Nomenclature.

Camera carrier has the starting point $p_{start}^{o} = [0.4 \quad 0.1 \quad -0.2][m]$, and the end point $p_{end}^{o} = [2.6 \quad 1.7 \quad -0.2][m]$. See Fig. 3a).
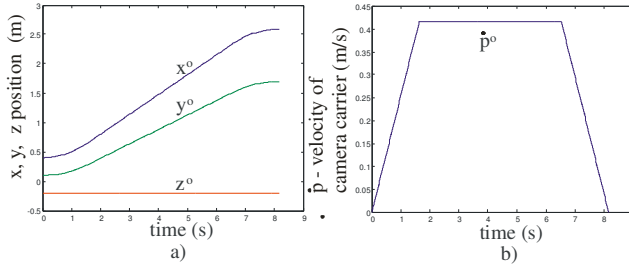
Figure 3. Reference frame a) position x^{o}, y^{o}, z^{o}, b) velocity of camera carrier $p_{max}^{o} = 0.417(m/s)$.

The level of control signals is given in Fig. 4f) and does not exceed the limits of $\pm 24[V]$. In Fig. 4c) there are three resultant forces that are not exceeding $34[N]$.
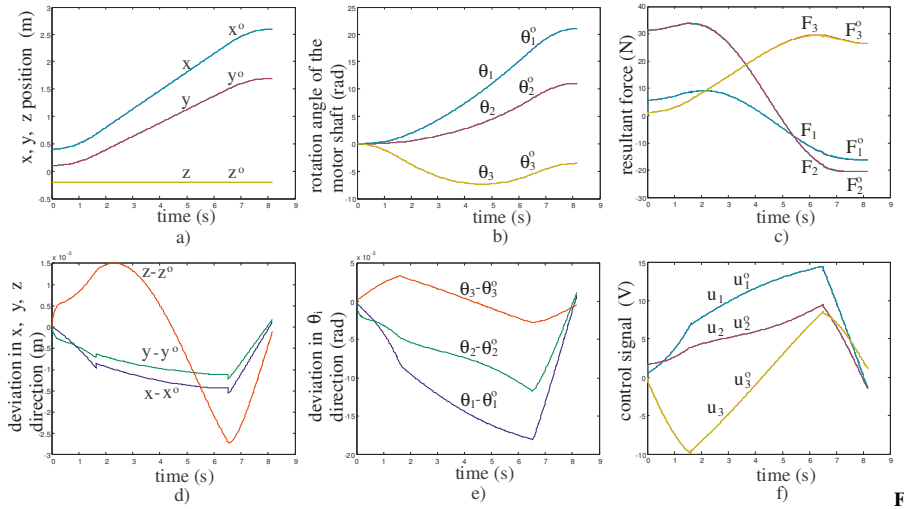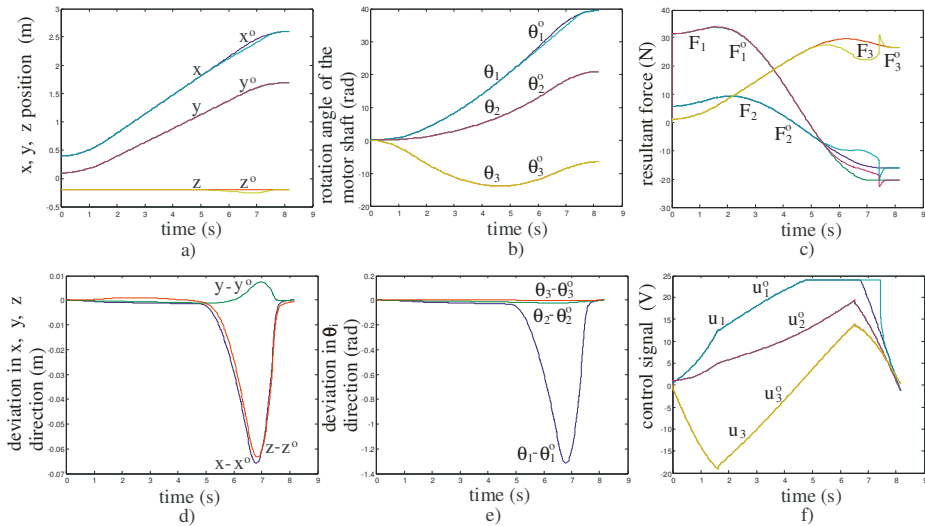

Figure 4. a) Reference frame and real coordinate x, y, z of camera carrier, b) reference and real coordinate θ_1, θ_2, θ_3 of motor shaft, c) reference frame and real resultant forces F_i, d) deviation real from the reference frame values of a motion trajectory of camera carrier, e) deviation real from the reference frame values of a motion trajectory of motor shaft, f) reference frame and real control signal u_i, *(for CPR-B, Example 1)*.

The camera moves in x and y directions, whiles the coordinate z is constant. Camera motion velocity has a trapezoid form and $\dot{p}_{max}^{o} = 0.417[m/s]$, as shown in Fig. 3b). The motors are of Heinzman SL100F type and gears are HFUC14-50-2A-GR+belt.

Example 1: The mathematical model of the system, at the reference frame, is defined by (12)-(24). The radius of motorized pulley is $R_1 = R_2 = R_3 = 0.15(m)$, in this Example. All three motor's angular positions θ_1, θ_2, and θ_3 are involved in the coordinated task generation. This is clearly shown in Fig. 4b), and it is a proof that all these motions are mutually coupled. There is a good tracking of a desired trajectory at the level of motor motions (in the order of about $10^{-3}[rad]$, see Fig. 4e)) and at the level of motion of the camera carrier (on the order of about $10^{-3}[m]$, see Fig. 4a) and Fig. 4d)).

Example 2: All system and control parameters are the same as in the Example 1. This example is done with one illogical assumption, which is the case when the system user assumes that the system at the reference level is uncoupled. In that case the Jacobi matrix has the diagonal form:

$$\dot{\phi} = J_{b\oplus} \cdot \dot{p} . \tag{26}$$

$$J_{b\oplus} = \begin{bmatrix} J_{b11} & 0 & 0 \\ 0 & J_{b22} & 0 \\ 0 & 0 & J_{b33} \end{bmatrix} . \tag{27}$$

$$u = G_v \cdot \ddot{\phi} + L_v \cdot \dot{\phi} + S_v \cdot M_{b\oplus} . \tag{28}$$

$$M_{b\oplus} = F_{b\oplus} \cdot R . \tag{29}$$

The resultant force is defined as:

$$F_{b\oplus} = \frac{\left(\left(J_{\Diamond b \oplus}\right)^T\right)^{-1}}{R} \cdot F . \tag{30}$$

$$C_{b\oplus} = \frac{\left(\left(J_{\Diamond b \oplus}\right)^T\right)^{-1}}{R} . \tag{31}$$

$$J_{\Diamond b\oplus} = \Diamond \cdot J_{b\oplus} . \tag{32}$$

$$u = G_v \cdot \ddot{\phi} + L_v \cdot \dot{\phi} + S_v \cdot R \cdot C_{b\oplus} \cdot F . \tag{33}$$

Directly follows that the matrix $C_{b\oplus}$ is diagonal like matrix $J_{b\oplus}$.

Unlike the previous example, the mathematical model of the system at the reference level in this example is defined by (26), (27), (14), (15), (28)-(30), (19), (20), (31)-(33). At the real level the system is coupled and its kinematic and dynamic model is defined by (12)-(24).

Fig. 5a) shows the results of the camera carrier motion in all three directions of the Cartesian coordinate frame x, y, z and the reference frame x^o, y^o, z^o.

Trajectory of motor angular positions at the real frame θ_1, θ_2, θ_3 and reference θ_1^o, θ_2^o, θ_3^o frame is given in Fig. 5b).
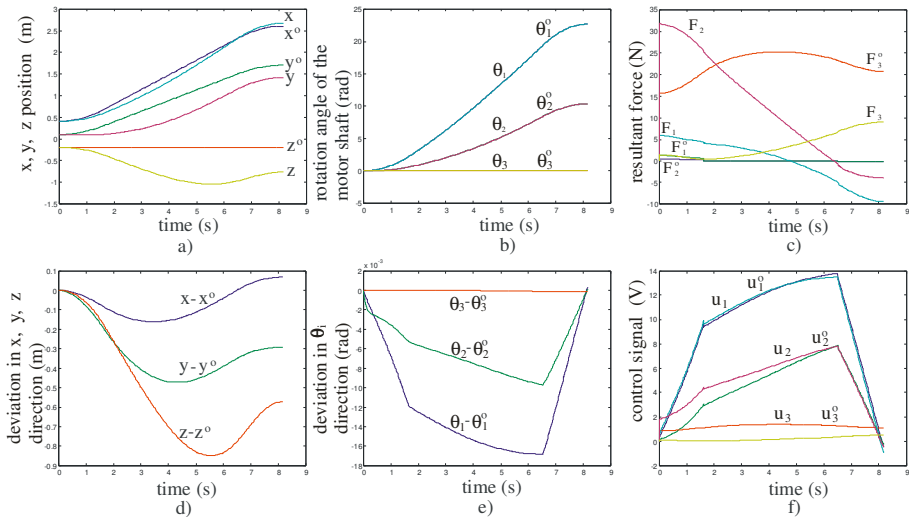
Figure 5. a) Reference frame and real coordinate x, y, z of camera carrier, b) reference and real coordinate θ_1, θ_2, θ_3 of motor shaft, c) reference frame and real resultant forces F_i, d) deviation real from the reference frame values of a motion trajectory of camera carrier, e) deviation real from the reference frame values of a motion trajectory of motor shaft, f) reference frame and real control signal u_i, *(for CPR-B, Example 2)*.

Since the positional control law is applied (with local feedback on the position and velocity) for each motor angular position, defined in equation (25), the control of motor motion is ideal, see Fig. 5b) and Fig. 5e). However, the coupling characteristics are not taken into the consideration at the reference frame, and because of that there is no good enough tracking of a real trajectory comparing to the reference signal in the Cartesian space, see Fig. 5a) and Fig. 5d). The unknown coupling characteristics significantly affect the accuracy of the trajectory tracking, which value reaches $(z - z^o)_{min} = -0.85(m)$. This will happen in the period of $5.3[s]$. The value of control signals is given in Fig. 5f). In Fig. 5c) there are three resultant forces, until to $32[N]$.

Example 3: The importance of this example is that the radius of motorized pulley is $R_1 = R_2 = R_3 = 0.08(m)$.

All other system parameters are the same comparing to the one in Example 1. The system mathematical model at the reference frame is defined by equations (12)-(24). It can be seen in Fig. 6d) and Fig. 6e) that the desired trajectory at the camera motion frame

and at the motor motion frame is worse than in Example 1. This is because the selected radiuses of motorized pulleys are smaller.

The first motor achieves the saturation point at $t = 4.7[s]$ referred to the real and reference frames. At the reference frame the signal goes out of saturation at $6.8[s]$, while at the real frame it goes out of saturation at $t = 7.45[s]$, see Figure 6f). The second and third motors do not enter saturation at all.

This causes a significant deviation of the real position of first motor comparing to the reference frame, which reaches value $(\theta_1 - \theta_1^o)_{min} = -0.137[rad]$, see Fig. 6b) and Fig. 6e). This is all reflected in a bad position tracking of the camera carrier in the Cartesian coordinates $((z - z^o)_{min} = -0.063[m], (x - x^o)_{min} = -0.068[m])$, see Fig. 6d). The resultant forces in Fig. 6c) are up to $35[N]$.

Reducing the radius of all three motorized pulleys significantly affects the dynamics of the motor i.e. it increases their speed.

This analysis shows that the motion dynamics of individual motors depends significantly on the choice of CPR-B construction type and its parameters.

This example confirms the property of the coupling between the motor motion and camera motion, as well.

Figure 6. a) Reference frame and real coordinate x, y, z of camera carrier, b) reference and real coordinate θ_1, θ_2, θ_3 of motor shaft, c) reference frame and real resultant forces F_i, d) deviation real from the reference frame values of a motion trajectory of camera carrier, e) deviation real from the reference frame values of a motion trajectory of motor shaft, f) reference frame and real control signal u_i, *(for CPR-B, Example 3)*.
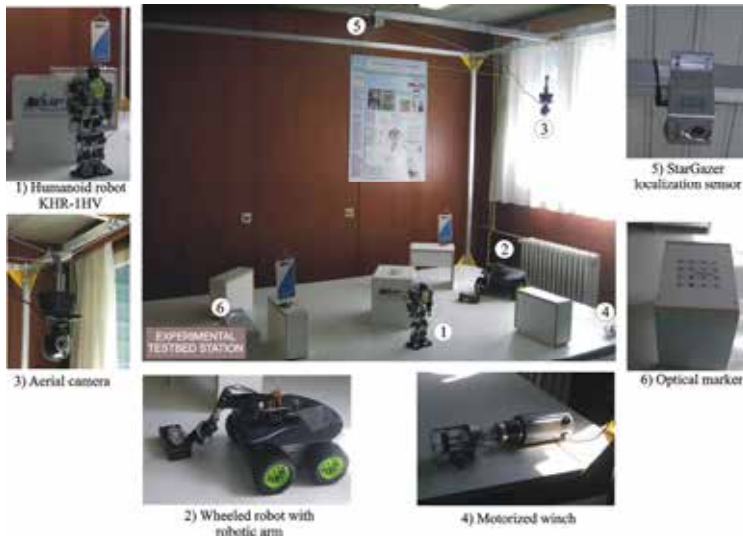
Figure 7. Organized work space with CPR system.

The CPR-B is modeled and analyzed by software package AIRCAMB.

The CPR device is developed in the Mihajlo Pupin Institute and is used to observe space. It is a part of more complex system presented in [13], see Fig. 7. The CPR observes the area in which the humanoid robot and robotic vehicle.

4. Conclusion

The unique general type of the CPR-B mathematical model is defined.

It is clear that the system has double led ropes that move the camera carrier through the 3D space. Another import specification of the system is reflected in the work done by the first and the second motor within construction. Each motor unwinds the rope on one side, and winds it on the other side, while the third motor unwinds or winds two ropes at the time only from one side. These properties have an important influence on the complexity of both kinematics and dynamics of the CPR-B model. Kinematic model is generated for the system via Jacobi matrix. The presented CPR-B model is functionality generated by formulating and applying its highly authentic kinematic and dynamic model during synthesis and analysis which will enable further development and implementation of the current control laws. Software packages AIRCAMB is developed and used for individual and comparative analysis of the CPR-B from various aspects. The influence of changing any parameters of the system (workspace dimensions, the mass of a camera carrier, change the size and dynamics of power disturbances, the choice of control law, the reference trajectory, and the presence of singularity avoidance system and a number of other characteristics) can be analyzed through this software package.

The selection of the motor components is extremely important for the CPR-B performance. The simulation results show the importance of the motor parameters

selection, especially for the cases when some system properties are unknown. Motor type can significantly affect the response of the system or accuracy of the desired trajectory tracking.

The general mathematical model of the CPR-B presented in this paper has been evaluated using several numerical examples. The model can be used for different applications, especially for following moving objects using integrated intelligence.

Future research intend at implementing the elastic ropes (type of nonlinear dynamic elasticity as defined in [14]-[31] in the mathematical model of the CPR-B. In this research several different models were developed and new models will be developing for different applications. All these models will be unified according to their similarities into one reconfigurable model, using the approached presented in [32] and [33].

References

[1] Gosselin C and Angeles J (March 1988) The Optimum Kinematic Design of a Planar Three-Degree-of-Freedom Parallel Manipulator, *Journal of Mechanisms, Transmissions, and Automation in Design,* Vol. 110/35-41.

[2] Fang J and Huang Z (1997) Kinematics of a three-degree-of-freedom in-parallel actuated manipulator mechanism, *Mech. Mach. Theory,* Vol. 32, No 7, pp. 789-796.

[3] Borgstrom P H, Borgstrom N P, Stealey M J, Jordan B, Sukhatme G, Batalin M A and Kaiser W J (Oct 29 - Nov 2, 2007) Discrete Trajectory Control Algorithms for NIMS3D, an Autonomous Underconstrained Three-Dimensional Cabled Robot, *Proceedings of the 2007 IEEE/RSJ International Conference on Intelligent Robots and Systems,* San Diego, CA, USA.

[4] Merlet J P, MARIONET (2010) A Family of Modular Wire-Driven Parallel Robots, *Advances in Robot Kinematics: Motion in Man and Machine*, Part 1, pp. 53-61.

[5] Gouttefarde M, Merlet J-P and Daney D (2006) Determination of the wrench-closure workspace of 6-DOF parallel cable-driven mechanisms," Advances in Robot Kinematics, Part 5, 315-322.

[6] Bruckmann T, Mikelsons L, Schramm D, Hiller M (December 2007) Continuous workspace analysis for parallel cable-driven Stewart-Gough platforms, *Special Issue: Sixth International Congress on Industrial Applied Mathematics (ICIAM07) and GAMM Annual Meeting*, Zürich 2007, Volume 7, Issue 1.

[7] Pott A (2008) Forward Kinematics and Workspace Determination of a Wire Robot for Industrial Applications, *Advances in Robot Kinematics: Analysis and Design,* Part 7, 451-458.

[8] Miermeister P, Pott A and Verl A (2012) Auto-Calibration Method for Overconstrained Cable-Driven Parallel Robots, *ROBOTIK 2012 - 7th German Conference on Robotics,* Munich, Germany.

[9] Higuchi T, Ming A and Jiang-Yu J (June, 6-8, 1988) Application of multi-dimensional wire crane in construction, *In 5th Int. Symp. on Robotics in Construction*, Tokyo, pp. 661–668.

[10] Duan BY (1998) A new design project of the line feed structure for large spherical radio telescope and its nonlinear dynamic analysis, *Mechatronics*, 9, 53-64.

[11] Su X Y, Duan BY (2000) The Application of the Stewart Platform in Large Spherical Radio Telescopes, *Journal of Robotic Systems by John Wiley & Sons*, 17(7), 375-383.

[12] Su X Y, Duan BY (2000) The mathematical design and kinematics accuracy analysis of a fine tuning stable platform for the large spherical radio telescope, *Mechatronics*, 10, 819-834.

[13] Rodic A, Jovanovic M, Popic S, Mester G (2011) Scalable Experimental Platform for Research, Development and Testing of Networked Robotic Systems in Informationally Structured Environments, Symposium Series on Computational Intelligence SSCI, Paris,France, pp. 136-143.

[14] Filipovic M (2008) New form of the Euler-Bernoulli rod equation applied to robotic systems, *Theoretical and Applied Mechanics,* Society Mechanics, Belgrade, Serbia, 35(4) 381-406.

[15] Filipovic M and Djuric A (2010) Whole analogue between Daniel Bernoulli solution and direct kinematics solution, *Theoretical and Applied Mechanics,* Society Mechanics, Belgrade, Serbia, 37(1), 49-78.

[16] Filipovic M (2010) Analogue between New Formulation of Euler-Bernoulli Equation and Algorithm of Forming Mathematical Models of Robot Motion, *Scientific Technical Review,* Military Technical Institute, Belgrade, Serbia, 60(1) 19-29.

[17] Filipovic M (2010) Differences between source and new form of the Euler-Bernoulli equation as well as its solution, *FACTA UNIVERSITATIS Series: Physics, Chemistry and Technology,* Nis, Serbia,8(1), 45-56.

[18] Filipovic M (2012) The Importance of Modelling an Aerial Robotic Camera, *Scientific – Technical Review,* Military Technical Institute, Belgrade, Serbia, 62(1) 28-37.

[19] Filipovic M (2011) Relation between Euler-Bernoulli Equation and Contemporary Knowledge in Robotics, *Robotica, International Journal,* Cambridge University Press, UK, 30,1-13 (2011).

[20] Filipovic M, Potkonjak V and Vukobratovic M (2007) Elasticity in Humanoid Robotics, *Scientific Technical Review,* Military Technical Institute, Belgrade, Serbia, 57(1), 24-33.

[21] Filipovic M and Vukobratovic M (2006) Contribution to modeling of elastic robotic systems, *Engineering & Automation Problems, International Journal,* 5(1) 22-35.

[22] Filipovic M and Vukobratovic M (2008) Complement of Source Equation of Elastic Line, *Journal of Intelligent & Robotic Systems, International Journal,* 52(2), 233-261.

[23] Filipovic M and Vukobratovic M (2008) Expansion of source equation of elastic line, *Robotica, International Journal,* Cambridge University Press, UK, 26(6), 739-751.

[24] Hedrih (Stevanovic) K (2009) Energy transfer in the hybrid system dynamics (energy transfer in the axially moving double belt system), *Special Issue, ARCH APPL MECH,* 79(6-7) 529-540.

[25] Hedrih (Stevanovic) K (2008) Transversal forced vibrations of an axially moving sandwich belt system, *ARCH APPL MECH, Springer,* 78(9) 725-735.

[26] Hedrih (Stevanovic) K (2008) Vibration Modes of a axially moving double belt system with creep layer, *J VIB CONTROL,*14(10-Sep) 1333-1347.

[27] Hedrih (Stevanovic) K (2008) Dynamics of multipendulum systems with fractional order creep elements, Special Issue Vibration and Chaos, *J THEOR APP MECH-POL, Warsaw, Poland,* 46(3) 483-509.

[28] Hedrih (Stevanovic) K (2008), Dynamics of coupled systems, *Nonlinear Analysis: Hybrid Systems,* 2(2) 310-334.

[29] Hedrih (Stevanovic) K (2007) Transversal vibrations of the axially moving sandwich belts, *ARCH APPL MECH,* 77(7) 523-539.

[30] Hedrih (Stevanovic) K (2010) Energy analysis in the hybrid system forced regimes, *Proceeding of Institute of Mathematics NANU Ukraine,* 7(3) 90-107.

[31] Hedrih (Stevanovic) K (2012) *Energy and Nonlinear Dynamics of Hybrid System*, Chapter in Book Dynamical Systems and Methods, Edited by Albert Luo, Springer, Part 1, 29-83.

[32] Djuric A, Al Saidi R, ElMaraghy W (2012) Dynamics Solution of n-DOF Global Machinery Model, *Robotics and Computer Integrated Manufacturing (CIM)" Journal*, Vol. 28, Issue 5, pp. 621-630.

[33] Djuric A, Al Saidi R, ElMaraghy W (August 21-24, 2010) Global Kinematic Model Generation for n-DOF Reconfigurable Machinery Structure, *6th IEEE Conference on Automation Science and Engineering, CASE 2010*, Toronto, Canada.

MIRJANA FILIPOVIĆ

ANALYSIS OF A RIGID BODY ROTATION AROUND TWO NO INTERSECTING AXES – VECTOR METHOD AND PARAMETER ANALYSIS OF PHASE TRAJECTORIES

Ljiljana Veljović
Faculty of Mechanical Engineering University of Kragujevac,
Sestre Janjić 6, 34000 Kragujevac, Serbia
E-mail: veljovicljilja@yahoo.co.uk

ABSTRACT Vector expressions for linear momentum and angular momentum and their corresponding derivatives with respect to time describe rigid body nonlinear dynamics with coupled rotations around axes without intersection. Vector method based on mass moment vectors coupled for pole and oriented axes was defined by K. Hedrih in 1991. and it is applied for analysis of a heavy gyrorotor nonlinear dynamics. Series of graphical presentations and their parametric transformations in relation with changing orthogonal distance between axes of coupled rotations is presented.

1.Introduction

Tern or a toy top is just a simple well-known toy with unusual property that when it rotates by high angular velocity about its axis of symmetry, it keeps in the state of stationary rotation around this axis. This feature has attracted scientists around the world and as a result of year's research many devices and instruments are created; from simple to very complex structures, which operate on the principle of a spinning top that plays an important role in stabilizing the movement. Ability gyroscope that keeps the line was used in many fields of mechanical engineering, mining, aviation, navigation, military industry, and in celestial mechanics because heavy bodies in motion, rotors of turbines, different mobile installations on ships, artillery projectiles in motion, aircraft propeller rotating possesses special properties known as properties of gyroscopes.

Each mechanical gyroscope is based on coupled rotations around more axes with one point intersection. Most of the old equipment was based on rotation of complex and coupled component rotations which resulting in rotation about fixed point gyroscopes. The classical books contain a classical and very important elementary dynamical model of the simple case of the gyrorotor, and present an analogous and useful dynamical and mathematical model of nonlinear dynamics. This work is different in that the equations of motion are derived using vector method proposed by K. Hedrih [1], and propose stability analysis for the system based on the derived model. The vector approach is very

suitable to obtain new view to the properties of dynamics of pure classical task, investigated by numerous generations of the researchers and serious scientists around the world.

2. Equations of rigid body dynamics

Mass moment vectors for axis and pole was introduced and defined by Hedrih (Stevanovic) K., and presented in the monograph [1] as well as in the series of papers [2-4] listed here.

Here is considered a heavy rigid body which rotates around two coupled axes without intersection and with orthogonal distance defined by vector $\vec{r}_0 = \overrightarrow{O_2 O_1}$. The body is eccentrically and inclined positioned on the self–rotation axis (Figure 1). Two angular velocities around two axes oriented by unit vectors $\vec{n}_1$ and $\vec{n}_2$ are denoted as $\vec{\omega}_1 = \omega_1 \vec{n}_1$ and $\vec{\omega}_2 = \omega_2 \vec{n}_2$. By using basic definitions for linear momentum and angular momentum as well as expression for velocity of elementary body mass particle rotation $\vec{v} = [\vec{\omega}_2, \vec{r}_0] + [\vec{\omega}_1 + \vec{\omega}_2, \vec{\rho}]$, the following vector expressions are presented: a* for linear momentum and b* for angular momentum.

a* $\vec{K} = [\vec{\omega}_2, \vec{r}_0]M + \vec{\omega}_1 \vec{S}_{\vec{n}_1}^{(O_1)} + \vec{\omega}_2 \vec{S}_{\vec{n}_2}^{(O_1)}$ (1)

b* $\begin{aligned} \vec{L}_{O_1} &= \omega_1 \vec{n}_1 r_0^2 M + \omega_1 [\vec{\rho}_C, [\vec{n}_1, \vec{r}_0]]M + \omega_1 [\vec{r}_0, S_{\vec{n}_1}^{(O_2)}] + \\ &+ \omega_2 [\vec{r}_0, \vec{S}_{\vec{n}_2}^{(O_2)}] + \omega_1 \vec{J}_{\vec{n}_1}^{(O_2)} + \omega_2 \vec{J}_{\vec{n}_2}^{(O_2)} \end{aligned}$ (2)

Where $\vec{S}_{\vec{n}_1}^{(O_1)} = \iiint\limits_V [\vec{n}_1, \vec{\rho}]dm$ and $\vec{S}_{\vec{n}_2}^{(O_1)} = \iiint\limits_V [\vec{n}_2, \vec{\rho}]dm$, $dm = \sigma dV$ are corresponding body mass linear moments of the rigid body for the axes oriented by direction of component angular velocities of coupled rotations through the movable pole O_2 on self rotating axis, $\vec{J}_{\vec{n}_1}^{(O_2)} = \iiint\limits_v [\vec{\rho}, [\vec{n}_1, \vec{\rho}]]dm$ and $\vec{J}_{\vec{n}_2}^{(O_2)} = \iiint\limits_v [\vec{\rho}, [\vec{n}_2, \vec{\rho}]]dm$ are corresponding body mass angular moments of the rigid body for the axes oriented by direction of component angular velocities of coupled rotations through the movable pole O_2 on self rotating axis.

Using first derivatives of linear momentum and angular momentum two vector equations of rigid body coupled rotation around axes without intersection are obtained.

$$\frac{d\vec{K}}{dt} = \dot{\omega}_2 [\vec{n}_2, \vec{r}_0]M + \omega_2^2 [\vec{n}_2, [\vec{n}_2, \vec{r}_0]]M + \dot{\omega}_1 \vec{S}_{\vec{n}_1}^{(O_1)} + \omega_1^2 [\vec{n}_1, \vec{S}_{\vec{n}_1}^{(O_1)}] + $$
$$+ \dot{\omega}_2 \vec{S}_{\vec{n}_2}^{(O_1)} + \omega_2^2 [\vec{n}_2, \vec{S}_{\vec{n}_2}^{(O_1)}] + 2\omega_1 \omega_2 [\vec{n}_2, \vec{S}_{\vec{n}_1}^{(O_1)}]$$ (3)

$$\frac{d\vec{L}_{O_1}}{dt} = \vec{\omega}_2 r_0^2 M + \omega_1 \omega_2 \{[\vec{n}_1, \vec{J}_{\vec{n}_2}^{(O_1)}] + [\vec{n}_2, \vec{J}_{\vec{n}_1}^{(O_1)}] + \Im^{(O_1)}[\vec{n}_2, \vec{n}_1]\} + $$
$$+ \omega_1^2 [\vec{n}_1, \vec{J}_{\vec{n}_1}^{(O_1)}] + \omega_2^2 [\vec{n}_2, \vec{J}_{\vec{n}_2}^{(O_1)}] + \dot{\omega}_1 \vec{J}_{\vec{n}_1}^{(O_1)} + \dot{\omega}_2 \vec{J}_{\vec{n}_2}^{(O_1)}$$ (4)

These vector expressions can be used in general case when considered system has two degree of freedom. Differential equation of self rotation and equation of phase expressions for kinetic pressures to bearings of self-rotation shaft with corresponding components as well as for corresponding vector rotators can be obtained [5-7].

The dynamical equations for motion on a straight inclined rotor can be easily obtained from the theorem of angular momentum derivative which in this case is in a form[5]:

$$\frac{dL_{O_1}}{dt} = \vec{M}_{O_1}\left(\vec{F}_i\right) - [[\vec{\omega}_2, \vec{r}_0],[\vec{\omega}_1 + \vec{\omega}_2, \vec{\rho}_C]]M \tag{5}$$

This leads to the two vector equations of rigid body coupled rotation around axes without intersection which can be used in general case when considered system has two degree of freedom[7]. In case when the second angle φ_2 is a rheonomic coordinate which is defined by a time function $\varphi_2 = \omega_2 t + \varphi_{20}$, we have one vector equation and it is in a form:

$$\ddot{\varphi}_1 + \Omega^2\left(\lambda - \cos\varphi_1\right)\sin\varphi_1 + \Omega^2\psi\cos\varphi_1 = 0 \tag{6}$$

Here, in differential equation there are some constants which are in following form:

$$\Omega^2 = \omega_2^2\frac{\varepsilon\sin^2\beta - 1}{\varepsilon\sin^2\beta + 1}, \ \varepsilon = 1 + \left(\frac{2e}{r}\right)^2, \ \lambda = \frac{g(\varepsilon - 1)\sin\beta}{e\omega_2^2\left(\varepsilon\sin^2\beta - 1\right)}, \ \psi = \frac{2ea\sin\beta}{er\left(\varepsilon\sin^2\beta - 1\right)} \tag{7}$$

Transforming previous nonlinear differential equation into system of two first order nonlinear differential equations it is possible to obtain stationary values which correspond to the relative equilibrium positions of the rotor on the self rotating axis. For each of relative equilibrium position Lyapunov criteria of stability can be applied and then it can be concluded about center or saddle points.

Relative nonlinear dynamics of heavy gyrorotor disc around self rotation shaft axis is possible to present by means of phase portrait method. Forms and transformations of phase trajectories by changing of initial conditions and for different cases of rotor eccentricity (ε), angle of inclination (β) or orthogonal distance between axes (a) express nonlinear phenomena.

The solution-first integral of differential equation (6) with the initial conditions $t_0 = 0$, $\varphi_1(t_0) = \varphi_{10}$, $\dot{\varphi}_1(t_0) = \dot{\varphi}_{10}$, is obtained in the following form:

$$\dot{\varphi}_1^2 = \dot{\varphi}_{10}^2 + 2\Omega^2\left(\lambda\cos\varphi_1 - \frac{1}{2}\cos^2\varphi_1 + \psi\sin\varphi_1\right) - 2\Omega^2\left(\lambda\cos\varphi_{10} - \frac{1}{2}\cos^2\varphi_{10} + \psi\sin\varphi_{10}\right) \tag{8}$$

The energy integral because the conservative system is analyzed is in a similar form.

$$\tilde{E}_P = \Omega^2(\varepsilon,\beta)\left[\lambda(\varepsilon,\beta)(\cos\varphi_1 - \cos\varphi_{10}) + \frac{1}{2}\left(\cos^2\varphi_{10} - \cos^2\varphi_1\right) + \psi(\varepsilon,\beta,a)(\sin\varphi_1 - \sin\varphi_{01})\right] \tag{9}$$

Some curves of potential energies are shown on Figure 2 where one can see extreme values that correspond to stable or nonstable relative equilibrium positions.

3. Phase portrait of the gyrorotor

Using obtained vector expressions by applying software tool, series of graphical presentations depending on the orthogonal distance between two axes of coupled disk rotations are obtained.

Characteristic potential energy curves, and corresponding homoclinic separatrix phase trajectories for different parameters values of the basic system correspond to the dynamic model illustrate the trigger of the coupled singularities and coupled triggers of the coupled singularities and homoclinic trajectories in the form of the number eight and also in the form of the duplicate number eight.
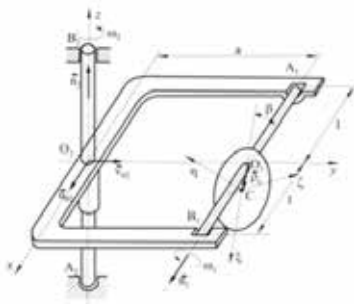
Figure 1- Model of gyrorotor who rotates around two no intersecting axes
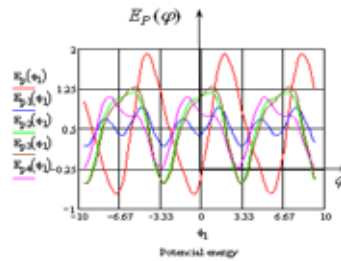
Figure 2 - Potential energy

Phase trajectories for different values of parameters of system and for different initial conditions are shown on Figure 4.There are many types of trajectories which are relared to oscilatory or progresive motion. One-sided separatrix, which are "prolating", and open phase trajectories, which are comprising enclosed phase trajectories which are matching to the periodical oscillator motion-rotations system around stability configurations of equilibrium positions for specific initial conditions when initial angular velocity are small and small angles elongation of rotations, and when that condition are satisfying for any time are illustrated on Figure 3.

In Figure 4. on phase portrait we notice augmentation of singular points, and it can be deduced by researching that for some kinetic parameters of system one stable equilibrium position loses stability and that positions now on phase portrait response to homoclinic point by type unstable saddle, but in symmetrical neighborhood appear two near-by stable equilibrium positions (configuration of masses), which on phase portrait response two singular points by center type. All of three points are coupled in one "trigger" (trigger of coupled singularities). Two stable singular points by type centers enclose one, and the new, closed homoclinic orbit which goes around three singularities, and passing trough one homoclinic point by type saddle in which it self-cross, that it is shaped like form of the number eight or in the form of duplicate of number eight or multiplication. Inside that new separatrix trajectory homoclinical orbit a series of common closed phase trajectories which los instability relative equilibrium positions or

relative rest positions, which correspond to periodic oscillatory motion for certain initial conditions, apropos oscillations around new stable position of equilibrium can be noticed.
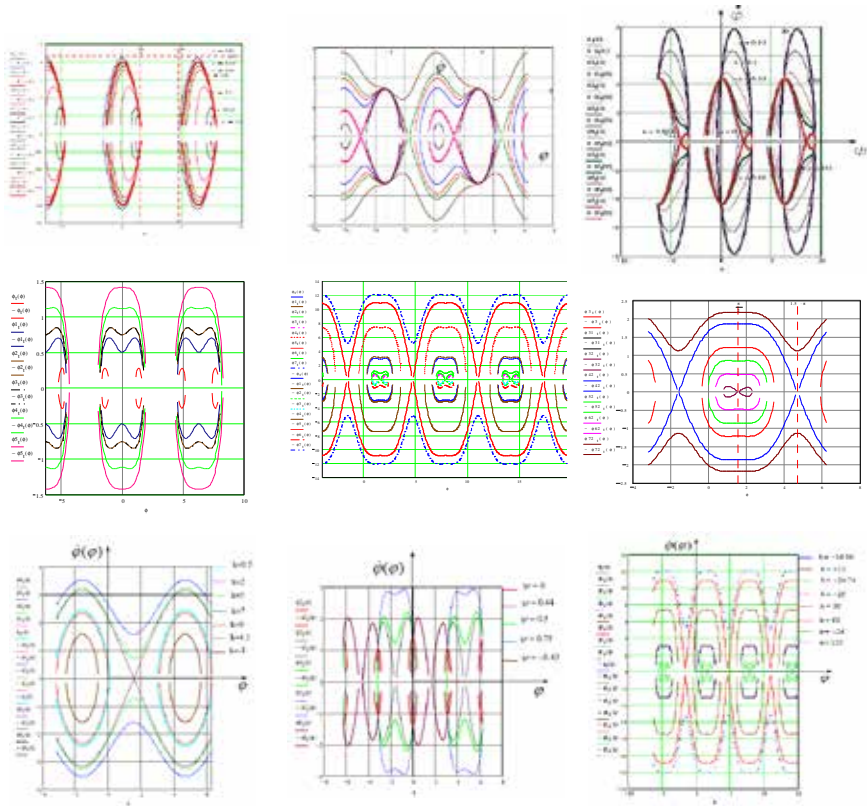
Figure 3 - Parametric transformation of phase trajectory for different values of orthogonal distance between axes
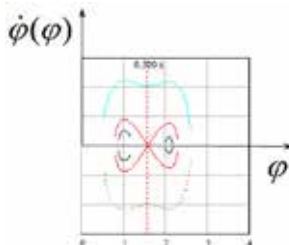
Figure 4 - Transformation of a closed phase trajectory of the heavy gyro-rotor-disk dy rotations inside a trigger of coupled singularities

4. Concluding remarks

By use derived vector expressions as well as graphical presentations of the system nonlinear dynamics, we can
conclude that body mass inertia moment vectors and vector rotators are very suitable for obtaining linear momentum and angular momentum and their derivatives of the system with coupled numerous rotations around axes without intersections, as well as for vector method analysis of system vector parameter dynamics. Analysis of rotation of a heavy gyro-rotor show us that in graphical presentations of the system kinetic parameters exits a set of the fixed points not depending of change of rigid body eccentricity or angle of inclination or of the orthogonal distance between axes of rigid body coupled rotations.

Keywords nonlinear dynamics, gyro-rotor, phase portraits, vector rotators

References

[1] Hedrih (Stevanović), K., *Vector Method of the Heavy Rotor Kinetic Parameter Analysis and Nonlinear Dynamics*, University of Niš 2001,Monograph, p. 252. (in English), YU ISBN 86-7181-046-1.
[2] Hedrih (Stevanović), K. (1998), *Vectors of the Body Mass Moments*, Monograph paper, Topics from Mathematics and Mechanics, Mathematical institute SANU, Belgrade, Zbornik radova 8(16), 1998, pp. 45-104. published in 1999 .(in English), (Zentralblatt Review).
[3] Katica (Stevanović) Hedrih, *Derivatives of the Mass Moment Vectors at the Dimensional Coordinate System N*, dedicated to memory of Professor D. Mitrinović, Facta Universitatis Series Mathematics and Informatics, 13 (1998), pp. 139-150. (1998, published in 2001. Edited by G. Milovanović).
[4] Hedrih (Stevanović), K., *Some vectorial interpretations of the kinetic parameters of solid material lines*, ZAMM. Angew.Math. Mech.73(1993) 4-5, T153-T156.
[5] Katica (Stevanović) Hedrih and Ljiljana Veljović, *Nonlinear dynamics of the heavy gyro-rotor with two skew rotating axes*, Journal of Physics: Conference Series, 96 (2008) 012221 DOI:10.1088/1742-6596/96/1/012221, IOP Publishing http://www.iop.org/EJ/main/-list=current/
[6] Hedrih (Stevanović) K, Veljović Lj., *The Kinetic Pressure of the Gyrorotor Eigen Shaft Bearings and Rotators*, The Third International Conference Nonlinear Dynamics – 2010, pp. 78-83
[7] Hedrih (Stevanović) K, Veljović Lj., *Vector Rotators of a Rigid Body Dynamics with Coupled Rotations around Axes without Intersection,* Mathematical Problem in Engineering, Volume 2011, Article 351269, 26 pages, doi:10.1155/2011/351269

THREE-PARAMETRIC TESTING OF SINGULARITY AND POSITION OF NON-LINEAR DYNAMICS RELATIVE BALANCE OF HEAVY MATERIAL PARTICLE ON ECCENTRICALLY ROTATING SMOOTH CIRCLE LINE

Marija Stamenković[1], Marija Mikić[1]

[1]Mathematical Institute SANU, Department of Mechanics,
11 000-Belgrade, Kneza Mihaila 36/III, Serbia,
e-mail: s_marija86@yahoo.com
[1]Mathematical Institute SANU, Department of Mechanics,
and Faculty of Mathematics, 11 000-Belgrade, Studentski trg 16, Serbia
e-mail: marijam@matf.bg.ac.rs

Abstract. The paper contains analytical descriptions of heavy material particle which moves on a rotating circular smooth line, radius R, which rotate around vertical axis, eccentrically positioned in relation to center of circle line on distance e, angular velocity Ω, (see Figure 1). By using software GeoGebra three-parametric testing of singularity and position of non-linear dynamics relative balance of heavy material particle on eccentrically rotating smooth circle line is examined.

1. Introduction

Dynamics of heavy material particle is a very old engineering problem with many different research results and discoveries of new nonlinear phenomena (see Refs. [1-3]). Many researchers pay attention and interest for research the nonlinear dynamics by using new analytical, numerical and experimental methods to discover the properties of nonlinear dynamics (see Refs. [4-10]).

2. Motion of the heavy material particle along circles

In Figure 1, for generalized coordinate we will take the angle φ, by which we mark relative position of material particle on circle line. The system has one degree of moving freedom, and two degrees of moving freedom because one reonomic relation is imposed-rotating by constant angular velocity.
Velocity of heavy material particle has two components:

1. component of relative rotation for circle line:

$$v_r = R\dot{\varphi} \tag{1}$$

2. component due to transmitting moving by rotation of circle line:

$$v_p = (e + R\sin\varphi)\Omega \tag{2}$$
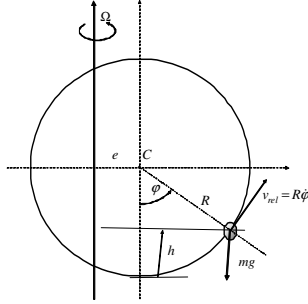
Figure 1. Moving of heavy material particle on circle line, radius *R*, which rotates around vertical axis, eccentrically positioned in relation to center of circle line on distance *e*, by angular velocity Ω.

The components are normal in relation to each other, so the square of angular velocity of material particle is presented in following form:

$$v^2 = v_{rel}^2 + v_p^2 = (R\dot\varphi)^2 + (e + R\sin\varphi)^2\Omega^2 \tag{3}$$

Expression of kinetic energy of the system is in the form:

$$E_k = \frac{1}{2}mv^2 = \frac{1}{2}m((R\dot\varphi)^2 + (e + R\sin\varphi)^2\Omega^2) \tag{4}$$

Potential energy of the system equals operation of weight force by improving height *h=R(1-cosφ)* and with changed mark.

$$E_p = mgh = mgrR(1 - \cos\varphi) \tag{5}$$

On the basis of Lagrange's equations: $\dfrac{d}{dt}\dfrac{\partial E_k}{\partial\dot\varphi} - \dfrac{\partial E_k}{\partial\varphi} + \dfrac{\partial E_p}{\partial\varphi} = 0.$

Differential equation of heavy material particle moving illustrated in figure is:

$$\ddot\varphi + \Omega^2\left(\frac{g}{R\Omega^2} - \cos\varphi\right)\sin\varphi - \Omega^2\frac{e}{R}\cos\varphi = 0 \tag{6}$$

If we introduce following symbols $\lambda = \dfrac{g}{R\Omega^2}$ and $\varepsilon = \dfrac{e}{R} = \psi$, previous differential equation is in the following form:

$$\ddot\varphi + \Omega^2(\lambda - \cos\varphi)\sin\varphi - \Omega^2\psi\cos\varphi = 0 \tag{7}$$

Using the previous ordinary nonlinear differential equations of second order, form non-linear system of differential equations of first order in the following form:

$$\frac{d\varphi}{dt} = u \tag{8}$$

$$\frac{du}{dt} = -\Omega^2(\lambda - \cos\varphi)\sin\varphi + \Omega^2\psi\cos\varphi$$

For angular velocity we introduce symbol *u*. We are interested in the values of the parameters λ and ψ leads to changes in dynamic systems. The paper deals with the specific parameter values λ and ψ for which there is a substantial change in the dynamical system.

3. Nonlinear differential equation

The initial problem that we had, describing of the dynamics movement of heavy material particle which moves as already described, reduced to solving nonlinear differential equation:

$$\ddot{\varphi} + \Omega^2 (\lambda - \cos\varphi)\sin\varphi - \Omega^2 \psi \cos\varphi = 0 \cdot \tag{9}$$

Introducing a shift $\dot{\varphi} = u$, $u = u(\varphi)$ we lower row of differential equation for one, i.e. we come to the equation:

$$u\dot{u} + \Omega^2 (\lambda - \cos\varphi)\sin\varphi + \Omega^2 \psi \cos\varphi = 0. \tag{10}$$

From there we get $u = \pm\sqrt{\Omega^2 (2\lambda\cos\varphi + \sin\varphi - 2\psi\sin\varphi) + c}$. From here we get connection between angle φ by which we denoted position of material particle on circle line and time t, i.e. we come to a general solution of starting differential equations.

$$t = \pm\int \frac{d\varphi}{\sqrt{\Omega^2 (2\cos\varphi + \sin^2\varphi - 2\psi\sin\varphi + c_1)}} + c_2, \quad \Omega \neq 0. \tag{11}$$

Of course, in our particular case we start from assumption that there is determined angular velocity Ω, and we will not consider case when $\Omega=0$.

4. Three-parametric testing of singularity

To determine the stationary points of differential equations system (8), which correspond to positions of relative heavy material point equilibrium on eccentrically-rotating smooth circle line, it's necessary to find position where relative angular velocity and relative angular acceleration of material points on the circle line equal zero. From there follows that it is necessary that the functions, i.e. expressions on the right side of the differential equations system (8) equals zero.

In order to determine the stationary points of differential equations system (8), we introduce next conditions:

$$u = 0 \tag{12}$$
$$-\Omega^2 (\lambda\sin\varphi - \sin\varphi\cos\varphi + \psi\cos\varphi) = 0$$

In order to determine the stationary points, it is necessary to solve next nonlinear equation:

$$\lambda\sin\varphi - \sin\varphi\cos\varphi + \psi\cos\varphi = 0 \tag{13}$$

However, a set of roots which we seek from the previous equation (13), having considered the fact that it depends on three parameters of systems, radius circle line R, eccentricity e, center's C circular lines in relation to the axis of rotations, as angular velocity Ω rotation around the circle line, we can express by using two coefficients $\lambda = \dfrac{g}{R\Omega^2}$ and $\varepsilon = \dfrac{e}{R} = \psi$ contained in previous equation.

This means that it is necessary to examine the influence of these two coefficients on the set of roots of nonlinear transcendental equation.

If $\sin\varphi = 0$ i.e. $\varphi = k\pi, k \in \mathbb{Z}$ then for $\psi = 0$ points $(0, k\pi), k \in \mathbb{Z}$ are stationary points of system of differential equations. Assuming that $\sin\varphi \neq 0$, and if we divide equations (13) with $\sin\varphi$ then follows:

$$\lambda = \cos\varphi - \psi ctg\varphi \qquad (14)$$

Coefficient $\lambda = \lambda(\varphi, \psi)$ we will observe as a function of two variables: coordinates φ and relative eccentricity $\varepsilon = e/R = \psi$ of the axis rotation from center around circle line. Depending on the properties and values of coefficient $\lambda(\varphi, \psi)$ in the function of the coordinates φ and relative eccentricity $\varepsilon = e/R = \psi$ of the axis rotation from center around circle line, we come to following conclusions.

5. Mathematical conclusion

First, it is necessary to explain what we mean when we say „Mathematical conclusion". Mathematical conclusion implies determining the stationary points of system differential equations, but when parameters λ, Ω and ψ can be of arbitrary values from the set of real numbers, i.e. when these values we do not observe as the physical size, but rather as mathematical constants.

For each fixed λ and $\Omega \neq 0$ we can find stationary points of the system. We will differ cases:

1. For $\psi < -1$ or $\psi > 1$ there will always be two stationary points on interval $[0, 2\pi)$. It can be seen in Figures 6 and 7.

2. For fixed $\psi \in [-1, 1]$ let's consider λ as a function of φ i.e. $\lambda = \lambda(\varphi)$. If $\lambda < \lambda_{\min}$ or $\lambda > \lambda_{\max}$, system dynamics will have two stationary points on interval $[0, 2\pi)$ (see Figures 2 and 4). If $\lambda = \lambda_{\min}$ or $\lambda = \lambda_{\max}$, system dynamics will have three stationary points on interval $[0, 2\pi)$ (See figure 8). If $\lambda_{\min} < \lambda < \lambda_{\max}$ system dynamics will have four stationary points on interval $[0, 2\pi)$ (See Figures 3 and 5).

3. For $\varphi = \arcsin\sqrt[3]{\psi}$, λ will reach extreme values. If we mark with $\varphi^* = \arcsin\sqrt[3]{\psi}$. Then it is $\lambda_{ekstremo} = \cos\varphi^* - \psi\, ctg\, \varphi^*$. Of course for fixed values of the parameters λ, Ω and ψ, i.e. on the concrete example, stationary points can be determined completely.

6. Conclusion about system dynamics properties

In our particular case, we consider the problem when $\Omega \neq 0$ and $\lambda > 0$. Then we can get a little closer information about the stationary points. We will differ cases:

1. For $\psi < -1$ or $\psi > 1$ there will always be two stationary points in interval $[0, 2\pi)$. If $\psi < -1$ then the first will be in interval $\left(0, \dfrac{\pi}{2}\right)$, and second will be in interval $\left(\pi, \dfrac{3\pi}{2}\right)$.

If $\psi > 1$ then the first will be in interval $\left(\frac{\pi}{2}, \pi\right)$, and second will be in interval $\left(\frac{3\pi}{2}, 2\pi\right)$.

2. For fixed $\psi \in [-1, 1]$ and if $\lambda < \lambda_{min}$ or $\lambda > \lambda_{max}$, system dynamics will have two stationary points on interval $[0, 2\pi)$. For fixed $\psi \in [-1, 0]$ then the first will be in interval $\left[0, \frac{\pi}{2}\right)$, and second will be in interval $\left[\pi, \frac{3\pi}{2}\right)$, and for fixed $\psi \in (0,1]$ then the first will be in interval $\left(\frac{\pi}{2}, \pi\right)$, and second will be in interval $\left(\frac{3\pi}{2}, 2\pi\right)$. For fixed $\psi \in [-1, 1]$ and if $\lambda = \lambda_{min}$ or $\lambda = \lambda_{max}$ system dynamics will have three stationary points in interval $[0, 2\pi)$. For fixed $\psi \in [-1, 0]$ in the interval $\left(\frac{\pi}{2}, \pi\right)$ will not be stationary points, and for fixed $\psi \in (0,1]$ in the interval $\left(\pi, \frac{3\pi}{2}\right)$ will not be stationary points. For fixed $\psi \in [-1, 1]$ and $\lambda_{min} < \lambda < \lambda_{max}$, system dynamics will have four stationary points on interval $[0, 2\pi)$. For fixed $\psi \in [-1, 0]$ in the interval $\left(\frac{\pi}{2}, \pi\right)$ will not be stationary points, and for fixed $\psi \in (0,1]$ in the interval $\left(\pi, \frac{3\pi}{2}\right)$ will not be stationary points.

This can be seen in Figures 2, 3, 4, 5, 6, 7 and 8.

7. Linearize of system and behavior of solutions in singular points environment

We are interested in behavior of solutions in singular points environment. Therefore we exert linearization of the starting system (8). Linearized system is:

$$\frac{d\varphi}{dt} = u$$
$$\frac{du}{dt} = -\Omega^2 (\lambda \cos \varphi_s - \cos^2 \varphi_s + \sin^2 \varphi_s - \psi \sin \varphi_s) \varphi \qquad (15)$$

Where we marked $(\varphi_s, 0)$ stationary points.

If we marked:
$$R = -\Omega^2 (\lambda \cos \varphi_s - \cos^2 \varphi_s + \sin^2 \varphi_s - \psi \sin \varphi_s). \qquad (16)$$

We will differ cases for:

1. If $R > 0$, then the equation will have real roots, and in such a way that the first is lower than zero, and second higher than zero, than in this case, stationary points will be saddles.

2. If $R < 0$, than the equation will have complexity-conjugated roots, and in such a way that their real parts equal zero, then in this case, stationary points will be centers.

We are interested in a change of dynamic system due to the value of parameter Ψ. For that reason we will observe next equation.

$$\lambda \cos \varphi_s - \cos^2 \varphi_s + \sin^2 \varphi_s - \psi \sin \varphi_s = 0. \tag{17}$$

For φ_s matter $\lambda = \cos \varphi_s - \psi \, ctg \varphi_s$ for $\varphi_s \neq k\pi, k \in \mathbb{Z}$. When we convert this in the previous equation (17), we obtain: $-\psi + \sin^3 \varphi_s = 0$. This equation will have solutions for $\psi \in [-1, 1]$. For $\lambda = \cos \varphi_s - \psi \, ctg \varphi_s$ and $\psi > \sin^3 \varphi_s$ system dynamics will have a different structure, then when is $\psi < \sin^3 \varphi_s$. If we marked $\psi_0 = \sin^3 \varphi_s$, we can see that for each fixed λ, we can determine ψ_0, such that for $\psi < \psi_0$ system dynamics has one structure, and for $\psi > \psi_0$ other structure.

We distinguish cases:

1. If $\psi > 1$ (then $-\psi + \sin^3 \varphi_s < 0$)
For $\varphi_z \in (0, \pi)$ $R > 0$, so in this case stationary point will be a saddle. For $\varphi_z \in (\pi, 2\pi)$ $R < 0$, so in this case stationary point will be a center. (See Figure 7)

2. If $\psi < -1$ (then $-\psi + \sin^3 \varphi_s > 0$)
For $\varphi_z \in (0, \pi)$ $R < 0$, so in this case stationary point will be a center. For $\varphi_z \in (\pi, 2\pi)$ $R > 0$, so in this case stationary point will be a saddle. (See figure 6)

3. If $\psi \in [0, 1]$
For $\varphi_z \in [0, \pi)$, if ψ is such that $-\psi + \sin^3 \varphi_s < 0$, then $R > 0$, so stationary points are saddles, while if ψ is such that $-\psi + \sin^3 \varphi_s > 0$, then $R < 0$, so stationary points are centers. For $\varphi_z \in [\pi, 2\pi)$ then $R < 0$ so stationary points are centers. (See Figures 3 and 2)

4. If $\psi \in (0, 1]$
For $\varphi_z \in [0, \pi)$ then $R < 0$, so stationary points are centers. For $\varphi_z \in [\pi, 2\pi)$ if ψ is such that $-\psi + \sin^3 \varphi_s < 0$, then $R > 0$, so stationary points are saddles, while if ψ is such that $-\psi + \sin^3 \varphi_s > 0$, then $R < 0$, so stationary points are centers (See Figures 5 and 4).

8. Figures
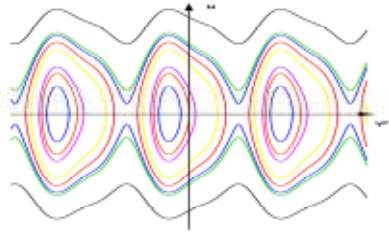
Figure 2. Portrait phase of dynamic system for
$\psi = 0.61$, $\Omega = 1$ and $\lambda = 0.71$
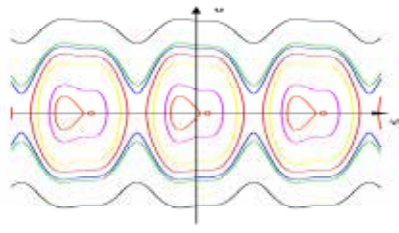
Figure 3. Portrait phase of dynamic system for,
$\psi = 0.08$, $\Omega = 1$ and $\lambda = 0.71$
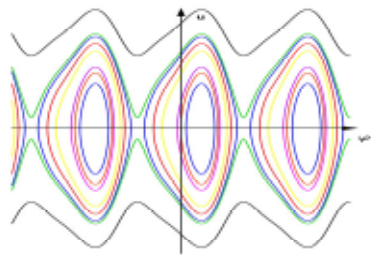
Figure 4. Portrait phase of dynamic system for
$\psi = -0.96$, $\Omega = 1$ and $\lambda = 0.71$
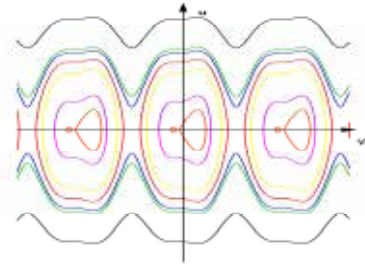
Figure 5. Portrait phase of dynamic system for
$\psi = -0.08$, $\Omega = 1$ and $\lambda = 0.71$
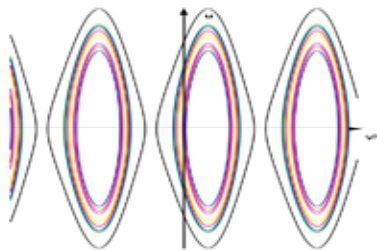
Figure 6. Portrait phase of dynamic system for
$\psi = -3$, $\Omega = 1$ and $\lambda = 0.71$
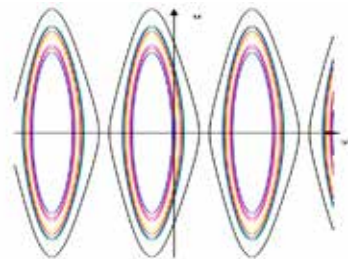
Figure 7. Portrait phase of dynamic system for
$\psi = 3$, $\Omega = 1$ and $\lambda = 0.71$
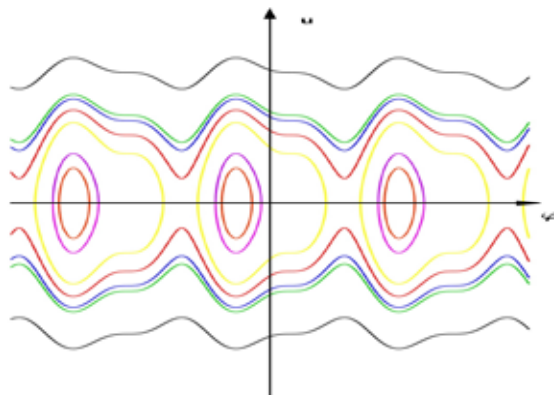
Figure 8. Portrait phase of dynamic system for
$\psi = 0.35, \Omega = 1$ and $\lambda = 0.35$

References

[1] Andronov, A.A., Vitt, A.A., Haykin, S.E., (1981), *Teoriya kolebaniy,* Nauka, Moskva., pp. 568

[2] Gerard I. and Daniel J., *Elementary Stability and BIfurcation Theory*, Springer Verlag, 1980.

[3] Guckenheimer, J. and Holmes, Ph. , (1983), Nonlinear Oscillations, Dynamical Systems, and Bifurcations of Fields , Springer-Verlag, pp. 461.

[4] Rašković D., Mehanika - Dinamika (Dynamics), Naučna knjiga, 1972.

[5] Rašković D., Teorija oscilacija (Theory of Oscillations), Naučna knjiga, 1952.

[6] Hedrih (Stevanović) K., (2004), *A Trigger of Coupled Singularities*, MECCANICA**,** Vol.39, No. 3, 2004., pp. 295-314. , DOI: 10.1023/B:MECC.0000022994.81090.5f

[7] Hedrih (Stevanović), K., *Trigger of Coupled Singularities (invited plenary lecture) ,* Dynamical Systems-Theory and Applications, Edited By J. Awrejcewicz and all, Lodz 2001, pp. 51-78.

[8] Hedrih (Stevanović), K., *Nonlinear Dynamics of a Gyrorotor, and Sensitive Dependence on initial Conditions of a Heav Gyrorotor Forced Vibration/Rotation Motion*, Semi-Plenary Invited Lecture, Proceednings: COC 2000, Edited by F.L. Chernousko and A.I. Fradkov, IEEE, CSS, IUTAM, SPICS, St. Petersburg, Inst. for Problems of Mech. Eng. of RAS, 2000., Vol. 2 of 3, pp. 259-266.

[9] Hedrih (Stevanoviж), K., *On Rheonomic Systems with Eqauivalent Holonomic Conservative System,* Int. Conf. ICNM-IV, 2002, Edited by W. Chien and all. Shanghai, *T*. Nonlinear dynamics. pp. 1046-1054.

[10] Hedrih (Stevanović), K., *The Vector Method of the Heavy Rotor Kinetic Parameter Analysis and Nonlinear Dynamics* , Monograph, University of Niš, 2001, pp. 252., YU ISBN 86-7181-046-1.

OPTIMAL PLACEMENT OF PIEZOELECTRIC ACTUATORS AND SENSORS FOR SMART STRUCTURES USING GENETIC ALGORITHM

S.M. Garmabi[1], M. Trajkov[2], T. Nestorović[3]

Institute of Computational Engineering, Mechanics of Adaptive Systems, Ruhr-Universität Bochum, Universitätsstr. 150, D-44801 Bochum, Germany

[1] seyed.garmabi@rub.de
[2] miroslav.trajkov@rub.de
[3] tamara.nestorovic@rub.de

Abstract. In this paper a method to find optimal places of piezoelectric actuators and sensors on different structures is presented. The genetic algorithm and multi-objective genetic algorithm are selected for optimization and H_∞ norm is defined as a cost function for the optimization process. To optimize the placement concerning the selected modes simultaneously, the multi-objective genetic algorithm is used. The optimization is investigated for two different structures: a cantilever beam and a simply supported plate. The vibrating structure is controlled in a closed loop with feedback gains obtained from optimal control. Finally, output of a structure with optimized placement is compared with output of the structure with not optimized placement of piezoelectric patches.

1. Introduction

In recent years, focus of many researchers in the field of vibration control has been concentrated on implementation of active piezoelectric materials due to their numerous advantages. For instance, they response very fast to changes of circumstances and they flexibly can be used as a sensor or an actuator. They are also lightweight materials and can be embedded on different structures.

The problem arises here to find the best location of the piezoelectric patches on structures to control the structure in an optimal way. Many researches have been done on this problem and lots of solutions have been recommended. Nevertheless all of them have some advantages and also disadvantages. The placement problem grows when not only optimization of one mode, but also some modes simultaneously are demanded.

Arbel [1], Hac [2], and Devasia [3] have used the grammian matrix as criterion for optimization propose to maximize the controllability and observability of the structure. For optimization process usually classical algorithms such as conjugate gradient and Newton-Raphson are used but they crash down when there is more than on local optima. To overcome this problem genetic algorithm (GA) has been proposed in several papers.

In this paper, the H_∞ norm is selected as a criterion or fitness function for optimization process within GA. The advantage of the GA over some other placement

methods can be seen in the fact, that many objectives can be optimized simultaneously (in our case norms of different modes) and it results in optimal locations of piezoelectric patches, whereby unlike with some other methods, there is no need to specify in advance limited number of predefined places.

2. Genetic algorithm

For very complicated cases, which cannot be optimized with other numeric optimization strategies, the evolution strategies are good choice of design optimization. The evolution strategies are slow and they have convergence problems. But they are well suited for complex situations: multi-modal problems that don't have only one single local optimum, problems where the objective function or the constraints or parts of constraints are not differentiable, problems with discontinuous solution spaces with local optima, etc. This strategy is a member of the down-hill-climbing methods since we are considering minimization as a goal of an optimization process.

The genetic algorithm is one method of the evolution strategies, which was introduced by John Holland and Kenneth around 1975. This method was introduced from natural science to mathematics and therefore lots of biological names are used in it. The GA has to code the phenotype information into bits using mostly the floating point representation known from computer science [4].

One genetic algorithm consists of three parts:

1. **Chromosomes** (Individuals) are selected from the solution space. They can be optima or non-optima but generally they are result of a problem. In GA the chromosomes are built of genes, which encode the independent variables. These codes can be Boolean, integers, floating point, string variables or any combination of them. Traditionally, genes or codes are binary numbers as strings of 0s and 1s. One set of different chromosomes forms a generation.
2. **Cost or Fitness function** is a criterion to evaluate each of chromosomes.
3. **Operators** are used to create new chromosomes from old ones.

The goal of GA is to minimize fitness function. The sequences of this optimization are listed in the following steps.

2.1. Initialization of population

In this step as a first guess to find the best result, an amount of chromosomes is randomly created. The number of these chromosomes P_s, depends on the number of variables of the problem. Usually two methods for P_s are suggested (n is the number of variables):

$$P_s > n+1 \tag{1}$$

$$P_s = 10n \tag{2}$$

2.2. Evaluation of chromosomes

In this step, each of chromosomes are evaluated according to the value of their fitness function, i.e. the chromosome **X** which has lower **F(X)** will have higher value and more chance to be chosen and to generate a new population.

2.3. Selection

Some of good chromosomes are selected in this step using usual selection procedures:
- Roulette Wheel
- Tournament selection
- Ranked-based selection

2.4. GA's Operators

With use of GA's operators, new individuals will be created. The GA's operators are: Mutation and Crossover.

2.4.1. Mutation

This is a random process where one allele of a gene is replaced by another to produce a new chromosome. This operator is mostly used to avoid the local optima but it can cause convergence problem and reduce the speed of convergence. Mutation is randomly applied with low probability in range of 0.001 and 0.01 [5].

Point Mutation: *11101001000* ⟶ *11101011000*

Figure 1. Sample of mutation in binary representation

2.4.2. Crossover

This operator uses an exploitation method to create new individuals, where with combining of two chromosomes of current population it creates new chromosomes. This combination is done by replacement of genes of parent chromosomes (Fig.2). This operator is important to reach the optimum point more quickly, therefore it executed with high probability in range of 0.5 to 0.9 [6].
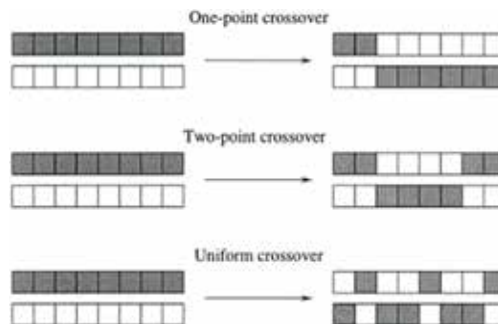
Figure 2. Three kinds of crossover operator

2.5. Termination factor

Two methods for termination of optimization iteration are introduced [5]:
- After reaching the specified number of generations.
- When not a big improvement for last N generations is observed.

An overview of a genetic algorithm is represented by the flowchart in Fig.3.
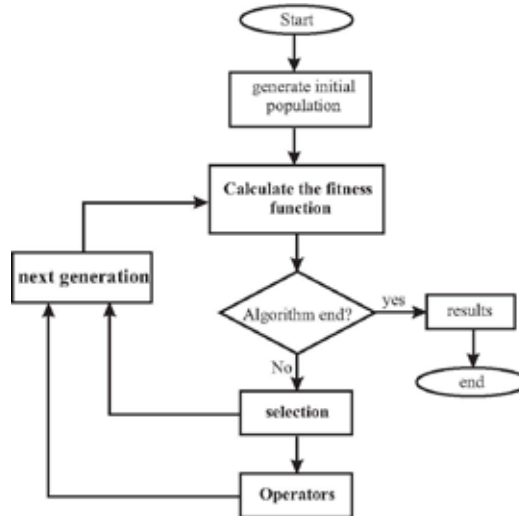
Figure 3. General scheme of a genetic algorithm or any evolutionary algorithms.

3. Multi-objective genetic algorithm

In many complex engineering problems simultaneous optimization of some objective functions is required, while optimizing one objective can cause an unaccepted result from other objectives. Traditionally GA was defined to solve one objective problem but lots of methods are developed to increase its capability. Generally there are two approaches for multi-objective optimization: Weighted sum method and Pareto optimal. In this paper, the Pareto optimal is used.

3.1. Pareto based approach
In many real-life problems, objectives are in conflict with each other. Hence, optimization with respect to one objective can cause unacceptable result for other objectives but a perfect multi-objective solution that simultaneously optimizes all objective functions is almost impossible. A reasonable solution to a multi-objective problem is to find a set of solutions, where each of them satisfies the objectives at an acceptable level without being dominated by any other solution.

To define a Pareto optimal, domination should be defined at first. A vector **v** dominates vector **u** if:

$$\forall i \in \{1, 2, ..., k\} : f_i(\mathbf{v}) \leq f_i(\mathbf{u}); \qquad (3)$$
$$\exists j \in \{1, 2, ..., k\} : f_j(\mathbf{v}) < f_j(\mathbf{u})$$

A vector $\mathbf{x} \in S$ (S: Solution space) is a Pareto optimal solution, if and only if there would be no vector like $\mathbf{y} \in S$, where $f(\mathbf{y}) = (f_1(\mathbf{y}),\ldots, f_k(\mathbf{y}))$ dominates $f(\mathbf{x}) = (f_1(\mathbf{x}),\ldots, f_k(\mathbf{x}))$ [7].

Finding the non-dominated set of solutions from a given set of solutions is similar in principle to finding the minimum of a set of a real numbers. Two approaches are presented in following for finding the non-dominated set from a given population.

3.2. Naive and slow approach
In this approach, each of solutions in population is compared with each other to see which one is dominated and which one not. If the solution i is found to be dominated by another solution, it means that there exists at least one solution which is better than i. A step-by-step
procedure of finding non-dominated set is given in the following [8]:
1. Set the solution counter $i=1$ and create an empty non-dominated set P´.
2. For a solution $j \in P$ (but $j \leq i$), check if solution j dominated solution i. if yes go to 4.
3. If more solution are left in P, increment j by one and go to 2; otherwise, set P´=P $\cup$ {i}.
4. Increment i by one. If $i \leq N$, go to step 2; otherwise stop and declare P´ as the non-dominated set.

3.3. Non-dominated Sorting of a Population
There exists some algorithm to classify the entire population into various non-dominated levels. The best non-dominated solutions are called non-dominated solutions of level 1. Once the best non-dominated set is identified, they are temporarily neglected from the population. The non-dominated solutions of the remaining population are then found and are called non-dominated solutions of level 2 and then it is neglected. This procedure
is continued until all population individuals are classified into non-dominated levels. The steps of procedure are represented in the following [9]:
1. Set all non-dominated sets P_j, ($j = 1, 2,\ldots$) as empty sets. Set non-domination level counter $j=1$.
2. Use non-domination approach like naive and slow to find the non-dominated set P of the population P.
3. Update $P_j = P´$ and $P = P/P´$.
4. If $P \neq P´$, increment j by one and go to 2. Otherwise, stop and declare all non-dominated sets P_i, for $i = 1, 2,\ldots, j$.

4. Controllability and observability

Controllability and observability are structural properties that carry useful information for testing and control.

Definition 1: System states given by state equation are controllable if it is possible by admissible inputs to steer the states from any initial value to any final value within some

time window. Observability is a measure for how well internal states of a system can be inferred by knowledge of its external outputs [10].

Definition 2: A structure is controllable if the installed actuators excite all its structural modes. It is observable if the installed sensors detect the motions of all the modes [11].

4.1. Continuous-time systems

A linear time invariant system (**A, B, C**) with s inputs is completely controllable when the controllability matrix

$$\mathbf{S}_{co} = \begin{bmatrix} \mathbf{B} & \mathbf{AB} & \mathbf{A^2B} & \cdots & \mathbf{A}^{N-1}\mathbf{B} \end{bmatrix} \qquad (4)$$

has rank N (N is number of states). And the system is completely observable if the observability matrix has rank N [10].

$$\mathbf{S}_{ob} = \begin{bmatrix} \mathbf{C} \\ \mathbf{CA} \\ \mathbf{CA}^2 \\ \vdots \\ \mathbf{CA}^{N-1} \end{bmatrix} \qquad (5)$$

The above criterion is simple but it has two disadvantages that first they answer the controllability and observability question in yes or no terms and second they are not useful for a system of big dimensions, since it causes numeric problems and enlarge the calculation time. Grammians are the alternative approach for determining the system properties. Grammians are nonnegative matrices which can express the controllability and observability in qualitative form and they are free of the numerical difficulties. The controllability and observability grammians are:

$$\mathbf{W}_c(t) = \int_0^t e^{\mathbf{A}t} \mathbf{B}\, \mathbf{B}^T e^{\mathbf{A}^T \tau} d\tau \qquad (6)$$

$$\mathbf{W}_o(t) = \int_0^t e^{\mathbf{A}t} \mathbf{C}\, \mathbf{C}^T e^{\mathbf{A}^T t} dt \qquad (7)$$

For a stable system, the grammians can be obtained by (9) which is called Lyapunov equations:

$$\begin{aligned} \mathbf{AW}_c + \mathbf{W}_c \mathbf{A}^T + \mathbf{BB}^T = 0 \\ \mathbf{A}^T \mathbf{W}_o + \mathbf{W}_o \mathbf{A} + \mathbf{C}^T \mathbf{C} = 0 \end{aligned} \qquad (8)$$

The eigenvalues of the product of grammians are independent of coordinate transformation and can be denoted as:

$$\gamma_i = \sqrt{\lambda_i(\mathbf{W}_c \mathbf{W}_o)} \qquad (9)$$

They are referred to as the Hankel singular values of the system [11].

4.2. Controllability and observability of a structural modal model

The modal state-space representation of flexible structures has specific controllability and observability properties, and its grammians are of a specific form.

338

When the damping is small, the grammians in modal coordinates are diagonally dominant and by using appropriate scaling they are approximately equal.

$$\mathbf{W}_c \cong diag(w_{ci}\mathbf{I}_2)$$
$$\mathbf{W}_c \cong diag(w_{ci}\mathbf{I}_2)$$
$$(10)$$

Therefore, the approximated Hankel singular values are obtained as a geometric mean of the modal controllability and observability factors.

$$\gamma_i \cong \sqrt{w_{cii}w_{oii}} \tag{11}$$

For flexible structures the grammians of each mode can be expressed in a closed form. This allows for their speedy determination for structures with a large number of modes, and allows for the insight into the grammian physical interpretation. In modal coordinates the diagonal entries of the controllability and observability grammians are in form:

$$w_{ci} = \frac{\|B_{mi}\|_2^2}{4\zeta_i\omega_i}, \qquad w_{oi} = \frac{\|C_{mi}\|_2^2}{4\zeta_i\omega_i} \tag{12}$$

and the approximated Hankel singular values are [11]:

$$\gamma_i = \frac{\|B_{mi}\|_2 \|C_{mi}\|_2}{4\zeta_i\omega_i} \tag{13}$$

The form of (14) is similar to norm of a system. System norm serves as a measure of intensity of its response to standard excitations such as unit impulse or white noise of unit standard deviation. Typical system norms are: H_2, H_∞, and Hankel. In this work H_∞ is used, which is defined as [12]:

$$\|G\|_\infty = \sup_{u(t)\neq 0} \frac{\|y(t)\|_2}{\|u(t)\|_2} \tag{14}$$

or alternatively as:

$$\|G\|_\infty = \max_\omega \sigma_{max}(G(\omega)) \tag{15}$$

where

$$G(\omega) = C(j\omega\mathbf{I} - \mathbf{A})^{-1} \tag{16}$$

is the transfer function of a system and

$$\sigma_{max}(G(\omega)) \tag{17}$$

is the largest singular value of G. The peak of the transfer function magnitude is the H_∞ norm of a single-input-single-output system.

The H_∞ norm in modal coordinate for each mode is expressed as following:

$$\|G\|_\infty = \sigma_{max}(G_i(\omega_i)) = \frac{\sigma_{max}(C_{mi}B_{mi}))}{2\zeta_i\omega_i} = \frac{\|B_{mi}\|_2 \|C_{mi}\|_2}{2\zeta_i\omega_i} \tag{18}$$

The acquired equation is similar to (14), hence it is a good criterion for measurement of controllability and observability of a system.

5. Application of optimal placement

This section includes the results for different host structures of piezoelectric patches. These host structures are a cantilever beam and a simply supported plate. At last, the frequency response of the different structures is depicted to show how well piezo-patches are placed on the structure. In Fig.4 the general algorithm, which has been used in this work to find optimal places of piezoelectric patches, is depicted.
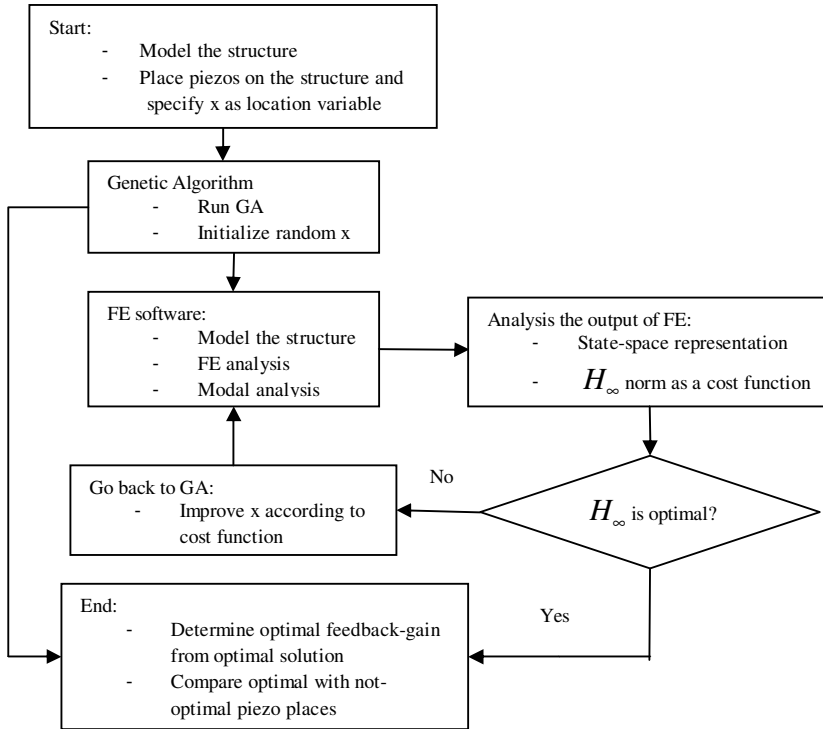
Figure 4. Flow-chart of the optimization procedure applied throughout this work

In this paper, when analyses are made on a beam, the beam has properties and size as shown in Fig.5.

5.1. Optimal locations of four piezo-patches on a cantilever beam

In this section, the optimization is done for optimal places of four piezoelectric patches based on the first mode of the system which is the most important mode, and then for first four modes of the structure with use of multi objective genetic algorithm.

5.1.1. Optimization based on first mode

It has been assumed that there are four patches, two of them act as sensors and other two act as actuators. The sensor and actuator are placed on the same location on the beam but on opposite sides. Therefore just finding the x_1, x_2 is enough.

In this case the genetic algorithm is run with population size of 20 in 100 generations. After 11 generations, the genetic algorithm converges to the best result (Fig.6) and gives x1 = 0.01; x2 = 0.07 as optimal places of piezoelectric patches. After finding the optimal places, it has been analyzed how well this optimization is done. For this propose, the output of system with optimized placement is compared with not-optimized one (Fig.7).

Length of beam	L	0.44 m
Width of beam	B	0.04 m
Height of beam	H	0.0028 m
Length of patch	L1	0.05 m
Width of patch	B1	0.03 m
Height of patch	H1	0.0005 m
Elastic modulus	E	$0.7 \times 10^{11}\ N/m^2$
Poisson's ratio	υ	0.33
Density	ρ	$2800\ kg/m^3$
Beam element type in Ansys		Solid45
Stiffness matrix	C	$\begin{bmatrix} 12.29\times10^{10} & 7.66\times10^{10} & 7.02\times10^{10} & 0 & 0 & 0 \\ 7.66\times10^{10} & 12.29\times10^{10} & 7.02\times10^{10} & 0 & 0 & 0 \\ 7.02\times10^{10} & 7.02\times10^{10} & 9.71\times10^{10} & 0 & 0 & 0 \\ 0 & 0 & 0 & 2.32\times10^{10} & 0 & 0 \\ 0 & 0 & 0 & 0 & 2.32\times10^{10} & 0 \\ 0 & 0 & 0 & 0 & 0 & 2.32\times10^{10} \end{bmatrix}$
Piezoelectric element type in Ansys		Solid5
Piezoelectric constant matrix d		$\begin{bmatrix} 0 & 0 & 7.07 \\ 0 & 0 & 7.07 \\ 0 & 0 & -13.82 \\ 0 & 0 & 0 \\ 0 & -11.91 & 0 \\ -11.91 & 0 & 0 \end{bmatrix}$
Permittivity matrix	ε	$\begin{bmatrix} 929 & 0 & 0 \\ 0 & 929 & 0 \\ 0 & 0 & 857 \end{bmatrix}$

Figure 5. A cantilever Beam with its properties.
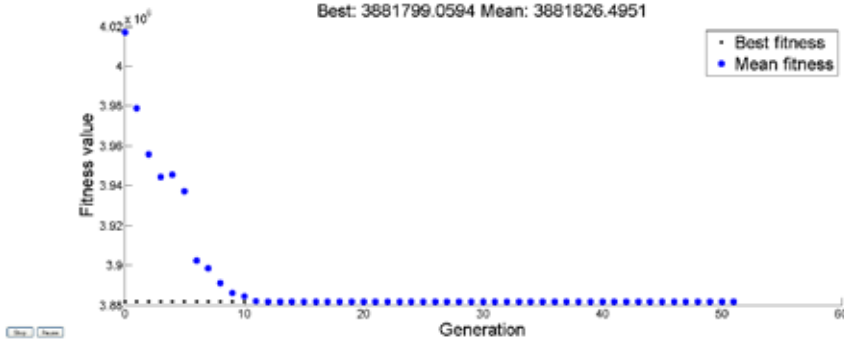
Figure 6. The genetic algorithm process for a cantilever beam with four patches (Pop.=20, Gen.=100).
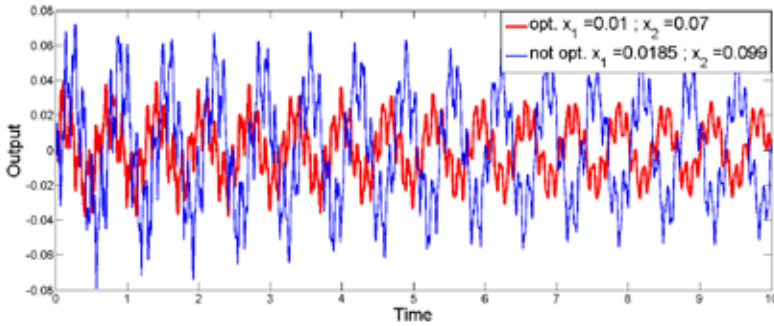
Figure 7. The outputs of optimized and not-optimized placement for the cantilever beam (opt. is based on first modes).

5.1.2. *Optimization based on first four modes*

The procedure of finding optimal places of four piezo-patches on a cantilever beam regarding the first four modes of the structure is almost like the previous procedure with some small changes. In this optimization process, the multi-objective genetic algorithm has

been used. The multi-objective GA has ran with 40 as population size in 200 generations. The multi-objective GA uses Pareto front approach and gives the best Pareto front as shown in Fig.8. The optimization process gives fourteen good places for piezo-patches. All these results are optima and are far better than not-optimized ones (Fig.9) but to see which result is the best one and which one is more compatible with our requests, the optimal control method is applied again, similarly as mentioned in the previous section (Fig.10).
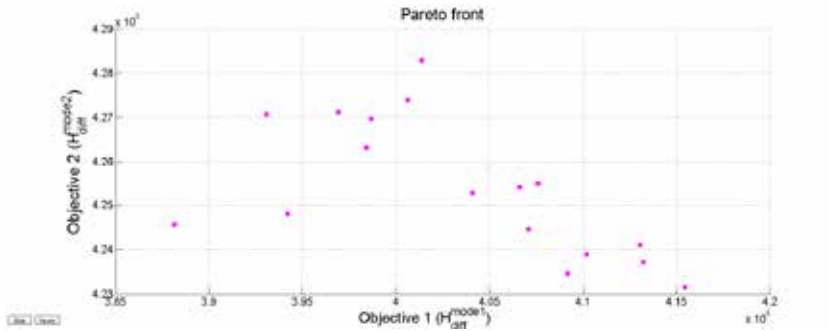
Figure 8. The best Pareto front after 150 generations for optimization based on first four modes (Pop.=40, Gen.=200).
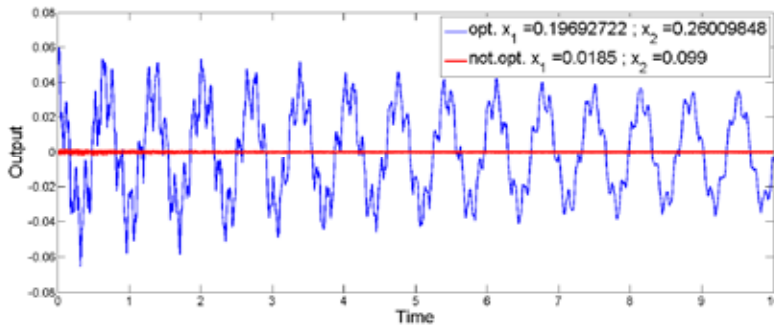
Figure 9. Comparison of opt. and not-opt. places of four patches on a cantilever beam regarding first four modes
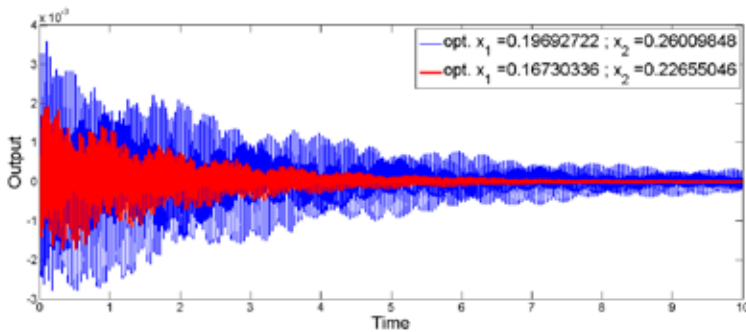
Figure 10. Comparison of two opt. places of four patches on a cantilever beam regarding first four modes.

5.2. *Optimal placement of four piezoelectric patches on a plate*

In this approach, the same procedure is followed as for the cantilever beam but now there are four design variables x_1, x_2, x_3, and x_4, which are defined as in Fig.11.

343
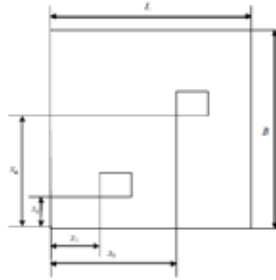
Figure 11. A schematic of the plate L = B = 0:44m.

5.2.1. Optimal places of piezo-patches for plate regarding first mode of the structure
After defining the geometry and material properties of the structure, the optimization of the placement for piezoelectric actuators and sensors is performed. The GA is used again to find these optimal places. The GA was run for population size 40 in 150 generations and it has converged to best result after 52 generations (Fig.12).

Fig.13 shows that the optimization is ended with very convenient results.
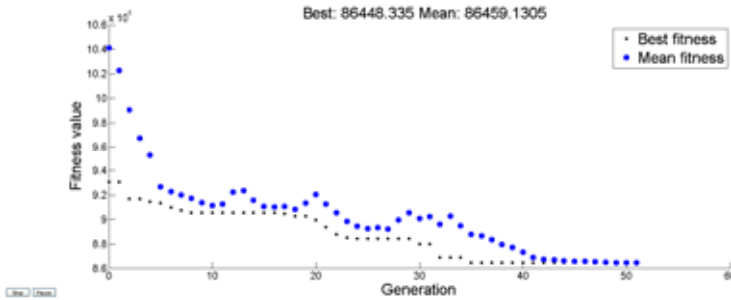
Figure 12. The GA performance to find optimal places of piezos on a plate regarding its first mode. (Pop.=40, Gen.=150).
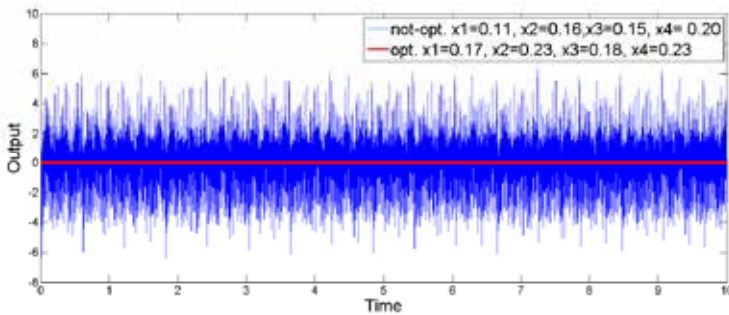
Figure 13. The comparison of output of two systems: one with optimal places and other one with random placement.

5.2.2. Optimal places of piezo-patches regarding first four modes of the structure

The multi-objective GA was executed with the 40 population size in 150 generations. This optimization process ends with giving final Pareto front which is depicted in Fig.14.

As Fig.15 shows, the best optimum placement is placement with: $x1 = 0.19$, $x2 = 0.25$, $x3 = 0.19$, $x4 = 0.23$.
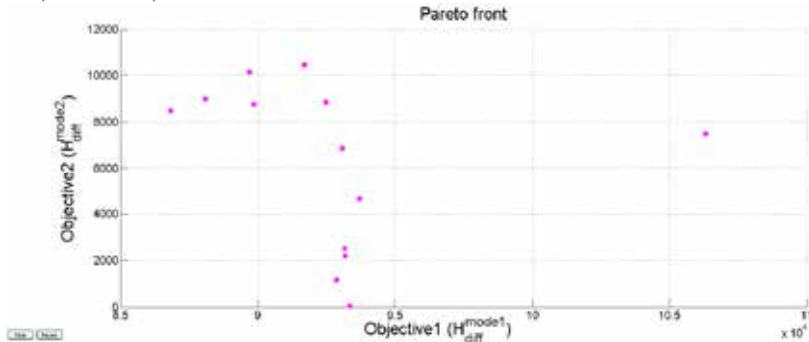
Figure 14. The final Pareto front (Pop.=40, Gen.=150).
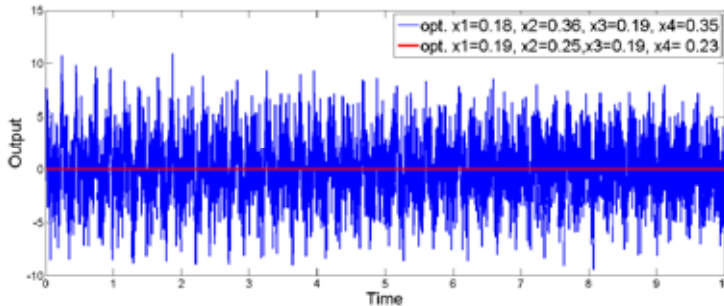
Figure 15. The comparison of output of optimized with not-optimized placement.

6. Conclusions and outlook

It is very important to find the places on the structure with the highest value of controllability and observability with limited number of piezoelectric patches. The GA has been used to find the optimal places. At first the structure has been analyzed with use of ANSYS to obtain the eigenmodes and eigenfrequencies of the structure. Afterwards, the output of ANSYS has been fed into MATLAB to build state space representation of the structure and at the end a criterion has been introduced for the optimization process with GA. The use of GA or multi-objective GA depends on the optimization purpose that whether optimization should be based on one mode or more than one mode. The process has been applied to two kinds of structures: a cantilever beam and a plate. The optimization process gives very convenient result as it can be seen from figures. The results show the different positions of piezopatches when optimization

based on one mode or more than one mode. From design point of view, it is very important beforehand to make a decision which mode shape or mode shapes are important to be controlled. In the GA, it is also possible to define some constraints regarding the position of piezo-patches since in some designs there are some predefined places that the patches cannot be embedded there. It is also possible to apply this optimization process to different types of structures.

In this paper, the optimization is done with limited numbers of piezo-patches but it is also possible to generalize the code to find optimal number of piezo-patches. Optimization of the number of pizo-patches as well as implementation of the procedure with complex geometries is a part of the ongoing research.

References

[1] Arbel, A., 1981, Controllability measures and actuator placement in oscillatory systems, International Journal of Control, 33, 565-574

[2] Hac, A., Liu, L., 1993, Sensor and actuator location in motion control of Fexible structures, Journal of Sound and Vibration, 167, 239-261

[3] Devasia, S., Meressi, T., Paden, B., Bayo, E., 1993, Piezoelectric actuator design for vibration suppression:
    placement and sizing, Journal of Guidance, Control and Dynamics, 16, 859-864

[4] Hartmann, D., 2010, Design Optimization (Ruhr-Universitaet Bochum)

[5] Deb, K., 2000, An enceinte constraint handling method for genetic algorithms computer methods in applied mechanics and engineering, 311

[6] Wehrens, R., Lutgarde, M.C., Buyden, S., Evolutionary optimisation: a tutorial Trends in analytical chemistry, 17

[7] Popov, Andrey, Genetic Algorithm for Optimization (Hamburg)

[8] Deb, K., Multi-objective optimization using evolutionary algorithms (s.l. Wiley)

[9] Andersson, J., A survey of multiobjective optimization in engineering design (Linkoeping University, Sweeden)

[10] Nestorović, T., Koppe, H., Gabbert, U., 2007, A direct model reference adaptive control system design and simulation for the vibration suppression of a piezoelectric smart structure, in Nonlinear Science and Complexity (editors A. Luo, L. Dai, H. Hamidzadeh, Transactions of Nonlinear Science and Complexity, Volume 1, World Scienti_c, Singapore) 375-381

[11] Gawronski, Wodek, K., Advanced Structural Dynamics and Active Control of Strutures (California Institute of Technology, Springer)

[12] Trajkov M., Nestorovic' T., July 2012, Optimal placement of piezoelectric actuators and sensors for smart structures, in "Experimental Mechanics, New Trends and Perspectives", J.F. Silva Gomes and Mário A.P. Vaz, Editors, Proceedings of the 15th International Conference on Experimental Mechanics ICEM15, Porto/Portugal, July 2012, Paper No. 2716, p. 1-13, ISBN: 978-972-8826-26-0

H_2 AND H_∞ BASED OPTIMAL PLACEMENT OF ACTUATORS AND SENSORS FOR ACTIVE VIBRATION CONTROL

Miroslav Trajkov [1], Tamara Nestorović [2]

[1, 2] Institute of Computational Engineering, Mechanics of Adaptive Systems
Ruhr-Universität Bochum, Universitätsstraße 150, D-44801 Bochum, Germany
e-mail: [1] miroslav.trajkov@rub.de, tamara.nestorovic@rub.de [2]

Abstract. This paper considers the problem of optimal actuator and sensor placement for active large flexible structures. The proposed placement optimization method is based on balanced reduced models. It overcomes disadvantages arising from demanding numeric procedures related with high order structural models. Optimization procedure relies on H_2 and H_∞ norms, as well as on controllability and observability Gramians, related with structural eigenmodes of interest. The optimization procedure was documented by several examples showing a good agreement between the results obtained using different placement indices.

1. Introduction

The study and development of piezoelectric smart structures involves a very important investigation of optimal actuator and sensor placement. Especially for piezoelectric smart structures and systems, the placement once applied cannot be changed easily and it is often related with the need to build a new structure in order to perform another placement constellation for actuators and sensors. Development of appropriate and reliable optimization procedures, which can be applied prior to real structure or a prototype building, is therefore the task of a great significance. In this paper we have proposed a reliable method for determining appropriate actuator/sensor placement, based on structural models developed using the finite element (FE) approach. Model based approach represents an indispensable tool in the optimization procedure due to requirement for iterative problem solution.

Optimization problem was treated by several authors and investigated for different structures. An overview of the optimization criteria for optimal placement of piezoelectric sensors and actuators on a smart structure was given in a technical review by Gupta et al. [1]. In [2] based on the modal approach, optimal geometrical conditions were obtained for several cases of active beams with different boundary conditions. Optimization criterion for finding optimal actuator/sensor positions for piezoelectric beams in [3] is the performance of an optimal LQR controller. In [4] efficiency indices

based on the mode shapes for a clamped piezoelectric beam were determined for typical eigenmodes.

Kumar and Narayanan [5] have applied the LQR controller based criteria to find optimal location of piezoelectric actuators/sensors for vibration control of plates and used genetic algorithm (GA) for solving a zero-one optimization problem. Peng et al. [6] involved maximizing of the controllability Gramian as the optimization criterion for optimal placement on a clamped plate using GA. Similar approach with modal controllability and observability Gramians and GA were also used in [7].

In this paper we present a general approach to optimal actuator and sensor placement applicable both for beam and plate structures, but also for other complex geometries of structures. The optimal placement procedure is based on the method for balanced model reduction, which assumes models with equally controllable and observable retained modes. The method has advantage over modal truncation and mathematical criteria for controllability and observability, since the retaining of the modes of interest is founded on their equal controllability and observability expressed in terms of appropriate Gramians. Further the paper deals with optimization criteria based on the H_2 and H_∞ norms, which are calculated for all possible candidate locations. In this way the fulfillment of the criteria is not limited to a narrow set of selected assumed favorable locations, but it relies on verification through all candidate positions by finding the placement indices with largest values.

2. Models and objective functions used for optimal placement

The procedure for finding optimal placement of actuators and sensors relies on the state space models of smart structures, which are obtained through the finite element (FE) modeling procedure and model order reduction.

2.1. FE based state space models

Applying general FE modeling procedure the model of a smart structure can be represented as a set of equations of motion in matrix form (1) obtained by assembling all finite elements of the structure (more details on FE modeling of piezoelectric structures can be found in [8,9]).

$$\mathbf{M\ddot{q}} + \mathbf{D}_d\mathbf{\dot{q}} + \mathbf{Kq} = \mathbf{F} \tag{1}$$

Vector $\mathbf{q}$ contains all degrees of freedom and it can be formed e.g. by node-wise arranging of degrees of freedom for all elements. For modeling of piezoelectric materials besides mechanical degrees of freedom, electric voltage or charge is included as additional degree of freedom to model electro-mechanical behavior.

The total load vector $\mathbf{F}$ is split, for the purpose of the control design later, into the vector of external forces $\mathbf{F}_E$ and the vector of control forces $\mathbf{F}_C$:

$$\mathbf{F} = \mathbf{F}_E + \mathbf{F}_C = \mathbf{\overline{E}\overline{f}}(t) + \mathbf{\overline{B}\overline{u}}(t) = \mathbf{B}_0\mathbf{u} . \tag{2}$$

The forces are here generalized quantities, which include also electric charges or electric potentials. Matrices $\mathbf{\overline{E}}$ and $\mathbf{\overline{B}}$ describe the positions of generalized external forces $\mathbf{\overline{f}}$

and the control parameters $\bar{\mathbf{u}}$ in the finite element structure, respectively. Matrix $\mathbf{B}_0$ represents the input matrix, and vector $\mathbf{u}$ includes all model inputs.

For the controller design purposes equation (2) is accompanied by the output equation in the form:

$$\mathbf{y} = \mathbf{C}_{0q}\mathbf{q} + \mathbf{C}_{0v}\dot{\mathbf{q}} \tag{3}$$

where in a general case $\mathbf{C}_{0q}$ represents the output displacement matrix, and $\mathbf{C}_{0v}$ the output velocity matrix. In the output equation (3) $\mathbf{q}$ represents a generalized displacement vector containing all degrees of freedom defined in the modeling procedure, like in (1). Matrices $\mathbf{C}_{0q}$ and $\mathbf{C}_{0v}$ are obtained through an FE procedure by defining appropriate sensor locations.

Solution of the equation (1) is determined in the form $\mathbf{q} = \boldsymbol{\varphi}e^{j\omega t}$ by solving the eigenvalue problem for a homogeneous case.

The nodal model representation (1) is transformed into a model in modal coordinates applying the following modal transformation:

$$\mathbf{q} = \boldsymbol{\Phi}\mathbf{q}_m \tag{4}$$

where $\mathbf{q}_m$ represents the vector of modal degrees of freedom or generalized modal displacements and $\boldsymbol{\Phi}$ is the modal matrix.

Introducing the modal coordinates (4) into (1) after normalization with respect to mass and appropriate transformations, taking into account the orthogonality properties the modal model is obtained, which after introducing the coordinate transformation in the state space form:

$$\mathbf{x} = \begin{bmatrix} \boldsymbol{\Omega}\mathbf{q}_m \\ \dot{\mathbf{q}}_m \end{bmatrix} \tag{5}$$

can be obtained as a state space realization:

$$\dot{\mathbf{x}} = \mathbf{A}\mathbf{x} + \mathbf{B}\mathbf{u}, \quad \mathbf{y} = \mathbf{C}\mathbf{x} + \mathbf{D}\mathbf{u} \tag{6}$$

Considering that flexible structures can be described in terms of independent coordinates, the modal state space model can be expressed in terms of state space realizations ($\mathbf{A}_{mi}$, $\mathbf{B}_{mi}$, $\mathbf{C}_{mi}$) for each mode i (7). With the coordinate transformation as in (5) corresponding matrices in the realization ($\mathbf{A}_{mi}$, $\mathbf{B}_{mi}$, $\mathbf{C}_{mi}$) are determined by [10]:

$$\mathbf{A}_{mi} = \begin{bmatrix} 0 & \omega_i \\ -\omega_i & -2\zeta_i\omega_i \end{bmatrix}, \mathbf{B}_{mi} = \begin{bmatrix} 0 \\ b_{m_i} \end{bmatrix}, \mathbf{C}_{mi} = \begin{bmatrix} \dfrac{c_{mq_i}}{\omega_i} & c_{mv_i} \end{bmatrix} \tag{7}$$

with natural eigenfrequencies ω_i and dampings ζ_i of the eigenmodes. The elements of the realization ($\mathbf{A}_{mi}$, $\mathbf{B}_{mi}$, $\mathbf{C}_{mi}$) are used for assessing the optimal actuator/sensor locations based on candidate input/output transfer functions relating corresponding actuators and sensors.

2.2. Norms – objective functions for optimal placement

Optimization of the actuator/sensor placement in this work is based on the properties of the H_2 and H_∞ norms and approximations for their determining, which enables norm

calculation in cases of large structures with high model orders. Exact calculation of the norms in such cases would require high computational effort and computational time. Proposed approach represents a suitable basis for optimal actuator and sensor placement in large structures due to reduced required computational time. The norms and their properties, which are considered and implemented in optimization procedure, are defined for a single mode, for a structure and for a system including a set of actuators and sensors. The main norm properties are summarized below. The proofs are derived in [10].

H_2 norm of a single mode. For a transfer function $G_i(\omega) = \mathbf{C}_{mi}(j\omega\mathbf{I} - \mathbf{A}_{mi})^{-1}\mathbf{B}_{mi}$ of the ith mode obtained from the realization (7), the H_2 norm of the mode is estimated as:

$$\|G_i\|_2 \cong \frac{\|\mathbf{B}_{mi}\|_2 \|\mathbf{C}_{mi}\|_2}{2\sqrt{\zeta_i\omega_i}} = \frac{\|\mathbf{B}_{mi}\|_2 \|\mathbf{C}_{mi}\|_2}{\sqrt{2\Delta\omega_i}} \cong \sigma_i\sqrt{2\Delta\omega_i} \tag{8}$$

where $\mathbf{B}_{mi}$, $\mathbf{C}_{mi}$ represent the input and the output matrices of the modal state space model defined in (7), ζ_i is the damping of the ith mode, σ_i the Hankel singular value corresponding to the ith mode, and $\Delta\omega_i = 2\zeta_i\omega_i$ is a frequency segment at the ith resonance for which the value of the power spectrum is one half of its resonance value.

H_∞ norm of a single mode. For an ith mode given by its modal realization $(\mathbf{A}_{mi}, \mathbf{B}_{mi}, \mathbf{C}_{mi})$ or by the parameters $(\omega_i, \zeta_i, b_{mi}, c_{mi})$ the H_∞ norm of the mode is estimated as:

$$\|G_i\|_\infty \cong \frac{\|\mathbf{B}_{mi}\|_2 \|\mathbf{C}_{mi}\|_2}{2\zeta_i\omega_i} = \frac{\|b_{mi}\|_2 \|c_{mi}\|_2}{2\zeta_i\omega_i} . \tag{9}$$

H_2 norm of a structure. Given a modal state space realization $(\mathbf{A}_m, \mathbf{B}_m, \mathbf{C}_m)$ of a structure, the H_2 norm of the structure can be determined approximately as the root mean square of the modal norms:

$$\|G\|_2 \cong \sqrt{\sum_{i=1}^{n} \|G_i\|_2^2} , \tag{10}$$

where n represents the number of the modes, and G and Gi are the transfer function (or the transfer matrix) of the structure and of the ith mode respectively.

H_∞ norm of a structure. Since the modes are almost independent, the norm H_∞ norm of a structure is approximately determined as the largest of the mode norms:

$$\|G\|_\infty \cong \max_i \|G_i\|_\infty , \quad i = 1,...,n . \tag{11}$$

For a system including a set of actuators and sensor, for the H_2 and H_∞ norms an additive property both for a single mode and for a structure is valid and can be used in the approximated calculation or the norms.

H_2 and H_∞ norms of a system with a set of actuators and sensors
for a single mode:

$$\|G_i\|_{2,\infty} \cong \sqrt{\sum_{j=1}^{s} \|G_{ij}\|_{(2,\infty)}^2}, \quad i = 1,...,n \tag{12}$$

for a structure:

$$\left\| G \right\|_{2,\infty} \cong \sqrt{\sum_{j=1}^{s} \left\| G_j \right\|_{(2,\infty)}^{2}} \ . \tag{13}$$

with s representing the number of actuators or the number of sensors, which may be different in a general case.

For a given structure the actuator/sensor placement problem requires the selection of optimal locations as a subset from a given set of possible candidate locations with regard to the specified objective function. The set of possible candidate locations consists of a larger number of elements then the subset of locations to be optimized.

In the first approach the placement is performed based on the placement indices and matrices, where the actuator and sensor placements are solved independently using similar procedures. Definition of placement indices and matrices is based on the additive properties of modal norms on the structural level.

For a flexible structure represented by a modal state space model, the norms of any mode i are determined based on appropriate input ($\mathbf{B}_{mi}$) and output ($\mathbf{C}_{mi}$) matrices of the corresponding mode, (8), (9). If s represents the total number of defined inputs (actuators) $j = 1,...,s$, and r the total number of outputs (sensors) $k = 1,...,r$, then the corresponding input and output matrices are:

$$\mathbf{B}_{mi} = \left[\mathbf{B}_{mi}^{1} \mid \mathbf{B}_{mi}^{2} \mid \cdots \mid \mathbf{B}_{mi}^{j} \mid \cdots \mid \mathbf{B}_{mi}^{s} \right]$$
$$\mathbf{C}_{mi}^{T} = \left[\mathbf{C}_{mi}^{1} \mid \mathbf{C}_{mi}^{2} \mid \cdots \mid \mathbf{C}_{mi}^{k} \mid \cdots \mid \mathbf{C}_{mi}^{r} \right] \tag{14}$$

where each of the matrices $\mathbf{B}_{mi}^{j}$ represents the 2×1 block of the jth actuator and $\mathbf{C}_{mi}^{k}$ represents the 1×2 block of the kth sensor, both having the form as in (7). Then according to the additive properties of the H_2 and H_∞ norms, the norm of a mode with a set of actuators (sensors) can be approximated by the root mean square sum of the norms of this mode with a single actuator (sensor), which can be expressed as:

for actuators:
$$\left\| G_i \right\|_{(2,\infty)}^{2} \cong \sum_{j=1}^{s} \left\| G_i^{j} \right\|_{(2,\infty)}^{2} \ , \tag{15}$$

for sensors:
$$\left\| G_i \right\|_{(2,\infty)}^{2} \cong \sum_{k=1}^{r} \left\| G_i^{k} \right\|_{(2,\infty)}^{2} \ . \tag{16}$$

Here the H_2 norms of the ith mode with a single actuator corresponding to the jth position, and of the ith mode with a single sensor corresponding to the kth position are given respectively by:

$$\left\| G_i^{j} \right\|_{2} = \frac{\left\| \mathbf{B}_{mi}^{j} \right\|_{2} \left\| \mathbf{C}_{mi} \right\|_{2}}{2\sqrt{\zeta_i \omega_i}} , \qquad \left\| G_i^{k} \right\|_{2} = \frac{\left\| \mathbf{B}_{mi} \right\|_{2} \left\| \mathbf{C}_{mi}^{k} \right\|_{2}}{2\sqrt{\zeta_i \omega_i}} . \tag{17}$$

Similarly the H_∞ norms of the ith mode with a single actuator corresponding to the jth position, and of the ith mode with a single sensor corresponding to the kth position are expressed as:

$$\left\|G_i^j\right\|_\infty = \frac{\left\|\mathbf{B}_{mi}^j\right\|_2 \left\|\mathbf{C}_{mi}\right\|_2}{2\zeta_i\omega_i}, \qquad \left\|G_i^k\right\|_\infty = \frac{\left\|\mathbf{B}_{mi}\right\|_2 \left\|\mathbf{C}_{mi}^k\right\|_2}{2\zeta_i\omega_i}. \tag{18}$$

Placement indices are defined in terms of H_2 or H_∞ norms for an actuator or a sensor placement. Each index $\eta_{i(2,\infty)}^k$ evaluates the kth actuator (or sensor) in the ith mode in terms of the H_2 or H_∞ norm and it is defined with respect to all modes $i = 1,...,n$ and all admissible actuators $k = 1,...,s$ (or sensors $k = 1,...,r$):

$$\eta_{i(2,\infty)}^k = \frac{\left\|G_i^k\right\|_{(2,\infty)}}{\left\|G\right\|_{(2,\infty)}}. \tag{19}$$

Here the norms $\left\|G_i^k\right\|_{(2,\infty)}$ are determined accordingly as in (17) or (18), and G is the transfer function of the system with all candidate actuators (or sensors). Placement indices determined according to (19) can be arranged in the form of matrix, where each row corresponds to the ith mode and each column to the kth actuator or sensor. Actuator and sensor placement indices are then obtained from the placement matrix by performing column-wise appropriate operations on the elements over all modes. For the objective function in terms of the H_2 norm, actuator (subscript a) or sensor (subscript s) placement indices are determined as the root mean square sum of the column-wise elements:

$$\eta_{(a,s)}^k = \sqrt{\sum_{i=1}^n \left(\eta_i^k\right)^2}, \quad k = 1,...,p \tag{20}$$

and $p = s$ (for s actuators) or $p = r$ (for r sensors). For the objective function in terms of the H_∞ norm, the actuator/sensor placement index is the largest index over all modes:

$$\eta_{(a,s)}^k = \max_i \left(\eta_i^k\right), \qquad i = 1,...,n, \qquad k = 1,...,p \tag{21}$$

where again $p = s$ (for s actuators) or $p = r$ (for r sensors). The placement indices $\eta_{(a,s)}^k$ determined in this way characterize the importance of the kth actuator or sensor, and represent therefore a criterion for the actuator/sensor placement in the presented approach, which treats the actuator and sensor placement individually.

Placement index for simultaneous actuator/sensor placement is defined as

$$\eta_i^{jk} = \frac{\left\|G_i^{jk}\right\|}{\left\|G_m^i\right\|}, \qquad i = 1,...,n \tag{22}$$

for each mode i, where G_i^{jk} characterizes the ith mode in the presence simultaneously of the actuator placed at the jth candidate location and of the sensor at the kth candidate location.

Besides the introduced placement indices, for the comparison purposes, the controllability index is introduced as an objective function for the optimal placement as well. The influence of the actuators to structural eigenforms is determined by the term $\mathbf{B}_m = \mathbf{\Phi}^{\mathrm{T}}\overline{\mathbf{B}}$, se Eq. (2). Different actuator configurations and their influence on the controllability of the ith mode $\boldsymbol{\varphi}_i$ are investigated by determining the value of $\boldsymbol{\tau}_i(j) = \boldsymbol{\varphi}_i^{\mathrm{T}}\overline{\mathbf{B}}_j$ for the jth actuator location. The controllability index is calculated based on the squared value of $\boldsymbol{\tau}_i$ and divided by the scalar product of the eigenvectors, in order to obtain the controllability index as a measure which is independent of the sign influenced by placement and independent of the eigenvector scaling. The controllability index can thus be determined as [19]:

$$\mu_i(j) = \frac{\boldsymbol{\varphi}_i^{\mathrm{T}}\overline{\mathbf{B}}_j\overline{\mathbf{B}}_j^{\mathrm{T}}\boldsymbol{\varphi}_i}{\boldsymbol{\varphi}_i^{\mathrm{T}}\boldsymbol{\varphi}_i} \ . \tag{23}$$

In a similar way the influence of the sensor placement can be considered through appropriate observability indices for the kth sensor location:

$$\nu_i(k) = \frac{\boldsymbol{\varphi}_i^{\mathrm{T}}\mathbf{C}_k^{\mathrm{T}}\mathbf{C}_k\boldsymbol{\varphi}_i}{\boldsymbol{\varphi}_i^{\mathrm{T}}\boldsymbol{\varphi}_i} \ . \tag{24}$$

3. Results of optimal placement for investigated beam and plate structures

To illustrate the optimization of the actuator/sensor placement, the results of the placement for a clamped piezoelectric beam and plate are presented in this section.
Clamped beam

In this example a steel beam clamped on both sides is considered. It is modeled as a 2D beam using the ANSYS software. As a result of the modal analysis, the eigenfrequencies and eigenvectors are determined, which represent an input to the algorithms for the optimal actuator/sensor placement procedures. Meshing the beam along its length results in 101 nodes, and possible candidate positions for this analysis are represented schematically in Figure 1 with pointed nodes 10, 20, … , 90.
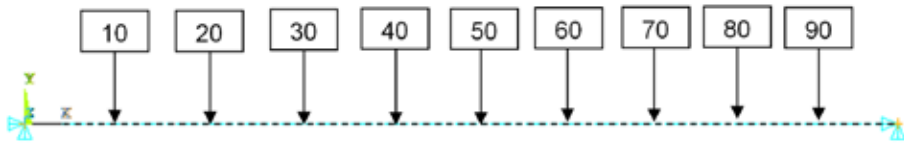
Figure 1. Candidate locations for actuator/sensor placement along the beam clamped on both sides

For the comparison purpose the optimal placement procedure was performed applying the algorithms for separate and simultaneous placement as well as the controllability/ observability indices. Several representative examples are presented below.
Qualitative representations of the curves presenting the values of the placement indices for different positions along the beam are similar for separate placement based on the H_2

and H_∞ norms. Depending on the number of eigenmodes, which should be considered (sensed or actuated) at the same time, the positions for optimal actuator/sensor placement may differ. Figure 2 shows different possible candidate positions with largest placement indices calculated based on the H_2 norm under consideration five bending eigenmodes of interest.
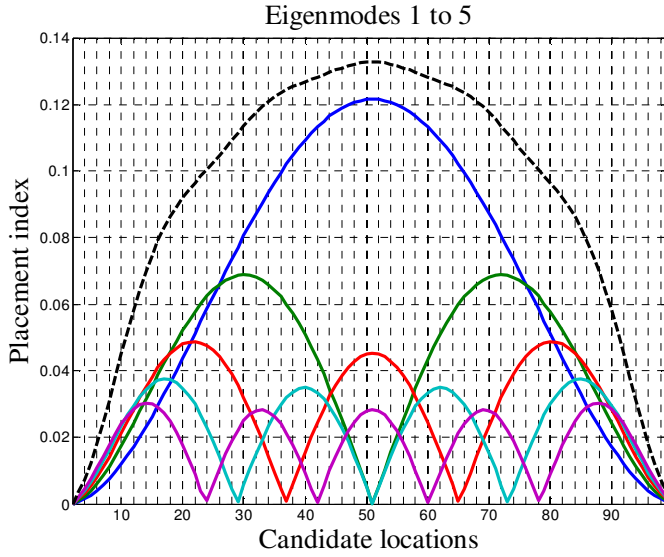

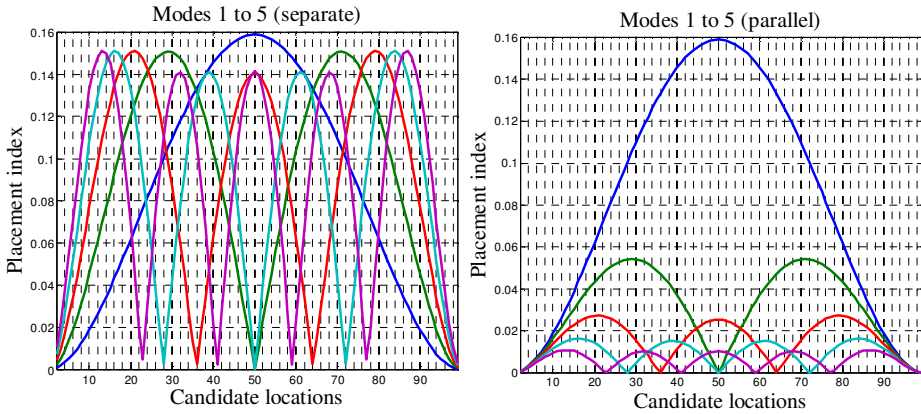**Figure 2.** Placement indices calculated based on the H_2 norm for the first five eigenmmodes

Figure 3. Placement indices based on the H_∞ norm for separate and parallel consideration of the eigenmodes

Placement indices determined based on the H_∞ norm are represented in Figure 3. Left hand side plot in represents the placement indices for individually considered eigenmodes 1 to 5. In the right hand side plot the placement indices were calculated based on parallel consideration of several eigenmodes of interest (here 1 to 5). Locations with largest placement indices indicate the candidates for optimal placement, depending on the number of employed actuators/sensors and on the number of considered modes of interest. Figures 2 and 3 represent the sensor placement indices. The forms of the placement indices curves for actuators are qualitatively the same and for the reason of brevity are omitted here. For the comparison, the method based on the controllability/observability indices is also applied. The results regarding the first five eigenmodes of the beam are summarized by the controllability index representation in Figure 4.
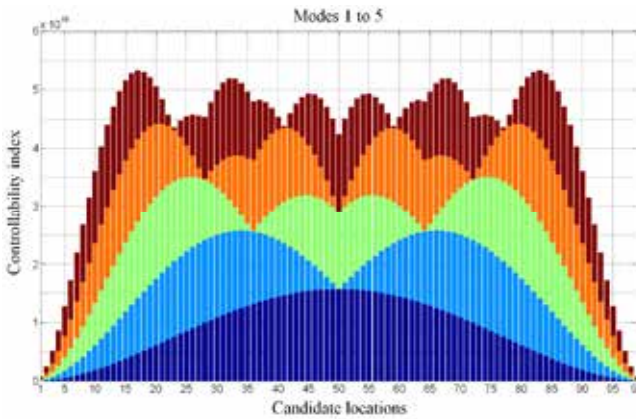
Figure 4. Controllability indices calculated for eigenmodes 1 to 5 for different candidate locations

The results of the three methods applied to the beam clamped on both ends are summarized in Table 1. It can be seen that all three methods provide identical results, when considering eigenmodes individualy. For parallel consideration of several eigenmodes of interest, optimal candidate locations depend on the performance index which was adopted as a criterion for placement.

Table 1. Candidate locations with largest placement indices (beam clamped on both sides)

Modes	Separate placement		Simultaneous placement		Controllability/observability indices
	H_2	H_∞	H_2	H_∞	
1	50	50	50	50	50
2	29, 71	29, 71	29, 71	29, 71	29, 71
3	21, 79	21, 79	21, 79	21, 79	21, 79
4	16, 84	16, 84	16, 84	16, 84	16, 84
5	13, 87	13, 87	13, 87	13, 87	13, 87
1, 2	43 to 57	50			34, 35, 36, 64, 65, 66
1 to 3	48 to 52	50			26, 74
1 to 4	47 to 53	50			21, 79, 41, 59
1 to 5	49 to 51	50			17, 83, 69, 31

Clamped plate

The plate structure in this example was modeled as a 3D plate in ANSYS software and corresponding eigenvectors of interest were obtained through modal analysis. The meshing of the plate, i.e. the nodes which correspond to candidate locations for actuator/sensor placement are represented in Figure 5. Here the corresponding rows and columns are numerated for a better preview.
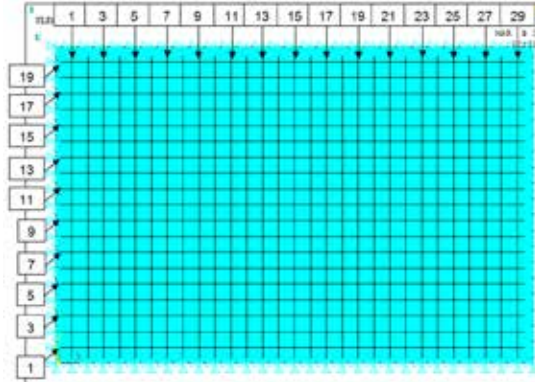
Figure 5. Candidate locations for the plate denoted by corresponding row and column numbers

Table 2. Candidate locations with largest placement indices (plate)

Modes	Separate placement		Controllability index
	H_2	H_∞	
1	(10,15)	(10,15)	(10,15)
2	(10,8), (10,9), (10,21), (10,22)	(10,8), (10,9), (10,21), (10,22)	(10,8), (10,9), (10,21), (10,22)
3	(14,15), (6,15)	(14,15), (6,15)	(14,15), (6,15)
4	(10,6), (10,15), (10,24)	(10,6), (10,15), (10,24)	(10,6), (10,15), (10,24)
5	(6,8), (6,22), (14,8), (14,22)	(6,8), (6,22), (14,8), (14,22)	(6,8), (6,22), (14,8), (14,22)
1, 2	(10,9), (10,10), (10,20), (10,21)	(10,15)	(10,10), (10,20)
1 to 3	(9,9), (9,10), (9,20), (9,21)	(10,15)	(7,11), (7,19), (13,11), (13,19)
1 to 4	(10,7), (10,22)	(10,15)	(12,8), (8,8), (12,22), (8,22)
1 to 5	(7,8), (13,8), (7,22), (13,22)	(10,15)	(13,8), (7,8), (13,22), (7,22)

Due to a very high number of nodes, i.e. candidate locations for the plate, the simultaneous placement procedure would not give a clear representation and therefore it is omitted from this analysis. The results of other two methods, separate placement and controllability index, are compared and summarized in Table 2. Besides, several representative results of the actuator/sensor placement for the clamped plate are shown in the figures below. Complete agreement of the results is available for individual

consideration of the eigenmodes. For parallel consideration of several structural eigenmodes of interest, the arising differences are based on the calculation, i.e. on the definition of the placement indices for the structure. Qualitative representations of the placement indices based on H_2 and H_∞ norms as well as of the controllability index for individually considered modes are the same. Actuator placement indices based on the H_2 norm for selected individual modes are represented in Figure 6.
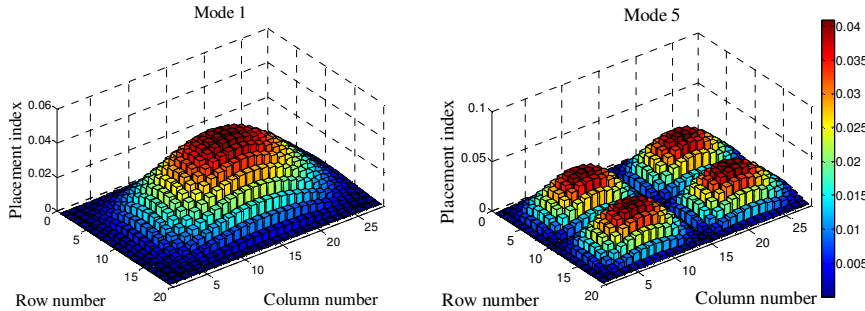
Figure 6. Placement indices based on H_2 norm for individually considered selected eigenmodes of the plate

Figure 7 represents the values of the placement indices calculated for all selected candidate locations based on the H_2 norm under parallel consideration of several eigenmodes of interest (*left*: modes 1 and 2; *right:* modes 1 to 5).
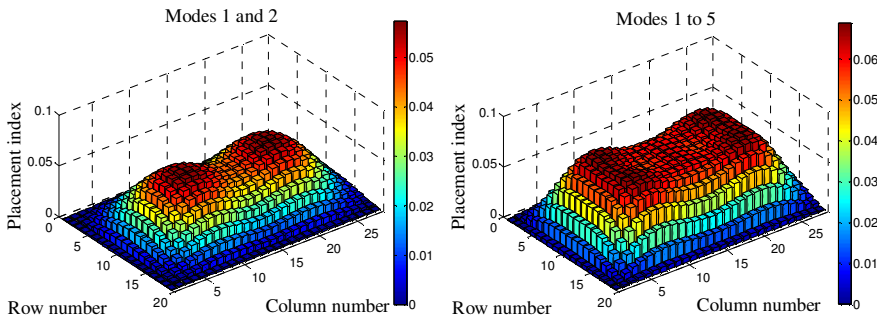
Figure 7. Placement indices for the plate based on the H_2 norm (parallel consideration of eigenmodes of interest)

4. Conclusion

In this paper the optimization methods for actuator/sensor placement for large flexible structures are presented, based on balanced reduction of structural models. Balanced modal reduction of the model orders for structures with large numbers of degrees of freedom is proposed as an efficient modeling procedure, which results in a realization with equally controllable and observable retained states. Optimal placement procedure is

based on the properties of the H_2 and H_∞ norms and approximations for their determining. Proposed approach represents a suitable basis for optimal actuator and sensor placement in large structures due to reduced required computational time.

Optimization procedure is proven by showing examples of a beam clamped on both sides and clamped plate. For these examples an extensive analysis was conducted and systematized results of separate and simultaneous placement procedures for individual and parallel consideration of the structural modes are shown. The efficiency of the proposed method is also proven by the comparison with the optimization results based on controllability and observability indices. This analysis has shown a compete agreement of the results. The method suggested in this paper also covers a broad spectrum of possible problems, which do not have to be necessarily limited only to piezoelectric actuators and sensors, but can be extended more generally to systems with integrated actuators and sensors, whose effect may be considered through actuation forces or moments.

References

[1] Gupta V., Sharma M. and Thakur N. (2010) Optimization Criteria for Optimal Placement of Piezoelectric Sensors and Actuators on a Smart Structure: A Technical Review, *Journal of Intelligent Material Systems and Structures*, 21(12), 1227-1243

[2] Barboni R., Mannini A., Fantini E. and Gaudenzi P. (2000) Optimal placement of PZT actuators for the control of beam dynamics, *Smart Mater. Struct.* 9, 110-120

[3] Kumar K. R. and Narayanan S. (2008) Active vibration control of beams with optimal placement of piezoelectric sensor/actuator pairs, *Smart Mater. Struct.* **17** 055008

[4] Liu J.J. and Liaw B.M. (2004) Efficiency of Active Control of Beam Vibration Using PZT Patches, *Proceedings of the SEM X International Congress & Exposition on Experimental and Applied Mechanics*, Costa Mesa, CA, June 7-10, 2004, Section 59: Smart Structures, Paper 385

[5] Kumar K. R. and Narayanan S. (2007) The optimal location of piezoelectric actuators and sensors for vibration control of plates, *Smart Mater. Struct.* 16, 2680-2691

[6] Peng F., Ng A. and Hu Y-R. (2005) Actuator Placement Optimization and Adaptive Vibration Control of Plate Smart Structures, *J. Intel. Mat. Syst. Str.*, 16, 263-271

[7] Sadri A.M., Wright J.R. and Wynne R.J. (1999) Modelling and optimal placement of piezoelectric actuators in isotropic plates using genetic algorithms, *Smart Mater. Struct.*, 8, 490-498

[8] Nestorović Trajkov T., Köppe H. and Gabbert U. (2006) Vibration control of a funnel-shaped shell structure with distributed piezoelectric actuators and sensors, *Smart Mater. Struct.*, 15, 1119-1132

[9] Nestorović T. (2005) *Controller Design for the Vibration Suppression of Smart Structures*, Fortschritt-Berichte VDI 8 1071, Düsseldorf, VDI Verlag

[10] Gawronski W. (2004) Advanced *Structural Dynamics and Active Control of Structures*, Springer New York

OPTIMAL DESIGN OF THIN-WALLED AIRCRAFT STRUCTURES USING TWO-LEVEL OPTIMIZATION APPROACH

S. Maksimović[1], K. Maksimović[2] I. Vasović[3],

[1] Military Technical Institute,
Ratka Resanovića 1, 11000 Belgrade, Serbia
e-mail: s.maksimovic@open.telekom.rs
[2]Republic Serbia, City Administration of City of Belgrade,
Secretariat for Utilities and Housing Services Water Management,
Kraljice Marije 1, 11000 Belgrade, Serbia
e-mail: katarina.maksimovic@beograd.gov.rs
[3] Institute Goša, Milana Rakica 35, Belgrade, Serbia
e-mail: ivanavvasovic@gmail.com

ABSTRACT. An attention in this investigation is focused on developing efficient optimization method for minimum weight design of thin-walled structures. Today, it is a common practice to use numerical optimization methodologies to deal with multidisciplinary industrial design problems. One of the major tasks in the design of aircraft structures is the sizing of the structural members to obtain the desired strength, weight, and stiffness characteristics. Optimization algorithms have been coupled with structural analysis programs for use in this sizing processThe efficiency of method is based on application of the two-level approach in optimization structural systems. This approach breaks the primary problem statement into a system level design problem and set of uncoupled component level problems. Two-level optimization approach is applied to structural design problems like: minimum weight of the complex aircraft composite structure under various strength, buckling and stiffness constraints. This paper considers a discrete model the buckling sensitivity analysis of thin multi-layered angle-ply composite structures. Angle-ply design variables and the thickness of each layer considered as design variables. Optimization method presented here is based on combining optimality criterion (OC) and mathematical programming (MP) algorithms. Finite element analysis (FEA) are used to compute internal forces at the system level. The local stress and local initial failure load in each independent element are defined as component constraints. The use of this MP algorithm is essential to two-level approach and local level, since it can handle the highly nonlinear component problem, such as local buckling or special initial failure constraints in mechanical fastened joints. Optimality criterion method significantly reduces time and cost the optimization process. The two-level optimization approach is applied to minimum-weight design of aircraft structural components such as aircraft nose landing gear, wing skins and parashute composite beam subject to

multiple constraints. Finally, several examples are shown to illustrate effectiveness of the two-level optimization model.

Key words: Optimization methods, multi-level approach, optimality criterions, displacement constraints, stress constraints, buckling constraints, finite elements

1 Introduction

The design of complex structures (which require a large finite element model (FE model) such as aircraft, require the use of optimization methods. The size of the optimization problem depends on the number of variables and constraints required, especially for the design of structures with large interactions between their various components. A multi-level approach is needed to decompose the entire system problem (system-level) into several sub-problems (element-level) taking into account the various coupling effects. The multi level approach allows individual system components to be optimized, thus significantly reducing the time needed for the computation and the design cycle. Various concepts have been proposed [1–7] to decompose large optimization problems down into sub-problems. It should be noted that the design parameters of the global structure affect both the structure and sub-structures (density, Young modulus, etc.), while the design parameters of the substructures can be local dimensions (e.g. geometric dimensions: thickness, length, width).The constraints on the structure are global (e.g. structural displacement), while the constraints on the sub-structures are local (e.g. local stress or strain). Today, it is a common practice to use numerical optimization methodologies to deal with multidisciplinary industrial design problems.   One of the major tasks in the design of aircraft wing structures is the sizing of the structural members to obtain the desired strength, weight, and stiffness characteristics. Optimization algorithms have been coupled with structural analysis programs for use in this sizing process. Most of the difficulties associated with large structural design are solution convergence and computer resources requirements. Structural optimization problems traditionally have been solved by using either the mathematical programming (MP) or the optimality criteria (OC) approach. More recently, the works in Refs [1-3,14] have illustrated the uniformity of the methods. Nevertheless, each approach offers certain advantages and disadvantages. The MP methods are extremely useful in defining the design problem in proper mathematical terms. When the design variables are few the these methods can be used quite effectively for optimization. However, in the presence of a large number of variables these methods are very slow. The rate of convergence for OC methods is initially very fast, step size determination is critical closer to the local optimum where the number of active constraints' increases and the computations of Lagrange multipliers becomes more complex. Power and weakness of the various MP methods are given in Ref. [8]. Ideally, a methodology that exploits the strength of both approaches could be employed in a practical system. The object of the present research effort is to develop such design method that can efficiently optimize large structures that exploit strengths (power) of the MP and OC methods. The motivation of this study is to come up with a multilevel optimization method using optimality criteria and mathematical programming techniques. Multilevel

optimization permits a large problem to be broken down into a number of smaller ones, at different levels according to the type of problem being solved. This approach breaks the primary problem statement into a system level design problem and set of uncoupled component level problems. Results are obtained by iteration between the system and component level problems. The decomposition of a complex optimization problem into a multilevel hierarchy of simpler problems often has computational advantages. It makes the whole problem more tractable, especially for the large engineering structures, because the number of design variables and constraints are so great that the optimization becomes both intractable and costly. The nature of an aircraft structure makes multilevel optimization highly practical, not only in terms of reducing the computing cost but also because the individual tasks in the traditional design process are preserved. The suitability of multilevel optimization in more complex design problem tested on a structure representative of a wing box in composite material, with buckling limitations in each panel, and another problem in which reliability requirements are included. Multilevel approach for optimization of the composite structures subject to stress, displacement, buckling and local failure constraints is developed.

2. Formulation of optimization problem

Structural optimization techniques have undergone many developments and refinements over the past few decades. More and more design problems can now be optimized using a variety of algorithms.

The general structural optimization problem of layered composite structures modeled by finite elements can be stated as follows:

Find the vector of design variables x such that

$$W = \sum_{i=1}^{n} \rho_i \, l_i \, x_i \quad \Rightarrow \min \tag{1}$$

subject to behavior and side constraints

$$G_j = C_j - \overline{C}_j \geq 0 \qquad j = 1,\ldots,m \tag{2}$$

where:

W - is the weight of structure

$\mathbf{x_i}$ - is design variable assigned to element i

$\mathbf{l_i}$ - is a geometrical parameter such that the product $l_i x_i$ is the volume of the element i

ρ_i - is the mass density

$\mathbf{G_j}$ - is constraint j

$\overline{C}_j$ - is limiting value of the constraint j

n - is total number of elements

m - is total number of constraints

The constraints imposed on the structure, defined by equation (2), may have the global and local character. The global constraints will be defined as system constraints. The system constraints imposed on the structure may include the maximum allowable stress in each element, the displacement limits at one or more locations, system stability, reactive forces,

dynamic stiffness, divergence, flutter etc. In addition to these there would be limitations on the minimum and maximum sizes of the elements.

In addition to system constraints there are local constraints. These include various buckling loads, various failure types in composite structures, etc.

Inclusion all these constraints in optimization process to large-scale structures are inefficient with computational aspect. However, to develop an efficient algorithm that effectively handles all types of constraints would be impractical and generally unnecessary. In the case of most structures it is likely that one can predict the type of constraint that will be the most active at the optimum and use the algorithm based on that constraint. The multilevel optimization approach may be very efficient for optimization large-scale structural systems because it breaks the primary problem statement into a system level design problem and a set of uncoupled component level problems. Results are obtained by iterating between the system and local level problems. The decomposition of a complex optimization problem into a multilevel hierarchy of simpler problems often has computational advantages. It makes the whole problem more tractable, especially for the large aircraft structures. The nature of an aircraft structure makes multilevel optimization highly practical, not only in terms of reducing the computing cost but also because the individual tasks in the traditional design process are then preserved.

3. Theory of multilevel optimization

Let D and d represent the sets of system and component design variables, respectively. Then the problem can be stated as:

Find vectors **D** and **d** such that

$$W(D) \Rightarrow \min \tag{3}$$

subject to

$$G_q(D,d) \geq 0 \quad , \quad q \in Q \tag{4}$$

and

$$g_{lj}(d_j, D) \geq 0 \quad , \quad l \in L \ ; \quad j \in M \tag{5}$$

The $G_q(D,d)$ represents constraints that are strongly dependent on the **D** vector and they are implicit functions except for the side constraints. The $g_{lj}(d_j, D)$ represent constraints that are primarily dependent on the j component variables d_j, and they are either explicit or implicit functions of d_j, depending on the type of constraints and the type of local failure analysis. The symbols **Q** and **L** denote the set of system and component level constraints respectively, **M** denotes the number of components and $\mathbf{d^T} = [\ \mathbf{d_1^T}, \mathbf{d_2^T}, ..., \mathbf{d_M^T}\ ]$.

The system design variables can be expressed symbolically as explicit functions of the detailed design variables, that is

$$D_j = \Psi(d_j) \qquad j = 1, ..., M \tag{6}$$

For each component the number of detailed design variables are larger than the number of corresponding system design variables.

Therefore, casting the problem entirely at the system level by expressing $\mathbf{D_j}$ as functions of $\mathbf{d_j}$ and solving it using mathematical programming methods are an impractical task for large-scale problems. The multilevel approach presented here is decomposed into two levels of design modification; one with the constraints that are strongly dependent

on system design **D** and the other with the constraints that are primarily dependent on local design variables **d$_j$**. Then system and local analyses and optimizations are carried out separately and tied together by an iterative scheme going from one level of design modification to the other and visa-versa seeking an overall optimum.

The structural optimization problem given by Eqs. (3)-(5) is recast as a multilevel optimization problem following form:

> **i.) System level:**
>
> Find vector D (7)
>
> such that $W(D) \Rightarrow \min$ (8)
>
> and $G_q(D, d^*) \geq 0 \quad ; \quad q \in Q$ (9)

where **d*** implies that the parameters strongly dependent on the detailed design variables **d** (i.e., failure loads and local buckling), do not change during a system level design modification stage.

> **ii.) Component level:**
>
> Find vectors **d$_j$** (10)
>
> such that m$_j$(d$_j$) $\Rightarrow \min$ (11)
>
> and $g_{lj}(d_j, D^*) \geq 0 \quad ; \quad l \in L$ (12)

where **D*** implies that the parameters strongly dependent on the system level design variables are kept constant during each component design modification stage.

4. The system level optimization

An efficient optimality criterion method is used for the system level optimization of large-scale complex structures subjected to constrains which are included at the system level. Optimality criteria approach will be used for the optimization structures with system level constraints. Optimality criteria methods for structural optimization involve:

1. derivation of set of necessary conditions that must be satisfied at the optimum design, and

2. the development of an iterative redesign procedure that drives the initial trial design toward a design which satisfies the previously established set of necessary conditions.

In order to establish the optimality conditions for the problem defined by (7)-(9) we need the associated Lagrangian which is given by the expression

$$L(D, \lambda) = \sum_{i=1}^{N} \frac{w_i}{D_i} + \sum_{j=1}^{Q} \lambda_j G_j \tag{13}$$

where λ_j's are the Lagrange multipliers. The Kuhn-Tucker optimality conditions are now obtained, in part, by differentiating the Lagrangian and the complete set is given by

> D* is possible (14)
>
> $\lambda_q G_q(D^*) = 0 \qquad \lambda \geq 0 \ , \ q \in Q$ (15)
>
> $\nabla W(D^*) + \sum_{q \in Q} \lambda_q \nabla G_q(D^*) = 0$ (16)

If the problem is assumed to be convex then these conditions are necessary and sufficient for the solution of vector D^*, λ^* to represent a global optimizing point otherwise they

define a local optimum. The optimum structure must satisfy Eqs. (14)-(16). These are the Kuhn-Tucker conditions or the optimality conditions. Equation (16) is the ratio of the weighted sum of the gradient of the constraints to the gradient of the objective function, which must be equal for all elements in an optimum design.

Equations (13) and (14) ensure satisfaction of the constraint equations. The constraints G_q in equation (9) may be displacement limits at the different node points in a structure, the relative nodal displacements corresponding to maximum allowable stress in each element, system stability, frequency constraints, flutter requirements, various failure criterions in layered composite structures such as the Tsai-Wu criterion.

The real optimum structure must satisfy conditions (15)-(16). To develop a computational algorithm that handles all these constraints efficiently would be difficult and generally unnecessary. In practical design problem what may be required is a design which is near minimum weight and not a design that exactly satisfies the mathematical optimality criteria. This can generally be achieved by designing the structure based on one or two of the must important constraints, and checking the design for the other constraints.

Problem optimization defined by Eqs (7)-(9) or (1)-(2) involves; large numbers of design variables, large numbers of inequality constraints and many inequality constraints that are computationally burdensome implicit functions of the design variables. These obstacles have been overcome by replacing the basic problem statement (7)-(9) with a sequence of relatively small, explicit, approximate problems that preserve the essential features of the original design optimization problem. This has been accomplished through the coordinated use of approximation concepts. The most important feature of the approximation concepts approach lies in the construction of simple explicit expressions for the set of constraints retained during each stage. This is achieved by linearization of these constraints with respect to linked reciprocal design variables. The linearized behavior constraints (9) are obtained by using a first order Taylor series expansion as:

$$G_q(D,d^*)=1-\sum_{i=1}^{n}C_{iq}\,D_i \qquad ; \quad i=1,...,Q \tag{17}$$

where $\mathbf{C_{iq}}$ is the partial derivative of $\mathbf{q}$-th constraint for $\mathbf{i}$-th design variable, a $\mathbf{Q}$ is the total number of constraints. Equation (17) represents the current linearized approximations of the retained behavior constraints. Using (17) the retained behavior constraints system level optimization problem (7)-(9) can be expressed as: Find vector $\mathbf{D}$ such that

$$W(D)=\sum_{i=1}^{N}\frac{w_i}{D_i} \Rightarrow \min \tag{18}$$

subject to constraints

$$G_q(D)=1-\sum_{i=1}^{n}C_{iq}\,D_i \qquad ; \quad q \in Q \tag{19}$$

and $D_i^L \le D_i \le D_i^U$ \hfill (20)

The $\mathbf{w_j}$ are positive fixed constants corresponding to the weight of the set of elements in the j-th linking group when $\mathbf{D_j=1}$. The set of independent design variables after linking is denoted by N and equation (19) represent the linear approximations of the behavior constraints. The $\mathbf{D_i^L}$ and $\mathbf{D_i^U}$ respectively denote lower and upper limits on the independent design variables.

In developing optimality conditions standard approach is to form a Lagrangian:

$$L(D, \lambda) = \sum_{i=1}^{N} \frac{w_i}{D_i} - \sum_{q \in Q} \lambda_q \left(1 - \sum_{i=1}^{n} C_{iq} D_i \right) \tag{21}$$

where λ_q are the undetermined Lagrangian multipliers. Approximation problem (18) - (20) is convex problem and therefore Kuhn-Tucker conditions are necessary that solutions $D*, \lambda *$ represent global minimum. Conventional optimality criteria methods for structural optimization involve; (i) the derivation of a set of necessary conditions that must be satisfied as the optimum design and (ii) the development of an iterative redesign procedure that drives the initial trial design toward a design which satisfies the previously established set of necessary conditions. Each approximate primal problem of the form given by equations (18)-(20) can be transformed to correspond an explicit dual problem. Detail solution methods and optimization algorithms are given in Refs [8,9,19].

4.1 Definition of strength constraints in layered composites

For analysis and optimization fibrous layered composite structures, modeled by laminated shell type finite elements, various failure criterions can be used. The Tsai-Wu criterion is used for failure analysis of orthotropic layers in composite shell. This criterion can be expressed as:

$$T_t = \left[\left(\frac{\sigma_1}{F_1} \right)^2 + \left(\frac{\sigma_2}{F_2} \right)^2 - \left(\frac{\sigma_1 \sigma_2}{R F_1 F_2} \right) + \left(\frac{\tau_{12}}{F_{12}} \right)^2 \right]^{\frac{1}{2}} \tag{22}$$

where σ_1, σ_2, τ_{12} are the components of stress tensor σ; F_1, F_2 and F_{12} are the stresses of failure in uniaxial tension, compression and shear, respectively and T_t is Tsai's number. By using eqns (19) and (22) linearized approximations of Tsai-Hill criterion can be written as:

$$G_q = 1 - \sum_{i=1}^{n} \frac{\partial T_t}{\partial D_i} D_i \tag{23}$$

where:

$$C_{iq} = \frac{\partial T_t}{\partial D_i} = T_1 \frac{\partial \sigma_1}{\partial D_i} + T_2 \frac{\partial \sigma_2}{\partial D_i} + T_3 \frac{\partial \tau_{12}}{\partial D_i} \tag{24}$$

with

$$T_1 = \frac{1}{2T_t} \frac{2\sigma_1 - \sigma_2}{\left(F_1 \right)^2}, \qquad T_2 = \frac{1}{2T_t} \left[\frac{2\sigma_2}{\left(F_2 \right)^2} - \frac{\sigma_1}{\left(F_1 \right)^2} \right]^2 \qquad \text{and} \qquad T_3 = \frac{1}{T_t} \frac{\tau_{12}}{\left(F_{12} \right)^2}.$$

In similar manner linearized constraints such as displacement, stability, frequency or other system constraints can be defined.

4.2 Definition of stability constraints

The linear stability of a structure is defined by eigenvalue problem.

$$[K - \lambda_j K_G] q_j = 0 \tag{25}$$

where K and K_G are respectively system stiffness and geometric matrix of the structure and q_j is the eigenvector associated with the j-th eigenvalue λ_j. For an efficient optimization of buckling problems it is essential to know the sensitivity of the buckling load parameter λ_j. The sensitivity with respect to changes in the design variable t_i (thicknesses of shell layers) is evaluated by

$$\frac{\partial \lambda}{\partial t_i} = q^T \left(\frac{\partial K}{\partial t_i} - \lambda \frac{\partial K_G}{\partial t_i} \right) q \tag{26}$$

The evaluation of sensitivities using equation (26) is not computational efficient. It is better to obtain the sensitivity of the buckling load parameter λ_j at the element load level using (26) in the form

$$\frac{\partial \lambda}{\partial t_i} = \sum_{l \in E} [q_l]^T \left(\frac{\partial K^e}{\partial t_i} - \lambda \frac{\partial K_G^e}{\partial t_i} \right)_l q^e{}_l \tag{27}$$

where E is the number of elements in the structure.

5. Local Level Optimization

Local level optimization process can include various types of failure modes in laminates or local buckling constrains. This optimization problem is solved by algorithms based on nonlinear mathematical programming methods. Classical optimization problem in local level are mechanically fastened joints in composites. Initial failure arises on characteristic curve, as shown in Fig. 1
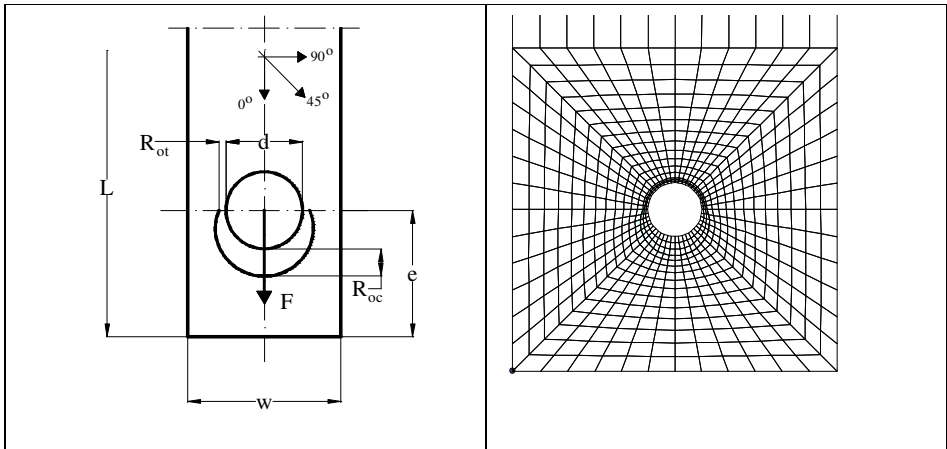
Fig. 1.   Description of the characteristic curve with FE mesh

The characteristic curve with finite element mesh, Fig. 1, is specified by the expression:

$$r_F(\Phi) = \frac{D}{2} + R_t + (R_c - R_t)\cos\Phi \ ; -\frac{\pi}{2} \le \Phi \le \frac{\pi}{2} \tag{28}$$

where $\mathbf{R_t}$ and $\mathbf{R_c}$ are referred to as the characteristic lengths for tension and compression. In order to determine the load at which a mechanical fastened joint fails and the mode of failure, the conditions for failure must be established. In this paper the joint is taken to have failed when certain combined stresses have exceeded a prescribed limit in any of plies along a chosen the characteristic curve. The combined stress limit is evaluated using the failure criterion proposed by Yamada- Sun in form [11]

$$\left(\frac{\sigma_1}{F_1}\right)^2 + \left(\frac{\tau_{12}}{F_{12}}\right)^2 \leq 1 \tag{29}$$

where σ_1 and τ_{12} are the longitudinal and shear stresses in a ply, respectively (1 and 2 being the directions parallel and normal to the fibers in the ply). F_{12} is the rail shear strength of a symmetric cross ply laminate $[0^o/90^o]_s$. F_1 is either the longitudinal tensile strength or the longitudinal compressive strength of a single ply.

This criterion is based on the assumption that just prior to failure of the laminate, every ply has failed due to cracks along the fibers. It is very important to say, that local constraints such as expressed by Eq. (29) or similar, can be included in optimization process as direct formulae using Fortran lingue notation in programme OPTIS [12]. Direct manner for defining very nonlinear constrains by using direct Fortran description is very efficient in practical optimization of composite or metal aircraft structure. Final dimensions are obtained at local optimization. Optimization algorithms are based on Nonlinear Mathematical programming methods such as: SUMT, CONMIN, method inscribed hypersphers [6], etc.

6. Numerical Examples

To illustrate the application and versatile multilevel approach to the weight structural optimizations composite structure subjected static loads are considered.

Example 1: Optimal Design of Composite Panel Subject to Buckling Constraints

Here laminated composite panel is optimized with respect buckling constrains. Geometry, loads, material properties and FE model of CFC composite panel are shown in Figure 2. The panel is modeled using 4-node layered shell finite elements based on higher order shear deformation theory (HOST) [16]. The complete optimization results are shown in Table 1.
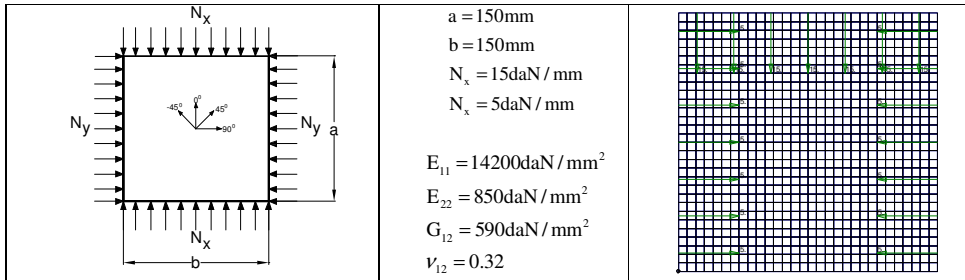
Figure 2 Geometry and FE model of laminated composite panel

Table 1: Optimal design of composite panel subject to buckling constraints

Sequences	W_{opt}	Condition	t_o [mm]	t_{90}[mm]	t_{45}[mm]	t_{-45}[mm]	t_{30}[mm]	λ_{min}
$[45/-45/0/90]_s$	0.09187	$t_{45} = t_{-45}$	0.59776	0.12849	0.31742			1.006
$[45/-45/0]_s$	0.09181	$t_{45} = t_{-45}$	0.73146		0.31514			1.0179
$[0/90/45/-45]_s$	0.09462		0.125	0.125	0.22735	0.92449		0.9966
$[45/-45/45/-45]_s$	0.08853				0.28935 0.125	0.80231 0.125		0.993
$[30/-30/0/90]_s$	0.09453	$t_{30} = t_{-30}$	0.57937	0.13951			0.3408	1.0126
$[0/90]_s$	0.10525			0.7796	0.7796			1.0009

$[45/-45/0/90]_s$, λ=1.006 $[45/-45/45/-45]_s$, λ=0.993
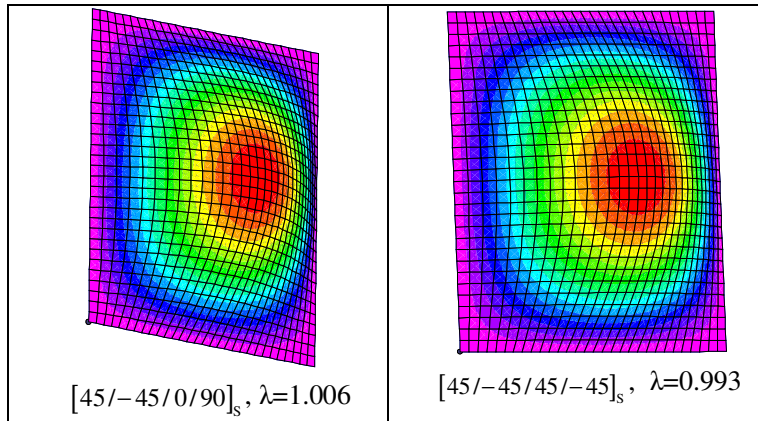
Fig. 3 Buckling modes of optimized panels with stability constraints

The effect of the stacking sequences on minimum weight of the composite panel, W_{opt}, is evident.

Example 2: Optimization of Aircraft Parachute Composite Beam

As very illustrative example for multilevel optimization procedure the fibrous composite parachute beam considered. The structure of parachute beam shown in Fig. 4 idealized with membrane finite elements. The elements consist of four layers in the 0°,90° and $\pm45^o$ directions. The 0° fibers are parallel to the length of the beam. The parachute composite beam was subject to static loading conditions. The aircraft parashute composite beam shown in Fig. 4 used for system level optimization.

Material of composite beam was graphite/epoxy NCHR 914/34%/132/ T300 with next mechanical properties:

E_{11}=126800   MPa F_{11}^t=1362 MPa
E_{22}=9220   MPa F_{11}^c=1333 MPa
E_{33}=9220   MPa F_{22}^t= 42 MPa

G_{12}=4620   MPa F_{22}^c= 172   MPa
G_{23}=G_{13}=720 MPa F_{12} = 100   MPa
v_{11}=v_{13}=v_{23} t_{layer}=0.13 mm

Fig. 4 Parachute CFC-composite beam

There are four mechanical fastened joints (holes) on the end of the parachute beam. The loads are introduced in these holes. Zone around each hole considered as substructure. This substructure has characteristic curve, as defined in Fig. 1, is modeled by very refined finite element mesh. The substructure (rectangular panel with central hole) is treated as optimization model on the local level. The Yamada-Sun criterion (29) around characteristic curve (28) used as constraints in local level optimization. For this purpose, in the local level, SUMT optimization algorithm is used. Optimization results of this substructure are thicknesses of layers:

$$t_1(\quad 0^o) = 2.08 \quad mm$$
$$t_2(+45^o) = 0.78 \quad mm$$
$$t_3(-45^o) = 0.78 \quad mm$$
$$t_4(\quad 90^o) = 0.26 \quad mm$$

Failure load that is in this analysis obtained: **F_f = 2297 daN**. Failure was initiated in layer 0°, with extension type of mechanism of failure $75^\circ \leq \Theta_f \leq 90^\circ$.

Failure loads that are experimentally obtained: (**F_1 = 2087 daN, F_2 = 2296 daN** and **F_3 = 2390 daN**).

Good agreement between numerical and experimental results is evident. Detail comparisons between numerical and experimental results are given in Ref. [13]. Difference between numerical and experimental results is maximum 5%. In this work optimization results of one substructure are presented only. These results illustrate multilevel optimization process.

Example 3: Minimum Weight Design of Nose Landing Gear with Stability Constraints

Here is illustrated minimum weight design of nose landing gear with stability constraints (See Section 4.2). This part is modeled by shell finite elements based on HOST [16].

| FE model of Nose Landing Gear | Part of landing gear modeled by shell finite elements |
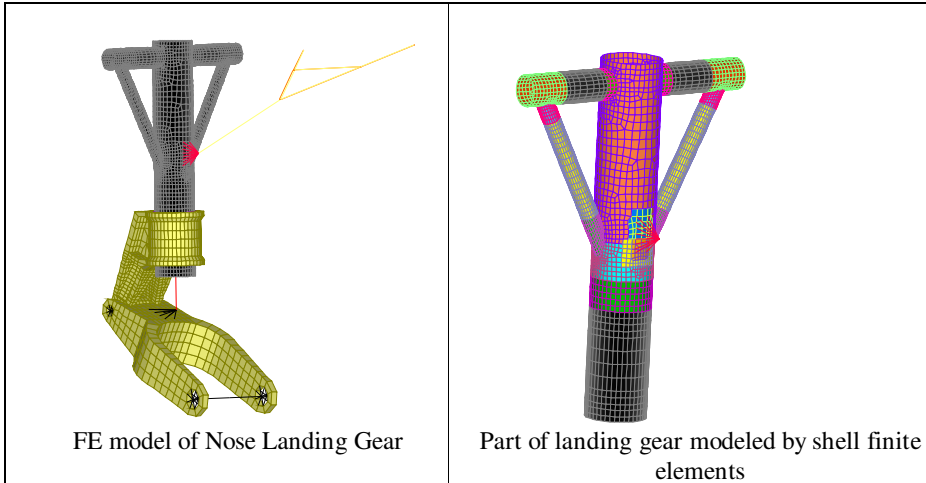
Figure 5 FE model of landing gear
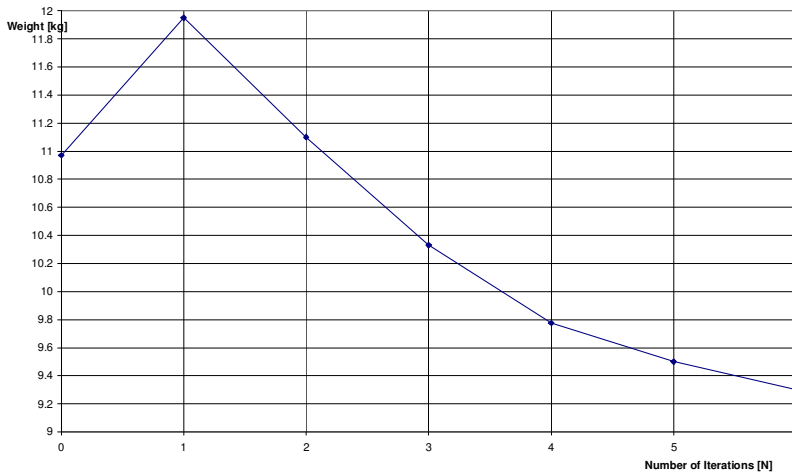
Figure 6 Weight history of part landing gear modeled by shell finite elements

Figure 6 shows weight history design of optimization process. The minimum weight of structure is obtained after 6 iterations only. Here is used dual algorithm based on OC approach.

7 Conclusions

The obtained results demonstrate the practicality of multilevel optimization approach in the design of the complex aircraft structures. In this study two-level optimization

algorithm is applied; system- and component level. From the various investigated test problems it becomes clear that the choice of various optimization algorithms at each level play a major role in the efficiency of the whole optimization process. Presented multilevel optimization approach uses optimality criteria's algorithm in conjunction with a Sequential Unconstrained Minimization Technique (SUMT). Optimality criteria's algorithms are used for system level optimization i.e. in case of weight minimization subject to global (system) constraints that can be displacements, system stability, frequencies, flutter etc. Nonlinear Mathematical Programming optimization algorithms are used for local (component) level optimization. Combining FEA, approximation concepts and OC or dual algorithms has led to a very efficient method for minimum weight sizing of large-scale structural systems. The proposed method is suitable for designing practical large-scale structures with a large number of design variables. Finally, minimum weight designs obtained for the aircraft parachute composite beam illustrate the application of the multilevel approach to a relatively large structural system.

References

[1]   Arora, J. S and Haug, E. J., Efficient Hybrid Methods for Optimal Structural Design, Journal of Engineering Mechanics Division, Proc. ASCE, 103 (EM3), pp 663-680, June 1974.

[2]   L.U. Hansen, P. Horst, Multi-level optimization in aircraft structural design evaluation, Computers and Structures 86, 2008, 104–118.

[3]   Maksimovic, S., Optimal Design of Composite Structures by Finite Elements, Proc. Int. Conf. Computer Aided in Composite Material Technology, Eds Brebbia, C. A., Wilde, W. P. and Blain, W.R., Springer-Verlag, Southampton 1988.

[4]   Haftka, R.T. and Starnes, J. H., Applications of a Quadratic Extended Interior Penalty Function for Structural Optimization, AIAA J, Vol. 14, No. 6, 1976.

[5]   Craig, R.R and Erbug, I.O., Application of a Gradient Projection Method to Minimum Weight Design of a Delta Wing with Static and Aero-elastic Constraints, Computers and Structures, Vol. 6, No.6, 1976.

[6]   Maksimović, S., Optimum Design of Composite Structures, Int. Conf. Composite Structures 3, Ed. Marshall, I.H., Elsevier Applied Science, London, 1985.

[7]   Schmit, L. A. and Miura, H., Approximation Concepts for Efficient Structural Synthesis, NASA CR- 2552, 1976.

[8]   Fleury, C. and Schmit, L. A., Dual Methods and Approximation Concepts in Structural Synthesis, NASA CR-3226, 1980.

[9]   Maksimović, S., Some Computational and Experimental Aspects of Optimal Design Process of Composite Structures, Int. J. Composite Structures, Vol 17, pp. 237-258, 1990.

[10]   Schmit, L.A. and Farshi, B., Optimum Laminate Design for Strength and Stiffness, I JNME, Vol. 7, pp 519 536, 1973.

[11]   Yamada, S. E., Analysis of Laminate Strength and its Distribution, J. Composite Materials, Vol. 12. pp. 275-284, 1978.

[12]   Maksimović S., Ilić I., Georgijević D., Bojanić M., Stefanović V., Structural Analysis and Static Strength Testing of Tactical Unmanned Aerial Vehicle, *Scientific Technical Review*, No. 2, 2013., pp.58-62.

[13] Maksimović, S. and Pejović, J., Strength Analysis of Aircraft Parachute Composite Beam, Raport of Aeronautical Institute, V9-492-P-S, 1991.

[14] Canfield, R.A, Grandhi, R.V and Venkayya, V.B, Optimum Design of Large Structures With Multiple Constraints, 27th Structures, Structural Dynamics and Materials Conference, May 19-21, San Antonio, Texas, 1986.

[15] Maksimović, S. and Maksimović, K., Optimal Design Method for Weight Minimization of Composite Structures with Stability Constrains, J. Technical Diagnostics, Vol. 3, No. 2, 2004.

[16] Maksimovic, S., *Improved geometrically nonlinear finite element analysis and failure of fiber reinforced composite laminates*, Proc. Int. Symp. Brittle Matrix Composites 4, Warsaw, Eds. A.M. Brandt, V.C. Li and I.H. Marshall, Woodhead Publ., 1994.

[17] Maksimovic, S., Zeljkovic, V., Multilevel Optimization Approach Applied to Aircraft Structures, *The First International Conference on Computational Mechanics (CM'04)*, November 15-17, 2004, Belgrade, Paper 55, 1-10, (Eds Mijuca D. and Maksimovic, S.)

[18] Maksimovic, S. and Zeljkovic, V., Multilevel Optimization of Large Scale Structures Based on Combining Optimality Criterion and Mathematical Programming Algorithms, Ed. B.H.V. Topping, Advances in Structural Engineering Optimization, Civil-Comp Press, Edinburgh, 1996.

[19] Kampolis I.,Giannakoglou K., A Multilevel Approach to Single- and Multiobjective Aerodynamic Optimization, Comput. Methods Appl. Mech. Engrg., 197 2963–2975, 2000.

DYNAMICS OF GEAR-PAIR SYSTEMS WITH PERIODIC VARYING MESH STIFFNESS - SPUR GEARS VS HELICAL GEARS

Ivana Atanasovska[1], M. Vukšić Popović[2]

[1, 2] Institute Kirilo Savić
Vojvode Stepe 51, Belgrade, Serbia
[1] e-mail: iviatanasov@yahoo.com
[2] e-mail: marija.vuksic@iks.rs

Abstract. *The modelling and calculation of parameters of involute gear pair dynamics is basic requirement for studying of gears stability and energy efficiency. In this paper, the dynamic model of involute gear pair is used in the comparative study of spur and helical involute gears with their stability as the dominant aspect. The stiffness and load distribution for research of gears dynamic behaviour have been calculated with the finite element method. The special attention was paid to define the procedure for time-varying mesh stiffness calculation. The obtained results shown as phase portraits confirm that the helical gear pair has more stabile work than the spur gear pair with same main geometry and load. Described procedure can be used for future investigation of optimal gears parameters (e.g. tooth profile, nominal load) with aspect of gear pair stability.*

1. Introduction

In order to study gears stability and energy efficiency, in recent years the focus is on nonlinear dynamics of gears. Many authors have investigated and discussed this problem from wide range of aspects, [1-4], and point out the importance of studying the nonlinear oscillations of gears from aspect of competitive limitations of noise level and vibrations. In this paper, the comparative study of spur and helical involute gears with their stability as the dominant aspect has been discussed.

The precise solution for involute gears oscillations can be obtained only if non-linear functions of stiffness and load are known. In the literature, the tooth stiffness and mesh stiffness are treated in different ways. In the simpler models, the gear mesh stiffness is assumed to be constant. In last decade, authors overcame this simplification and presented various methods for teeth deformation, teeth stiffness and load calculation. Thus, some of them determined the dynamic load between two elastic helical gears with excitation from new incoming contacts and calculated the total deformation of contact teeth as sum of numerical calculated (with Finite Element Method) teeth bending

deformations and analytical calculated Hertz's teeth contact deformations. But, they neglected influence of load value on contact deformations. The importance of determination of variable contact area in simulation of contact problems in gears is discussed by Ulaga, [5]. They presented a new Finite element technique for more accurate contact stress predictions, while Pedrero et al. [6] described minimum elastic potential criterion as method for calculation of load distribution in involute gears mesh. But they still used Hertz's formulae for contact in one point and neglected influence of load value. This is not appropriate calculation methods for teeth total deformations, because contact deformation depends of the magnitude of load and must be determined through iterative procedure [7]. In the new series of papers, [3,8,9,10,11] have been confirmed the Finite Element Method (FEM) as out of competition method for investigations of deformations and load distribution for involute gears.

The main objective of this paper is to present a method to determine the load in a gear pair considering the actual positions of the contacts and the actual deformations of the gear teeth. The determination of positions of the contacts and the actual deformations of the gear teeth are then used to determine the mesh stiffness and load distribution between the meshed teeth pairs. These values are used in gear pair dynamic model to obtain the analysis of involute spur and involute helical gears motion.

2. Theoretical gear pair dynamic model

A pair of gears is simulated with two disks coupled with non-linear mesh stiffness and mesh damping. Many authors confirmed this simplified dynamic model and focus their investigation resources on various influence factors [12,13,14,15]. In this model one disk (driving gear) has radius r_1 and mass moment of inertia J_1 and the other (driven gear) has radius r_2 and mass moment of inertia J_2. The radii r_1 and r_2 correspond to the radii of the base circles of the two gears, respectively (Fig.1a). The dynamic transmission error is the difference between the actual and ideal position of the driven gear and can be expressed as a linear displacement along the line of action (x). It is very important to calculate the $x(t)$ function (t - time) to predict gear noise and increase gears life. Reduction to the line of action [16,17], transforms the gear model II (model with two steps of freedom, Fig.1a) to gear model I (model with one step of freedom, Fig.1b).
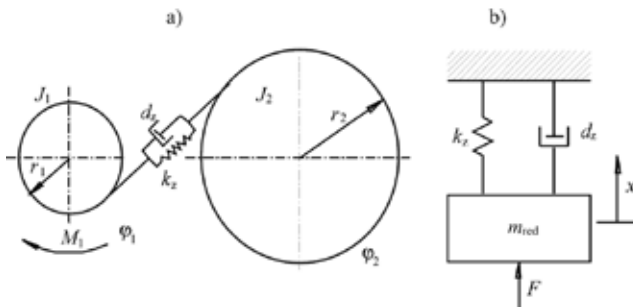
Figure 1. Dynamic model of gear pair.

a) model II - with two steps of freedom, b) model I - with one step of freedom

Nonlinear dynamic analytical model of involute gears motion for model II can be given with equations:

$$m_1 \ddot{x}_1 + d_z(t)(\dot{x}_1 - \dot{x}_2) + c_0(t)(x_1 - x_2) = F_n(t) \,. \tag{1a}$$

$$m_2 \ddot{x}_2 - d_z(t)(\dot{x}_1 - \dot{x}_2) - c_0(t)(x_1 - x_2) = -F_n(t) \,. \tag{1b}$$

and for model I with equation:

$$m_{red} \ddot{x} + d_z(t)\dot{x} + c_0(t)x = F_n(t) \,. \tag{2}$$

In these equations: m_i (i=1,2) are equivalent masses of gears and m_{red} is reduced mass of gears, $c_0(t)$ is the gear mesh stiffness function, $d_z(t)$ is the gear mesh dumping function and $F_n(t)$ is the function of normal load distribution between the gear teeth in mesh, during gear meshing period. The mathematical models can be used for the analysis of the gears oscillation parameters, only if all functions are known. In the research presented in this paper, the stiffness and load distribution are calculated using the true contact geometry of the involute gears as elastic bodies. The developed finite element model presented in previous papers [11,18] have been used. Damping value is assumed to be equal to 1 which excludes its influence on the gears oscillation characteristics, [17]. The calculation of nonlinear damping in dynamics of gear mesh is subject that requests widely access and research, [19].

2.1. Teeth stiffness and mesh stiffness

In general, stiffness is the force that causes unit deformation. There are different variables that describe stiffness for meshed gears. In this paper, the few of them are used. The tooth stiffness can be defined as ratio of differential of unit normal load in tooth face plane section $d(F_b/B)$ and appropriate elastic deformation:

$$c = \frac{d(F_b / B)}{du} \,. \tag{3}$$

The tooth stiffness depends of many influence factors (gears geometry, load value, material characteristics etc.) and varies along length of action, as well as along line of contact of a teeth pair. Determination of tooth stiffness function is very important point in involute gears investigations, especially for helical gears. The complex helical gears geometry and variable length and position of teeth contact lines during mesh period require complex study of teeth contact and stiffness, [20]. Contact lines are not parallel to gears axis during meshing period for helical gears. Therefore, teeth pairs coming in mesh gradually. This leads to continuously changing of contact line length and makes load distribution calculation very complex. Zone of action (contact zone) for involute parallel-axis gears with helical teeth is the rectangular area in the plane of action bounded by the length of action and the effective face width, Fig.2.
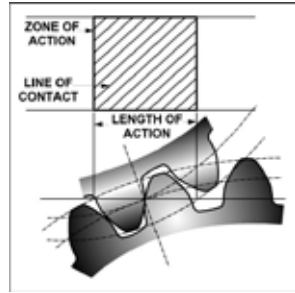
Figure 2. Zone of action for involute parallel-axis gears with helical teeth.

The tooth stiffness at each point of line of teeth pair contact is called **specific tooth stiffness** and can be obtained as ratio of unit load and tooth deformation for any specific point:

$$c_{sp} = q/u .$$ (4)

For calculation of unit stiffness for i[th] teeth pair (when m teeth pair are simultaneously in contact), contact is simulated with serially connected springs, which is in accordance with contact modelling in mechanics. So, the specific teeth pair stiffness for any contact point when unit specific tooth stiffness for pinion tooth c_{sp1}, and wheel tooth c_{sp2} are known has following form:

$$c_{sp(i)} = \frac{c_{sp1} \cdot c_{sp2}}{c_{sp1} + c_{sp2}} .$$ (5)

In many theoretical calculations, the assumption of constant teeth pair stiffness along line of contact exists. The average teeth pair stiffness along line of contact is used as constant teeth stiffness and can be calculated for every of m teeth pair in contact as average value of specific teeth pair stiffness along line of contact:

$$c' = \overline{q/u} .$$ (6)

The previous mentioned dynamic models of gears motion [14,15] use simplified stiffness variable called total mesh stiffness c_0 that is sum of total teeth pair stiffness for all simultaneously meshed teeth pairs.
For involute spur gears, that means:

$$c_0 = B \cdot \sum c_i' , \ i=1 \text{ for single tooth pair contact period}$$

$$i = 1,2 \text{ for period with two teeth pair in contact.}$$ (7)

where: c_i' is average teeth pair stiffness for i[th] teeth pair in contact and B is length of line of contact, i.j. gear facewidth.
For involute helical gears, that means:

$$c_0 = \sum (c_i' \cdot B_i) , \ i = 1,2 \text{ for two teeth pair in contact}$$

$$i = 1, 2, 3 \text{ for three teeth pair in contact.} \qquad (8)$$

where B_i is length of line of contact for i^{th} teeth pair.

3. Analytical solution of nonlinear load distribution for spur gears

3.1. Load distribution over simultaneously meshed tooth pairs

For cylindrical involute straight-tooth gears (spur gears), the problem of load distribution in mesh could be solved with separately solved two load distributions: the load distribution over simultaneously meshed tooth pairs and the load distribution over a gear facewidth. Paper [21] describes the solution of load distribution over simultaneously meshed tooth pairs. This solution is used as the starting point in research described in this paper.

The following equations describe the gear load distribution in an analytical form [21,22]:

$$\overline{q}_1 = \frac{c_1'}{c_1' + c_2'} \cdot \frac{F_{bn}}{B} = \frac{c_1' F_{bn}}{c_0} \;;\; \overline{q}_2 = \frac{c_2'}{c_1' + c_2'} \cdot \frac{F_{bn}}{B} = \frac{c_2' F_{bn}}{c_0} \;. \qquad (9)$$

3.2. Load distribution over gear facewidth

In real working conditions, the load distribution over gear facewidth is non-uniform and can be described with function $q(z)$, which defines the unite load change along the tooth pair contact line. The system of integral equation, which consists of the contact equation and balance equation, represents the starting point for determination of real load distribution over gear facewidth. This system can be presented in the following form:

$$\int_0^B q(z) \cdot K(z,u) dz = \Delta + F_\beta(z) \;; \qquad (10)$$

$$\int_0^B q(z) dz = F_{bn} \;. \qquad (11)$$

Where: $q(z)$ – is the function of unite load change along the tooth pair contact line; $K(z,u)$ – is influence function, which defines the relation between u (elastic deformation at one particular point on the contact pattern) and $q(z)dz$ (concentrated load at the same point); z – is the coordinate of the studied point along contact pattern; Δ – is total tooth pair deformation in the direction normal to tooth pair contact pattern; $F_\beta(z)$ – is mesh initial misalignment (deviation between pinion tooth facewidth direction and wheel tooth facewidth direction when the gear pair is nonloaded); F_{bn} – is total normal load value for gear pair in mesh.

It's very hard or almost impossible to determine real values for many factors and variables that have crucial influence on the accurate form of the function $q(z)$, as well as

on the value of real tooth pair bearing pattern length *B*. Also, there is very small possibility to determine and to take into the calculation the real values for gear body deformation, gear rim deformation and deformations of all other parts of gear transmission. Therefore, the determination of function $q(z)$, with very high level of accuracy, is impossible and a system of integral equations defined with the expressions (10) and (11) could be solved only by numerical method usage with the same simplification and assumptions.

The discrete method for solving the problem of load distribution over gear facewidth is used in this paper. During single meshed tooth pair period, the main principle of this method defines tooth pair contact pattern like the final number of equal segments. Generally, a length of these segments is nearly a value of gear pair module *m*, Fig. 3. Then, value of load $q_j(z)$ that acts on the jth segment (part) of tooth pair contact pattern substitutes with uniform unite load $\overline{q_j}$, i.e. with concentrated force $F_j = \overline{q_j} \cdot \Delta z_j$. Finally, the discrete method gives the system of integral equations that can be translated to the equivalent system of algebraic equations. A lot of numerical methods can be use for this translation.

The matrix form of the mentioned equivalent system of algebraic equations is:

$$\begin{bmatrix} K_{11} & K_{12} & . & . & . & K_{1n} \\ K_{21} & K_{22} & . & . & . & K_{2n} \\ \vdots & \vdots & & & & \vdots \\ K_{n1} & K_{n2} & . & . & . & K_{nn} \\ 1 & 1 & . & . & . & 1 \end{bmatrix} \cdot \begin{bmatrix} F_1 \\ F_2 \\ \vdots \\ F_n \end{bmatrix} = \begin{bmatrix} \Delta_1 + F_{\beta 1} \\ \Delta_2 + F_{\beta 2} \\ \vdots \\ \Delta_n + F_{\beta n} \\ F_{bn} \end{bmatrix}. \tag{12}$$

where each matrix element K_{jk} represents the sum of all influence factors for both gears, i.e. the total coefficient for influences of force that acts on the kth segment of tooth pair contact pattern to the deformation of the jth segment of the tooth pair contact pattern.
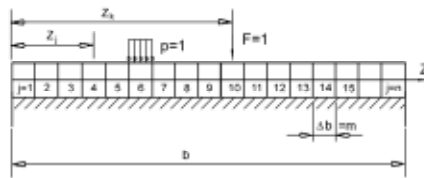
Figure 3. Partition of tooth pair contact pattern on finale number of equal segments.

In equation (12), F_j, $j=1,n$ are unknown forces that act on the center points of segments and their values define the load distribution over gear facewidth, and Δ_j, $j=1,n$ is the displacements of the center points of contact pattern segments which are increased for corresponding mesh misalignments due to manufacturing and assembly ($F_{\beta j}$, $j=1,n$). Δ_j and $F_{\beta j}$ are corresponding values in the direction which is identical to the direction of normal load. The solution of the system of algebraic equations (12) gives values F_j and this define the real load distribution over facewidth and real length of tooth bearing pattern during transmission of external load defined with force F_{bn}.

4. Analytical solution of nonlinear load distribution for helical gears

The helical gears nonlinear load distribution in gear mesh could be solved only by resolving the load distribution between simultaneously meshed teeth pairs and the load distribution along each of teeth pair contact line, at the same time. For mathematical definition of load distribution in helical gear mesh, the expanded procedure for load distribution over gear facewidth for involute spur gear could be used.

For every moment (contact position P) during helical gears meshing period m tooth pairs are simultaneously in contact. System of integral equations, which consists of the contact equation and balance equation, can be defined for each ith of m simultaneously meshed tooth pairs for single contact position. This system can be presented in the following form:

$$\int_0^{B_i} q_i(z) \cdot K_i(z,u) dz = \Delta_i + F_{\beta i}(z).$$

(13)

$$\int_0^{B_i} q_i(z) dz = F_{bni}.$$

(14)

Where: $q_i(z)$ – is function of unit load change along the ith tooth pair contact line, B_i – is length of ith teeth pair contact line for a contact position P, $K_i(z,u)$ – is influence function, which defines relation between u (elastic deformation at one particular point on the contact pattern) and $q_i(z)dz$ (concentrated load at the same point), z – is coordinate of studied point along contact pattern, Δ_i – is total tooth pair deformation in the direction normal to tooth pair contact pattern, $F_{\beta i}(z)$ – is mesh initial misalignment (deviation between pinion tooth facewidth direction and wheel tooth facewidth direction when the gear pair is unloaded), F_{bni} – is total normal load value for i^{th} tooth pair in mesh.

Systems of equations (3) and (4) for all m simultaneously meshed tooth pairs and equation of load balance:

$$F_{bn1} + F_{bn2} + ... + F_{bnm} = F_{bn}.$$

(15)

give system of $(2m+1)$ equation for load distribution solution. It's very hard or almost impossible to determine real values for many factors and variables that have crucial influence on accurate form of the function $q_i(z)$, as well as on value of real tooth pair bearing pattern length B_i. Therefore, this system of integral equations can be solved only by numerical method usage with same simplification and assumptions.

The main difference between discrete method developed for spur gear pair and helical gear pair is in the number of tooth pairs that are simultaneously in mesh and in variable tooth pair bearing pattern length. It is consider that the n_i is the number of segments on the ith tooth pair contact line, so the equation (15) takes the following form:

$$\sum_{i=1}^{m} \sum_{j=1}^{n_i} q_{ij} \cdot B_{ij} = F_{bn} \ . \tag{16}$$

where q_{ij} – is normal unit load along the jth segment of ith tooth pair contact line; B_{ij} – is length of the segment. The numerical Finite Element Method is used for calculation of these values.

5. Finite Element Analysis for load distribution calculation

This chapter of the paper describes Finite Element Analysis (FEA) of spur and helical gears. Appropriate analysis is performed in order to select meshed gears model which is sufficiently economic and in same tame sufficiently geometrically accurate, [18]. The chosen FEM models each consist of three gear's teeth. The special algorithm for tooth's involute profile drawing is developed and built in present FEM software to assure drawing of real involute flanks contact geometry. Also, choice of optimal mesh size level is performed, [18]. Described FEM models are made for one particular gear pair with high value of transmission ratio, that enable us to perceive all potential problems during stress and strain calculations. The main characteristics of the gear pair are: number of teeth z_1=20, z_2=96; standard tooth involute profile, addendum modification coefficients x_1=0.3, x_2=0.2; face width b=175 mm; module m_n=24; pressure angle α_n=20°; rotational wheel speed n_2=4.1596 min^{-1}; wheel torque T_2=1264.4 KN·m, material: steel with $E = 206\ 000$ N/mm^2; ν =0.3; helix angle β=15° and pinion teeth inclination – right, wheel teeth inclination – left (for the investigated helical gear pair only). For defined geometry characteristics and torque, the normal nominal load that this gear pair transmits is F_{bn}= 1168.0354 KN. The appropriate Finite Element Analysis gives the possibilities for monitoring of deformation and stress variables during tooth pair meshing period.

5.1. FEA for a spur gear pair

Finite Element Analysis for the spur gear pair with previous defined characteristics is performed by FEM model shown in Fig.4a,b and in detail described in previous papers, [11,18]. For solving the stiffness and load distribution for gear pair dynamic model the specific iterative procedure has been used: In the first iteration, for the period with two teeth pairs in contact, the uniform distribution of normal load F_{bn} between simultaneously meshed teeth pairs is assumed ($\overline{q_1} = \overline{q_2}$). For this load case, the FEA gave results for total pinion tooth deformation and total wheel tooth deformation (u_{z1} and u_{z2}) – equal to displacements of contact points in the direction of the path of contact. Sum of these values represents the total deformation for a teeth pair in mesh u'. Then, equation (6) gives the values of tooth pair stiffness c_i' for both of simultaneously meshed teeth pairs, as well as the equation (7) for the total mesh stiffness c_0. When the obtained values are inserted in equations (9) the unit loads $\overline{q_i}$, i=1,2 result in corrected values. Then new FEA with same gear models, but with corrected loading, produce results for

the next iteration of unit load values. Number of iterations depends on the partcular level of accuracy required.

In the last iteration, the developed methodology and FEM calculations give all the values necessary for determination of the key parameters: tooth deformations, tooth stiffness, load distribution, maximum equivalent stress in tooth roots and maximum equivalent stress on the meshing tooth flanks, Fig.4c.
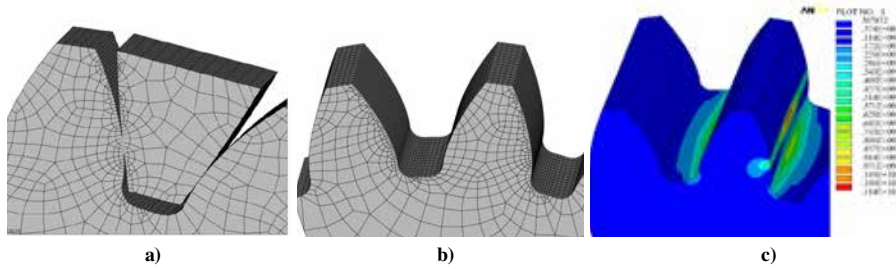
Figure 4. The spur gear FEM model and equivalent stresses for pinion gear.

5.2. FEA for a helical gear pair

Finite Element Analysis for the helical gear pair with previous defined characteristics is performed by FEM model shown in Fig.5a,b and in detail described in previous papers, [10]. For solving the stiffness and load distribution for gear pair dynamic model a similar iterative procedure has been used: In first step (iteration), total normal load for a contact position P is divided on simultaneously meshed tooth pairs in proportion of appropriate bearing pattern lengths, which are scanned from FEM nonlinear contact solution for the investigated gear pair. Therefore, the normal load on i^{th} meshed tooth pair is:

$$F_i = B_i \cdot F_{bn} / \sum_{i=1}^{m} B_i . \tag{17}$$
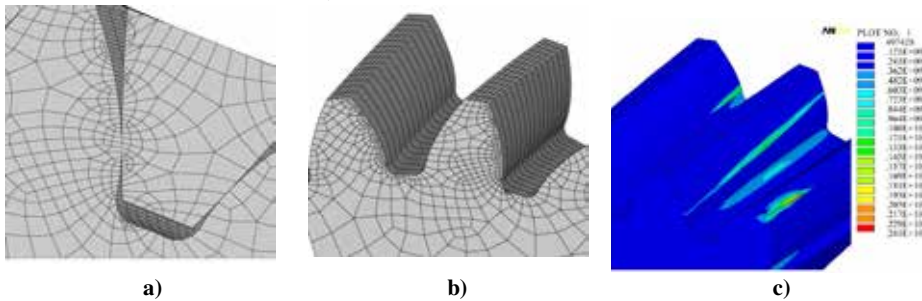
Figure 5. The helical gear FEM model and equivalent stresses for pinion gear.

Then, tooth pair stiffness of jth segment on i^{th} line of contact is calculated as ratio of unit normal load and total teeth deformations in the direction of line of contact scanned from FEA results, Eq.4. For the next iteration normal load is divided on tooth pairs in mesh in accordance with stiffness values and bearing pattern lengths:

$$F_{bti} = \frac{c_i' \cdot F_{bt}}{\sum\limits_{i=1}^{m}(c_i' \cdot B_i)} \cdot B_i \ .$$

(18)

In the last iteration, the developed methodology and FEM calculations give results needed for dynamic behaviour modelling: tooth deformations, tooth stiffness, load distribution, maximum equivalent stress in tooth roots and maximum equivalent stress on the meshing tooth flanks, Fig.5c.

6. Results and discussion

For the investigated spur gear pair the results are obtained by described procedure and displayed in this chapter for the middle teeth pairs of modelled gear segments.

On Fig.6 obtained distribution of specific tooth stiffness is presented: along path of contact (Fig.6a) and along gear facewidth for the contact point with maximum stresses, Fig.6b. On this diagrams the variable y/p_b [-] is ratio of contact point position on line of contact (measured from start contact point) y and base pitch p_b. The appropriate load distribution obtained from shown stiffness distribution is calculated with Eq.9 and shown on Fig.6c. Total mesh stiffness for a spur teeth pair is shown on Fig.7. The mesh stiffness variation is presented during two time periods of the gear pair motion.

For the investigated helical gear pair, results for the specific stiffness and normal load distribution are obtained by described procedure and shown on Fig.8. The results are displayed for one tooth pair meshing period. On this diagrams the variable y/p_{bt} [-] is ratio of contact point position on line of contact (measured from start contact point) y and transverse base pitch p_{bt}, and the variable z [mm] is distance of contact point form tooth face surface.
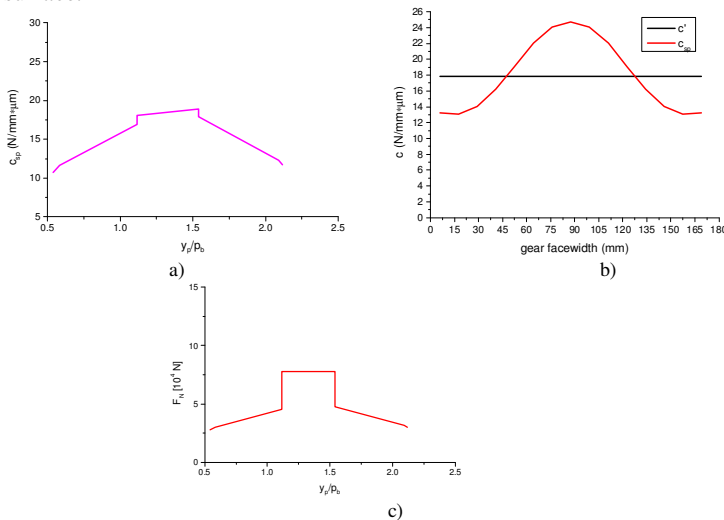
Figure 6. The results for spur gear stiffness and load distribution.
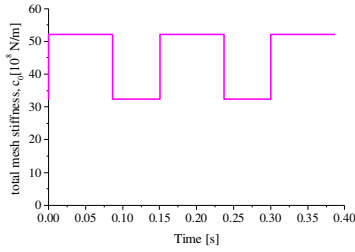
Figure 7. Total mesh stiffness during spur gear meshing.

The specific stiffness that is calculated and shown at Fig.8 and the real teeth pair bearing pattern lengths B_i (i=1,2,3) taken from the FEM helical gears model are used for the calculation of total mesh stiffness c_0 (N/m) by Eq.8. The trend of the total mesh stiffness change during the periods with two and three simultaneously meshed gear pairs is shown in Fig.9. Results shown in this diagram correspond to three tooth pair mesh periods. The diagrams shown in Fig.7 and Fig.9 have the expected form in accordance with results of other authors, [17].
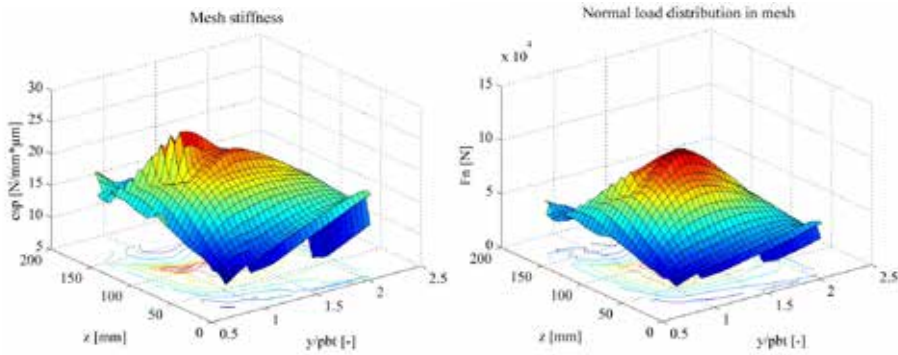
Figure 8. Mesh stiffness and normal load distribution for helical gear pair.
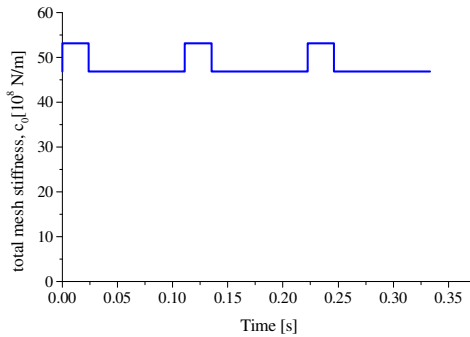
Figure 9. Total mesh stiffness during helical gear meshing.

383
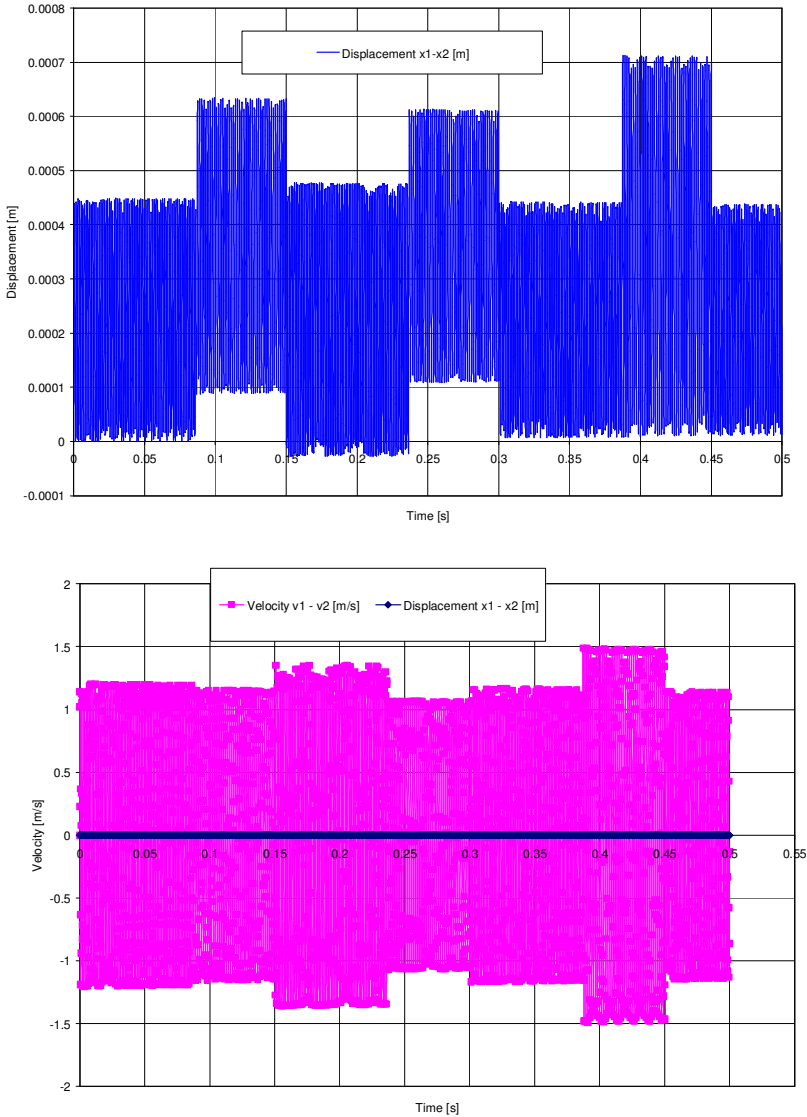
Figure 10. Variation of spur gear pair displacement and velocity.

Obtained results for total mesh stiffness and normal load distribution for both of gear pairs (spur and helical) are then put in nonlinear dynamic analytical model of involute gears motion described with equation (1a,b) for model II and equations (2) for model I. In that way these analytical models become solvable. The Runge-Kutta numerical
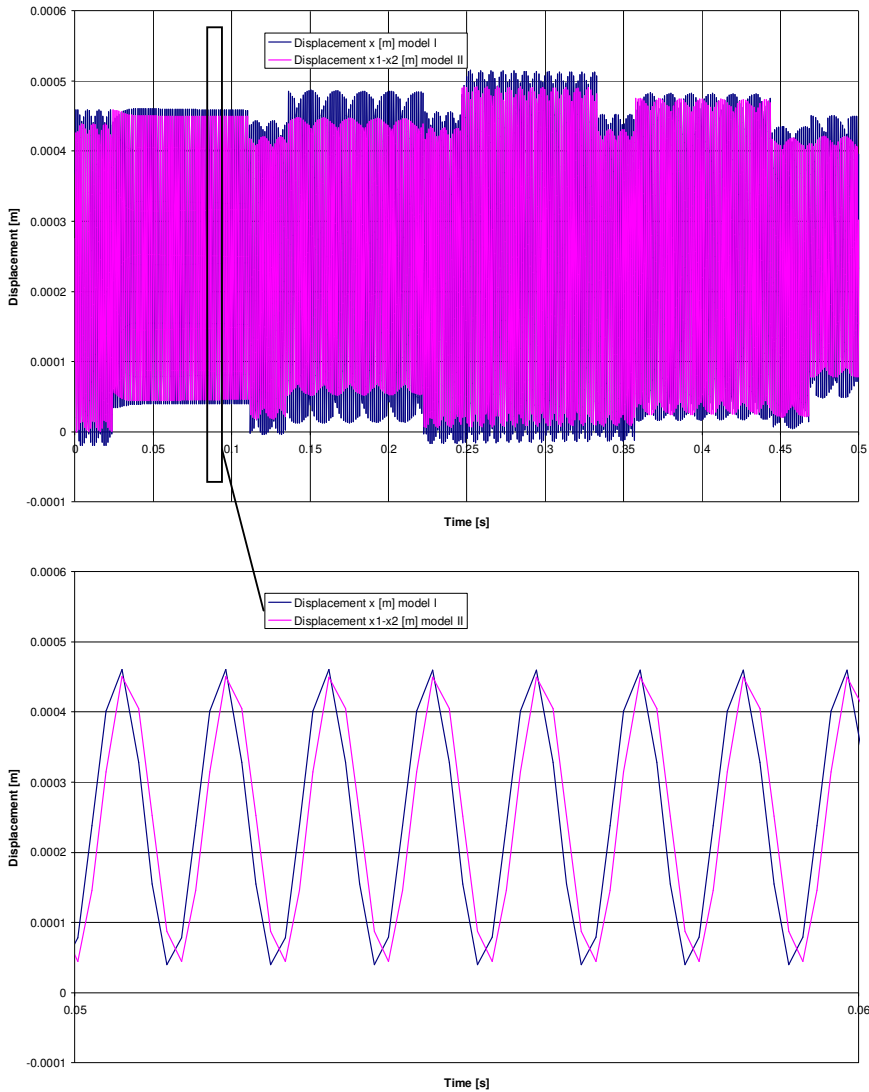
Figure 11. Variation of helical gear pair displacement.

iterative methods are used for solving the obtained differential equations. The commercial MATLAB software is used for calculations.

The variation of displacements and velocity for the spur gear pair calculated with model II are shown in Fig.10. For the helical gear pair appropriate diagrams are shown in Fig.11 and Fig.12. The results obtained for dynamic gear models I and II, are shown in

385

comparative diagrams with the zooming details. Results in Fig.11 correspond to three meshing periods and results in Fig.12 correspond to gear pair velocity for the same time period.
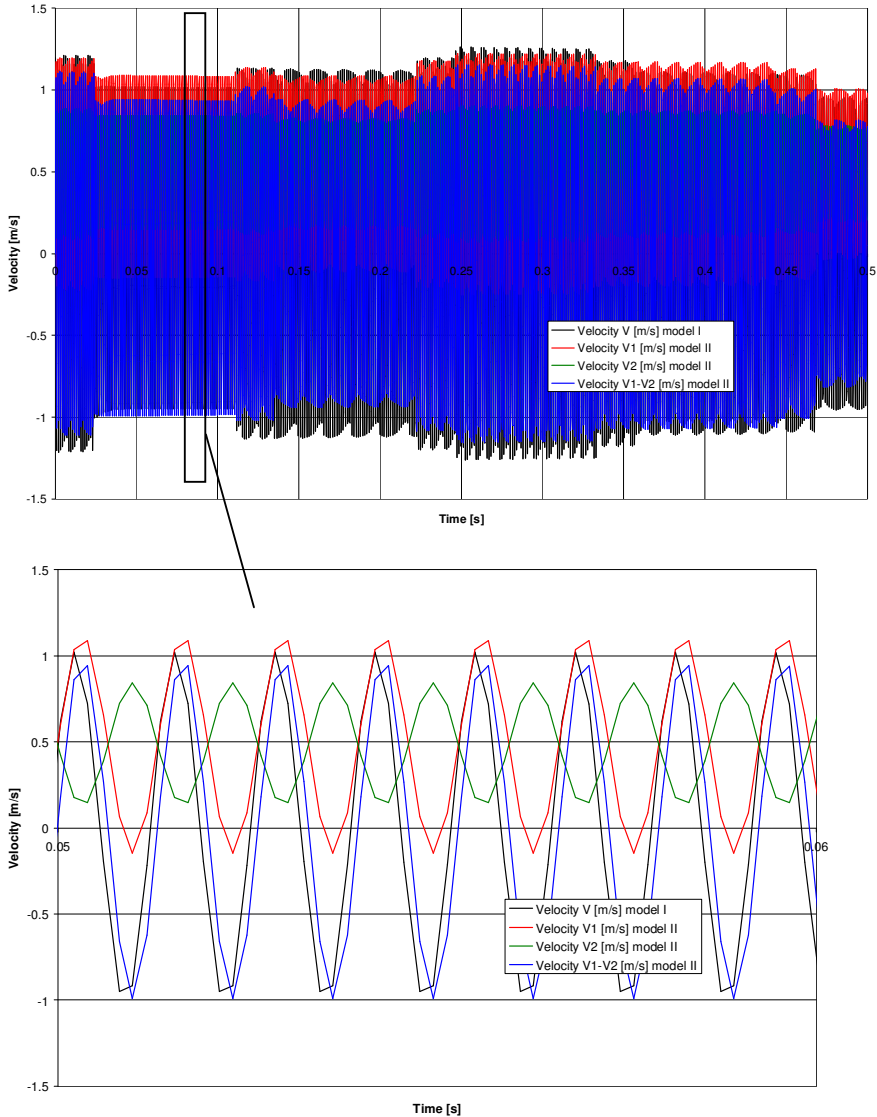
Figure 12. Variation of helical gear pair velocity.

7. Conclusions

This paper shows the calculation of total mesh stiffness and nonlinear load distribution for spur and helical involute gears with a new methodology and Finite Element Analysis. The presented research successfully put together numerical methods for stress and strain calculations and numerical iterative methods for differential equations solving. Excellent qualitative superposition of results with results of other authors, [2], led to the conclusion that developed models and procedures are suitable for future research. The obtained results shown as phase portraits in Fig.13 confirm that the helical gear pair has more stabile work than the spur gear pair with same main geometry and load.
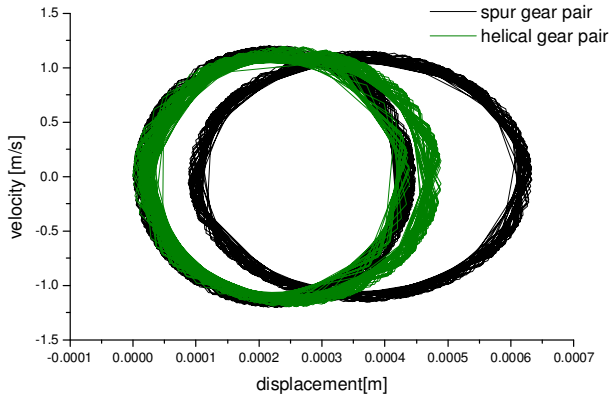
Figure 13. Comparative phase portraits.

Although this fact has been known in theory of gears, the presented research is important because the developed procedure gives the accurate assessment of the differences between spur and helical gear pairs and can be used for future investigation of optimal gears parameters (e.g. tooth profile, nominal load) with aspect of gear pair stability. Also, the time-varying meshing damping could be incorporate in developed model of gears dynamics.

8. References

[1] Dimitrijević D. et al., Dynamic analysis of the stress and strain state of the spur gear pair, *Scientific Technical Review*, LVII 3-4 (2007), pp.20-25.

[2]   Amezketa M. et al., Dynamic model of a helical gear pair with backlash and angle-varying mesh stiffness, *Multibody Dynamics, ECCOMAS Thematic Conference Warsaw*, Poland, (2009), 29 June–2 July

[3]   Li S. et al., Nonlinear dynamic simulation of coupled lateral-torsional vibrations of a gear transmission system, *IJCSNS International Journal of Computer Science and Network Security*, 6 (8A) (2006), pp.27-35.

[4]   Andersson A., Vedmar L., Dynamic model to determine vibrations in involute helical gears, *Journal of Sound and Vibration,* 260 (2003), pp.195–212.

[5]   Ulaga, S., Ulbin, M., Flasker, J., Contact problems of gears using Overhauser splines, International *Journal of Mechanical Sciences*, Volume 41 (1999), pp. 385-395.

[6]   Pedrero, J. I., Pleguezuelos, M., Aguiriano, S., Load distribution model of minimum elastic potential for involute internal gears, *Machine Design*, (2007), pp. 245-250

[7]   Atanasovska et al., Analysis of the nominal load effects on gear load capacity using the finite element method, *Proceedings of the Institution of Mechanical Engineers, Part C: Journal of Mechanical Engineering Science*, Volume 224, Number 11 (2010), pp. 2539-2548.

[8]   Li, S., Finite Element Analyses for contact strength and bending strength of a pair of spur gears with machining errors, assembly errors and tooth modifications, *Mechanism and Machine Theory,* Volume 42 (2007), pp. 88–114.

[9]   Li, S, Effect of addendum on contact strength, bending strength and basic performance parameters of a pair of spur gears, *Mechanism and Machine Theory*, Volume 43 (2008), pp. 1557–1584.

[10] Atanasovska I., Nikolić V., 3D spur gear FEM model for the numerical calculation of face load factor, *The Scientific Journal: Facta Universitatis, Series: Mechanics, Automatic Control and Robotics*, Vol 6, No 1 (2007), pp.131-143.

[11] Atanasovska I., Nikolić V., Dimitrijević D., Momčilović D., Finite element model for stress analysis and nonlinear contact analysis of helical gears, *Scientific Technical Review*, Vol.LVIX, No.1 (2009), pp.61-69.

[12] Umezawa, K., Suzuki, T., Sato, T., Vibration of power transmission helical gears (Approximate equation of tooth stiffness), *Bulletin of JSME*, Volume 29 (1986), pp. 1605–1611.

[13] Parker R. G., Vijayakar S. M., Imajo T. Non-linear dynamic response of a spur gear pair: Modelling and experimental comparisons*, Journal of Sound and Vibration* 237(3) (2000), pp.435-455.

[14] Atanasovska I., Vukšić Popović M., Starčević Z., The dynamic behaviour of gears with high transmission ratio, *International Journal for traffic and transport engineering IJTTE,* Volume 2, Number 2 (2012), pp.153-160.

[15] Walha, L. et al., Effects of eccentricity defect on the nonlinear dynamic behavior of the mechanism clutch-helical two stage gear, *Mechanism and Machine Theory*, Volume 46 (2011), pp. 986–997.

[16] Faggioni M., Samani F., Bertacchi G., Pellicano F. Dynamic optimization of spur gears, *Mechanism and Machine Theory* 46 (2011), pp.544–557.

[17] Lakota M. and Stajnko D., Application of Joint Time Frequency Analysis for Early Crack Detection on One-stage Gear Drive, *Strojarstvo* 51 (6) (2009), pp.565-574.

[18] Atanasovska I. et al., Developing of gear FEM model for nonlinear contact analysis, *Proceedings of 1. International Congress of Serbian Society of Mechanics, Kopaonik* (2007), pp.695-703.

[19] Hortel M., Skuderova A. Linear and nonlinear damping in dynamics of gear mesh of the parametric systems with impacts, *Engineering MECHANICS*, Vol. 14, No. 1/2 (2007), pp.91–104.

[20] Jelić M., Atanasovska I., The New Approach for Calculation of Total Mesh Stiffness and Nonlinear Load Distribution for Helical Gears, *The 4th International Conference on Power Transmissions*, Sinaia,Romania (2012).

[21] Nikolić V, Atanasovska I.: The finite element method solution of the load distribution over simultaneously meshed tooth pairs for cylindrical involute straight-tooth gears, *Conference with international participation IRMES'04*, Kragujevac, (2004).

[22] Moriwaki I., Saito K.: Calculation of tooth deflection by global local finite element method (sampling points for accurate interpolation), *International congress – Gear Transmissions'95*, Sofia (1995), pp. 95-98.

ELEMENTS OF DYNAMIC MODIFICATIONS AND SENSITIVITY CONSIDERING THE EFFECT OF STRUCTURAL PARAMETERS UNCERTAINTY

Nataša Trišović[1], Wei Li[2], Taško Maneski[1], Mirjana Misita[1], Ljubica Milović[3]

[1] University of Belgrade, Faculty of Mechanical Engineering,
Kraljice Marije 16, 11120 Belgrade, Serbia;
[2] Department of Mathematics, Xidian University, Xi'an, Shaanxi, 710071, China
[3] University of Belgrade, Faculty of Technology and Metallurgy, Karnegijeva 4, 11000 Belgrade, Serbia
Corresponding author: ntrisovic@mas.bg.ac.rs

Abstract. The present paper deals with the problem of improving of dynamic characteristics some structures. Dynamic modification procedure is given as using distribution of potential and kinetic energy in every finite element is used for analysis. Also, the paper will discuss the introducing of a probabilistic treatment of important problem parameters. Most numerical simulations of physical systems are rife with sources of uncertainty. Uncertainty in simulations stems from the stochastic nature of geometric and physical parameters, indeterminate nature of initial/boundary conditions, and inadequacy of physical models coupled with discretization errors. Structural modifications can cause changes in the matrices of some elements. Depending on the type of structure, or a desired change, a group of elements can be modified

Key words: dynamic modification, reanalysis, uncertainty

1 Introduction

Dynamic response of mechanical systems depends on structural parameters. The objective is to evaluate the structural response for successive modifications in the design avoiding the difficult solution of the modified equations. The structural modifications may be caused by external factors or by the designer in order to improve the characteristic of the response (eigenvalues and eigenvectors). Modification of dynamic characteristics means change of corresponding design variables to get desired dynamic behavior of structure. The design variables depend on the type of optimization problem. In the design of structural components, such as stiffened panels and cylinders, the design parameters represent the spacing of the stiffeners, the size and shape of the stiffeners, and the thickness of the skin. The thickness of plates, cross-sectional areas of bars, areas, moments of inertia, and torsion constants of beams represent sizes of the elements. Joints and members could be eventually added or deleted during the design

procedure so that the geometry of the structures may be modified. Reanalysis methods can include the next activities:

(a) Modification in the geometry with no further change in the number of degrees of freedom.

(b) Modification of design variables (mass, damping and stiffness).

(c) Increase or reduction of the number of DOFs by changing the supporting manner and addition or deletion of joints and members.

(d) Alteration of the kind of material on some places if modification is possible. The main purpose of dynamic reanalysis is to provide numerical procedures to evaluate the structural response after modifications of design variables.

The development of a new, simple procedure for structural reanalysis of mechanical system must be capable of modifying its dynamic properties while achieving requested characteristics with conveniently fast convergence of the whole process. The analytical method with a clear concept, based on distribution of kinetic and potential energies is used for modifying the dynamic properties of main vibration (oscillation) forms, occurring in individual components or in grouped assemblies. The analysis of complex structures begins with initial rough analysis of a structure that is followed by the analysis of grouped structural assemblies. The final phase is the precise analysis based on sensitivities of individual elements. The selection of structural parameters for dynamic properties improvement through eventual modification according to energy distribution includes geometry, supporting system and material characteristics. Based on this approach, the corresponding algorithm is proposed and applied. One of the important performances of this algorithm is convenience for rational implementation in computer systems, using appropriate software. In this way, relevant data for structural system dynamic response during reanalysis can be obtained and considered in the optimization. The main purpose of dynamic reanalysis is to provide numerical procedures to evaluate the structural response after modifications of design variables.

1.1 Literature Overview

The basic theory for determining the existence of solution for frame structure optimization with frequency limits is found in Ref. (Tong at all, 2000). According to this theory, natural frequencies do not change with uniform frame modification and key limitation for determination of optimal dynamic solution of frame structure modification is mostly that of eigenfrequencies. The optimization criteria for space frame structure with multiple limitations in its natural frequencies are considered in (Wang at all, 2004). Knott coordinates and cross sections of elements, although of different nature, have been treated simultaneously in unified design specification for a minimum weight of structure. Optimum first criterion, developed for one limitation based on differentiation of the Lagrange function, indicates that at optimum all the variables are of the same efficiency. In order to solve multiple limitations of frequencies global numbers are introduced, avoiding in this way the calculation of Lagrange's multiplicators.

In the final stage, the most efficient variables are identified and modified as priority. Using the minimal weight increment, optimal solution can be obtained from initial design solution. The procedure is also effective for repeated values of frequency. In

paper (Nair at all, 1998) the model for modified dynamic structural system is presented, based on reduced appreciative concept of improved method for the approximation of eigenvalues and eigenvectors of first order. The expressions for local approximation based on Taylor's series are used as base vectors for eigenparameters perturbance approximation. The reduced system of eigenvalues is generated for each eigenvector using eigenvectors as a base and Ritz's vector approximation of first order. The equations for reanalysis are algebraic (Wamg at all, 1986). A new function to limit eigenvalues approximation in the procedure of structural optimization is introduced in (Canfield, 1990). Applied Reyli ratio increases the approximation quality for frequency limitations since it approximates eigenforms energy and kinetic energy instead eigenvalues, producing faster and stable convergent solutions.

The application of iterative method for sensitivity determination in reanalysis of structure due to small perturbances of design variables is applied in numerical procedure, discussed in (Yoon, 1988). In this paper the algorithms for displacements and stresses are given, as well as for eigenvalues and forms. The scheme of iteration is modified saving matrix coefficients as constant and using only one decomposition. Implementation of algorithm is simple, and the convergence fast. The extension of the method to the sensitivity of eigenfrequencies with repeated values is convenient to avoid the conditions of matrix coefficients close to bifurcation points, which occurs when non-linear response of a structure is considered.

It should be noted that dynamic response is given primarily through corresponding eigenfrequencies and main oscillation forms as characteristic (typical) variables. Changing them, by changing the design parameters of a structure, it is possible to achieve the required structural dynamic response.

Sensitivity analysis is an important point within the *dynamical modification* procedure. Sensitivity analysis represents a collection of mathematical methods for reanalyzing structures which is, within dynamical modification, related to sensitivity of eigenvalues and eigenvectors. Therefore, the application of sensitivity analysis is limited to construction of segments for which necessary mathematical relations can be determined. If this is not possible, sensitivity analysis is only partially applicable. Dynamical analysis of complex structures can easily be conducted via finite elements modeling. Therefore, while finite element analysis method is highly adequate for modeling complex structures, one of its major drawbacks lies in the usage of large number of degrees of freedom in calculating the exact eigenpairs. This number can amount to few tens of thousands, or even more. To reduce the calculation time it is possible to divide the complex structure into connected substructures and analyze each one separately. The dynamical behavior of each substructure is represented only by a reduced set of eigenpairs of interest, which contributes to significant problem simplification. A more general problem of structural dynamic analysis has three important aspects. *Firstly*, the observed physical structure is represented by initial finite element model. Modeling is based on numerous idealizing approximations within an exaggerated elaboration of details, which in essence does not significantly improve the accuracy of output data, especially having available powerful computers and appropriate software packages. Optimal alternative is to have the possibility of verifying outputted data that were measured on a prototype or real structure. *Secondly*, the dynamic characteristics of

construction under reanalysis are analyzed. What is basically observed are eigenvalues and main forms of oscillations as characteristic variables that can invoke inadequate actual dynamic behavior. *Thirdly*, on the basis of the analysis of actual dynamic behavior, modification steps are proposed after which a modified model is obtained. Having in mind that mechanical structures are most often very complex, the most convenient modification steps are not easily obtained.

1.2 *Uncertainty quantification*

Uncertainty quantification in structures is a very important field of investigation, due to its influence on subjects such as structures reliability and model validation amongst others. Uncertainty quantification in structures can be used where the uncertainties introduced by random forces were applied to the structure Lin (1969). Cacciola at all (2005) did research on the procedure for the dynamic reanalysis of linear systems subjected to deterministic or stochastic loads. The structural modifications may be imposed by external factors (e.g. design alterations for operational reasons, or discrepancies between the predicted and measured properties of the structures) or by the designer in order to improve the characteristic of the response (e.g. layout optimization). Joints and members could be eventually added or deleted during the design procedure so that the topology of the structures may be modified. Reanalysis techniques are commonly devoted to efficiently determine the structural response produced by the following events:

1. modification in the geometry with no further change in the number of degrees of freedom (DOFs);
2. alteration of dynamic characteristics of structural components (mass, damping and stiffness);
3. variation of the number of DOFs due to addition or deletion of joints and members;
4. alteration of loads due to both modification of the original number and position of joints and for changing in the intensity of external excitations.

Cacciola at all (2005) stated that most reanalysis methods are not able to deal with the last two modifications, which are usually named topological modifications as they imply a change in the dimension of the system due to addition or deletion of DOFs.

Kirsch and Liu (1997) focused a static reanalysis method by researching the characteristic of a modified initial design for the case of layout modification (no changes in the number of degrees of freedom).

Lecomte (2013) investigated the response of uncertain vibro-acustic and structural dynamic systems. In this paper, it is shown the comparison of the exact means, variances, covariances, as well as the exact stochastic and covariance coefficients, with their estimates obtained through Monte-Carlo simulations that confirmed the advantages of the analytical approach.

2. PROBLEM SETUP

Sensitivity examination on real examples still presents a troublesome task so that the analysis of distribution of specified values is performed instead. The distribution of optimization elements is an example of reanalysis which is expressed in percentages of

specified quantities from a chosen group of elements. By posing the task of obtaining the desired first or other eigenfrequency of a system, construction analysis often requires the calculation of a great number of construction alternatives. However, through reanalysis, which is based on balancing the distribution of kinetic and potential energy of all finite elements in the model, it is possible to efficiently obtain the desired eigenfrequencies of a system. The main goal of dynamic optimization is to increase natural frequencies and to increase the difference between them. Some information should be prepared, before you set up the FE model.

The matrix form of differential equations of motion for a system that is not subjected to external forces is:

$$[M] \cdot \left\{ \ddot{Q}(t) \right\} + [K] \cdot \left\{ Q(t) \right\} = \{0\} \tag{1}$$

Eigenvalue of this differential equation for i-th mode is:

$$[K]\left\{ \underline{Q}_i \right\} - \lambda_i [M]\left\{ \underline{Q}_i \right\} = \{0\} \tag{2}$$

Given that $[\Delta K]$ and $[\Delta M]$ are the corresponding changes in rigidity and mass matrices respectively, then the formula (2) can be applied to the modified system and so called modified equation for the case of free oscillations is: $[K]'\left\{ \underline{Q}_i \right\}' = \lambda_i '[M]'\left\{ \underline{Q}_i \right\}'$,

where we have substituted

$$[K] = [K]' - [\Delta K], \quad [M] = [M]' - [\Delta M],$$
$$\left\{ \underline{Q}_i \right\} = \left\{ \underline{Q}_i \right\}' - \left\{ \Delta \underline{Q}_i \right\}, \quad \lambda_i = \lambda_i ' - \Delta \lambda_i \tag{3}$$

where $\Delta \lambda_i$ and $\left\{ \Delta \underline{Q} \right\}_i$ are changes of eigenvalues and eigenvectors, respectively.

Assuming that the changes in the construction are small, it can be expected that the changes of values of vectors of eigenvalues and eigenvectors will also be small. Therefore, the higher order members in the following equations can be neglected (Ki, 1983). After mathematical transformation it is possible to express the change of i-th eigenvalue under system modification, which was the final purpose of this procedure:

$$\frac{\Delta \lambda_i}{\lambda_i '} = \frac{\frac{1}{2}\left\{ \underline{Q}_i \right\}'^T [\Delta K]\left\{ \underline{Q}_i \right\}' - \frac{1}{2}\lambda_i '\left\{ \underline{Q}_i \right\}'^T [\Delta M]\left\{ \underline{Q}_i \right\}'}{\frac{1}{2}\lambda_i '\left\{ \underline{Q}_i \right\}'^T [M]'\left\{ \underline{Q}_i \right\}'} . \tag{4}$$

The previous formula can be considered as *basic expression in construction reanalysis* aimed at improving dynamic characteristics. The expression in the nominator represents the difference of increases in potential and kinetic energy between modified and unmodified states. Since the increase in i-th eigenvalue is directly proportional to this difference, each member of the nominator is of vital importance for analysis, which will be shown in detail further in the text. Another important question arises from analyzing the previous formula. The designations " ' " depict the values which are related to the modified state. Often, due to large size of a certain problem, it is not possible to easily obtain those values. If those changes are small, which is a prerequisite for obtaining accurate solution it is possible, with great degree of reliability, to use the expression with values that are related to unmodified system:

$$\frac{\Delta\lambda_i}{\lambda_i} = \frac{\frac{1}{2}\{\underline{Q}_i\}^T[\Delta K]\{\underline{Q}_i\} - \frac{1}{2}\lambda_i\{\underline{Q}_i\}^T[\Delta M]\{\underline{Q}_i\}}{\frac{1}{2}\lambda_i\{\underline{Q}_i\}^T[M]\{\underline{Q}_i\}} \tag{5}$$

$$E_{p,r} = \frac{1}{2}\{\underline{Q}_r\}^T[K]\{\underline{Q}_r\}, \quad E_{k,r} = \frac{1}{2}\lambda_r\{\underline{Q}_r\}^T[M]\{\underline{Q}_r\}, \quad E_{p,r} = E_{k,r} = E_r$$

The expression in the denominator of equation (5) represents the kinetic energy of a certain oscillation mode and having in mind equation (2), it also represents the potential energy, for reasons of energy balance in the main oscillation modes.
where:

  If the energy distribution over groups of elements is expressed in percentages for each main oscillation mode, it is possible to obtain rough information that can be used in modification. The basic goal of dynamic modification is to increase the eigenvalues and their distances. The formula (5) is important for understanding the procedure that requires modification of a certain construction. The denominator of previous formula is not changed in the procedure of modification, so the main point of analysis is placed on the nominator. The modification of construction assumes the change in only but few segments that are most responsive to change. This sensitivity is expressed in the fact that the change of certain construction parameters of these segments will result in greatest difference in the nominator of previous formula, and consequently in greatest effect on increasing the observed eigenfrequency of the system. Since the observed structures are already in exploitation, the essence of improving dynamic behavior is to achieve maximum change with minimal "intervention". The question is how to determine segments or substructures of a construction that are most sensitive to small changes in their parameters?

The problem of dynamic modification of a construction with the goal of improving dynamic characteristics has been a worldwide challenge for many researchers in previous decades (Trisovic (2007), Trisovic at all (2010), Allaboudi at all (2013).

The methods thereby used are widely different, from strictly mathematical do entirely experimental. Dynamic response of a mechanical structure must be improved by either (i) load control, or (ii) change in dynamic characteristics of a structure. Loads are often the result of interaction of the structure and its environment, so they are not easily controlled. In that case, it is important to know that the dynamic response can be improved by redesigning (reanalyzing) the dynamical characteristics of the structure. Having this in mind, the application of the techniques of reanalysis in obtaining the desired conditions for FE model of mechanical structures has shown a rapid improvement in previous decades. There are numerous techniques that are applied in dynamic reanalysis of mechanical structures. One of them has been already mentioned, *sensitivity analysis* that is successfully applied in general as well as in specific dynamical problems. The success of the procedure of dynamical modification depends on many factors, most important of which are: complexity of a structure including the boundary conditions, and modification method that a research team will choose to apply.

3.1. *Dynamic analysis and diagnostics of a model and its groups*
Dynamic analysis and diagnosis of a model implies the analysis and interpretation of

model behavior and its modification. On the basis of the analysis of energy distributions in main oscillation modes for all construction elements, the following cases are observed, on the grounds of which it is possible to derive the algorithm for reanalysis of similar structures.

I   Elements in which the kinetic and potential energies (and the difference in their increase) are negligible with respect to other elements.

II Elements in which the kinetic energy is dominant compared to potential energy

III Elements in which the potential energy is dominant compared to kinetic energy

IV Elements in which the potential and kinetic energy exist and are not negligible in comparison with other elements

4. CASE STUDY

Using the example of a cantilever beam, the application of the reanalysis formula has been demonstrated in determining the zones of the construction that are most sensitive to changes. Two models are observed: original and arbitrarily modified. The condition is that the modification be small, otherwise the linearization of modification equations, presented in the previous section, would not hold. Note that during the reanalysis, instead of eigencalculations for the changed construction, the corresponding reanalysis formula can be applied, where it is necessary to calculate the coefficients of modification α and β, as well as relative modification ratios ψ and ζ. It is thus possible to considerably save calculation time, and it will be particularly demonstrated that by the line finite elements the reanalysis formula generates entirely reliable results. The type of modification is determined by the type of finite elements, type of boundary conditions, model geometry, and the like.

a. Deterministic input

Consider a cantilever beam of length $1\,m$, rectangular cross-section, $b \times h = 100mm \times 50mm$, divided into 5 finite elements (Fig. 1). In designations, in the tables and diagrams, this cantilever beam is referred to as the original cantilever beam. For the analysis of sensitivity to changes, the *original cantilever beam* is modified across the entire length, with small modifications[1].

Table 1. Few initial eigenvalues for the original cantilever beam and the modified one, where the height, as a construction variable, is increased by 10%

Original cantilever beam		Height increased by 10% across the entire length		Modified shape, I, II,III,IV,V $\Delta h[\%]$, Mat Lab: 8.6, +4, +0.97, -0.98, -2.59	
Frequencies, $f_{0i}[Hz]$	Eigenvalues, λ_i	Frequencies, $f_{0i}[Hz]$	Eigenvalues, λ_i	Frequencies, $f_{0i}[Hz]$	Eigenvalues, λ_i
1443.94	82311011.93	1588.33	99596324.43	1472.33	85579889.95

---

[1] In the literature dealing with dynamic reanalysis it is stressed that modifications should be small, so that the chosen modification process converges to the desired eigenvalues of the pairs, however it is not easy to determine what is 'small';

730.93	21091661.91	804.02	25520910.91	748.59	22122917.88
260.24	2673654.72	286.26	3235122.21	270.70	2893010.45
41.51	68010.88	**45.66**	82293.17	**45.82**	82876.53

That cantilever beam is called a *modified cantilever beam* (Fig. 2). In this case, the chosen construction variable is the height of the rectangular cross-section *h*. Calculations are performed with the software package MatLab that possesses the function for calculating eigenvalues and eigenvectors. The lowest frequencies are always of the utmost interest for analysis. The table below (table 1) shows a few initial eigenvalues for the original cantilever beam and the modified one, where the height, as a construction variable, is increased by 10%.

Fig. 3 displays the diagram of potential, E_p, and kinetic, E_k, energy distributions, and their mutual difference, $E_p - E_k$, original cantilever beams for all elements in a row, for the first oscillation mode, where the first eigenfrequency is f_{01} = 41.51Hz, and the first eigenvalue is λ_1=68010.88 s^{-2}.
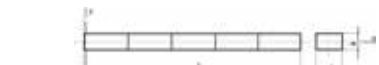
Fig. 1 Original cantilever beam
ρ=7833kg/m^3, E=206840000000 N/m^2;
b=0.1m, h=0.05m, l=1m
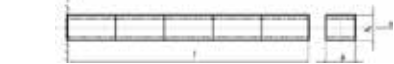
Fig. 2 Arbitrarily modified cantilever beam
b_1=b, h_1=1.1h

Fig. 6 Modified cantilever beam after the first iterative step
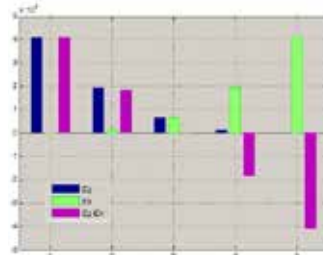
Fig. 3 Diagram of potential and kinetic energy distributions and their mutual difference for the original cantilever beam [J].

Fig. 4 Diagram of potential and kinetic energy growth rate distributions and their mutual difference for modified and original cantilever beam [J].
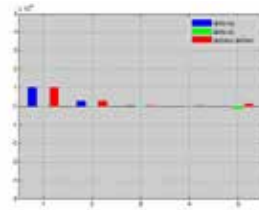
Fig. 5 Diagram of potential and kinetic energy growth rate distributions and their mutual difference for the modified cantilever beam after the first iterative step (Fig. 4.5), and the original cantilever beam [J].

Fig. 4 shows a digram of potential, ΔE_p, and kinetic, ΔE_k, energy growth rates and their difference ΔE_p - ΔE_k for the increased height across the entire beam length, by 10 %, for the first oscillation mode. The first frequency of a modified cantilever beam is f'$_{01}$ = 45.66Hz, while the first eigenvalue is λ'$_1$=82293.17s^{-2}. It is noticeable that the first eigenvalue growth rate is $\Delta\lambda_1$ = +21 %, and the corresponding eigenfrequency growth rate is Δf$_{01}$ = f'$_{01}$ - f$_{01}$ = +10 %

Fig. 5 displays a diagram of potential, ΔE_p, and kinetic, ΔE_k, energy growth rates and their difference ΔE_p - ΔE_k for the modified cantilever beam after the first iterative step (Fig. 6) for the first oscillation mode. The aim of modification is to increase the frequency by 10 %. Note the convergence compared to the previous diagram, which is evidenced by reduced 'columns' characterizing the change in potential and kinetic energy growth rates. Also, a significant conclusion related to the cantilever beam cross-section modification is that stiffness, i.e. cross-section height, should be increased in the fixed-point zone, while the beam's free end should be loosened, i.e. mass should be decreased in that zone.

Based on distribution of difference ΔE_p - ΔE_k between growth rates E_p and E_k individually per element (Fig. 4), the shape of the optimized cantilever beam is obtained (Fig. 7). It is possible to arrive at desired changes, respectively, per element of a cantilever beam in the way as follows. First, the values of differences ΔE_p - ΔE_k per element are arranged in the table below:

$$\alpha_j = \left(1+\psi_j\right)^3 - 1, \quad \beta_j = \psi_j, \quad \psi_j = \frac{\Delta h_j}{h};$$

After substituting data individually for each finite element, there follows $\Delta\lambda_1$ = 15165.96.

When this value and the first eigenvalue of the initial beam are summed, it follows that: $\lambda_{1,\text{rean}}$ = 15165.96+ 68010.88= 83176.84, a $f_{1,\text{rean}}$ = 45.90 Hz

Comparing these results with those presented in Tab. 1, after eigenvalues were obtained by applying the MatLab software program (45.82), it can be concluded that there is a remarkable coincidence.

3.2. UNCERATINITY QUANTIFICATION AND SIMULATION

3.2.1 Stochastic input

Further research included the execution of simulations *Ek, Ep*, growth rates *Ek* and *Ep*, differences in growth rates, first frequency in a cantilever beam and a modified beam for 1000 values of Young's modulus of elasticity according to the Gaussian distribution.

On the basis of simulation, the following results were obtained, as presented in the figures (Fig.7-11). The figures show the diagrams of distribution *Ek*, Ep, growth rates *Ek* and *Ep*, and differences in growth rates for each element separately.

The biggest difference in potential and kinetic energy growth rates was registered in the first finite element (nearest to the fixed point). In other finite elements the differences in kinetic and potential energy growth rates are decreased respectively, however on the very free end the values of kinetic energy are dominant, so that the difference in growth rate is negative. It is noticeable that the first element is the most sensitive to any change because the growth rate difference declines or rises very fast. The elements located in the middle of the beam length are almost non-sensitive, which means they are not suitable for the reanalysis. In order to increase eigenfrequencies, the free-end element is sensitive, but it is needed to decrease its kinetic energy, which can be achieved by decreasing its mass (reduction of height).

Fig.7-11. Diagrams of distribution Ek, Ep, growth rates Ek and Ep, and differences in growth rates per element

Element 1	
Element 2	
Element 3	
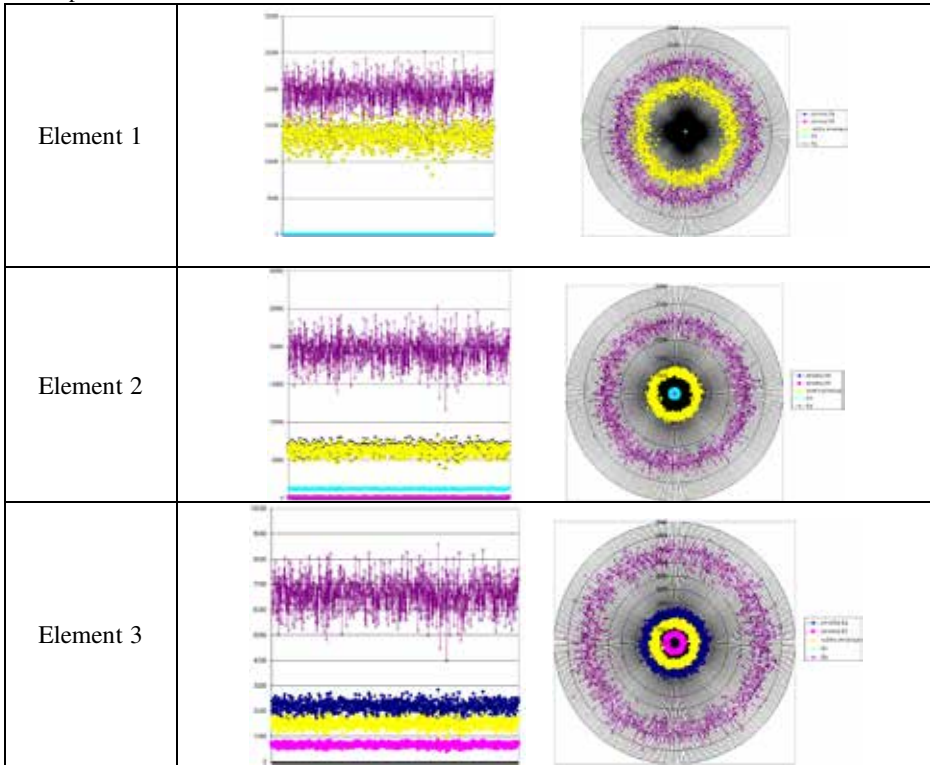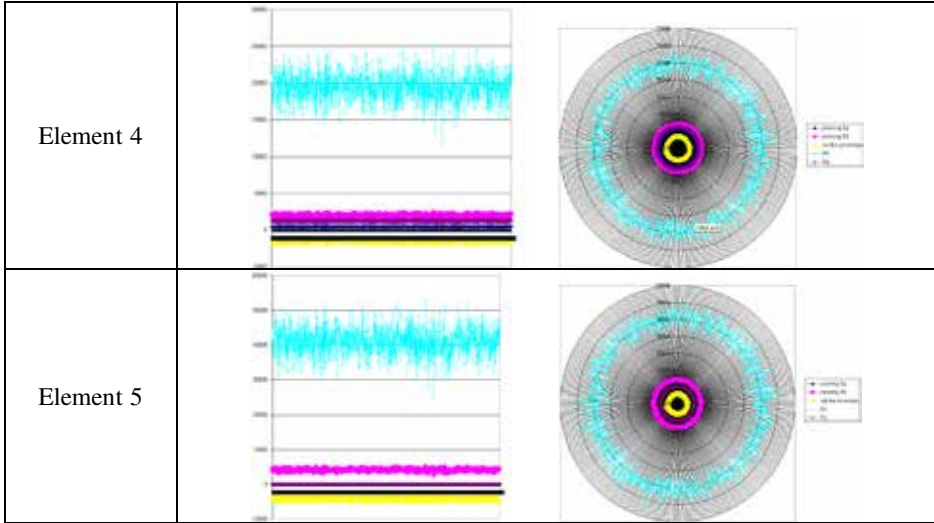
Element 4		
Element 5		

The figure below (Fig. 12) displays distributions of differences in potential and kinetic energy growth rates on the beam for all five finite elements and for 1000 simulation results.
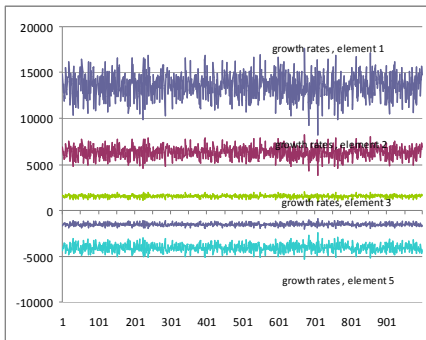
Fig. 12. Difference in potential and kinetic energy growth rates for five finite elements for 1000 simulation results for the cantilever beam
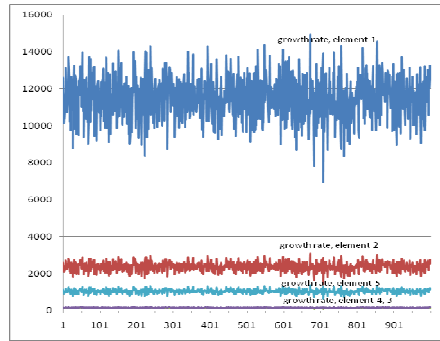
Fig. 13. Difference in potential and kinetic energy growth rates for five finite elements, for 1000 simulation results, for the optimized beam

The figure 13 shows the distributions of differences in potential and kinetic energy growth rates on the optimized beam (Fig. 13), for all five finite elements and for 1000 simulation results.

399

4.2.3 Comparison of frequency sensitivity between original and modified cantilever beams

Further analysis explored the dependence between the first frequency and Ek and Ep in each element of the original beam and the modified one.

The largest change in kinetic energy was found with respect to the change in the first frequency of the fifth element, and the largest change in potential energy was found with respect to the change in the first frequency of the first element, which is in agreement with the deterministic theory. Identical regularities were established for both the original and the modified beam, however with different values.

4.2.4 Uncertainty in cantilever beam redesign calculations and frequency calculations

Table 2 shows the simulation results for the original beam frequency (frequency) and the modified beam frequency (frequency 1) for different values of Young's modulus of elasticity. Frequency growth rate was calculated as a difference between the modified beam frequency and the original beam frequency.

Tab. 2 The simulation results for the original beam frequency (frequency) and the modified beam frequency (frequency 1) for different values of Young's modulus of elasticity

No	Young's modulus	Frequency	Frequency 1	Frequency growth	Frequency rounded growth rate
1	216008194057,00	43,52331847	47,87565032	4,352331847	4,4
2	221020777903,00	40,47158724	44,51874596	4,047158724	4
3	209951519584,00	41,8644712	46,05091832	4,18644712	4,2
4	213280508641,00	38,98414442	42,88255887	3,898414442	3,9
5	204137145899,00	39,82625243	43,80887767	3,982625243	4
6	218644848354,00	39,47510831	43,42261914	3,947510831	3,9
…					
1000		43,37335183	47,71068701	4,337335183	4,3

A set of 1000 results obtained by the normal distribution (program $\mathbf{R}^2$) was used for further analysis where the Laplace criterion was applied to determine the uncertainty.

The Laplace criterion assumes equal probability for certain states to take place, so that probability represents

$$v\left(s_{ij}\right) = \frac{1}{m}$$

where m is the number of likely states (1000 in this case). Therefore the expected value is:

---

[2] $\mathbf{R}$ is a free software programming language and a software environment for statistical computing and graphics. The R language is widely used among statisticians and data miners for developing statistical software and data analysis. Polls and surveys of data miners are showing R's popularity has increased substantially in recent years.

$$\overline{p_i} = \sum_{j=1}^{m} p_{ij} * v\left(s_{ij}\right) = \frac{1}{m}\sum_{j=1}^{m} p_{ij}$$

In Table 3 a division into the confidence intervals was performed and frequency of the observed quantities occurrence was calculated. The result for the occurrence of the oscillation frequency rounded growth rate indicates normal distribution.

Table 3. Confidence intervals

Frequency rounded growth rate	3,2	3,4	3,5	3,6	3,7	3,8	3,9	4	4,1	4,2	4,3	4,4	4,5	4,6	4,7
Frequency of occurrence	1	1	2	5	18	49	80	135	180	206	163	104	35	19	2

Fig. 14 shows normal distribution of the probability of the frequency of occurrence of eigenfrequencies growth rate difference. It is evident from the diagram that the highest probability of the occurrence of eigenfrequencies growth rate difference is 4.2, with the occurrence probability of 20.6%.
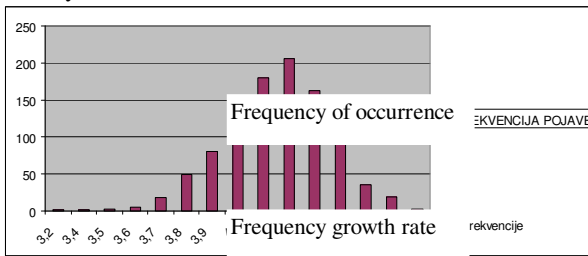
Fig 14 Normal distribution of occurrence probability of frequencies growth rate difference

By transforming the frequencies of occurrence of eigenvalues growth rate difference according to the Laplace criterion, we will obtain normal distribution of the occurrence probability, i.e. the degrees of uncertainty of the occurrence of eigenfrequencies growth rate difference.

Tab. 4. Occurrence probability (%)

Frequency growth rate	3,2	3,4	3,5	3,6	3,7	3,8	3,9	4	4,1	4,2	4,3	4,4	4,5	4,6	4,7
Occurrence probability (%)	0,10	0,10	0,20	0,50	1,80	4,90	8,00	13,50	18,00	20,60	16,30	10,40	3,50	1,90	0,20

The above text gives the probability of eigenfrequencies differences distribution in the original and the modified beam. Given that the normal distribution of eigenfrequencies growth rate difference was obtained, it is interesting to take a look at the probability distribution of eigenfrequencies in the original and the modified beam.

5. CONCLUDING REMARKS

Studying the dynamic behavior of a construction can predict its response to change in shape, changes in size of its elements or change in materials used. Generally, the aim of

system modification with respect to improvements in dynamic behavior is to increase eigenfrequencies and widen the distance between two neighboring frequencies. The specific importance lies in lowest frequencies and those close to the system exciting frequencies.

Developed procedure for dynamic modification represents the essence of methodology for improving the dynamic behavior of a construction. Originality of this methodology is that in analyzing the dynamic behavior of construction it uses the distribution of kinetic and potential energy in main oscillation modes. On the basis of analyzing the percentages of distributions for kinetic and potential energy in main oscillation modes, a rough estimate for adequacy is obtainable across zones and construction subgroups. This is especially important for complex structures. When groups suitable for reanalysis are located, a detailed (fine) analysis of a separated subgroup is undertaken. Most often it is necessary to make a modified model which is used for comparison to the original one, and on the basis of thus derived reanalysis formula, new guidelines are reached. There are clear, mathematically expressed, unambiguous guidelines for further conducting the modification procedure – which is described in the algorithm, and there are segments where the form of modification is not clearly seen. Then, on the basis of the analysis of sensitivity to certain changes, a clearer image of further steps is obtained. Based on these cases an algorithm for reanalysis is derived and its essence is in the following. If it is necessary to improve the dynamic behavior of a construction, most often to avoid the resonance with exciting dynamic loads, it is necessary to create the initial finite element model of a given construction and perform the basic calculation of dynamical properties in order to obtain the basic frequencies and main oscillation modes. Kinetic and potential energy of the entire construction can be represented as an algebraic sum of the energies of all elements, which is also given here. In order to conduct a rough analysis, the distributions of kinetic and potential energy for construction subgroups in *r*-th main oscillation mode can be expressed in the values of percentages. Therefore, on the basis of analyzing the energy distributions in the main oscillation modes of the main construction elements, it is possible to depict the following cases, on the basis of which it is possible to derive the algorithm for reanalysis of similar structures. Following are the characteristic areas:

I   Elements in which the kinetic and potential energies (and the difference in their increase) are negligible with respect to other elements.

II   Elements in which the kinetic energy is dominant compared to potential energy

III   Elements in which the potential energy is dominant compared to kinetic energy

IV   Elements in which the potential and kinetic energy exist and are not negligible in comparison with other elements

A great number of examples illustrate the cases mentioned. Also, a great number of empirical correlations are given for certain changes that may lead to desired improvement of dynamic behavior of the construction.

The application of developed procedure on real structures illustrated its practical aspects. The procedure developed in this paper can be classified as iterative and having great reliability for fast convergence. The convergence of modification procedure assumes relatively fast achievement of proposed goals. Most often, the proposed goals are: elevation of eigenfrequencies and increase of distance between two neighboring

frequencies. Special importance lies in the lowest frequencies and those whose values are close to excitation frequencies of the system.

Assuming that Young's modulus of elasticity has normal distribution for 1000 simulation results, it is obtained that the frequency of free oscillations also has normal distribution in both the initial cantilever beam and modified beam and optimized beam. The results indicate that the behavior of the frequency of oscillations distribution correlates with the frequency of distribution of Young's modulus of elasticity and that the dependency exits irrespective of the cantilever beam design and shape respectively.

Comparison of differences in potential and kinetic energy growth rates in the beam and optimized cantilever beam indicated differences in finite elements sensitivity, whereby the segments for reanalysis were identified.

Middle-zone elements are unsuitable for reanalysis, while fixed-point and end-zone ones are suitable. The element in the fixed-point end is the most critical from a number of viewpoints. Dynamically, it is only by increased stiffness of the element that better effects are achievable.

The analysis of uncertainty in the original, modified and optimized beams established for all three cases normal probability distribution in the rate of frequency occurrence. Difference was found in the interval of frequency normal distribution in the original cantilever beam compared to the distribution interval in modified and optimized beams. A broader confidence interval in modified and optimized beams indicates adverse effects of non-ideal material on the procedure of dynamic modification.

A versatile procedure for conducting reanalysis studies in the presence of uncertainty has been developed by combining Monte Carlo simulation tools with finite element modeling modules.

References

[1]   Allaboudi, E., Maneski, T., Trisovic, N., Ergić, T., „Improving Structure Dynamic Behaviour Using a Reanalysis Procedures Technique", Journal: Technical Gazette vol.20, no.2, str. 297 - 304 , April, 2013, ISSN 1330-3651.

[2]   Canfield, R.A., *High-Quality Approximation of Eigenvalues in Structural Optimization*, AIAA Journal, Vol. 28, No. 6, 1990, pp. 1116-1122.

[3]   Dragojlovic P., Misita M., Milanovic D.D., Tadic D., Kirin S., Risk management and multicriteria optimization of production program, Revista Metalurgia International, 2012, Vol. 17, No. 6, pp. 35-39. ISSN 1582-2214

[4]   Ki, I.K., *Nonlinear Inverse Perturbation Method in Dynamic Redisgn,* PhD, Thessis, Michigen University, USA, 1983.

[5]   Kirsch U, Liu S. Structural reanalysis for general layout modifications. AIAA J 1997;35:382–8.

[6]   Lecomte, C., Exact statistics of szstem with uncertainties: Am analytical theory of rank-one stohastics dynamics systems, Journal of Sound and Vibration 332 (2013), 2750-2776.

[7]   Lin YK. Probabilistic thoery of strcutural dynamics. NY, USA: McGraw-Hill Inc; 1967.

[8]   Maneski T., KOMIPS software, Monograph computer modeling and structures calculation, Faculty   of Mechanical Engineering, University of Belgrade, 1998 [ISBN 86-7083-319-0].

[9]   Mateus, H.C., Mota Soares, C.M., and Mota Soares, C.A., *Sensitivity Analysis and Optimal Design of Thin Laminated Composite Structures*, Computers and Structures, Vol. 41, No. 3, 1991, pp. 501-508.

[10]   Milanović D.D., Misita M, Decision support and management support systems, FME, Belgrade, 2008. ISBN 978-86-7083-642-6.

[11]   Nair, B.P., Keane, A.J., and Langley, R.S., *Improved First-Order Approximation of Eigenvalues and Eigenvectors,* AIAA Journal, Vol. 36, No. 9, September 1998, pp. 1722-1727.

[12]   Pascual, B. Adhikari S., Combined parametric–nonparametric uncertainty quantification using random matrix theory and polynomial chaos expansion, Computers and Structures 112–113 (2012) 364–379.

[13]   Pierfrancesco Cacciola, Nicola Impollonia, Giuseppe Muscolino, A dynamic reanalysis technique for general structural modifications under deterministic or stochastic input, Computers and Structures 83 (2005) pp. 1076–1085.

[14]   Rao, S.S., and Reddy, C.P., *Optimum Design of Stiffened Conical Shells with Natural Frequency Constraints*, Computers and Structures, Vol. 14, Nos.1-2, 1981, pp 103-110. Conference, 2001.

[15]   Rao, S.S., and Reddy, C.P., *Optimum Design of Stiffened Cylindrical Shells with Natural Frequency Constraints*, Computers and Structures, Vol. 12, Aug. 1980, pp 211-219.

[16]   Rao, V.R., Iyengar, N.G.R., and Rao, S.S., *Optimization of Wing Structures to Satisfy Strength and Frequency Requirements*, Computers and Structures, Vol. 10, No. 4, 1979, pp. 669-674.

[17]   Sedaghati, R., Suleman, A., and Tabarrok, B., *Structural Optimization with Frequency Constraints Using the Finite Element Force Method*, AIAA Journal, Vol. 40, No. 2, 2002, pp. 382-388.

[18]   Sergeyev, O., and Mroz., Z., *Sensitivity Analysis and Optimal Design of 3D Frame Structures for Stress and Frequency Constraints, Computers and Structures*, Vol. 75, No. 2, 2000. pp. 167-185

[19]   Stanojevic Petar Orlic Branislav Misita Mirjana Z Tatalovic Nada Lenkey Gyoengyver Online monitoring and assessment of emerging risk in conventional industrial plants: possible way to implement integrated risk management approach and KPI's (Article J, JOURNAL OF RISK RESEARCH, (2013), vol. 16 br. 3-4, str. 501-512)

[20]   Tadic D., Djapan M., Misita M., Stefanovic M., Milanovic D.D. A Fuzzy Model for Assessing Risk of Occupational Safety in Processing Industry, The International Journal of Occupational Safety and Ergonomics, 2012, Vol.18, No.2, 115-126.

[21]   Tadic D., Milanovic D.D, Misita M., Tadic B., A new integrated approach to the problem of ranking and supplier selection under uncertainties, Proceedings of the Institution of Mechanical Engineers, Part B, Journal of Engineering Manufacture, London, UK, 2011. Vol. 225, No. B9, oo. 1713-1724, ISSN 0954-4089.

[22]   Thomson, W.T., *Theory of Vibration with Applications*, Prentice-Hall, Inc., Englewood Cliffs, New Jersey, 1972.

[23]   Tong, W.H., Jiang, J.S., and Liu, G.R., *Solution Existence of the Optimization Problem of Truss Structure with Frequency Constraints*, Int. Journal oj Solids and Structures, Vpol. 37., No. 30, 2000, pp. 4043-4060

[24]   Tong, W.H., and Liu, G.R., *An Optimization Procedure for Truss Structure with Discrete Design Variables and Dynamic Constraints*, Computers and Structures, Vol. 79, No. 2, 2001, pp. 155-162

[25]   Trišović, N., Maneski, T., Kozak, D. „Developed procedure for dynamic reanalysis of structures", Strojarstvo - Journal for Theory and Application in Mechanical Engineering, Vol. 52, Number. 2, pp: 147-158, 2010; ISSN 0562-1887.

[26]   Trisovic, R., N., Modification of the Dynamics Characteristics in the Structural Dynamic Reanalysis, PhD, Thessis, University of Belgrade, Serbia, 2007

[27]   Voormeeren S.N., Klerk d., Rixen D.J., Uncertainty quantification in experimental frequency based substructuring, Mechanical Systems and Signal Processing 24 (2010) pp. 106–118.

[28]   Wang, B.P., and Pilkey, W. D., *Eigenvalue Reanalysis of Locally Modified Structures Using a Generalized Rayleigh's Method*, AIAA Journal, Vol. 24, No.6, 1986, pp. 983-990.

[29]   Wang, D., Zhang, W.H., and Jiang, J.S., *Truss Optimization on Shape and Sizing with frequency Constraints*, AIAA Journal, Vol. 42, No. 3, 2004, pp. 622-630.

[30]   Yoon, B.G. and Belegundu, A.D., *Iterative Methods for Design Sensitivity Analysis*, AIAA Journal, 26, November 1988., pp. 1413-1417.

DYNAMIC MODEL OF BUCKET WHEEL EXCAVATOR MAIN SUBSYSTEMS

Z. Golubović[1], Z. Lekić[1], S. Makragić[1]

[1] Faculty of Technical Sciences
The University of Pristina, Knjaza Milosa bb, 38220, Kosovska Mitrovica
e-mail: zoran.golubovic@pr.ac.rs, zlatibor.lekic@pr.ac.rs, slobodan.makragic@pr.ac.rs

In this paper, dynamics models of bucket wheel excavator (BWE) superstructure in the vertical plane, the boom hoisting drive system and bucket wheel drive system describes in a mathematical model or single program. This model allows to evaluate the effects of structural changes in one subsystem to its dynamic behavior as well as a dynamic behavior of the other subsystems on the BWE. Mathematical model solving provides the basic mechanical characteristics that define the dynamic behavior of a BWE in the process of digging. The obtained moments, angular velocity, displacement and force time functions are graphically represented. Results analysis of BWE dynamic calculations indicates that the appropriate reconstruction must be made to improve such a negative dynamic behavior in the process of digging.

Keywords: *bucket-wheel excavator, dynamic model, mathematical model, digging.*

1. Introduction

Dynamic model of BWE is represented by dynamic models of its major subsystems that are most loaded in the excavation process. Dynamic models of digging [1,2,3,4], hoisting [5] and superstructure [6] subsystems were examined separately without considering the impact of one subsystem dynamics behavior to another. These three subsystems are in the process of digging exposed load that comes from digging forces[7]. Number of influential parameters whose individual contribution to a very different and mutually conditioned affects on character of digging force. The main parametars are: specific resistance to excavation (SFRE) presented in reference [8] , cutting conture length (kL) , cutting speed. According to researches[9], value of SFRE is greatly influenced by cutting speed, too. From the ather side cutting conture depends on bucket wheel vibration in vertical plane [10,11]. Electric motor torque according to

[4] is described by an exponential function. Moments of inertia, stiffness and damping are calculated according to [12].The results obtained using the dynamic model presented in this paper can be used to identify the optimal retrofit solution [13].

2. Dynamics model of BWE main subsystems

Figure 1 shows the kinematics scheme of the boom hoisting drive system, consisting of: an asynchronous electric motor (EM), mechanical coupling (S), gearbox (R), brakes (K) and drum for rope winding (D). For this work interesting is the case where the balance established between the braking and load torque. Because of the changing nature of the torque load at the catch is only a few teeth of gears coupled. This leads to very rapid wear of the gears tooth flanks, and therefore to a relatively small gear life. Oscillatory system is represented as five rotating mass on a single shaft wedged: J_r - the reduced gearbox moment of inertia on the shaft brake, J_5 - the reduced gear number 5 moment of inertia on the shaft brake, J_6 - the reduced gear number 6 and drum moment of inertia on the shaft brake, J_7 - the reduced boom and bucket wheel moment of inertia on the shaft brake.
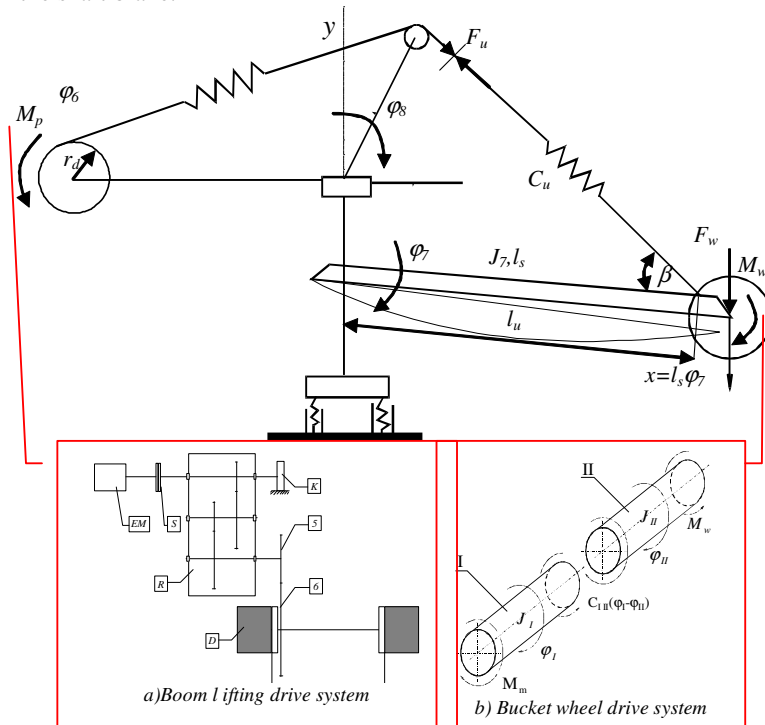
Figure 1. Mechanical model of bucket wheel excavator

Dominant influence of the oscillations of the system has upper supporting structure. According to analysis [6], the upper supporting structure accumulates around 85%, portal sheet 10%, suspension system about 3% while all other substructure (boom, the drive bucket wheel system and lower supporting structure) accumulated less than 1% of the system potential energy in its oscillations. Those facts suggests that, in the analysis of the systems low-frequency oscillations, the deformability of the lower support structure, boom and bucket wheel drive system can be ignored.

For the mechanical model shown in Figure 1, we write the system of differential equations for the boom hoisting drive system motion [5]:

$$J_k \cdot \ddot{\varphi}_k + c_{kr}\left(\varphi_r - \varphi_k\right) + d_{kr}\left(\dot{\varphi}_r - \dot{\varphi}_k\right) = M_k$$
$$J_r \cdot \ddot{\varphi}_r + c_{r5}(\varphi_5 - \varphi_r) + d_{r5}(\dot{\varphi}_5 - \dot{\varphi}_r) - c_{kr}(\varphi_r - \varphi_k) - d_{kr}(\dot{\varphi}_r - \dot{\varphi}_k) = 0$$
$$J_5 \cdot \ddot{\varphi}_5 + c_{56}(\varphi_6 - \varphi_5) + d_{56}(\dot{\varphi}_6 - \dot{\varphi}_5) - c_{r5}(\varphi_5 - \varphi_r) - d_{r5}(\dot{\varphi}_5 - \dot{\varphi}_r) = 0 \qquad (1)$$
$$J_6 \cdot \ddot{\varphi}_6 + F_u\, r_d - c_{56}(\varphi_6 - \varphi_5) - d_{56}(\dot{\varphi}_6 - \dot{\varphi}_5) = 0$$

Boom oscillations can be described by equation:

$$J_7 \cdot \ddot{\varphi}_7 - F_u\, l_u \sin\beta = -(l_s + r_t)F_w \qquad (2)$$

Force in the rope (F_u) can be determined as the product of stiffness and rope elongation:

$$F_u = c_u\left(\frac{l_u \varphi_7}{\sin\beta} - r_d i_k \varphi_6\right) \qquad (3)$$

Where is: $\varphi_k, \varphi_r, \varphi_5, \varphi_6, \varphi_7\,[rad]$ - absolute angles of rotation reduced on the shaft brake, $M_K\,[KNm]$ - braking torque, $c_i\,[Nm/rad]\,(i = k, r, 5, 6, 7)$ - reduced stiffness on the shaft brake, $d_i\,[Nm/rad^2]\,(i = k, r, 5, 6, 7)$ - dumping reduced on the shaft brake, c_u, d_u - rope stiffness and dumping; $F_u\,[KN]$ - Force in the rope reduced on the shaft brake, $l_s\,[m]$ - boom length, $x\,[m] = l_s \cdot \varphi_7$ - vertical movement of bucket wheel, $r_d\,[m]$ - radius of the drum, $r_t\,[m]$ - bucket wheel radius, $l_u\,[m]$ - distance from the boom rotation axis and rope hanging point. $F_w = 1,1\cdot Ft\,[KN]$ -digging force(tangential force increased by 10% due to other resistance).

Oscillatory system of bucket wheel drive system [2] is represented as two rotating mass J_I - Electric motor moment of inertia, J_{II} - Bucket wheel and bucket wheel drive system gearbox moment of inertia.

Differential equations for the bucket wheel drive system motion [5]:

$$J_I \cdot \ddot{\varphi}_I + C_{I\,II}\left(\varphi_I - \varphi_{II}\right) = M_m$$
$$J_{II} \cdot \ddot{\varphi}_{II} - C_{I\,II}\left(\varphi_I - \varphi_{II}\right) = -M_w \qquad (4)$$

where is: $\varphi_I, \varphi_{II}\,[rad]$ - absolute angles of rotation reduced on the electric motor shaft, $M_m\,[KNm]$ - electric motor torque, $M_w\,[KNm]$ - load torque reduced on the electric motor shaft.

Electric motor torque according to [4] is described by an exponential function and thair graphic interpretation is given on figure 2.

$$M_m = \sum_{j=1}^{9} C(j) \cdot e^{-\lambda(j) \cdot \omega_m} \tag{5}$$

where is: C(j) – interpolation coefficient, $\lambda(j)$ - interpolation coefficient, ω_M - angular velocity of the electric motor shaft.
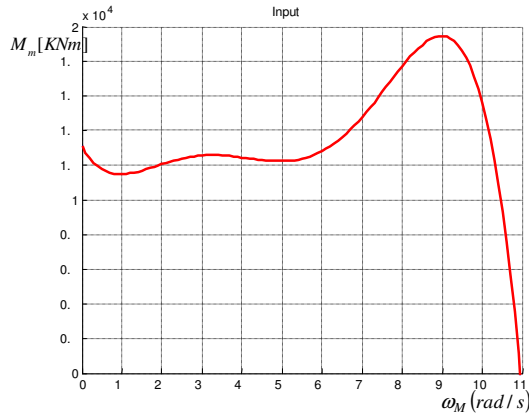

Figure 2. Electric motor torque (P=900 KW)

Tangential component of a load force, which presents 90% of total load of bucket wheel drive system, according [7] is given by the following equation:

$$Ft(\psi) = k_L \cdot L_{sr} f(\psi) \tag{6}$$

Where is:

$$f(\psi) = \begin{cases} \sin\psi & za\ 0 \le \psi \le \pi/2 \\ (\alpha - \psi)/(\alpha - \pi/2) & za\ \pi/2 \le \psi \le \alpha \\ 0 & za\ \psi > \alpha \end{cases}$$ - Function of tangential component

changes, $k_L = random[K_L]$ - Randomly selected value from a range of specific resistance measured, values L_{sr} - Length of a bucket cutting contours.

According to experimentally obtained the values of SFRE [K_L] in the Kosovo coal basin for gray compact clay excavation [14] tangencial component of load force is presented graphically in figure 3.

Torque load of bucket wheel drive system cab be calculated according to equation:

$$M_w = F_w \cdot \frac{d_t}{2} \tag{7}$$

where is: d_t - diameter of bucket wheel. Solving systems of differential equations (1), (2), (4) using the Runge-Kutta methods in Matlab software package Simulink Modul (fig. 4) obtained the results that will be graphically represented.
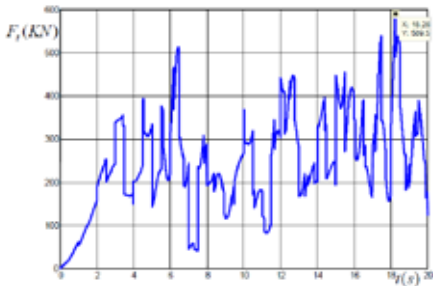
Figure 3. Tangencial component of digging
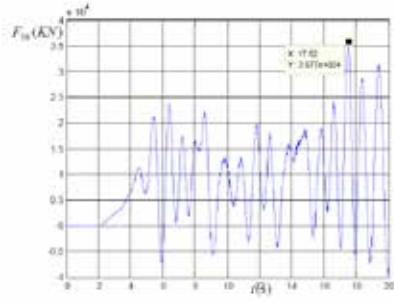
Figure 5. Load force at the last pair of toothed gears (hoisting subsystem)
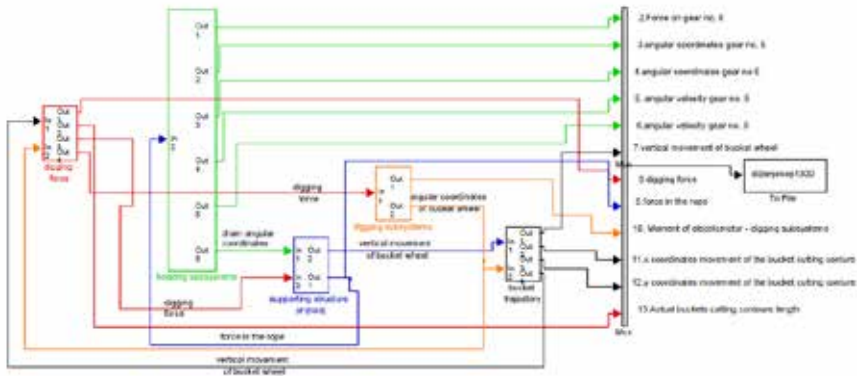
Figure 4. Simulink model of BWE dynamics model

Figure 5 graphically presented the load force at the last pair of toothed gears. Dynamic load on the bucket wheel in excavation process, despite the elasticity of the rope has a decisive influence on the vibrations of boom hoisting drive system.

Angular velocity oscillations of large amplitude at the last pair of toothed gears, where are in the process of digging in conjunction only two possibly three gear tooth, resulting in rapid wear of the teeth. From the figure 6 and figure 7 it can clearly be seen that the coupled gears 5 and 6, with a stiff shaft motors, much moved. This process leads to wear on their hips, so they lose their involute shape. In addition, as the latest gears pair is outside the gearbox housing, weather conditions affect the removal of grease from their contact surfaces. That enhances their wear. High-frequency oscillations are particular expressed in gear no.5.

Time function of electric motor (Fig. 9) and bucket wheel angular velocity (Fig. 10) shows that the coupling elements of the gear have very little influence on the reduction of vibration caused by the stochastic load on the bucket wheel. A large gear which is connected with shaft to a bucket wheel has the largest angular velocity oscilations, so it can be concluded that the impact loads on its tangent is greatest.

The oscilation of electric motor torque (Fig. 8), after starting period which is not the subject of this analysis, is consistent with the load torque oscillations (Fig. 3). It speaks of gear and coupling small absorption capacity.
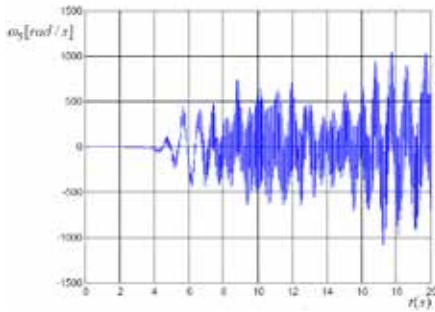
Figure 6. Angular velocity of gear no.5
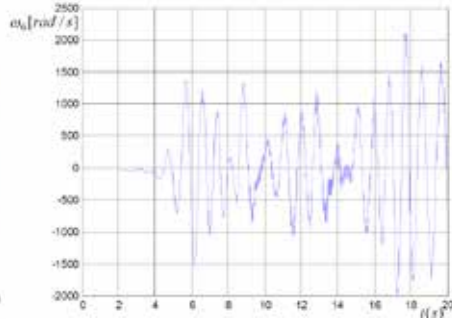
Figure 7. Angular velocity of gear no.6

Oscillations amplitude $\omega_6[rad/s]$ greatly exceeds the nominal value of the electric motor torque, which shows that he is constantly overloaded and under the influence of heavy loads.
The difference of electric motor shaft and gearbox input shaft angular speed that reaches up to 10 $[rad/s]$ shows that the coupling which establishes a connection between gear units and motors exposed to high torque twisting.
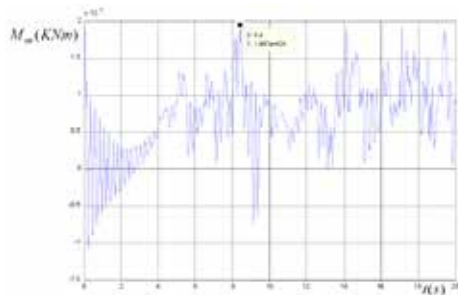
Figure 8. Electric motor torque
(bucket wheel drive system)
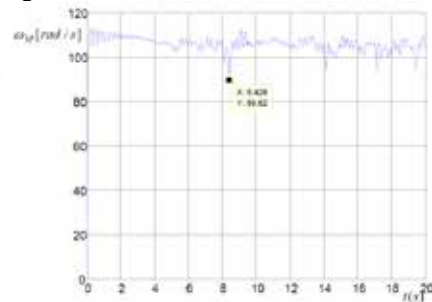
Figure 9. Angular velocity of electric motor shaft
(bucket wheel drive system)

4. **Conclusion**

Results analysis of BWE dynamic calculations indicates that the appropriate reconstruction must be made to improve such a negative dynamic behavior in the process of digging. As done in the module SIMULINK of software package MATLAB (Fig. 4) program provides easily changes of some or all program sub-elements and quickly obtain the results. That is an opportunity to examine the effect of individual subsystem reconstruction on BWE dynamic behavior in process of digging .
Reconstruction may involve the following intelligent retrofit solutions:

- additional holding brake system independent of the boom hoisting drive system to reduced vertical movement of bucket wheel,

- coupling and gearbox replacing in digging drive subsystem to reduced the oscillations amplitude and frequence of bucket wheel drive system, design changes of bucket wheel construction to reduced displacement under load
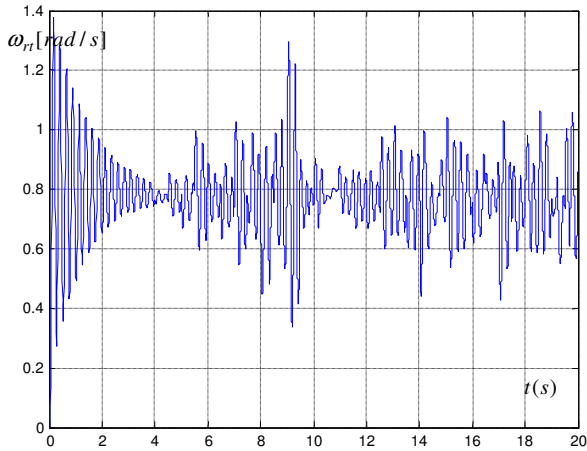

Figure 10. Angular velocity of bucket wheel

.

5. References

[1] V. Jevtić, Z. Golubović., Z. Lekić. (1996): Mathematical modeling of resistance moment as the basic component for the dynamic behavior of the BWE, *XIV international conference on material handling and handling and warehousing*, Belgrade.

[2] V. Jevtić, Z. Golubović., Z. Lekić, S. Makragić: The analysis of dynamic processes in the BWE working wheel drive system with a hydrodynamic coupling, *6th Sever symposium on mechanical gears*, Subotica(1997). pp. 179-185

[3] Z. Golubović, V. Jevtić, Z. Lekić (1997): Dynamic behavior of planetary gear in BWE drive systems , *Yugoslav Congress of Theoretical and Applied Mechanics 97 XXII*, Vrnjačka Banja, 2-7 jun.

[4] Z. Golubović (2009): Contribution of drive system reconstruction feasibility for middle class BWE, *master's thesis*, Kosovska Mitrovica.

[5] V. Jevtić (1979)   Theoretical and experimental studies of flow stresses in hoisting subsystem structural elements, *master's thesis*, Niš-Bohum.

[6] Volkov, D.P , Čerkasov V.A. – Dynamics and strength of excavators, translated from the Russian, *Department of Mining Institute for Informatics and Economics* , Beograd, 1989.

[7] K. Hitzschke (1984) Experimentelle Analyse der Belastung des Schaufelrades durch den Grabvorgang, *Hebeyeuge u. Fördermittel*, H.9

[8] V. Raaz (1999) Assessment of the Digging Force and Optimum Selection of the Mechanical and Operational Parameters of Bucket Wheel Excavators for Mining of Overburden, *Coal and Partings, Krupp Fordertechnik*, Esen.

[9] N. G. Dombrovski, (1972) Multi –bucket excavators: theory, construction, calculation, (In Russian), *Mashinostroenie*.

[10] S. Bošnjak, N. Zrnić, Z. Petković, (2006) Bucket wheel excavators and trenchers - Computer added calculation of loads caused by resistance to excavation. *Machine Design*, University of Novi Sad, pp.121-128.

[11] S. Bošnjak, N. Zrnić, D. Oguamanam, (2006) On the dynamic modeling of bucket wheel excavators, *FME Transactions 34*, pp 221-226.

[12] V. Batinić, (2008) Determination of gear mesh stiffness in planetary gearing, *Military Technical Courier, vol. 56*, no. 2, pp. 227-236.

[13] M. Gnilke (2006) Intelligent retrofit solutions for bucket wheel excavators, *MAN TAKRAF Fördertechnik GmbH*, Lauchhammer

[14] D. Ljamić, M Arsić, B. Ćirković, (1995) Experimental analysis of BWE SchRs 650/5x24 bucket wheel load, *Mining Machinery - scientific Meeting*, Beograd

FORCED OSCILLATIONS OF A MEMBRANE ON NONLINEAR ELASTIC FOUNDATION

Nikola Nešić [1]

[1] Mathematical Institute SANU, Department of Mechanics,
11 000-Belgrade, Kneza Mihaila 36/III, Serbia,
e-mail: nnesic@gmail.com

Abstract. In this research, forced transversal oscillations of a rectangular membrane on nonlinear elastic foundation are considered, and for special case an analytical approximations of the solutions are given. Based on numerical experiment specific visualizations of the asymptotic approximation of amplitude-frequency and phase frequency curves which correspond to the asymptotic approximation of solutions are conducted, which describes qualitative properties of one frequency nonlinear oscillation stationary and no stationary regimes.

1. INTRODUCTION

Membranes as a structural elements have application in many fields of industry and science. Some examples are microfiltration systems in biological, medical, food, dairy and beverage products industry. Besides that, they also have application in, aerospace, civil and mechanical engineering [1, 2]. To analyze oscillations of membrane systems is important from both, theoretical and practical point of view. Rašković [3] gave brief study of linear analysis of dynamics of structures. Using the mathematical analogy complex membrane systems can be studied similar like plats, beams or belts systems [4]. Nonlinear vibrations as phenomenon that appears in real systems can be studied analytically using the methods that are different from linear analysis. The transverse vibration of rectangular and circular plates connected with an elastic and visco-elastic layer has been studied [4-11] for linear as well for non-linear dynamics. In the linear analysis of coupled systems multi-frequency regimes of time functions appears corresponding to one eigen amplitude function of one mode, and also that time functions of different vibrations modes are uncoupled.

In this research, forced transversal oscillations of a rectangular membrane on nonlinear elastic foundation are considered, and for special case an analytical approximations of the solutions are given. To be able to deal with forced oscillation problem in such a structure, the dynamic behavior of the structure for the free vibrations

of the system needs to be understood well. Then it is necessary to develop an accurate structural model that would describe such a system. The obtained structural model consists of nonlinear partial differential equation. The equation is separated to time and shape functions by using the classical Bernoulli-Fourier method of separation of variables [3]. Then, asymptotic method is used to obtain analytical solutions of the membrane displacements for the forced nonlinear vibrations of the system.
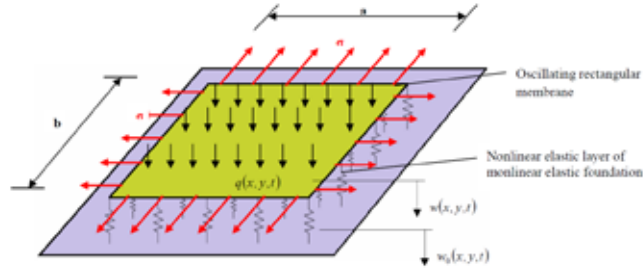

Fig. 1 The physical model of the membrane on the nonlinear elastic foundation loaded by external distributed excitation

2. SOLUTION OF THE NONLINEAR FORCED VIBRATION RECTANGULAR MEMBRANE SYSTEM

In this paper, as a model problem, we consider one rectangular membrane connected with the support via nonlinear elastic layer. The scheme of such a mechanical model is shown on Fig. 1. We are neglecting the thickness of a membrane and assume that membrane is thin with mass density $\rho[kg/m^3]$. The membrane is stretched and fixed along its entire boundaries in xy plane. The tension of membrane per unit length $\sigma_i[N/m]$ is same at all points in all directions and does not change during the motion. We assumed small transverse displacements of the membrane $w(x,y,t)$ and of the support $w_0(x,y,t)$. Also, it is assumed that the mass of the layer between membrane and support is neglected where with $\tilde{c}[N/m]$ we denote constant stiffness coefficient per surface unit area of the elastic layer. Using the D'Alambert principal, the governing partial differential equation for the forced nonlinear membrane vibration is expressed in the following form:

$$\frac{\partial^2 w(x,y,t)}{\partial t^2} = c_0^2 \Delta w(x,y,t) - \frac{c}{\rho}[w(x,y,t)-w_0(x,y,t)] - \frac{\tilde{c}}{\rho}[w(x,y,t)-w_0(x,y,t)]^3 + \frac{q(x,y,t)}{\rho} \quad (1)$$

where $c = \sqrt{\sigma/\rho} \ [m/s]$ is velocity of transverse wave propagation of membrane and $\Delta = \partial^2/\partial x^2 + \partial^2/\partial y^2$ is Laplacian operator. Where for $\varepsilon\beta_i = \beta/\rho_i$ we have that ε is so

called small parameter which is always positive and β is coefficient of the nonlinearity of the elastic layer.

Assuming that displacement of the foundation and external force are given by

$$w_0(x, y, t) = \sum_{m=1}^{M} \sum_{n=1}^{N} w_{0nm} W_{nm}(x, y) \cos \Omega_{nm} t \tag{2}$$

$$\frac{q(x, y, t)}{\rho} = \sum_{m=1}^{M} \sum_{n=1}^{N} h_{0nm} W_{nm}(x, y) \cos(\Omega_{nm} t + \vartheta) \tag{3}$$

we can rewrite eq(1) and apply Bernoulli-Fourier method of separation of variables:

$$w(x, y, t) = W_{nm}(x, y) T_{nm}(t) \tag{4}$$

Then we obtain:

$$W_{nm}(x, y)\ddot{T}_{nm}(t) = c_0^2 \Delta W_{nm}(x, y) T_{nm}(t) - \frac{c}{\rho} \left[W_{nm}(x, y) T_{nm}(t) - w_{0nm} W_{nm}(x, y) \cos \Omega_{nm} t \right] - \tag{5}$$

$$- \frac{\tilde{c}}{\rho} \left[W_{nm}(x, y) T_{nm}(t) - w_{0nm} W_{nm}(x, y) \cos \Omega_{nm} t \right]^3 + h_{0nm} W_{nm}(x, y) \cos(\Omega_{nm} t + \vartheta)$$

Displacement functions can be written in the form:

$$\Delta W_{nm}(x, y) - k_{nm}^2 W_{nm}(x, y) = 0 \tag{6}$$

We can write eq(6) in the form

$$\frac{\Delta W_{nm}(x, y)}{W_{nm}(x, y)} = k_{nm}^2 \tag{7}$$

Solution of Eq.(7) can be assumed in the form

$$W_{nm}(x, y) = \sin \frac{n\pi x}{a} \sin \frac{m\pi y}{b} \tag{8}$$

Multiplying (5) with $W_{sr}(x, y)$ and integrating over the surface A of the membrane:

$$\ddot{T}_{nm}(t) \int_0^a \int_0^b W_{nm}(x, y) W_{sr}(x, y) dx dy = c_0^2 k_{mn}^2 T_{nm}(t) \int_0^a \int_0^b W_{nm}(x, y) W_{sr}(x, y) dx dy -$$

$$- \frac{c}{\rho} \left[T_{nm}(t) - w_{0nm} \cos \Omega_{nm} t \right] \int_0^a \int_0^b W_{nm}(x, y) W_{sr}(x, y) dx dy - \tag{9}$$

$$- \frac{\tilde{c}}{\rho} \left[T_{nm}(t) - w_{0nm} \cos \Omega_{nm} t \right]^3 \int_0^a \int_0^b [W_{nm}(x, y)]^3 W_{sr}(x, y) dx dy +$$

$$+ h_{0nm} \cos(\Omega_{nm} t + \vartheta) \int_0^a \int_0^b W_{nm}(x, y) W_{sr}(x, y) dx dy$$

Using orthogonality condition

$$\int_0^a \int_0^b W_{nm}(x, y) W_{sr}(x, y) dx dy \begin{cases} = 0 \longrightarrow nm \neq sr \\ \neq 0 \longrightarrow nm = sr \end{cases} \tag{10}$$

we can easily calculate this integral in the case when nm=sr, and return this value in (9). Then we obtain expresion for the time function in the following form:

$$\ddot{T}_{nm}(t) \frac{ab}{4} = c_0^2 k_{mn}^2 T_{nm}(t) \frac{ab}{4} - \omega_0^2 \left[T_{nm}(t) - w_{0nm} \cos \Omega_{nm} t \right] \frac{ab}{4} - \tag{11}$$

$$- \tilde{\omega}_{0F}^2 \left[T_{nm}(t) - w_{0nm} \cos \Omega_{nm} t \right]^3 \int_0^a \int_0^b [W_{nm}(x, y)]^4 dx dy + h_{0nm} \cos(\Omega_{nm} t + \vartheta) \frac{ab}{4}$$

with

$$\frac{c}{\rho} = \omega_0^2 \quad \text{and} \quad \frac{\tilde{c}}{\rho} = \tilde{\omega}_{0F}^2 \tag{12}$$

Dividing (11) by

$$\int_0^a \int_0^b [W_{nm}(x,y)]^2 \, dxdy = \frac{ab}{4} \tag{13}$$

and rearranging terms, we obtain

$$\ddot{T}_{nm}(t) + (\omega_0^2 - c_0^2 k_{mn}^2) T_{nm}(t) = \omega_0^2 w_{0nm} \cos\Omega_{nm}t - $$
$$- \tilde{\omega}_{0F}^2 \tilde{g}_{nm} T_{nm}^3(t) - 3\tilde{g}_{nm} T_{nm}^2(t) w_{0nm} \cos\Omega_{nm}t + 3\tilde{g}_{nm} T_{nm}(t) w_{0nm}^2 \cos^2\Omega_{nm}t +$$
$$+ \tilde{g}_{nm} w_{0nm}^3 \cos^3\Omega_{nm}t + h_{0nm} \cos(\Omega_{nm}t + \vartheta) \tag{14}$$

with

$$\tilde{g}_{nm} = \frac{\iint_A [W_{nm}(x,y)]^4 \, dxdy}{\iint_A [W_{nm}(x,y)]^2 \, dxdy} \tag{15}$$

If disturbance of the foundation has small amplitude and introducing analysis of small parameter, (14) can be simplified to:

$$\ddot{T}_{NM}(t) + (\omega_0^2 + c_0^2 k_{NM}^2) T_{NM}(t) = -\tilde{\omega}_{0F}^2 \tilde{g}_{NM} T_{NM}^3(t) + h_{0NM} \sin(\Omega_{NM}t + \vartheta_{NM}) \tag{16}$$

If we consider that excitation is small [12]:

$$h_{0nm} \approx \varepsilon \tilde{h}_{0nm} \quad \text{and} \quad \tilde{\omega}_{0F}^2 = \varepsilon \tilde{\tilde{\omega}}_{0F}^2 \tag{18}$$

where ε is small parameter. Then (16) can be written as

$$\ddot{T}_{NM}(t) + (\omega_0^2 + c_0^2 k_{NM}^2) T_{NM}(t) = -\varepsilon \tilde{\tilde{\omega}}_{0F}^2 \tilde{g}_{NM} T_{NM}^3(t) + \varepsilon \tilde{h}_{0NM} \sin\theta \tag{19}$$

Solution of this equation (19) is assumed in the form

$$T_{NM}(t) = a_{NM}(t) \cos\left(\frac{p}{q}\theta + \varphi\right) \tag{20}$$

In case of main resonant state in first approximation $p = q = 1$.

$$T_{NM}(t) = a_{NM}(t) \cos(\theta_{NM} + \varphi_{NM}) + \varepsilon u_{NM1}(a_{NM}, \theta_{NM}, \Phi_{NM}) + \varepsilon^2 u_{NM2}(a_{NM}, \theta_{NM}, \Phi_{NM}) + ... \tag{21}$$

where $u_{NM1}(a_{NM}, \theta_{NM}, \Phi_{NM})$ do not contain first vibration mode with

$$\Phi_{NM} = \theta_{NM} + \phi_{NM} \tag{22}$$
$$\theta_{NM} = (\Omega_{NM}t + \vartheta_{NM}) \tag{23}$$

We are linearizing nonlinear differential equation by assumption that the frequency of the excitation force is in frequency domain of the main frequency of the coresponding linear system:

$$\frac{d\theta_{NM}}{dt} = \Omega_{NM} \approx \omega_{0NM} = \sqrt{(\omega_0^2 + c_0^2 k_{NM}^2)} \tag{24}$$

Amplitudes and phases of harmonics, $a_{NM}(t)$ and $\Phi_{NM}(t)$ we are determining from the following system of differential equations:

$$\frac{da_{NM}(t)}{dt} = +\varepsilon A_1(a,\phi) + \varepsilon^2 A_2(a,\phi) + ... \tag{25}$$

$$\frac{d\phi_{NM}(t)}{dt} = \omega_{0NM} - \Omega_{NM} + \varepsilon B_1(a,\phi) + \varepsilon^2 B_2(a,\phi) + ... \tag{26}$$

where we are neglacting terms of the higher order, since they are close to zero.
The first asymptotic approximation is:

$$T_{NM}(t) = a_{NM}(t)\cos(\theta_{NM} + \varphi_{NM}).$$ (27)

The first corrected asymptotic approximation is:

$$T_{NM}(t) = a_{NM}(t)\cos(\theta_{NM} + \varphi_{NM}) + \varepsilon u_{NM1}(a_{NM}, \theta_{NM}, \Phi_{NM}).$$ (28)

with

$$\frac{da_{NM}(t)}{dt} = \varepsilon A_1(a, \phi)$$ (29)

$$\frac{d\phi_{NM}(t)}{dt} = \omega_{0NM} - \Omega_{NM} + \varepsilon B_1(a, \phi)$$ (30)

The second asymptotic approximation is:

$$T_{NM}(t) = a_{NM}(t)\cos(\theta_{NM} + \varphi_{NM}) + \varepsilon u_{NM1}(a_{NM}, \theta_{NM}, \Phi_{NM}).$$ (31)

The second corrected asymptotic approximation is:

$$T_{NM}(t) = a_{NM}(t)\cos(\theta_{NM} + \varphi_{NM}) + \varepsilon u_{NM1}(a_{NM}, \theta_{NM}, \Phi_{NM}) + \varepsilon^2 u_{NM2}(a_{NM}, \theta_{NM}, \Phi_{NM})$$ (32)

with

$$\frac{da_{NM}(t)}{dt} = +\varepsilon A_1(a, \phi) + \varepsilon^2 A_2(a, \phi)$$ (33)

$$\frac{d\phi_{NM}(t)}{dt} = \omega_{0NM} - \Omega_{NM} + \varepsilon B_1(a, \phi) + \varepsilon^2 B_2(a, \phi)$$ (34)

If we find time derivatives of the (31) :

$$\dot{T}_{NM}(t) = -a_{NM}(t)\omega_{0NM}\sin\Phi_{NM} +$$

$$+ \varepsilon \left\{ A_1(a, \phi)\cos\Phi_{NM} - B_1(a, \phi)a_{NM}(t)\sin\Phi_{NM} + \frac{\partial u_1}{\partial \theta_{NM}}\Omega_{NM} + \frac{\partial u_1}{\partial \Phi_{NM}}\Omega_{NM} \right\} + \varepsilon^2 ......$$ (35)

$$\ddot{T}_{NM}(t) = -a_{NM}(t)\omega_{0NM}^2\cos\Phi_{NM} +$$

$$+ \varepsilon \{ \left\langle [\omega_{0NM} - \Omega_{NM}]\frac{\partial A_1(a, \phi)}{\partial \varphi} - 2a_{NM}(t)\omega_{0NM}B_1(a, \phi) \right\rangle \cos\Phi_{NM} -$$ (36)

$$- \left\langle [\omega_{0NM} - \Omega_{NM}]a_{NM}(t)\frac{\partial B_1(a, \phi)}{\partial \varphi} - 2\omega_{0NM}A_1(a, \phi) \right\rangle \sin\Phi_{NM} +$$

$$+ \frac{\partial^2 u_1}{\partial \theta_{NM}^2}\Omega_{NM}^2 + \frac{\partial^2 u_1}{\partial \Omega_{NM}^2}\omega_{0NM}^2 \} + \varepsilon^2 ...$$

Finnaly, we obtain:

$$\frac{da_{NM}(t)}{dt} = -\frac{h_{0NM}}{\omega_{NM} - \Omega_{NM}}\cos\phi_{NM}(t)$$ (37)

$$\frac{d\phi_{NM}(t)}{dt} = \omega_{NM} + \frac{3}{8}\frac{\tilde{\omega}_{0F}^2 \tilde{g}_{nm}}{\omega_{NM}}[a_{NM}(t)]^2 + \frac{h_{0NM}}{a_{NM}(t)[\omega_{NM} - \Omega_{NM}]}\cos\phi_{NM}(t)$$ (38)

3. CONCLUSIONS

In the present paper the nonlinear forced vibration of a membrane system connected nonlinearly with nonlinear elastic layer were analyzed analytically. From the obtained solutions of amplitude and phase time derivatives one can notice the effect of nonlinearity of the elastic layer on behavior of system. With differential equation (14) is

which is rheononlinear, we open a new research task for next investigation of different types of vibration regimes.

REFERENCES

[1] J. Postlethwaite, S.R. Lamping, G.C. Leach, M.F. Hurwitz, G.J. Lye (2004) Flux and transmission characteristics of a vibrating microfiltration system operated at high biomass loading. Jornal of Membrane Science 228: 89-101.

[2] M.Y. Jaffrin (2008) Dynamic shear-enhanced membrane filtration: A review of rotating disks, rotating membranes and vibrating systems. Journal of Membrane Science 321: 7–25.

[3] D. Rašković (1965) Theory of oscilations. Naučna knjiga, Belgrade.

[4] J. Simonović (2008) Dynamics of Mechanical Systems of complex Structure. Magister thesis (In Serbian), University of Niš.

[5] K. (Stevanović) Hedrih, J. Simonović (2012) Multi-frequency analysis of the double circular plate system non-linear dynamics. Nonlinear Dynamics 67 : (3) 2299-2315.

[6] K. (Stevanović) Hedrih, J. Simonović (2010) Non-linear dynamics of the sandwich double circular plate system. International Journal of Non-linear Mechanics 45: (9) 902-918.

[7] K.S. Hedrih (2006) Transversal vibrations of double plate systems, Acta Mechanica Sinica 22: 487-501.

[8] K.S. Hedrih, J. Simonović (2007) Transversal vibrations of a non-conservative double circular plate system. Facta Universitatis, Series Mechanics, Automatic Control and Robotics 6: 19-64.

[9] Hedrih (Stevanović) K., (2008), Energy transfer in double plate system dynamics. Acta. Mech. Sin. 24, 331–344, 2008.

[10] Hedrih (Stevanović) K., (2009), Energy transfer in the hybrid system dynamics (energy transfer in the axially moving double belt system), Special Issue, Arch. of Applied Mech., (2009) vol.79, No.6-7 pp. 529-540. DOI 10.1007/s00419-008-0285-7.

[11] Hedrih (Stevanović) K. and Simonović J., (2011), „*Multi-frequency analysis of the double circular plate system non-linear dynamics*", Nonlinear Dynamics, DOI 10.1007/s11071-011-0147-7.

[12] Mitropolyskiy, Yu.A and Mosseenkov, B.I., (1976), *Assimptoticheskie recheniya uravnyeniya v chastnih proizvodnih*, Vichaya chkola Kiev. (in Russian)

PRECISE TRAJECTORY TRACKING OF ROBOTIC MECHANISM

Ljubinko Kevac[1], Mirjana Filipović[2]

[1] School of Electrical Engineering
The University of Belgrade, Bulevar Kralja Aleksandra 73, 11000 Belgrade
e-mail: ljubinko.kevac@gmail.com
[2] Mihajlo Pupin Institute,
The University of Belgrade, Volgina 15, 11000 Belgrade
e-mail: mira@robot.imp.bg.ac.rs

Abstract. *In this paper the problem of path tracking is considered. Through the history of robotic mechanisms, path tracking was considered one of the hardest tasks, due to many different problems. One of the biggest problems is elasticity, for an example of the joint or link and therefore the elasticity of robotic mechanism. An example of simplified robotic mechanism is examined in this paper. This robotic mechanism has one motor that controls the movement. It has one gear and one link on top of it and rigidity and elasticity of these two parts represents the biggest problem. When model of robotic mechanism is idealized, which means that everything is rigid, the trajectory tracking is easy, but if elasticity is included this problem gets complicated and predefined trajectory is not very well followed. In this paper a new way of trajectory tracking is shown. Method is sufficiently easy and it can be used on more complex mechanism which is a subject for future work.*

1. Introduction

The modeling of a modern robot system as a rigid mechanical system is an unrealistic simplification. Many applications, such as spray painting, plasma cutting and assembly, require good path tracking. Modeling and control of robotic mechanism is very popular and important part of today's Robotics, therefore, there are many papers and books related to this topic. First one who introduced this problem was Spong [1]-[3].There are two sources of vibration in robot manipulators: 1) joint elasticity, due to the elasticity of motion transmission elements such as harmonic drives, gear-boxes, belts or long shafts [9], and 2) link elasticity, introduced by a long and slender/lightweight construction of the arm, [4]-[8].
Elasticity of robotic mechanism represents one of the biggest problems in path tracking. There are many papers dealing with modeling of robotic mechanism and its elasticity problems. In [11]-[15] authors present a new way of motor modeling and therefore

control of the robotic mechanism. Depending on a robotic mechanism, it is controlled by one or more motors. Robotic mechanism shown on Fig. 1. is idealized (everything is rigid) and path tracking is not an issue. More realistic model of a robotic mechanism is shown on Fig. 2. This mechanism does not track the motors movement very well, because of the robots elasticity. In this paper this problem is considered and robotic mechanism on Fig. 2. is controlled to follow the motor, and therefore manage the desired path. Used method is a new approach and, although, this is a simplified mechanism, this method can be used on a complicated robotic mechanism.

2. Robotic mechanism

It is common to make a robotic mechanism to follow predefined trajectory. Usually, this trajectory is defined by another robotic mechanism and this trajectory is called referent trajectory. The purpose of this paper is to make a robotic pair consisting of elastic gear and rigid link (hereinafter referred to as the elastic robotic mechanism) to follow a trajectory generated by a robotic pair consisting of rigid gear and rigid link (hereinafter referred to as the rigid robotic mechanism).

2.1. Modeling of the rigid robotic mechanism

As a first step, modeling of the rigid robotic mechanism is conducted. The rigid robotic mechanism is shown on Fig. 1. Model is sufficiently easy, because everything is idealized and therefore only kinetic energy is spent. From Fig. 1. it is chosen that θ is used as generalized coordinate. θ represents the angle originated by the movement of the motor and because everything is rigid, link is rotating with the same angle. Also, it is important to know that the link is long $a = 0.3\,m$, and mass in link tip is $m = 2kg$. Mass in link base is $m_b = 1kg$.
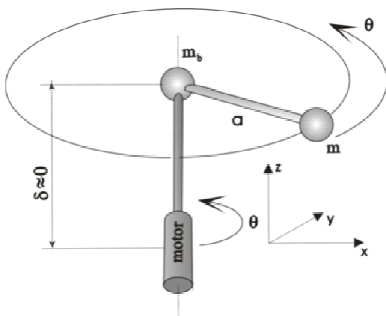

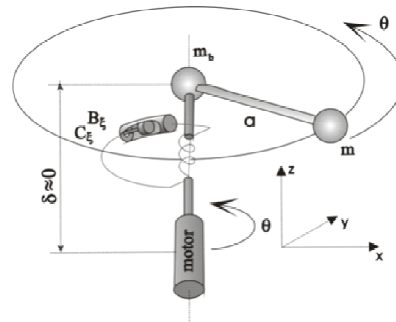**Figure 1.** The rigid robotic mechanism.   **Figure 2.** The elastic robotic mechanism.

From Fig. 1. the Equation for kinetic energy is derived

$$E_k = \frac{1}{2}ma^2\dot{\theta}^2 + \frac{1}{2}J_{zz}^2\dot{\theta}^2 + \frac{1}{2}J_{zb}^2\dot{\theta}^2 \tag{1}$$

From (1) the first Equation of the model is conducted

$$\frac{\partial}{\partial t}\frac{\partial E_k}{\partial \dot{\theta}} = ma^2 \ddot{\theta}^2 + (J_{zb} + J_{zz})\ \ddot{\theta}\ = (ma^2 + J_{zb} + J_{zz})\ddot{\theta}\ = 0 \tag{2}$$

Where $I_{zz} = 0.0025\,(kgm^2)$- inertia moment of mass m, $J_{zb} = 0.0013\,(kgm^2)$- inertia moment of mass m_h. Equation (2) represents the essential part of the rigid robotic mechanism model. For the complete model, Equation of the motor is needed. Firstly new constants are defined

$$G_v = \frac{J_r R_r}{C_m},\ L_v = \frac{R_r B_c}{C_m},\ S_v = \frac{R_r}{C_m} \tag{3}$$

Where $R_r = 0.272\,(\Omega)$- rotor circuit resistance, $J_r = 4.52\,(kgm^2)$ - inertia moments of the rotor and reducer, $C_m = 6.1(Nm/A)$- proportionality constants of the moment, $B_c = 0(Nm/(rad/s))$ - coefficient of viscous friction. Now, Equation of motor is written

$$Cm_i = G_v\ \ddot{\theta}\ + L_v\ \ddot{\theta}\ + S_v[(ma^2 + J_{zb} + J_{zz})\ddot{\theta}\ ] \tag{4}$$

Where Cm_i – electromotive force of motor [V]. With (2) and (4), model of the rigid robotic mechanism is complete. For better representation of the results, Cartesian coordinates are needed. Fig. 1. shows that only x and y coordinates are important and change during the rotation of the robotic mechanism, while z coordinate is 0. Therefore, relation between generalized and Cartesian coordinates is, as on Fig. 1.

$$x = a \cdot \cos\theta \quad . \tag{5}$$
$$x = a \cdot \sin\theta . \tag{6}$$

During the rotation of the link, knowledge of the velocity is important, so from (5) and (6) Cartesian coordinates of velocity are

$$\dot{x} = -a \cdot \sin\theta \cdot \dot{\theta} \tag{7}$$
$$\dot{y} = a \cdot \cos\theta \cdot \dot{\theta} \tag{8}$$

2.2. Modeling of the elastic robotic mechanism

In *2.1* model of the rigid robotic mechanism is concluded with Equations (2) i (4). Created model represents referent model (referent trajectory) and next step is modeling of the elastic robotic mechanism. The elastic robotic mechanism is shown on Fig. 2. Creating model of the elastic robotic mechanism is slightly harder, because this mechanism has elastic gear and as a result, with kinetic energy, potential and dissipative energy are spent. It is important to notice that characteristic variables and constants are the same as in the rigid robotic mechanism.

For easier understanding of the problem, the view from above is shown on Fig. 3. Because of the elastic gear, link of this robotic mechanism does not follow the motor, as the mechanism with rigid gear. As Fig. 3. shows, the link rotates with angle q and is ahead of the motor. q is greater than θ for ξ and it is because of the joints elasticity
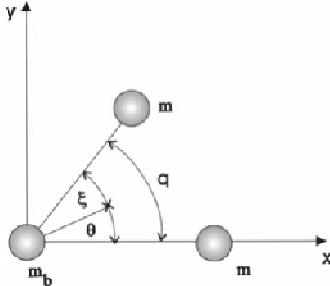
$$q = \theta + \xi. \tag{9}$$

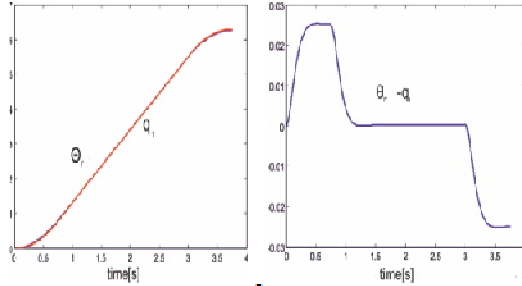**Figure 3.** The view from above

Figure 4. $\dot{\theta}_r$ and q_1

For purpose of modeling the elastic mechanism q and θ are used as generalized coordinates. Firstly, using Fig. 2. and Fig. 3., kinetic energy is derived

$$E_k = \frac{1}{2}ma^2 \dot{q}^2 + \frac{1}{2}J_{zz}^2 \ddot{q}^2 + \frac{1}{2}J_{zb}^2 \dot{q}^2 . \tag{10}$$

Potential and dissipative energy as a result of elasticity are, respectively

$$E_{p\xi} = \frac{1}{2}C_\xi \xi^2 \tag{11}$$

$$\phi_\xi = \frac{1}{2}B_\xi \xi^2 . \tag{12}$$

Where $C_\xi = 1.8143 * 10^1 \in R^1 (Nm / rad)$-characteristics of stiffness of the gear, $B_\xi = 3 \in R^1 (Nm /(rad / s))$ - characteristics of damping of the gear. All Equations must be represented with generalized coordinates. From (9) it is shown that

$$\xi = q - \theta. \tag{13}$$

When (13) is substituted in (11) and (12) potential and dissipative energy are, respectively

$$E_{p\xi} = \frac{1}{2}C_\xi (q - \theta)^2 \tag{14}$$

$$\phi_\xi = \frac{1}{2}B_\xi (q - \theta)^2 \tag{15}$$

After defining the energies, next step is determination of the model. From (10) it can be written

$$\frac{\partial}{\partial t}\frac{\partial E_k}{\partial \dot{\theta}} = ma^2 \ddot{q}^2 + (J_{zb} + J_{zz}) \ddot{q} = (ma^2 + J_{zb} + J_{zz})\ddot{q} = 0 \tag{16}$$

Now, from (14) and (15), four Equations are derived

$$\frac{\partial E_{p\xi}}{\partial q} = C_\xi (q - \theta) \tag{17}$$

$$\frac{\partial E_{p\xi}}{\partial \theta} = -C_\xi (q - \theta) \tag{18}$$

$$\frac{\partial \phi_\xi}{\partial q} = B_\xi (\dot{q} - \dot{\theta}) \tag{19}$$

$$\frac{\partial \phi_\xi}{\partial \theta} = -B_\xi (\dot{q} - \dot{\theta}) \tag{20}$$

Using (16), (17) and (19) the first Equation of model of the elastic robotic mechanism is derived

$$(ma^2 + J_{zb} + J_{zz})\ddot{q} + C_\xi q - C_\xi \theta + B_\xi \dot{q} - B_\xi \dot{\theta} = 0 \tag{21}$$

From (18) and (20) it is obvious that the Equation of the motor is

$$Cm_i = G_v \ddot{\theta} + L_v \ddot{\theta} - S_v [C_\xi (q - \theta) + B_\xi (\dot{q} - \dot{\theta})] \tag{22}$$

Using (21) and (22) matrix form can be derived

$$\begin{bmatrix} 0 \\ u \end{bmatrix} = \begin{bmatrix} H_{11} & 0 \\ 0 & H_{22} \end{bmatrix} \begin{bmatrix} \ddot{q} \\ \ddot{\theta} \end{bmatrix} + \begin{bmatrix} C_{11} & C_{12} \\ C_{21} & C_{22} \end{bmatrix} \begin{bmatrix} q \\ \theta \end{bmatrix} + \begin{bmatrix} B_{11} & B_{12} \\ B_{21} & B_{22} \end{bmatrix} \begin{bmatrix} \dot{q} \\ \dot{\theta} \end{bmatrix} \tag{23}$$

Where,

$$H_{11} = ma^2 + J_{zb} + J_{zz}, H_{22} = G_v, C_{11} = C_\xi, C_{12} = -C_\xi, C_{21} = -S_v C_\xi. C_{22} = S_v C_\xi,$$

$$B_{11} = B_\xi, B_{12} = -B_\xi, B_{21} = -S_v B_\xi$$

and $B_{22} = S_v B_\xi + L_v$. It is important to have information about the second derivative of generalized coordinates

$$\begin{bmatrix} \ddot{q} \\ \ddot{\theta} \end{bmatrix} = \begin{bmatrix} H_{11} & 0 \\ 0 & H_{22} \end{bmatrix} \left(\begin{bmatrix} 0 \\ u \end{bmatrix} - \begin{bmatrix} C_{11} & C_{12} \\ C_{21} & C_{22} \end{bmatrix} \begin{bmatrix} q \\ \theta \end{bmatrix} - \begin{bmatrix} B_{11} & B_{12} \\ B_{21} & B_{22} \end{bmatrix} \begin{bmatrix} \dot{q} \\ \dot{\theta} \end{bmatrix} \right) \tag{24}$$

The relation between generalized coordinates and Cartesian coordinates is needed. As Fig. 2. shows, only x and y coordinates are important

$$x = a \cdot \cos q . \tag{25}$$

$$y = a \cdot \sin \theta . \tag{26}$$

During the rotation of the link, knowledge of the velocity is important, so from (25) and (26) Cartesian coordinates of velocity are

$$\dot{x} = -a \cdot \sin q \cdot \dot{q} \tag{27}$$

$$\dot{x} = a \cdot \cos q \cdot \dot{q} \tag{28}$$

3. Simulation results

In second section models of two robotic mechanisms are derived. It is indicated that trajectory tracking is needed. The rigid robotic mechanism rotates around z axis and generalized coordinate for tracking of that rotation is angle θ. The elastic robotic

mechanism, also rotates around z axis, but it is in front of the motor by ξ, because of an elastic joint. It is desired that the elastic robotic mechanism rotates like the rigid robotic mechanism.

3.1. Initial results

Using MATLAB a referent model is created and therefore referent (rigid) trajectory of angle is generated (hereinafter referred to as θ_r). Afterwards, model of elastic mechanism is created and used referent trajectory is θ_r. Using classic PD regulator, whose gains are adjusted with *Pole placement* method [10], robotic mechanism with elastic gear is controlled to follow θ_r. After this simulation, the results are gathered and shown on Fig.4. (these results have index *1 (first)*)
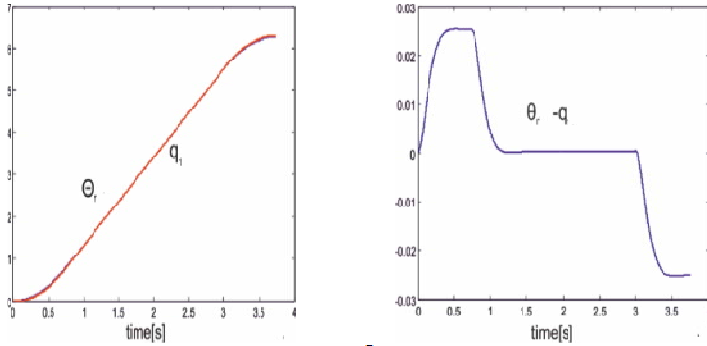

Figure 4. θ_r and q_1.

Fig. 4. shows that q_1 has slightly big error, and this is because of the ξ. These results are proved by showing Cartesian coordinates of referent and the first model, Fig. 5. and Fig. 6.
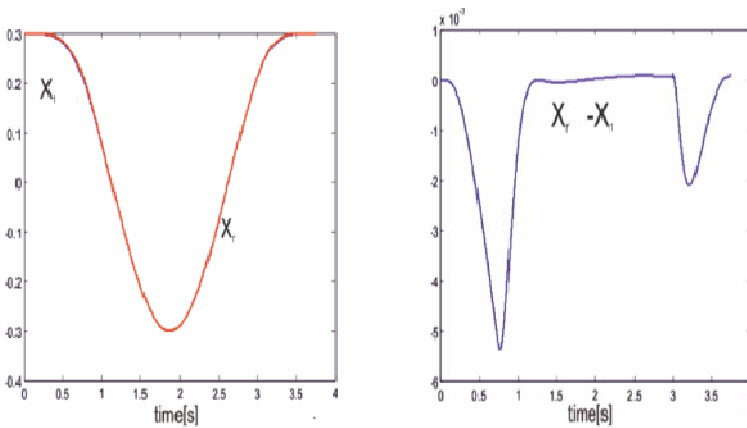

Figure 5. *X* coordinate of *rigid* and *the initial* model

3.2. Final results

Usually, ξ is in practice estimated using the known parameters and its estimation is often *99 %* correct as the real value. In this paper, Equation (9) will be used for estimation of ξ_r,
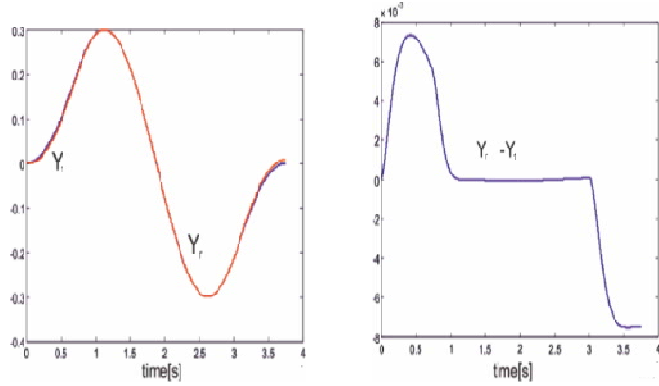
$$\xi_r = q_1 - \theta_r \tag{29}$$

Figure 6. *Y* coordinate of *rigid* and *the initial* model

Now, from (29) new referent trajectory is derived. As Fig. 3. shows q is in front of θ by ξ, so as a new referent trajectory $\theta_r - \xi_r$ is used. It means that when new nominal trajectory is used, because of the ξ_r, output result will be near θ_r. These results are shown on Fig. 7. (it is indexed as *2(second)*)
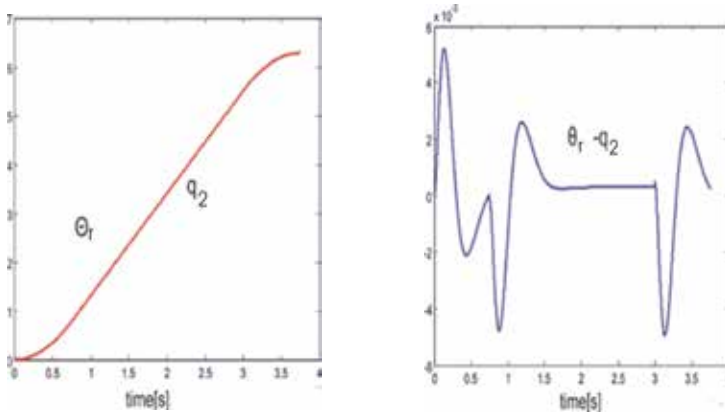

Figure 7. θ_r and q_2.

As Fig. 7. shows the error between output result and θ_r is very small, so with this nominal trajectory robotic mechanism with elastic gear follows mechanism with rigid one very good. Comparative results of Cartesian coordinates are shown on Fig. 8. and Fig. 9.
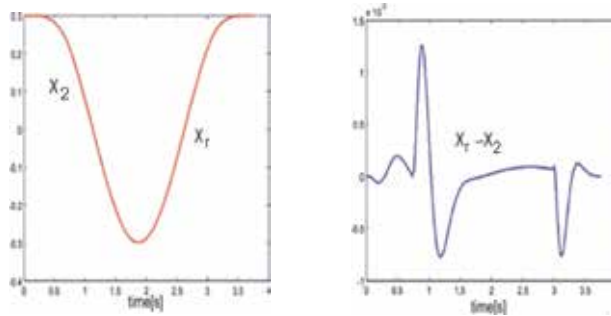

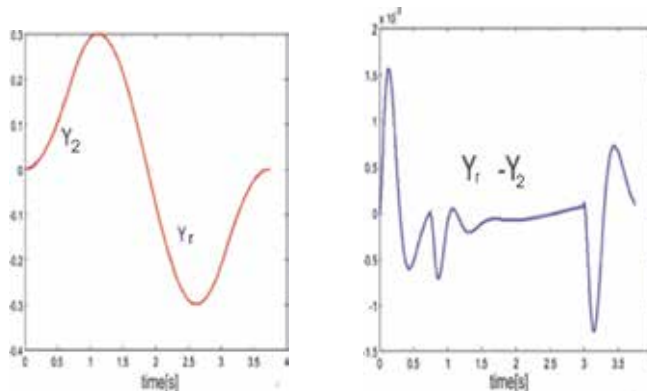**Figure 8.** *X* coordinate of *rigid* and *final(second)* model

Figure 9. *Y* coordinate of *rigid* and *final(second)* model

Fig. 8. and Fig. 9. show that Cartesian coordinates of *final(second)* model are very similar to Cartesian coordinates of the rigid model (θ_r), therefore the final model tracks trajectory generated by the rigid robotic mechanism very well, while the *initial* model has larger error. It is shown that the influence of elasticity is removed, the only error is due to controllers imperfection and with usage of another regulator, this error might be smaller.

4. Conclusion

In this paper a new approach for path tracking of a robotic mechanism is presented. Path tracking is one of the major issues in Robotics, due to the elasticity and other

imperfections. The main advantage of the method used in this paper is its simplicity and expandability on more complex robotic mechanisms.

Firstly, the model without elasticity is determined and therefore a desired trajectory. Desired trajectory is used as a referent trajectory with model that has elastic gear. Obtained results have quite a deviation from the referent trajectory. Deviations are present due to the elasticity of the robotic mechanism. This elasticity is usually determined by using know parameters of mechanical object (robotic mechanism), but in this paper it is calculated by subtracting resulted and desired trajectory, which represents one of theoretical ways of calculating mentioned error. With this error, new referent trajectory is determined and it represents previous referent trajectory reduced by the calculated deviation.

With this approach, error due the elasticity is used in good purpose and after applying new referent trajectory, the result is very similar to desired trajectory. The new error is present only due the imperfection of PD regulator. Obtained results are shown on Fig. 4. – Fig. 9. and they show that used method of path tracking is very precise and simple which is important in these applications, because of the possible use in more complicated systems.

Acknowledgment

References

[1] Spong, W.M. Modeling and control of elastic joint robots, ASME J.of Dynamic Systems¸ Measurement and
    Control. 109, 310-319 (1987)

[2] Spong, W.M. On the Force Control Problem for Flexible Joint Manipulators, IEEE Transactions on
    Automatic Control. 34, (1), 107-111 (1989) January

[3] Ghorbel, F., Spong, W.M. Adaptive Integral Manifold Control of Flexible Joint Robot Manipulators, IEEE
    International Conference on Robotics and Automation, Nice, France, (1992) May

[4] Book W.J. (1988) Modeling, design, and control of flexible manipulator arms: A tutorial review ,
    Proceedings of the 29th IEEE Conference on Decision and Control, Honolulu, HI, pp.500-506.

[5] De Luca A (1998a) Trajectory Control of Flexible Manipulators, *Control problems in Robotics and*

[6] *Automation,* pp. 83-104, Editors: B. Siciliano and K.P. Valavanis, Springer.

[7] De Luca A. (1998b) Dynamic Control of Robots with Joint Elasticity, *Proceedings of 29th IEEE Conference*

on Decision and Control, Honolulu, HI, pp.500-506.

[8] De Luca A. (1998c) Control Properties of Robot Arms with Joint Elasticity, In: Byrnes C.I.. Martin C.F.,

 Saeks R.E. (eds), *Analysis and Control of Nonlinear Systems,* North-Holland, Amsterdam, The Netherlands,

 pp. 61-70.

[9] Fraser A.R. and Daniel R.W. (1991) *Perturbation Techniques for Flexible Manipulators,* Kluwer, Boston,

 MA.

[10]   Sweet L.M. and Good M.C. (1985) Redefinition of the Robot Motion Control Problem, *IEEE Control*

 System Magazine, Vol. 5, No. 3. Pp. 18-24.

[11]   Astrom K.J. and Hagglung T (1995) *PID Controllers: Theory, Design, and Tuning,* Instrument Society of

 America, Research Triangle Park, North Carolina.

[12]   Filipovic M, Potkonjak V and Vukobratovic M (2007) Humanoid robotic system with and without elasticity

 elements walking on an immobile/mobile platform, *Journal of Intelligent & Robotic Systems, International*

 Journal 48, pp. 157-186.

[13]   Filipovic M and Vukobratovic M (April 2008) Complement of Source Equation of Elastic Line, *Journal of*

 Intelligent & Robotic Systems, International Journal, 52(2), pp. 233-261.

[14]   Filipovic M and Vukobratovic M (April 2008) Expansion of source equation of elastic line, *Robotica,*

 International Journal, Cambridge University Press, 26(6), pp. 739-751.

[15]   Filipovic M (2009) Euler-Bernoulli Equation Based on the Knowledge of the Classical Dynamics,

 Engineering & Automation Problems, International Journal, No 1, pp. 18-34.

[16]   Filipovic M (2011) Relation between Euler-Bernoulli Equation and Contemporary Knowledge in Robotics ,

 Robotica, International Journal, Cambridge University Press, 30, pp. 1-13.

INFLUENCE OF DISC BRAKE INSTALLATION ONTO THE ROPE DRUM ON DYNAMIC BEHAVIOR OF BUCKET WHEEL EXCAVATOR

Z. Golubović[1], Z. Lekić[1], S. Makragić[1]

[1] Faculty of Technical Sciences
The University of Pristina, Knjaza Milosa bb, 38220, Kosovska Mitrovica
e-mail: zoran.golubovic@pr.ac.rs,   zlatibor.lekic@pr.ac.rs,
slobodan.makragic@pr.ac.rs

One of the intelligent retrofit solutions for bucket wheel excavator (BWE) is installation of an additional holding brake system independently of the drives. The main function of the brake in boom hoisting subsystem of BWE, during the process of horizontal cut digging, is to achieve sufficient breaking torque which will hold boom and working wheel. Within classical solutions of hoisting subsystem, positioned to the input shaft of the gear box, gives a certain freedom of gear movement during excavating. When the brake is activated, only two or three gear teeth are loaded. This process leads to wear on their hips, so they lose their involutes shape. In addition, as the latest gears pair is outside the gearbox housing, weather conditions affect the removal of grease from their contact surfaces. That enhances their wear. Disc brake installation onto the rope drum will primarily eliminated gears moving and completely will unload the last couple of gears. As installation of additional brake system to boom hoisting subsystem affect the dynamic behavior of BWE in the excavation process will be presented in this document.

Keywords: disc brake, bucket wheel excavator, dynamic behavior, gears.

1. Introdaction

Proper and reliable functioning of the hoisting gear is vital for the safety of an BWE. Intelligent retrofit solutions represented in [5] proposes to implement an additional holding brake system independent of the drives. Caliper disc brakes [6,16] applying the brake forces to a disc directly mounted onto the rope drum. As positive side-effect of this arrangement the winch drives are relieved of load during excavating. Influence of disc brake installation onto the rope drum on dynamic behavior of BWE superstructure[8,15] and digging subsystem [2,3,4] will be examine on dinamic model presented in [11]. Hoisting drive system is modeling according to [7]. Method of determining the BWE digging force considering the characteristics of excavated soil, bucket cutting contour, cutting speed and vertical vibration of the bucket wheel is described in [1,9,10,12,15] Moments of inertia, stiffness and damping are calculated according to [12].

2. CALIPER BRAKE ON ROOP DRUM

Hoisting subsystem with independent dick brake system is show on figure 1. Holding brake on gearbox input shaft is replaced by disk brake on the roop drum. The caliper brakes in the SHI series (figure 2) consist of two independent halves with facing spring loaders and hydraulic cylinders. The brake lining support is held by guide bolts which absorb brake energy. The lining support is hydraulically retracted during operation of the brakes. The brakes can be used horizontally or vertically, predominantly as an emergency brake. Any lining wear can quickly be manually compensated. The friction lining is glued and riveted onto the lining support. Special linings are available for particular requirements.
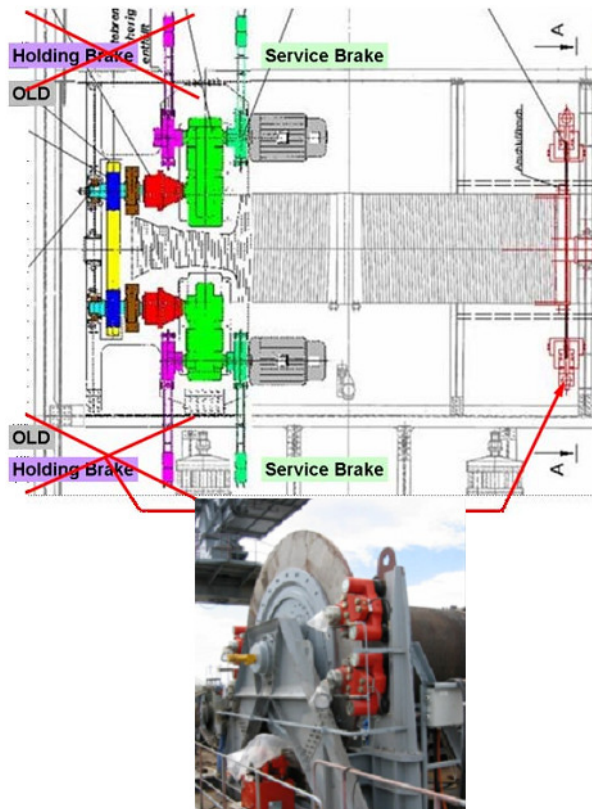

Figure1. Emergency back-up brake on rope drums

Applications: emergency stop brakes for heavy duty operation and coasting. Ideal for hoists on container cranes and casting cranes, for large belt conveyor systems, cable cars, etc.

Design Advantages:
• fast response time for maximum safety
• suitable for different disc thicknesses
• no tangential forces onto pistons and seals during dynamic braking
• low spare parts and maintenance requirement due to using only one dynamic seal per cylinder
• simple and fast manual wear compensation
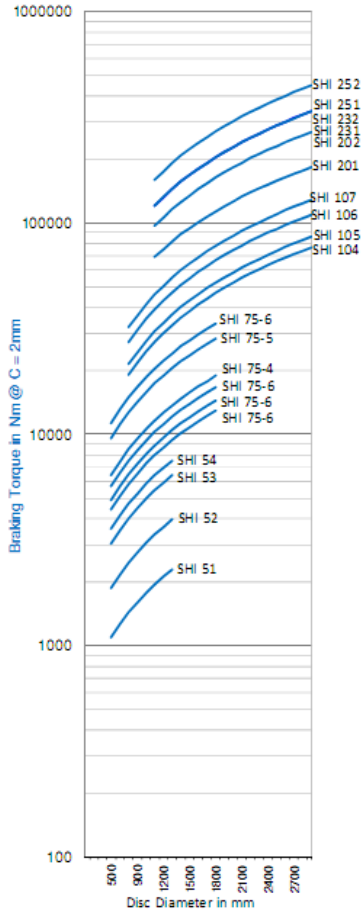• easy and quick replacement of pad carriers

Figure 2. Caliper disc brake SHI series

3. Dynamic model of BWE hoisting subsystem

Dynamic model of BWE main subsystems is the same as the one represented in [11]. Only changes are in kinematics of boom hoisting drive system. **Figure 3** shows the kinematics scheme of the boom hoisting drive system, consisting of: an asynchronous electric motor (EM), mechanical coupling (S), gearbox (R), holding brakes (K)on input shaft (figure 3.*a*) or caliper brake (C) (figure3.*b*) and drum for rope winding (D). For this work interesting is the case where the balance established between the braking and load torque, so the (EM) will not be included in dinamics models.
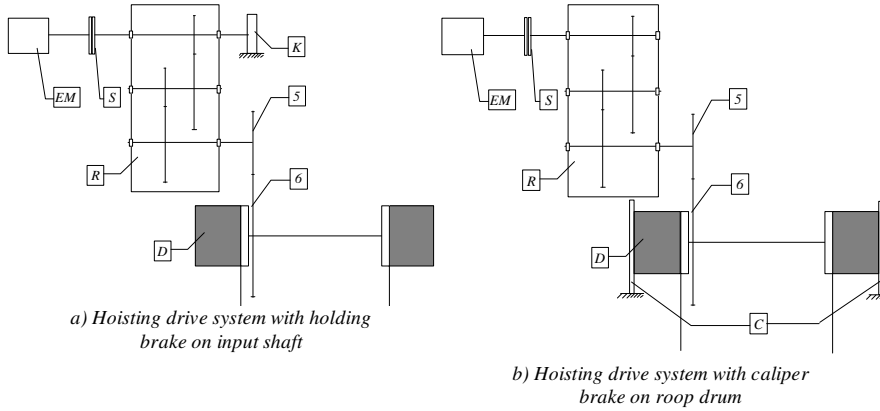
a) Hoisting drive system with holding brake on input shaft

b) Hoisting drive system with caliper brake on roop drum

Figure 3. Kinematics scheme of the boom hoisting drive system

Oscillatory system is represented in **Figure 4** as five (fig. 4.*a*) or four (fig. 4.*b*) rotating mass on a single shaft wedged: J_r^* - the reduced gearbox moment of inertia on the shaft brake, J_5^* - the reduced gear number 5 moment of inertia on the shaft brake, J_6^* - the reduced gear number 6 and drum moment of inertia on the shaft brake, J_7^* - the reduced boom and bucket wheel moment of inertia on the shaft brake. M_K - braking torque, F_u - Force in the rope reduced on the shaft break,

a) holding brake on input shaft

b) caliper brake on roop drum

Figure 4. Dinamic model of hoisting drive system
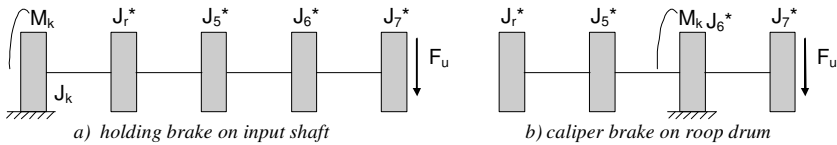
Solving systems of differential equations presented in [11] using the Runge-Kutta method in Simulink Module of Mathlab software package will obtain graphically presented results.

Results in case of hoisting drive system with holding brake on input shaft (blue curve) and system with caliper brake on rope drum (red curve) are given on the same charts, for easy comparison.

Vibrations amplitude of bucket wheel in a vertical plane (figure 5), in case of installed disc brakes on roop drum, are reduced to only 1 [cm] with more than 27 [cm] for system with holding brake on input shaft.
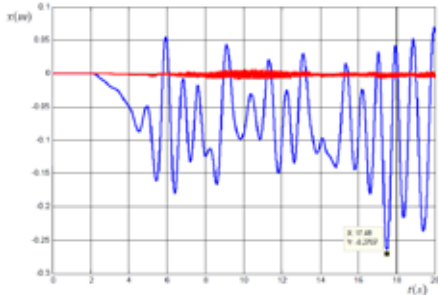

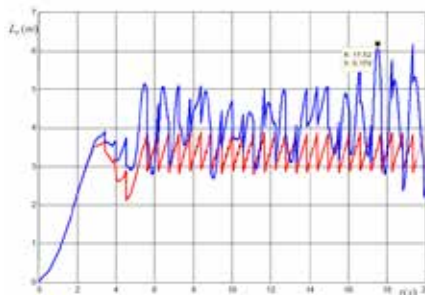**Figure 5**. Vertical movement of bucket wheel

Figure 6. Total length of the cutting contours

In addition, gears of hoisting drive system are relieved of load during excavation process.

Total length of the cutting contours (figure 6), for buckets that dig simultaneously , in case of hoisting system with disc brakes has a jagged shape ranges between 3 to 4 meters (red curve). That length for old system with holding brake on input shaft has maximum values of 6,2 meters, which is almost double.
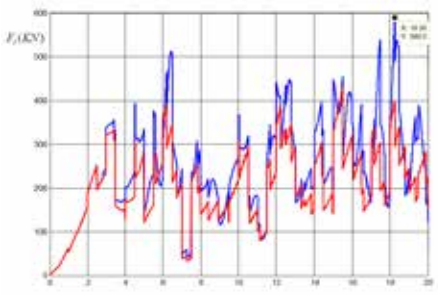
Figure 7. Digging force
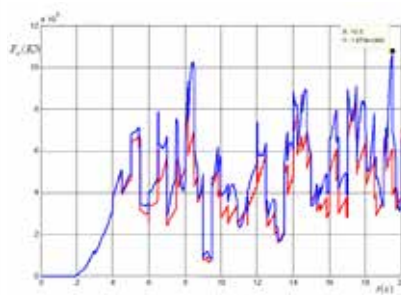
Figure 8. Force in the roop

The increasing of the cutting length or deeper buckets invasion into excavation terrace produced additional load for digging subsystem already stochastically loaded due to the in homogeneity of excavation materials. This leads to uneven filling of excavator buckets and finally causes additional load for belt conveyor.

Digging force (figure 7) directly dependents on the total length of buckets cutting contours. For drive system without disc brakes digging force reaches a maximum value greater than 30% compared to system with disc brakes.

Time function of rope load (figure 8) is very similar to the digging force time function, but the values are much higher due to the weight of the boom and working wheel. Lower values of rope load when hoisting drive system have disc brakes on roop drum ensure their longer exploitation and better safety of an BWE.

4. Conclusion

Disc brake installation onto the rope drum will primarily eliminated hoisting drive system gears moving and completely will unload the last couple of gears. Installation affects of additional brake system to boom hoisting subsystem are: vibration amplitudes of bucket wheel in a vertical plane are reduced, uncontrolled increase of cutting contours length is prevented, 30% less load of rope and digging drive system. The dynamic behavior of BWE in the excavation process clearly suggests installation of disc brake on the rope drum.

5. References

[1] Jevtić V, Golubović Z, Lekić Z, Mathematical modeling of resistance moment as the basic component for the dynamic behavior of the BWE, *XIV international conference on material handling and handling and warehousing*, Belgrade (1996).
[2] Jevtić V, Golubović Z, Lekić Z, Makragić S, The analysis of dynamic processes in the BWE working wheel drive system with a hydrodynamic coupling, *6th Sever symposium on mechanical gears,* Subotica (1997). pp. 179-185
[3] Golubović Z, Jevtić V, Lekić Z, Dynamic behavior of planetary gear in BWE drive systems , *Yugoslav Congress of Theoretical and Applied Mechanics 97 XXII*, Vrnjačka Banja (1997).
[4] Golubović Z, Contribution of drive system reconstruction feasibility for middle class BWE, *master's thesis*, Kosovska Mitrovica (2009).
[5]   Gnilke M, Intelligent retrofit solutions for bucket wheel excavators, *MAN TAKRAF Fördertechnik GmbH*, (2006)Lauchhammer,
[6] SIBRE Siegerland-Bremsen GmbH, *Product catalogues* D-35708 Haiger, (2011) Germany
[7] Jevtić V, Theoretical and experimental studies of flow stresses in hoisting subsystem structural elements, *master's thesis*, Niš-Bohum (1979).
[8] Volkov D.P , Čerkasov V.A., Dynamics and strength of excavators, translated from the Russian, *Department of Mining Institute for Informatics and Economics* , Beograd (1989),
[9] Hitzschke K, Experimentelle Analyse der Belastung des Schaufelrades durch den Grabvorgang, *Hebeyeuge u. Fördermittel*, H.9. (1984)
[10] Raaz V. Assessment of the Digging Force and Optimum Selection of the Mechanical and Operational Parameters of Bucket Wheel Excavators for Mining of Overburden, *Coal and Partings, Krupp Fordertechnik*, Esen (1999).
[11] Golubović Z, Lekić Z, Makragić S (2012) Dynamic model of bucket wheel excavator main subsystems, *Symposium Non-linear Dynamics with Multi and Interdisciplinary Applications (SNDMIA 2012)*, Belgrade
[12] Bošnjak S, Zrnić N, Petković Z, Bucket wheel excavators and trenchers - Computer added calculation of loads caused by resistance to excavation, *Machine Design, University of Novi Sad* (2006), pp.121-128.
[13] Bošnjak S, Zrnić N, Oguamanam D, On the dynamic modeling of bucket wheel excavators, *FME Transactions 34* (2006), pp. 221-226.
[14] Batinić V, Determination of gear mesh stiffness in planetary gearing, *Military Technical Courier*, vol. 56, no. 2, (2008) pp. 227-236.
[15] Ljamić D, Arsić M, Ćirković B, Experimental analysis of BWE SchRs 650/5x24 bucket wheel load, *Mining Machinery - scientific Meeting*, (1995) Beograd
[16] Mannesmann Demag, *SSB safety disc brekes*, Ba/0689/2T, Germany

_____

CHAOTIC OCCURRENCE OF THE RECORDED EARTHQUAKE MAGNITUDES IN SERBIA

Srdjan Kostić[1], N. Vasović[2]

[1] University of Belgrade Faculty of Mining and Geology, Djusina 7, Belgrade, Serbia, e-mail: srdjan.kostic@rgf.rs
[2] University of Belgrade Faculty of Mining and Geology, Djusina 7, Belgrade, Serbia, e-mail: kisi@pharmacy.bg.ac.rs

Abstract. In this paper, we demonstrate that the earthquake magnitude frequency per month, recorded between 1970 and 2011 in Serbia, evolved as a chaotic process, by conducting the nonlinear time series analysis of 760 recorded seismic events, according to Northern California Earthquake Data Center. The main idea was to reconstruct the phase space of the system under study, solely by analysing the time course of one of its variables. In that way, some characteristic quantities, like maximal Lyapunov exponent or determinism factor, could be extracted, defining the dynamics of the observed process. The applied algorithm consisted of several steps. Primarily, the optimal value of embedding delay (τ=3) was determined using the mutual information method. In the second step, false nearest neighbor method, for calculating the optimal embedding dimension, gave rather high value of minimal false nearest neighbor (0.88), due to the small inital data set. This was the reason why optimal value of embedding dimension was chosen to be equal to the number of degrees of freedom of the observed process (m=3). The determinism test, as the next step in our analysis, showed relatively low value of determinism factor (κ=0.71), due to the small number of earthquakes recorded in the period 1970-1980, which is confirmed through the deterministic analysis of the seismic events in 1980-2011 (κ=0.949). In the following stage of our analysis, we conducted stationarity test in order to show that the parameters of the system do not change during the measurement (i.e. the system has the same dynamics during the observed period). Relatively low percent of cross prediction error (12,41%) indicates that the system under study is stationary, even though the sampling of data was insufficient. As the final step, the assumed chaotic dynamics was confirmed by positive maximal Lyapunov exponent (λ_{max}=0.001257). Also, broadband noise in the Fourier power spectrum once more corroborates the deterministically chaotic dynamics of the recorded seismic events. This type of dynamical behavior could be associated with the crustal ''heterogeneity'', in which fault zones might have fluctuations in strength due to pore pressure variation.

1. Introduction

Earthquakes represent complex feature of the deformation of the earth's brittle crust. Their complexity reveals itself in power-law (fractal) scaling [1,2], with fractal spatial distribution of epicentres and fractal-like structure of faults [3,4]. Fractal property of earthquakes is also reflected through power-law distribution of magnitudes, which is commonly given by Gutenberg-Richter and Omori-Utsu law [5]. In the same time, earthquakes show complex temporal behavior, in the way that recorded seismic time series exhibits chaotic dynamics. Regarding this, Beltrami and Mareschal [6] tried to reconstruct the strange attractor for the earthquake time series recorded in the Parkfield seismic region between 1969 and 1987. They came to ambiguous results – either this

series cannot be distinguished from a random one, or it has a strange attractor with dimension higher than 12. Tiwari et al. [7] applied a nonlinear forecasting approach in a reconstructed phase space of the earthquake frequency in the Central Himalayan Region, and found a low positive correlation between predicted and observed data suggesting that the earthquake dynamics in the studied area is characterised by a mix of stochastic and chaotic behaviour. Applying the same nonlinear time series analysis technique, used in this paper, Mohammadi and Noorzad [8] calculated the value of maximal Lyapunov exponent from the earthquake time series in Tabriz seismic region in Iran, between 1949 and 2007. The positive value of maximal Lyapunov exponent indicated the presence of a strange attractor. De Santis et al. [9] showed that the seismic sequence of foreshocks culminating with the M_w = 6.3 main shock on April 6, 2009 in L'Aquila (Central Italy) evolved as a chaotic process, by using the method based on the Accelerated Strain Release analysis in time and on the nonlinear approach in a reconstructed phase space.

In this paper we apply commonly used technique for studying the possible chaotic nature of experimentally observed irregular behavior, which is given by nonlinear time series analysis theory [10,11,12]. This technique enables extraction of characteristic quantities, such as the maximal Lyapunov exponent, of a particular system solely by analyzing the time course of one of its variables. It was already successfully applied for confirming the chaotic behavior of a simple periodically driven resistor-inductor diode [13], human electrocardiographic recording and human locomotory apparatus [14,15]. Also, this kind of analysis, in an idealized phase space after a time delay reconstruction, was already applied in some other fields of geophysics, like geomagnetism [16,17]. Here we apply this nonlinear time series analysis technique, in order to reconstruct the phase space from an earthquake time series in Serbia, between 1970 and 2011from the Advanced National Seismic System composite earthquake catalog (ANSS), hosted by Northern California Earthquake Data Center [18]. The original data consisted of 760 recorded earthquakes, which is a relatively small data set. For the numerical calculation, we used the open-source program package, developed in [13]. The applied algorithm consisted of several steps: firstly, the mutual information method, initially suggested by Fraser and Swinney [19], was used to determine the appropriate value of embedding delay. Secondly, we applied the ''false nearest neighbor technique'' of Kennel et al. [20] to determine the proper value of embedding dimension. After that, we applied determinism test, developed by Kantz and Schreiber [11], in order to show that the observed system originates from a deterministic, not a stochastic process. Subsequently, we conducted the stationarity test, suggested by Schreiber [21], so as to ensure that the recorded data originate from system whose parameters are constant during the measurements. In the last part, we calculated the maximal Lyapunov exponent, applying the method proposed by Wolf et al. [22]. Furthermore, deterministicallz chaotic distribution of the recorded earthquakes was confirmed by broadband noise in Fourrier power spectrum.

The scheme of this paper is as follows. In section 2, we describe the applied technique, step by step, from mutual information method through false nearest neighbor method, determinism and stationarity test to calculation of maximal Lyapunov exponent and Fourrier power spectrum. This is followed by the analysis of the obtained results,

regarding the dynamics of the examined time series. In the third section we give brief discussion on the applied method and techniques, with suggestions for further research.

2. Nonlinear analysis of earthquake time series in Serbia

The recordings of seismic events in Serbia represent the source of data of various levels of reliability [23]. During the period 1900-1970, the macrosesmic location of epicentres was performed (stronger earthquakes: Rudnik, Lazarevac, Juhor, Krupanj, Svetozarevo, Vranje, Vitina, were determined as I=8-9). From 1970 until the present, the instrumental recording and evaluation of earthquake magnitude has been performed. During this period, only four moderate-magnitude earthquakes with M=5.2-5.6 (Kopaonik, Mionic, Trstenik and Kraljevo) have occurred. In other words, quantitative data about the earthquakes with epicenters in Serbia exist after 1970, which is the reason why we investigated the sequence of 760 recorded seismic events between 1970 and 2011, from [18]. We are aware of the fact that studying of this relatively small data set could lead to ambiguous results. Another important issue is the analysis of the short period of seismicity, which is not a standard approach in research on seismicity in one area. Usually, the reccurrence time of great earthquakes is taken as an optimal period (100 years in Serbia). However, regarding the research on chaotic dynamics of the recorded earthquakes, the short time series analysis is not an exception. De Santis et al. [9] also considered limited number of data (782 earthquakes) and demonstrated that it had evolved as a chaotic process. Our decision to focus the attention only to the recorded earthquakes in the period 1964-2011 is motivated by the fact that this period could be considered to have reliable data about the recorded earthquakes. Instrumental seismology started significantly to develop in Serbia during the 1950's, so the data before that period should be taken with great caution. Also, analogous time period was considered in [8].
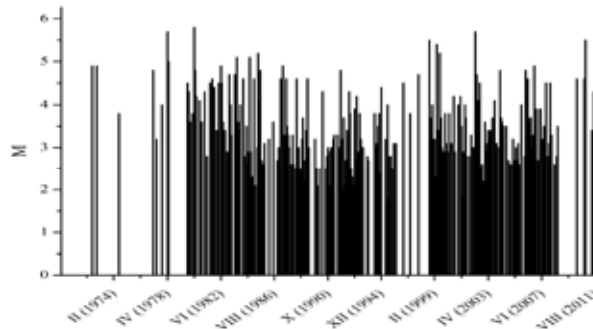

Figure 1. Time series of recorded earthquakes in Serbia for the period 1970-2011.

The original data consisted of 760 recorded earthquakes, with the maximum magnitude of 5.8, and the minimum magnitude of 1.2. 526 earthquakes occurred with the magnitudes between 2.3 and 3.5. We performed a nonlinear time series analysis,

considering the recorded earthquake magnitudes for every month, since 1970. For the months without any registration, we assumed zero value of magnitude, which was already proposed by Mohammadi and Noorzad [8]. If there was more than one registration during a month, then the largest recorded magnitude was assigned. In that way, we obtained a series of 504 data (Figure 1).

2.1. Determining embedding delay

According to Takens' delay embedding theorem, phase portraits are constructed by expanding a scalar time series $s(t)$, i.e. seismic time series in this case, into a vector time series $X(t)$ using time delays τ: $X(t) = \{x_0(t), x_1(t), ..., x_n(t),...\}$, where $x_n(t) = s(t+n\tau)$. For an infinite amount of data, the time delay τ can in principle be chosen almost arbitrarily. However, when we deal with real limited data, contaminated with a certain amount of noise, an appropriate value of τ must be chosen [19]. A suitable embedding delay τ has to fulfil two criteria. First, τ has to be large enough so that the information got from measuring the values of variable (magnitude in this case) at time t+τ is relevant and significantly different from the information we already have by knowing the value of the measured variable at time t. Second, τ should not be larger that the typical time in which the system looses memory of its initial state. If τ would be chosen larger, the reconstructed phase space would look more or less random since it would consist of uncorrelated points. The latter condition is particularly important for chaotic systems which are intrinsically unpredictable and, hence, loose memory of the initial state as time progresses.
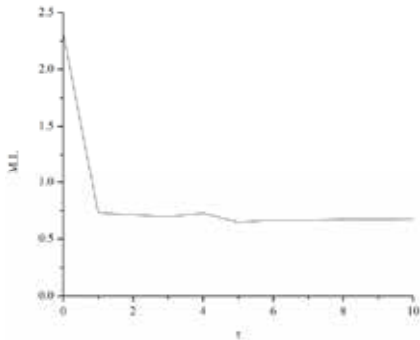
Figure 2. Determination of the proper embedding delay - the mutual information has the first minimum at $\tau = 3$.
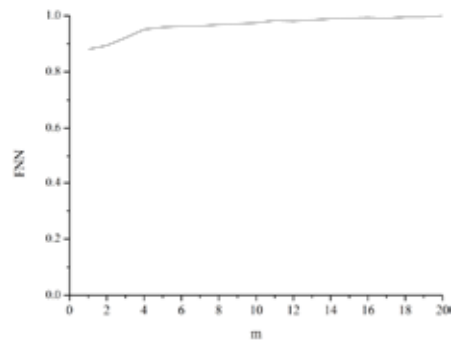
Figure 3. Fraction of false nearest neighbor versus the optimal embedding dimension.

There are two ways of choosing an appropriate embedding delay. The first approach is based on calculating the autocorrelation function of data, where the delay τ represents the time when this function takes a zero value, e.g. when x_0 and x_1 are completely decorrelated. However, autocorrelation function measures only the linear dependence of two variables, so it would be more efficient if we use a technique which measures the

general dependence of two variables, like mutual information method. According to [19], the value of τ that produces the first local minimum of mutual information should be used for phase portraits.

As apparent form figure 2, the first minimum of the mutual information appears at τ=3, which is taken as the optimal value of embedding delay.

Regarding the dynamics of the time series being reconstructed, finite value of Shannon entropy (2.326) suggests that the time series is non-random in nature. Indeed, lower entropy values represent an orderly/chaotic behavior of system dynamics, which is, in general, the case for the earthquake time series under study [7].

2.2. Determining embedding dimension

The next step in our analysis, after calculating the optimal value of embedding delay, is to determine the minimal required embedding dimension m in order to fully resolve the complex structure of the attractor. We use the procedure that identifies the number of ''false nearest neighbors'', points that appear to be nearest neighbors because the embedding space is too small. This method relies on the assumption that an attractor of a deterministic system folds and unfolds smothly with no sudden irregularities in its structure. In other words, two points that are close in the reconstructed embedding space have to stay sufficiently close also during forward iteration. If this criterion is met, then under some sufficiently short forward iteration, originally proposed to equal the embedding delay, the distance between two points of the reconstructed attractor, which are initially close, will sty approximately the same. However, if some point has a close neighbor that doe not fulfil this criterion, then this point is marked as having a false nearest neighbor. Our aim is to minimize the fraction of points having a false nearest neighbor by choosing a sufficiently large m. In this case, the results indicate that the lowest value of FNN is 0.88, obtained for embedding dimension $m = 1$ (Figure 3).

This could not be considered as an appropriate value of embedding dimension, because the criterion of FNN ≈ 0 is not fulfilled. Also, it is observed that a FNN increases with the embedding dimension, which could indicate the high level of stochasticity in the system under study, or it could be a consequence of a relatively small realistic data set, already reported in [20]. Concerning this, we assume that the minimum embedding dimension is equal to the number of degrees of freedom of the observed system, since the embedding dimension tells us how many autonomous first-order ordinary differential equations are necessary to model the behavior of the system [13]. In our case the earthquake nucleation mechanism is modeled with three first-order ordinary differential equations (velocity, distance and state variable), so the embedding dimension, used in further calculation, equals 3, which confirms the fact that a chaotic process is often characterized by having a small embedding dimension [24]. This assumption corresponds well to the suggestion of Sitharama et al. [25] that the false nearest neighbor method cannot be applied in small sample data sets. Apparently, all developed methods for finding a proper embedding dimension are inconvenient to apply on these types of time series.

Having calculated the optimal embedding delay and embedding dimension, we are able to successfully reconstruct the attractor (Figure 4).
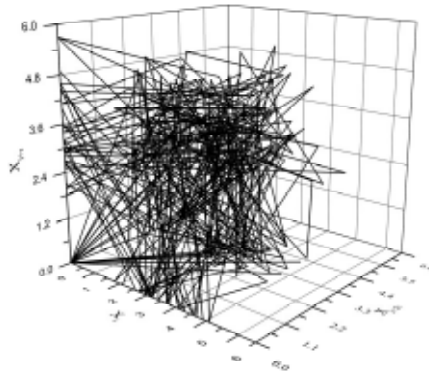
Figure 4. Reconstructed phase space obtained with the optimal embedding parameters: $\tau = 3$ and $m = 3$.

If we compare the return map for the system under study with the return map obtained by Tiwari et al. [7] for the earthquake data northeastern India regions, we would gain qualitatively the same graph (Figure 5). This fact indicates the possibility that temporal distribution of recorded earthquakes exhibits chaotic behavior, considering the fact that Tiwari et al [7] confirmed the earthquake processes in the northeastern india region evolve on a non-random high-dimensional chaotic system.
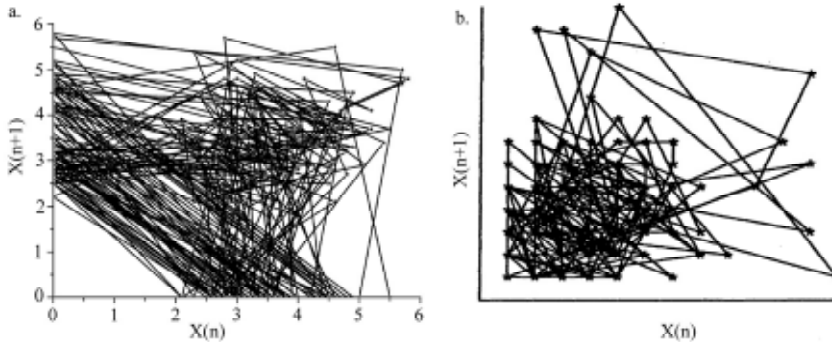
Figure 5. Comparison of the return map obtained for the earthquake data in Serbia (a) and earthquake data in Northeastern India (b).

2.3. Determinism test.

After calculating the embedding delay and embedding dimension, it is possible to apply a determinism test, in order to show that a time series originates from a deterministic process, since, according to [26], the time series must originate from a determinstic process in order to justify the calculation of the maximal Lyapunov exponent. The method developed by Kaplan and Glass [26] assumes that a time series

more or less complex first-order ordinary differential equations. The relevant consequence of this fact is that if a system is described by a set of ordinary differential equations, its vector field can be drawn easily. The length as well as the rotation of each vector in every point of the phase space is uniquely determined with the differential equations. In order to construct the vector field of the system directly from the time series, the phase space has to be coarse-grained into equally sized boxes with the same dimension as the embedding space. To each box that is occupied by the trajectory, a vector is assigned, which will finally be our approximation for the vector field. The vector pertaining to a particular box is obtained as follows. Each pass of the trajectory through the box generates a unit vector, whose direction is determined by the phase space point where the trajectory first enetrs the box and the phase space point where the trajectory leaves the box, determining the average direction of the trajectory through the box during a particular pass. The approximation for the vector field in one box of the phase space is now simply the average vector of all passes. If the time series originated from a deterministic system, and the coarse grained partitioning is fine enough, the obtained vector field should consist solely of vectors that have unit length. If solutions in the phase space are to be unique, then the unit vectors inside each box may not cross, since that would violate the uniqueness condition at each crossing. In other words, if the system is deterministic, the average length of all directional vectors κ will be 1, while for a completely random system $\kappa \approx 0$.

Considering the fact that we investigate the limited number of data, that are not evenly distributed, we coarse grained our three-dimensional embedding space into the largest 41x41x41 grid. For this calculation the three-dimensional embedding space was coarse grained into 68921 boxes. The pertaining determinism factor of the approximated vector field presented in figure 6 is $\kappa = 0.71$. The total amount of 298 vectors was obtained for this embedding space. We are aware of the fact that a number of vectors is significantly smaller than the total number of boxes, which could cause the average vector length to be different from 1.

The results of the determinism test could be ascribed to three possible reasons: chaos is present but i) magnitude errors in the seismic catalogue may slightly affect the results; ii) a stochastic contribution to the dynamics is present as well; or iii) chaos in not present. To exclude or accept one of the possible three cases, and to further discriminate and quantify the possible chaos in the seismic data, we conducted additional analysis, excluding the first several spikes, until 1980. The additional analysis was done because small number of earthquakes was recorded in the period 1970-1980, which could be one of the possible reasons of relatively low determinism factor. The results of the determinism test for this data set are shown in Figure 7. For this analysis, the determinism factor is $\kappa = 0.949$, which is closer to the value of 1 and confirms the deterministic nature of the system under study.
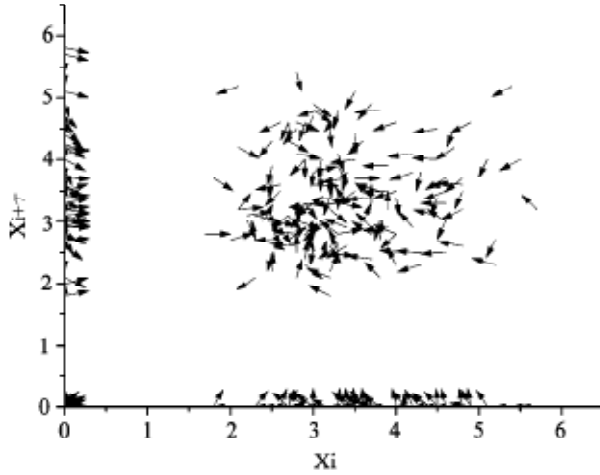
Figure 6. Determinism test. The approximated vector field for the embedding space reconstructed with $\tau = 3$ and $m = 3$. The pertaining determinism factor is $\kappa = 0.71$.
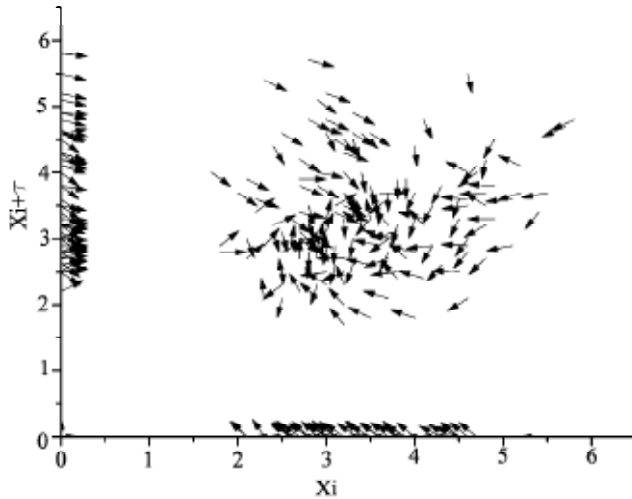
Figure 7. Determinism test, for data in the period 1980-2011. The approximated vector field for the embedding space reconstructed with $\tau = 3$ and $m = 3$. The pertaining determinism factor is $\kappa = 0.949$.

2.4. Stationarity test.

In order to determine whether the studied time series originated from a stationary process, we apply a stationarity test, originally proposed by Kantz and Schreiber [11], based on the cross-prediction error statistics. According to Perc [14,27] the maximal Lyapunov exponent cannot be considered as an indicator for chaos, if the studied time series does not result from a stationary process, which represents a system whose

prediction of unknown data value, using similar events happened in the past, which are considered as neighboring points. For each point of the equally sized non-overlapping segment i at time t, predictions of the value of an unknown data are performed in the segment j at the time $t+\Delta t$. The accuracy of obtained predictions is evaluated then, by calculating the average prediction error δ_{ij}, which is repeated for all combinations of i and j. The resulting high prediction error δ_{ji} is a clear indicator that the stationarity requirements in the examined time series are not fulfilled [27].

The colour of each map segment indicates the cross-prediction error of using segment i as the neighbour source for making predictions in segment j. We divided the original data set into short series each occupying 10 points, because of the small number of data and the limited value of cross-prediction error. In this way, we obtained a total of 58 segments and exactly 58^2 possible combinations to evaluate the statistics.

The average cross-prediction errors for all possible combinations of i and j are presented in Figure 8. The average value of all δ_{ij} is 1.885, while the minimum and maximum values are 0 and 2.4783 respectively.
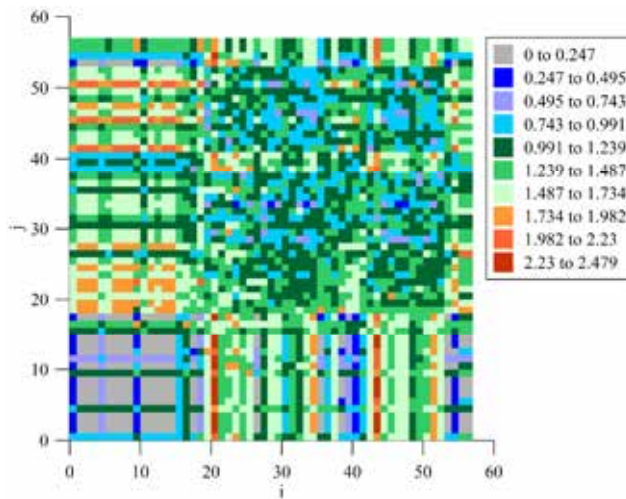
Figure 8. Stationarity test. The whole time series was partitioned into 58 non-overlapping segments each occupying 10 data points. The colour map displays average cross-prediction errors δ_{ij} in dependence on different segment combinations.

As it can be seen, the minimal cross prediction error is when $i = j$ on the diagonal, since x_t and the neighbours pertain the same data segment, so the possibility of an altered dynamics is small [27]. Also, it can be observed that δ_{ij} remains basically around the average value (green) and lower (blue and gray), approximately 87.59%, except for some isolated cases of high prediction error (yellow and red), without any evident pattern. Moreover, since all cross-prediction errors differ maximally by a factor of 2, we can clearly refute non-stationarity in the studied time series.

2.5. Largest Lyapunov exponent.

Lyapunov exponents are determined according to the algorithm developed by Wolf et al. [22], which is based on the evaluation of the distance evolution between two nearest points (L_0), for a fixed evolution time (t_{evolve}). If the final distance is larger than the starting one ($L_{evolve} > L_0$), the attractor is chaotic. However, if t_{evolv} is too large, it is possible that the two trajectories defining L_0 pass through a folding region of the attractor ($L_{evolv} < L_0$), leading to underestimation of the largest Lyapunov exponent. Hence, according to Perc [27], after each t_{evolv} a replacement step is attempted in which we look for a new point in the embedding space whose distance to the evolved initial point is as small as possible, until the initial point reaches the end of the time series. Finally, λ_{max} is calculated according to the equation (1):

$$\lambda_{max} = (1/Mt_{evolv})\sum_{i=0}^{M} ln(L_{evolv}^{(i)}/L_0^{(i)}) \tag{1}$$

where M is the total number of replacement steps.

The largest Lyapunov exponent converges well to $\lambda_{max}=0.001257$, confirming the deterministically chaotic behavior. Also, the largest positive Lyapunov exponent is very important because it gives an idea of the length of time over which a chaotic system is predictable [16].

At the end, broadband noise in Fourier power spectrum once more approves the chaotic temporal distribution of the recorded seismic events (Figure 9).
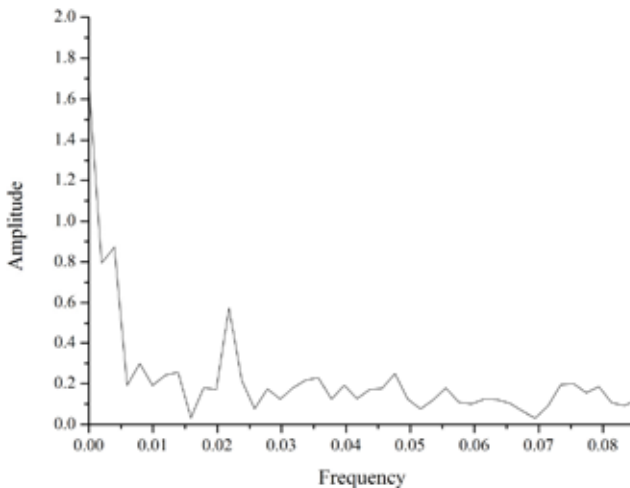

Figure 9. Broadband noise in the Fourier power spectrum indicates chaotic behavior.

3. Conclusion.

In this paper, we demonstrate that the distribution of the earthquake magnitudes in the period 1970-2011 evolved as a chaotic process. The obtained embedding delay (τ = 3) and embedding dimension (m = 3), verified through the determinism and stationarity test, led to the positive value of maximal Lyapunov number, for various values of evolution times. The main challenge in this analysis was the limited number of data. This was especially the case with determining embedding dimension, where we assigned the value of 3 to optimum embedding dimension, since the earthquake nucleation process is a system with three degrees of freedom. Also, an increase of FNN parameter with increased embedding dimension could indicate a high level of stochasticity in the system. This was the main reason why the deterministic test was deployed. However, determinism test did not completely confirm the uniqueness of solutions in the phase space, concerning the fact that the calculated pertaining determinism factor was 0.71. Hence, the additional analysis was done only for the recorded earthquakes in the period 1980-2011, showing that the determinism factor, in this case, is 0.949, which is near the value for purely deterministic system. In other words, denser data set should be analyzed in order to evaluate the deterministic nature of the original system.

However, the results obtained by applying the nonlinear time series analysis to an earthquake time series must be interpreted with great caution: the measurement error and stochastic component could largely influence the original data, which could make the analysis more difficult.

Next step in our research will be the application of this technique to the seismic sequence before and after Kraljevo M = 5,4 earthquake on November 3, 2010 in order to show that the seismic sequence during the great event also evolves as a chaotic process.

References

[1] Mandelbrot B B (1992) *The fractal geometry of nature*, Freeman, San Francisco.

[2] Turcotte D L (1997) *Fractals and Chaos in Geology and geophysics*, 2nd edition, Cambridge University Press, Cambridge.

[3] Marsan D, Bean C J, Steacy S and McCloskey J (2000) Observation of diffusion processes in earthquake populations and implications for the predictability of seismicity systems, *Journal of Geophysical Research*, **105**, pp. 28,081–28,094.

[4] Okubo P G and Aki K (1987) Fractal Geometry in the San Andreas Fault System, Jorunal of Geophysical Research, **92**, pp. 345–355.

[5] Turcotte D L, Newman W I and Gabrielov A (2000) A statistical physics approach to earthquakes. In ''Geocomplexity and the Physics of Earthquakes'' *Geophysical monograph 120*, J B Rundle, D L Turcotte and W Klein (Eds.), pp. 83-97.

[6] Beltrami H and Mareshal J (1993) Strange seismic attractor? Pure and Applied Geophysics, **141**, pp. 71-81.

[7] Tiwari R K, Sri Kakshmi S and Rao K N N (2004) Characterization of earthquake dynamics in northeastern India regions: a modern nonlinear forecasting approach. *Pure and Applied Geophysics,* **161**, pp. 865-880.

[8] Mohammadi S and Noorzad A (2009) Detecting chaos in earthquake time series for seismic hazard prediction. *Proceedings of the 3rd IASME/WSEAS International Conference on Geology and Seismology*, pp. 17-20.

[9] De Santis A, Cianchini G, Qamili E and Frepoli A (2010) The 2009 L'Aquila (Central Italy) seismic sequence as a chaotic process. *Tectonophysics*, **496**, pp. 44–52.

[10] Abarbanel H D I (1996) *Analysis of observed chaotic data*, Springer, New York.

[11] Kantz H and Schreiber T (1997) *Nonlinear time series analysis*, Cambridge University Press, Cambridge.

[12] Sprott J C (2003) *Chaos and time-series analysis*, Oxford University Press, Oxford.

[13] Kodba S, Perc M and Marhl M (2005) Detecting chaos from a time series. *European Journal of Physics,* **26**, pp. 205-215.

[14] Perc M (2005) The dynamics of human gait. European Journal of Physics, **26** pp. 525-534.

[15] Perc M (2005) Nonlinear time series analysis of the human electrocardiogram. *European Journal of Physics* **26**, pp. 757-768.

[16] Barraclough D R and De Santis A (1997) Some possible evidence for a chaotic geomagnetic field from observational data. *Physics of Earth and Planetary Interiors*, **99**, pp. 207-220.

[17] De Santis A, Barraclough D R and Tozzi R (2002) Nonlinear variability of the recent geomagnetic field, *Fractals*, **10**, pp. 297-303.

[18] http://quake.geo.berkeley.edu/cnss/

[19] Fraser A and Swinney H (1986) Independent coordinates for strange attractors from mutual information, *Physical Review A*, **33**, pp. 1134-1140.

[20] Kennel M, Brown R and Abarbanel H (1992) Determining embedding dimension for phase-space reconstruction using a geometrical construction, *Physical Review A*, 45, pp. 3403-3411.

[21] Schreiber T (1997) Detecting and analyzing nonstationarity in a time series with nonlinear cross-predictions, *Physical Review Letters*, **78**, pp. 843-846.

[22] Wolf A, Swift J, Swinney H and Vastano J (1985) Determining Lyapunov exponents from a time series, *Physica 16D*, pp. 285-317.

[23] Marović M., Đoković I., Pešić L., Radovanović S., Toljić M. and Gerzina N., (2001) Neotectonics and Seismicity of the Southern Margin of the Pannonian Basin in Serbia, Monography: Horvath F., Cloetingh S. and Bada G. (Eds.): Neotectonics and Seismism of the Pannonian Basin and Surrounding Orogens: A memoir on the Pannonian Basin. EGS Special Publication Series, pp. 277-295.

[24] May R M (1976) Simple mathematical models with very complicated dynamics, *Nature*, **261, pp.** 459-467.

[25] Sitharama I S, Cho E C and Phoha V V (2002) *Foundation of wavelet networks and applications*, Chapman and Hall/CRC, London.

[26] Kaplan D and Glass L (1992) Direct test for determinism in a time series, *Physical Review Letters* **68**, pp. 427-430.

[27] Perc M (2006) Introducing nonlinear time series analysis in undergraduate courses, *Fizika A* **15**, pp. 91-112.

SIMPLE MODEL OF EARTHQUAKE NUCLEATION WITH TIME-DELAY

S. Kostić[1], I. Franović[2], K. Todorović[3], N. Vasović[4]

[1] University of Belgrade Faculty of Mining and Geology, Djusina 7, Belgrade, Serbia, e-mail: srdjan.kostic@rgf.rs
[2] University of Belgrade Faculty of Physics, Studentski trg 12, Belgrade, Serbia, e-mail: igor.franovic@gmail.com
[3] University of Belgrade Faculty of Pharmacy, Vojvode Stepe 450, Belgrade, Serbia, e-mail: kisi@pharmacy.bg.ac.rs
[4] University of Belgrade Faculty of Mining and Geology, Djusina 7, Belgrade, Serbia, e-mail: kisi@pharmacy.bg.ac.rs

Abstract. In this paper we introduce the time delay τ in friction term in the Madariaga model of stick-slip motion coupled with Dieterich-Ruina's rate and state dependent friction law. Madariaga's system of equation describes the motion of the Burridge-Knopoff model, which is today recognized as a common model for earthquake nucleation mechanism. It consists of one block of a certain rock type, connected through harmonic spring to a moving plate and driven along the rough surface, which causes the whole system to move in a stick-slip fashion. The introduction of time delay in friction term is motivated by the fact that the observed spring-block model exhibits memory effect that commonly appears during the stick-slip motion of the block along the rough surface. Standard local bifurcation analysis of delay-differential equations is performed, indicating the dynamical change of the system state from stable equilibrium through periodic (first Hopf bifurcation) and quasiperiodic motion (second Hopf bifurcation) and eventually to deterministic chaos. The results are confirmed by using the software package DDE-BIFTOOL. The corresponding Hopf bifurcations are locally of the direct or inverse type which depends on the sign of the derivatives along the bifurcation curves. These dynamical changes are confirmed by the calculation of Fourier power spectra. We believe that this new approach, concerning the involvement of time-delay in the friction term in the Burridge-Knopoff model reveal some aspects of underlying physics of earthquake nucleation.

1. Introduction

Understanding the development and initial stages of an earthquake rupture is a major goal of earthquake science. Some researchers suggest that the nucleation process, specifically the size of the nucleation zone, is related to the ultimate size of the resulting earthquake [1-3], while others support the view that the size of the nucleation zone is unrelated to the final magnitude of an earthquake [4-6]. However, the influence of the nucleation mechanism on the final impact of earthquake certainly exists, so the modeling of this phenomenon could lead to new insights on the nature of earthquakes. A common approach in the description of seismic sources is their approximation by a model of equivalent forces that correspond to the linear wave equations, neglecting

nonlinear effects in the source area [7-11]. Equivalent forces are defined as producing displacements at a given point that are identical to those from the real forces acting at the source. However, this body-force equivalent is a formal concept and it is necessary to relate its characteristics to some physical concepts of the real earthquake source. One such concept is the elastic rebound theory, formulated by Reid [12], suggesting that earthquakes are the result of fracture of the Earth's material caused by tectonic stresses. Today, it is commonly accepted that vast majority of shallow tectonic earthquakes arise from faulting instabilities. In other words, dynamic faulting is widely accepted as the origin of the majority of seismic events [13]. However, the earthquake origin is not accessible to direct observation, so research in this area is conducted by studying the recorded time series, propagation of seismic waves through Earth's interior or by simulating the earthquakes in laboratory conditions. In this paper, we follow the suggestion of Brace and Byerlee [14], that stick-slip occurring in laboratory experiments may be analogous to the mechanism of crustal earthquakes. This stick-slip motion is well simulated by Burridge-Knopoff model [15], which is today recognized as a common model for earthquake nucleation mechanism. Originally, it consisted of several blocks interconnected by harmonic springs and attached to a moving plate, which drives the system along the rough surface, causing it to move in a stick-slip fashion. In this paper, we observed only one block, attached through harmonic spring to a driving plate, which causes the block to miove along the rough surface of the lower plate (Figure 1).
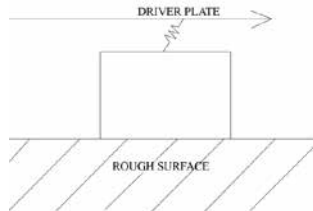
Figure 1. The Burridge-Knopoff block and spring model, represented by a slider coupled through a spring to a loader plate.

The main nonlinearity of this system comes from the friction between the block and the rough surface of the lower plate, which also causes many aspects of earthquake phenomena. Concerning this, some specific constitutive laws for rock friction has been developed based on laboratory studies. These laws have been successfully used to explain various aspects of stable and unstable sliding between elastic solids as observed in the laboratory [16-18]. In this paper we use Dieterich-Ruina rate-and state dependent friction law [19,20], based on experimental observations. One formulation of the Dieterich-Ruina friction law was proposed by Ruina [16] and is known as the ,,slip law'' [21]:

$$\tau = \sigma\left[\mu_o + \theta + A ln\left(\frac{V}{V_c}\right)\right]$$

$$\frac{d\theta}{dt} = -\frac{V}{D_c}\left[\theta + B ln\left(\frac{V}{V_c}\right)\right]$$

(1)

where the friction stress τ is a function of the normal stress σ, μ_0 is a constant coefficient of friction, D_c is the critical slip distance in order for friction to change from static to dynamic values [22]. V is the slip rate, V_c is a constant introduced for dimensional consistency [16]. A and B are positive frictional parameters corresponding to the response to a step change in the imposed velocity of a single block configuration [23] and θ is the state variable (Fig. 2).

The Dieterich-Ruina friction law (1) includes a state variable θ, which, in effect, represents the delayed reaction of the friction to instantaneous changes in velocity. It is this parameter that describes the memory effect in the model, or the so-called ''aging''[23,24]. In our paper we model this effect by including the time-lag in the friction term, which was not explicitly considered in previous papers.

The basis of our model is represented by the system of equations proposed by R. Madariaga, already used in [25], where we introduce the time-lag in the friction term. The results are obtained through standard local bifurcation analysis and confirmed by using the software package DDE-BIFTOOL, which represents a collection of Matlab routines for numerical bifurcation analysis of systems of delay differential equations with several constant and state-dependent delays [26,27].
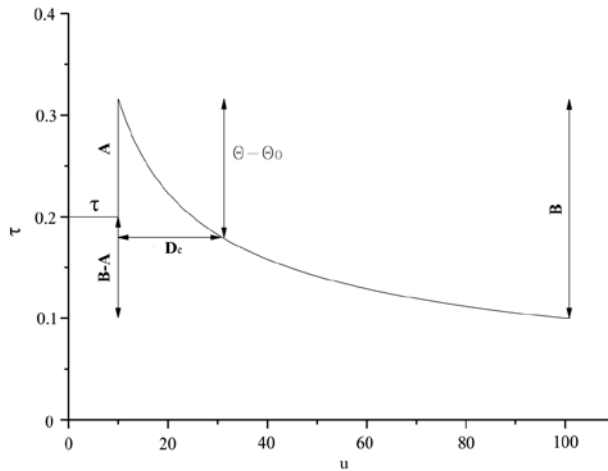
Figure 2. Schematic diagram, illustrating the response to a step change in the imposed velocity, V, of a single block. The imposed velocity, initially maintained constant at V_0, is suddenly incremented by ΔV and subsequently held constant at $V_0 + \Delta V$. The friction stress τ, initially constant at τ_0, suddenly increases to A when the velocity is incremented by ΔV and then decreases exponentially to a new value B. The length scale D_c, characterizes the distance.

The scheme of this paper is as follows. In section 2, we present the original model suggested by Madariaga [25], including the modification with introduced time delay. In section 3, we examine the one-block model, coupled with Dieterich-Ruina friction law, including the time delay term, by applying the standard local bifurcation analysis. The results are validated using the sofware package DDE-BIFTOOL. Moreover, we confirm the existence of chaotic motion through the calculation of the Fourrier power spectrum

and maximal Lyapunov exponent. In section 4 we give the possible correlation of the obtained results with the earthquakes. Concluding remarks are given in section 5, together with the suggestions for further research.

2. The earthquake model

Our numerical simulations of a spring-block model are based on the system of equations proposed by Madariaga [25]. These equations of motion coupled with Dieterich- Ruina rate and state dependent friction law are originally given in the following way:

$$\dot{\theta} = -v\big(\theta(1+\varepsilon)log(v)\big)$$

$$\dot{u} = v - 1 \tag{2}$$

$$\dot{v} = -\gamma^2\Big[u + (1/\xi)\big(\theta + log(v)\big)\Big]$$

where the parameter M is the mass of the spring block, u represents displacement of the block and v is the block's velocity. Parameter $\varepsilon=(B-A)/A$ measures the sensitivity of the velocity relaxation, $\xi =(kD_c)/A$ is the nondimensional spring constant, and $\gamma = (k/M)^{1/2}(D_c/v_0)$ is the nondimensional frequency [25]. Parameter k represents spring constant, connecting the block, while A, B and D_c are the same as in equation (1).

The system has only one stationary solution, $(\theta,u,v)=(0,0,1)$, which corresponds to steady sliding. In this paper, we introduce time delay τ concerning the retardation time between the movement of the upper plate and the block, due to complex friction force between the block and the rough lower plate. In this way, we obtain the following system of delay differential equations:

$$\dot{\theta} = -v\big(\theta(1+\varepsilon)log(v-\tau)\big)$$

$$\dot{u} = v - 1 \tag{3}$$

$$\dot{v} = -\gamma^2\Big[u + (1/\xi)\big(\theta + log(v)\big)\Big]$$

We shall proceed in the standard way to determine and analyze the characteristic equation of (4) around a stationary solution (0,0,1).

3. Local stability and bifurcations of the stationary solution

Linearization of the system of equations (3) and substitution $\theta=Ae^{\lambda t}$, $u=Be^{\lambda t}$, $v=Ce^{\lambda t}$ and $v(t-\tau)=Ce^{\lambda(t-\tau)}$ results in a system of algebraic equations for the constants A, B and C. This system has a nontrivial solution if the following is satisfied:

$$-\lambda^3 - \lambda^2\left(\frac{\gamma^2}{\xi}+1\right) - \lambda\gamma^2\left(\frac{1}{\xi}+1\right) - \gamma^2 + \lambda(1+\varepsilon)\frac{\gamma^2}{\xi}e^{-\lambda\tau} = 0 \tag{4}$$

The equation (4) is the characteristic equation of the system (3). Further, we substitute $\lambda=i\omega$ in equation (4) to obtain:

$$\frac{i\omega^3 + \omega^2\left(\dfrac{\gamma^2}{\xi}+1\right) - i\omega\gamma^2\left(\dfrac{1+\xi}{\xi}\right) - \gamma^2}{i\omega(1+\varepsilon)\dfrac{\gamma^2}{\xi}} = -\left(\cos\omega\tau - i\sin\omega\tau\right) \tag{5}$$

The resulting two equations for the real and imaginary part of equation (5) after squaring and adding give an equation for each of the parameters, ε and ξ in terms of the other parameters, ω and γ, and after division for τ in terms of the parameters ω, γ and ξ. In this way, one obtains parametric representations of the relations between τ and the other parameters, which correspond to the bifurcation values $\lambda=i\omega$. The general form of such relations is illustrated by the following formulas: for ε as a function of ω:

$$\varepsilon = -1 + \sqrt{C} \tag{6}$$

where:

$$C = \frac{\left[\omega^3 - \omega\gamma^2\left(\dfrac{1+\xi}{\xi}\right)\right]^2 + \left[\omega^2\left(\dfrac{\gamma^2}{\xi}+1\right)-\gamma^1\right]^2}{\left(\omega\dfrac{\gamma^2}{\xi}\right)^2} \tag{7}$$

On the other hand, for ξ as a function of ω:

$$\xi = \frac{\left[\omega\gamma^2\sin(\omega\tau) + \omega^2\gamma^2\cos(\omega\tau)\right]}{\left(\omega^3 - \omega\gamma^2\right)\sin(\omega\tau) + \left(\gamma^2 - \omega^2\right)\cos(\omega\tau)} \tag{8}$$

For τ as a function of ω:

$$\tau = \tau_c = \frac{1}{\omega}\left[arctg\left(\frac{-\omega^2\left(\dfrac{\gamma^2}{\xi}+1\right)}{-\omega^3 + \omega\gamma^2\left(\dfrac{1+\xi}{\xi}\right)}\right) + 2k\pi\right] \tag{9}$$

where k is any nonnegative integer such that $\tau_k \geq 0$.

The previous parametric equations for ε, ξ and τ give the Hopf bifurcation curves that are illustrated in Fig.3, for the fixed values of the parameters ξ (0,5) and γ(0.8). We adopted the value of γ=0,8, because for commonly used values of $\gamma = 10^4 - 10^{12}$ according to Madariaga [25] the system under study becomes very stiff in numerical sense. Another reason for taking the constant value of γ is that, in this case, the trajectory for a Hopf bifurcation depends only on ε, ξ and τ. In that way, we can observe a transition to chaos by simply increasing the value of those parameters.

As apparent from Fig.3, the fixed point undergoes a supercritical Hopf bifurcation, i.e. by enchancing the time delay τ, stable fixed point turns into an unstable one, and a limit cycle is born. Moreover, as we change the value of time delay, periodic motion turns into quasiperiodic and finally to deterministically chaotic behavior. The critical value of the time delay τ_c, when the bifurcation from stable into unstable fixed point occurs, is given by the relation in equation (9). In other words, our system exhibits quasiperiodic (Ruelle-Takens-Newhouse) route to chaos [28,29]. However, the derivatives of the solutions of the characteristic equation (5) with respect to τ at the
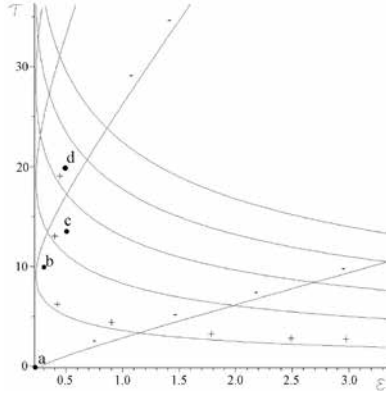
Figure 3. Hopf bifurcation curves $\tau(\varepsilon)$, for the fixed values of parameters $\xi = 0.5$, and $\gamma = 0.8$. The signs +/- represent the supercritical or subcritical Hopf bifurcation, respectively. Appropriate time series and phase plots for points 1, 2, 3 and 4 are shown in figures 4 and 5.
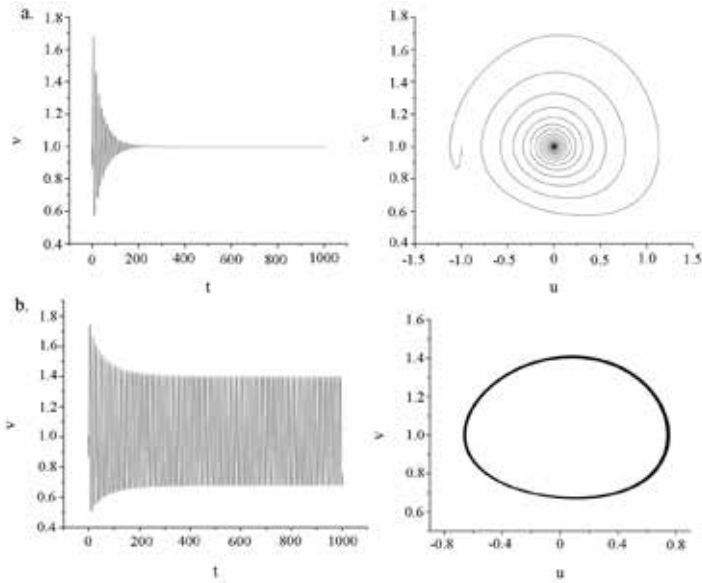
Figure 4. Temporal evolution of variable v and appropriate phase portrait for a. $\tau=0$, $\varepsilon = 0.2$, $\xi = 0.5$ and $\gamma = 0.8$ – point 1 form Fig.3 (equilibrium state); b. $\tau=10$, $\varepsilon = 0.3$, $\xi = 0.5$ and $\gamma = 0.8$ – point 2 from Fig. 3 (periodic motion).

bifurcation values in the Fig. 3 are not always positive, so that for $\tau \in (\tau_c, \tau_{c+1})$, by crossing the bifurcation curve, two already existing unstable directions could be lost in a sufficiently small neighbourhood of $(0,0,1)$, causing the dynamic state of the system to

change from oscillatory behavior to stable equilibrium state, which is known as time-delay induced amplitude death [30,31].

Fig. 4 and 5 represent temporal evolution of variable v for the fixed values of ε, ξ, γ and τ (corresponding time series and phase portraits for points 1, 2, 3 and 4 from Figure 3).
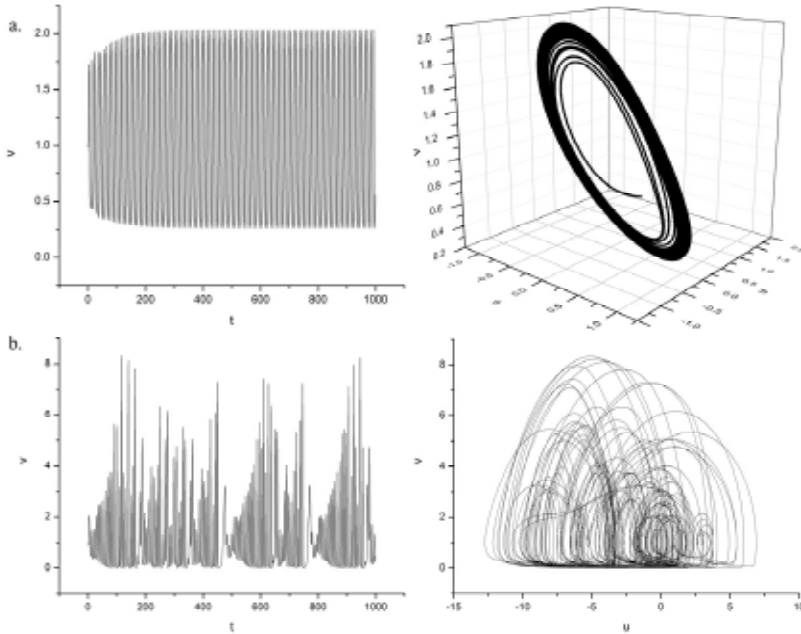
Figure 5. a. Temporal evolution of variable v and appropriate phase portrait for a. $\tau=13$, $\varepsilon = 0.5$, $\xi = 0.5$ and $\gamma = 0.8$ – point 3 from Fig. 3 (quasiperiodic motion); b. $\tau=20$, $\varepsilon = 0.5$, $\xi = 0.5$ and $\gamma = 0.8$ – point 4 from Fig.3 (deterministic chaos).
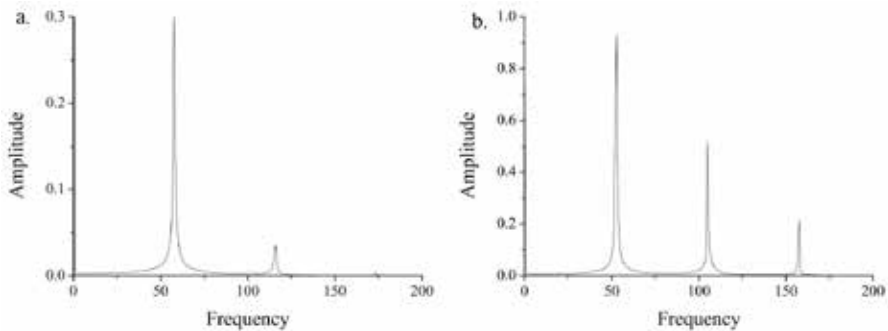
Figure 6.a. Single peak in power indicates the oscillatory behavior of the model. **b.** Two peaks in power indicate the appearance of torus (second Hopf bifurcation).

The presence of chaos was confirmed by calculation of the Fourier power spectrum for oscillations, torus and chaotic orbits, shown in fig. 4 and 5. The single peak in power in fig.6a indicates the oscillatory behavior of the system under study, while the second peak in fig.6b indicates a presence of torus. The broadband noise in fig. 7 indicates that the attractor is strange.
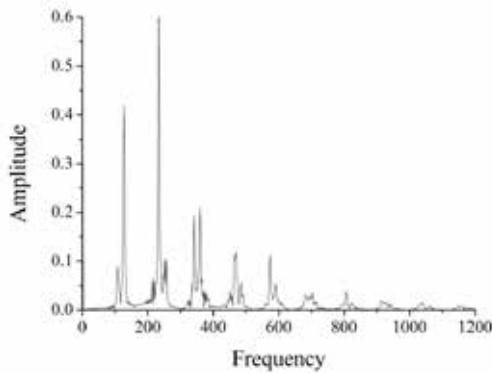
Figure 7. The broadband noise in the Fourier power spectrum indicate the chaotic behavior of the system.

Moreover, the deterministically chaotic behavior was further validated by calculating the maximal Lyapunov exponent for the $v(t)$ time series. As apparebt form Fig. 8, the value of maximal Lyapunov exponent converges well to $\lambda_{max}=0.095$.
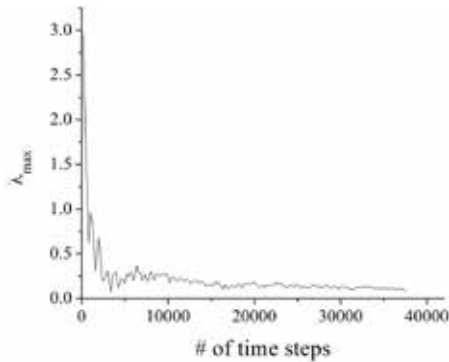
Figure 8. Calculation of the maximal Lyapunov exponent for $v(t)$ time series. The parameter value corresponds to the plot shown in figure 5.a. maximal Lyapunov exponents converge well to $\lambda=0.095$.

4. Seismological interpretation

Although parameter values used in this paper are exclusively of theoretical character, without looking for the relation with the observed data for laboratory and natural fault

zones, it is possible to give a qualitative interpretation of the obtained results. In the context of seismology, the spring-block model illustrated in Fig. 1 can be understood as a representation for one-dimensional earthquake motion, where the spring stiffness k corresponds to the linear elastic properties of the rock mass surrounding the fault [23]. According to [32], the parameter D_c corresponds to the critical sliding distance necessary to replace the population of asperity contacts. The parameters A and B are empirical constants, which depend on material properties, directly included in parameter ε defined by the ratio of parameters B-A and A. These parameters also change during the slip, as it is shown in Fig. 2. As apparent from this figure, parameter A reflects the rise of the friction coefficient, when the block is subjected to sudden velocity increase. For every succeeding slip phase, this parameter gain a new value, concerning a different nature of the contact between the block and the rough surface. This parameter is also reflected through parameter ξ, defined as the nondimensional spring constant.

On the other hand, the results of the bifurcation analysis imply that the transition from periodic motion to equilibrium state, known as ''amplitude death'' (inverse Hopf bifurcation) is observed only by increasing the value of τ (Fig. 3). This time-dependence of the studied system could be related to ''self-healing process'' along the fault zone, and it corresponds well to previously obtained laboratory observations [33] as well as the seismic estimates of fault healing [34,35], which show that frictional healing proceeds linearly with log time during quasistationary contact.

In the end, the analogy with earthquake motion suggests that the friction law can be a potential source for the observation of aperiodicity in earthquake dynamics. If we assume that the friction law is the main physical process regulating the frequency of earthquakes, then the presence of a strange attractor suggests that earthquakes are typically aperiodic. Thus aperiodic orbits on the strange attractor may exhibit dynamics analogous to the dynamics during an earthquake. Furthermore, it is important to note that aperiodic behavior observed in the system under study may be partially responsible for irregular ground motion during the earthquakes.

5. Concluding remarks

We analyzed the properties of a system of equations, describing the Burridge-Knopoff model coupled with Dieterich-Ruina friction law, with the time-delay introduced in the state friction term. In order to examine the possibility of deterministically chaotic behavior we performed the standard local bifurcation analysis and obtained exact parametric representation of the Hopf bifurcation curves in the general case of the introduced time-lag. The derivatives along the obtained Hopf bifurcation curves indicate the transition from equlibrium state through periodic and quasiperiodic motion and finally to deterministic chaos. The corresponding Hopf bifurcations are of direct or inverse type. Supercritical or subcritical Hopf bifurcation could not be diversed, since we conducted only the local analysis (near the fixed point).

On the other hand, even though we examined the model with only one block, our results reveal some characteristics of the general physics that is behind the generation of the earthquakes in terms of a chaotic process. Also, they confirm the fact that the memory effect included in this model represents the important feature of the real

earthquakes, since the chaotic motion is already observed for the recorded eartquakes. Moreover, the strategy applied here can be replicated for other models, e.g. with greater number of blocks, in order to better understand the chaotic behavior of earthquakes in general.

Concerning this, we will expand our future studies, including two or three blocks, interconnected by harmonic springs, and coupled with different friction laws, in order to compare the obtained results and observe how the dynamics of the system under study changes under different conditions.

References

[1] Ohnaka M (1993) Critical size of the nucleation zone of earthquake rupture interred from immediate foreshock activity, *Journal of Physics of the Earth*, **41**, pp. 45– 56.

[2] Ellsworth W L and Beroza G C (1995) Seismic evidence for an earthquake nucleation phase, *Science*, **268**, pp. 851– 855.

[3] Dodge D A, Beroza G C and Ellsworth W L (1996) Detailed observations of California foreshock sequences: implications for the earthquake initiation process, *Journal of Geophysical Research*, **101**, pp. 22,371– 22,392.

[4] Abercrombie R and Mori J (1994) Local observations of the onset of a large earthquake: 28 June 1992 Landers, California, *Bulletin of the Seismological Society of America*, **84**, pp. 725–734.

[5] Mori J and Kanamori H (1996) Initial rupture of earthquakes in the 1995 Ridgecrest, California sequence, *Geophysical Research Letters*, **23**, pp. 2340 – 2437.

[6] Kilb D and Gomberg J (1999) The initial subevent of the 1994 Northridge, California, earthquake: Is earthquake size predictable? *Journal of seismology*, **3**, pp. 409– 420.

[7] Geller R J (1976) Body force equivalents for stress-drop seismic sources, *Bulletin of Seismological Society of America*, **66**, pp. 1801-1804.

[8] Aki K and Richards P G (2004) *Quantitative Seismology*, *Theory and Methods*, Freeman, San Francisco.

[9] Ben-Menahem A and Singh S J (1981) *Seismic waves and sources*, Springer-Verlag, New York.

[10] Kennet B L N (1983) *Seismic wave propagation in stratified media*, Cambridge University Press, Cambridge.

[11] Bullen K E and Bolt B A (1985) *An introduction to the theory of seismology*. Cambridge University Press, Cambridge.

[12] Reid H F (1910) The mechanism of the earthquake, the California earthquake of April 18, 1906, *Report of the state earthquake investigation commission*, Vol. 2. Washington DC: Carnegie Institution.

[13] Gibowicz S J and Kijko A (1994) *An introduction to Mining Seismology*, Academic Press, USA.

[14] Brace W and Byerlee J (1966) Stick-slip as a mechanisms for earthquakes, *Science*, **153**, pp. 3739, 990-992.

[15] Burridge R and Knopoff L (1967) Model and theoretical seismicity, *Bulletin of the Seismological Society of America*, **57**, pp. 341-371.

[16] Ruina A L (1983) Slip instability and state variable friction laws. *Journal of geophysical research*, **88**, pp. 10359-10370.

[17] Rice J R and Ruina A L (1983) Stability of steady frictional slipping. *Journal of Applied Mechanics*, **50**, pp. 343-349.

[18] Tullis T E and Weeks J D (1986). Constitutive behavior and stability of frictional sliding in granite. *Pure and Applied Geophysics*, **124**, pp. 383-414.

[19] Dieterich J H (1997). Modeling of rock friction, 1. Experimental results and constitutive equations. *Journal of Geophysical Research.* **84**, 2161-2168.

[20] Dieterich J H (1981). Constitutive properties of faults with simulated gouge. Mechanical Behavior of Crustal Rocks, *Geophysical Monograph Series 24,* Carter N L (Ed), pp. 103-120.

[21] Ampuero J P and Rubin A M (2007) Earthquake nucleation on rate and state faults-aging and slip laws. *Journal of Geophysical Research*, **113**, pp. 1-21.

[22] Erickson B A (2010) *Complexity in the nonlinear Dieterich-Ruina friction law.* PhD thesis. Universtiy of California, Santa Barbara, 132 p.

[23] Scholz C H (2002) *The mechanics of earthquakes and faulting*, Cambridge University Press, Cambridge.

[24] Szkutnik J, Kawecka-Magiera B and Kulakowski K (2003) History-dependent synchronization in the Burridge-Knopoff model. *Tribology Series*, **43**, pp. 529–536.

[25] Erickson B, Birnir B and Lavallee D (2008) A model for aperiodicity in earthquakes, *Nonlinear processes in geophysics*, **15**, pp. 1-12.

[26] Engelborghs K, Lemaire V, Belair J and Roose D (2001) Numerical bifurcation analysis of delay differential equations arising from physiology modeling, *Journal of Mathematical Biology,* **42**, pp. 361-385.

[27] Pieroux D, Erneux T, Haegeman B, Engelborghs K and Roose D (2001) Bridges of periodic solutions and tori in semiconductor lasers subject to delay, *Physical Review Letters,* 87, 193901/1-193901/14.

[28] Ruelle D and Takens F (1971) On the nature of turbulence, *Communications in Mathematical Physics,* **20**, pp. 167-172.

[29] Newhouse S, Ruelle D and Takens F (1978) Occurrence of strange axiom-A attractors near quasiperiodic flow on 7, m > 3, *Communications in Mathematical Physics*, **64**, pp. 35-44.

[30] Yamaguchi Y and Shimizu H (1984) Theory of self-synchronization in the presence of native frequency distribution and external noises, *Physica D: Nonlinear Phenomena*, **11**, pp. 212-226.

[31] Aronson D G, Ermentrout G B and Kopell N (1990) Amplitude response of coupled oscillators, *Physica D: Nonlinear Phenomena*, **41**, 403-449.

[32] Dieterich J H and Kilgore B D (1994) Direct observation of frictional contacts: new insights for state dependent properties, *Pure and Applied Geophysics,* **143**, pp. 283–302.

[33] Marone C (1998). Laboratory derived friction laws and their application to seismic faulting. *Annual Review of Earth and Planetary Science*, **26**, pp. 643-696.

[34] Scholz C H, Aviles C and Wesnousky S (1986) Scaling differences between large interplate and intraplate earthquakes, *Bulletin of Seismological Society of America*, **76**, pp. 65- 70.

[35] Vidale J, Ellsworth W, Cole A and Marone C (1994) Variations in rupture process with recurrence interval in a repeated small earthquake, *Nature,* **368**, pp. 624-626.

Serbian Scientific Society

Symposium

Symposium Nonlinear Dynamics – Milutin Milanković

Multidisciplinary and Interdisciplinary Applications
(SNDMIA 2012), Belgrade, October 1-5, 2012.
(Eight Serbian Symposium in area of Non-linear Sciences)

APPENDIX I

Abstracts Invited Lectures published as full papers in other Journals

Beograd, October 1-5, 2012.
Venue: Mathematical Institute SANU

PL-1. ID-60.

DYNAMICS OF MULTI-VALUED VECTOR FIELDS WITH BOUNCING FLOWS IN DISCONTINUOUS DYNAMICAL SYSTEMS

Albert C. J. Luo
Department of Mechanical and Industrial Engineering, Southern Illinois University Edwardsville
Edwardsville, IL62026-1805, USA
Tel: 1-618-650-5389, Fax: 1-618-650-2555
Email: aluo@siue.edu

In this presentation, a classification of discontinuity in discontinuous dynamical systems will be discussed first. To discuss the singularity to the boundary, the grazing and inflexional singular sets on the boundary will be presented, and the real and imaginary singular sets will be also discussed. With permanent flow barriers, the forbidden boundary and the boundary channel will be presented. The forbidden boundary will not allow any flows passing through the boundary, and the boundary channel will not allow any boundary flows getting into the corresponding domains. Further, the domain and boundary classification will be addressed. Sink and source domains will be discussed. Similarly, the sink and source boundary will be also presented. Because of C^0-discontinuity, the flow barriers, the isolated domains and the boundary channels, the transport laws are needed to continue the flow in discontinuous dynamical systems. Multi-valued vector fields in a single domain will be introduced. With the simplest transport law (i.e., the switching rule), the bouncing flow on the boundary will be presented, and the extendable flows will be discussed as well. A controlled piecewise linear system will be presented as an application, and the vector fields on both sides of the boundary will be switched at the boundary. The bouncing flows will be illustrated in such a controlled piecewise linear system.

Naučno društvo Srbije — Serbian Scientific Society

http://afrodita.rcub.bg.ac.rs/~nds/   http://afrodita.rcub.bg.ac.rs/~nds/indexe.html

Symposium **Non-linear Dynamics – Milutin Milanković**
with Multi and Interdisciplinary Applications, **(SNDMIA 2012)**, Belgrade, October1-5, 2012
(Eigth Serbian Symposium in area of Non-linear Sciences)

PL-3. ID-67.

EXPERIMENTAL INVESTIGATESIONS OF ANALYSIS AND CONTROL OF NONLINEAR PEHNOMENA IN SOME MEHCANICAL SYSTEMS

H. Yabuno
Faculty of Science and Technology
Keio University 223-8522, JAPAN
e-mail: yabuno@mech.keio.ac.jp

In this presentation, positive utilizations of nonlinear phenomena are considered for establishing high performance mechanical systems [1]. Because nonlinear phenomena are generally very complex and not predictable of their occurrences, many control methods to avoid the occurrences have been proposed. On the other hand, most mechanical systems have inherently nonlinear characteristics in their inertia or restoring forces. In this presentation, we do not suppress the nonlinear phenomena due to the nonlinearity, but try to positively utilize nonlinear phenomena produced due their nonlinearity. First, we deal with an under actuated manipulator of which fist joint has actuator and sensor but second joint does not have actuator nor sensor. In most researches on under actuated manipulators, the assumption that the second

joint does not have actuator but has sensor is given, i.e., the feedback with respect to the angle of the free link connected to the second joint is possible, are given. On the other hand, we consider the case when the angle of the free link is not measurable, i.e. the feedback control with respect to the angle of the free link cannot be applied [2]. By high-frequency excitation of the first link to the second joint, the supercritical and subcritical, and their perturbed pitchfork bifurcations can be produced and many kinds of stable steady states can appear. We analytically show the motion control strategy by using the amplitude equation and confirm the validity through experiments. The second topic is related to the realization of a high performance atomic force microscope (AFM) [3]. For measuring soft materials as biological samples, we have to keep small amplitude in the self-excited micro-cantilever probe not to give the damage to the sample due to the contact between the cantilever and the samples. To this end, we utilize the nonlinear dynamics of van der Pol oscillator which has a limit cycle depending on the magnitude of the nonlinearity. We apply the nonlinear feedback proportional to the velocity and the deflection squared to realize the dynamics of van der Pol oscillator in the micro-cantilever probe in AFM. The validity is experimentally confirmed from the practical sample images.

Keywords: Bifurcation, bifurcation control, amplitude equation, underactuated manipulator, Atomic force microscope.

References
[1] Yabunho, H., Stabilization and utilization of nonlinear phenomane based on bifurcation control of slow dynamics, *Journal of Sound and Vibration*, **315** (2008), pp. 766-780.
[2] Yabuno, H. Matsuda, T., and Aoshima, N., Reachable and stabilizable area of an underactuated manipulator without state feedback control, *IEEE/ASME Transactions on Mechatronics*, **10** (2005), pp. 397-403.
[3] Yabuno, H., Kuroda, M., Someya, T., Nishimura, K., Hayashi, K., and Ashida, K., *Japanese Journal of Applied Physics*, **50** (2011), 076601.

THE NEW COMPLETE BIFURCATION THEORY OF NONLINEAR DYNAMICAL SYSTEMS AND CHAOS. RARE ATTRACTORS AND APPLICATION TO GLOBAL ANALYSIS

Mikhail V. Zakrzhevsky

Prof.,Dr.habil.sc.ing, Institute of Mechanics,
Riga Technical University, email: mzakr@latnet.lv

A new *complete bifurcation theory of nonlinear dynamical systems (CBT NDS)* and its application, intended for direct global bifurcation analysis of dynamical periodic systems is presented. The bifurcation theory is established for essential nonlinear dynamical periodic systems, described by models of ODE equations or by map-based models of discrete-time equations. Our approach is based on ideas of Poincaré, Andronov and other scientists' results concerning global dynamics, structural stability and bifurcations and chaotic responses of dynamical nonlinear systems and their topological properties.

The main idea of the new CBT is a fact that the NDS in a given parameters and state spaces has finite number (usually not so many) of independent bifurcation groups S(p) with their own complex topology and bifurcations, chaotic behavior, and, in many cases, with rare regular and chaotic attractors (RA). For each point of parameter space it is possible to find all essential fixed points of the periodic orbits (stable and unstable). This periodic skeleton allows to mark out the bifurcation groups and to start global analysis in state and parameter spaces.

The main concepts of the new CBT are: complete bifurcation group (BG); unstable periodic infinitium subgroups (UPI), responsible for chaos; complex protuberances; and periodic skeletons for a system with parameter p. For illustration of the advantages of the new bifurcation theory we use in this presentation several typical nonlinear models: Duffing driven double-well oscillator, a pendulum driven and parametrical excited oscillator (see Figs 1, 2). Besides we consider using the method of complete bifurcation groups for several different models of driven 2DOF systems: a flat system with one mass suspended by nonlinear springs in a plane, two masses chain system with non-unique equilibrium positions, and a simple rotor system with asymmetric suspension.

The last 2DOF systems were investigated for comparing two approaches: traditional analytical approximate methods (harmonic balance methods, average and many scale methods, the nonlinear normal mode's method) and the method of complete bifurcation groups and approaches of the bifurcation theory. In all considered examples we have found that the complete bifurcation theory's methods allow finding important unknown regular or chaotic attractors and/or new bifurcation groups with rare attractors RA. Additional illustration of the bifurcation theory, it is possible to find in the author's and hiss colleague's papers where there is rather complete bibliography on the bifurcation theory and rare attractors (see references).

464
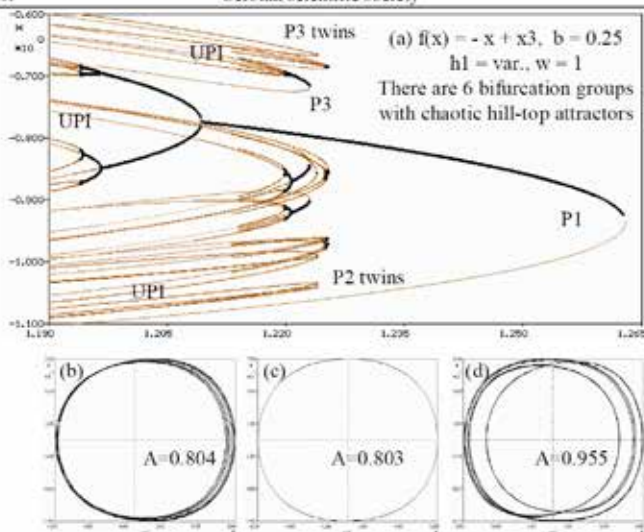
Fig. 1 Driven damped double-well Duffing oscillator. (a) Bifurcation diagrams (black –stable, reddish – unstable) with hilltop (HT) rare periodic and chaotic attractors (ChA) galore; amplitude of excitation $h1$ = var. (b) asymm. HT ChA, $h1$ = 1.2193; (c) P1 HT; h = 1.2195; (d) HT ChA-3 rare attractor, $h1$ = 1.2195.
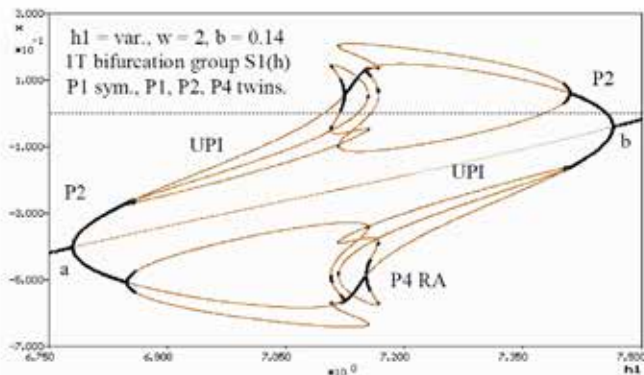
Fig. 2 Driven damped pendulum oscillator. Fragment of 1T bifurcation group (black –stable, reddish – unstable) with complex protuberance (a, b), P1 – P4 stable and unstable orbits, UPI and rare periodic P4 attractors (dark dots in the middle of the figure). Amplitude of excitation $h1$ = var.

References:

[1] M. Zakrzhevsky, New concepts of nonlinear dynamics: complete bifurcation groups…, JVE 10/4, 2008, 421-441.

[2] M. Zakrzhevsky et al, Nonlinear dynamics and chaos. Bifurcation groups and rare attractors, Riga, RTU, 181p, 2012 (in Russian).

465

Naučno društvo Srbije

http://afrodita.rcub.bg.ac.rs/~nds/

Serbian Scientific Society

http://afrodita.rcub.bg.ac.rs/~nds/indexe.html

Symposium **Non-linear Dynamics** – Milutin Milanković
with Multi and Interdisciplinary Applications, **(SNDMIA 2012)**, Belgrade, October 1-5, 2012
(Eigth Serbian Symposium in area of Non-linear Sciences)

PL-6. ID-18.

CHAOS IN MULTIPLE-TIME-SCALE DYNAMICS OF THE BRAY-LIEBHAFSKY OSCILLATORY REACTION

Ž. Čupić[1] and Lj. Kolar-Anić[2]

[1] Institute of Chemistry, Technology and Metallurgy, University of Belgrade, Center of Catalysis and Chemical Engineering, Njegoševa 12, Belgrade, Serbia
e-mail: zcupic@nanosys.ihtm.bg.ac.rs
[2] Faculty of Physical Chemistry, University of Belgrade, Studentski trg 12-16, Belgrade, Serbia
e-mail: lkolar@ffh.bg.ac.rs

ABSTRACT. Any reaction system starting from some arbitrary initial conditions tends to final steady or equilibrium state that plays the role of an attractor, passing through distinct regions of the phase space while its different chemical species simultaneously transform through the reaction network. Since, almost all complex many variable dynamical systems are characterized by multiple-time-scales, various forms of attractors and transitions between different dynamical states were studied in such systems. Typical example is an oscillatory reaction, known as the Bray-Liebhafsky (BL) one, that consists of a complex homogeneous catalytic oscillatory process involving numerous iodine intermediates such as I_2, I^-, HIO, HIO_2 and I_2O, that all oscillates [1]-[4]. The concentrations of mentioned species in the considered process differ for several orders of magnitudes among themselves. Thus, typical concentration of hydrogen peroxide during oscillatory state of the system is between 10^{-2} and 10^{-1} mol dm^{-3}, the concentration of iodine is between 10^{-5} and 10^{-4} mol dm^{-3}, whereas the concentrations of other species are much lower, between 10^{-9} and 10^{-6} mol dm^{-3}. Consequently, their simultaneous time variations are different, resulting in dissimilar behaviors characteristic for multiple-time-scale systems with, at least, slow (large-concentration) and fast (low-concentration) species. In systems, where concentrations of crucial species differ significantly, the relaxation oscillations are common. Furthermore, in multiple-time-scale systems with more than one slow variable, mixed-mode oscillations may appear in the region with simple sustained oscillations. [5] They generally consist of two types of oscillations with distinct amplitudes: large-amplitude oscillations (LAO-s) and small-amplitude oscillations (SAO-s). Depending on numbers of small (S) and large (L) oscillations in a period, different periodic dynamical states can be identified and assigned

by state enumeration L^S. Between every two successive periodic states with different dynamical assignation, the chaotic states appear. [6] Here we analyze emerging of chaotic atractor in the model [7] of BL reaction with multiple-time-scale dynamics. With aim to explain the mixed-mode oscillations obtained by numerical simulations of the various dynamical states of a model for the Bray-Liebhafsky reaction under CSTR conditions, the folded singularity points on the critical manifold of the full system and Andronov-Hopf bifurcation of the fast subsystem are calculated. The interaction between those singularities causes occurrence of tourbillion structure and canard solutions.

Keywords: Bray-Liebhafsky oscillatory reaction, mixed mode oscillations, critical manifold, multiple time scale dynamics

References

[1] W.C. Bray, A periodic reaction in homogeneous solution and its relation to catalysis, J. Am. Chem. Soc. 43 (1921) 1262-1267.

[2] W.C. Bray, H.A. Liebhafsky, Reaction involving hydrogen peroxide, iodine and iodate ion. I. Introduction, J. Am. Chem. Soc. 53 (1931) 38.

[3] Lj. Kolar-Anić, Ž. Čupić, S. Anić, G. Schmitz, Pseudo-steady states in the model of the Bray-Liebhafsky oscillatory reaction, J. Chem. Faraday Trans. 93 (1997) 2147-2152.

[4] G. Schmitz, Models for the oscillating reactions nullclines and steady states, in: Physical Chemistry '98, S. Ribnikar, S. Anić (Eds.), Soc. Phys. Chemists of Serbia, Belgrade, 1998, pp.173-179.

[5] M. Desroches, J. Guckenheimer, B. Krauskopf, C. Kuehn, H. Osinga, M. Wechselberger, Mixed-mode oscillations with multiple time-scales, SIAM Review 54 (2012) 211-288.

[6] A.Z. Ivanović-Šašić, V.M. Marković, S.R. Anić, Lj.Z. Kolar-Anić, Ž.D. Čupić, Structures of chaos in open reaction systems, Phys. Chem. Chem. Phys. 13 (2011) 20162-20171.

[7] Lj. Kolar-Anić, Ž. Čupić, G. Schmitz, S. Anić, Improvement of the stoichiometric network analysis for determination of instability conditions of complex nonlinear reaction systems, Chem. Eng. Sci. 65 (2010) 3718-3728.

Naučno društvo Srbije
http://afrodita.rcub.bg.ac.rs/~nds/

Serbian Scientific Society
http://afrodita.rcub.bg.ac.rs/~nds/indexe.html

Symposium **Non-linear Dynamics – Milutin Milanković**
with Multi and Interdisciplinary Applications, **(SNDMIA 2012),** Belgrade, October1-5, 2012
(Eigth Serbian Symposium in area of Non-linear Sciences)

PL-8. ID-50.

WAVE PROPAGATION IN FIBRE REINFORCED COMPOSITE LAMINATES

D. Milosavljević[1], G. Bogdanović[2]

[1] Faculty of Engineering
The University of Kragujevac, Sestre Janjić 6, 34000 Kragujevac, Serbia
e-mail: dmilos@kg.ac.rs
[2] Faculty of Engineering
The University of Kragujevac, Sestre Janjić 6, 34000 Kragujevac, Serbia
e-mail: gocab@kg.ac.rs

ABSTRACT. Composite materials consist of at least two constituents one of which is matrix and another fibre usually lay up through layers mutually bonded to make multilayered composite in the forms of laminates. Fibres carry loads giving strength and matrix bonds fibres together play important role in load transfer to fibres and forms outer shape of composite.

Prediction of dynamic behavior of laminated composites is rapidly assuming considerable importance to industry. Thus, here we deal with such composites, and analysis relates to fibre reinforced materials in which continuous strong and stiff fibres, such as carbon, boron etc., are embedded in a relatively soft matrix, such as resin.

If material is reinforced with one family of fibres it has one privileged direction making material locally transversally isotropic in relation to that direction. Fibre direction may be defined as unit vector field a which may vary from point to point. Trajectories of unit vectors a are defined as fibres in relation to which material is locally transversally isotropic. Since fibre direction depends on position, here we consider coordinate free formulation of constitutive equations [1].

The non-linear dynamic theory of finite elasticity is quite difficult and still today relatively few analytical solutions have been obtained for the full governing equations. These are based on early work of Hadamard and there have been examined cases simple enough to involve only a very limited material response. In the search of more complex motions only partial results seem to be possible [2].

In recent times, researchers interested in continuum mechanics have usually restricted their attention to special classes of response functions such as neo-Hookean or Moony-Rivlin

materials. On the other hand, researchers interested in acoustics have concentrated their interest towards the theory of small, but finite amplitude, waves. Possibility to obtain exact solutions of nonlinear dynamic elasticity is important in many fields of applications. These solutions often give opportunity to investigate more complex theories of material behavior where dissipative and dispersive phenomena are taken into account. Here we are going to provide partial survey of some results and methods of approximations made to search governing equations.

Here it is going to be made sort of parallel between nonlinear and linear elasticity, and to derive in a rigorous and general way the nonlinear equations, which describe fibre reinforced composites and laminates. Constitutive relations of finite elasticity are given for models of materials reinforced by one or two families of fibres. Linearization leads to constitutive relations same as those developed by introduction of strain energy function, which make relatively easy search through wave phenomena.

For given deformation strain energy function depends on both strain $\boldsymbol{\varepsilon}$ and fibre direction $\boldsymbol{a}$. Here is given list of matrix products whose traces make proper orthogonal group basis leading to set of invariants which may be used to form general quadratic form of strain energy function. This may be used to form stress strain relations leading to elasticity tensor for material reinforced by one or two families of fibres.

Dynamic behavior of anisotropic media may be seen the best through its behavior during bulk wave propagation. Bulk waves exist in infinite homogeneous bodies and propagate unbounded without disturbances caused by either boundaries or inter-layers. Such waves may be decomposed into finite plane waves propagating along arbitrary direction $\boldsymbol{n}$ in solid.

Properties of these waves are determined by dependence between propagation direction and constitutive properties of media. Three types of such waves may be distinguished in connection to three displacement vectors, which determine acoustic polarization. Three polarization vectors are mutually orthogonal, but in most cases they are neither perpendicular nor parallel to propagation direction.

The most of dynamical systems are naturally nonlinear and, since it is not easy to find closed solutions of such systems, here we are going to write Reimann-Christoffel equation, leading to three non-homogeneous linear equations which determine displacement amplitudes. This equation represents propagation condition of bulk waves as set of three homogeneous linear equations. Proper values of Reimann-Christoffel equation give phase speed of propagation of plane waves, and proper vectors represent polarization vector. This equation is the most important equation of entire theory of elastic wave propagation in crystals. Since acoustic tensor is symmetric tensor of second order, proper values are real and proper vectors are mutually orthogonal. Reimann-Christoffel equation may be solved analytically only for the simplest cases of material symmetry [3].

For successful display of three dimensional wave surfaces numerical analysis, which contain all propagation directions, phase velocities and polarization vectors, has been performed. The most appropriate approach in this consideration is fibre reinforced material for which proper axes coincide with global coordinate system. That is always used when crystallographic axes are known in advance. Materials used in present analysis are fibre reinforced with one or two families of continuous fibres. Since fibres are much stronger than matrix anisotropic properties are very strong.

After examination of bulk waves we are going to restrict our attention to stress free infinite plate, developing dispersion relations. We are going to use developed dispersion relations to examine laminate structures, and then to consider dynamic behavior of such structures.

Keywords: Waves, Composites, Strongly Anisotropic, Slowness surfaces, Acoustic tensor,

References

[1]. Spencer, A. J, M.,Constitutive theory for strongly anisotropic solids, in *Continuum theory of the mechanics of fibre reinforced materials*, ed. by A.J.M. Spencer, Springer-Verlag Wien-New York, 1984, pp. 1-33.
[2]. Ogden, R. W., *Non-Linear Elastic Deformations*, John Wiley & Sons, New York, 1988.
[3]. Nayfeh, A.H., *Wave Propagation in Layered anisotropic media*, Elsevir, (1995).

SOME PROBLEMS OF DYNAMICS OF A HEAVY RIGID BODY CARRYING A MATERIAL POINT

A. Markeev

Ishlinski Institute for Problems in Mechanics of
the Russian Academy of Sciences,
Prospect Vernadskogo, 101, block 1, 119526, Moscow, Russia
e-mail: markeev@ipmnet.ru

A system consisting of an outer rigid body (a shell) and an inner body (a material point) which moves according to a given law along a curve rigidly attached to the shell is considered. The system moves in a uniform gravity field over a fixed absolutely smooth horizontal plane. During its motion, the shell may collide with the plane. The coefficient of restitution at impact is supposed to be arbitrary.

If the shell executes free flight over the plane, the system mass center moves in a parabola or along a vertical straight line.

The paper presents differential equations governing the motion of the shell relative to its center of mass; they describe both stages of free flight over the plane and instances of collisions of the shell with the plane [1].

The shell is found can execute translational motion, if the material point moves according to the special law. The second Lyapunov method was used to investigate stability of this shell motion.

A general solution of the equations governing the rotational motion of the shell was obtained for the case where the shell is dynamically symmetric and the point moves along its symmetry axis according to an arbitrary law.

Two special cases of the system motion are also considered. In the first case the relative motion of the material point is assumed to be fast and the point mass small in comparison with the shell mass, and in the second one the point executes fast motion in a small neighborhood of a given point of the shell.

Using the classical perturbation theory methods approximate systems of differential equations governing the shell rotation are obtained for these cases. Difference between solutions of these systems and the corresponding exact systems of equations is estimated. First integrals of the approximate systems are found, their integrability is proved, and some special solutions are considered.

The paper also presents the results obtained in the problem of existence and stability of periodic motions of a dynamically symmetric shell colliding with a plane [2].

Keywords: rigid body, collisions, stability, rotational motion, fast motions, perturbation theory

References

[8] Markeev A.P., On the Dynamics of a Rigid Body Carrying a Material Point, *Nonlinear Dynamics*, **8** (2012), No 2, pp. 219 – 229. (in Russian)

[9] Markeev A.P., On Periodic Motion of a Rigid Body Carrying a Material Point in the Presence of Impacts with a Horizontal Plane, *Nonlinear Dynamics*, **8** (2012), No 1, pp. 71 – 81. (in Russian).

ONE APPLICATION OF REGULARLY VARYING FUNCTIONS TO FRIEDMANN EQUATIONS

Žarko Mijajlović

University of Belgrade – Faculty of Mathematics, Belgrade, Serbia
e-mail: zarkom@matf.bg.ac.rs

ABSTRACT. In this paper we analyze the asymptotic solutions of the acceleration equation

$$\frac{\ddot{a}}{a} = -\frac{4\pi G}{3}\left(\rho + \frac{3p}{c^2}\right)$$

related to the Friedman cosmological equation

$$\left(\frac{\dot{a}}{a}\right)^2 = \frac{8\pi G}{3}\rho - \frac{kc^2}{a^2}$$

which describes the expansion scale factor $a(t)$ of the universe. Here, $p = p(t)$ is the energy pressure in the universe, $\rho = \rho(t)$ is the density of matter in the universe, k is the space curvature, G is the gravitational constant and c is the speed of light. The variable t represents the cosmic time. We are particularly interested in the solutions satisfying the generalized power law $a(t) = t^\alpha L(t)$, where $L(t)$ is a regularly varying function in the sense of J. Karamata, see [3]. For this reason we introduced a new parameter $\mu(t) = q(t)(H(t)t)^2$ where $q(t)$ is the deceleration parameter and $H(t)$ is the Hubble parameter. We prove that the acceleration equation has an asymptotical solutions that satisfy the generalized power law if and only if the integral limit

$$\gamma = \lim_{x\to\infty} x\int_x^\infty \frac{\mu(t)}{t^2}dt$$

exists and $\gamma < 1/4$. Thus, the values of the constant γ determine the asymptotical behavior at the infinity of the solutions of the acceleration equation, i.e. of the expansion scale factor $a(t)$ of the Universe. Our approach presented in the paper covers all results on cosmological parameters for Standard model of the universe, as presented in [1] or in [2]. Our analysis is based on the theory of regularly

varying solutions of the linear second order differential equation developed by V. Marić, see [4].

Keywords: Friedmann equations, regular variation, cosmology, power law.

References

[1] Liddle, A.R., Lyth, L.H., *Cosmological Inflation and Large-Scale Structure*, Cambridge Univ. Press, Cambridge, 2000.
[2] Peacock, J.A., *Cosmological Physics*, Cambridge Univ. Press, Cambridge, 1999.
[3] Bingham, N.H., Goldie, C.M., Teugels, J.L., *Regular variation*, 491, Cambridge Univ. Press, Cambridge (1987)
[4] Marić, V., *Regular Variation and Differential Equations*, 127, Springer, Berlin (2000).

Naučno društvo Srbije
http://afrodita.rcub.bg.ac.rs/~nds/

Serbian Scientific Society
http://afrodita.rcub.bg.ac.rs/~nds/indexe.html

Symposium **Non-linear Dynamics – Milutin Milanković**
with Multi and Interdisciplinary Applications, **(SNDMIA 2012)**, Belgrade, October1-5, 2012
(Eigth Serbian Symposium in area of Non-linear Sciences)

PL-11. ID-84.

FRACTIONAL DERIVATIVE VISCOELASTIC MODELS IN THE WAVE THEORY OF IMPACT

Yury A. Rossikhin and Marina V. Shitikova
Research Center on Dynamics of Solids and Structures
Voronezh State University of Architecture and Civil Engineering
20-letija Oktjabrja Street 84, Voronezh 394006, Russia
Tel./Fax: +7-4732-773992, e-mail: yar@vgasu.vrn.ru, shitikova@vmail.ru

The recently published state-of-the-art article [1] devoted to the analysis of new trends and recent results in the field of fractional calculus application to dynamic problems of structural mechanics has shown that during the last decade fractional calculus entered the mainstream of engineering analysis and has been widely applied to structural dynamics problems both in discrete and continuous equations. Among many engineering problems considered in [1], the problems of dynamic contact interaction play the important role.

In the present paper, different approaches are reviewed for solving the problems dealing with the shock interaction of thin viscoelastic bodies, such as beams, plates and shell, with bodies of finite dimensions [2]. It is emphasized that fractional derivative viscoelastic models of the shock interaction possess some advantages, since they allow one to obtain the solution in the analytical form. Two approaches are discussed for studying the impact response of fractionally damped systems.

The first one is based on the assumption that viscoelastic properties of the target manifest themselves only in the contact domain, while the other part of the target remains elastic one and its behavior is described by the equations of motion which take rotary inertia and shear deformations into account. It is assumed that transient waves generate in the target at the moment of impact, the influence of which on the contact domain is considered using the theory of discontinuities. To determine the desired values behind the transverse shear wave front, one-term ray expansions are used, as well as the equations of motion of the falling mass and the contact region. This approach results in defining the contact force and the local penetration of target by an impactor from the set of linear fractional differential equations.

The second approach is the immediate generalization of the Timoshenko approach, wherein the internal viscoelastic properties of the whole target and Hertz's contact law are taken into account using Volterra correspondence principle. This approach

results in the nonlinear functional equation for determining the contact force or the impactor's relative displacement.

The examples of implementing these two approaches are presented, in so doing several procedures are suggested for the analysis of the impact response of fractionally damped systems depending on the different combinations of magnitudes of its mechanical and viscous features.

References

1. Yu. A. Rossikhin, M.V. Shitikova, Application of fractional calculus for dynamic problems of solid mechanics: Novel trends and recent results. *Applied Mechanics Reviews* 63 (1) (2010) 010801-1-52.
2. Yu. A. Rossikhin, M.V. Shitikova, Transient response of thin bodies subjected to impact: Wave approach. *The Shock and Vibration Digest* 39 (4) (2007) 273-309.

PL-12. IF-14.

HOMOGRAPHICAL SOLUTIONS OF HAMILTONIAN SYSTEMS AND COMPUTER ALGEBRA

E. Grebenikov[1] , N. Zemtsova[2]

Institution of Russian Academy of Sciences Dorodnicyn Computing
Centre of RAS, Vavilov st. 40, 119333 Moscow, Russia
[1] e-mail: e-greben@yandex.ru. [2] e-mail: zemni@yandex.ru

ABSTRACT. It is known that Hamilton differential equations of cosmic dynamics under certain conditions, imposed on geometrical and dynamic parameters of model, have the homographic solutions in Wintner sense [1,2,3,4,5].

The constructive theory of such solutions (that is ̄finding of the exact conditions guaranteeing their existence) have been implemented by us and our colleagues on the basis of application of system of computer algebra Mathematica[5].

In particular we have proved the existence of new classes homographic solutions for models with various number n gravitating bodies (n=4,5,6,7,8,9,10, ets.). We have developed a method of search of equilibrium points for such models and on the basis of the KAM-theory [6,7] have received sufficient conditions of their stability in Lyapunov's sense.

Keywords: dynamic systems, differential equations, stationary solutions, stability, computer algebra.

References
[1] Wintner A., The analytical foundations of celestial mechanics. MIR, Moscow, (1967), (in Russian).
[2] Grebenikov, E.A., Kozak-Skovorodkin, D., Jakubiak M., The Methods of Computer Algebra in Many-Body Problem. RUDN, Moscow, (2002), (in Russian).
[3] Zemtsova N.I., Stability of the stationary solutions of the differential equations of restricted Newtonian problem with incomplete symmetry, Nonlinear Dynamics and Systems Theory, **3**(1) (2003),pp. 121-130.
[4] Gadomski L., Grebenikov E.A., Prokopenya A.N., Studying the stability of equilibrium solutions in the planar circular restricted four-body problem, *Nonlinear oscillations*, **10**(1), (2007), 66-82
[5] Wolfram S., The Mathematica book. Wolfram Media, Cambridge University Press, (1999).
[6] Arnold V.I., Small denominators and problems of stability of motion in classical and celestial mechanics, Uspekhi Math.Nauk, 18(6), (1963), pp. 91-192, (in Russian).
[7] Markeev A.P., Libration points in celestial mechanics and cosmodynamics, Nauka, Moscow, (1978), (in Russian)

PHENOMENOLOGICAL MAPPING AND MATHEMATICAL ANALOGY IN NONLINEAR DYNAMICAL SYSTEMS

K. (Stevanović) Hedrih [1]

[1] Mathematical Institute SANU, Department of Mechanics,
and Faculty of Mechanical Engineering University of Niš, Serbia,
Priv. address: 18000- Niš, Serbiam ul. Vojvode Tankosića 3/22,
e-mail: khedrih@eunet.rs

ABSTRACT. On the basis of this phenomenological mapping and mathematical analogy, we present that analysis for one type of the system nonlinear dynamics is possible to applied for qualitative analysis of nonlinear phenomena appeared in dynamics of other disparate model or nature system nonlinear dynamics. The linearizations as well as nonlinear approximations of nonlinear differential equations around stationary points correspond to equilibrium positions or relative equilibrium positions of mechanical system dynamics with trigger of coupled singularities are obtained. First approximations of a nonlinear differential equation obtained by different methods and around different known analytical solutions were compared and corresponding conclusions are presented. As special examples are used nonlinear differential equations describing nonlinear dynamics of the mechanical system with coupled rotations in damping field

Keywords: Nonlinear dynamics, nonlinear phenomenon, trigger of coupled singularities, phenomenological mapping, approximation.
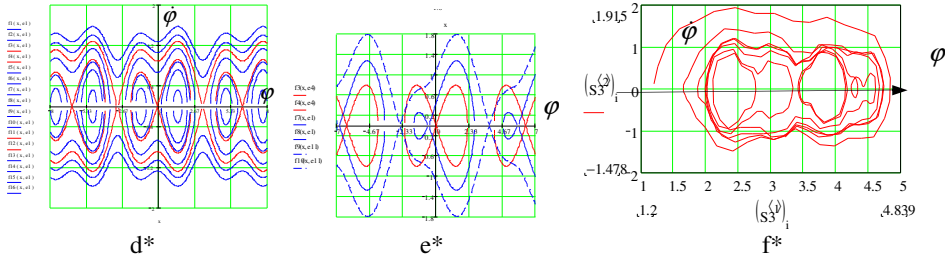
a*   b*   c*

d* e* f*
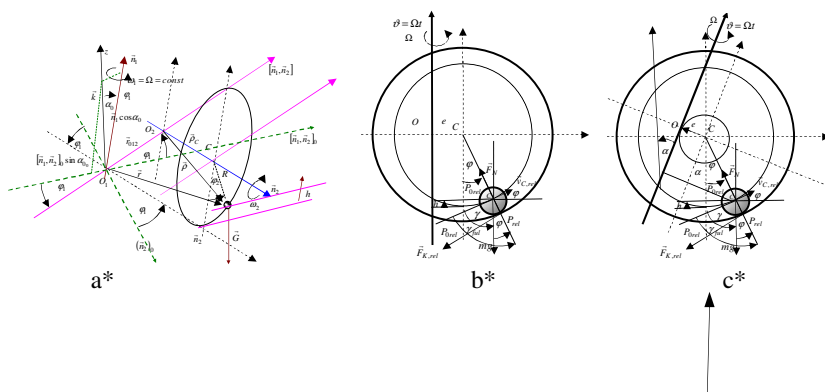
Figure 1. Three characteristic models (a*,b*,c*) of nonlinear dynamical systems abstractions of real nonlinear dynamical systems and three visualiyation of nonlinear dynamics in phase plane(d*,e*, f*).

Some characteristic nonlinear differential equations and approximations around stationary points: Nonlinear differential equations describing nonlinear dynamics of a heavy mass particle or a heavy disk rolling along rotating circle about axis inclined to the vertical direction with constant angular velocity are in the forms (see Figure 1 . a*, b* and c*, and also References [1-8]):

a* $\ddot{\varphi}_2 + 2\delta\dot{\varphi} + \Omega^2 (\lambda \cos\beta_0 - \cos\varphi_2)\sin\varphi_2 - \Omega^2 \dfrac{r_{012}}{R}\cos\varphi_2 = \Omega^2 \lambda \cos\varphi_2 \sin\beta_0 \sin\Omega t$, $\lambda = \dfrac{g}{R\Omega^2}$ (1)

b* $\ddot{\varphi} + \dfrac{\Omega^2}{\kappa}\langle\lambda - \cos\varphi\rangle\sin\varphi - \varepsilon\dfrac{\Omega^2}{\kappa}\cos\varphi = 0$, for $\varepsilon = 0$, $\ddot{\varphi} + \dfrac{\Omega^2}{\kappa}\langle\lambda - \cos\varphi\rangle\sin\varphi = 0$ (2)

c* $\ddot{\varphi} + \dfrac{\Omega^2}{\kappa}\langle\lambda\cos^2\alpha - \cos\varphi\rangle\sin\varphi - \dfrac{\Omega^2}{\kappa}\left(\varepsilon + \dfrac{\lambda}{2}\sin 2\alpha\right)\cos\varphi = \dfrac{\Omega^2}{2\kappa}\lambda\cos(\alpha + \varphi)\sin\alpha\cos\Omega t$ (3)

$$\varepsilon = \frac{e}{(R-r)} \text{ , } \kappa = \left(\frac{\mathbf{i}^2_{C,rel}}{r^2} + 1\right) = \frac{\mathbf{i}^2_{P,rel}}{r^2} \text{ , } \lambda = \frac{g}{(R-r)\Omega^2} \text{ , } \frac{\mathbf{J}_{P,rel}}{M} = \mathbf{i}^2_{P,rel} = \mathbf{i}^2_{C,rel} + r^2 \text{ , } \ell_{red} = \left(\frac{\mathbf{i}^2_{C,rel}}{r^2} + 1\right)(R-r)$$

Previous differential equations, also, represent the analogous differential equations of the self rotation heavy rigid body, skew and eccentrically positioned to the axis of self rotation, with coupled rotations about two no intersecting orthogonal axes.

Taking into account possible approximation of nonlinear differential equations (1)-(2)-(3) around stationary points (see trigger of coupled singularities and homoclinic orbit in the form of number "eight" in phase planes in Fig. 1. c*, e(and f*), we obtain series of the approximations and for this these examples, we separate the three following types of linearized approximations as results of linear mapping around stationary states (see Refs. [7]):

$$\ddot{\varphi} + \Omega^2(\lambda - 1)\varphi \approx \Omega^2 \lambda ctg\,\alpha\cos\Omega t \text{ ; } \ddot{\varphi} + 2\delta\dot{\varphi} + \omega^2_{0,lin}\varphi = \kappa_2\varphi^2 + \kappa_3\varphi^3 \text{ and}$$

$$\ddot{\varphi}_2 + 2\delta\dot{\varphi} + \varphi_2[\lambda + \gamma\sin\varphi_{s2}\cos\Omega t] + f = h_s\cos\Omega t$$

It is possible to obtain corresponding nonlinear approximations of of nonlinear differential equations (1)-(2)-(3) around stationary points. Then by using known analytical solutions of linearized nonlinear differential equations around stationary point, as the starting solutions, by application Krilov-Bogolyubov-Mitropolyski asymptotic methods and method of variation constants and averaging, different expressions, it is possible to obtain the first approximations of nonlinear differential equation solutions. For nonlinear differential equation: $\ddot{x}_1(t) + 2\delta_1\dot{x}_1(t) + \omega^2_1 x_1(t) = \mp\tilde{\omega}^2_{N1} x^3_1(t)$, (4)

By use two methods starting by known analytical solutions $x_1(t) = R_1(t)e^{-\delta_1 t}\cos(p_1 t + \phi(t))$, $p_1 = \sqrt{\omega^2_1 - \delta^2_1}$ and $x(t) = a(t)\cos[\omega_1 t + \phi(t)]$, and we obtained the first approximations of the solution in the different forms (see Refs. [9]):

$$x_1(t) = R_{01}e^{-\delta_1 t}\cos\left[p_1 t \mp \frac{3}{16\delta_1 p_1}\omega^2_{N1}a^2_o\left(e^{-2\delta_1 t} - 1\right) + \Phi_o\right] \text{. for } \delta_1 \neq 0 \text{ , } \varepsilon \neq 0 \text{ , } \omega^2_1 > \delta^2_1 \text{ , } p_1 = \sqrt{\omega^2_1 - \delta^2_1}$$ (5)

479

$$x_1(t) = a_o e^{-\delta_1 t} \cos\left[\omega_1 t \mp \frac{3}{16\delta_1\omega_1} \omega_{N1}^2 a_o^2 \left(e^{-2\delta_1 t} - 1\right) + \Phi_o\right] \quad \text{for } \delta_1 \neq 0, \ \varepsilon \neq 0, \ \omega_1^2 > \delta_1^2 \tag{6}$$

For the case that damping coefficient tends to zero, from both first approximations (5) and (6), we obtain same analytical approximation of the solution for conservative nonlinear system dynamics. For the case that coefficient of the cubic nonlinearity tends to zero, from first approximation (5), we obtain known analytical solution of the linear no conservative system dynamics, but the second obtained approximation (6) give not correct solution. Then we can conclude that, starting different known analytical solutions, for obtaining first approximations are acceptable, but limited by corresponding conditions.

References

[10] Andronov, A.A., Vitt, A.A., Haykin, S.E., (1981), *Teoriya kolebaniy,* Nauka, Moskva., pp. 568.

[11] Hedrih (Stevanović) K., (2005), *Nonlinear Dynamics of a Heavy Material Particle Along Circle which Rotates and Optimal Control*, Chaotic Dynamics and Control of Systems and Processes in Mechanics (Eds: G. Rega, and F. Vestroni), p. 37-45. IUTAM Book, in Series *Solid Mechanics and Its Applications, Editerd by G.M.L. Gladwell, Springer.* 2005, XXVl, 504 p., ISBN: 1-4020-3267-6.

[12] Hedrih (Stevanović) K., (2004), *A Trigger of Coupled Singularities*, MECCANICA, Vol.39, No. 3, 2004., pp. 295-314. , DOI: 10.1023/B:MECC.0000022994.81090.5f,

[13] Hedrih (Stevanović K., (2008), Dynamics of coupled systems, Nonlinear Analysis: Hybrid Systems, Volume 2, Issue 2, June 2008, Pages 310-334.

[14] Hedrih (Stevanović) K R. (2012), Energy and Nonlinear Dynamics of Hybrid Systems, Book Chapter, in *Dynamical Systems and Methods, Edited by Albert Luo, Tenreiro Machado and D Baleanu, , 2012, Part 1, Pages 29-83,* 2012, DOI: 10.1007/978-1-4614-0454-5_2 , ISBN 978-1-4614-0453-8. e-ISBN 978-1-4614-0454-5,

[15] Mitropolyskiy, Yu.A, (1964), Problemi asimptoti-cheskoy teorii nestashionarnih kolebaniy, Nauka Moskva.

[16] Petrović, M., Fenomenološko preslikavanje (Phenomenological mapp), SKA, Beograd, 1933. str. 33.

[17] Rašković D., Teorija oscilacija (Theory of Oscillations), Naučna knjiga, 1952.

SL-1. ID-70.

DIGITIZATION OF SCIENTIFIC AND CULTURAL HERITAGE IN SERBIA

Žarko Mijajlović

University of Belgrade – Faculty of Mathematics, Belgrade, Serbia
e-mail: zarkom@matf.bg.ac.rs

ABSTRACT. The aim of this paper is to present the efforts in the area of digitization and digital preservation of scientific and cultural heritage of a group of Serbian scientists. They are from the Faculty of Mathematics of the University of Belgrade, the Mathematical Institute and since recently the Faculty of Natural Sciences of the University in Priština, now situated in Kosovska Mitrovica. Digitized cultural heritage is one of the most important contemporary components of the study of our history and culture. On the other hand, digitized scientific works are the crucial resource and tool for scientific works and fast exchange of scientific information. Also, we understand that every scientific work becomes after some time the part of history and the part of cultural heritage as well. Due to the fast development of computer technologies and Internet, there are many advantages for using digitized works. Besides easy and fast access and exchange of information, the protection of scientific and cultural values is also one of the most important elements.

First Serbian mathematical book: Aritmetika, 1767

Vasilije Damjanović
mathematical book

Some digitization projects started in Serbia already in the middle of the nineties of the previous century. The aim of these early projects was the digitization of national cultural heritage and retro-digitization of mathematical books of old Serbian scientists. The principal participating institutions were Faculty of Mathematics, Belgrade, and Mathematical Institute of

481

the Serbian Academy of Science and Arts, but the other institutions were involved too (Archaeological Institute, Institute of musicology, Institute for monument protection of Serbia, National library, National museum, etc.). The projects were financed by the Ministry of Science of Serbia and Faculty of mathematics. The project *Computer archiving and multimedia presentation of cultural values and national heritage*, see [1], was the most important and comprehensive project in our country in the area of digitization until now. The project consisted of two parts:

- Infrastructure, standards and methodology of design and the architecture of data.
- Design and building of archive databases and program implementation.

In this presentation we describe **Virtual Library**, one of these sub-projects. It concerns digitization of mathematics-related books, theses, manuscripts, and mathematical journals somehow related to Serbia or our region of South Eastern Europe. The project's goal is to form digital archives, databases and presentations of digitized scientific editions in mathematical sciences (mathematics, mechanics, astronomy) and offer easier on-line access both to old and recent mathematical works. The

Virtual Library. The overall objective of the *Virtual Library of the Faculty of Mathematics*, University of Belgrade, http://elibrary.matf.bg.ac.rs, is to implement an as much as possible complete collection of retro-digitized books and other digital documents from the past, see [2]. The main part of this project relates to an electronic archive which contains first of all old manuscripts electronic form and their presentation to the general public.

The project was initially inclined towards mathematics, but since 2009 the books from other areas are also deposited in the Library. The preference is given to the Serbian authors and works that are related to the scientific and cultural region of Southeast Europe. Some of the books in the Library are rare and it is known that only a few copies of them are left in the printed form. Practically they are inaccessible to the general public. We felt it was important to preserve their existence in some way. Not only as a cultural and scientific heritage important for Serbia, but also as part of the World Heritage. We decided to contribute to the preservation of these books and present them to the general public in electronic, digitized form.

The Library has strong support from the Faculty of Mathematics, University of Belgrade, Mathematical Institute of Serbian Academy of Sciences and Arts (SASA), the National Center for Digitization and the Ministry of Science of Serbia.

Virtual Library of the Faculty of Mathematics is the largest Internet oriented database in Serbia of digitized texts with free access. At the time of this writing, the library contains almost 2,000 books. In the Library there are several important collections. For example, the Library contains an important collection consisting of 400 doctoral dissertations in mathematical sciences (most of them are defended at the Faculty of Mathematics). Another important collection consists of rare books from the 18th and 19th century. There are also small collections of digitized books from every republic of former Yugoslavia.

The important part of the Library make the collected works of some leading Serbian scientists from the past: Atanasije Stojković, Bogdan Gavrilović, Milutin Milanković, Đuro Kurepa, Đorđe Stanojević and several others.

Works related to the archive in the Virtual Library are published in the journal NCD Review (SEEDI Communication), issued by the Faculty of Mathematics in Belgrade.

Keywords: digitization, old mathematical books, scientific heritage

References

[1] Ž. Mijajlović, Z. Ognjanović, *A survey of certain digitization projects in Serbia*. Review of
   the National Center for Digitization, 4 (Proc. Symp. Digital Preservation of Cultural Heritage, 16–17 Sept. 2003, Borovets, Bulgaria), 52–61, 2004, http://elib.mi.sanu.ac.rs.
[2] Ž. Mijajlović, Z. Ognjanović, A. Pejović, *Digitization of Mathematical Editions in Serbia*,
   Mathematics in Computer Science, Vol. 3, Issue 3, 251-263, 2010. ISSN 1661-8270.

APPENDIX II

The 50th Anniversary Conference of the ICNO-ENOC in Rome 2011.

ICNO I	**September 1961 Kiev (USSR) Chair: Mitropolsky**
ICNO II	**September 1962 Warsaw (Poland) Chair: Ziemba**
ICNO III	**May 1964 Berlin (GDR) Chair: Reißig**
ICNO IV	**September 1967 Prague (Czechoslovakia) Chair: Djadkov**
ICNO V	**August 1969 Kiev (USSR) Chair: Mitropolsky**
ICNO VI	**September 1972 Poznan (Poland) Chair: Ziemba**
ICNO VII	**September 1975 Berlin (GDR) Chair: Schmidt**
ICNO VIII	**September 1978 Prague (Czechoslovakia) Chair: Pust**
ICNO IX	**September 1981 Kiev (USSR) Chair: Mitropolsky**
ICNO X	**September 1984 Varna (Bulgaria) Chair: Brankov**
ICNO XI	**August 1987 Budapest (Hungary) Chair: Farkas**
ICNO XII	**September 1990 Cracow (Poland) Chair: Gutowski**
ENOC I	**Hamburg, August 16 - 20, 1993, Chairman Professor Edwin Kreuzer**
ENOC II	**Prague, September 9 - 13, 1996, Chairman Professor Ladislav Pust, Secretary Professor Frantisek Peterka**
ENOC III	**Copenhagen, August 8 - 12, 1999, Chairman Professor Hans True**
ENOC IV	**Moscow, August 19 - 23, 2002, Chairman Professor Klimov**
ENOC V	**Eindhoven, August 7 - 12, 2005, Chairman Professor Dick van Campen**
ENOC VI	**St. Petersburg, June 30 - July 4, 2008, Chairman Professor Alexander Fradkov**
ENOC VII	**Rome, July 24 - 29, 2011, Chairman Professor Giuseppe Rega**
ENOC VIII	**Wien 2014.**

ICNO I:

September 12-18, 1961, Kiev, USSR
IUTAM Symposium on the Theory of Non-Linear Vibrations
Academy of Sciences of the Ukrainian SSR
Institute of Mathematics
Chairman: Prof. Dr. Yu. Mitropolsky

Committee: N.N. Bogolyubov (USSR, Chair),
M.L. Cartwright (UK), C. Hayashi (Japan), K. Klotter (USA),
S. Lefschetz (USA), Yu.A. Mitropolski (USSR), T. Vogel

Participants: 92 scientists from 13 countries, amongst them
A.I. Lurie (USSR), A.N. Tikhonov (USSR), Yu.A.
Mitropolski (USSR), M.L. Cartwright (UK), S. Lefschetz
(USA), S. Smale (USA)

Yu. A. Mitropolski

485

APPENDIX III

SYMPOSIUMS ON
NONLINEAR MECHANICS IN SERBIA

Symposium NONLINEAR DYNAMICS – Milutin Milanković, Belgrade October 2012 - НЕЛИНЕАРНА ДИНАМИКА 2012 organized by the Department of natural-mathematical sciences of Serbian Scientific Society is the eighth in Serbia in area of donlinear dynamics.

First symposium in area of Nonlinear mechanics was held in Aranđelovac in 1984 and was organized by Serbian society of mechanics. A leading scientist in the area of Nonlinear mechanics, academician RAS and NANU Yu.A. Mitropolskiy was an invited participant with a Plenary Lecture.

Symposium, entitled *Sixth International Symposium on Nonlinear Mechanics Nonlinear Sciences and Applications Niš 2003* (The 6th ISNM NSA NIŠ'2003), as was the case with the previous one, entitled '*Nonlinear Sciences at the Threshold of the Third Millenium*', is organized with the wish to unite in a single symposium, on the basis of the M*athematical Phenomenology* of *Mihajlo Petrovic Alas*, quite disparate sciences with the aim of integrating the knowledge of the participants of our symposium. This is a serious and long-term task of science.

How did it all start? It started here, at the Faculty of Mechanical Engineering, University of Niš.

Prof. dr *Danilo P. Rasković* (Ph.D. in mechanical engineering and BS in mathematics), the first head of the Chair for Mechanics and Automatics, while teaching mechanics at the Department for Mechanical Engineering at the newly founded Faculty of Technical sciences, directed his youngest and most talented students towards studying nonlinear oscillations and nonlinear mechanics. Thereafter, he initiated a cooperation with the academician *Jury Aleksejevitch Mitropolsky* and a leading school of nonlinear mechanics, asymptotic methods and nonlinear oscillations at the Institute for Mathematics in Kiev, Ukraine. That is how a centre for nonlinear mechanics was established at the Chair for Mechanics, Faculty of Mechanical Engineering in Niš. They were supported by the Institute for Mathematics – SANU from Belgrade and by the scientist from all the Universities in Yugoslavia, especially Universities in Belgrade and Novi Sad. The organization of symposiums on nonlinear sciences followed.

The *first symposium on nonlinear mechanics - Nonlinear Dynamics*, organized by YUSM and Serbian Society for Mechanics, was held in Arandjelovac. Prof. Jury Aleksejevitch Mitropolskiy gave the invited plenary lecture. All the members of the Chair for Mechanics and the Chair for Hydraulic Engineering of the Faculty of Mechanical Engineering University of Niš took part in this and other symposiums; they were co-organizers as well.

486

The *Second Yugoslav Symposium on Nonlinear Mechanics* entitled: ***"The First Yugoslav Conference on Nonlinear Deterministic and Stochastic Processes in Dynamical Systems with Applications YCNP Niš'91",*** organized by the Faculty of Mechanical Engineering was held in Niš. The Chairman of the Scientific Committee was Prof. dr V. Vujičić, while the Chairman of the Organizing Committee was Prof. Katica (Stevanović) Hedrih. Proceedings of Abstracts was printed; the papers and invited lectures which were approved were printed in the first and the following issues of the **University Journal – *Facta Universitatis, new Series – Mechanics, Automatic Control and Robotics with Editor-in-Cief*** Katica (Stevanović) Hedrih**.** This Series was the third Series, which was being published, besides the *Series Mathematics, Informatics and Electronics, and Energetics*. William Nash, Kazuyuki Yagasaki ..., gave the invited lectures, at this international symposium.

The invited plenary lectures were given by the following Yugoslav scientists: *Veljko A. Vujičić, Vladan Djordjević, Ljubomir Grujić, Božidar Vujanović, and other.*.

Prof*. dr Slobododan Laković*, the Dean of the Faculty of Mechanical Engineering University of Niš and a member of the Organizing Committee, has significantly contributed to the success of this symposium.

The ***Third Yugoslav Symposium on Nonlinear Mechanics*** was held in the form of a *Minisymposium*, as a part of the *XXII Yugoslav Conference on Mechanics in Ni*š in 1995. The Faculty of Mechanical Engineering in Niš, with co-organization by the Faculty of Civil Engineering organized this Congress as well.

The Chairman of the Organizing Committee was Prof. *Katica (Stevanović) Hedrih*. The Dean of the Faculty of Mechanical Engineering, was very hospitable. Academician ***Vladan Djordjević****,* the President of YUSM has contributed to the successful organization of this Congress and the Minisymposium. Professors *Yu. A. Mitropolskiy, V.V. Rumyantsev, Felix Chernousko, Anatoliy Martinyuk, Valentina Filchakova, Dan Stamatiu*, ... were guest at this symposium.

The ***Fourth Symposium on Nonlinear Mechanics*** was held in 1997, again in the form of a *Minisymposium*, as a part of the *XIII Yugoslav Congress on Theoretical and Applied Mechanics.* This Congress, held in the Congress Center – Zvezda in Vrnjacka Banja, was organized by the Yugoslav Society for Mechanics. The organization of this Symposium was helped by the Institute for Mathematics – SANU and the Faculty of Mechanical Engineering in Niš and in Belgrade.

The Chairman of the Scientific Committee was the academician ***Nikola Hajdin***, and the Chairman of the Organizing Committee was Prof. *Katica Hedrih*. Professors Anthony Kounadis, Guiseppe Rega, Anton Baltov, Ilya Blekhman .. ... were guest at this symposium.

The ***Fifth Symposium on Nonlinear Mechanics- Nonlinear Sciences at the Threshold of the Third Millenium*** was organized with the wish for it to become a tradition and to gather the connoisseurs of nonlinear phenomenology from disparate sciences and dynamic systems and for it to become renown all over the world.

The Chairmen of the Scientific Committee were academicians ***Jury A. Mitropolsky, V. M. Matrosov and V. Vujičić***, and the Chairmen of the Organizing Committee was Prof. *Katica Hedrih*. Academicians N. Hajdin, V.V. Rumyantsev and M. Prvanović and Professors D.S. Sophianopoulos, G.T.Michaltos, Ji Huan He, I. Finogenko, P.S. Krasil'nikov ..... were guests at this symposium.

The year of the Fifth Symposium was the year of the 10th **Jubilante issue** of the University Journal – ***Facta Universitatis, new Series – Mechanics, Automatic Control and***

487

Robotics. These symposiums and the Journal Facta Universitatis are a permanent characteristic of the University of Niš, Faculty of Mechanical Engineering in Niš and scientific achievements of Yugoslav and Serbian scientists in international relations.

Two last Mini-symposia on Non-linear Dynamics were at Third Serbian (28th Yu) Congress on Theoretical and Applied Mechanics, Vlasina lake, Serbia, 5-8 July 2011 and Forth Serbian (29th Yu) Congress on Theoretical and Applied Mechanics, Vrnačka Banja , Serbia, 4-7 Juny 2013. Between invited lecturers were Professor Subhash C. Sinha, Director, Nonlinear Systems Research Laboratory at Auburn University and Founding Editor, ASME Journal of Computational and Nonlinear Dynamics and Professor John T. Katsikadelis, President of Hellenic Society of Mechanics and Professor Pavel Krasilnikov, head of department of differential equation at Moscow Aviation Institute and ,e,be rod Scientific Council for evaluation Doctoral Dissertation in Russian Federation, in Russia.
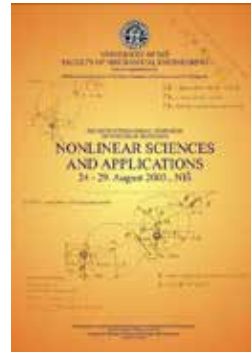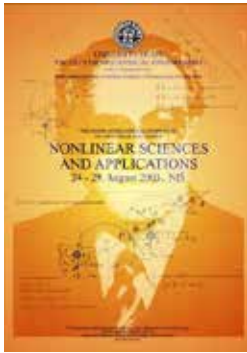
Katica (Stevanović) Hedrih

Serbian Symposium on Nonlinear Mechanics, Aradjelovac, 1984;

Invited Lecturer *Academician RAN and NANU Yu. A. Mitropolskiy* (KIEV) *in Niš with Serbian Scientists*

Invited Lecturer: Professor Willam Nash from MTI Massachusetts,
Founder of Journal Non-Linear Mechanics at
Yugoslav Conference on Deterministic and Stochstic Processes in Dynamical Systems
with Applications Nis 1991

THE FIFTH YUGOSLAV SYMPOSIUM ON NONLINEAR MECHANICS -NONLINEAR SCIENCES AT THE THRESHOLD OF THE THIRD MILLENNIUM (YUSNM NIŠ '2000)

held in Niš, Yugoslavia at October 2-5, 2000. at Faculty of Mechanical Engineering, and it dedicated to the 40th Anniversary of the Faculty of Mechanical Engineering and
Faculty of Civil Engineering and Architecture, as well as to the 35th Anniversary of the
University of Niš. The Symposium is organized under the patronage of the Departmentof Technical Sciences, Serbian Academy of Sciences and Arts.

*Academician RAS **V. Rumyantsev** (Moscow, Russia) in Niš*
(YUSNM NIŠ '2000-October 2-5, 2000.) at Faculty of Mechanical Engineering.

Participants of
The Fifth Yugoslav Symposium on Nonlinear Mechanics -NONLINEAR SCIENCES AT THE THRESHOLD OF THE THIRD MILLENNIUM (YUSNM NIŠ '2000)
from Russia, Greece, China, Bulgaria, Rumania, Ukraine and Yugoslavia. mr D. Jovanović (Niš,YU), Professor P. Krasil'nikov (Moscow, Russia), Professor Ji Huan He mr D. Jovanović (Niš,YU), , Academician UHEAS K. Hedrih (Niš, YU), Academician SASA M. Prvanović (Belgrade, YU), Professor G. Michaltsos (Athens, Greece), Z. Vosika (Belgrade YU), Professor D. Sophianopoulos (Athens, Greece), Academician SASA N. Hajdin (Belgrade, YU), Ass. Professor P. Rajkovi ć (Niš, YU), Professor G. T. Konstantakopoulos (Athens, Greece), Academician RAS V. Rumyantsev (Moscow, Russia), Professor D. Miki či ć (Belgrade, YU), Academician ANS V.A. Vujičić,....

Participants of the 6th International Symposium on Nonlinear Mechanics
Nonlinear Sciences and Applications 6th INM NSA NIŠ 2003.

(in middle professor A. Vatsala –USA, V. Lakshmikanthan-prsident of IFNA, Professor Leela-USA, Professor T. Kawaguchi-presinet of Tensor Society-Japan, Professor L. Bareteu- Romania, Professor F. Peterka-Prague, J. Warminski –Lublin, Professor U. Gabbert-Magdeburg and T. Nestorovic-now Professor in Bochum,... and Serbian participants)

Participants of the 6th International Symposium on Nonlinear Mechanics
Nonlinear Sciences and Applications 6th INM NSA NIŠ 2003.

D. Jovanović. K. (Stevanović) Hedrih (Niš), J. Warminski (Lublin), F. Peterka (Prague) and G. Rega (Roma)

6th International Symposium on Nonlinear Mechanics
Nonlinear Sciences and Applications 6th INM NSA NIŠ 2003.

Last Mini-symposia Non-linear Dynamics at Third Serbian (28th Yu) Congress on Theoretical and Applied Mechanics, Vlasina lake, Serbia, 5-8 July 2011. Between invited lecturers were Professor Subhash C. Sinha, Director, Nonlinear Systems Research Laboratory at Auburn University and Founding Editor, ASME Journal of Computational and Nonlinear Dynamics and Professor John T. Katsikadelis, President of Hellenic Society of Mechanics.

Invited Lectured Professor Pavel Krasilnikov, head of department of differential equation at Moscow Aviation Institute and ,e,be rod Scientific Council for evaluation Doctoral Dissertation in Russian Federation, in Russia.

Same of Participants of Minisymposium Nonlinear Dynamics – Milutin Milankovič at Forth Serbian (29th Yu) Congress on Theoretical and Applied Mechanics, Vrnačka Banja , Serbia, 4-7 Juny 2013.

A number of Participants of Symposium
Symposium Nonlinear Dynamics – Milutin Milanković
Multidisciplinary and Interdisciplinary Applications
(SNDMIA 2012), Belgrade, October 1-5, 2012.
(Eight Serbian Symposium in area of Non-linear Sciences)

Plenary and Invited Lecturers: Alber Luo, Katica (Srevanović) Hedrih, Ivana Kovačić and Hiroshi Yabuno

Plenary and Invited Lecturers: Hiroshi Yabuno, Alber Lu,Marina Shitikovam Katica (Srevanović) Hedrih, Marinko Ugrčićm Atevan Maksimović and young researcher Marija Stamenković

A number of Participants of Symposium

Symposium Nonlinear Dynamics – Milutin Milanković

Multidisciplinary and Interdisciplinary Applications
(SNDMIA 2012), Belgrade, October 1-5, 2012.
(Eight Serbian Symposium in area of Non-linear Sciences)

Plenary Lecturer Professor Pavel Krasilnikov

Professor Slobodan Anić and Professor Žarko Mijajlović

A number of Participants of Symposium
Symposium Nonlinear Dynamics – Milutin Milanković
Multidisciplinary and Interdisciplinary Applications
(SNDMIA 2012), Belgrade, October 1-5, 2012.
(Eight Serbian Symposium in area of Non-linear Sciences)

Plenary Lecturer: Tamara Nestorović

Plenary Lecturer and Chaurman: Mihail Zekrzhevski and Dragomir Zeković

Chaurman and Inviter Lecturer: Dragan Milosavljević and Dragomir Zeković

A number of Participants of Symposium
Symposium Nonlinear Dynamics – Milutin Milanković
Multidisciplinary and Interdisciplinary Applications
(SNDMIA 2012), Belgrade, October 1-5, 2012.
(Eight Serbian Symposium in area of Non-linear Sciences)

Plenary Lecturers: Marina Shitikova and Mihailo Lazarević

A number of Participants of Symposium
Symposium Nonlinear Dynamics – Milutin Milanković

A number of young researchers - participants of Symposium
Symposium Nonlinear Dynamics – Milutin Milanković

Inviter Lecturer: Ilya Simonovsky

Plenary Lecturer: Boris Malomed

APPENDIX IV

Chair of Mechanics Faculty of Mechanical Engineering Niš (1963–2005)

dr Ing. Dipl. Math. Danilo P. Rašković

(1910-1985)

The First Head of Chair of Mechanics and Automatic
at Faculty of Mechanical Engineering in Niš
(1963-1974)

Prof., Dr., Eng., B.Sc. Mathematician,

DANILO P. RAŠKOVIĆ,

full-professor at the Faculties of Mechanical Engineering in Belgrade, Niš, Kragujevac and Mostar, and the Faculties of Science in Belgrade and Novi Sad

Danilo Rašković, a doctor of technical sciences and mathematician with a university degree, was the founder of the first scientifically based courses of mechanics at the Faculty of Mechanical Engineering in Belgrade. He also introduced courses on the subject of resistance of material, elasticity theory, and oscillation theory all of which he taught, too. He was the author of many high-circulation textbooks of high scientific level and good mathematical foundation. He introduced vector, matrix and tensor calculus in the studies of mechanics at the Faculty of Mechanical Engineering in Belgrade and, later on, did the same at the mechanical engineering faculties in Niš, Kragujevac and Mostar. He enabled the Faculty in Belgrade, and similar schools elsewhere, to produce highly qualified and educated engineers which was one his greatest contributions. He wrote the first university textbook in Serbia on oscillation theory containing his original accomplishments in the field. He achieved considerable scientific results in the fields of elasticity theory and oscillation theory. With a good human resource base at Niš Faculty, which he had set up, he started research work into the field of nonlinear mechanics. His scientific work is important because in all of his projects he succeeded in connecting theories of elasticity and oscillation, and engineering practice. He wrote 25 university textbooks which covered the entire field of mechanics and related areas. Almost all of them had been reprinted several times, with some of them having 20 reprints. His excellent textbooks were in use on the territory of the entire former Yugoslavia, which was in tatters under the powerful influence of fascism during the Second World War.

Thanks to Professor Danilo Rašković, the faculties of mechanical engineering of Serbia, Bosnia and Herzegovina, and all the other republics of the once unified Yugoslavia, which are now separate states, produced excellent mechanical engineers. Rašković was a patriot and an honourable man. He was the recipient of the October award of the city of Niš for his contributions to the development of science at the city's university.

This distinguished scientific figure of exquisite creative energy and inspired enthusiasm, a scholar deeply attached to the Yugoslav and Serbian scientific and cultural heritage, and an exquisite pedagogue of high moral principles is in the living memory of many generations of students whom he taught how to learn and love mechanics, as a basic scientific branch of mechanical engineering either directly, through his lectures, or through his various and numerous textbooks and compilation of problems. His disciples and colleagues are glad that he had the ability to pass onto them his great enthusiasm permeated with his sincere devotion for mechanics and his exquisite scientific eagerness.

Professor Danilo P. Rašković was born in 1910, in Užice. Upon completing elementary school and six grades of high school, he graduated from the Military Academy in 1930. As an engineering military officer he enrolled in the department of mechanical and electrical engineering at the Faculty of Engineering in Belgrade, in 1933. Having graduated in 1938, he enrolled in the department of theoretical mathematics at the Faculty of Philosophy and graduated from it in 1941. As a graduate mechanical engineer he was appointed assistant section head of the Military Technical Institute in Čačak. He remained in that position during 1941. In 1942 he was appointed assistant at the Faculty of Engineering in Belgrade where he earned hid doctorate's degree in the same year, upon presenting his thesis entitled *Tangential Strains of Normally Profiled Beams.*

Professor Rašković lectured mechanics, strains of materials and oscillation theory at the faculties of mechanical engineering in Belgrade, Niš, Kragujevac, Novi Sad and Mostar, as well as at the Faculty of Science in Belgrade, Faculty of Philosophy in Novi Sad, Faculty of Electronics in Niš, and at the Military Technical College in Belgrade. More details on the research work of Professor Rašković can be found in the Belgrade University Bulletin no.75 of 1957, issued on the occasion of his appointment as a full professor at the Faculty of Mechanical Engineering in Belgrade. During his

university career, he was twice elected Vice-Dean of the Faculty of Mechanical Engineering of Belgrade University. In the mechanical engineering department at the Faculty of Engineering in Niš, he lectured statistics, kinetics, kinematics, dynamics, oscillation theory, resistance of material, theory of elasticity, as well as analytical mechanics, theory of nonlinear oscillations and continuum mechanics at the postgraduate level. He was the first head of the department of mechanics and automatics at the Faculty of Mechanical Engineering in Niš. He was an extremely inspired professor, scientist and practitioner much favoured among his students and respected by his colleagues both as a professor and an engineer, because he knew how to relate engineering theory to practice.

Professor Rašković was a very fertile writer. While still in the military service he wrote five professional papers. In the period before 1957, when he was appointed full professor, he published 26 scholarly papers. As a full professor he wrote 37 pieces of scientific work that were published in scientific journals of the Serbian Academy of Sciences and Arts, Polish Academy of Science, German Society of Mechanics ZAMM and some other foreign journals. He took part in a number of scientific meetings in the country and abroad. He reviewed papers for four leading referral journals in the world: *Applied Mechanics Review* (USA), *Mathematical Review* (USA), *Zentralblatt für Mathematik* (Germany) and *Referativnii žurnal* (Moscow). Professor Rašković was a member of several professional and scientific societies/association in the country and abroad, the GAMM being one of them. He initiated the foundation of the Yugoslav Society of Mechanics during 1952.

He wrote a considerable number of university textbooks which ran through numerous editions. Some of them still hold records as for the number of editions and copies printed within the group they belong to. In addition, he wrote a series of textbooks on the subject of mechanics for secondary technical schools, as well as a number of chapters in professional technical handbooks, mimeographed course materials and textbooks for post-secondary schools of mechanical engineering. He also wrote several textbooks for postgraduate studies.

Among the publications for postgraduate studies the following should be mentioned: *Analytical Mechanics, Theory of Elasticity and Tensor Calculus.*

Most of his university textbooks and publications were at the time of their first edition the only professional literature on the subject, in the Serbian language. So, his publications played an important part in spreading of the knowledge in the field of technical mechanics among students, and mechanical and other kinds of engineers in Serbia and Yugoslavia. It is particularly worth mentioning that he has interpreted all the material by the most modern mathematical apparatus and has illustrated it by numerous examples from the engineering practice. Many of the cited university publications are being reprinted even nowadays and are still used by both students of engineering and engineers themselves.

Although it has been ten years since he left us, Professor Rašković is still present among new generations of students, and engineers, through his renowned textbooks that bear the memory of his merits and which have also left an indelible imprint on the development of mechanical engineering science and practice, and on the formation of many a generation of university professors. His life and work have set an example to future generations of students educated at the University of Niš and provided them with a creative impulse. He is an everlasting paradigm and a proof of how one's deeds can outlive one's physical existence by far.

In 1962 Professor Rašković, **as the head of mechanics department at the Institute of Mathematics of the Serbian Academy of Sciences and Arts**, organized research work in four different study groups, each one dealing with a particular subject, which were: ***Stability of motion*** - supervised by Dr Veljko Vujičić, ***Boundary layer theory -*** supervised by Dr Victor Saljnikov, ***Problems of anisotropic incompatible materials with finite strain*** - supervised by Dr Rastko Stojanović and ***Optimal problems of mechanics*** -supervised by Prof. Dr. Danilo Rašković.

According to records from the mechanical engineering faculties in Belgrade and Niš, as well as those from the Zentralblatt's data base, he traveled abroad on several occasions in order to participate in international scientific gatherings or to expend his knowledge. In 1957 he went to Berlin to do his specialization studies with a piece of work which was published in the *Proceedings of the 20th International Congress of Applied Mechanics*. In September 1956, in Brussels, he participated in the working of the said congress. He took part in international congresses of applied mathematics and

mechanics of the German society GAMM a few times: 1957 - in Hamburg and 1958 - in Saarbrücken. Also, in 1959, 1961 and 1962 he was delegate of the Yugoslav Society of Mechanics. In 1963, in Karlsruhe, he represented Mathematical Institute of the Serbian Academy of Sciences. In 1966, in Darmstadt, he "*produced a scientific statement in the field of oscillation theory*" and in 1968 in Prague, Czechoslovakia, he had a paper entitled *Second order acceleration (jerk) for the relative motion of a body expressed by a matrix method*.

He also participated, several times, in the working of the International Conference of Nonlinear Oscillation (ICNO): 1962 in Warsaw, as a delegate of the Council of Science of the People's Republic of Serbia; 1969 in Kiev; 1972 in Krakow, at the '72 ICNO.

Between the 1963/64 and 1973/74 academic years he was Head of the mechanics section of the mechanical engineering department at the Technical Faculty in Niš, while giving lectures on all subjects from the mechanics group. Simultaneously, he taught mechanics at technical faculties in Kragujevac and Mostar and, for a while, also the subject of applied mathematics at Novi Sad Faculty of Mathematics. He accepted the position in Niš after being acquitted of the duty as a lecturer at the Faculty of Mechanical Engineering in Belgrade. The said acquittal was brought in by the Faculty in Belgrade, and was registered under the no. 67/8, in January 1964. Comments on the controversial decision are left to the others. For further reference readers should look into the book (*).

In 1974/75 he was arrested in Mostar, Bosnia-Herzegovina, and unjustly sentenced. Following the experience, he worked on new editions of his high-circulation textbooks, out of which the 10th edition of *Mechanics I* for university studies deserves a special mention as does the 15th edition of his handbook containing tables from the strength of materials. Last months of his life he spent preparing his textbook *Elasticity Theory* for publishing. It came out in 1985 but he did not live to see it.

He died, unexpectedly, on January 29, 1985 in Belgrade.

Content (continued)